Uncovering novel factors involved in the maintenance of genome integrity through functional genomics: Focus on DNA interstrand crosslink repair.

By

Edgar Alberto Pinedo Carpio

Division of Experimental Medicine, Faculty of Medicine

McGill University

Montreal, Quebec, Canada

Winter 2023

A thesis submitted to McGill University in partial fulfilment of the requirements of the degree of Doctor in Philosophy in Experimental Medicine

© Edgar Pinedo Carpio, 2023

Abstract

DNA interstrand crosslinks (ICLs) are considered one of the most deleterious DNA lesions due their impact on both DNA replication and transcription. ICLs are of clinical relevance since several chemotherapeutic agents, such as platinum-based agents or nitrogen mustards (e.g cyclophosphamide) generate ICLs as part of their antineoplastic mechanism-of-action. Cells employ a complex array of interconnecting DNA repair pathways to deal with ICLs, including the Fanconi anemia (FA) and Homologous Recombination (HR) repair pathways. To gain insight into the factors involved in the cellular response to ICL, I performed a series of genome-wide CRISPR-based screens in cells treated with mafosfamide, a chemical analog to cyclophosphamide. My thesis first focuses on the characterization of C1orf112 as a novel modulator of the response to ICL-inducing agents. Depletion of C1orf112 impairs genomic stability by increasing spontaneous levels of γ-H2AX, micronuclei and 53BP1-nuclear bodies. In fact, C1orf112 acts in the HR-mediated phase of the FA pathway and is required for the resolution of ICL-induced RAD51 foci. Furthermore, proximal mapping of C1orf112 using miniturboID identified the AAA+ ATPase FIGNL1 as a constitutive interactor and functional characterization of this complex shows that C1orf112 and FIGNL1 cooperate in the unloading of RAD51 at ICL-induced lesion. The second part of my thesis focuses on the characterization of a series of poorly characterized open-reading frames using targeted mini-screening. This systematic approach identified C1orf27 as a novel factor involved in the modulation of ICL repair. Secondary validation, chemogenomic profiling, proteomic analysis delineated C1orf27 as a potential regulator of ubiquitin-like post-translation processes during the ICL response. Specifically, my analysis suggested that C1orf27 collaborates with UFM1-specific peptidase UFSP2 in modulating UFMylation during ICL repair. Notably, C1orf27 have prognosis potential in ovarian cancer in which RNA expression correlates with poorer patient outcome. Altogether, my findings reveal that C1orf112 is a previously

unidentified regulator of the AAA+ ATPase FIGNL1 in the resolution of ICLs by homology-directed DNA repair pathways. Second, my CRISPR-based targeted approach and proteomic analysis has uncovered C1orf27 as a novel factor involved in the UFM1 pathway through its cooperative role with UFSP2. These studies harbors implications for the diagnosis and the treatment of diseases characterized by alterations in the FA/HR repair pathways. Furthermore, the synthetic lethality signatures uncovered in our screens represent an important consensus dataset for the ICL response that could be further explored for revealing other novel factors involved in FA- and HR- mediated DNA repair.

Abrégé

Les liaisons interbrins (LIBs) de l'ADN sont considérées comme l'une des lésions d'ADN les plus délétères, car elles entravent toute réplication et transcription subséquentes. Les LIBs sont d'importance clinique puisque plusieurs agents chimiothérapiques, tels que les agents à base de platine ou les moutardes azotées (par exemple le cyclophosphamide), génèrent des LIBs dans le cadre de leur mécanisme d'action antinéoplasique. Les cellules utilisent un réseau complexe de voies de réparation de l'ADN interconnectées pour réparer les ICL, y compris les voies de réparation de l'anémie de Fanconi (FA) et de la réparation dirigée par homologie (HDR). Afin de mieux comprendre les facteurs impliqués dans la réponse cellulaire aux LIBS, j'ai effectué une série de criblage par CRISPR à l'échelle du génome dans des lignées cellulaires malignes traitées *in vitro* avec du mafosfamide, un analogue chimique du cyclophosphamide, pour induire la formation de lésions ICL intracellulaires. Ma thèse porte d'abord sur la caractérisation du cadre de lecture ouvert « C1orf112 » en tant que nouveau modulateur de la réponse cellulaire aux agents inducteurs de LIBs. La déplétion de C1orf112 entraine une altération de la stabilité génomique en augmentant les niveaux spontanés de g-H2AX, de micronoyaux et de corps nucléaires 53BP1. En fait, C1orf112 agit au niveau la phase médiée par HDR de la voie FA et est nécessaire à la résolution des foyers RAD51 induits par les ICL. De plus, l'analyse des interactions protéiques de C1orf112 à l'aide du miniturboID a identifié la AAA+ ATPase FIGNL1 comme une protéine qui interagit constitutivement avec C1orf112 et la caractérisation fonctionnelle de ce complexe démontre que C1orf112 et FIGNL1 coopèrent dans le déchargement de RAD51 au niveau de la lésion induite par l'ICL. La deuxième partie de ma thèse porte sur la caractérisation d'une série de cadres de lecture ouverts mal caractérisés à l'aide d'écrans CRISPR ciblés. Cette approche systématique a identifié C1orf27 comme un nouveau facteur impliqué dans la modulation de la réparation de l'ICL. La validation secondaire, l'exposition de cellules malignes à des agents chimiothérapiques, et l'analyse des interactions protéiques, ont identifiée C1orf27 comme un

régulateur de modification post-traductionnelle de l'ubiquitine pendant la réparation d'ICL. Plus précisément, mon analyse à l'aide du miniturboID suggéré que C1orf27 collabore avec la peptidase UFSP2 spécifique à UFM1 pour moduler l'UFMylation pendant la réparation d'ICL. Notamment, C1orf27 est considéré comme un potentiel biomarqueur du pronostic pour le cancer de l'ovaire. En effet, des hauts niveaux d'expression de l'ARN de C1orf27 à des mauvais pronostics pour les patients. Dans l'ensemble, mes découvertes révèlent que C1orf112 est un régulateur précédemment non identifié de l'AAA + ATPase FIGNL1 impliqué dans la résolution des ICL par des voies de réparation de l'ADN dirigées par homologie. Deuxièmement, mon approche ciblée basée sur la technologie CRISPR a identifié C1orf27 comme un nouveau facteur impliqué dans la modulation de l'UFMylation au cours de la réparation des ICL. Ces études auront des implications sur le diagnostic et le traitement de maladies caractérisées par des altérations des voies de réparation FA/HDR. De plus, les signatures de létalité synthétique découvertes dans nos écrans CRISPR représentent un important ensemble de données consensuelles pour la réponse ICL qui pourrait révéler de nouveaux facteurs impliqués dans la réparation de l'ADN médiée par FA et HDR qui pourraient potentiellement être exploités dans un cadre clinique.

Preface

This is a manuscript-based thesis which consist of one research article submitted and under review and one research article to be submitted. Text included in the Chapter I which is a general introduction was adapted from published reviews.

Chapter II:

Edgar Pinedo-Carpio[#], Julien Dessapt[#], Romain Villot, Lauralicia Sacre, Abba Malina, Jonathan Boulais, Elise G. Lavoie, Vincent Luo, Anna-Maria Lazaratos, Jean-François Côté, Frédérick Mallette, Alba Guarné, Amelie Fradet-Turcotte[§], and Alexandre Orthwein[§]. C1orf112/FIRRM is a novel regulator of interstrand crosslink repair that decreases FIGNL1-RAD51 interaction. bioRxiv **doi:** https://doi.org/10.1101/2022.10.06.511186

Chapter III:

Edgar Pinedo-Carpio, Abba Malina, and Alexandre Orthwein. Genome-wide CRISPR-based screening identifies C1orf27 as a novel regulator of DNA interstrand cross-link repair through its role in UFMylation.

Dedication

To my kids, Gerardo and Isabella,
my essential flames which daily fire me up to move forward in life.

Acknowledgments

Following an analogy with the adage "*takes a village to raise a kid*", I truly believe that it takes great effort and plenty of work and contributions from colleagues, friends, and family to finish a PhD. As such, it is with great pleasure that I dedicate these lines to everyone who has supported me and encouraged me to pursuit this scientific endeavour. First and foremost, I would like to start my expression of gratitude with my supervisor and mentor, Dr. Alexandre Orthwein, who allowed me to learn and explore my curiosity during all these years of graduate studies. It is through hard work and challenging goals that he prompted me to become a better scientist. Thanks for the long discussions, Alex, and the considerable patience with my stubbornness when pursuing and tackling scientific problems.

I also would like to thank our collaborators and friends at the Université of Laval: Dr. Amélie Fradet-Turcotte and Julien Dessapt, whose work and scientific drive allowed us to ellaborate together a wonderful piece of research for which I feel privileged and deeply grateful. I would like to also thank my co-supervisors: Dr. Nathalie Johnson, Dr. Raquel Aloyz, and the members of my thesis committee: Dr. Stephanie Lehoux, Dr. Francois Mercier, Dr. Koren Mann, Dr. Lawrence Panasci, Dr. Russell Jones and Dr. Gerardo Ferbeyre, for their valuable scientific advice and constructive criticism during my years of graduate studies.

I am also grateful to my friends and colleagues of the Orthwein laboratory, Vincent, Estelle, Oded, Anna-Maria, Arash, Steven, Damien, Manon, Elise, Zara, and special gratitude to Dr. Abba Malina, colleague and friend who has advised me throughout these years and has always found the time to discuss science in company of a good beer. Thanks to my friends at the Lady Davis institute, Luca, Barbara, Tamiko, Christian, Ryan, Maria, Sahil, Martin, Cesar, Carlos, Janette, and Sofia, for their continuous support and friendship. I would like to express my deepest gratitude to my parents, siblings, and grandmother back home in Peru for always believing in me and encouraging me to continue with my dreams. Last, but not least important, I would like to finish thanking my beloved

wife Milagros and my two kids Gerardo and Isabella, for always being there, for their unconditional love and support and for giving me the strength to continue and successfully finish this scientific journey. Parenthood during graduate studies can be challenging, but it is also true that a smile or laughter of your kids gives you joy and fortitude to move forward, thanks Mila for being my partner and wife, for your support and for showing me by example how to merge graduate studies and parenting successfully.

Contribution of Authors

Chapter I

I wrote the general introduction presented in this chapter using published reviews and articles related to the topics covered. Text presented in this chapter was completed under the supervision of Dr. Alexandre Orthwein.

Chapter II

Experiments were conceived, designed, and performed by both me and Julien Dessapt. Specifically, I generated the Cas9-expressing cells, optimized the Burkitt lymphoma screen pipeline, and executed the Namalwa and Raji genome-wide screens. I processed the screen genomic DNA and prepared the NGS libraries. I conducted the bioinformatic screen analysis and selected the hits for further characterization. I conducted the GSEA, GO and network analysis. I conducted the initial validation of C1orf112 using the competition assay. I generated the C1orf112 KO cells in the RPE1-hTERT p53-/- background. I performed the DR- and SA-GFP assays in U2OS and Hela cells. I conducted the senescence-associated β-Gal assay in RPE1 cells. I conducted the apoptosis and SRB experiments. I generated the stable C1orf112- and FIGNL1-miniturboID cells and executed the proteomic experiments. I functionally validated the epistatic relationship between C1orf112 and FIGNL1 using the DR-GFP and competition assay. I cloned the full-length cDNA into the pENTR221 vectors and generated the siRNA resistance and C1orf112 mutants and truncations used in the protein-structure analysis. Finally, I performed the expression-drug sensitivity analysis for C1orf112. Julien Dessapt conducted immunofluorescent experiments: Fok1, LacO/LacR, micronuclei, 53BP1, γ-H2AX and RAD51 persistance; drug-sensitivity assay in U2OS. Romain Villot conducted the senescent experiments in IMR90 cells. Jonathan Boulais conducted the bioinformatic analysis of the proteomic data. Elise G. Lavoie generated the FIGNL1 mutants, truncations, performed qPCR experiments and assisted with molecular cloning. Anna-Maria Lazaratos assisted with molecular cloning. Abba Malina optimized the general pipeline used in the genome wide screens and assisted with the bioinformatic analysis. All work presented in this chapter was completed under the supervision of Dr. Alexandre Orthwein and Dr. Amelié Fradet-Turcotte.

Chapter III

Experiments were conceived, designed, and performed by me. Specifically, I generated the Cas9-expressing cells, optimized the Burkitt lymphoma screen pipeline, and executed the Ramos genome-wide screen. I processed the screen genomic DNA and prepared the NGS libraries. I conducted the bioinformatic screen analysis and selected the hits for further characterization. I conducted the GSEA, GO and network analysis. I designed and generated the minilibraries used in the mini-screening validation. I conducted the miniscreens, processed the genomic material, generated the NGS libraries and conducted their analysis. I conducted the multi-omics analysis and identified the interacting partners of C1orf27. I performed the DR-GFP assays in Hela cells. I performed the correlation analysis between patient outcome and gene expression for C1orf27 in ovarian cancer cohorts. I generated the C1orf27-, UFSP2- and UFL1-miniturboID stable cells and executed the proximity labelling proteomic experiments. I conducted the bioinformatic analysis of the proteomic data. Abba Malina optimized the general pipeline used in the genome wide screens and assisted with the bioinformatic analysis. All work presented in this chapter was completed under the guidance and supervision of Dr. Alexandre Orthwein.

Chapter IV

I wrote the general discussion presented in this chapter. Text presented in this chapter was completed under the guidance and supervision of Dr. Alexandre Orthwein.

Contribution to original knowledge

Chapter II

- We have successfully conducted two genome-wide CRISPR-based screens in Burkitt lymphoma cells and have uncovered an important dataset of genetic vulnerabilities associated with mafosfamide treatment.
- Our CRISPR screening approach identified C1orf112 as a novel player in the response to interstrand crosslink agents.
- We demonstrate that C1orf112 controls cellular fate by regulating replicative stress-induced senescence and apoptosis.
- We demonstrate that C1orf112 collaborates with the AAA+ ATPase anti-recombinase FIGNL1 to promote the resolution of both interstrand crosslinks and double strand breaks by homologous recombination.
- We showed that C1orf112 facilitates the unloading of the recombinase RAD51 at DSBs in a FIGNL1-dependent manner, thereby promoting ICL repair.

Chapter III

- We have successfully conducted a genome-wide CRISPR-based screens in Ramos Burkitt lymphoma cells and have uncovered an important complementary dataset of genetic vulnerabilities associated with mafosfamide treatment.
- Our CRISPR screening approach using tailored minilibraries focus on poorly characterized ORFs allowed us to identify C1orf27 as a novel factor involved in the response to diverse interstrand crosslink agents.

- Integrated analysis of CRISPR-screen, proteomics and co-evolutionary data have allowed us to position C1orf27 as a novel factor involved in UFMylation.

- Chemogenomic profiling of C1orf27 and canonical members of the UFM1 pathway indicates that this ubiquitin-like modification plays an important role in the response to DNA damage induced by replication stress and ICL agents.

- Using the Hela DR-GFP reporter cell line we have uncovered a previously unknown role of C1orf27 in homologous recombination.

- Using biotinylation-based proximity proteomics we have mapped the protein interactome of C1orf27, UFSP2 and UFL1, which indicates a cooperation between C1orf27 and the peptidase UFSP2 during UFMylation.
- Expression analysis of C1orf27 correlates with patient outcome in cohorts of ovarian cancer patients.

Table of Contents

ABSTRACT…… i
ABREGE…….iii
PREFACE……....v
DEDICATION……...vi
ACKNOWLEDGMENTS…….vii
CONTRIBUTION OF AUTHORS……....ix
CONTRIBUTION TO ORIGINAL KNOWLEDGE…… .xi
TABLE OF CONTENTS……..xiii
LIST OF FIGURES…….....xvi
LIST OF TABLES……...…….xviii
LIST OF ABBREVIATIONS……....xix

Chapter I: General Introduction……..……...27

1.1 DNA replication and genome integrity……27
1.2 Genomic stability maintenance……27
1.2.1 Replication stress ……..……...…….…...27
1.2.1.1 Replication fork barriers……..28
1.2.2 DNA Double strand break repair……32
1.2.2.1 Canonical NHEJ ……33
1.2.2.2 alt-EJ……..35
1.2.2.3 HR…….…….36
1.2.2.4 SSA…….……42
1.2.3 Nucleotide Excision Repair…….43
1.2.4 Translesion synthesis……...45
1.2.5. Ubiquitin and ubiquitin-like modifications in DNA repair…….……..48
1.2.5.1 UFM1 pathway……50
1.2.6 DNA damage checkpoints……..53
1.2.7 DNA damage and senescence…….56
1.3 Fanconi Anemia: Disease and diagnosis……..58
1.4 Interstrand crosslinks and FA/BRCA ICL repair pathway……..63
1.4.1 Molecular mechanisms in FA/BRCA ICL repair……64
1.5 ICL-inducing agents and Cancer therapy……70
1.6 Cyclophosphamide and Cisplatin……72
1.7 Functional genomics and DNA repair research……...74
1.7.1 CRISPR/Cas9-based genome-wide screening…….…….77
1.7.1.1 The Toronto KnockOut library……...80
1.7.1.2 MAGeCK and DrugZ……81
1.8 Biotinylation-based proximity labelling proteomics and TurboID……..……82
1.9. Open-reading frames ……..…83
1.9 Summary and rationale……....85

Chapter II: C1orf112/FIRRM is a novel regulator of interstrand crosslink repair that decreases FIGNL1-RAD51 interaction.

2.1 Abstract……90
2.2 Introduction……91
2.3 Results
2.3.1 CRISPR screening identifies C1orf112 as a modulator of ICL repair in BL cells.....93
2.3.2 C1orf112 depletion induces genomic instability and cellular senescence in a p53-dependent manner……100
2.3.3 C1orf112 acts downstream of the FA pathway during ICL repair……108
2.3.4 C1orf112 interacts and acts with FIGNL1 in ICL repair……116
2.3.5 C1orf112 regulates FIGNL1 interaction with RAD51 and RAD51 resolution at ICLs……125
2.4 Discussion……135
2.5 Material and Methods……138
2.6 Acknowledgements……149
2.7 Author Contributions……149
2.8 Conflict of interest……149
2.9 References……150

Chapter III: Genome-wide CRISPR-based screening identifies C1orf27 as a novel regulator of DNA interstrand cross-link repair through its role in UFMylation.

3.1 Abstract……158
3.2 Introduction……159
3.3 Results
3.3.1 Genome-wide CRISPR screening identified open-reading frames as novel factors involved in the response to mafosfamide ……161
3.3.2 Secondary validation positioned C1orf27 as novel factor involved in the response to ICL……169
3.3.3 Multiomics data integration analysis delineated C1orf27 as a novel factor involved in the UFM1 pathway……177
3.3.4 C1orf27 interacts with UFSP2, and they collaborative operate in the UFM1 pathway ……183
3.3.5 Probing the UFM1 protein network upon ICL damage through miniturboID proximity labeling……189
3.3.6 Proposed model for C1orf27's role in the UFM1 pathway and its potential clinical relevance as a biomarker. ……196

3.4 Discussion……201
3.5 Materials and Methods……206
3.6 Acknowledgements……210
3.7 Author Contributions……211
3.8 Conflict of interest……211

3.9 References……212

Chapter IV: General Discussion**……..……...**219
Future Directions……..……234
Final Conclusion and Summary……..……...…237
References……...…...239
Appendix……...……....278

List of Figures

Figure 1.1 Schematics of the different sources of DNA Replication Stress.

Figure 1.2 Overview of DSB repair pathways.

Figure 1.3 Overview of DNA Damage repair pathways.

Figure 1.4 Overview of UFM1 pathway.

Figure 1.5 Replication-dependent ICL/FA repair pathway.

Figure 2.1 CRISPR-based genome-wide screening identifies C1orf112 as a novel modulator of mafosfamide sensitivity.

Figure 2.2 Depletion of C1orf112 lead to genomic instability and senescence-induced cell death.

Figure 2.3 C1orf112 is not a core FA gene but is required for HR.

Figure 2.4 FIGNL1 is a functional interactor of C1orf112.

Figure 2.5 The C1orf112-FIGNL1 complex regulates RAD51 unloading in HR.

Figure 2.S1 Additional analysis of CRISPR screen performed in Raji and Namalwa cells, related to Fig. 2.1.

Figure 2.S2 Validation of C1orf112 knockdowns and knockouts, 53BP1 nuclear bodies in analysis and additional senescence assay in IMR90 cells, related to Fig 2.2.

Figure 2.S3 Characterization of C1orf112 knockdown and knockout cells related to Fig. 2.3

Figure 2.S4 Validation of protein expression and cell lines for mTurboID and LacO/LacR analysis, and characterization of C1orf112 and FIGNL1 in survival assays.

Figure 2.S5 Expression levels and cellular localization of mCherry-LacRnls-FIGNL1 and GFP-C1orf112 constructs used in Fig. 5.

Figure 2.S6 Chemogenomic profiling of C1orf112, FIGNL1 and literature-curated relevant genes.

Figure 3.1 Genome-wide CRISPR-based dropout screen identifies C1orf27 as a novel regulator of the response against mafosfamide.

Figure 3.2 Secondary validation using targeted CRISPR-based screens and DNA damaging agents position C1orf27 as novel factor involved in ICL repair.

Figure 3.3 Multiomics analysis of C1orf27 and its interacting partners and its potential role in Homologous recombination.

Figure 3.4 C1orf27 interacts with UFSP2, and they collaborative operate in the UFM1 pathway.

Figure 3.5 Probing the UFM1 protein network upon ICL damage through miniturboID proximity labeling.

Figure 3.6 Proposed Model of C1orf27's role in the UFM1 pathway.

Figure 3.S1 Additional information about screen parameters assessed for Ramos-Cas9 BL cells used in the Ramos- CRISPR screen related to Figure 3.1

Figure 3.S1.1 Normalized read count distribution of all samples.

Figure 3.S2 Gene-set enrichment Analysis (GSEA) and Network analysis of Ramos screen.

Figure 3.S3 Additional information of multiomics, mutational, DR-GFP assay and protein structure analysis of C1orf27.

Figure 3.S4 Biotinylation and fusion-protein expression assessment of C1orf27-, UFSP2- and UFL1-miniturboID stable cells.

Figure 3.S5 Integrative analysis of the proximal interactomes of C1orf27, UFSP2 and UFL1.

Figure 3.S6 C1orf27 expression correlates with poor survival in ovarian cancer.

List of Tables

Table 1.1 Fanconi Anemia and FA-associated genes and their molecular functions.

Table 2.S1 NormZ values for Namalwa and Raji CRISPR-screens.

Table 2.S2 Genes Ontology analysis, related to figure 2.1D.

Table 2.S3 NormZ values figure 2.5, 2.S3F and 2.S6**.**

Table 2.S4 Hits from mTurboID Figure 2.4 and 2.5.

Table 2.S5 Primers, sgRNAs, shRNAs and siRNAs sequences used in this study.

Table 2.S6 Antibodies used in this study.

Table 2.S7 Plasmids used in this study.

Table 2.S8 Bioinformatic packages and algorithms used in this study.

Table 3.S1 Mapped read Statistics-Count Report Ramos Screen.

Table 3.S2 Zero counts and Gini-Index Statistics-Count Report Ramos Screen.

Table 3.S3 NormZ values for Ramos CRISPR-screen related to figure 3.1 B.

Table 3.S4 GSEA-Gene Ontology analysis related to figure 3.1 C and 3.S2 A.

Table 3.S5 MAGeCK MLE Z-scores values for Ramos miniscreens related to figure 3.2 A.

Table 3.S6 Gene Ontology analysis related to figure 3.3 C & 3.S3 A.

Table 3.S7 High confidence hits obtained in C1orf27-miniturboID proteomics.

Table 3.S8 High confidence hits obtained in UFSP2-miniturboID proteomics.

Table 3.S9 High confidence hits obtained in UFL1-miniturboID proteomics.

Table 3.S10 Gene ontology analysis of C1orf27-miniturboID dataset related to figure 3.4 D.

Table 3.S11 Gene ontology analysis related to figure 3.5 D and E.

Table 3.S12 Triple intersection of proteomics datasets related to figure 3.S5 B.

Table 3.S13 Primers and sgRNAs sequences used in this study.

Table 3.S14 Software and packages used in this study.

List of Abbreviations

53BP1	p53-binding protein 1
6-4PPs	6-4 pyrimidine-pyrimidone photoproducts
ADH5	Alcohol dehydrogenase 5
ADP	Adenosine di-phosphate
aEJ	Alternative end-joining
ALDH2	Aldehyde dehydrogenase, mitochondrial
APEX2	Apurinic/Apyrimidinic Endodeoxyribonuclease 2
ATM	Ataxia telangiectasia mutated
ATP	Adenosine triphosphate
ATR	Ataxia telangiectasia and Rad3-related
BARD1	BRCA1-associated RING domain protein 1
BER	Base excision repair
BIR	Break-induced replication
BLM	Bloom syndrome helicase
BMI1	Polycomb complex protein BMI-1
BRCA1	Breast cancer type 1 susceptibility protein
BRCA2	Breast cancer type 2 susceptibility protein, also known as FANCD1
BRCT	BRCA1 C terminus
C1orf112	Chromosome 1 Open Reading Frame 112
C1orf27	Chromosome 1 Open Reading Frame 27
C12orf23	Chromosome 12 Open Reading Frame 23
CHK1	Checkpoint kinase 1
CHK2	Checkpoint kinase 2
CMG	DNA helicase (CDC45, MCM2–7 and GINS)

cNHEJ	Classic nonhomologous DNA end-joining
CO	Crossover
CPDs	Cyclobutene-pyrimidine dimers
CRISPR	Clustered Regularly Interspaced Short Palindromic Repeats
crRNA	CRISPR RNA
CSR	Class switch recombination
CtIP	CtBP-interacting protein
D-loop	Displacement loop
DDC	DNA damage checkpoint
DDR	DNA-damage response
DDRGK1	DDRGK domain-containing protein 1
dHJ	Double Holliday junction
DNA	Deoxyribonucleic acid
DNA-PKcs	DNA-dependent protein kinase catalytic subunit
DPC	DNA-protein crosslink
DSBs	DNA double-strand breaks
DTT	DNA damage tolerance
DUBs	Deubiquitylating enzymes
E. coli	Escherichia coli
E1	Ubiquitin-activating enzyme
E2	Ubiquitin-conjugating enzyme
E3	Ubiquitin ligase
EME1	Crossover junction endonuclease EME1
ER	Endoplasmic reticulum
EXO1	Exonuclease 1

FA	Fanconi anemia
FAAP100	Fanconi anemia core complex-associated protein 100
FAAP20	Fanconi anemia core complex-associated protein 20
FACS	Fluorescent activated cell sorting
FAN1	Fanconi-associated nuclease 1
FANCD2	Fanconi anemia group D2 protein
FANCI	Fanconi anemia group I protein
FANCJ	Fanconi anemia group J protein, also known as BRIP1
FANCL	Fanconi Anemia RING-type E3 ligase
FANCM	Fanconi anemia group M protein
FBH1	F-box DNA helicase 1
FDA	Food and Drug administration
FDR	False Discovery Rate
FIGNL1	Fidgetin-like 1 protein
FIRRM	FIGNL1 Interacting Regulator of Recombination And Mitosis
FR	Fork reversal
G1	Gap1 cell cycle phase
G2	Gap2 cell cycle phase
G2/M	Gap2/mitosis cell cycle phase
GEN1	Flap endonuclease GEN homolog 1
GOI	Gene of interest
GSEA	Gene Set Enrichment Analysis
HDR	Homology-directed repair
HELQ	Helicase POLQ-like
HERC2	HECT domain and RCC1-like domain-containing protein 2

HJ	Holliday junction
HR	Homologous recombination
HROB	Homologous recombination OB-fold protein
IC25	Inhibition concentration twenty-five
ICLs	DNA interstrand crosslinks
IR	Ionizing radiation
KO	Knock-ut
Ku70/Ku80	Ku heterodimer
LIBs	Liaisons interbrins
LIG4	DNA ligase IV
lncRNA	long non-coding RNA
LOH	Loss of heterozygosity
MAF	Mafosfamide
MAGeCK	Model-based Analysis of Genome-wide CRISPR/Cas9 Knockout
MCM8	Minichromosome maintenance 8
MCM9	Minichromosome maintenance 9
MDC1	Mediator of DNA damage checkpoint protein 1
MDM2	Mouse double minute 2 homolog
MGE	Mobile genetic elements
MLE	Maximum likelihood estimation
MMC	Mitomycin C
MMS	Methyl methanesulfonate
MOI	Multiplicity of infection
MRE11	Meiotic recombination 11 homolog 1
MRN	MRE11-RAD50-NBS1 complex

MS	Mass spectrometry
mTOR	Mammalian target of rapamycin
MUS81	Crossover junction endonuclease MUS81
NBS1	Nijmegen breakage syndrome protein 1
NCO	Non-crossover
NEDD8	Neural precursor cell-expressed and developmentally downregulated 8
NEIL3	Nei-like protein 3
NER	Nucleotide excision repair
NGS	Nex-generation sequencing
NIPBL	Nipped-B-like protein
NormZ	Normalized Z-score
ORF	Open-reading frame
p53	Tumor suppressor p53
PALB2	Partner and localizer of BRCA2
PAM	Protospacer adjacent motif
PARP	Poly (ADP-ribose) polymerase
PAXX	Paralogue of XRCC4 and XLF
PCNA	Proliferating cell nuclear antigen
Pol d	Polymerase d
Pol e	Polymerase e
POLQ	Polymerase Polq
PrimPol	Primase and DNA-dependent polymerase
PTM	Post-translational modification
R-loops	RNA-DNA hybrid
RAD50	DNA repair protein RAD50

RAD51	Rad51 homolog
RAD52	Rad52 homolog
RB	Retinoblastoma
RECQL	ATP-dependent DNA helicase Q1
REV1	DNA repair protein REV1
REV3	DNA polymerase zeta catalytic subunit
REV7	REV7 homolog, also known as MAD2L2
RIF1	Rap1-interacting factor 1 homolog
RNA	Ribonucleic acid
RNF168	Ring finger 168
RNF8	Ring finger 8
ROS	Reactive oxygen species
RPA	Replication protein A
RPE1	Retinal pigmented epithelial cell line
S	S cell cycle phase in which DNA is replicated
SCAI	Suppressor of cancer cell invasion protein
SCE	Sister chromatid exchange
SDSA	Synthesis-dependent DNA strand annealing
seDSB	Single-ended double-stranded breaks
sgRNA	Single-guide RNA
shRNA	Short hairpin RNA
SIOD	Schimke immune-osseous dysplasia disorder
siRNA	Short interfering RNA
SLX1	Structure-specific endonuclease subunit SLX1
SLX4	SLX4 structure-specific endonuclease subunit homolog, also known as FANCP

SpCas9	Streptococcus pyogenes Cas9
SPIDR	Scaffolding protein involved in DNA repair
SPRTN	DNA-dependent metalloprotease SPRTN
Srs2	Saccharomyces cerevisiae S288C DNA helicase
SSA	Single strand annealing
ssDNA	Single-stranded DNA
SUMO	Small Ub-like modifier
SWSAP1	ATPase SWSAP1
TALENs	Transcription activator-like effector nucleases
TEX264	Testis-expressed protein 264
TKO	Toronto KnockOut genome-wide library
TLS	Translesion synthesis
TMEM263	Transmembrane protein 263
tracrRNA	Trans-activating CRISPR RNA
TRAIP	E3 ubiquitin-protein ligase TRAIP
TRC	Transcription-replication conflict
TS	Template switching
TTD	Trichothiodystrophy
U2OS	Human Bone Osteosarcoma Epithelial Cells
UAF1	USP1-associated factor
UBA5	E1 ubiquitin activating enzyme 5
UBDs	Ubiquitin-binding domains
UBE2T	Fanconi Anemia E2 ubiquitin-conjugating enzyme
UBLs	Ubiquitin-like proteins
UDS	Unscheduled DNA synthesis

UFC1	E2 UFM1-conjugase 1
UFL1	E3 UFM1-ligase 1
UFM1	Ubiquitin fold modifier 1
UFMylation	Ubiquitin-fold modifier 1 protein modification
UFSP2	UFM1 Specific peptidase 2
USP1	Ubiquitin-specific-processing protease 1
UV	Ultraviolet light
WRN	Werner helicase
XLF	XRCC4-like factor
XP	Xeroderma pigmentosum
XPA	Xeroderma pigmentosum group A-complementing protein
XPC	Xeroderma pigmentosum group C-complementing protein
XRCC1	X-ray repair cross-complementing protein 1
XRCC4	X-ray repair cross-complementing protein 4
ZNFs	Zinc-finger nucleases
γ-H2AX	Histone 2 A.X phosphorylated on Ser139

Chapter I: General Introduction

1.1 DNA replication and genome integrity

The rise of complex multicellular forms of life on earth was allowed by the evolution of molecular structures and regulatory pathways that carry out the faithful and rapid duplication of large genomes. Eukaryotic genomes initiate replication from many replication origins which are localized across the genome [1]. During the S phase, thousands of origins are activated (fired) serially in a timely coordinated fashion to secure the completion of DNA replication before chromosome segregation. Just a fraction of all licensed origins is used during a regular S phase, and the remaining "licensed" but inactive origins serve as backup in case of fork slow down or complete stalling [2, 3]. Although the molecular machinery involved in DNA replication is highly accurate, the fidelity of this cellular event is often challenged and stressed by exogenous and endogenous agents. This phenomenon, broadly termed replication stress, is characterized by transient slowing or complete stalling of replication forks is an important source of genome instability and a hallmark of cancer cells [2-4].

1.2 Genomic stability maintenance

1.2.1 Replication stress

Genome instability arises as a result of DNA lesions originated from errors during DNA replication, from exposure to genotoxic compounds including cellular metabolites, or from genetic insults caused by exogenous agents such as ultraviolet (UV) and ionizing radiation (IR) [2]. Due to its nature as source of genome instability in pre-neoplastic lesions, elucidating the molecular events involved in replication stress is critical for our better understanding of cancer. Depending on the type of stress impairing the replisome, cells triggered the activation of multiple cellular pathways to stabilize, repair and restart the replication fork; pointing to safeguard genomic

duplication and preserve genome integrity [5]; A detailed scheme of the multiple sources of replication stress is described in Figure 1.1.

1.2.1.1 Replication fork barriers

DNA lesions and adducts are considered among the most common recognized replication blocks [6, 7]. These insults/adducts are the result of exposure to multiple endogenous and exogenous sources, including chemical mutagens, reactive oxygen species (ROS), by-products of metabolism, UV radiation and non-canonical nucleotides [8]. DNA alkylating agents such as methyl methanesulfonate (MMS) or UV can cause DNA lesions that represent roadblocks to replicative DNA polymerases, forcing the replisome machinery to bypass these lesions using tolerance repair pathways such as TLS [9]. DNA adducts and interstrand cross-links (ICLs) generated by reactive metabolites (e.g., aldehydes or formaldehydes) or DNA cross-linkers(e.g., cyclophosphamide and cisplatin), as well as DNA-protein cross-links(DPCs) which are formed by a variety of agents that trap proteins on DNA(e.g., poly(ADP-ribose) polymerase(PARP) and topoisomerase I(TOP1) inhibitors), also act as detrimental roadblocks for replication fork progression [5, 10-12].

Single-stranded DNA (ssDNA) breaks or nicks are generated by ROS, ionizing radiation, free radicals and as intermediates in base excision repair (BER) [13, 14]. When replication forks encounter ssDNA breaks in the leading strand template this cause replication fork collapse with the formation of a single-ended double-stranded breaks (seDSB) [4, 5, 13]. In addition, secondary DNA structures such as hairpins, guanine-rich DNA sequences(G-quadruplexes) and cruciform structures can arise in the genomic DNA during regular physiological processes that generate ssDNA, such as replication, transcription, and DNA repair. These structures represent physical fork barriers and cause replication stress as well [5, 15-17]. Another source of replication stress is the transcription-replication conflict (TRC). R-loops are three-stranded polynucleotide structures containing DNA-RNA hybrids and ssDNA and they also represent a physical barrier for fork

progression. Abnormal accumulation of R-loops is linked to loss of certain DNA repair proteins and increased genomic instability; hence, cells have evolved multiple pathways to deal with R-loops and prevent TRC [5, 18].

1.2.1.2 Replication stress response

In general, replication stress elicits three major interconnected responses at replication forks: (i) replication checkpoint; (ii) remodelling of stressed or stalled forks and (iii) activation of DNA repair or tolerance pathways [5]. For instance, replication stress can hinder the coupling between the replicative helicase and polymerases, augmenting the exposure of single-stranded DNA (ssDNA) at replication forks [5, 19]. Single-stranded DNA is coated by replication protein A (RPA) and this allows the recruitment and activation of ataxia telangiectasia and Rad3-related (ATR) checkpoint kinase [5, 20]. Once activated, ATR stabilizes stressed forks, suppresses origin firing and induces cell-cycle arrests, aiming to reduce deleterious consequences of replication stress [5, 21]. A second line of response upon replication stress is a remodelling process called fork reversal. Replication fork reversal is a protecting remodelling response that allows forks to setback their course when the replisome encounter DNA lesions and resume DNA synthesis without chromosomal breakage [22, 23]. The fork reversal model can be divided into two stages: (i) conformation of reverse forks through the annealing of the two newly synthetized strands, leading to four-way junction structures (chicken foot structure), which resemble Holliday junctions (HJ) intermediates and (ii) restart of reversed forks. This remodelling allows for removal of the original lesion before reversed fork restart or the bypassing through a template-switching mechanism [22, 23]. Multiple DNA repair and tolerance pathways are activated at stressed or stalled forks that allows cells to bypass or recover from this cellular stress. These pathways include Translesion synthesis (TLS), primase and DNA-dependent polymerase (PrimPol)-mediated repriming, template switching (TS), break-induced replication (BIR), homologous recombination (HR) and

others [5, 24, 25]. This orchestrated stress response at replication forks enables the completion of DNA replication and prevents genomic instability.

Upon replication fork collapse and generation of seDSBs a subpathway of homologous recombination (HR) known as break-induced replication (BIR) becomes activated. In BIR, resection undergoes at the broken end, then invasion into the sister chromatid and replication follow until the end of the chromosome or until a converging fork is encountered. Loss of key FA/HR proteins such as RAD51, BRCA1, BRCA2 is lethal in non-transformed cells, which is in line with the fact that an estimated of around 50 replication forks collapse in every DNA synthesis(S-phase), highlighting their importance in fork protection and cell viability [13, 26-29]. Furthermore, other FA/HR proteins such FANCD2, FANCM and the RAD51 paralogs have been also implicated in the fork protection pathway and their loss results in increased fork degradation and augmented levels of spontaneous replication stress [5, 30-32].

DNA replication is intimately linked to DNA repair and sister chromatin cohesion, therefore a group of genetic syndromes described as DNA repair disorders are connected with defective S-phase progression and abnormal processing of replication fork intermediates upon stalling. Notable examples of these disorders are the RECQL helicase, Bloom and Werner syndrome, Fanconi anemia and Schimke immune-osseous dysplasia disorder (SIOD) [33-35]. Worth noting, various distinctive features of these disorders encompass reduced growth, developmental abnormalities, hematological/immune dysfunctions, and increased risk of developing malignancies such as leukemias, lymphomas, breast, ovarian, skin cancers and sarcomas [36, 37].

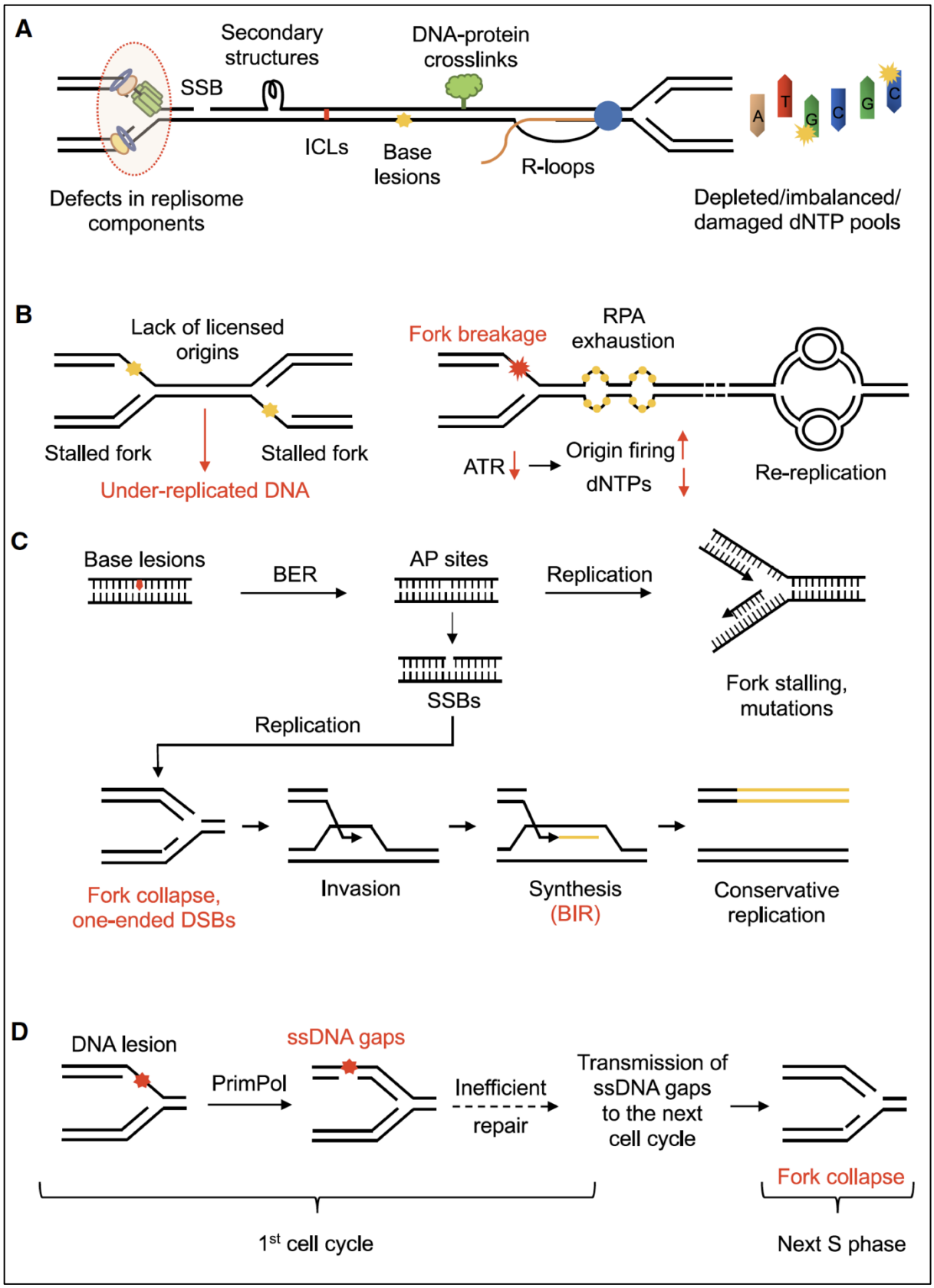

A
Secondary structures
DNA-protein crosslinks
SSB
ICLs
Base lesions
R-loops
Defects in replisome components
Depleted/imbalanced/ damaged dNTP pools
B
Lack of licensed origins
Stalled fork
Stalled fork
Under-replicated DNA
Fork breakage
RPA exhaustion
ATR
Origin firing
dNTPs
Re-replication
C
Base lesions
BER
AP sites
Replication
SSBs
Fork stalling, mutations
Replication
Fork collapse, one-ended DSBs
Invasion
Synthesis (BIR)
Conservative replication
D
DNA lesion
PrimPol
ssDNA gaps
Inefficient repair
Transmission of ssDNA gaps to the next cell cycle
Fork collapse
1st cell cycle
Next S phase

Figure 1.1 Schematics of the different sources of DNA Replication Stress. A) Replication fork progression can be compromised by different types of lesions or obstacles such as SSBs, DNA secondary structures, DNA interstrand crosslinks, DNA-protein crosslinks, etc. B) Diminished rescue of stalled replication forks due to lack of licensed origins results in under-replicated DNA regions; in opposition to this, increased origin firing compromises fork progression by depletion of dNTPs, excessive amount of ssDNA and RPA exhaustion, which altogether leads to genome-wide breakage of replication forks. C) Excessive repair intermediates such as AP sites and SSBs operate as replication roadblocks to replication forks. D) Replication forks can bypass DNA lesions by PrimPol-mediated repriming, which if left unrepaired, can persist into the next cell cycle and trigger fork collapse. (Adapted with permission from Elsevier, Molecular Cell [5]).

1.2.2 DNA double-strand break repair.

Even before the discovery of the DNA structure in 1953, it was known that in our daily life, exposure to exogenous agents such as ultraviolet light (UV), X-rays and certain chemicals could cause genetic changes in our genome and promote malignancies [7, 8]. It took another decade to recognize that our genome is also constantly challenged by endogenous sources of DNA damage [38-40]. Although both DNA lesions from endogenous and exogenous sources have the potential to damage and modify our genome, the relative contribution of each source to the development of cancer remains to be clarified [8, 41, 42].

It has been estimated that each human cell is subject to approximately 70,000 DNA lesions per day [43]. Most of these insults (~75%) are single-strand DNA (ssDNA) breaks caused by oxidative damage or base hydrolysis during metabolism. Notably, ssDNA breaks can be converted to DNA double-strand breaks (DSB), which although they are less frequent, they are considered the most deleterious form of DNA damage [8]. DSBs are particularly dangerous because they do not leave an undented complementary strand to be used as template for repair. If not properly repaired,

they could lead to chromosome breaks and translocations which are linked to developmental disorders, neurodegeneration, immunodeficiency, radiosensitivity, sterility and cancer predisposition [44, 45]. DSBs are generated in response to ionizing radiation (IR) or radiomimetics drugs, treatment with topoisomerase I/II inhibitors and they could also arise during replication stress as discussed above. In addition, DSBs are also produced by the activity of specific nucleases during V(D)J and class switch recombination in B lymphocytes and meiotic recombination in germinal cells. Finally, naturally occurring DSBs also occurs when cells face replicative senescence during telomere shortening, and when endogenous metabolites such genotoxic aldehydes buildup and lead to endogenous generation of ICL [45, 46].

At least two independent DNA repair pathways can deal with DSBs: homologous recombination (HR) and classic nonhomologous DNA end-joining (cNHEJ. The critical factor influencing the pathway choice is the extent of DNA end processing and the two dominant pathways repairing DSBs are HR and cNHEJ [7]. During HR, the DSB is repaired by interchanges of equivalent genomic regions of DNA between homologous or sister chromosomes. In contrast, cNHEJ ligates the ends without the need of a DNA template [8].

1.2.2.1 Canonical NHEJ

Canonical NHEJ is the predominant pathway involved in DSB repair and is estimated that it repairs around 80% of all DSBs in human cells [47, 48]. During cNHEJ, DNA ends are welded together by a multiprotein complex and directly ligated [49]. In contrast, during homologous recombination (HR), end-resection at DSB generates a 3' single-stranded DNA to serve as template for repair. Due to this template repair requirement HR primarily operates in the S and G2 phases of cell cycle, whereas cNHEJ is active throughout the cell cycle [47, 50]. In cNHEJ the repair is initiated when the DSB ends are bound by the Ku heterodimer (Ku70/Ku80), which has a toroidal structure that encircles DNA break ends and function as recruitment hub for many

downstream NHEJ factors. Ku localizes within seconds to DSBs and activates the DNA-dependent protein kinase catalytic subunit (DNA-PKcs) to form the DNA-PK holoenzyme [7, 45, 47]. Ku nucleates also the recruitment of other factors, including DNA ligase IV(LIG4), and the scaffolding factors XRCC4, XRCC4-like factor (XLF) and paralogue of XRCC4 and XLF(PAXX). XRCC4 has a critical role in the stability and functioning of LIG4, whereas XLF and PAXX have somewhat redundant scaffolding functions [51-56]. DNA binding stimulates DNA-PKcs kinase activity leading to a cascade of phosphorylation events of multiple NHEJ and DNA repair factors. Although the functional significances of these phosphorylation events remain uncertain, autophosphorylation of DNA-PKcs appears to be crucial for DSB repair [47]. As such, DNA-PKcs autophosphorylation on the six-residue ABCDE cluster results in the destabilization of the DNA-PKcs interaction with DNA ends, leading to end processing by nucleolytic activity of enzymes such as ARTEMIS. In the other hand, excessive end processing is prevented by DNA-PKcs autophosphorylation on the five residue PQR cluster, which safeguards and protects DNA ends. Interestingly, ABCDE phosphorylation could also be a target of ATM, and this event facilitates the access of DSB resecting enzymes to promote HR when NHEJ fails [7]. Recent work at Harvard using single-molecule imaging of cNHEJ has revealed the existence of a two-stage mechanism of synapsis of the two ends of the DSB [57]. First Ku and DNA-PKcs form a long-range synapse; followed by a second short-range stage, in which the two DNA ends become closely aligned in a process mediated by XLF, LIG4 and the kinase activity of DNA-PKcs. This synaptic reaction can alternate between these two stages and this reversible dynamic process undergoes until ligation is completed [51, 58].

Among the physiological roles of NHEJ are included the repair of spontaneous DSBs arising from multiple sources as well as dealing with developmentally programmed DSBs in lymphocytes. It is estimated that spontaneous DSBs occur around 50 times per day in mammalian somatic cells

[59], and they can be caused by multiple sources such as: (i) reactive oxygen species (ROS); (ii) environmental ionizing radiation; (iii)nuclease activity; (iv) unfinished topoisomerase activity and (v) misrecognition as DSB of unprotected telomeres [47]. The diversity needed for our adaptative immune system is generated in part through programmed DSBs. These controlled gene shuffling involved in V(D)J recombination and class switch recombination (CSR) is originated through the repair of DSB intermediates by NHEJ [47].

1.2.2.2 alt-EJ

In addition, when canonical NHEJ does not operate due to mutations or deregulation, alternative end-joining pathways are triggered. These alternative end-joining pathways frequently rely on terminal microhomologies for the joining reaction and require the participation of factors that are also involved in homologous recombination and SSB repair, such as MRE11-RAD50-NBS1(MRN) complex, poly (ADP-ribose) polymerase I(PARP1), XRCC1, and DNA ligase I or III [45, 60]. The alt-EJ pathway (also known as microhomology-mediated end joining and Pol θ-mediated end joining) requires microhomology ranging between 2 bp and 20 bp [61].Overcoming inhibition of extensive end resection mediated by Ku, 53BP1 and RIF1 is the first limiting step necessary to trigger alt-EJ. Due to the scarce number of humans harboring NHEJ mutations, it is still unclear if alt-EJ constitutes a standalone pathway or if its components play roles in other functions in dsDNA processing (replication, recombination & repair) and becomes activated only when NHEJ is compromised. Critical factors for alt-EJ are Pol θ, poly (ADP-ribose) polymerase 1(PARP1), CtIP and the MRN complex. Phosphorylated CtIP stimulates the endonuclease activity of MRN leading to processing of DNA ends and generation of 15-100-nucleotides 3' overhangs necessary for alt-EJ [61]. In addition, PARP1 seems to have a DNA damage sensing and facilitator role in alt-EJ [61, 62]. Further work is necessary to identify the rest of factors involved in alt-EJ and how distinctive this pathway is from cNHEJ.

1.2.2.3 Homologous recombination (HR)

Besides NHEJ, the second major pathway in charge of repairing DSBs is homologous recombination (HR). As mentioned above, HR differs from NHEJ in several mechanistic aspects. Due to its requirement of repair template HR is largely restricted to S and G2 phases of the cell cycle. Besides its role in DSB repair in somatic cells, HR also mediates the pairing and crossing over of homologous chromosomes in meiosis and allows proper meiotic division and generation of genetic diversity [50, 63]. The decision of which pathway operates upon DSBs is tightly regulated during the cell cycle. A major determinant of this pathway choice and therefore a differential regulator of DNA end-resection is p53-binding protein 1(53BP1). Indeed, the restriction on resection modulated by 53BP1 renders NHEJ as the default DSB pathway in G1 cells. This inhibition of resection is lifted in the S phase of the cell cycle and this positive regulation of the 53BP1-mediated inhibition of resection requires BRCA1 [50, 64]. As such, a fine-tuned balance between BRCA1 and 53BP1 modulates pathway choice by either promoting or inhibiting end resection [65].Loss of 53BP1 partially rescues the HR defect of BRCA1 mutant cells, suggesting that BRCA1 could overcome 53BP1 functions at DSBs in order to promote DSB resection. Additionally, defective DSB resection in BRCA1 mutant cells results in NHEJ-mediated chromosomal rearrangements [66, 67]. Furthermore, DSB resection promoted by 53BP1 depletion was reported to promote alternative end-joining during class-switch recombination in G1 phase B lymphocytes [68]. Therefore, alterations of the correct balance between DSB repair pathways leads to genomic instability. Moreover, chromosomal defects and DNA damage sensitivity observed in Fanconi anemia mutant cells have been linked to aberrant NHEJ activity, suggesting that FA proteins could promote faithful repair through homologous recombination and supress NHEJ [7, 69, 70].

HR does not always comprise a single mechanism suitable to all type of lesions. This complexity in the HR response is based on the diversity and size of single-stranded DNA gaps and DSBs, their cause and origin, the phase of the cell cycle and the cell type [71, 72]. Therefore, recombination repair does not comprise a linear process such as replication or transcription, instead, is a collection of potentially parallel and alternative processes [71, 73]. In despite of this complexity, HR comprises core biochemical events that include: (i) "initiation", which consist of DNA end resection or enlargement of DNA breaks by nucleases and DNA helicases that allow the generation of single-stranded DNA (ssDNA); (ii) "homologous DNA pairing and strand exchange", consisting in the search for sequence complementarity mediated by the RAD51 nucleoprotein filament and the reciprocal exchange of DNA strands; (iii) "branch migration" of three or four-stranded recombination intermediates and finally (iv) separation of the joined chromosomes by nucleolytic resolution or by topological dissolution involving a type IA topoisomerase and DNA helicase. These core HR steps are mostly conserved in Bacteria, Archaea, Eukarya and Phage [71, 73-76].

1.2.2.3.1 End Resection

In Eukarya DNA end resection is initiated by the MRE11-RAD50-NBS1(MRN) complex, which promotes the activation of ATM and the preparation of DNA for HR. RAD50 contains ATPase domains which interact with MRE11 and associates with the DNA ends of the DSB [7, 51, 77]. Besides its role in stabilization of DNA ends, MRE11 has endonuclease and exonuclease activities critical for the initiation of DNA end resection. Through its endonuclease activity, MRE11 nicks the strand that ends at a DSB with a free 5' terminus, then through its 3'-5' exonuclease activity, MRE11 extends the nick to the DNA end. This step of "short range resection" by MRE11 is mediated by its interaction with CtBP-interacting protein (CtIP) and is stirred by proteins blocking the DNA such as Ku, replication protein A(RPA) or nucleosomes [51, 78-85]. This initial

processing step allows the recruitment of factors involved in "long-range resection". This subsequent step is mediated by two somewhat redundant mechanisms which are dependent on either the 5' →3' exonuclease 1(EXO1) or the DNA helicase/endonuclease Dna2. Both nucleases rely on other factors for proper functioning, specifically, Dna2 rely on interaction with RPA and the Bloom syndrome helicase (BLM), whereas EXO1 is enhanced by RPA and work together with BLM as well. Interestingly, the helicase Werner helicase (WRN) can replace BLM in the Dna2-dependent nucleolytic resection activity [50, 51, 86-91]. Oddly, DNA end resection of the chicken foot structure arising from stressed replication fork appear to rely in different mechanisms than the ones described at DSBs [50, 92, 93].

1.2.2.3.2 Presynaptic Filament Assembly

DSB end resection and generation of 3'-tailed ssDNA leads to RPA accumulation. RPA is a critical heterotrimeric complex (RPA1, RPA2, RPA3) involved in the stabilization and protection of ssDNA regions generated during DNA replication and repair [7, 94]. Upon DNA damage, the complex RPA initially competes with RAD51 for ssDNA binding, however, it also has a pro-recombinogenic role once RAD51 is loaded onto ssDNA, since it is involved in the elimination of secondary structures and the protection of DNA ends. Furthermore, RPA also participates in SSA in which it also binds to ssDNA but the annealing of the resected ssDNA is mediated by RAD52 in a RAD51-independent manner [7, 65].

Some important proteins termed HR mediators regulate RPA displacement, RAD51 nucleofilament formation and strand exchange activity. The most important and characterized are BRCA2, the RAD51 paralogs and RAD52 in budding yeast [7, 50, 51, 65]. BRCA2 is considered the key recombination mediator in vertebrates and some fungal species, and it is constitutively bound to the 26S proteosome complex subunit DSS1. BRCA2 interacts with ssDNA, RAD51 monomers and with BRCA1-BARD1 through partner and localizer of

BRCA2(PALB2) [51, 95]. BRCA2 harbors a series of eight evolutionary conserved motifs called BRC repeats. BRCA2 BRC domains promote RAD51 loading onto ssDNA by disrupting self-assembled RAD51 oligomers and promoting binding of RAD51 monomers in a one-to-one fashion [65]. In addition, the human RAD51B-RAD51C complex enhances presynaptic filament assembly on RPA-coated ssDNA, suggesting that these complexes of RAD51 paralogs are HR mediators as well [50, 96].

1.2.2.3.3 Homologous DNA pairing and strand exchange

The RAD51-ssDNA nucleofilament mediates homology search by invading duplex DNA and allowing base-pairing with complementary sequences. Recent findings have identified the BRCA1-BARD1 complex as the HR factor that enhance the assembly of the synaptic complex [97], highlighting that BRCA1 promotes multiple critical steps during HR. The synaptic complex contains a three-stranded DNA helix intermediate that allows the conformation of heteroduplex DNA comprising the invading strand and the complementary strand of the invaded molecule [98]. If sufficient base-pairing occurs, the synapse undergoes stabilization, and the non-base-paired strand of the invaded molecule is displaced to form a displacement loop(D-loop) structure, this process relies in coordinated RAD51-mediated ATP hydrolysis and RAD51 nucleofilament dismantling [51, 99]. Upon D-loop formation, a DNA polymerase gets involved and DNA synthesis starts from the free 3' end of the invading nascent strand to copy sequence information from the donor DNA molecule [50, 51]. Although DNA polymerase δ(Pol δ) is the canonical polymerase involved in nascent strand synthesis, translesion DNA polymerases have been reported to compete with Pol δ for this function [51, 100-102]. Intriguingly, the extended D-loop structure can be resolved by mechanistically distinct pathways: canonical double-strand break repair (DSBR), synthesis-dependent DNA strand annealing (SDSA) and double Holliday junction(dHJ) dissolution. From these pathways only DSBR can generate recombinants harboring

chromosome arm exchange or crossover. SDSA is thought to be mediated by the RTEL helicase after displacement of the RAD51 filament and D-loop disassembly [7, 103]. Alternatively, to SDSA, recombinational repair often leads to the formation of intermediates in which the DNA structures are covalently linked by the formation of four-way DNA junctions or Holliday junctions (HJs) [104-106].

1.2.2.3.4 Recombination intermediates processing

These recombination intermediates require processing to allow proper chromosome segregation during mitosis [107]. Until now, three pathways for HJ processing have been described. The first involved the Bloom syndrome helicase BLM, Topoisomerase IIIα, RMI1 and RMI2, which together conformed the BTR complex. This complex stimulates the convergent migration of two HJs to produce a hemicatenane which is later processed by topoisomerase activity [107, 108]. This HJ dissolution pathway generates exclusively non-crossover outcomes, as such, it plays a critical role in preventing aberrant sister chromatid exchange (SCE) and regulates the potential for loss of heterozygosity (LOH). Individuals with mutations in BLM suffer from Blood syndrome and display elevated levels of SCE, genomic instability and are predisposed to early onset cancers [107, 109, 110]. The second and third pathways involved in the processing of recombination intermediates rely on the activities of structure-specific endonucleases also called "resolvases" that cleave HJs and generate crossover (CO) and non-crossover (NCO) events. Indeed, the aberrant frequency of SCE observed in BLM-deficient cells is thought to be a consequence of resolution processing undergoing in the absence of the dissolution pathway [107]. The endonucleases involved in this processing are SLX1-SLX4 and MUS81-EME1, which together form the SLX-MUS complex [107, 111-117], and GEN1 [107, 118, 119]. Because of the inherent risk surrounding the generation of crossover in mitotic cells, the resolution pathway and the activity of these nucleases is tightly regulated, and the BTR-mediated HJ dissolution pathway is

prioritized [106, 107]. In addition, the DNA translocase FANCM and proteins of its family such as Fml1 or Mph1, are reported to play a role in D-loop dismantling, crossover regulation and promoting SDSA [107, 120-123].

1.2.2.3.5 Negative regulation of RAD51-mediated recombination

Conversely, many factors play a negative regulatory role in RAD51 nucleofilament formation to properly fine-tune strand exchange and avoid hyper-recombination and crossover (CO)-dependent rearrangements [65]. Yeast Srs2 was the first described negative regulator of Rad51 function. The Srs2 DNA helicase removes RAD51 from presynaptic filaments through its ATP hydrolyzing activity coupled with DNA disentangling function [124, 125]. Human cells do not have an identified ortholog of Srs2, however, there is an important number of human helicases orthologs involved in the dissociation of RAD51-ssDNA filaments: BLM, RECQ5, FANCJ and FBHI [71, 126-130]. In addition to the above-mentioned factors, the helicase and proliferating Cell nuclear Antigen (PCNA)-interacting factor, PARI has been reported to dissemble RAD51 nucleofilaments in a process requiring ATP hydrolysis [131]. More recently, another factor, the polymerase Polθ(also known as POLQ) was shown to play an anti-recombinogenic role. Although Polθ cannot remove RAD51 already bound to ssDNA, it can still negatively modulate the formation of RAD51 nucleofilaments [132]. Intriguingly, Srs2, PARI and Polθ can also promote alternative error-prone repair mechanism such as alt-EJ, TLS and SSA [133-136]. Despite this exciting new knowledge about these HR negative regulators, how they operate and interact with HR positive mediators are interrogates remaining to be answered.

1.2.2.4 Single-strand Annealing (SSA)

Although this is not a requirement, NHEJ often uses 1-4bp of microhomology, by contrast, SSA and alt-EJ require extensive resection to unveil microhomology. SSA does not rely on Ku activity and actually, attenuation of Ku binding to break end is thought to be required for SSA to occur [61]. SSA also rely on the induction of extensive resection conducted by the MRN complex and CtIP. This resection generates between 15-100 nucleotide 3' ssDNA tails and this stage is where aEJ and SSA pathways differ. While in aEJ annealing of microhomology seems to be enough for Pol θ to extend the DNA strand and allow the stabilization of the intermediate and posterior ligation, SSA is more demanding in terms of sequence homology and additional extensive resection is needed [61, 86]. The 3' ssDNA tails are further extended by nuclease EXO1, BLM or DNA2. These 3' ssDNA ends are coated by multiple copies of RPA for protection and to prevent the formation of secondary structures. SSA is a RAD51-independent pathway that, however, rely on the presence of 3' ssDNA tails which share adequate sequence homology to form a stable annealing intermediate and the annealing of complementary tails is mediated by RAD52 [61]. Before ligation, the unannealed non-homologous sequence portions of the 3' ssDNA tails required to be processed and removed, this excision step is performed by the nucleotide excision repair complex XPF-ERCC1 and the mismatch repair complex MSH2-MSH3, which indicates the intimate crosstalk among repair pathways [61, 137-139]. A scheme of the DNA repair pathways involved in DSB repair is described in Figure 1.2.

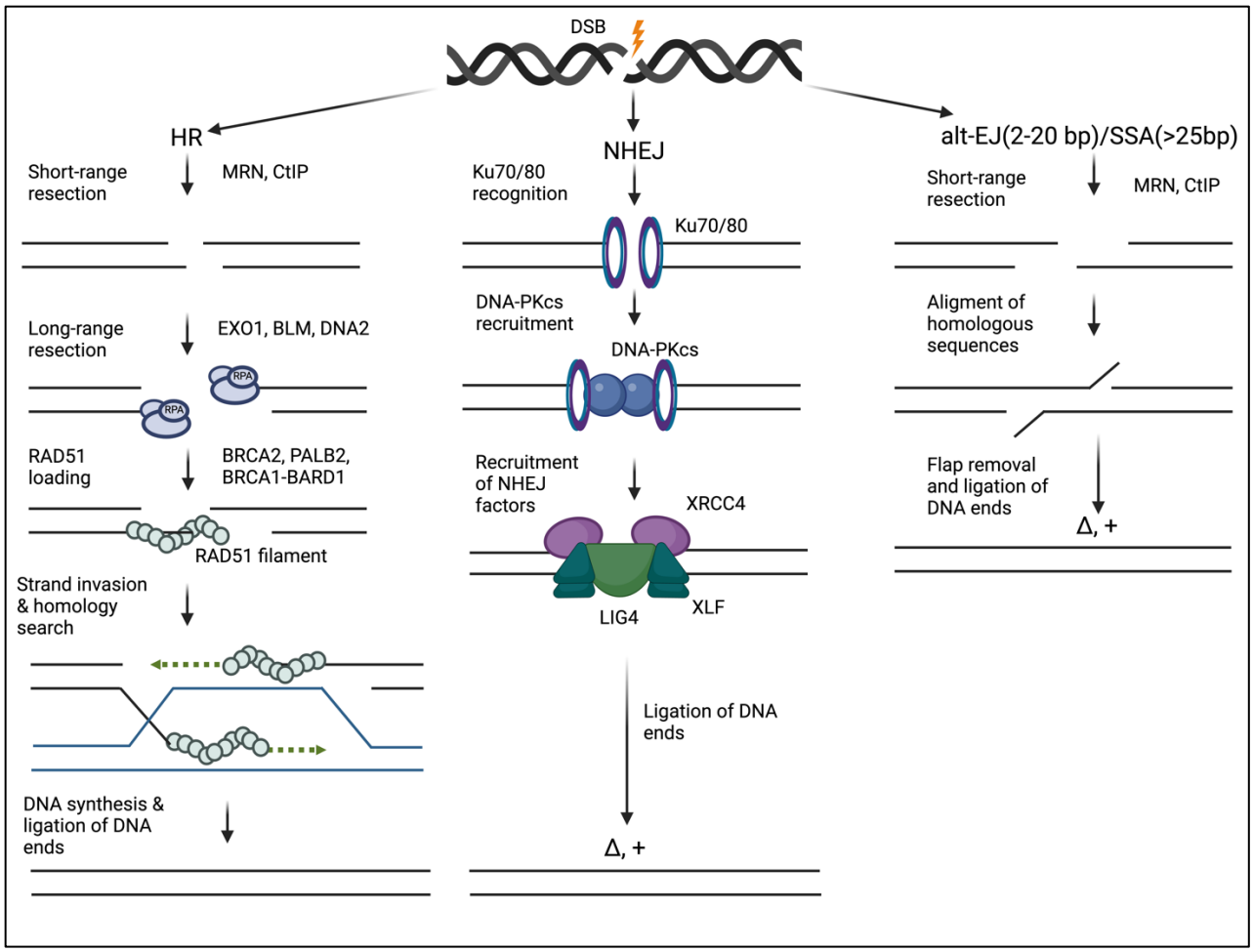


Figure 1.2 Overview of DSB repair pathways (Adapted from [140] & [95]).

1.2.3 Nucleotide Excision Repair

Nucleotide excision repair (NER) is the central DNA repair pathway involved in the removal of bulky DNA lesions induced by UV irradiation, environmental genotoxic compounds, and certain chemotherapeutic agents [141]. In the earliest studies of NER, it was observed that when a short, damaged oligonucleotide was released from DNA, this gap was filled during repair synthesis [141-145]. The gap-filling step in NER can be assessed by unscheduled DNA synthesis (UDS) and this assay, which is still used to date in the clinic, allowed the connection between NER and the genetic disorder Xeroderma pigmentosum (XP) to be made [141, 146]. Patients with this rare condition display an extreme sensitivity to sunlight and around 2000-fold increased risk of developing skin

cancer because they are unable to repair lesions induced by solar UV-irradiation [141, 147]. In addition to XP, two others genetic disorders associated with NER are: Cockayne syndrome and trichothiodystrophy (TTD), however, patients with these disorders do not display skin cancer predisposition, instead, they present developmental and neurological abnormalities [141, 148].

Based on the striking clinical heterogeneity associated with its impairment, the mammalian NER can serve as a paradigm for the clinical influence of many process involved in the DNA-damage response(DDR).This clinical heterogeneity can now be explained by our understanding that NER is exceptional among the DNA repair pathways in its capacity to deal with the widest range of structurally unrelated DNA lesions, including: cyclobutene-pyrimidine dimers(CPDs) and 6-4 pyrimidine-pyrimidone photoproducts(6-4PPs)-which are the major UV-induced lesions-; bulky chemical adducts, intrastrand crosslinks caused ICL drugs such as cisplatin or cyclophosphamide, endogenous byproducts such as aldehydes; and ROS-derived cyclopurines [141, 149, 150].

NER can be initiated by two subpathways: (i) global genome NER(GG-NER) or (ii) transcription-coupled NER(TC-NER) [151, 152]. In GG-NER the genome is scanned for helix distortions (aberrant base pairing) linked to structural changes to nucleotides, while TC-NER is triggered when RNA polymerase II (RNA Pol II) is stalled by a lesion in the template strand during transcription [149]. In *Escherichia coli*, both NER and HR are involved in ICL repair. *Escherichia coli* UvrABC proteins involved in NER are also involved in resolving ICLs [153, 154]. After ICL recognition, the endonuclease complex $UvrA_2B$ recognizes and binds to the ICL, then UvrC and UvrB make incisions flanking the ICL and release the adduct from one DNA strands in a process called unhooking [155-157]. The NER mechanism in human cells harbors more complexity than in *E.coli* and the following NER proteins have been reported to participate in ICL repair: XPA, RPA, XPC-RAD23B, ERCC1, XPF and XPG [155, 158]. It is acknowledged that ICLs are sensed by the XPC-RAD23B complex [155, 159-161] and that XPF-ERCC1 and XPG are endonucleases

that generate incisions flanking the DNA adduct [155, 162], highlighting the critical role of NER proteins in ICL repair, the ICL repair pathway will be described extensively in section 1.4.

1.2.4 Translesion synthesis

When the main DNA polymerases in charge of DNA replication, polymerase ε (Pol ε) on the leading strand and polymerase δ (Pol δ) on the lagging strand, encounter DNA damage in the template strand, these highly processive enzymes cannot accommodate slanted template structures and get blocked [163]. As stalled replication forks are dangerous and can lead to permanent cell cycle arrest, fork collapse and genomic instability; DNA damage tolerance (DTT) pathways have evolved in virtually all organisms, and they allow replication to continue and bypass the blocking DNA lesions without removing the damage [164-167]. There are two main DTT pathways described in eukaryotes: (i) Translesion synthesis (TLS) and (ii) homology-directed DDT. In response to DNA damage, monoubiquitination of the clamp protein proliferating cell nuclear antigen (PCNA) allows the recruitment of specialized TLS polymerases [167-169]. Due to their relaxed active sites and their tendency to mis incorporate bases on both damaged and undamaged templates, TLS polymerases contribute to mutagenesis and TLS is considered an error-prone DDT pathway [167, 168, 170, 171]. As such TLS polymerases have been implicated in cancer development and in promoting chemotherapeutic resistance in cancer cells [167, 172-174]. In addition to TLS, DNA damage bypass can also occur through homology-directed DDT, which consist of two subpathways: fork reversal (FR) and template switching (TS). Both FR and TS are triggered upon polyubiquitination of PCNA and involve a temporary switch from the damaged template strand to the use of the newly synthetized copy of the complementary strand on a homologous sister chromatid. As such, and because an undamaged template is copied, FR and TS are considered error-free tolerance pathways [167, 175]. Human TLS polymerases are grouped in 4 families: the Y-family (Rev 1, Pol η, Pol ι, and Pol κ); the A-family (Pol θ); the B-family(Pol ξ)

and the archaeo-eukaryotic primase(AEP) family(PrimPol) [9, 169, 176-178]. The molecular mechanism governing TLS appears to be conserved from *E.coli* to humans. In this model, initially proposed by Bridges and Woodgate in 1985 [179, 180], it is believed that TLS occur in two kinetically separable steps: (i) misincorporation followed by (ii) extension. It is assumed that a single TLS polymerase, such as *E.coli* Pol V or human Pol η, could mediate both steps [181]. Nevertheless, it is now known that some TLS polymerases are more proficient at DNA extension (Pol η and Pol ξ) than base incorporation, consequently, TLS repair not only occurs in two steps, but it also may require two coordinated polymerases for efficient DNA lesion bypass [181]. REV7(also identified as MAD2L2 or FANCV) is a highly conserved multifunctional protein. It was initially identified in *Saccharomyces cerevisiae* as a gene promoting UV-induced mutagenesis, and later on reported to be a conserved component of the DNA polymerase ξ Translesion synthesis (TLS) complex [182, 183]. Maybe the more described function of REV7 is its role as the small non-catalytic subunit of the DNA Polξ complex involved in TLS repair, in which the catalytic subunit REV3 and REV7 form Polξ [184, 185]. Subsequently, Polξ in cooperation with REV1 form the Polξ-REV1 complex, which is believed to be responsible for most damage-induced mutations during DNA replication, which highlights its mutagenic role in TLS. Following the two-step model of TLS, REV1 is thought to play a role as recruitment module and base-incorporating polymerase, whereas Polξ is the extension polymerase, which carryout DNA synthesis using a damaged primer terminus [184, 186, 187]. As part of this role in TLS repair, REV7 also is critical for repair of intra and interstrand crosslinks (ICLs), either as Polξ alone or in cooperation with REV1, is it reported to be important for DNA extension past an ICL-lesion [185, 188, 189]. Expectedly, cells deficient in REV1, REV3 or REV7 displayed hypersensitivity to ICL agents such as cisplatin [168, 185, 188-194]. Furthermore, bi-allelic mutations of REV7 were identified in a

patient displaying clinical features of Fanconi anemia (FA) [195]. Fanconi anemia (which will be described extensively in section 1.3) is a rare genetic disorder linked to hypersensitivity to DNA crosslinking agents and defects in genes that are responsible for DNA ICL repair through homologous recombination (HR). Based on these studies, REV7 was included in the FA gene-family an received a complementation group name as FANCV. Further *in vivo* studies supported the role of REV7 in FA, in this study REV7 mutant mouse displayed disrupted Polξ activity, human-like FA features and hypersensitivity to ICL agents [185, 196].

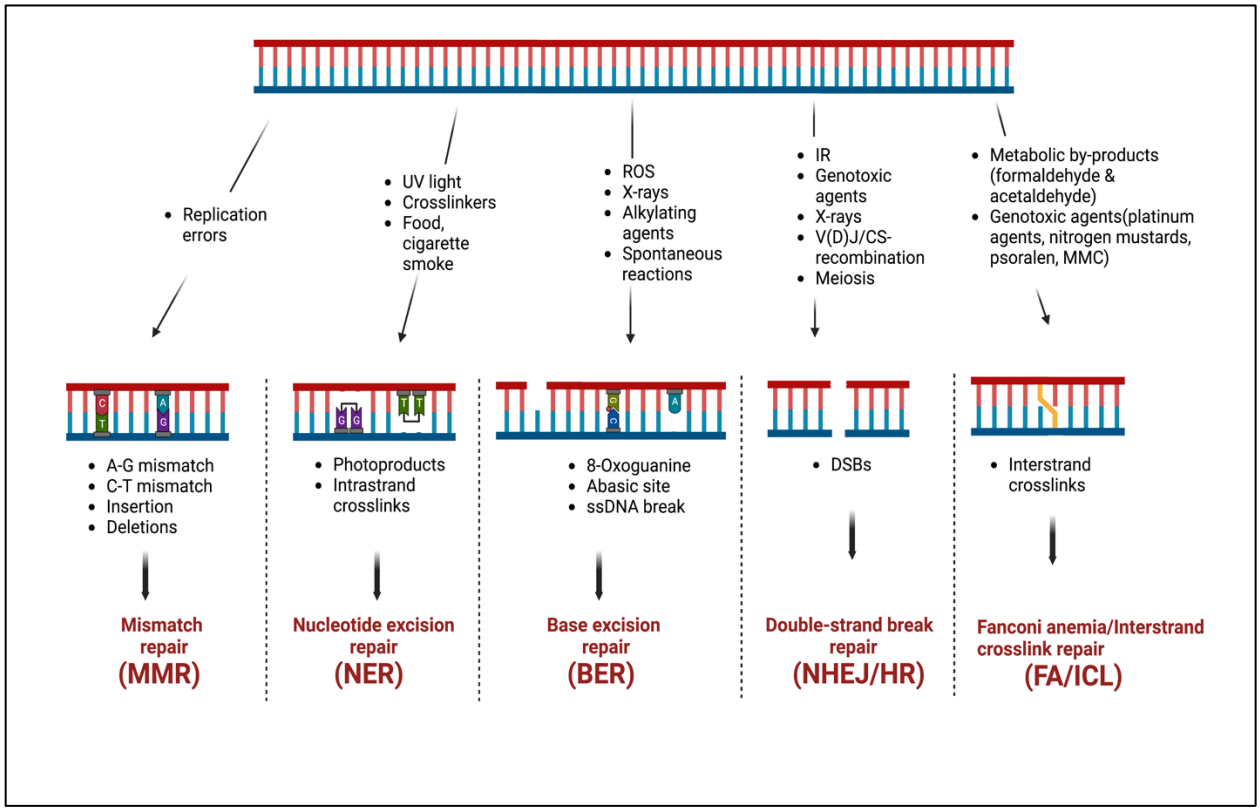


Figure 1.3. Overview of DNA Damage repair pathways. (Adapted from [197] and [198]).

1.2.5 Ubiquitin and ubiquitin-like modifications in DNA repair

Although it was initially discovered as a post-translational modification (PTM) in charge of directing the targeting of proteins and their respective obliteration by the proteasome, now ubiquitin and ubiquitin-like proteins are considered essential post-translation modifiers that regulate stability, activity, localization, and interactions of proteins in a broad range of cellular processes [199-202]. Furthermore, the existence of more than 1000 factors in the ubiquitin system and around 10,000 knowns individual ubiquitylation sites on human proteins, is a clear indication of the biological significance of ubiquitin-dependent signaling in biology [203-205]. Ubiquitin is a highly conserved protein of 76 amino acid expressed in all Eukaryotes [201]. In addition to ubiquitin, vertebrate cells express more than a dozen of ubiquitin-like proteins (UBLs). Some important UBLs include small Ub-like modifier (SUMO), neural precursor cell-expressed and developmentally downregulated 8 (NEDD8), interferon-stimulated gene 15 (ISG15) and the recently identified Ubiquitin fold modifier 1 (UFM1) [202, 203, 206]. Although most UBLs have no obvious sequence similarity with ubiquitin, they all share a similar tertiary structure [202, 206]. Ubiquitin and most UBLs are covalently linked to target proteins via a three-step enzymatic cascade involving a ubiquitin-activating enzyme(E1), a ubiquitin-conjugating enzyme(E2) and a ubiquitin ligase(E3). These enzymes first catalyze the formation of an isopeptide bond between the C-terminus of ubiquitin and Lysine residues on target proteins [200, 202, 203]. Ubiquitylations are for the most part, dynamic and reversible modifications, thanks to the regulatory activity of deubiquitylating enzymes (DUBs) [203, 207]. Ubiquitin modifications are decoded by effector proteins that harbor domains capable of identifying these PTMs. Moreover, around 20 different types of ubiquitin-binding domains (UBDs) have been identified in around 250 mammalian proteins [203, 208]. Interestingly, certain UBDs display a striking enrichment among proteins involved in DNA damage response (DDR) [208]. A paradigmatic example that illustrates the

importance of ubiquitin in intracellular signaling in DNA damage response, is the coordinated recruitment of DNA repair proteins such as 53BP1 and BRCA1 onto chromatin surrounding DSB sites [202, 209]. This recruitment is initiated by phosphorylation of the histone variant H2AX (generating γH2AX) by phosphatidylinositol-3- kinases [210], then γH2AX is recognized by mediator of DNA damage checkpoint protein 1(MDC1) and this allows subsequent accumulation of MDC1 at DSBs [202, 203, 211]. Subsequently, the E3 ligase RNF8 gets recruited to DSB sites via its fork head associated (FHA) domain, which binds to ataxia telangiectasia mutated (ATM)-mediated phosphorylation residues in MDC1 [203, 212-214]. Once recruited to DSB sites, RNF8 promotes histone ubiquitylation that allows the recruitment of another important E3 ligase via its UBD domains: RNF168 [203, 215-217]. As resulting outcome, the RNF8/RNF168-dependent ubiquitylation signaling allows the recruitment of several DSB factors such as BRCA1, 53BP1, RAD18, RAP80(BRCA1-A) complex, HERC2, BMI1, RIF1, RNF169, FAAP20 and NIPBL [202, 218]. Finally, another critical DNA repair response in which ubiquitylation plays an important role is DNA ICL repair by the Fanconi Anemia pathway (described with more detail in section 1.3). In the initiation repair events of FA, the convergence of replication forks at an interstrand crosslink triggers the ubiquitination of the replicative DNA helicase CMG (CDC45, MCM2–7 and GINS) by the recently characterized E3 ubiquitin ligase TRAIP; once ubiquitylated, CMG is unloaded and ICL repair proceeds [159, 219]. Furthermore, as part of the central FA pathway, nine FA proteins assemble into a multi-subunit ubiquitination module called the FA core complex. FANCL is the RING-type E3 ligase and in coordination with the UBE2T (E2) and UBE1(E1) mediates the monoubiquitylation of the heterodimer ID2(FANCI and FANCD2), and this event is the central activating protein modification that triggers FA ICL repair [220-224]. Finally, the DUB reported to be important for FA is USP1, which is the protein involved in the deubiquitylation of ID2, and whose inactivation leads to FA characteristic features [225].

1.2.5.1 UFM1 pathway

Ubiquitin-like proteins (UBLs) are classified in two sub-families: (i) type-1 UBL, which are conjugated to their target protein in a ubiquitin-like manner, such as: SUMO, NEDD8 and UCRP/ISG15 (ii) type-2 UBL(also known as Ub domain proteins(UDP)), which contain a ubiquitin-like structure entrenched in different large proteins, such as : Rad21, Elongin B. Scythe, Parkin and HOIL-1 [206, 226-230]. A novel UBL type 1 modification discovered by a Japanese group 18 years ago is Ubiquitin fold modifier 1(UFM1) [230]. UFM1 is an 85 amino acid protein modifier highly conserved in metazoans but not in fungi [231]. Although UFM1 does not exhibit a clear similarity in sequence identity with ubiquitin, its tertiary structure displays a remarkable resemblance to human ubiquitin [230]. Like ubiquitin, UFM1 is covalently attached to a target protein following a three-step E1-E2-E3 enzymatic reaction. The UFM1 signaling starts with the maturation of the UFM1-precursor(proUFM1) by UFM1-specific cysteine proteases (UFSP1 and UFSP2) [231-234], which cleave the C-terminal dipeptide Ser-Cys and expose a single glycine residue [230-232]. Following maturation, in an ATP-dependent reaction, UFM1 is activated by the E1 ubiquitin activating enzyme 5(UBA5), forming a thioester bond with the Cysteine (Cys) 250 of UBA5 [230]. Next, the E2 UFM1-conjugase 1(UFC1) interacts with the Ub-fold domain of UBA5, and the activated UFM1 gets transferred to UFC1 forming a thioester bond with Cys116 in UFC1 [206, 231, 235]. Interestingly, while most of the UFM1 components are reported to be located on the cytosolic side of the endoplasmic reticulum (ER) membrane, the E1 UBA5 and E2 UFC1 are both reported to have cytosolic and nuclear localization [230, 231, 236]. In the final step of the UFM1 conjugating reaction, the E3 UFM1-ligase 1(UFL1) recruits both the target protein(substrate) and the UFM1-charged E2 and catalyzes the formation of a covalent isopeptide bond between a Lysine residue of the target protein and UFM1. UFL1 is an atypical E3 ligase that lacks a catalytic cysteine, and it is classified as a scaffold-like E3 ligase [231, 237]. The final outcome

of the above-described reaction is a protein modification termed UFMylation [206, 231, 237]; A detailed scheme of the UFM1 pathway is described in Figure 1.4. Although the molecular mechanism involved in the UFM1 conjugation is well characterized, the biological significance and diverse functions of UFMylation have just started to be characterized, hence, just a small pool of UFMylation putative targets have been identified. Six years after their discovery of the UFM1 pathway, Dr. Masaaki Kumatsu's research group, using a proteomic approach, identified the E3 UFL1 ligase but also C20orf116 as the first UFM1 substrate. Further independent confirmation by other group, revalidated this and C20orf116 was named UFM1-binding protein 1 containing a PCI domain (UFBP1), these and posterior research showed that UFBP1 and the UFM1 pathway are essential for cell survival and differentiation of hematopoietic stem cells through the maintenance of ER homeostasis [237-240]. Another interesting target of UFMylation is the putative tumor suppressor ASC1. It was recently reported that UFMylation of ASC1 promotes breast cancer development through a transcriptional activation of ERα target genes, leading to proliferation and tumor formation [237, 241]. Furthermore, a subsequent murine study showed that the E3 UFL1(also known as RCAD) is essential for hematopoietic stem cell survival and erythroid differentiation. Specifically, they showed that germline and somatic deletion of UFL1 lead to severe anemia and death, due to elevated levels of ER stress, ROS, DNA damage and aberrant p53 activation [242]. More recently, in an interesting study a chinese group reported that p53 was a target of UFMylation. Mechanistically, researchers found that UFL1 competes with MDM2 for binding the N-terminal region of p53, and UFMylation of p53 was reported to play a role in preventing its ubiquitylation, enhancing its stability and supporting its role as master tumor suppressor [243].

Finally, and of interest for genomic stability, recent reports showed for the first time the link between UFM1 pathway and the DNA damage response. First it was observed that the E3 ligase

UFL1 co-localized with γH2AX at DSB sites upon UV-induced DNA damage. Posterior characterization showed that MRE11 is UFMylated on K282, and that this protein modification is required for the assembly of the MRN complex. Altogether, they reported that MRE11 UFMylation promotes ATM activation, DSB repair through HR-mediated repair and genome stability [244]. Later in a second MRE11-related study using zebrafish models, a research group uncovered that UFMylation of MRE11 is essential for telomere length maintenance and hematopoietic stem cell survival. Zebrafish models deficient in *Ufm1*and *Ufl1* displayed telomere shortening, impaired hematopoiesis and premature aging. Mechanistically, they showed that UFMylation of MRE11 was critical for the recruitment of phosphatase PP1-α, which triggers the dephosphorylation of NBS1. Without UFM1-MRE11 conjugation, NBS1 remains phosphorylated and diminishes the recruitment of MRN complex to telomeres [245]. Lastly, another study identified Histone H4 as a novel target of UFMylation. Specifically, they showed that UFL1 is recruited to DSBs by the MRN complex and mediates UFMylation of H4, which triggers recruitment of Suv39h1 and Tip60, leading to ATM activation. In addition, they showed that ATM phosphorylates UFL1 at serine 462, and this PTM boost ATM activation in a positive feedback loop mechanism [246]. Regarding the clinical relevance of the UFM1 pathway in human disease, genetic studies of different human populations have identified genetic variants of several members of the UFM1 pathway in broad range of diseases including neurodevelopmental diseases, such as child encephalophaty, microencephaly, ataxia [247-249]; hip-displasia [250-252] and carcinomas [206, 241].

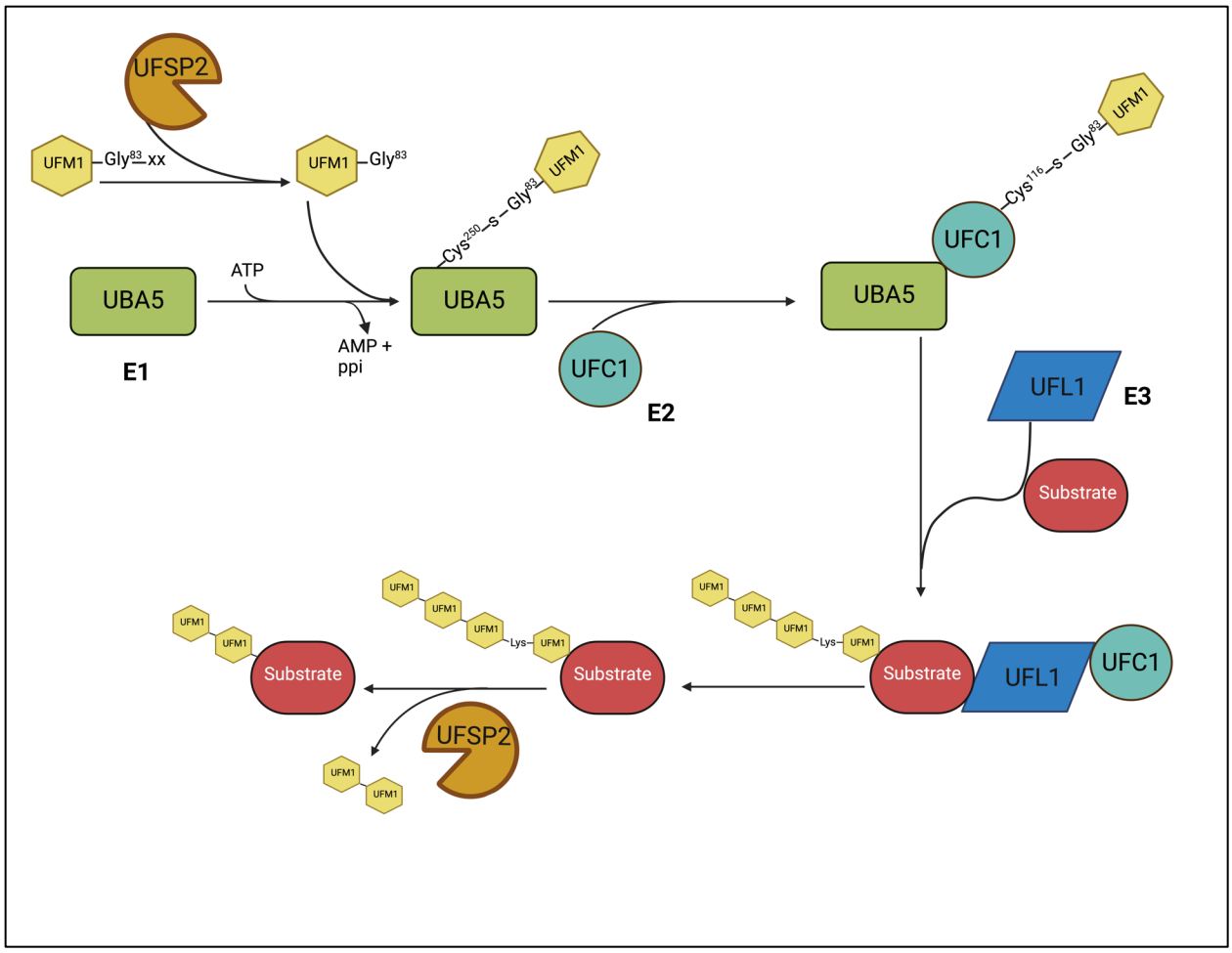


Figure 1.4 Overview of UFM1 pathway (Adapted from [206]).

1.2.6 DNA damage checkpoints

All eukaryotic cells have four phases during the cell cycle: G1, S, G2 and M, and one outside called G_0. In mammals these four phases are well defined, and each have distinct biochemical process undergoing. Depending on the nature of the lesion and the phase of the cell cycle in which the injury is detected, the cell cycle can be stopped at three checkpoints: G1/S transition, within S-phase or at the G2/M transition [253, 254]. A major component of the DNA-damage response (DDR) is a signaling transduction pathway called DNA damage checkpoint (DDC) [255-257].

Originally a checkpoint was defined as 'determined point during the cell cycle in which the integrity of DNA was "checked" before allowing cell cycle progression' [253, 258, 259].

As any other signaling transduction pathway, DDC has 4 components: (i) sensors, (ii) signal transducers (iii) effectors and (iv) mediators. However, there is not absolute demarcation of the roles, as some proteins can be both sensor and transducer, and some mediators can be placed in between role or play participate in more than one role during DDC [253]. In mammals the DDC is elicited by two members of the phosphoinositide 3-kinase-related kinase (PIKK) family of proteins: ataxia telangiectasia mutated (ATM) and ATM-related (ATR). Another kinase reported to be part of this response is DNA-PKcs, however, its role in the signaling is less understood [256]. ATM and ATR phosphorylate SQ/TQ residues in effector proteins, and this triggers a signaling cascade that establishes a transcriptional program and impedes cell division [256, 260, 261]. The initiation event of DSB repair and checkpoint activation is the detection or sensing of broken DNA ends. An essential modulator of repair and DDC is the MRN(MRE11-RAD50-NBS1) complex, which plays roles in DNA end recognition and end processing, as detailed previously. In addition, MRN complex plays an essential role in the recruitment and activation of ATM to blunt, unresected DSB ends. In the other hand, ATR cannot be recruited to blunt ends and its recruitment requires previous DSB end resection. As such, in G1 or in in any other condition in which end-resection is prevented, ATR is not recruited nor is activated [256, 262-264]. Once end resection occurs, the checkpoint signaling is switched from ATM- to ATR-dependent. ATR recruitment is mediated by its essential binding partner ATRIP, which binds to RPA-coated ssDNA [20, 265]. Upon activation, ATM and ATR trigger a signaling cascade that results in the phosphorylation of several factors, many of which are kinases themselves. In mammals the kinase activated by ATM is CHK2, while ATR activates the kinase CHK1, both kinases are essential players in DDC response. In addition, an essential and one of the most

prominent histone modifications upon DDC activation is the phosphorylation of the C-terminal SQ site of histone variant H2AX, yielding γ-H2AX [266-269]. All three PIKK kinases involved in DDC, ATM, ATR and DNA-PKcs have been reported to phosphorylate H2AX [256, 266, 267]. Eukaryotic cells subjected to DNA damage rely on the transcription factor p53 as the master genome guardian orchestrating cellular fate decisions, and enforcing cells to undergo cell cycle arrest, apoptosis, or senescence. p53 is phosphorylated and activated by all PIKK DDC kinases and this highlights the central role of p53 as the crucial DDC effector [256]. The G1/S checkpoint stops cells from entering the S phase when DNA damage is detected by inhibiting replication. If the DNA damage are DSBs caused by IR or radiomimetic compounds, ATM is recruited, activated and it phosphorylates downstream key targets such as p53 and CHK2. This ATM-CHK2 signaling cascade triggers signals involved in both initiation and maintenance of the G1/S arrest [253, 270, 271]. If the DNA damage is produced by agents such as UV light or UV-mimetic drugs, the lesion is sensed by ATR, Rad17-RFC and the 9-1-1 complex, resulting in phosphorylation and activation of CHK1. In both axes (ATM-CHK2-CDC25A or ATR-CHK1-CDC25A) the signal is followed by p53-mediated maintenance of G1/S arrest [253]. The intra-S-phase checkpoint is initiated by DNA damage either during S phase or by unrepaired lesions that were able to bypass the G1/S checkpoint, in both cases this leads to a block in replication [253, 272]. The predominant accepted molecular mechanism involved in S-phase arrest is the inhibition of firing of late origins of replication [253, 273-278]. The factors involved in sensing DNA damage during the S-phase checkpoint comprises a large set of checkpoint and DNA repair proteins, such as ATM, MRN complex and BRCA1, all essential for the activation of this checkpoint [253, 279]. Contrary to the ATM-mediated response for DSBs, when DNA damage is caused by UV, genotoxic agents causing bulky lesions, or replication stress, the main damage sensor is the ATR protein in tight cooperation with its partner ATRIP, when these two factors ensemble they conform the ATR-

ATRIP heterodimer [280, 281]. Once activated ATR phosphorylates CHK1 and triggers the activation of the ATR-CHK1-CDC25A axis resulting in inhibition of firing of replication origins [278]. In addition, ATR-mediated signaling results in phosphorylation of BRCA1, NBS1, among other DNA repair factors, that together participate in the recovery of stalled/collapsed replication forks, inhibition of replication initiation and altogether in the recovery of active replication by HR and related DNA repair events [253, 282, 283]. Finally, the G2/M checkpoint is the process that upon DNA damage detections impedes cells to undergo mitosis. And as the other two checkpoints mentioned above, depending on the type of lesion, either the ATM-CHK2-CDC25 and/or the ATR-CHK1-CDC25 get elicited [284-286]. Similarly, with other cell cycle controls, if lesion is induced by UV, bulky adducts, or replication stress, ATR-CHK1 initiates the cell cycle arrest, but the maintenance is conducted by the ATM-CHK2 signaling [280].

1.2.7 DNA damage and senescence

Cellular senescence was initially described in 1961 by Leonard Hayflick, using human fibroblast he observed that these cells stopped proliferation after a certain number of cellular divisions (nowadays called the Hayflick limit) [287, 288]. Since then, cellular senescence has been recognised as a cellular state in response to different damaging stimuli including replicative exhaustion, exposure to endogenous or exogenous DNA-damaging agents, nutrient deprivation, hypoxia, mitochondrial dysfunction, and oncogene activation [287, 289-296]. Although cellular senescence and aging are intimately linked, they are not synonymous. Cells can undergo a senescence program regardless of the age of the organism [290]. The state of cellular senescence is characterized by a stable and generally irreversible cell-cycle arrest and the acquisition of distinctive morphological, metabolic, and transcriptional changes [287, 295]. In mammalian cells, the stable cell-cycle arrest triggered in senescent cells is controlled by the retinoblastoma (RB) family and p53 proteins [290]. In this tightly controlled response, RB1, p107(RBL1) and p130(RBL2) are phosphorylated by

cyclin-specific kinases (CDK4, CDK6 and CDK2) and this hypo-phosphorylation represses E2F-dependent gene expression, which is essential for normal cell-cycle progression and DNA replication [287, 297, 298]. The transcriptional target of p53 and CDK2 inhibitor p21(CDKN1A), and p16(CDKN2A) accumulate during senescence and this protein increase leads to persistent activation of RB family proteins, E2F inhibition and subsequent permanent cell cycle arrest [287, 298-300]. Seminal cytogenetic work conducted by Barbara McClintock [301-303], along with concepts proposed by Hayflick [288, 304] and Olovnikov [305], paved the way for the identification and molecular characterization of telomeres and their posterior association with cellular senescence. Even though the majority of DNA damage foci in senescent cells is localized at telomeres, other genotoxic agents can also trigger senescence by inducing irreversible DNA damage. Indeed, several genotoxic agents such as UV and ionizing irradiation, chemotherapeutic drugs such as Topoisomerase inhibitors or DNA crosslinkers, mitochondrial dysfunction, and oxidative stress can trigger senescence as well [287]. Oncogene activation is a hallmark of cancer and cellular transformation [306, 307]. Yet, oncogene activation in normal cells does not result in transformation, instead, triggers cellular senescence [291, 308]. Hence, oncogene-induced senescence (OIS) is a tumor-suppressive response triggered in cells which expressed elevated levels of a deviant oncogene, and this senescence response is independent of telomere attrition [291, 309]. Although OIS is often mediated by the tumor suppressors p16 and ARF, leading to a permanent cell-cycle arrest; the DDR also plays a pivotal role in triggering this response [287, 291, 292, 296]. A possible mechanistic explanation of this oncogene-induced DDR response linked to senescence is the speculation that this is caused by replication fork collapse as a result of oncogene-driven hyperproliferation. In this proposed [310] model it is suggested that oncogenes induce an increased usage of DNA replication origins, reduced processivity of fork replication leading to

increased rates of fork stalling, fork collapse and altogether replication stress and genomic instability [291].

1.3 Fanconi Anemia: Disease and diagnosis

In 1927, the Swiss pediatrician Guido Fanconi described three brothers with congenital physical abnormalities, pancytopenia, and a fatty aplastic bone marrow. The three children between the age of 5-7 displayed microcephaly, intense brown pigmentation of the skin, hypogonadism, hyperreflexia and died of a condition termed back then as 'Familial infantile pernicious-like anemia' [311]. Fanconi's observations formed the diagnostic criteria for Fanconi anemia (FA) for many years and it included: pancytopenia, hyperpigmentation, skeletal malformations, small stature, urogenital abnormalities and familial occurrence [312]. An important step forward in the diagnosis of FA patients was the incorporation of chromosomal break assays using DNA crosslinking agents such as diepoxybutane or mitomycin C [313, 314]. This assay showed that FA patients cells displayed a striking hypersensitivity to ICL agents, and this was found to be a unique marker of FA genotype. This diagnostic assay led to the identification of pre-anemic cases, along with patients displaying anemia, leukemia but did not present physical abnormalities, resulting in improved diagnostic and medical management [312]. Fanconi anemia is a rare genetic syndrome (1 in 100,000 in US) [315] often diagnosed upon presentation of progressive bone marrow failure (BMF) in early childhood [222, 315]. Additionally, FA has been found in all ethnic groups and it is reported to have a carrier frequency of around 1 in 300, as such, it is estimated that up to 0.5 % of the general population may be heterozygous for one of current reported FA locus [312]. In addition, due to genetic founder effects FA is prevalent in certain genetically isolated populations, for instance, it is estimated that in Afrikaners [316] the birth incidence of FA approximates 1 in 22,000; around 1 in 45,000 in Israel [317] and the Spanish Gypsy [318] population is reported to have the highest FA prevalence in the world with approximately 1 in 64 carrier frequency owed to

a FANCA founder mutation [37]. Even though FA is usually described specially linked to BMF, it is right to define it as a multisystemic disease. In the phenotypic heterogeneity currently reported in patients some commonalities found include a broad variety of skeletal and developmental defects such as skin hyperpigmentation, infertility, congenital deformities, osteopenia, hearing failure, endocrine and gastrointestinal anomalies [319]. As a whole, it is estimated that around 90% of FA patients develop BMF [320], 70% display endocrine disorders [321], and between 60-70% have a type of congenital defect [319, 322]. Another distinct feature of FA is that it is a genetic disorder with strikingly elevated cancer predisposition risk, with a particular susceptibility to develop acute myeloid leukemia (AML), as well as solid tumors of the head and neck (HNSCC) [319, 323]. It is estimated that FA patients have >700 fold-risk of developing AML early in life in comparison to normal population, and for FA patients that progress into their 20-30s it is estimated that they have around ~500-fold increased risk of developing head and neck squamous cell carcinomas (HNSCC) and ~ 2300-fold risk oesophageal cancer ([222, 319, 323-326]. Due to clinically overlapping symptoms, FA can occasionally be indistinguishable from other genetic syndromes such as Seckel and Nijmegen, Bloom, RECQL4(Baller-Gerold, Rothmund-Thomson and RAPADILINO) or Xeroderma pigmentosum (XP). And this could be explained by the significant crosstalk and complementary functions of FA proteins and factors involved in multiple genome maintenance pathways [37]. Although FA is a rare disease, the clinical relevance of FA to cancer in the general population came to the spotlight with the identification of biallelic mutations in breast and ovarian cancer susceptibility genes in FA patients [222]. Whereas *BRCA2* germline heterozygous mutations increases the lifetime risk of developing breast cancer to around 50% and 15% for ovarian cancer, biallelic mutations of *BRCA2* cause FA with brain tumours, including medulloblastoma and Wilms [37, 279, 327, 328]. Likewise, biallelic mutations of *BRCA1* cause FA, whereas heterozygous *BRCA1* mutations also predisposes to hereditary breast and

ovarian cancer syndrome (HBOC) [37, 322, 329-331]. In addition, other FA/HR genes with reported increased cancer risk include *PALB2* (breast [332, 333] and pancreatic cancer [334]*)*, *FANCM* (triple negative breast cancer [335]), *FANCA* (familial breast cancer [336]), *RAD51C* (breast and ovarian cancer [337]), *FANCC* & *FANCG* (early-onset pancreatic [338]) and *UBE2T* (breast cancer [339]) [222]. Homozygous germline mutations(biallelic) of any one of the 22 currently known FA genes (designated as complementation groups *FANCA-FANCW*) causes FA, with the notable exceptions of *FANCB*, which is X-linked and *RAD51(FANCR),* whose dominant-negative mutations were reported in rare patients with FA [37, 329, 340]. FA proteins, along with FA-associated proteins (FAAPs), cooperate in a common DNA repair pathway involved in the repair of ICLs known as the FA or FA/BRCA pathway.

		Gene	Alias	Established molecular fuction	Patient frequency
Genes mutated in FA patients	FA Core Complex	FANCA		FA core complex assembly	64%
		FANCB		FA core complex assembly	2%(X-linked)
		FANCC		FA core complex assembly	12%
		FANCE		FA core complex assembly	1%
		FANCF		FA core complex assembly	2%
		FANCG		FA core complex assembly	8%
		FANCL		E3 ubiquitin ligase that monoubiquitylates FANCD2 and FANCI	0.4
		FANCM		FA core complex assembly	0.1
				5'-3' DNA translocase/helicase	
				Branch migration & repair of HJ intermediates and replication forks	
				Recruits the BLM helicase during the DDR	
		FANCT	UBE2T	E2 ubiquitin-conjugating enzyme for the FD2 monoubiquitylation by FANCL	0.1
	ID2	FANCD2		Recruits DNA repair proteins	4%
				Monoubiquitylated by the FA core complex	
				Forms a heterodimer with FANCI	
		FANCI		Recruits DNA repair proteins	1%
				Monoubiquitylated by the FA core complex	
				Forms a heterodimer with FANCD2	
		FANCP	SLX4	Resolution of Holliday junctions	0.5%
				Master scaffold and regulator of ERCC1-XPF, MUS81-EME1/2, SLX1	
	FA/HR	FANCD1	BRCA2	DNA repair control and effector recruitment, RAD51 loading onto DNA	2%
		FANCJ	BRIP1/BACH1	3'-5' DNA helicase essential for BRCA1-dependent DNA repair	2%
		FANCN	PALB2	Regulates BRCA1 localization and DNA repair activity	0.7%
		FANCO	RAD51C	DNA repair via homologous recombination	0.1%
		FANCR	RAD51	DNA repair via homologous recombination	Rare(Dominant-negative)
		FANCS	BRCA1	DNA repair via homologous recombination	0.1%
		FANCU	XRCC2	DNA repair via homologous recombination	0.1%
	Recent	FANCV	REV7	Translesion DNA synthesis	One patient
		FANCW	RFWD3	E3 ubiquitin ligase involved in turnover of RPA and RAD51 during HR/ICL	One patient
		FANCQ	XPF/ERCC4	DNA repair nuclease involved in ICL unhooking	0.1%
FA-associated genes		FAAP10	STRA13/CENPX/MHF2	FA core complex; histone fold-containing protein, localization of FANCM	Unknown
		FAAP16	APITD1/CENPS/MHF1	FA core complex; histone fold-containing protein, localization of FANCM	Unknown
		FAAP20	C1orf86	FANCA stability; binds ubiquitylated TLS polymerase REV1	Unknown
		FAAP24	C19orf40	FA core complex; interacts with FANCM	Unknown
		FAAP100	C17orf70	FA core complex	Unknown
		FAN1		Nuclease; restart of stalled replication forks	Unknown
		UAF1		ID2 deubiquitination	Unknown
		UHRF1		Lesion recognition	Unknown
		USP1		ID2 deubiquitination	Unknown
					Unknown

	Gene	Alias	Established molecular fuction	Patient frequency
Involved in ICL repair	MUS81-EME1		Structure-specific endonuclease with a preference for 3' flaps	Unknown
	SNM1A		5' exonuclease	Unknown
	SNM1B		5'exonuclease	Unknown
	HELQ		Helicase required for ICL repair	Unknown
	BLM		DNA helicase(5'-3'); HJ dissolution and inhibition of RAD51 stand invasion	Unknown
	RMI2		Cooperates with BLM in HJ dissolution	Unknown
	MRE11		Component of the MRN complex; involved in HR	Unknown
	NBS1		Component of the MRN complex; involved in HR	Unknown
	RAD50		Component of the MRN complex; involved in HR	Unknown
	ATR		Kinase important for DDR; cell cycle checkpoint	Unknown
	CTIP	RBBP8	End-resectiong during HR	Unknown
	TOPIIIα		Topoisomerase involved in relaxing supercoiled DNA during HR	Unknown

Table 1.1. Fanconi Anemia and FA-associated genes and their molecular functions.(Adapted from [222]& [37]).

1.4 Interstrand cross-links and FA/BRCA ICL repair pathway

Although FA proteins have essential roles in multiple housekeeping responses related to maintenance of genomic stability, the interstrand crosslink repair pathway is the canonical FA-dependent DNA damage response (DDR) pathway and loss of function in FA genes results in hypersensitivity to ICL-inducing agents. ICLs are DNA lesions that covalently link two bases on complementary DNA strands. Due to the complex chemical nature governing ICL-formation, cross-linking agents can form not only ICLs but also monoadducts, DNA-protein cross-links (DPC) and intrastrand cross-links [341]. ICLs impede the separation of the two DNA strands, and as a result they represent an utter barrier for transcription and replication, two essential cellular processes. Consequently, ICLs are considered among the most deleterious type of DNA damage, and they are particularly detrimental to rapidly dividing cells [329, 341]. The structural diversity found in ICLs results from the numerous agents that can form DNA adducts and their multiple reactive functional groups found in DNA bases [159]. Preference for adduct sites depends on the ICL agent and all four nucleotides have been observed to form ICLs. Yet, purine nucleotides (dG and dA) tend to be more reactive than pyrimidine nucleotides (dT and dC), and dG-related lesions make up for the majority of physiological and clinically relevant ICLs [159]. ICLs can be crudely subclassified in 3 different groups: (i)chemotherapeutics;(ii) endogenous metabolites and (iii)microbial-derived metabolites [159]. ICL-inducing agents commonly used in chemotherapy include platinum compounds (e.g., cisplatin, carboplatin, oxaliplatin), nitrogen mustards (e.g., cyclophosphamide, melphalan, chlorambucil, bendamustine), psoralen (e.g., furocumarins from plants and fungi), and chlroethyl nitrosoureas (e.g., carmustine) [159, 341]. Although most of our knowledge about ICL repair comes from the use of chemotherapeutic agents, biological systems did not evolve a plethora of sophisticated DNA repair pathways to deal with compounds developed in the last century. So, with the goal of filling this knowledge gap

research groups have recently identified several sources of endogenous ICL agents. It is now acknowledged that certain cellular metabolic processes such as lipid peroxidation, alcohol metabolism, histone demethylation and nitrous acid metabolism, can produce by-product intermediates such as formaldehyde, acetaldehyde, or nitric oxide, which are now recognized as endogenous sources of ICLs [342-345].Furthermore, in seminal studies supporting this, researchers showed that in murine models with double K.O. for Fancd2 and Aldh2 (acetaldehyde-detoxifying enzyme), animals displayed severe aplastic anemia along with elevated levels of DNA damage in the HSC compartment; thus firmly establishing that acetaldehyde is a potent endogenous ICL agent [46, 222, 346, 347]. Moreover, in a follow up study, Patel's group at Cambridge recently showed that mitochondrial ALDH2 and cytosolic ADH5, are both essential for removing formaldehyde, and that loss of these detoxifying enzymes leads to BMF and development of leukemia in mice and humans [348].

1.4.1 Molecular mechanisms in FA/BRCA ICL repair

FA interstrand cross-link repair is a multistep response that requires involvement and tight coordination of several different DNA repair pathways including homologous recombination (HR), nucleotide excision repair (NER) and Translesion synthesis (TLS) [222, 323]. Four crucial insights contribute to the elaboration of the first model of FA ICL repair: first (i) it was the notion that ICL repair was couple to DNA replication [349], and this was supported by the observations that ICL-inducing agents trigger cell cycle arrest in late S/G2 and they elicits DSBs formation only after entering S phase; (ii) FA ICL repair require involvement of homologous recombination, based on the role of BRCA2(FANCD1) [279] in FA and epistatic observations between FANCC and XRCC2 [350]; (iii) FA ICL requires the involvement of TLS, supported by epistasis between TLS DNA polymerase Rev1 and FANCC for ICL repair [350-352] & (iv) observation that cells deficient in XPF, a canonical NER endonuclease, displayed hypersensitivity

to ICL [159, 162]. Altogether, these critical observations led to the proposal of a replication-dependent ICL repair model in which the (a)encounter of replication forks with an ICL triggers a XPF/ERCC1-mediated unhooking of the ICL [353] and generation of a DSB; (b) TLS polymerases are recruited to bypass the lesion and execute DNA synthesis; (c) the adduct is removed by NER; and finally (d) homologous recombination repair mediates a faithful repair of the lesion [159].

Sensing and ICL recognition. In this broadly accepted model, supported by mechanistic analysis using Xenopus egg extracts [188], replication-dependent ICL repair starts when replication fork convergence on an ICL, triggers the ubiquitylation of the Cdc45-MCM2-7-GINS(CMG) helicase by the E3 ubiquitin ligase TRAIP [219]. Once ubiquitylated, CMG is evicted from the chromatin by the p97 ATPase in cooperation with BRCA1 [354, 355]. This event then triggers ICL sensing by the FA anchoring complex containing the translocase FANCM and its interacting partners FAAP24, FAAP16(also known as MHF1/CENP-S) and FAAP10 (MHF2/CENP-X), [329, 340, 356]. FANCM binding to ICLs is dependent on its phosphorylation by ATR, and once recruited, FANCM functions as a landing platform for the FA core complex [224, 329]. In addition, FANCM recruitment to ICLs trigger RPA accumulation at ICL [11, 357], subsequent ATR stimulation and activation of DNA damage checkpoint [20]. The FA core complex which comprises FANCA, FANCB, FANCC, FANCE, FANCF, FANCG, FANCL, FANCM, FANCT and accessory proteins including FAAP100, FAAP16, FAAP10, FAAP20 and FAAP24 [222-224, 341]. This complex harbor an enzymatic module containing FANCL (E3 ubiquitin ligase) and FANCT(UBE2T) (E2 ubiquitin-conjugating enzyme) that catalyze the monoubiquitylation of the heterodimer composed of FANCI and FANCD2, known as the ID2 complex, which is the central activating event of the FA pathway [222, 358, 359]. Monoubiquitinated ID2 is then recruited to the chromatin, accumulated at ICLs and colocalized

with additional downstream FA/HR proteins [222, 360]. In addition, as a negative regulation of the signaling, ID2 deubiquitylation by the ubiquitin carboxy-terminal hydrolase 1(USP1) in cooperation with USP1-associated factor (UAF1) is critical for completion of the ICL repair response [360, 361].However, the dynamics of this reversible ID2-Ub conjugation are still poorly understood [222, 224]. Two other important post-translation modifications affecting ID2 have been reported. First the SUMOylation of ID2 by the PIAS1 and PIAS4 SUMO E3 ligases triggers its recognition, and second, ubiquitylation by the SUMO-targeted ubiquitin ligase RNF4, resulting in ID2 eviction from ICL sites mediated by p97 [224, 329, 362]. Upon ID2 localization at ICLs, important downstream reactions are triggered including: endonucleolytic incision, translesion synthesis (TLS) and HR-mediated DSB repair.

DNA incision: ICL unhooking. Once the ubiquitinated ID2 complex is bound to chromatin, it functions as a recruitment platform for structure-specific endonucleases (SSE) and translesion synthesis (TLS) polymerases. As such, ID2-Ub controls the nucleolytic ICL incision from one of the parental strands and this incision process commonly called "unhooking' is a central event in ICL repair [159, 222, 363]. Unhooking of DNA adducts usually requires two (5' and 3') incisions on the same strand of DNA. Although this dual incision is not sufficient to completely removed the adduct, it is enough to permit TLS polymerases perform DNA synthesis and bypass the lesion [329, 341, 364]. Three different structure-specific endonucleases (SSE) including SLX1-SLX4, MUS81-EME1, XPF(ERCC4)-ERCC1, and three endo/exonucleases including Fanconi associated nuclease 1 (FAN1), SNM1A and SNM1B have been implicated in ICL repair [111, 112, 114, 223, 341, 365-373]. SLX4(FANCP) is a scaffold FA protein that gets recruited to the ICL lesion through its interaction with FANCD2 [365, 370, 374, 375]. SLX4 functions as a landing 'tool-belt' and recruits and activates the SSE nucleases XPF(ERCC4)-ERCC1, MUS81-EME1 and SLX1. XPF-ERCC1 is 3' endonuclease essential for NER of bulky adducts, but

interestingly, XPF and ERCC1 mutants are highly sensitive to ICL-inducing agents and this higher sensitivity with respect to other NER factors, suggest that they may have a distinct role in ICL repair. In line with this relevance for ICL repair, XPF was identified as a complementation group of Fanconi anemia (FANCQ) [341, 376, 377]. XPF-ERCC1 once docked with SLX4 forms a complex and makes the incision that unhooks the ICL, XPF endonuclease role is essential for ICL repair and the other SSE seems to have redundant roles in ICL repair [222, 329, 341, 372]. Recent studies [378, 379] reported that purified XPF does not cleave X-structures and instead, it cleaves efficiently fork structures several nucleotides from the ssDNA, which suggest that XPF may need fork reversal events which convert X-shaped DNA into a suitable structure for XPF incision [159]. Currently the endonuclease involved in the cleavage of the ICL from the other strand has not been identified, however, SNM1A seems a good candidate. This endonuclease displays suitable specificity for this role, and it is able to degrade a DNA strand past an ICL starting from a 5' ICL incision. In addition, recent epistatic evidence [373] of a potential collaboration between XPF and SMN1A and CRISPR-based chemogenomic profiling [380] showing strong clustering and correlation with other FANC genes, support this hypothesis [159].

Translesion synthesis. An important advance in our understanding of FA ICL repair has been the recognition that TLS polymerases play an essential role in ICL repair. Hence, TLS is crucial as this event generates the critical DNA template necessary for faithful HR repair in the next phase of FA ICL repair. Upon unhooking, the resulting lesion on one of the parental DNA strands remains and the nucleotide containing the damaged base needs to be bypassed to allow DNA synthesis [341]. TLS polymerases are recruited to ICL intermediates by ubiquitylated PCNA and the FA core complex. In addition to PCNA-Ub, the FA core complex mediates the recruitment of TLS polymerases through the interaction of FAAP20 and REV1, specifically, the UBZ4 domain of FAAP24 recognizes both, ubiquitin and the BRCT (BRCA1 C terminus)

domain of REV1 [189, 224, 381, 382]. Although, the polymerase in charge of the nucleotide incorporation during TLS has not been yet identified, the bypass TLS step is executed by REV1 and the error-free extension step is conducted by REV3 and REV7(FANCV), both subunits of Pol ζ [159, 224, 329, 383]. Although HR and NHEJ are the most important DSB repair pathways with an expected function in the final steps of ICL processing, the FA pathway is thought to have a role in pathway choice, channeling most of DSB intermediates created by ICL processing into high fidelity HR repair [223, 329]. As previously described in detail in section 1.2.2.2, the HR repair pathway encompasses three key phases: DSB end resection, strand invasion and Holliday junction resolution [87, 222, 329, 384, 385]. In the last phase of HR, after second-end capture and DNA synthesis, a double Holliday junction structure is formed. Then branch migration promotes Holliday junction resolution by GEN1 or SLX4-MUS81-EME1-SLX1 resolvases or junction dissolution executed by the BTR(BLM-TOPIIIα-RMI1) complex [329]. However, these intermediates processing outcomes are equally possible, there is a pathway choice preference for the BTR-mediated dissolution, likely promoted by the interaction of the translocase FANCM with this complex, this key event links the completion of ICL repair back to the proteins involved in its initial sensing and detection [319]. Finally, the unhooked ICL in the other strand of the DNA is believed to be removed by NER, however this still requires further verifications [159, 222, 224]. A detailed scheme of the replication dependent ICL/FA pathway is described in Figure 1.5.

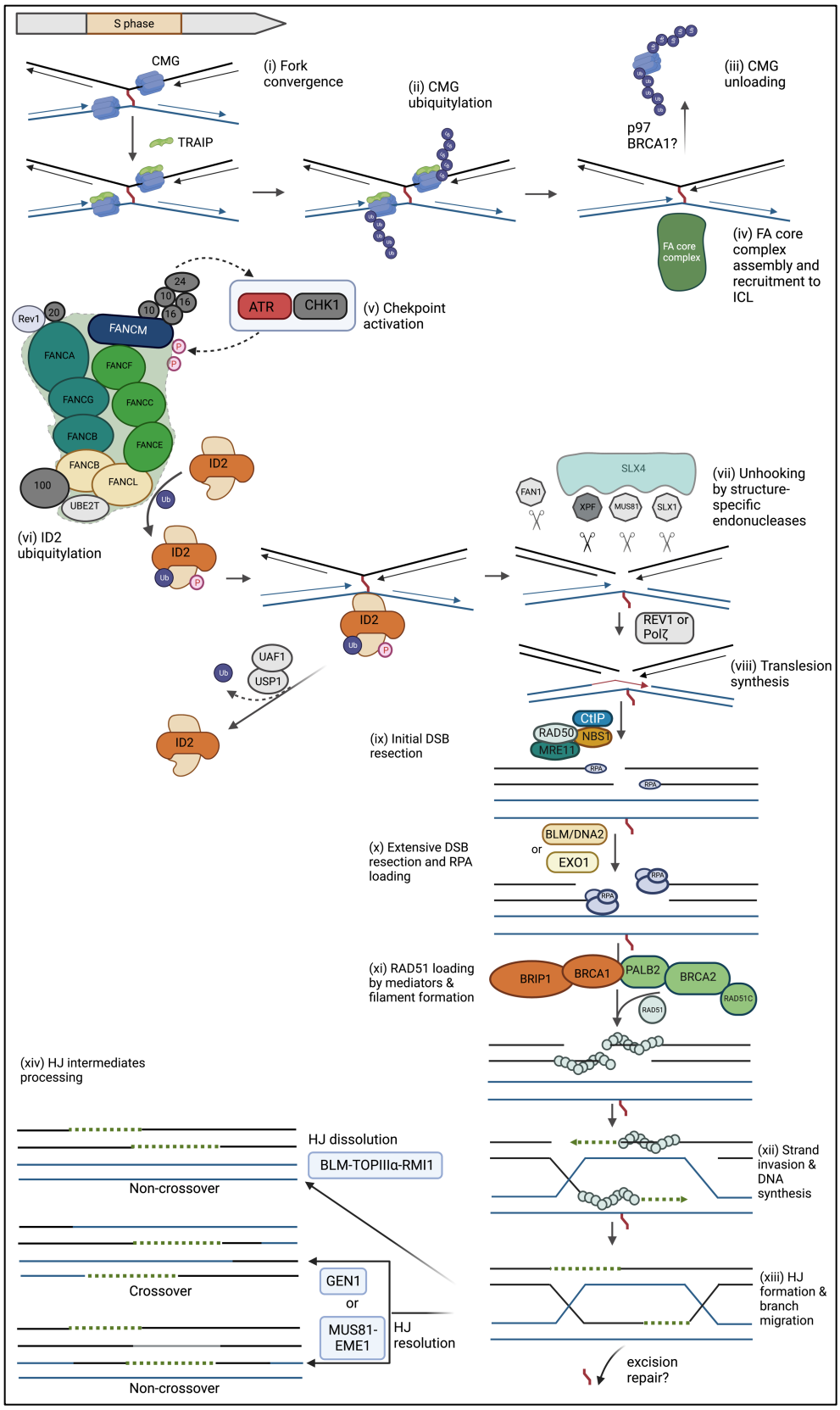


Figure 1.5 Replication-dependent ICL/FA repair pathway.

1.5 ICL-inducing agents and Cancer therapy

The use of DNA interstrand crosslinking agents has its origins in one of the multiple barbaric events that occurred during the Second World War. In December of 1943, the Allied ship S.S John Harvey which was anchored in the small Italian harbor of Bari carrying a secret deadly cargo, was attacked by the German Luftwaffe. As result of the attack massive explosions were triggered and an estimated of 60 tonnes of American mustard gas bombs were released and contaminated the port and surrounding area [323]. Although the tragic incident was handled with the highest secrecy by the allied authorities in a cover-up effort, a stubborn and talented military physician called Stewart Alexander started a throughout investigation into the Bari disaster. As part of his findings Alexander and his team observed that affected patients or diseased victims displayed very low levels of white blood cells. As a trained physician in chemical weapons, he hypothesized that the toxic mustard gas could have a great therapeutic potential in the treatment of leukaemia [386]. Officials never acknowledged Alexander's Bari reported, nevertheless, Col. Cornelius Rhoads, chief of the Medical Division of the US Chemical Warfare Service, along with other Eisenhower's senior medical advisers, lauded the exceptional job performed by Alexander. Furthermore, prompted by the Bari 'report and a top-secret clinical trial done at Yale university using nitrogen mustard, Col. Rhoades went on and convinced the chairman of General Motors, Alfred P. Sloan Jr. and its famous engineer Charles F. Kettering, to establish a new research institute fully dedicated to launch a war on cancer. As result of these efforts, in August 7th of 1945, the same day of the infamous atomic attack on Japan, they announced their plans to build the Sloan Kettering Institute for Cancer research [386]. Then in 1946 after turning the military weapon into a scientific breakthrough, researchers announced the first report therapeutic use of nitrogen mustards in clinic [387]. Remarkably, seventy-two years later, and with minimal chemical modifications, nitrogen mustards such as cyclophosphamide

and melphalan are still core components of chemotherapeutic regimens used in the treatment of lymphomas, leukeamias and solid tumours. Few years later other ICL-inducing agents were also incorporated in cancer clinical treatment, the Streptomyces caespitosus isolate mitomycin C(MMC) was included in 1956, platinum compounds such as cisplatin in 1971 and psoralens in 1989 respectively [323].

The incapacity to repair ICL is a hallmark in FA patients, but these DNA lesions are also deleterious to many cancer cells, and this make ICL-inducing agents very effective as treatments. The mechanism of action of each DNA crosslinker compound is similar but they also display specific differences regarding the base specificity of the compound and the structural distortion caused on the DNA helix. For instance, DNA damage caused by cisplatin, the most used crosslinker, is estimated to comprise mostly (~90%) of intrastrand crosslinks and just less than 5% ICLs. In addition, nitrogen mustards and MMC are also reported to cause only around 5%-10% of ICLs [319, 388, 389].

Despite their efficacy in clinic, crosslinker-based chemotherapy has limitations due to its side effects and the capacity of cancer cells to develop chemotherapeutic resistance. Patients displaying relapse or refractory disease have dismal outcomes and this remains an unmet clinical challenge for several types of cancer [390-398]. Due to their broad usage in cancer treatment, there has been a considerable amount of research efforts focus on finding new ICL-inducing agents and increasing the sensitivity of current treatments. Therefore, the identification of factors involved in the modulation of sensitivity of tumor cells to ICL-inducing agents could have enormous therapeutic implications. Upregulation of FA pathway results in chemotherapeutic resistance to a range of DNA crosslinkers [319, 399-402]. Therefore, inhibiting FA repair to make tumor cells behave as FA cells and sensitizing them against ICL-inducing agent is a reasonable therapeutic approach. Direct targeting of FANC proteins or the

identification of synthetic lethal nodes in ICL repair are some strategies that could help in tackling this clinical challenge.

1.6 Cyclophosphamide and Cisplatin

1.6.1 Cyclophosphamide

Cyclophosphamide is considered one of the most successful chemotherapeutic agents ever synthetized. Pharmacology efforts aimed at modifying the chemical structure of nitrogen mustards and achieving higher selectivity for cancer cells led to the synthesis of cyclophosphamide in 1958 [403, 404]. After satisfactory clinical trials conducted in 1958, cyclophosphamide was approved as cytotoxic cancer agent by the FDA in 1959 [392, 405]. Sixty-three years after its approval, cyclophosphamide is still widely used as chemotherapeutic agent in the treatment of lymphomas, leukemias, solid tumours and as a conditioning agent for blood and marrow transplantation [392, 405]. In addition, in low-income regions of sub-Saharan Africa, cyclophosphamide has been intensively used as monotherapy for pediatric endemic Burkitt lymphoma during the past 50 years [406].

Cyclophosphamide is an inactive prodrug that requires metabolic processing and chemical activation to release its active metabolite: phosphoramide mustard. Metabolic activation in the liver by cytochrome P-450 yields 4-hydroxycyclophosphamide and aldophosphamide. Then, these two precursors are diffuse into the cells and further metabolized into two metabolites: phospharamide mustard and acrolein [407]. Phosphoramide mustard is the metabolite responsible for generating DNA crosslinks and acrolein is a by-product unsaturated aldehyde linked to hemorrhagic cystitis as toxic secondary effect of cyclophosphamide treatment [392]. In addition, one novel synthetized nitrogen mustards tested in preclinical and clinical studies [408-413] is mafosfamide (MAF), which is a preactivated cyclophosphamide analog. MAF is a stable 4-thioethane sulfonic acid salt of 4-hydroxicyclophosphamide, that in contrast to

cyclophosphamide, does not require metabolic activation in the liver. Interestingly, MAF is spontaneously metabolized into 4-hydroxycyclophosphamide and a thiol called mesna. Then following the same metabolic route used for cyclophosphamide, 4-hydroxycyclophosphamide and its tautomer aldophosphamide, are metabolized into the active metabolite phospharamide mustard and acrolein [408]. Consequently, the mechanism of action responsible for the cytotoxity of MAF in cells is similar to the one reported for cyclophosphamide.

1.6.2 Cisplatin

Cisplatin was first synthetized by the Italian chemist Michele Peyrone in 1844 and it was called Peyrone's chloride [414], but it was not until 1965 that its therapeutic potential caught the attention of the scientific community. Barnett Rosenberg, a biophysicist at Michigan state university discovered by accident that platinum mesh electrodes were capable of inhibiting cell division in E. coli, sparkling the interest of the chemotherapeutic potential of these products. Further chemical analysis led to the identification of two active complexes: the neutral cis-isomer [PtII (NH3)2Cl2] later termed as cisplatin, and the platinum analogue cis-diamminetetrachloro-platinum(V). Followed up studies and clinical research conducted in United Kingdom and by the US National Cancer Institute, led to the approval of Cisplatin by the FDA in 1978, as chemotherapeutic agent for the treatment of testicular, ovarian and bladder cancer [415]. A decade after, the second platinum drug carboplatin received FDA approval, and more recently, in 2002, another platinum (Pt) agent, oxaliplatin, received authorization in US and Europe as well [416]. Cisplatin, carboplatin and oxaliplatin, the three most prominent platinum-based drugs in clinic, generate monoadducts, DNA intrastrand and interstrand crosslinks as part of their cytotoxic mechanism against cells. Inside cells cisplatin requires to be activated, and this happens through aquation to monoaqua species, in which chlorine groups are replaced by water. Once activated cisplatin can bind to DNA and form Pt-DNA adducts or

crosslinks [417]. Although there are estimates as mentioned before, there is still continuous debate regarding which of the multiple Pt-DNA adducts is the most prominent and have the highest biological relevance [415, 418]. Multiple mechanisms are reported to be involved in driving the resistance against platinum-based ICL agents, including drug uptake, DNA-damage damage recognition & repair, and apoptosis. The discovery of novel mechanism involved in the sensitivity and resistance against both nitrogen mustards and platinum-based ICL-inducing agents will greatly valuable and translated into a better management and treatment of cancer patients.

1.7 Functional genomics and DNA repair research

Among the therapeutic options available for oncologic treatment, chemotherapy and radiation are two great examples about how to exploit the exquisite sensitivity of cancer cells to DNA damage. Yet, despite their efficacy and our increasing knowledge in cancer biology, we are just starting to uncover the molecular mechanisms involved in their efficacy at selectively killing malignant cells, and why they eventually fail upon relapse or refractory disease. While there is not a straightforward route to identify cancer drug targets and predict functional oncogenic nodes, solutions will likely arise from holistic initiatives, including recent efforts in functional cancer genomics [419]. A crucial goal in Biology is the identification of genes underlying a specific cellular process or pathology. Reverse genetics is a 'genotype-to-phenotype' approach that requires previous knowledge to test the consequence of a specific genetic perturbation. In contrast, forward genetic screens are "phenotype-to-genotype" methods that in unbiased manner involve the perturbation of many genes (even at genome-wide scale), the selection of specific phenotypes, and the further characterization of the genetic manipulations causing the phenotypic changes [420]. Forward genetic approaches historically relied on random mutagenesis of the genome and subsequent selection of the aberrant phenotype. Although

laborious, these methods have uncovered the genetic bases of many fundamental biological process such as cell cycle control [421, 422], embryogenesis [423, 424], apoptosis [425], development [426-428], as well as NOTCH and Ras signaling [429]. However, a disadvantage of these approaches, is that due to the random nature of the method, the causal mutations selected in the clones is in principle unknown. Additionally, the identification and linkage of these random mutations with a specific phenotype, is expensive and labour intensive. A major breakthrough that helped with these technical challenges was the incorporation of novel techniques in genome sequencing, such as next-generation-sequencing (NGS), which facilitated the identification and mapping of the mutations involved in the target phenotype [420, 430]. Along with NGS technologies, the development of embryonic stem cells (ESC) and the improvement of methods for efficient genetic manipulation sparked research efforts aiming to generate loss-of-function alleles for virtually every gene in mouse or humans. Consequently, all these developments, along with the extensive experience in mammalian cell culture methods, led to the development of refined high-throughput screening. Initial forward genetic screens were driven by the use of RNA interference (RNAi) technology [431]. This approach generated valued information on gene functions in different cellular and animal models [432-436], but it was also hampered by its extensive off-target activity and the often-incomplete gene knockdown observed [420, 437-439]. Aiming to solve the problems found with RNAi in genetic perturbation endeavours, two other technologies were developed: Zinc-finger nucleases (ZFNs) and transcription activator-like effector nucleases (TALENs). ZNFs were engineered enzymes harboring a FokI endonuclease domain which was fused to an array of DNA-binding domains that allow site-specific mutagenesis upon DSB generation. Although ZNFs represented an improvement in the gene editing field, the method was time-consuming, expensive, and technically complicated. In the other hand, while TALENs were easier to design than ZNFs

and were considered an improved technology over ZNFs, yet, their cargo capacity and low efficient delivery, make them also unsuitable for efficient HTS applications [420, 440-442]. This technical challenges in genome editing reached a turning point in 2012, when CRISPR-Cas9 technology was uncovered and a revolution in life sciences started. A continuous battle between prokaryotes and their viral predators have allowed the evolution of sophisticated defense systems. Prokaryotic CRISPR (clustered regularly interspaced short palindromic repeats)-Cas9(CRISPR-associated-9) adaptive immune systems have the capacity to store information of previous infections and upon rencounter with their viral predators or mobile genetic elements (MGE), deploy RNA-guided nucleases for sequence-specific silencing [443]. In a landmark 2012 study by Jinek et al. [444], the teams of Emmanuelle Charpentier and Jennifer Doudna, isolated the components of the CRISPR-Cas9 system and adapted it to function in-vitro. In this ground-breaking study they showed that this prokaryotic defense system could be programmed to cleave at specific sites in a target DNA. This seminal work along with other key initial and late contributions by Francisco Mojica [445-448], Alexander Bolotin [449], Philippe Horvath [450], Christine Pourcel [451], Rodolphe Barrangou [452, 453], Sylvain Moineau [450, 452, 454], Luciano Marraffini [455, 456], Virginijus Siksnys [457, 458], Elitza Deltcheva [459], Feng Zhang [460-462], George Church [463], and others basic science researchers, paved the way for one of most important breakthroughs in life sciences, with implications in basic science, medicine, agriculture and industry. The huge relevance of this scientific work was translated into the awarding of Emmanuelle and Jennifer Doudna with the Nobel prize of Chemistry in 2020.

The Streptococcus pyogenes Cas9(SpCas9) was the first CRISPR system to be adapted and used in mammalian cells [460, 463], and it remains the most used gene-editing system nowadays. Upon sequence recognition in the DNA target region, SpCas9 cleaves and generates a blunt double-strand break (DSB) [454]. Class-II CRISPR system, comprises of a Cas endonuclease

and one target-specific CRISPR RNA (crRNA). In this system, Cas9 recognize DNA sequences through base pairing between the target DNA and the guide sequence of the crRNA in the presence of a protospacer adjacent motif (PAM) 5'-NGG (N representing any nucleotide) next to the target DNA sequence. SpCas9 specifically requires a trans-activating CRISPR RNA (termed tracrRNA) which is fused with the crRNA and together form the single-guide RNA (sgRNA) [444, 464]. The DSB generated by Cas9 are usually repaired by NHEJ, which is an error-prone repair pathway that introduces insertion/deletions(indels), resulting in out-of-frame genetic perturbations. Alternatively, if in the editing system a donor-template with homologous arms to the target DNA is used, CRISPR-Cas9 system can allow precise genome edition, although with reduced frequency [464].

1.7.1 CRISPR/Cas9-based genome-wide screening

The great efficiency of Cas9 and the relative non complicated methodology while designing guides to target specific genes have prompted to the design and generation of multiple genome-wide CRISPR-Cas9-Knockout libraries for both human and mouse which are now available in public repositories [465-472]. Most of these libraries require the generation of Cas9-stable cell lines and optimization of genome editing efficiency. All-in-one systems are also available; however, separate delivery is recommended as it permits the optimization of Cas9 activity without confounding effects from the KO generated [473]. Lentiviral transduction of genome-wide libraries is carried-out at low multiplicity of infection (MOI, ~0.2-0.3) which allows that in the targeted mutant cell pool most of cells are only transduced with 1 plasmid (~1sgRNA per cell), in accordance with the Poisson distribution. Normally, CRISPR-lentiviral libraries include between 4-10 sgRNA targeting each gene, this redundancy allows to maximise statistical power and keep cell culture conditions scaled to reasonable size. Because sgRNA encoding specific sequences are integrated into the genome, each targeted mutant cell harbors a unique barcode

identification (integrated sgRNA sequence=unique cellular barcode) which can be link later to a specific aberrant phenotype. This direct linkage between the genetic perturbation traced with the barcode-NGS readout and the aberrant phenotype, is the basis of what it is now define as CRISPR-based functional genomics [473].

CRISPR-Cas9-based forward genetic screens have shown great efficacy in identifying cancer genetic vulnerabilities against specific compounds and gene essentiality for different types of cancer. CRISPR-based screening aimed to assess cellular fitness are considered the most straightforward type of screening regarding pipeline design, execution and posterior identification of fitness genes under specific growth conditions [473]. Still, fitness screens currently represent the most robust and abundant CRISPR-based screen data so far generated. Furthermore, essential screens have allowed the identification of essential genes in human cancer cell lines [467, 472, 474-478], human haploid cells [479], and human pluripotent stem cells [480, 481]. In addition, a collaboration between the Broad institute (Aquilles project) in US and the Sanger institute (Score project) in UK have led to the creation of the Cancer Dependency Map effort [482-484], whose objective is to map cancer vulnerabilities in every possible type of cancer, and make a comprehensive database available for academic and pharmaceutical scientist and help them in their pursuit of a better identification of therapeutic targets. So far, the pilot of this ambitious project has been executed in around 1000 cell lines, and it is estimated that this is just the beginning, and a complete dependency map would require the screening of around 20,000 cancer models in the next decade [476, 485].

Targeted therapies usually display good initial response, however, they often have only a modest effect on overall survival. In contrast, cytotoxic chemotherapy which is mostly based on DNA-damaging agents, often yields long-term remission and in some cancers even cure of the disease. Regrettably, many patients treated with cytotoxic chemotherapy eventually display acquired

drug-resistance, relapse and perish from the disease. Therefore, research efforts aiming to understand the mechanism involved in drug resistance, refractory disease and sensitization against chemotherapeutic agents are of great importance. A second type of CRISPR-based screening focus on tackling this problem is called chemogenomic profiling or drug-based screening. These screens are particularly useful in uncovering oncogenic nodes responsible for drug resistance and identifying novel targets which sensitize cells against the tested chemotherapeutic agent, these latter are called sensitizer hits and are the basis of what it is called now synthetic lethal-based CRISPR-Cas9 screening. The concept of synthetic lethality goes back to experiments with Drosophila melanogaster conducted by Calvin Bridges in the early 20th century [486]. In his crossing experiments Bridges observed that combined inheritance of specific mutant gene pairs was lethal, whereas single inheritance of either mutant gene result in viable normal progeny [487]. The termed was coined by Theodore Dobzhansky two decades later [488] when he observed the same phenomenon in Drosophila pseudoobscura [489].
Recent work using CRISPR-based synthetic lethal screening have nicely demonstrated the power of these unbiased systemic approaches in identifying novel vulnerabilities to a broad spectrum of compounds such as PARP [490-493] and ATR inhibitors [494-496], ICL-inducing agents [497-499], DNA alkylators [461], UV [380, 500], IR, and doxorubicin [501, 502]. Among these research efforts, the seminal work by Olivieri et al. [380], from the Durocher group in Toronto, have demonstrated the power of charting the DNA damage response against dozens of genotoxic agents and have contribute with the elaboration of chemogenomic databases and a genetic map of the DDR in human cells.

Taking advantage of the versatility of CRISPR-Cas systems at targeting the genome and guided by protein engineering methods such as phage-assisted continuous evolution (PACE), several

modified variants of the Cas nuclease have been added to the CRISPR-toolbox. From removal of the nuclease activity(dCas9), expansion of PAM recognition, to transcription-modifying domains of Cas9, has led to the development of CRISPR-mediated transcriptional inhibition (CRISPRi) or activation (CRISPRa) [503-507], direct RNA editing [508, 509], and Cas9-mediated base editing [510-514]. For instance, in a good illustration of the power of base editing screening, Cuella-Martin et al. [515], showed how these screens enable large-scale characterization of mutations in genes that are usually essential for cell viability. Many DDR genes display this behaviour, and when using conventional dropout screens, the characterization of their function is compromised, and they do require point-mutation analysis for fully dissecting their biological role. Additionally, fluorescent activated cell sorting (FACS) and flow cytometry have been coupled with CRISPR-Cas9 screening to execute different sort of phenotypic screens [473]. FACS-bases genetic screening relies on the use of genetic reporters and/or fluorophore-conjugated antibodies. These types of screens are particularly useful when working with primary cells or cells that are resilient to genomic perturbation, and when intermediate phenotypes rather than endpoints need to be interrogated. FACS-based screening has been proven useful assessing cellular differentiation or immune cell maturation, as well as uncovering novel regulators of WNT and mTOR signaling [473, 516-518].

Finally, recent reports have pointed out that genetic interactions screens in patient-derived organoids, co-culture or 3-D systems, better recapitulate in vivo phenotypes in comparison to regularly used 2-D culture systems [487, 519-521].

1.7.1.1 The Toronto KnockOut library

The Toronto KnockOut (TKO) genome-wide library v1 was designed and developed by the laboratory of Dr. Jason Moffat at the University of Toronto [467]. This library was optimized using previous experimental approaches used in first-generation CRISPR screens [461, 472] and

focussed on high-performing guide RNAs targeting essentials and non-essential genes. Furthermore, and to minimize potential off-target effects they excluded candidate sgRNAs with more than one genomic off-target site within two mismatches of the guide-plus-PAM sequence. This library targeted 17,232 genes with a total of six sgRNAs per gene. In addition, it also includes control sgRNAs targeting LacZ, EGFP, luciferase, and two sets of sgRNAs targeting random loci on Chr10:584(highly specific with no predicted off-target activity) and 796 promiscuous sgRNAs with 20 or more binding sites across the genome. Altogether, the TKO v1 Moffat library contains 91,320 sequences and for this reason is called the 90k genome-wide library [467].

1.7.1.2 MAGeCK and DrugZ

CRISPR-based genome-wide screening showed superior advantages over old technologies such as RNA interference, still, the NGS data generated posed technical challenges for its computational analysis. Some of the difficulties are the limited number of replicates used in these experiments which requires a proper statistical model to estimate the variance of the read counts and assess the statistical significance of comparisons between treatment and control samples [522]. Another challenge is that the observed sgRNA abundance displays great variability in both depletion and enrichment experiments and it is over-dispersed. Finally, another difficulty observed in these analyses is that different sgRNAs targeting the same gene might have different specificities and KO efficiencies. To tackle these computational challenges observed in CRISPR-based data, the laboratory of Dr. Shirley Liu at Harvard developed a statistical approach called Model-based Analysis of Genome-wide CRISPR/Cas9 Knockout (MAGeCK) which allow researchers to identify essential genes or pathways. MAGeCK outperforms existing computational methods with respect of FDRs and its high sensitivity and

it displayes great statistical power across different sequencing depths and number of sgRNAs used [522].

Analysis of CRISPR-based chemogenomic data can be challenging. Positive selection- or enrichment screens which identify genes that confer resistance to cellular perturbation usually display a high signal-to-noise ratio because only resistant-related mutant survive. In the other hand, negative selection- or dropout screens requires a minimum of 10-14 doubling times to allow sensitive detection of genes whose perturbation results in cellular fitness defects. DrugZ is an algorithm designed for the analysis of CRISPR-mediated chemogenetic interactions and it was developed by the laboratory of Dr. Traver Hart [523]. As proof of principle of the statistical robustness of this method, they used the algorithm to identify genes that drive normal cellular resistance to PARP inhibition and found synthetic lethal interactions between PARP inhibition and known and novel DNA repair factors. Their study showed greater sensivity of DrugZ over other approaches such as MAGeCK [522], edgeR [524], and equivalent results as the ones obtained using RIGER [525].

1.7.2 Biotinylation-based proximity labelling proteomics and TurboID

Enzyme-mediated proximity labelling is an alternative method to immunoprecipitation and biochemical fractionation for proteomic assessment of cellular complexes and protein-protein interaction networks. This method is based on the use of a promiscuous labeling enzyme which is fused genetically to a specific protein of interest. The addition of exogenous substrates such as biotin, triggers the covalent tagging of endogenous proteins in the vicinity of the promiscuous protein within a few nanometers distance range. Biotinylated proteins are later collected using streptavidin-coated beads and identify by mass spectrometry (MS). The two most commonly used enzymes used for proximity labelling are APEX2 [526, 527] and BioID [528, 529], a promiscuous mutant of *Escherichia coli* biotin ligase. While APEX2 has some

advantages such its tagging speed- protein tagging is observed within a 1 minute- and its versatility, as it does not only tag proteins but also RNAs and can generate contrast for electron microscopy. Nevertheless, APEX2 tagging requires the use of H_2O_2 which is toxic for living cells. In the other hand, BioID tagging is simple and non-toxic, and for these reasons has been extensively used in the study of protein-protein interactions in mammalian cells, plants protoplasts, parasites, mouse, and yeast [530]. Still, a major disadvantage of BioID labeling is its slow kinetics which requires biotin incubation times of around 24 h to obtain sufficient material and suitable sensitivity during the proteomic assessment [530]. This dynamic limitation in labeling limits its application to study process that occur on the range of minutes or few hours, such as DNA repair responses. To tackle these technical limitations and through the use of directed evolution of E. coli ligase, the laboratory of Dr. Alice Ting in Harvard has developed two new promiscuous ligase mutants: TurboID and miniturboID [530]. These improved ligases combine the catalytic efficiency of APEX2 and the simplicity and non-toxicity of BioID, and displayed greater efficiency than BioID, enabling proximity labeling within 10 minutes of activity. Although TurboID is the most active between these two new ligases, if optimization of labeling time is required, miniturboID is preferentially recommended. While miniturboID is less active than TurboID, it displays less background activity in the biotin-lacking conditions, and it is also smaller (28 vs 35kDa) which is preferred to avoid interference in biological function and cellular trafficking in the tested fusion protein [530].

1.7.3 Open-reading frames (ORFs)

Biomedical research has been reported to be focused on a relatively small fraction of human genes, recent reports indicated that most of research has been concentrated on approximately only 2,000 genes of the nearly 20,000 human protein-coding genes. The reasons behind this

genetic-focus bias remain unknown but researchers suggest that social forces, gene and protein inequality annotation and funding mechanisms reinforce this bias of present-day science towards past-research topics [531, 532]. The completion of the human genome project two decades ago was expected to prompt an expansion of the scope of scientific research beyond the small fraction of genes studies since the 1980s, however and besides the increasing availability of novel technologies this problem has persisted. As consequence of this, around 18,000 genes remain poorly characterized. Research efforts combining genomic, transcriptomic, and proteomic approaches have been the driving forces behind gene and protein discovery. Open reading frames (ORFs) are defined as stretches of DNA sequences harboring a start and stop codon. A seminal study [533] back in 2011 generated the most extensive and updated collection (hORFeome V8.1) of human open-reading frames encompassing 16,100 ORFs encoded in a Gateway vector system, this research effort was aimed to provide the necessary tools to the research community to conduct functional characterizations of the human genome. Furthermore, recent techniques such as ribosome profiling have revealed that translation if widespread at many annotated long non-coding RNA (lncRNA) transcripts and predicted untranslated regions of mRNAs [534-536]. This data suggests that the human genome harbours many more protein-coding regions than initially predicted. As a result of this consortium-driven study 7,264 novel Ribo-Seq ORFS have been catalogued and incorporated into references databases for further characterization [537]. In order to be classified as a canonical protein-coding region, a novel protein-coding gene should comply with certain requirements: a reliable transcript, intact ORF, indications of evolutionary conservation at the coding region, and evidence of protein levels [538]. Therefore, research efforts focused on the systemic characterization of these old and recently uncovered ORFs

and their potential significance as drivers of human disease and development, are of great importance and required the full attention of the scientific community.

1.8 Summary and Rationale

Despite the remarkable progress achieved in our understanding of the HR and ICL/FA DNA repair pathways, further research is needed to uncover the molecular mechanisms regulating these biological processes. For instance, the use of novel approaches such as functional genomics and proximity-labelling proteomics have allowed researchers recently to uncover several novel factors involved in ICL/FA repair and other DNA repair pathways, highlighting their complexity and still poorly understood biology. In this thesis I have used genome-wide CRISPR-based screens and focused my attention on the characterization of novel factors involved in ICL-repair. In chapter II, I described work regarding the characterization of C1orf112 as novel factor involved in the response to ICL-inducing agents. C1orf112 acts in the HR-mediated phase of the FA pathway and is required for the resolution of ICL-induced RAD51 foci. Furthermore, we mapped the proximal interactome of C1orf112 using miniturboID and identified the AAA+ ATPase FIGNL1 as a constitutive interactor. Although our knowledge regarding the mediators of RAD51 loading and the positive regulation of this critical step in HR is considerable, the knowledge of the factors involved in the anti-recombinogenic role is scarce. Altogether this chapter describes a novel function of C1orf112 in HR/ICL repair by promoting the unloading of RAD51, highlighting the contribution of this work in further understanding the fine-tuning regulation of HR upon ICL-induced DNA damage. In chapter III, I described my work using targeted CRISPR-based screening focusing in poorly characterized open-reading frames. This systemic approach allowed me to identify C1orf27 as novel factor involved in the modulation of ICL repair. Secondary validation and

chemogenomic profiling delineated C1orf27 as potential regulator of the recently uncovered ubiquitin-like UFM1 pathway during the ICL repair response. Proteomic analysis interrogating the proximal interactome of C1orf27 using miniturboID technology identified UFSP2 as strong constitutive interacting partner of C1orf27. Furthermore, we extended this proteomic analysis and mapped the proximal interactome of this peptidase and the E3 ligase UFL1, allowing us to better defyne the protein network involved in UFMylation under genotoxic conditions such as ICL-induced DNA damage. Our integrative proteomice analysis of C1orf27, UFSP2 and UFL1 allowed us to identify two constitutive interacting partners of these 3 baits: DDRGK1, which was previously identified as UFM1-related adapter protein, and TMEM263(C12orf23) a novel uncharacterized factor likely involved in UFMylation. Altogether, this thesis showed how our CRISPR-based screening approach allowed us to identify and characterized two novel factors involved in ICL-repair and our work here described contributes to our better understanding of this DNA repair response.

Chapter II: C1orf112/FIRRM is a novel regulator of interstrand crosslink repair that decreases FIGNL1-RAD51 interaction.

C1orf112/FIRRM is a novel regulator of interstrand crosslink repair that decreases FIGNL1-RAD51 interaction.

Edgar Pinedo-Carpio[1,2,#], Julien Dessapt[3,4,#], Romain Villot[5,6], Lauralicia Sacre[7], Abba Malina[1,8], Jonathan Boulais[9], Elise G. Lavoie[3,4], Vincent Luo[1,10], Anna-Maria Lazaratos[1,3,9,10], Jean-François Côté[3,9], Frédérick A. Mallette[5,6,11], Alba Guarné[7], Amelie Fradet-Turcotte[3,4,§], and Alexandre Orthwein[1,2,8,10,§]

[1] Lady Davis Institute for Medical Research, Segal Cancer Centre, Jewish General Hospital, 3755 Chemin de la Côte-Sainte-Catherine, Montréal, QC H3T 1E2, Canada;

[2] Division of Experimental Medicine, McGill University, Montréal, QC H4A 3J1, Canada;

[3] CHU de Québec Research Center-Université Laval (L'Hôtel-Dieu de Québec), Cancer Research Center, Québec, QC G1R 3S3, Canada;

[4]Department of Molecular Biology, Medical Biochemistry and Pathology, Université Laval, Québec, QC G1V 0A6 Canada;

[5]Departement de Médecine, Université de Montréal, Montréal, QC H3C 3J7 Canada;

[6]Maisonneuve-Rosemont Hospital Research Centre, Montréal, QC H1T 2M4 Canada;

[7]Department of Biochemistry, McGill University, Montréal, QC H3G 0B1 Canada;

[8] Gerald Bronfman Department of Oncology, McGill University, Montréal, QC H4A 3T2, Canada;

[9]Montreal Clinical Research Institute (IRCM), Montreal, QC, H2W 1R7, Canada;

[10]Department of Microbiology and Immunology, McGill University, Montréal, QC H3A 2B4 Canada;

[11]Departement de Médecine, Université de Montréal, Montréal, QC H3C 3J7 Canada.

[#]co-first authors

[§]co-corresponding authors

Running title: C1orf112/FIRRM promotes interstrand crosslink DNA repair.

Address correspondence to:

Alexandre Orthwein, M.Sc., Ph.D.

Lady Davis Institute, Segal Cancer Centre

Jewish General Hospital

Montreal, QC, H3T 1E2 Canada

e-mail: alexandre.orthwein@mcgill.ca

Amelie Fradet-Turcotte, Ph.D.

Oncology Division, CHU de Québec Research Center-Université Laval

Cancer Research Center - Université Laval

Quebec, QC, G1R 2J6 Canada

e-mail: Amelie.Fradet-Turcotte@crchudequebec.ulaval.ca

2.1 Abstract

Interstrand DNA crosslinks (ICLs) represent complex lesions that block essential biological processes, including DNA replication, recombination, and transcription. Several pathways have been involved in ICL repair, in particular nucleotide excision repair (NER), translesion DNA synthesis (TLS), Fanconi anemia (FA), and homologous recombination (HR). Still, the extent of factors involved in the resolution of ICL-induced DNA double-strand breaks (DSBs) remains poorly defined. Using CRISPR-based genome-wide screening, we identified the poorly characterized C1orf112 (also known as Apolo1) as a novel sensitizer to the clinically relevant ICL-inducing agent mafosfamide. Consistently, we noted that low expression of C1orf112 correlates with increased sensitivity to a series of ICL agents and PARP inhibitors in a panel of cell lines. We showed that lack of C1orf112 does not impact the initial recruitment and ubiquitylation of FANCD2 at the ICL site but rather impairs the resolution of RAD51 from ICL-induced DSBs, thereby compromising homology-directed DNA repair pathways. Our proximal mapping of C1orf112 protein neighbours coupled to structure-function analysis revealed that C1orf112, through its WCF motif, forms a complex with the N-terminal domain of the AAA+ ATPase FIGNL1 and regulates the interaction of FIGNL1 with RAD51. Our work establishes the C1orf112-FIGNL1 complex as an integral part of the HR-mediated response to ICLs by regulating the unloading of RAD51 during ICL repair.

Keywords: DNA repair, interstrand crosslink, homologous recombination, DNA double-strand break, RAD51 unloading.

2.2 Introduction

Interstrand crosslinks (ICLs) are highly cytotoxic DNA lesions that produce physical obstacles for vital biological processes, including DNA replication, transcription, and recombination. ICLs can emerge from endogenous reactive aldehydes, but more often occur upon exposure to either naturally occurring compounds (e.g., mitomycin C), or chemically synthesized drugs, such as cisplatin or cyclophosphamide (reviewed in [1]). These ICL-inducing drugs are widely used as chemotherapeutic agents in the treatment of both solid tumours and blood cancers [2]. Aside from compromising essential biological processes, ICLs, if left unrepaired, result in a variety of genomic abnormalities, ranging from point mutations to chromosome breakage or mis-segregation, up to mitotic catastrophe (reviewed in [3]).

Each type of ICL-inducing agents leads to different types of intra- and interstrand cross-links that distort the double helix to different levels [1]. To detect, signal and repair these lesions, cells rely on a complex response which typically gets triggered when the replication machinery encounters the ICL, and involves the precise and coordinated effort of multiples pathways, including the Fanconi Anemia (FA), Nucleotide Excision Repair (NER), and the Homologous Recombination (HR) repair pathways, alongside the ATR checkpoint signaling pathways [1]. ICLs are initially recognized by the FANCM complex (FANCM, FAAP24, MHF1 and MHF2) that serves as a platform for the docking of seven additional FANC proteins (FANCA-C, FANCE-G, FANCL) as well as two additional associated proteins (FAAP20 and FAAP100) that altogether form the FA core complex. Together with FANCT (UBE2T), the E3-ubiquitin ligase FA core complex promotes the monoubiquitylation of the effector FANCI/FANCD2 (ID2) heterodimer, a critical step in the processing and subsequent repair of the ICLs. Once assembled and activated at the lesion, the ID2 heterodimer recruits structure-specific nucleases that promote ICL unhooking; and acts as a molecular hub for the recruitment of translesion synthesis (TLS) DNA polymerases which bypass the ICL adduct, and

the subsequent recruitment of HR factors involved in the repair of the DNA double-strand breaks (DSBs) generated during this process [1]. The last few years witnessed the discovery of an important decision point during the detection and early processing of ICL, named the ICL repair pathway choice. This decision is made between replication-independent and -dependent pathways and appears to be dictated by the structure and the location of the ICL as well as the phase of the cell cycle in which it is detected [1]. Recent dissection of the replication-dependent ICL repair pathway has identified a series of novel players such as TRAIP [4, 5] , NEIL3 [6] , and SCAI-REV3 [7, 8] that act before the TLS and HR pathways, respectively.

Aside from a better understanding of ICL repair pathway choice, several reports have highlighted the complexity of the final stages of ICL repair, such as the resolution of RAD51-mediated strand invasion. For instance, the AAA^+ ATPase FIGNL1 has been shown to bind RAD51 and promote its unloading from DNA [9], a function that is limited by the SWSAP1-SWS1-SPIDR complex [9, 10] . More recently, the helicase HELQ [11] and the HROB–MCM8–MCM9 [12-14] complex have been shown to contribute to parallel pathways that promote DNA repair synthesis following D-loop formation. However, the spatiotemporal regulation of these functions is still unknown.

Although the first model of ICL repair was drawn in the early 2000's, the extent of factors involved in the regulation of this repair pathway remains largely unclear. Here, our CRISPR-based genomic screens identified the poorly characterized C1orf112 as a novel player in the response to ICLs. In-depth characterization delineated its contribution to the regulation of the HR pathway during the ICL response. Proximal mapping of C1orf112 proximity interactors coupled to structure-function validation identified the AAA+ ATPase FIGNL1 as a constitutive partner in the unloading of RAD51 at ICL-induced DSBs. Our model defines the C1orf112-FIGNL1 complex as an integral component of the resolution of ICL-induced DSBs by promoting the dissociation of RAD51.

2.3 Results

2.3.1 CRISPR screening identifies C1orf112 as a modulator of ICL repair in BL cells.

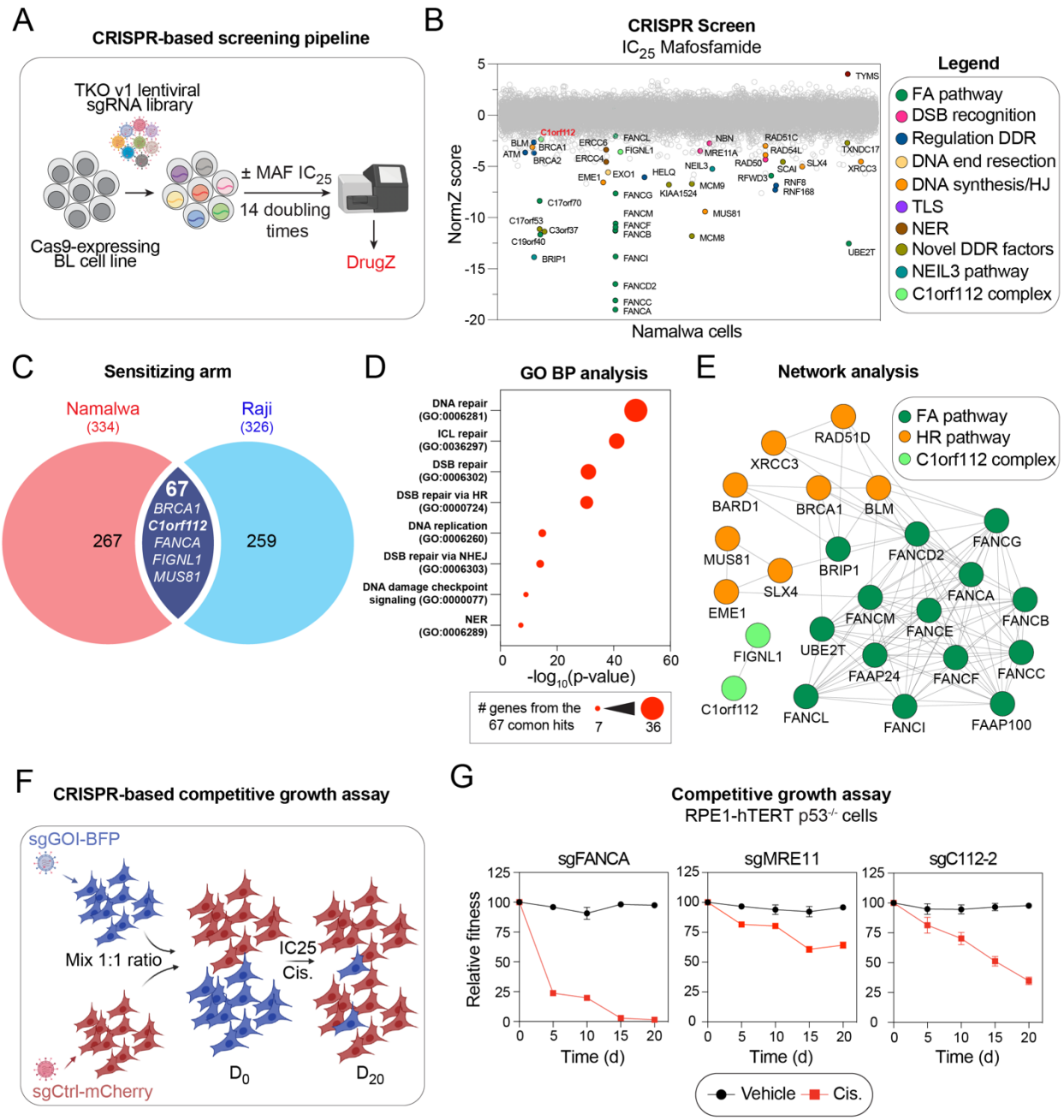
To better understand the factors influencing ICL repair, we undertook CRISPR/Cas9 dropout screens in two human Burkitt's lymphoma (BL) cell lines, Namalwa and Raji, using the metabolized version of the ICL agent, cyclophosphamide, as a selective drug (Mafosfamide (MAF)). First, we generated stable Namalwa and Raji cell lines expressing Cas9 using lentiviral transduction and confirmed genome editing efficiency by targeting the FAM83G gene as previously described [15]. Next, CRISPR-based genome-wide screening was initiated by transducing the TKO v1 sgRNA library in both human BL Cas9-cell lines [16, 17] and transduced cells were amplified under puromycin (2 μg/ml) selection for 7 days (**Fig. 2.1A**). Both Namalwa and Raji transduced cell lines were subsequently treated with either preoptimized doses of MAF (IC25) (1.30 μM and 1.57 μM, respectively) or with DMSO as a vehicle for 14 doubling time (14 days for both cell lines) before being processed for next-generation sequencing (NGS). The DrugZ algorithm was used to determine the relative abundance of each sgRNA and identify genes whose knockout sensitizes cells to MAF (NormZ score < -2.5, $p < 0.005$ [18]) (**Fig. 2.1B, 2.S1A and Table 2.S1**). In both screens, pathway enrichment analysis identified ICL repair and HR as two biological pathways statistically enriched among our identified genes of interest (**Fig. 2.S1B, data not shown**). As expected, most factors of the Fanconi Anemia core complex and factors implicated in HR repair emerged as top sensitizers in both cell lines (**Fig. 2.1B, 2.S1A and Table 2.S1**), validating our CRISPR-based screening approach to identify new genes influencing ICL repair. Of note, the recently characterized *FIGNL1* [9, 19]*, HROB-MCM8-MCM9* [12-14] *and SCAI* [7, 8] scored significantly on both of our screens (**Fig. 2.1B, 2.S1A, Table 2.S1)**.

We identified 67 target genes that function as sensitizers in both BL cell lines (**Fig. 2.1C, Table 2.S1**). Gene ontology analysis of these hits revealed enrichment for specific biological

processes related to DNA repair, DNA replication and DNA damage checkpoint (**Fig. 2.1 C-D, Table 2.S2**) and the network constructed with these common sensitizers shows high connectivity between genes of the FA and HR pathway (**Fig. 2.1E and 2.S1C**). According to this network, we found that C1orf112 behaves similarly to factors of the cellular response to ICL agent in BL cell lines. Previous reports identified C1orf112(currently recognized as FIRRM: FIGNL1 interacting regulator of recombination and mitosis), as a modulator of chromosome segregation through the regulation of PLK1 activity [20]. As no other genes associated with mitosis progression were enriched in our screens, we reasoned that a different function of C1orf112 may be important for the cellular response to ICL.

To validate the C1orf112 contribution in the response to ICL agents, we targeted it using a single-guide RNA (sgRNA) in a twenty-day CRISPR-based growth competition assay [21] that was performed in hTERT immortalized non-transformed human retinal pigmented epithelial cell line RPE-1 (henceforth termed RPE-hTERT $p53^{-/-}$ cells) (**Fig. 2.1F**). Briefly, stable cell lines expressing a sgRNA of interest along with a BFP-reporter or a control sgRNA against LacZ along with a mCherry reporter were established. At D_0, the cell line expressing the sgGOI-BFP was mixed to a 1:1 ratio with the sgCtrl-mCherry cell line and treated for 20 days (D_{20}) with an IC25 of the ICL-inducing agent cisplatin (2.4 nM) before BFP and mCherry measurement at different time points. For comparison, we also tested sgRNAs that target representative genes of the FA (sgFANCA) and the HR pathways (sgMRE11). In this assay, C1orf112 knockout hypersensitizes RPE-hTERT $p53^{-/-}$ cells to cisplatin, demonstrating that the phenotype associated with C1orf112 depletion is neither cell line nor ICL agent specific (**Fig. 2.1F and 2.S1E**). The effect of C1orf112 depletion on the cellular fitness of cisplatin-treated cells is intermediate of a core FA protein and MRE11 (**Fig. 2.1F**), suggesting that C1orf112 is important for cellular survival to ICL-inducing agent but may not be a core FA gene. Together, this work demonstrates that our CRISPR-based screening approach is

effective for identifying genes that impact the response to ICL agents, including C1orf112 as a new modulator of this response.



Pinedo-Carpio, Dessapt *et al.* Figure 2.1

Figure 2.1 CRISPR-based genome-wide screening identifies C1orf112 as a novel modulator of mafosfamide sensitivity.

(A) Schematic representation of the CRISPR-based screening pipeline used in Burkitt lymphoma cells and the screen analysis using the DrugZ algorithm.

(B) Horizontal scatter plot of DrugZ-generated ranking of the Namalwa mafosfamide CRISPR screen. NormZ values are plotted on the Y-axis, and gene names are plotted on the X-axis. FA: Fanconi Anemia, DSB: Double-Strand Break, DDR: DNA Damage Response, HJ: Holliday Junction, TLS: Translesion Synthesis, NER: Nucleotide Excision Repair.

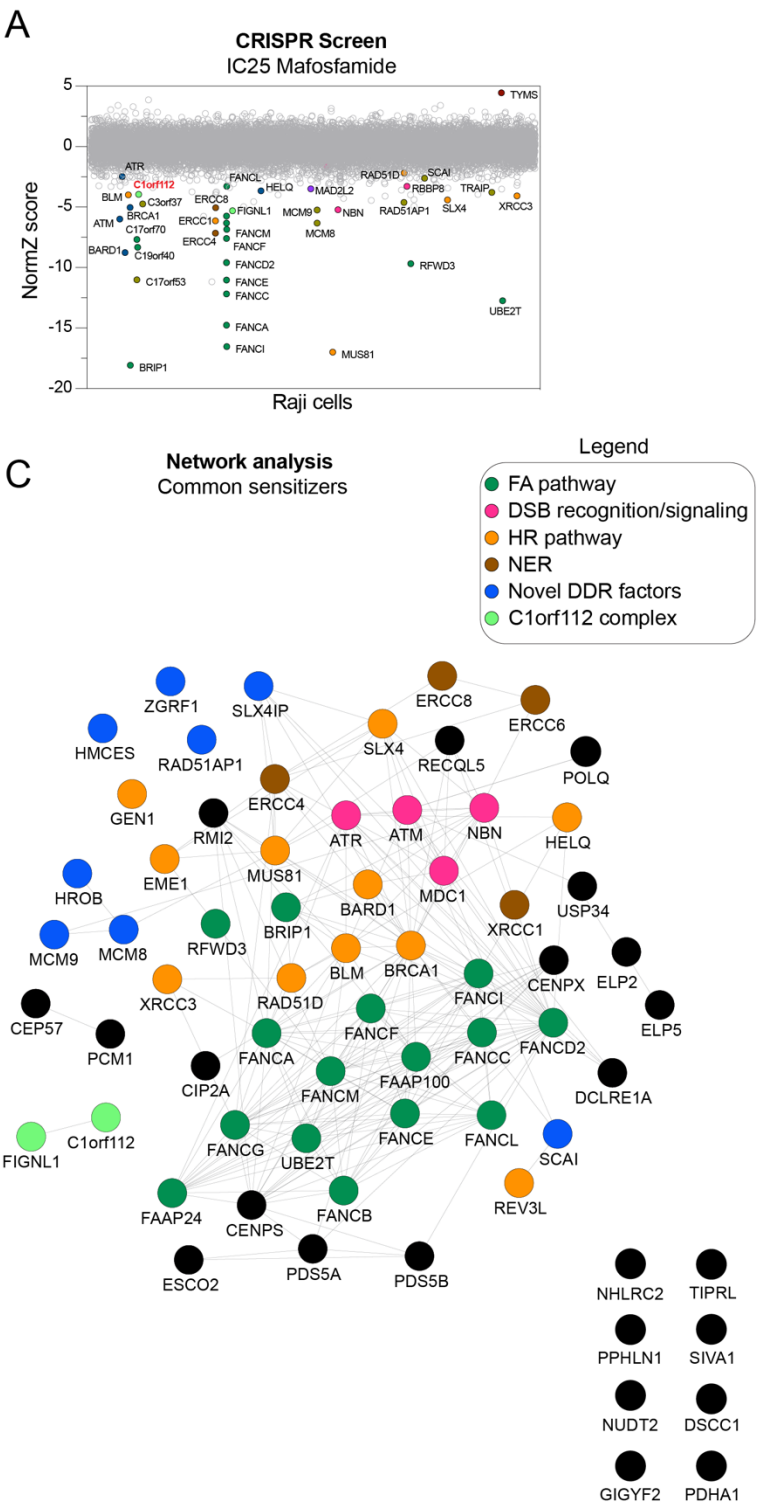
(C) Venn diagram displaying common sensitizing genes from Namalwa and Raji screens (for genes with NormZ ≤ 2)

(D) Gene ontology biological processes (GO BP) diagram obtained from common sensitizing genes from Namalwa and Raji screens. GO term enrichments are ranked by statistical significance (p-value). The size of the circle indicates the number of the 67 common gene hits within a pathway.

(E) Network analysis displaying protein physical interactions using Cytoscape and the GeneMANIA package. The C1orf112-FIGNL1 complex is represented in the vicinity of FA and HR repair networks.

(F) Schematic representing the pipeline used in the two-color competition assay. RPE1-hTERT $p53^{-/-}$ cells were transduced with a sgRNA targeting either the gene of interest (GOI) coupled with Blue Fluorescent Protein (BFP) or LacZ gene coupled with mCherry. BFP- and mCherry-expressing cells were mixed at a 1:1 ratio at day 0 (D_0) and treated with IC25 cisplatin (Cis.). BFP-positive over mCherry-positive cells ratio was followed over 20 days (D_{20}).

(G) Competitive growth results obtained in RPE1-hTERT $p53^{-/-}$ cells targeted with sgRNA against FANCA, MRE11 or C1orf112 (C112). Cells were either treated with DMSO as a vehicle or cisplatin at its IC25 (2.4 μM). Data are represented as the mean ± SEM (n = 3 technical replicates).



Pinedo Carpio, Dessapt *et al.* Figure 2.S1

Figure 2.S1 Additional analysis of CRISPR screen performed in Raji and Namalwa cells, related to Fig. 2.1

(A) Horizontal scatter plot of DrugZ-generated ranking of the Raji mafosfamide CRISPR screen. NormZ values are plotted on the Y-axis, and gene names are plotted on the X-axis.

(B) Gene Set Enrichment Analysis (GSEA) analysis of the score obtained in the Namalwa and Raji screens for ICL repair, and recombinational repair.

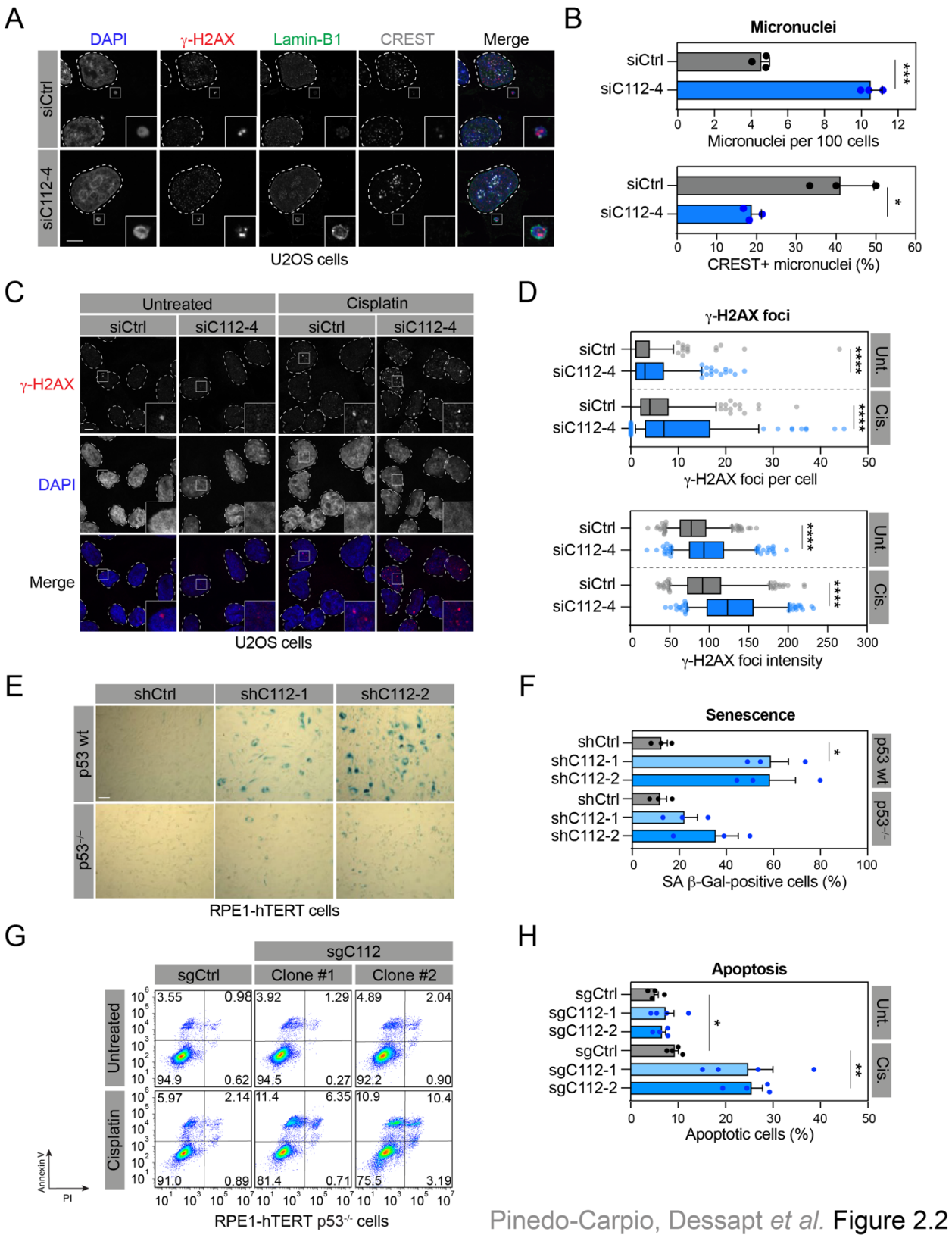
(C) Network analysis displaying protein physical interactions for sensitizer genes common to Namalwa and Raji CRISPR screens using Cytoscape and the GeneMANIA package.

2.3.2 C1orf112 depletion induces genomic instability and cellular senescence in a p53-dependent manner.

In a first attempt to define the role of C1orf112 on genomic stability, we depleted it by using small-interfering RNA (siRNA) in Human Bone Osteosarcoma Epithelial Cells (U2OS) cells (**Fig 2.S2A**). At 48 hrs post-transfection, C1orf112-depleted U2OS cells accumulated micronuclei (MNi). MNi formation is triggered by unresolved genomic instabilities, such as DSBs and lagging chromosomes [22]. In C1orf112-depleted cells, we observed that most MNi show negative staining for centromeres and positive staining for the DSB marker γ-H2AX (**Fig. 2.2 A-B**), suggesting that they arise from improperly segregated acentric chromosome fragments induced by DSBs [22]. 53BP1 nuclear bodies (NBs) are another marker of genomic instability, representing subnuclear structures assembled around DNA lesions caused by replication stress and transmitted during mitosis to the daughter cells [23]. Interestingly, C1orf112-depleted cells exhibit a 2-fold increase in the number of 53BP1-NBs in the G1 phase of the cell cycle (**Fig. 2S2 B-C**) suggesting that C1orf112 plays a role in preventing replication of stress-induced DNA breaks in mammalian cells. To further explore the impact of C1orf112 on genomic stability, we quantified the number and the intensity of γ-H2AX foci that accumulate in interphase of C1orf112-U2OS depleted cells. We found that both the number and the intensity of γ-H2AX were remarkably increased in C1orf112-depleted cells treated with 1 μM of cisplatin for 3 hours compared to the control (cells treated with siCtrl) (**Fig. 2.2 C-D**). Interestingly, depletion of C1orf112 is sufficient to increase the number and the intensity of γ-H2AX in untreated cells, indicative of a contribution of C1orf112 to protect cells from endogenous DNA damage (**Fig. 2.2 C-D**).

In mammalian cells, the presence of DNA damage activates checkpoints that promote cell cycle arrest, senescence or ultimately apoptosis in a p53-dependent manner [24-27]. Consistent with our previous observations, that C1orf112 depletion results in the accumulation of DNA breaks, we

noticed that its depletion by two distinct small-hairpin RNAs (shRNAs) is sufficient to induce senescence in two p53 WT cell lines, RPE1 hTERT and IMR90 (**Fig. 2.2 E-F and 2.S2 D-F**). This phenotype was greatly reduced in RPE1 hTERT cells where TP53 was inactivated by CRISPR technology. In fact, all our attempts to generate p53 WT C1orf112 knockout cells line were unsuccessful. In contrast, we were able to isolate two C1orf112$^{-/-}$ clones in RPE1 hTERT p53$^{-/-}$ that we validated by immunoblotting analysis (**Fig. 2.S2I**). In this context, increased levels of apoptosis detected in C1orf112$^{-/-}$ cells by Annexin V/propidium iodide staining showed that both clones are more prone to cell death upon cisplatin treatment (**Fig. 2.2 G, H**), confirming the protective role of C1orf112 against cell death following ICL induction.



Pinedo-Carpio, Dessapt *et al.* Figure 2.2

Figure 2.2 Depletion of C1orf112 lead to genomic instability and senescence-induced cell death

(A) Representative images of U2OS cells depleted or not for C1orf112 and processed for γ-H2AX (red), Lamin-B1 (green) and centromeres (CREST) (grey) immunofluorescence. Nuclei were counterstained with DAPI. Scale bar = 5 μm.

(B) Quantification of micronuclei Lamin-B1-positive (upper panel) and CREST-positive (lower panel) in cells treated as in (A). Data are represented as the mean ± SD (n = 3 independent experiments). A minimum of 100 cells were analyzed per condition per experiment. Data were analyzed with an unpaired t-test with Welsh's correction.

(C) Representative images of cells depleted or not for C1orf112 and exposed to 1 μM cisplatin or DMSO as a vehicle for 3 hrs. Cells were processed for γ-H2AX (red) immunofluorescence and counterstained with DAPI. Scale bar = 5 μm.

(D) Quantification of γ-H2AX foci per cell (top) and γ-H2AX foci intensity (bottom) in cells treated as in (C). Data are represented as the mean ± SD (n = 3 independent experiments). A minimum of 100 cells or foci were analyzed per condition per experiment. Data were analyzed with an unpaired t-test with Welsh's correction.

(E) Representative scatter plot of apoptosis analysis upon treatment with cisplatin in RPE1-hTERT $p53^{-/-}$ cells depleted or not for C1orf112 using shRNA. Apoptosis was induced with pulse treatment of 4 μM cisplatin and compared to vehicle-treated cells (DMSO). Annexin-V/PI staining was conducted 48 hrs post cisplatin treatment and reported as PI content versus Annexin-V intensity in scatter plots.

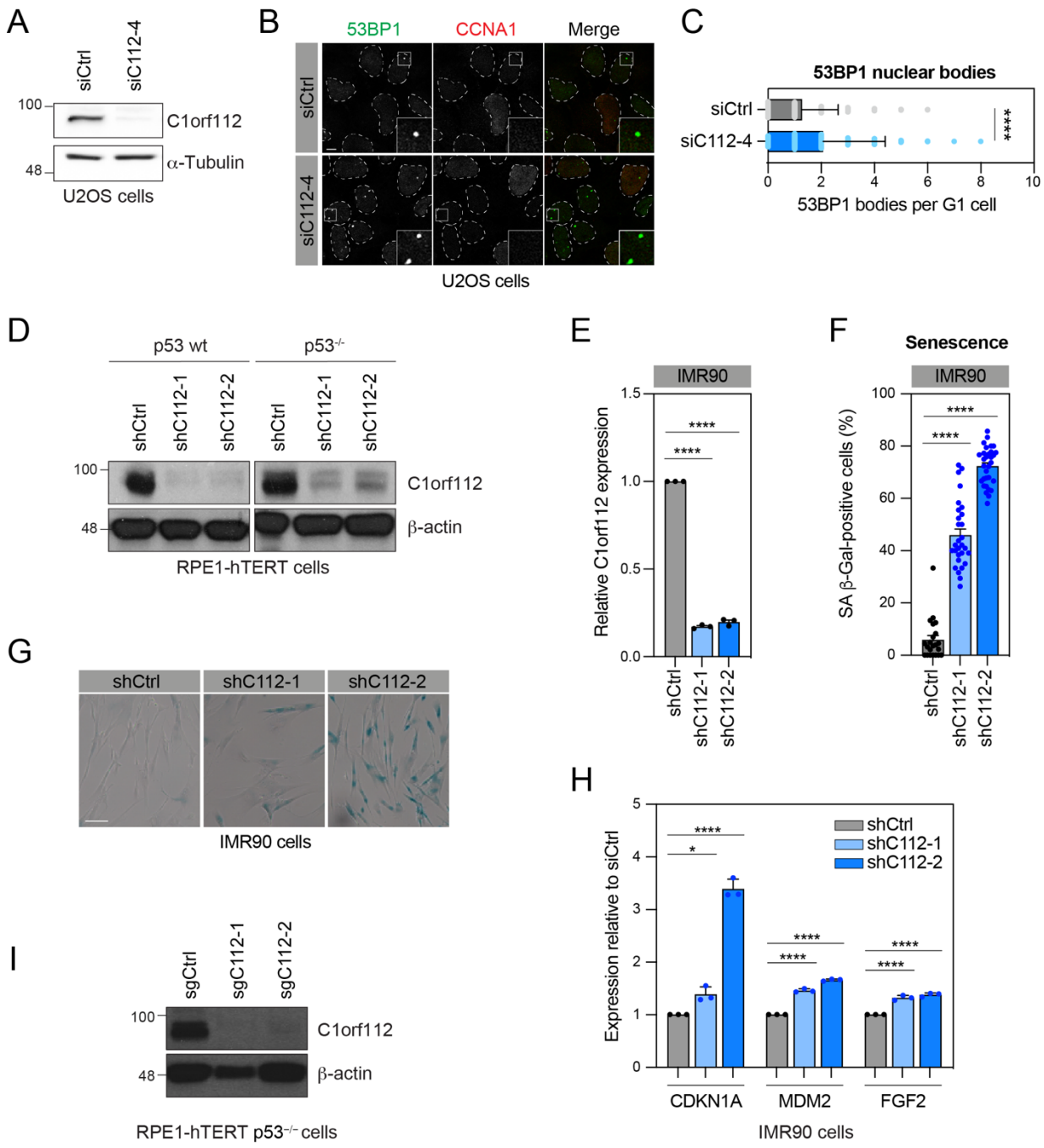
(F) Quantification of apoptotic RPE1-hTERT $p53^{-/-}$ cells depleted or not for C1orf112 and treated or not with cisplatin. Data are represented as the mean ± SEM (n = 4, 30,000 cells measured per

experiment in each condition). Data were analyzed using a one-way Welch's ANOVA test and Dunnett's multiple comparison tests.

(G) Representative images of RPE1-hTERT WT and $p53^{-/-}$ cells depleted or not for C1orf112 and stained with senescence-associated (SA) β-Galactosidase. Cells were grown for 24 hrs and stained for SA β-galactosidase. Scale bar = 100 μm.

(H) Quantification of SA-β-gal positive cells as shown in (G). Data are represented as the mean ± SEM (n = 3 independent experiments). Data were analyzed using a one-way Welch's ANOVA test and Dunnett's multiple comparison tests.

*p<0.05, **p<0.01, ***p<0.001, ****p<0.0001



Pinedo Carpio, Dessapt *et al.* Figure 2.S2

Figure 2.S2. Validation of C1orf112 knockdowns and knockouts, 53BP1 nuclear bodies in analysis and additional senescence assay in IMR90 cells, related to Fig 2.2

(A) WCE of U2OS cells depleted or not for C1orf112 were analyzed by immunoblot with an anti-C1orf112 antibody. Anti-α-Tubulin was used as a loading control.

(B) Representative images of U2OS cells treated with a siC1orf112 or non-targeting siRNA for 48 hrs were processed for 53BP1 and CCNA1 (Cyclin A) immunofluorescence. Scale bar = 5 μm.

(C) Quantification of 53BP1 nuclear bodies per CCNA1-negative cell as shown in (B). Data are represented as the mean ± SD (n = 3 independent experiments. A minimum of 100 cells were analyzed per condition per experiment). Data were analyzed with an unpaired t-test with Welsh's correction.

(D) WCE of RPE1-hTERT WT or $p53^{-/-}$ cells depleted or not for C1orf112 with the indicated shRNA were analyzed by immunoblot with an anti-C1orf112 antibody. Anti-β-actin was used as a loading control.

(E) RT-qPCR for C1orf112 was performed on IMR90 cells. Expression was normalized against GADPH and reported as a percent relative to shCtrl. Data are represented as the mean ± SD (n = 3 independent experiments). Data were analyzed with an ordinary one-way ANOVA test with Dunnett's multiple comparison tests.

(F). Quantification of IMR90 cells depleted or not for C1orf112 and stained with SA β-galactosidase. Data are represented as the mean ± SEM (n = 3 independent experiments). Data were analyzed with an ordinary one-way ANOVA test with Dunnett's multiple comparison tests.

(G) Representative images of IMR90 cells depleted or not for C1orf112 and stained with SA β-galactosidase. Scale bar = 5 μm.

(H) RT-qPCR for CDKN2A (p21), MDM2 and FGF2 was performed on RPE1-hTERT cells. Expression was normalized against GADPH and reported as a percent relative to shCtrl. Data are

represented as the mean ± SD (n = 3 independent experiments). Data were analyzed with an ordinary one-way ANOVA test with Dunnett's multiple comparison tests.

(I) WCE of RPE1-hTERT $p53^{-/-}$ clonal cells depleted or not for C1orf112 with the indicated sgRNA were analyzed by immunoblot with an anti-C1orf112 antibody. Anti-β-actin was used as a loading control.

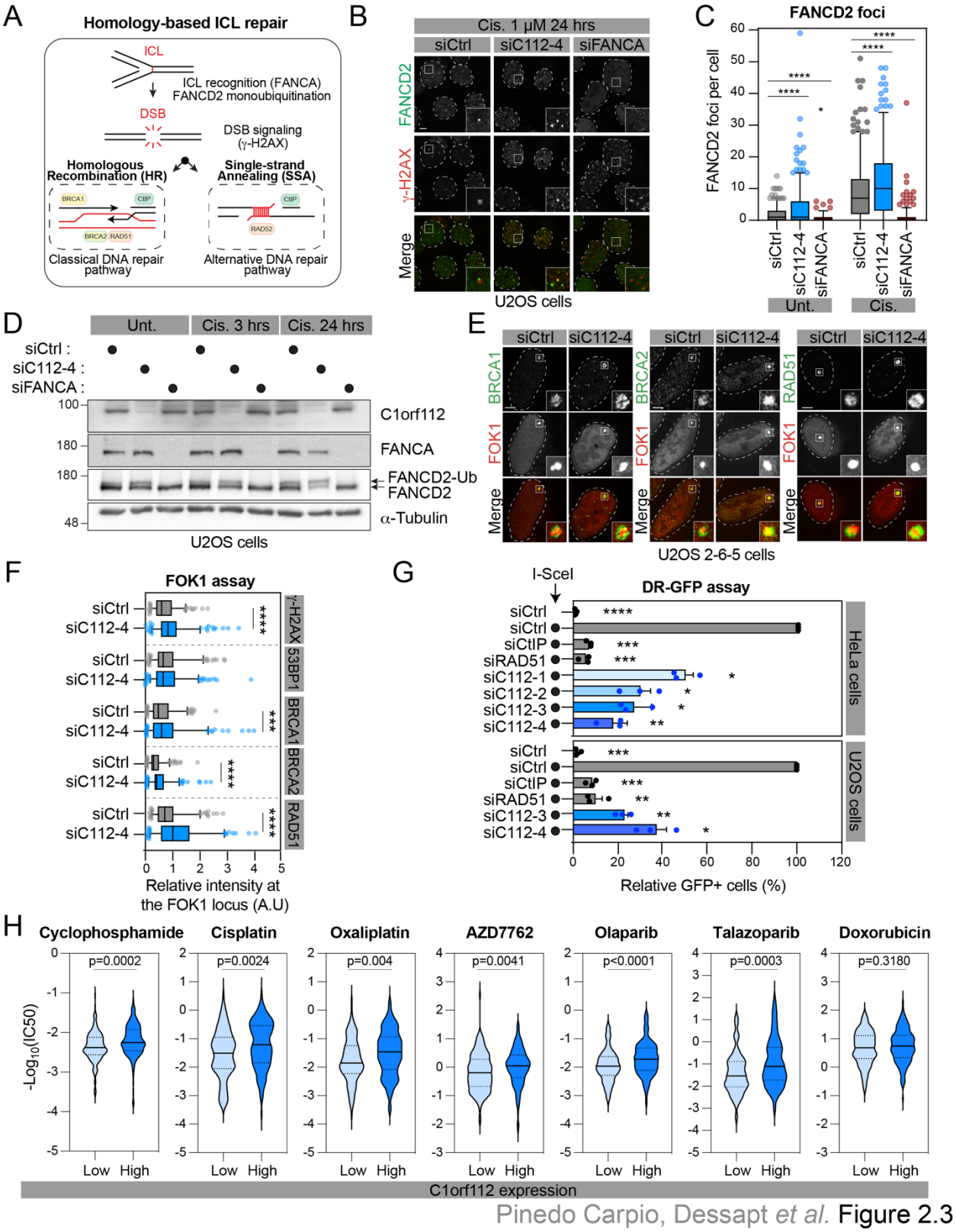
*p<0.05, ****p<0.0001

2.3.3 C1orf112 acts downstream of the FA pathway during ICL repair

The response to ICLs relies on the FA pathway to detect covalently linked DNA strands and promote the recruitment of specific nucleases that release the ICL from one of the two parental strands [28]. DSBs left behind by nucleolytic processing are then repaired by homology-directed recombination pathways such as HR and SSA (**Fig. 2.3A**). To delineate at which step(s) C1orf112 is participating in the ICL response, we first assessed its involvement in the recruitment and the activation of FANCD2 at ICLs. As expected, both FANCD2 accumulation and ubiquitylation at ICLs were abrogated upon depletion of FANCA in U2OS cells, serving as a control (**Fig. 2.3 B-D**). In contrast, C1orf112 depletion had a limited impact on the detection of FANCD2 at γ-H2AX foci (**Fig. 2.3 B-C**), and on its mono-ubiquitylation post-cisplatin treatment (**Fig. 2.3D**). These data suggest that C1orf112 plays a role downstream of the FA pathway during the response to ICLs. In fact, we noticed that FANCA-depleted cells were hypersensitive to both ICL agents MAF and cisplatin in our viability assay, unlike C1orf112-targeted cells, which displayed a much milder response to these drugs (**Fig 2.S3G**).

As for γ-H2AX foci (**Fig. 2.2 C-D**), we noted that more FANCD2 foci accumulate in C1orf112 depleted cells (**Fig. 2.3 B-C**). To further dissect the stage at which C1orf112 influences the ICL response, we focused our attention on key HR factors and their accumulation at DSBs in absence of C1orf112. We took advantage of a DSB reporter system in which the recruitment of these factors can be quantified at a single genomic locus. Briefly, DSBs are rapidly induced by the recruitment of the ER-mCherry-LacRnls-FOK1-DD fusion protein at a *LacO* array integrated on chromosome 1p3.6 in U2OS cells (U2OS 2-6-5 cell line) [29, 30]. In this assay, depletion of C1orf112 correlated with an exacerbated accumulation of several HR factors at FOK1-induced DSBs, including BRCA1, BRCA2 and RAD51 (**Fig. 2.3 E-F and 2.S3 A-B**). Of note, C1orf112 depletion did not affect the recruitment of the NHEJ factor 53BP1, suggesting that C1orf112 is primarily involved in HR-

mediated processes. To directly assess this question, we used well-established HeLa and U2OS DR-GFP reporter cell lines [31], as well as the U2OS SA-GFP reporter cell line [32] to measure DNA repair by HR and single-strand annealing (SSA), respectively (**Fig 2.3 G and Fig. 2.S3 C-E**). Depletion of C1orf112 with a series of siRNAs resulted in a marked decrease in both assays, particularly with siRNA-3 and -4, which results in efficient depletion of the protein as determined by immunoblotting analysis (**Fig 2.S3C**). Of note, C1orf112 depletion had a much milder impact in both the DR- and SSA-GFP assays, in comparison to CtIP or RAD51 depletion, suggestive of a regulatory rather than a core contribution of C1orf112 in homology-directed DNA repair pathways. Consistent with these observations, expression of C1orf112 correlated with the cellular response to ICL-inducing agents in the Genomics of Drug Sensitivity in Cancer Project dataset (CCLE repository-DepMap), where cells expressing higher levels of C1orf112 are more resistant to ICL-inducing agents (**Fig 2.3H**). Interestingly, high levels of C1orf112 also protect cells from other genotoxic agents that indirectly lead to the formation of DSBs: the Poly [ADP-ribose] polymerase 1 inhibitor (PARPi) Talazoparib and ATR inhibitor (AZD7762). In contrast, higher expression of C1orf112 is not an advantage in treatment that directly induces DSBs such as the topoisomerase II poisoning agent doxorubicin (**Fig 2.3H**). Chemogenomic profiling of CRISPR screens performed in RPE1 hTERT $p53^{-/-}$ cells with different genotoxic agents showed that C1orff112 depletion impairs predominantly cell survival (NormZ < -2.3) upon exposure to agents that induce replication roadblocks (e.g. cisplatin), base alkylation (MNNG), and oxidative damage ($KBrO_3$, H_2O_2) (**Fig 2.S3F, Table 2.S3**) [33]. Altogether, these results support a model where C1orf112 is specifically involved in the repair of DSBs indirectly generated by a subtype replication stress induced by replication fork roadblocks.



Pinedo Carpio, Dessapt *et al.* Figure 2.3

Figure 2.3. C1orf112 is not a core FA gene but is required for HR.

(A) Schematic of ICL repair pathways in mammalian cells. ICL: Interstrand Crosslink.

(B) Representative images of U2OS cells depleted or not for C1orf112 or FANCA. Cells were treated with the indicated siRNA for 48 hrs and treated or not with 1 μM cisplatin for 24 hrs before fixation. Cells were processed for γ-H2AX and FANCD2 immunofluorescence. Scale bar = 5 μm.

(C) Quantification of FANCD2 foci per cell in cells depleted or not for C1orf112 or FANCA. Data are represented as the mean ± SD (n = 3, 100 cells quantified per experiment in each condition). Data were analyzed using a one-way Welch's ANOVA test and Games-Howell's multiple comparison tests.

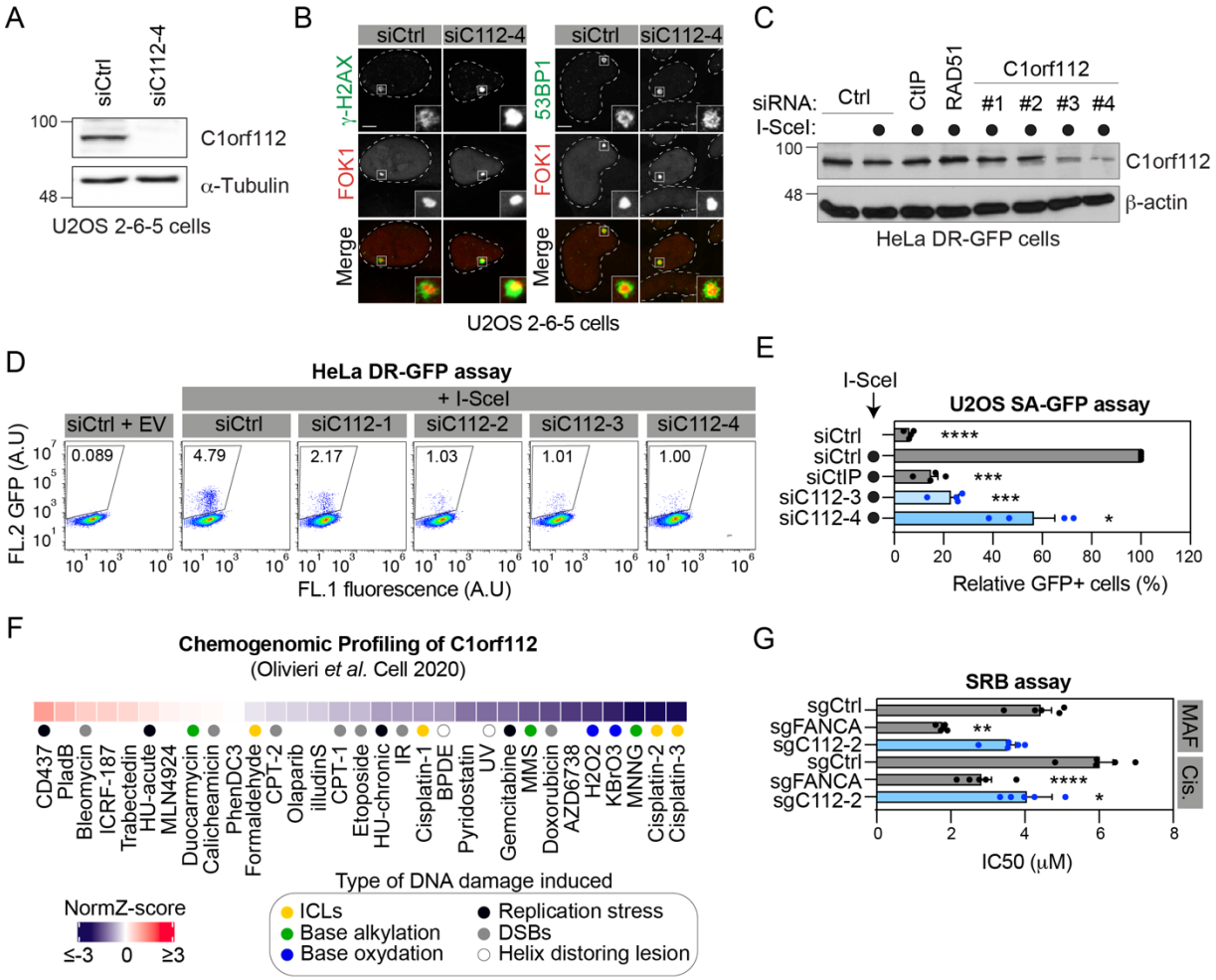
(D) U2OS cells were depleted or not for C1orf112 or FANCA and treated with cisplatin or DMSO. Whole Cell Extracts (WCE) were analyzed by immunoblot with anti-C1orf112, anti-FANCA or anti-FANCD2 antibodies. Anti-α-tubulin was used as a loading control. FD2: FANCD2, FD2-ubi: FANCD2 ubiquitinated.

(E) U2OS 2-6-5 cells were depleted or not for C1orf112 (for 48 hrs and ER-mCherry-LacR-FOK1-DD expression was induced for 4 hrs before fixation. Cells were then processed for BRCA1, BRCA2 or RAD51 immunofluorescence. Scale bar = 5 μm.

(F) Quantification of the ratio of indicated protein foci intensity over ER-mCherry-LacR-FOK1-DD foci intensity as shown in (E). Data are represented as the mean ± SD (n = 4 independent experiments, 50 foci quantified per experiment in each condition). Data were analyzed with an unpaired t-test with Welsh's correction.

(G) Quantification of GFP-positive HeLa and U2OS DR-GFP cells depleted or not CtIP, RAD51 or C1orf112. Twenty-four hours after transfection of the indicated siRNA, cells were transfected with the I-SceI expression plasmid (•) or an empty vector. Data are represented as the mean ± SEM

(n = 3 independent experiments, 30,000 cells quantified per experiment in each condition). Data were analyzed using a one-way Welch's ANOVA test and Dunnett's multiple comparison tests. (H) Drug sensitivity analysis using expression data for C1orf112 from the CCLE repository-DepMap and IC50 values using the GDSC database. Drug sensitivity of high (dark blue) and low (light blue) C1orf112 expressing cells is shown. Data were analyzed with an unpaired t-test (Cisplatin, Oxaliplatin, Olaparib & Doxorubicin) or a Mann-Whitney test (Cyclophosphamide, AZD7762 & Talazoparib) based on data normality assessed with a Shapiro-Wilk test.
*p<0.05, **p<0.01, ***p<0.001, ****p<0.0001



Pinedo Carpio, Dessapt *et al.* Figure 2.S3

Figure 2.S3 Characterization of C1orf112 knockdown and knockout cells related to Fig 2.3

(A) WCE of U2OS 2-6-5 cells depleted or not for C1orf112 were analyzed by immunoblot with an anti-C1orf112 antibody. Anti-α-Tubulin was used as a loading control.

(B) Representative images of U2OS 2-6-5 cells depleted or not for C1orf112. Cells were treated as in Figure 3E and processed for γ-H2AX (left) and 53BP1 (right). Scale bar = 5 μm.

(C) WCE of HeLa DR-GFP depleted or not for CtIP, RAD51 or C1orf112 were analyzed by immunoblot with an anti-C1orf112 antibody. Anti-β-actin was used as a loading control.

(D) Representative scatter plots of GFP-positive HeLa DR-GFP cells analyzed by flow cytometry and presented in Figure 3G. Flow cytometric profiles where green fluorescence (FL2) and auto orange fluorescence (FL1) are plotted on the y-axis and x-axis, respectively.

(E) Quantification of GFP-positive U2OS SA-GFP cells depleted or not for CtIP or C1orf112 Twenty-four hours post siRNA transfection, cells were transfected with the I-SceI expression plasmid (•) or an empty vector. Data are represented as the mean ± SEM (n = 4 independent experiments, 30,000 cells quantified per experiment in each condition). Data were analyzed using a one-way Welch's ANOVA test and Dunnett's multiple comparison tests.

(F) Chemogenomic profiling using the NormZ-score from the CRISPR screens performed in RPE1 hTERT Cas9 $p53^{-/-}$ cells with the indicated DNA damaging agents as detailed in [33].

(G) Quantification of RPE1-hTERT $p53^{-/-}$ cells survival in response to ICL-inducing agent. Cells were transduced with lentiviral particles containing sgRNAs against C1orf112, FANCA or a non-targeting control (sgCtrl). After selection with puromycin, cells were seeded in 96-well plates and treated with mafosfamide (MAF) or cisplatin (Cis.). Both drugs were added at a maximum concentration of 50 μM in a two-fold serial dilution until 0.097 μM. Data are represented as the mean ± SEM (n = 5 independent experiments). Data were analyzed using a one-way Welch's ANOVA test and Dunnett's multiple comparison tests.

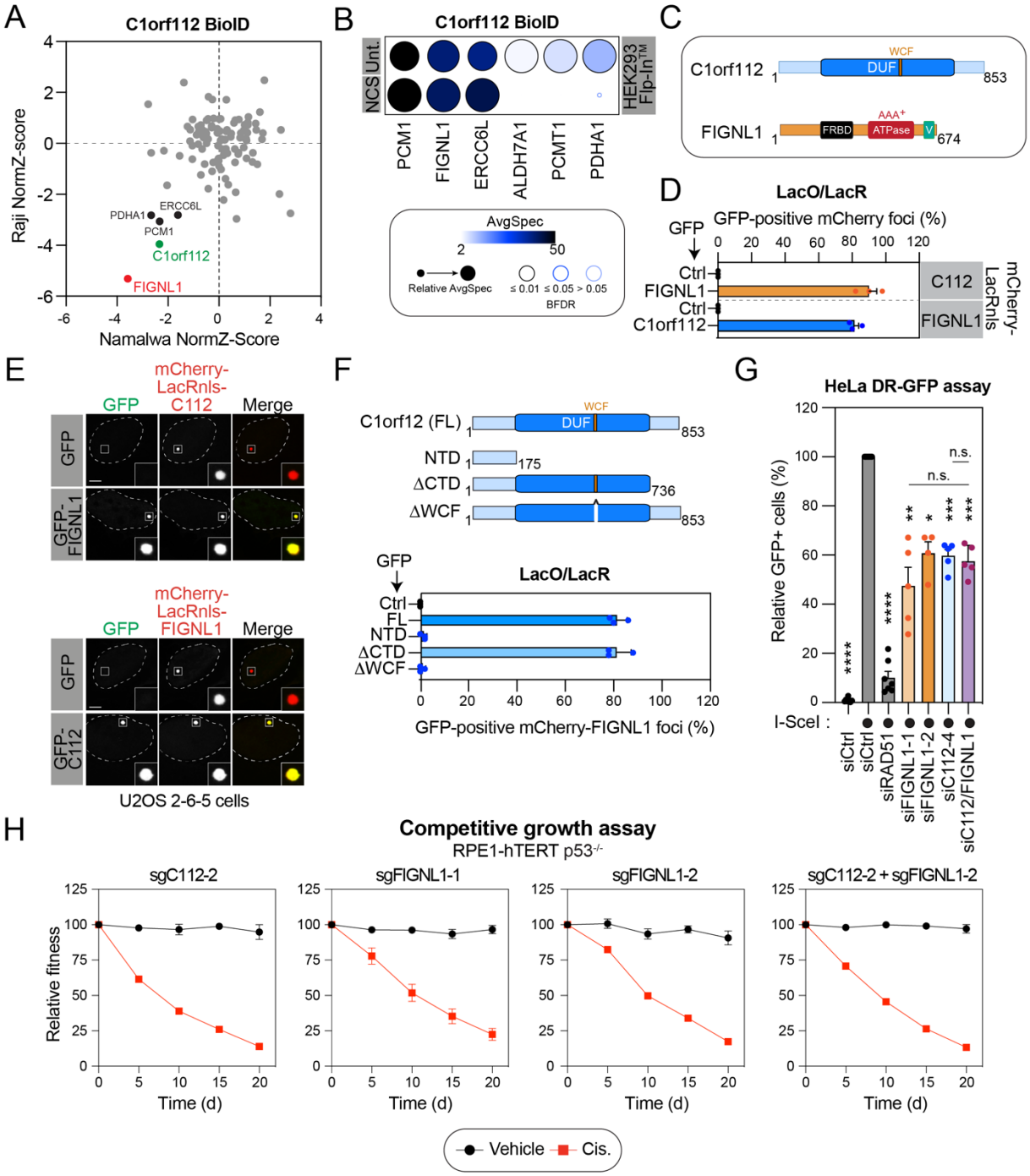
*p<0.05, **p<0.01***p<0.001, ****p<0.0001

2.3.4 C1orf112 interacts and acts with FIGNL1 in ICL repair.

To gain insight into the role of C1orf112 in DNA repair, we mapped its proximal interactome by taking advantage of the miniTurboID technology [34]. Briefly, C1orf112 was N-terminally tagged with the promiscuous biotin ligase miniTurbo (mTurboID) and stably expressed in HEK293 Flp-In™ cells (**Fig 2.S4A**). This construct was validated for its ability to efficiently biotinylate proximal partners by immunoblotting analysis (**Fig 2.S4B**). The proximity interacting network of C1orf112 was generated in both untreated cells and cells treated with the radiomimetic drug Neocarzinostatin (NCS) for 3 hrs. A total of 153 high-confidence C1orf112 interactors found in 3 technical replicates were identified (**Table 2.S4**). To pinpoint the interactors that are functionally relevant to the role of C1orf112 in DNA repair, we intersected the list of high-confidence prey obtained by mTurboID (BFDR < 0.01, Saint score = 1) with the NormZ scores obtained from Namalwa and Raji screen datasets (**Fig 2.4A**). Using this approach, we identified 4 interactors, 3 of which were identified in both treated and untreated cells suggesting that they are constitutive partners of C1orf112 (**Fig 2.4B**). Two of these interactors, the Pericentriolar material 1 protein (PCM1) and the DNA excision repair protein ERCC6-like (ERCC6L, also known as PICH), play a role in mitosis where they respectively contribute to the proper assembly of functional centrosomes and the resolution of anaphase bridges [35-37]. Therefore, we reasoned that they most likely play a role in the mitotic function of C1orf112/Apolo1 [20]. Interestingly, the AAA+ ATPase Fidgetin Like 1 (FIGNL1) was also identified as a constitutive interactor of C1orf112 using mTurboID. Although FIGNL1 has also been detected at centromeres, two studies support a role for the protein in regulating RAD51 filament during HR repair [9, 19]. The interaction between FIGNL1 and C1orf112 has been previously detected with two orthogonal approaches (Yeast two-hybrid [38], AP-MS [19, 39]) which strengthen our findings.

To validate and further characterize the interaction between FIGNL1 and C1orf112, we took advantage of the U2OS 2-6-5 cell line that contains a *lacO* array integrated into a single locus. In this context, transiently transfected mCherry-LacRnls-bait fusion proteins accumulate at the array in U2OS 2-6-5 cells, and the colocalization of preys is quantified at the mCherry locus. Of note, no FOK1 nuclease is expressed in these experiments. When fused to mCherry-LacRnls, both C1orf112 and FIGNL1 were able to respectively trigger the accumulation of GFP-tagged FIGNL1 and C1orf112 at the LacO array (**Fig 2.4 C-E and 2.S4 C-D**). In contrast, neither of the mCherry-LacRnls-tagged proteins recruited GFP alone, which was used as a negative control, at the LacO array. C1orf112 is a protein of 853 amino acids that contains a domain of unknown function (DUF) and a highly conserved WCF tripeptide motif (**Fig 2.4C**) [38]. Structure-function analysis of C1orf112 truncation and deletion mutants in this experiment revealed that the conserved WCF tripeptide motif is essential for the interaction with FIGNL1 while the C-terminal region of C1orf112 is not required (**Fig 2.4F and 2.S4 E-F**). Next, we used the DR-GFP reporter assay to investigate the functional relevance of the interaction between C1orf112 and FIGNL1 during DNA repair. Both C1orf112 and FIGNL1 were depleted using siRNA, and the efficiency of the siRNA for FIGNL1 was verified by RT-PCR (**Fig 2.S4G**). As reported in Fig 3, depletion of C1orf112 led to a mild but significant defect in HR repair when compared to the positive control siRAD51 (40 % vs 90 % decrease) (**Fig 2.4G**). Interestingly, both siRNAs targeting FIGNL1, as well as a double knockdown of FIGNL1 and C1orf112, lead to a similar defect in HR than C1orf112 with 50 %, 40 % and 40% decrease, respectively. This result supports a model where functions of FIGNL1 and C1orf112 are functionally epistatic in the HR pathway. In support of this hypothesis, FIGNL1-depleted and FIGNL1-C1orf112-depleted cells exhibit similar sensitivity to cisplatin in CRISPR-based growth competition assay (**Fig 2.4H**). Furthermore, the depletion of either protein in U2OS cells specifically reduced cell viability in the presence of ICL-inducing agents such as cisplatin,

formaldehyde, mitomycin C, chronic exposure to hydroxyurea and PARPi (**Fig 2.S4H**). Altogether, these findings suggest that C1orf112 and FIGNL1 act as a complex in the resolution of DNA breaks that are indirectly created by replication stress.



Pinedo Carpio, Dessapt *et al.* Figure 2.4

Figure 2.4 FIGNL1 is a functional interactor of C1orf112.

(A) Functional validation of mturboID data using Namalwa and Raji screen datasets. Scatter plots of preys obtained in mturboID proteomic (Fold-change ≤ 1.5) intersect with normalized Z (NormZ) values obtained from both CRISPR screens. High-confidence preys (BFDR < 0.01 & Saint score = 1) behaving like C1orf112 are highlighted.

(B) High-confidence proximal interactors of C1orf112 identified by mturboID with or without DNA damages induced with neocarzinostatin (NCS). The spectral counts for each indicated prey protein are shown as AvgSpec. The circle size represents the relative abundance of preys over baits, and node edge color corresponds to the Bayesian False Discovery Rate (BFDR).

(C) Schematic representation of C1orf112 and FIGNL1 protein domains. DUF: Domain of Unknown Function. WCF: WCF tripeptide sequence. FRBD: FIGNL1's RAD51 Binding Domain. V: vps4 domain.

(D) Quantification of the colocalization of C1orf112 and FIGNL1 at a *LacO* array. U2OS 2-6-5 cells were transfected with the indicated mCherry-LacRnls and GFP constructs. GFP alone was used as a negative control (Ctrl). Twenty-four hours post-transfections, cells were fixed and mounted for confocal analyses. Data are represented as the mean ± SD (n = 3 independent experiments, 50 cells quantified per experiment in each condition).

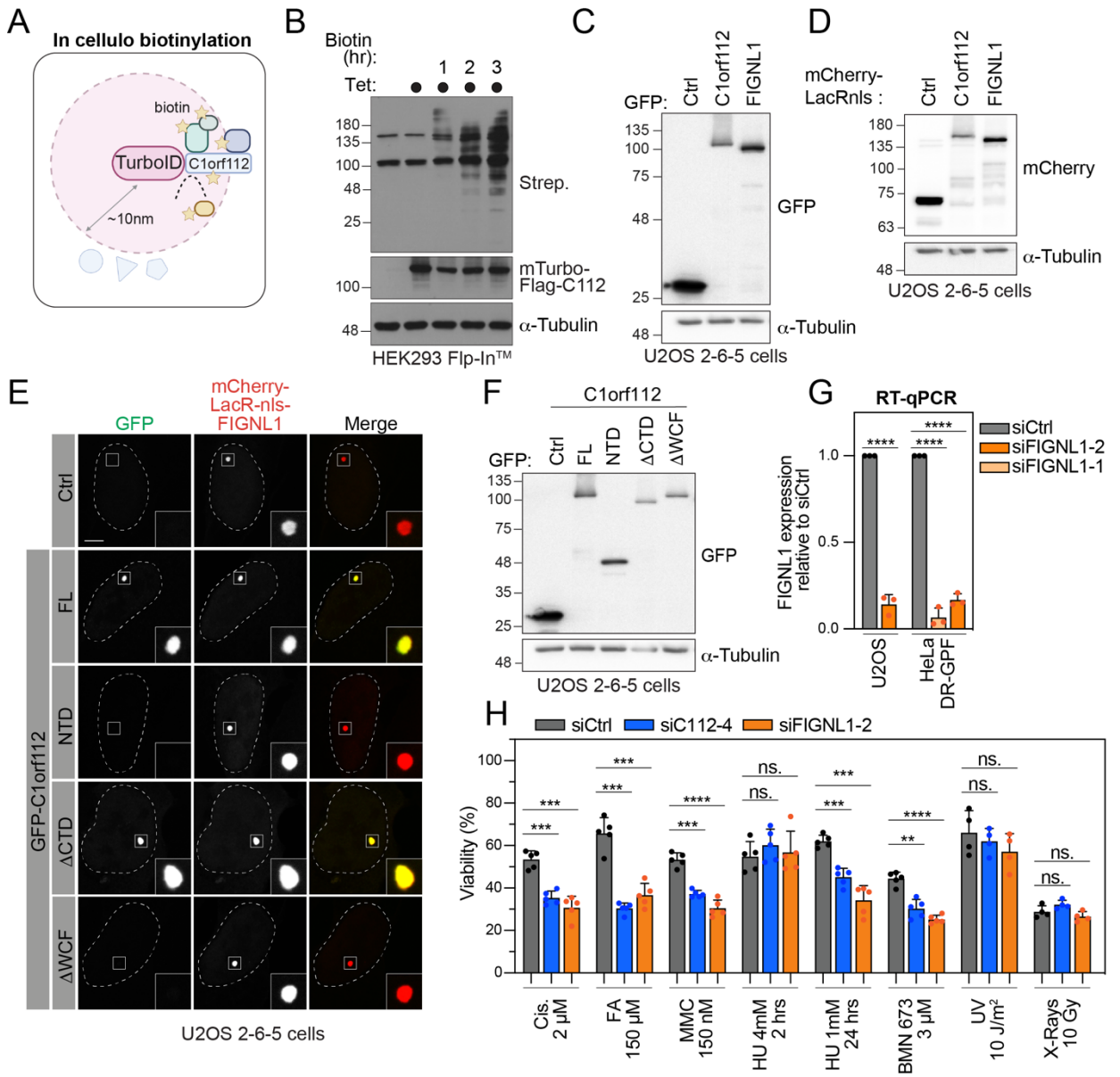
(E) Representative images of data quantified in (D). Scale bar = 5 μm.

(F) Schematic representation of C1orf112 full length (FL) and truncated proteins (upper panel). NTD: N-Terminal Domain. CTD: C-Terminal Domain. Quantification of GFP-tagged proteins colocalizing with mCherry-LacRnls-FIGNL1 in U2OS 2-6-5 cells is presented (lower panel). Cells were transfected and processed as in (D). Data are represented as the mean ± SD (n = 3 independent experiments, 50 cells quantified per experiment in each condition). Data were analyzed with an unpaired t-test with Welsh's correction.

(G) Quantification of GFP-positive HeLa DR-GFP cells depleted or not for RAD51, FIGNL1 and/or C1orf112. HeLa cells containing a DR-GFP reporter cassette were transfected and analyzed as described in Figure 3G. (•) represent I-SceI transfected cells. Data are represented as the mean ± SEM (n = at least 5 independent experiments, 30,000 cells quantified per experiment in each condition). Data were analyzed using a one-way Welch's ANOVA test and Dunnett's multiple comparison tests.

(H) Competitive growth results in FIGNL1 and/or C1orf112 depleted RPE1-hTERT $p53^{-/-}$ cells. Cells were assayed and treated as in Figure 1F and G. For dual targeting analysis, RPE1-hTERT cells were transduced with a colorless-sgRNA-non targeting control (LacZ), a sgC1orf112 coupled with BFP- and a sgFIGNL1 coupled with mCherry. Data are represented as the mean ± SEM (n = 3 technical replicates).

*p<0.05, **p<0.01, ***p<0.001, ****p<0.0001



Pinedo Carpio, Dessapt *et al.* Figure 2.S4

Figure 2.S4 Validation of protein expression and cell lines for mTurboID and LacO/LacR analysis, and characterization of C1orf112 and FIGNL1 in survival assays.

(A) Schematic representation of the biotinylation of C1orf112 proximal endogenous proteins using TurboID technology. Cutoff for proximity tagging is reported at 10nm [34].

(B) WCE extracts of HEK293T FL/IN cells induced or not for mturbo expression with 1μM tetracycline and supplemented or not for 50 μM biotin were analyzed by immunoblot with anti-streptavidin and anti-Flag antibodies. Anti-α-tubulin was used as a loading control.

(C-D and F) WCE extracts of U2OS 2-6-5 cells transfected with the indicated GFP- (C and F) or mCherry-LacRnls- (D) proteins were analyzed by immunoblot with anti-GFP or anti-mCherry antibodies. GFP. Anti-α-tubulin was used as a loading control.

(E) Representative images of U2OS 2-6-5 cells transfected with mCherry-LacRnls-FIGNL1 and the indicated GFP-C1orf112 constructs. GFP is used as control (Ctrl). Cells were fixed and mounted for confocal analyses. Scale bar = 5 μm

(G) RT-qPCR for FIGNL1 was performed on U2OS cells. Expression was normalized against GADPH and reported as a percent relative to siCtrl. Data are represented as the mean ± SD (n = 3 independent experiments). Data were analyzed with an unpaired t-test with Welsh's correction.

(H) Viability assay in cells treated with DNA damage-inducing agent. U2OS cells were treated with the indicated siRNA. Forty-eight hours later, cells were either exposed to 2 μM cisplatin (Cis.), 150 μM formaldehyde (FA), 150 nM mitomycin C (MMC), 3 μM Talazoparib (BMN-673) for 48 hrs, to 2 hrs of 4 mM hydroxyurea (HU) followed by 46 hrs recovery, to 24 hrs of 1 mM HU followed by 24 hrs recovery, to 10 J/m^2 UV or 10 Gy followed by 48 hrs recovery. Cells were counted with a hemacytometer and normalized against the number of cells quantified in the untreated condition. Data are represented as the mean ± SD (n = 4 independent experiments). Data were analyzed using a one-way Welch's ANOVA test and Dunnett's multiple comparison tests.

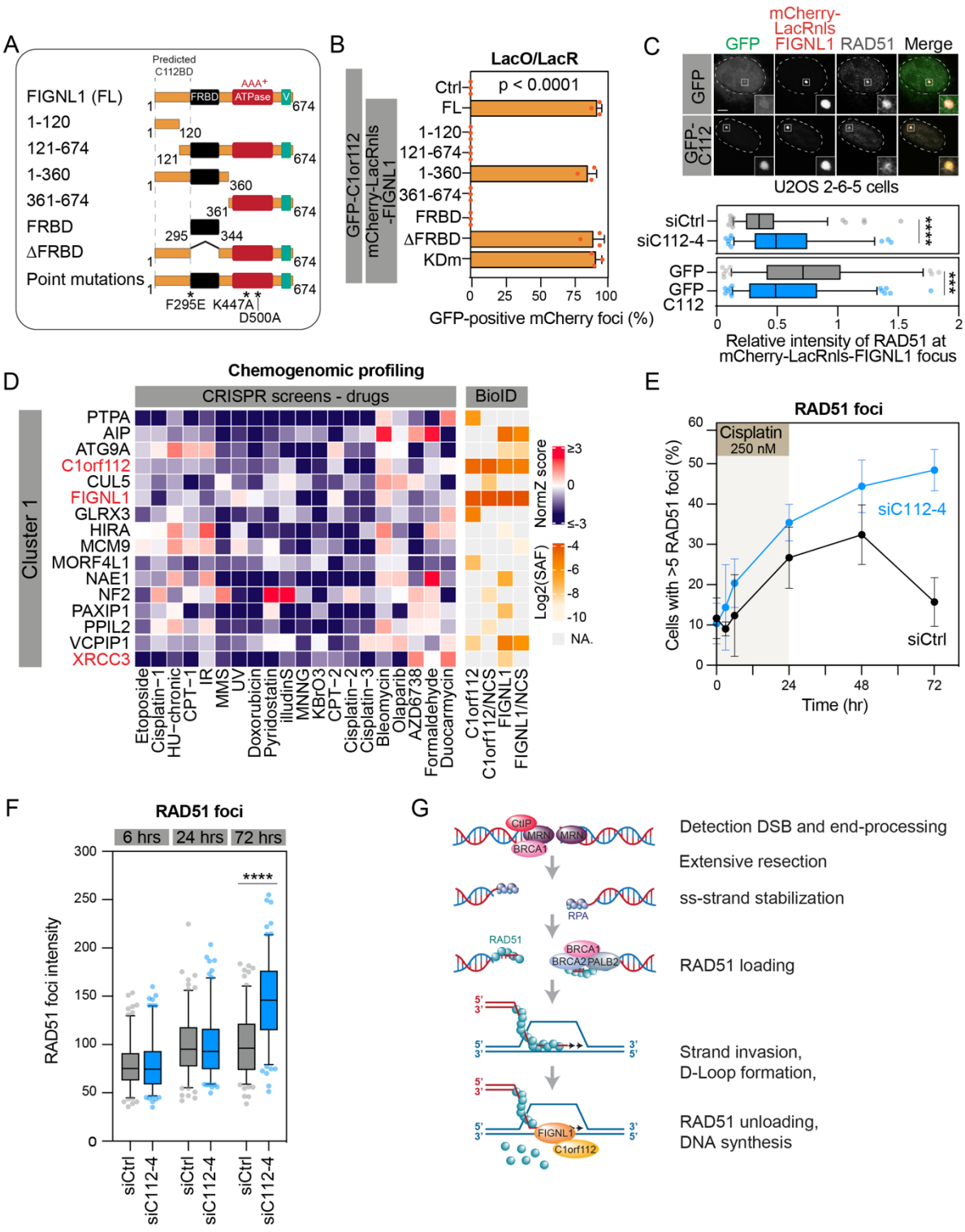
**p<0.01, ***p<0.001, ****p<0.0001

2.3.5 C1orf112 regulates FIGNL1 interaction with RAD51 and RAD51 resolution at ICLs.

FIGNL1 is a protein of 674 amino acids with three conserved domains, i) a RAD51 binding domain (FIGNL1's RAD51 binding domain, FRBD), ii) an AAA^+ ATPase domain, and iii) a C-terminal Vps4 domain [9, 19]. Interestingly, FIGNL1 has been shown to promote RAD51 dissociation from ssDNA [9, 19]. To gain insight into how C1orf112 and FIGNL1 may collaborate during ICL repair, we first took advantage of our ability to detect the interaction of GFP-C1orf112 with mCherry-LacRnls-FIGNL1 in the LacO/LacR assay (**Fig 2.4D**) to rapidly screen a panel of FIGNL1 truncation and mutant proteins (**Fig 2.5A**). mCherry-LacRnls-FIGNL1 constructs were designed to remove or abolish the function of the previously described FIGNL1's RAD51 binding domain (FRBD) [19] and AAA^+ ATPase activity of FIGNL1 [9] (**Fig 2.5A and 2.S5A**). In this experiment, FIGNL1 constructs lacking the FRBD (ΔFRBD) or the ability to interact with RAD51 (F295E) still efficiently recruited GFP-C1orf112 to the LacO array (**Fig 2.5B, Fig 2.S5 B-C**). Similarly, none of the single (K447A and D500A) and double (KDm: K447A/D500A) mutations of residues that are highly conserved within the AAA^+ ATPase domain impacted the interaction of FIGNL1 with C1orf112 (**Fig 2.5B, Fig 2.S5 B-C**). Consistent with the model that RAD51 is not required for the interaction, similar levels of GFP-C1orf112 were detected at the mCherry-LacRnls-FIGNL1 in cells treated with siRNA control or against RAD51 (**Fig 2.S5 D-E**). Interestingly, the fact that FIGNL1 constructs encompassing amino acids 1-120 or 121-674 are unable to recruit C1orf112 to the array, suggest that the C1orf112 binding motif (C112BM) of FIGNL1 spans over the intersection of these constructs (**Fig 2.5A**). Consistently, the FIGNL1 fragment 1-360 efficiently promoted the accumulation of C1orf112 in our assay.

In the LacO/LacR assay, mCherry-LacRnls-FIGNL1 efficiently recruits RAD51 to the array (**Fig 2.5C, Fig 2.S5F**). Interestingly, we observed a significant increase of RAD51 intensity at the mCherry locus in C1orf112 depleted U2OS 2-6-5 cells (**Fig 2.5C**), suggesting that C1orf112

negatively regulates the interaction of FIGNL1 with RAD51. Consistent with this hypothesis, ectopic expression of GFP-C1orf112 had the opposite effect and resulted in a reduced signal of RAD51 at the LacO array when compared to the expression of GFP alone (**Fig 2.5C**). These findings support a model where the C1orf112-FIGNL1 complex control RAD51 dynamics at the site of DNA breaks. In line with this model, clustering of TurboID preys based on their chemogenomic profiles [33] revealed that C1orf112 and FIGNL1 cluster with RAD51 paralog XRCC3 (**Fig 2.5D, Table 2.S4**). To further test this model, we investigated whether C1orf112 impacts the dynamic of RAD51 foci formation and resolution in cells treated with an ICL-inducing agent. RAD51 foci rapidly appeared 3-6 hours after the addition of cisplatin to the media (**Fig 2.5E and 2.S5G**). While more foci accumulated in cells depleted for C1orf112, their intensity were like the intensity of the foci in cells treated with a siRNA control (**Fig 2.5F**), suggesting that RAD51 is properly loaded at ICLs in these cells. In contrast, more than 40% of C1orf112-depleted cells still exhibited more than 5 RAD51 foci 72 hours post-treatment, a time frame that was sufficient to resolve these foci in the control condition. Altogether, these findings demonstrate that C1orf112 regulates RAD51 unloading at ICLs following strand invasion by regulating its interaction with FIGNL1 (**Fig 2.5G**).



Pinedo Carpio, Dessapt *et al.* Figure 2.5

Figure 2.5 The C1orf112-FIGNL1 complex regulates RAD51 unloading in HR.

(A) Schematic representation of FIGNL1 full length (FL), proteins fragments and mutant proteins used in this study.

(B) Quantification of mCherry-LacRnls constructs colocalizing with GFP-C1orf112 in U2OS 2-6-5 cells. Cells were treated and processed as described in Figure 4D. Data are represented as the mean ± SD (n = 3 independent experiments, 50 cells quantified per experiment in each condition). Data were analyzed with an unpaired t-test with Welsh's correction.

(C) Upper panel: Representative images of U2OS 2-6-5 cells transfected with mCherry-LacR-FIGNL1 and GFP-C1orf112. GFP was used as a negative control. Fixed cells were processed for RAD51 (grey) immunofluorescence. Scale bar = 5 μm. Lower panel: Ratio of the intensity of RAD51 over mCherry signal at the *LacO* array foci. Cells were either transfected with mCherry-LacR-FIGNL1 alone or with a GFP-tagged construct 24h before fixation. When indicated, cells were treated with siRNA 24 hrs prior to plasmid transfection. Data are represented as the mean ± SD (n = 3 independent experiments, 50 foci quantified per experiment in each condition). Data were analyzed with an unpaired t-test with Welsh's correction.

(D) Left panel: Chemogenomic profiling using the NormZ-score from the CRISPR screens performed in RPE1 hTERT Cas9 $p53^{-/-}$ cells with the indicated DNA damaging agents as detailed in [33]. Right panel: Heatmap indicating proximity interaction network of C1orff112 and FIGNL1, treated or not with NCS, with the protein expressed from the indicated gene (Log2SAF: spectral abundance factor).

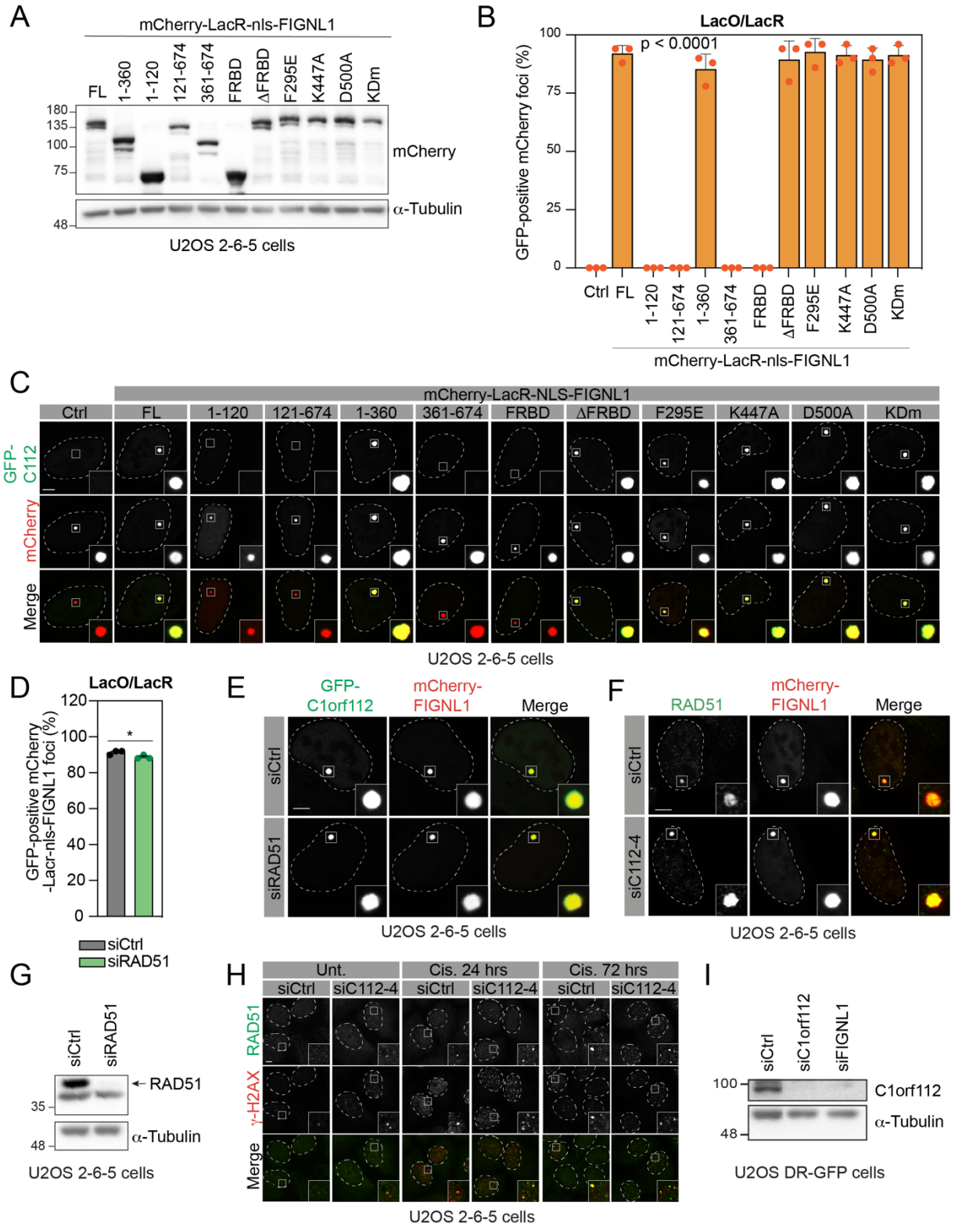
(E) Quantification of U2OS cells with ≥ 5 RAD51 foci following treatment with cisplatin. Cells were depleted or not for C1orf112 prior to treatment with 250 nM cisplatin (t = 0). Twenty-four hours later, cells were washed with PBS and left for recovery. Cells were fixed and then processed for RAD51 immunofluorescence for every time point. Data are represented as the mean ± SD (n =

3 independent experiments, 50 cells quantified per experiment in each condition). Data were analyzed with an unpaired t-test with Welsh's correction.

(F) Quantification of the intensity of RAD51 foci analyzed in (E). Data are represented as the mean ± SD (n = 3 independent experiments, 50 foci quantified per experiment in each condition). Data were analyzed with an unpaired t-test with Welsh's correction.

(G) Proposed model of the FIGNL1-dependent role of C1orf112 in RAD51 unloading following DNA strand invasion. ss: single strand.

***p<0.001, ****p<0.0001



Pinedo Carpio, Dessapt *et al.* Figure 2.S5

Figure 2.S5 Expression levels and cellular localization of mCherry-LacRnls-FIGNL1 and GFP-C1orf112 constructs used in Fig. 5.

(A) WCE of U2OS 2-6-5 cells transfected with the indicated mCherry-LacRnls-FIGNL1 constructs were analyzed by immunoblot with an anti-mCherry antibody. Anti-α-tubulin antibody was used as a loading control. KDm: K447A / D500A double mutant.

(B) Quantification of mCherry-LacRnls constructs colocalizing with GFP-C1orf112 in U2OS 2-6-5 cells. Cells were treated and processed as described in Figure 4D. Data are represented as the mean ± SD (n = 3 independent experiments, 50 cells quantified per experiment in each condition). Data were analyzed with an unpaired t-test with Welsh's correction.

(C) Representative images of data from (B). U2OS 2-6-5 cells were transfected with indicated mCherry-LacR construct and then fixed and mounted for confocal analyses. Scale bar = 5 μm.

(D) Quantification of the colocalization between mCherry-LacRnls-FIGNL1 and GFP-C1orf112 in U2OS 2-6-5 cells depleted or not for RAD51. Data are represented as the mean ± SD (n = 3 independent experiments, 50 foci quantified per experiment in each condition). Data were analyzed with an unpaired t-test.

(E) Representative images of data quantified in (D). Cells were fixed and mounted for confocal analyses. Scale bar = 5 μm.

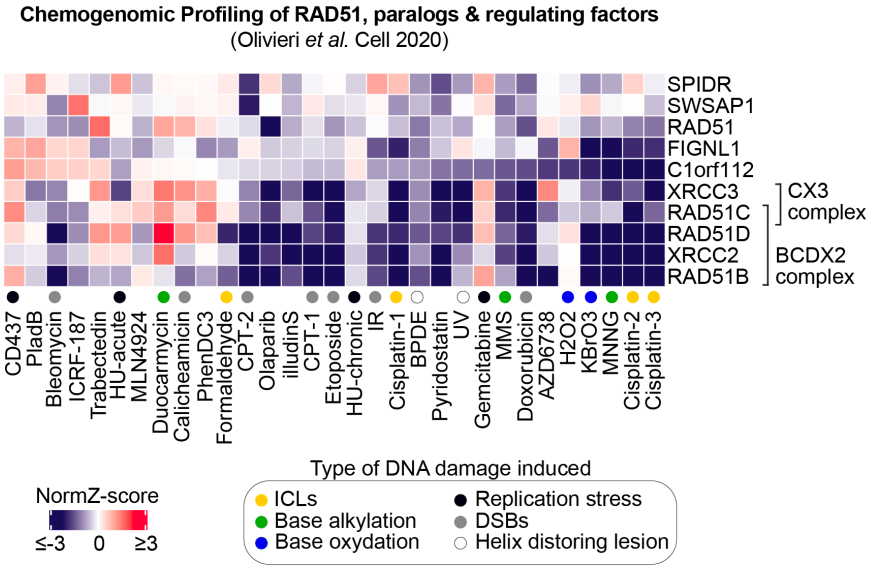
(F) Representative images of the colocalization of mCherry-LacRnls-FIGNL1 with RAD51 in U2OS 2-6-5 cells depleted or not for C1orf112. Cells were fixed and processed for RAD51 immunofluorescence. Scale bar = 5 μm.

(G) WCE of U2OS 2-6-5 cells depleted or not for RAD51 were analyzed by immunoblot with an anti-RAD51 antibody. Anti-α-Tubulin was used as a loading control.

(H) Representative images of the data quantified in figure 5 E. Cells were fixed and processed for RAD51 (green) and γ-H2AX (red) immunofluorescence. Scale bar = 5 μm.

(I) WCE of U2OS DR-GFP cells depleted or not for C1orf112 or FIGNL1 were analyzed by immunoblot with an anti-C1orf112 antibody. Anti-α-Tubulin was used as a loading control. *$p<0.05$

A



Pinedo Carpio, Dessapt *et al.* Figure 2.S6

Figure 2.S6 Chemogenomic profiling of C1orf112, FIGNL1 and literature-curated relevant genes.

(A) Chemogenomic profiling using the NormZ-score from the CRISPR screens performed in RPE1 hTERT Cas9 $p53^{-/-}$ cells with the indicated DNA damaging agents as detailed in [33].

2.4 Discussion

2.4.1 C1orf112 is a novel regulator of HR-mediated ICL-repair.

While the initial steps involved in ICL repair have been extensively described, it remains largely unclear how ICL intermediates are processed and subsequently resolved. CRISPR-based functional genomics have been a powerful strategy to gain novel insight into several DNA repair pathways [33], including the recent characterization of SCAI as a modulator of repair pathway choice during ICL processing [7, 8]. In this work, we delineated the contribution of the poorly characterized C1orf112 in the latter stage of ICL repair using a similar strategy. We show that lack of C1orf112 impairs cell survival in response to a series of ICL-inducing agents. In these conditions, C1orf112 acts downstream of the FA pathway where it is functionally epistatic with the AAA+ ATPase FIGNL1 for the resolution of HR-mediated intermediate. Specifically, our findings reveal that C1orf112 is required for the resolution of RAD51, a phenotype that is reminiscent of the RAD51 unloading activity of FIGNL1 [9]. Consistent with a coordinated role of C1orf112 and FIGNL1 in regulating HR-mediated DNA repair, mutation in *figl1-1*, the ortholog of FIGNL1 in plants, is epistatic with *flip-1* mutation, the ortholog of C1orf112, in limiting meiotic crossover formation [38]. While we were unable to detect the recruitment of C1orf112 at ICLs, previous studies identified this factor at stalled replication fork by iPOND [40-42], suggesting that they specifically contribute to ICL-induced replication fork collapse [1]. The fact that C1orf112 limits the formation of micronuclei, the accumulation of 53BP1 nuclear bodies, and prevents the induction of senescence, supports a model where C1orf112 may act in the response to replication stress.

2.4.2 C1orf112 forms a heterodimer with FIGNL1 to regulate RAD51 accumulation upon repair.

Previous reports identified FIGNL1 as key regulator of the resolution of RAD51 foci in different biological contexts [9, 19, 38]. Interestingly, our systematic proteomics analysis of C1orf112 identified FIGNL1 as a constitutive proximal interactor that we validated *in cellulo*. Our preliminary data suggest that this heterodimer is necessary for the stability of the complex (**Fig. 2.S5I**), reminiscent of what has been previously observed with the BRCA1/BARD1 heterodimer, where each member of the heterodimer controls the abundance, stability, and function of the other [43, 44]. Our findings suggest that C1orf112 acts as a scaffolding platform for FIGNL1 in complex with RAD51, thereby regulating its unloading. Furthermore, our proximal mapping of FIGNL1 identified the RAD51 paralog XRCC3, a component of the CX3 complex, which has been suggested to act downstream of RAD51 loading [45]. Although RAD51 was recently involved in the protection of cells from transcription-replication conflicts [46], either C1orf112- or FIGNL1- depleted cells are not sensitized to transcription-interfering agents such as Trabectedin and illudinS (**Fig 2.S6**), suggesting that the heterodimer specifically regulates RAD51 dynamics following strand invasion and not at stalled replication forks per se. Interestingly, cells depleted from either one of these factors are specifically sensitive to chemical agents that generate replication roadblocks, which requires a specific processing before repair such as ICL-agents and agents that promote either base oxidation or base alkylation (**Fig 2.S6**) [47-49]. Of note, our data suggest that C1orf112 and the SWS1-SWSAP1-SPIDR complex, which inhibit FIGNL1-dependent RAD51 unloading [9, 19], play opposite roles in response to replication stress. Consistently, both complexes cluster differently when analysed by chemogenomic profiling (**Fig 2.S6**).

2.4.3 FIGNL1-independent function of C1orf112

Chemogenomic profiling of both FIGNL1 and C1orf112 highlights the differential contribution of each factor to cell survival upon genotoxic stress, suggesting that C1orf112 and FIGNL1 also have distinct functions in cells. Consistent with this hypothesis, FIGNL1 is highly conserved in a range of eukaryotic species while C1orf112 is not conserved in Fungi as well as in model organisms such as C. elegans and D. melanogaster [38]. In line with this observation, the predicted C1orf112 interacting region is located in a less conserved region of FIGNL1. Alike other scaffolding proteins such as REV7, it is possible that C1orf112 forms different molecular complexes, depending on the cellular context, thereby preserving genomic stability (reviewed in [50]). In fact, our proteomic analysis also identified ERCC6L as one of the top constitutive interactors of C1orf112, which may likely reflect a role during mitotic progression [20].

2.4.4 Clinical relevance of C1orf112 in cancers

So far, no mutation in C1orf112 has been linked to a FA-related phenotype. However, high levels of C1orf112 have been associated with poor outcomes in a series of cancers, including gliomas [51], and therefore may be a potential prognostic marker in multiple tumor types [52]. Our data further suggest that C1orf112 expression may modulate the response to different well-established chemotherapeutic agents, thereby influencing patient outcome.

2.5 Material and Methods

Cell Culture and plasmids transfections.

All cell lines were maintained at 37°C and 5% CO_2. Namalwa and Raji Burkitt lymphoma cell lines (kind gift of Dr. Jerry Pelletier, McGill university) were cultured in Roswell Park Memorial Institute (RPMI) 1640 medium (Wisent) and supplemented with 20% fetal bovine serum (FBS, Sigma) and 1% Penicillin-Streptomycin (Wisent). RPE1-hTERT p53 WT and $p53^{-/-}$ cells (kind gift of Dr. Daniel Durocher, University of Toronto) and IMR90 cells (obtained from the NIGMS Human Genetic Cell Repository I90-10) were cultured in Dulbecco's modified Eagle medium (DMEM) medium (Wisent) and supplemented with 10% FBS and 1% Penicillin-Streptomycin. U2OS (purchased from ATCC) and U2OS 2-6-5 cell lines (a kind gift from Roger Greenberg (University of Pennsylvania, [29]) were cultured in McCoy's medium (Life Technologies) and supplemented with 10% fetal bovine serum (FBS). Hela DR-GFP cells, U2OS DR-GFP and U2OS SA-GFP cells (kind gift of Dr. Jeremy Stark, City of Hope) were cultured in DMEM and McCoy's medium (Wisent), respectively. These cells were supplemented with 10% FBS and 1% Penicillin-Streptomycin.

RPE1-hTERT Cas9 $p53^{-/-}$ $C1orf112^{-/-}$ cells were generated by transduction of the parental cell line with lentiviral vectors harboring C1orf112-sgRNAs targeting exon 5 and exon 13 (**Table 2.S5**). Cells were selected with puromycin for 4 days, and single clones isolated by single-cell sorting. Knockout cells were validated using immunoblotting. Stable Cas9-expressing Burkitt lymphoma cell lines (Namalwa and Raji Burkitt cells) were generated using the LentiCas9-Blast vector as previously described [53] and validated for Cas9 expression by immunoblotting analysis. Cell lines used for all mturboID-MS experiments were generated in HEK293 Flp-In™ T-REx™ cells as previously described [16] and pool of stable transfectants selected with 200 μg/mL hygromycin (Multicell) and 5 μg/mL blasticidin (Invivogen). Expression of bait proteins were induced with 1 μg/mL

tetracycline for 24 h. Plasmid transfections were done using Lipofectamine™ 2000 (Invitrogen) and TransIT-LT1 (Mirus) transfection agents according to the manufacturer's instructions. All cell lines were validated using short tandem repeat (STR) markers and tested negative for mycoplasma contamination.

RNA interference

The pLKO shRNA plasmids against C1orf112 were obtained from the McGill Platform for Cellular Perturbation (MPCP) as part of the TRC/RNAi Consortium from the Broad institute. Non-targeting shRNA control was purchased from Addgene. Single siRNA duplex sequences targeting C1orf112, FIGNL1, FANCA, a custom non-targeting sequence, and SMARTPool siRNAs targeting RAD51 or CtIP were purchased from Dharmacon. Unless stated otherwise, all siRNAs were transfected at a concentration of 25 nM in a forward transfection for 48 hours using RNAimax (Invitrogen) according to the manufacturer's instructions. Knockdowns were confirmed by immunoblotting or qPCR analyses. All siRNA and shRNA sequences are detailed in **Table 2.S5**.

RNA extraction and RT-qPCR

Total RNAs were extracted using the RNeasy mini kit according to the manufacturer's instruction (QIAGEN) and quantified using a NanoDrop™ spectrometer. 500 ng of total RNA was reversed transcribed with the High-Capacity cDNA reverse transcription (RT) kit (Invitrogen) in accordance with the manufacturer's instructions. Prior to the RT, contaminant genomic DNA was removed by DNaseI (ThermoFisher) treatment and confirmed by GAPDH RT-PCR on DNaseI-treated reactions. qPCRs were performed on a LightCycler 480 apparatus (Roche) with the LightCycler 480 SYBR Green 1 qPCR master mix (Roche) using the following program: 40 cycles of 94°C denaturation for 15 seconds, 56°C annealing for 5 seconds and 72°C elongation for 15 seconds. 5%

of the RT-PCR reaction was used as a template. The standard curve was calculated with serial dilution of the U2OS cDNA as templated and used to determine the relative expression of each gene before normalization to the relative expression of GAPDH. The PCR primers are listed in **Table 2.S5**.

Chemicals and sources of DNA damage

In the FOK1 system, DSBs were induced at the *LacO* array by inducing the nuclear localization (4-Hydroxytamoxifen (4-OHT, 100 nM, #3412, Tocris)) and stabilization (Shield-1 ligand, 0.5 μM, CIP-S1-0001, CheminPharma)) of the ER-mCherry-LacR-FOK1-DD nuclease for 4 hrs prior to immunofluorescence sample preparation. DNA damages were induced by exposing cells to either ionizing irradiation (IR 1 or 10 Gy) with a CellRad (Precision X-Ray Inc.), cisplatin treatments (Tocris 1 μM for 3 or 24 hrs, 250 nM in time course experiment, and 2 μM in survival assay), mafosfamide (MAF, Toronto Research chemicals, 1.30 μM and 1.57 μM in Namalwa and Raji screens respectively), neocarzinostatin (NCS) (Sigma-Aldrich, 100 ng/mL), hydroxyurea (HU, Sigma-Aldrich, 4 mM and 1 mM in survival assay), formaldehyde (Sigma-Aldrich, 150 μM), mitomycin C (MMC, Sigma-Aldrich, 150 nM), Talazoparib (BMN 673, Selleck Chemicals, 3 μM), or UV (10 J/m^2). UV irradiations were carried on with a germicidal lamp (243 nm).

Cell viability assays

U2OS cells were seeded in 6-well plate (75 000 cells/wells) 24 hrs prior to siRNA transfection (siCtrl, siC1orf112 or siFIGNL1). Forty-eight hrs post-transfection, cells were exposed to the indicated treatment. Following a recovery of 48 hrs, cells were harvested and counted using an hematocyter.

Plasmids

DNA sequences of sgRNAs were cloned into a modified form of LentiGuide-puro with BFP or mCherry marker as described in [54]. The cDNA for C1orf112 (MHS1010-202739778, *Horizon Discovery*) and FIGNL1 (MHS6278-202759761, *Horizon Discovery*) were obtained from Dharmacon, and coding sequences with respective attB1/B2 adapters were PCR-amplified and subcloned into pDONR221 vectors using a BP clonase II reaction according to the manufacturer's instructions (Invitrogen), to generate ENTRY vectors. ENTRY clones containing C1orf112 constructs (aa 1-175, aa 1-735) and FIGNL1 constructs (aa 1-120, aa 121-674, aa 1-360, aa 361-674, aa 295-344) were generated using the same approach. FIGNL1 mutations and depletion construct (Δ295-344, F295E, K447A, D500A and K477A/D500A) were directly introduced in ENTRY vectors using the Quick-change approach. Quick-change Site-Directed Mutagenesis was conducted using primers listed in **Table 2.S4** using the Quick-change (Agilent) or Q5-Site-directed mutagenesis kit (NEB) following the manufacturer's protocol. LR recombining reactions were then conducted to transfer ENTRY constructs into pDEST-mturboID (kind gift from Dr. Anne-Claude Gingras, University of Toronto), pDEST-mCherry-LacRnls (kind gift from Dr. Daniel Durocher, University of Toronto), or pDEST-FRT-TO-eGFP-nls. All sequences were validated through Sanger sequencing. A list of plasmids used in this study is provided in **Table 2.S7**.

CRISPR-Cas9-based genome-wide screening

Namalwa and Raji genome-wide screens were executed as previously described [16]. Briefly, 245 millions Namalwa and Raji cells expressing Cas9 were transduced with TKOv1 sgRNA lentiviral library at MOI (0.2), ensuring coverage of at least 500-fold for each individual sgRNA represented in the cell population. Two days later, the selection of fully edited transduced cells was achieved by adding puromycin to the media at a final concentration of 2 μg/ml for 7 days. Following a 2-day

recovery in fresh media without selection, cells were split into 2 pools, in triplicate, at a cell density of 45 million cells (D0). The first pools were treated with mafosfamide at its IC25 (1.30 μM and 1.57 μM in Namalwa and Raji screens respectively) and the second pool with DMSO as a vehicle. Cells were then cultured for 14 doubling times with puromycin at a concentration of 1 μg/ml. Cells were counted and passaged every 3 days at a cell density of 0.37 million cells per mL to maintain fold coverage of 500 cells per sgRNA, until D14. At each time point, cell pellets were frozen for subsequent genomic DNA purification. Genomic DNA isolation was performed as described in [16]. For next-generation sequencing (NGS) library preparation, sgRNAs were amplified from genomic DNA using two rounds of nested PCR with inner oligo and outer oligo annealing. The initial outer PCR was performed with TaKaRa ExTaq® DNA Polymerase Hot-Start Version polymerase (Takara) using forward (FW) and reverse (RV) outer primers (**Table 2.S5**). PCR products were pooled, and ~2% of the input was amplified using Hot start Q5 polymerase to add Illumina HiSeq adapter sequences (**Table 2.S5**). The resulting product from each pooled sample was further purified following separation on an 8% 0.5× TBE polyacrylamide gel. The library NGS was quantified using qPCR and analyzed by deep-sequencing on the HiSeq 2500 Illumina platform. Reads were trimmed of NGS adapter sequences using the Cutadapt tool. Reads were aligned to the sgRNA library index file using Bowtie2. BAM files were generated using samtools, and total read count tables were subsequently generated using the MAGeCK count command. DrugZ algorithm was used to identify gene knockouts which were depleted or enriched from D14 populations in comparison to D0 [18].

Gene Set Enrichment Analysis (GSEA) and Network interaction analysis

GSEAs were conducted individually for each DrugZ-ranked list from the Namalwa and Raji screens using the GSEA v4.3.0 package and using the Gene Ontology biological process gene sets. For the

integrated pathway enrichment analysis, an average of the NormZ values acquired individually for both screens using DrugZ was obtained, and a merged ranked list was generated. Pathway enrichment analysis on the integrated ranked list was conducted using the package Enrichr as previously described [55, 56]. Network interaction analysis was performed using Cytoscape v 3.9.1 and the GeneMANIA package [57, 58].

Construction of heatmaps

All heatmaps were generated with the ComplexHeatmap R package [59] by performing hierarchical clustering on drugs NormZ-scores derived from published CRISPR screens [33] and limited to preys identified by our miniturboID assays. In legends, dark blue indicates NormZ scores ≤ -3 while bright red indicates scores ≥ 3. Similarly, we created a heatmap out of our miniturboID results using the log2-transformed SAF (Spectral Abundance Factor) metric, a normalization method calculated by dividing average spectral counts of preys by their respective protein length in amino acids.

Acquisition of immunoblotting images

All immunoblot images were acquired with an Azure Biosystems c300 Imaging System instrument. Briefly, membranes were exposed to Azure Radiance ECL (VWR) for 1 min before acquisition on the Azure apparatus with the sensitivity parameter set to "Normal" (1108x834). Whole pictures were adjusted for luminosity and contrast with the Adobe Photoshop software.

CRISPR-based competition growth assay

Growth competition assays were conducted as described in [21] and [54]. Briefly, RPE1-hTERT Cas9 $p53^{-/-}$ were transduced with lentiviral particles of Lenti-mCherry-sgRNA-LacZ or Lenti-BFP-sgRNA-GOI (C1orf112/FIGNL1/FANCA/MRE11). Twenty-four hours post-transduction, cells

were selected with 15 μg/mL of puromycin for 4 days. BFP and mCherry labelled cells were mixed at a 1:1 ratio and seeded in a 6-well plate. At the initial time point (T0), cells were treated with cisplatin at 6 μM (IC25) or vehicle (DMSO), and the levels of each fluorophore were measured via flow cytometry. Cells were maintained under these conditions and subcultured for 20 days. The ratio of BFP to mCherry fluorescent cell population were assessed via flow cytometry every 5 days.

Apoptosis

RPE1-hTERT Cas9 $p53^{-/-}$ $C1orf112^{-/-}$ clones 1 and 2 were seeded in 6-well plates and treated with an overnight treatment of 4 μM cisplatin. The next day, cells were washed with Dulbeccos's PBS and fresh media added to the plate. Forty-eight hours post cisplatin treatment, cells were processed for Annexin-V (Biolegend) and PI staining, following the manufacturer's instructions. Analyses of Annexin-V and PI signals were done on at least 30 000 events acquired on a BD Fortessa (Becton Dickinson). Data were analyzed using the FlowJo software as previously described [60].

Senescence-associated β-Galactosidase Assay

Senescence-associated β-galactosidase (SA β-gal) assays were performed as previously described [61]. Briefly, shRNA expressing REP1 hTERT p53WT or $p53^{-/-}$ or IMR90 cells were fixed with 0.5% glutaraldehyde in PBS, washed and kept at 4 °C in PBS supplemented with 1 mM $MgCl_2$ (pH 6). Cells were stained with X-Gal solution containing potassium ferricyanide in PBS supplemented with 1 mM of MgCl2 (pH 6). Images were acquired, and the percentage of SA β-gal positive cells was quantified.

GFP-based DNA repair Assays

DNA repair by HR (DR-GFP) or SSA (SA-GFP) of I-SceI-generated DSB were measured as previously described [16, 31]. Briefly, HeLa DR-GFP, U2OS DR-GFP or U2OS SA-GFP cells were seeded in 6-well plates at a density of 100,000 cells/well and were transfected with 25 nM of siRNA. Twenty-four hours later, cells were transfected with pCBA-SceI plasmid using Lipofectamine 2000 (Invitrogen). Cells were harvested 48 hrs post-transfection, and the percentage of GFP-expressing cells was measured by flow cytometry. Analysis of GFP-positive signal was done on at least 30 000 events acquired on a BD Fortessa (Becton Dickinson). Data were analyzed using the FlowJo software and presented as previously described [16].

Expression profiling IC50

The correlation between gene expression and drug sensitivity was conducted using expression datasets for each gene of interest available from the Cancer Cell Line Encyclopedia (CCLE) project as part of the Cancer Dependency Map (DepMap). IC50 values were obtained from the Genomics of Drug Sensitivity in Cancer (GDSC) database (Release 8.4, GDSC2 datasets) [62].

Sulforhodamine B (SRB) Assay

RPE1-hTERT cells were seeded in 96-well plates at a density of 1000/cells per well. Twenty-four hours later, cisplatin and mafosfamide were added in a two-fold serial dilution from 50 to 0.097 μM. Survival was assessed four days after treatment using the sulforhodamine B (SRB) colorimetric assay as described previously [63, 64]. Briefly, after drug treatment cells were fixed by adding 100 μL of 10% trichloroacetic acid (TCA, Bioshop Canada) and incubated at 4°C for 1 hr with gentle agitation. Cells were washed four times and plates were left air-drying overnight at room temperature. The next day, cells were stained with 100 μL of 0.057% SRB (Sigma Aldrich) and incubated at room

temperature for 30 minutes. Plates were then rinsed four times using 1% acetic acid and were left air-drying overnight. Protein content was solubilized by adding 200 μL of 10 mM Tris base solution (pH 10.5) for 30 minutes at room temperature. Measurement of optical density (OD) at 510 nm was conducted using a FLUOstar Optima microplate reader. Background correction was conducted using the measurement of control wells with media. Treatments were performed in triplicate, averaged, and normalized to untreated control. IC50 concentrations were obtained using the slope's equation for log (concentration of drug) vs normalized OD.

Immunofluorescence Microscopy

U2OS and U2OS 2-6-5 cells were grown on glass coverslips in 24-well plates and fixed with 2% (wt/vol) paraformaldehyde (PFA) in PBS for 20 minutes at RT. Exceptionally, cells used in the time course experiments were fixed with 100% MeOH for 20 minutes at -20°C. When indicated, PFA-fixed cells were processed for immunofluorescence by further permeabilizing cells with 0.3% (vol/vol) Triton X-100 for 20 minutes at RT. Cells were then incubated with blocking buffer (10% goat serum, 0.5% NP-40, 0.5% saponin in 1X PBS) for 30 minutes at RT and then incubated with primary antibodies (**Table 2.S6**) in blocking buffer for 2 hrs at RT. After three washes with PBS, cells were incubated for 1 hr at RT with secondary antibodies (**Table 2.S6**) and 4',6-diamidino-2-phenylindole (DAPI, 0,4 μg/mL) blocking buffer. Coverslips were mounted onto glass slides with ProLong™ Diamond Antifade Mountant agent (Invitrogen). Images were acquired using a Zeiss LSM900 laser-scanning microscope equipped with a 48X and 63X oil lens. In all micrographs, dashed lines indicate the nucleus outline, and insets represent a 10-fold magnification of the indicated fields. Each quantification was done on at least 3 biological replicates, and at least 100 cells or 50 foci were counted in each experiment. Unless stated otherwise, significance was assessed by performing a t-test with Welch's correction.

mturboID sample preparation for mass spectrometry

HEK293 Flp-In^{tm} cells expressing mTurboID-tagged protein or mTurbo tag alone were seeded in 150 mm plates in technical duplicates. Induction of fusion protein and proximity biotinylation were conducted as previously described [16, 60, 65]. Briefly, induction of mturboID-tagged protein expression was done by adding 1 μM tetracycline to the media for 24 h. Then, the medium was supplemented with 50 μM biotin for 1 hr and incubated for an additional 3hrs with 100 ng/mL neocarzinostatin (NCS). Cells were harvest, washed and lysed in ice-cold RIPA buffer (50 mM Tris-HCl pH 7.4, 150 mM NaCl, 1% NP-40, 1 mM EDTA, 0.1% SDS and 0.5% sodium deoxycholate, 1 mM PMSF, 1 mM DTT) supplemented with 1:500 Sigma-Aldrich protease inhibitor cocktail P8340. and sonicated on ice. After sonication, 250 units of benzonase (EMD) were added sample prior to a 30 minutes centrifugation at 12,000 xg at 4°C. Supernatants were transferred to pre-washed streptavidin-Sepharose beads (GE, #17-5113-01) and incubated at 4°C on a rotator for 3 hrs. Beads were centrifuged at 400 xg for 1 minute and sequentially washed 2 times with RIPA buffer and 3 times with of 50 mM ammonium bicarbonate (ABC, pH 8.0). Beads were then resuspended in 100 μL of ABC, and on-bead digestion was achieved by adding 10 μg of trypsin (Sigma) to the suspension for overnight digestion at 37°C. The next day, an additional 10 μg of trypsin was added to each sample, and further digested for 3 hrs. Beads were pelleted by centrifugation for 1 min at 400 g, and the supernatant-containing peptides were pooled with supernatants from two subsequent rinses with 100 μL of mass spectrometry grade H_2O. Formic acid was added to the pooled samples to a final concentration of 5% to end digestion. Samples were centrifuged at 16,000 xg for 10 minutes at room temperature and supernatants were lyophilized using vacuum centrifugation. Dried peptides were kept at −80°C.

Analysis of MS data was conducted as described before with minor modifications [60]. Briefly, samples were injected into an Orbitrap Fusion (Thermo Fisher), and raw files were analyzed with the

Comet, XTandem! and Mascot search engines using the human RefSeq database (version 20170518) supplemented with "common contaminants" from the Max Planck Institute (http://maxquant.org/downloads.htm), the Global Proteome Machine (GPM; http://www.thegpm.org/crap/index.html) and decoy sequences. The search parameters were set with trypsin specificity (two missed cleavage sites allowed), variable modifications involved Oxidation (M) and Deamidation (NQ). The mass tolerances for precursor and fragment ions were set to 10 ppm and 0.6 Da, respectively, and peptide charges of +2, +3, +4 were considered. Search results were individually processed by PeptideProphet [66], and peptides were assembled into proteins using parsimony rules first described in ProteinProphet [67] using the Trans-Proteomic Pipeline (TPP). TPP settings were the following: -p 0.05 -x20 -PPM –d "DECOY", iprophet options: pPRIME and PeptideProphet: pP. To estimate the interactions statistics, we used SAINTexpress (PMID 24513533) (version 3.6.1) on proteins with iProphet protein probability ≥ 0.9 and unique peptides ≥ 2. Each bait was compared against its respective negative control (treated or not with NCS). These controls comprised of pulldowns from HEK cells expressing the empty vector (without the BirA*-Flag) in triple technical replicates. SAINT analyses were performed with the following compression settings: nControl:2, nCompressBaits:2. Interactions displaying an average probability (AvgP) ≥ 0.7 were considered as statistically significant (Supplementary Table X). Unfiltered contaminants, such as Keratin, BirA* and beta galactosidase were discarded in every bioinformatics analyses. Using the ProHits-Viz online tool (prohits-viz.org), we generated a dot plot representing the relative AvgSpec of identified proteins for both baits.

2.6 Acknowledgments

We are grateful to members of the Orthwein and Fradet-Turcotte laboratories for critical reading of the manuscript; Daniel Durocher, Roger Greenberg, Anne-Claude Gingras, Jerry Pelletier and Jeremy Stark for plasmids and other reagents. EPC is a recipient of a doctoral fellowship from the Fonds de Recherche Santé Québec (FRQS). Work in the A.O. laboratory was supported by a CCSRI Innovation Grant (#706389), a Transition Grant from the Cole Foundation and an internal Operating Fund from the Sir Mortimer B. Davis Foundation of the Jewish General Hospital. Work in the A.F.-T laboratory was supported by a Canadian Institutes of Health Research Grant (PDT_152948 to A.F.-T.). Work in the J.-F.C. laboratory is supported by a Canadian Institutes of Health Research Grant (PJT-178241). A.F.-T. is a Tier 2 Canada Research Chair in Molecular Virology and Genomic Instability and is supported by the Foundation J.-Louis Lévesque. J.-F.C. holds the Tier 1 Canada Research Chair in Cellular Signalling and Cancer Metastasis and is supported by the Alain Fontaine Chair in Cancer Research from the IRCM Foundation.

2.7 Author Contributions

E.P.C., J.D., F.M., A.G., A.O. and A.F-T. designed research; E.P.C., J.D., R.V., L.S., A.M., J.B., E.G.L., V.L., A-M.L., and J-F.C. performed research and analyzed data; A.F.-T. and A.O. wrote the original draft and E.P.C. and J.D. edited the manuscript**.**

2.8 Conflict of interest

The authors declare that they have no conflict of interest.

2.9 References

1. Semlow, D.R. and J.C. Walter, *Mechanisms of Vertebrate DNA Interstrand Cross-Link Repair.* Annu Rev Biochem, 2021. **90**: p. 107-135.
2. Deans, A.J. and S.C. West, *DNA interstrand crosslink repair and cancer.* Nat Rev Cancer, 2011. **11**(7): p. 467-80.
3. Lopez-Martinez, D., C.C. Liang, and M.A. Cohn, *Cellular response to DNA interstrand crosslinks: the Fanconi anemia pathway.* Cell Mol Life Sci, 2016. **73**(16): p. 3097-114.
4. Wu, R.A., et al., *TRAIP is a master regulator of DNA interstrand crosslink repair.* Nature, 2019. **567**(7747): p. 267-272.
5. Li, N., et al., *Cooperation of the NEIL3 and Fanconi anemia/BRCA pathways in interstrand crosslink repair.* Nucleic Acids Res, 2020. **48**(6): p. 3014-3028.
6. Semlow, D.R., et al., *Replication-Dependent Unhooking of DNA Interstrand Cross-Links by the NEIL3 Glycosylase.* Cell, 2016. **167**(2): p. 498-511 e14.
7. Adeyemi, R.O., et al., *The Protexin complex counters resection on stalled forks to promote homologous recombination and crosslink repair.* Mol Cell, 2021. **81**(21): p. 4440-4456 e7.
8. Schubert, L., et al., *SCAI promotes error-free repair of DNA interstrand crosslinks via the Fanconi anemia pathway.* EMBO Rep, 2022. **23**(4): p. e53639.
9. Matsuzaki, K., et al., *Human RAD51 paralogue SWSAP1 fosters RAD51 filament by regulating the anti-recombinase FIGNL1 AAA+ ATPase.* Nat Commun, 2019. **10**(1): p. 1407.
10. Prakash, R., et al., *Distinct pathways of homologous recombination controlled by the SWS1-SWSAP1-SPIDR complex.* Nat Commun, 2021. **12**(1): p. 4255.
11. Adelman, C.A., et al., *HELQ promotes RAD51 paralogue-dependent repair to avert germ cell loss and tumorigenesis.* Nature, 2013. **502**(7471): p. 381-4.
12. Hustedt, N., et al., *Control of homologous recombination by the HROB-MCM8-MCM9 pathway.* Genes Dev, 2019. **33**(19-20): p. 1397-1415.
13. Huang, J.W., et al., *MCM8IP activates the MCM8-9 helicase to promote DNA synthesis and homologous recombination upon DNA damage.* Nat Commun, 2020. **11**(1): p. 2948.
14. Wang, C., et al., *C17orf53 is identified as a novel gene involved in inter-strand crosslink repair.* DNA Repair (Amst), 2020. **95**: p. 102946.
15. Steinhart, Z., et al., *Genome-wide CRISPR screens reveal a Wnt-FZD5 signaling circuit as a druggable vulnerability of RNF43-mutant pancreatic tumors.* Nat Med, 2017. **23**(1): p. 60-68.

16. Findlay, S., et al., *SHLD2/FAM35A co-operates with REV7 to coordinate DNA double-strand break repair pathway choice.* EMBO J, 2018. **37**(18).
17. Hart, T., et al., *High-Resolution CRISPR Screens Reveal Fitness Genes and Genotype-Specific Cancer Liabilities.* Cell, 2015. **163**(6): p. 1515-26.
18. Colic, M., et al., *Identifying chemogenetic interactions from CRISPR screens with drugZ.* Genome Med, 2019. **11**(1): p. 52.
19. Yuan, J. and J. Chen, *FIGNL1-containing protein complex is required for efficient homologous recombination repair.* Proc Natl Acad Sci U S A, 2013. **110**(26): p. 10640-5.
20. Xu, L., et al., *Feedback control of PLK1 by Apolo1 ensures accurate chromosome segregation.* Cell Rep, 2021. **36**(2): p. 109343.
21. Hustedt, N., et al., *A consensus set of genetic vulnerabilities to ATR inhibition.* Open Biol, 2019. **9**(9): p. 190156.
22. Bizard, A.H. and I.D. Hickson, *Anaphase: a fortune-teller of genomic instability.* Curr Opin Cell Biol, 2018. **52**: p. 112-119.
23. Lukas, C., et al., *53BP1 nuclear bodies form around DNA lesions generated by mitotic transmission of chromosomes under replication stress.* Nat Cell Biol, 2011. **13**(3): p. 243-53.
24. Reinhardt, H.C. and B. Schumacher, *The p53 network: cellular and systemic DNA damage responses in aging and cancer.* Trends Genet, 2012. **28**(3): p. 128-36.
25. Bartkova, J., et al., *Oncogene-induced senescence is part of the tumorigenesis barrier imposed by DNA damage checkpoints.* Nature, 2006. **444**(7119): p. 633-7.
26. Di Micco, R., et al., *Oncogene-induced senescence is a DNA damage response triggered by DNA hyper-replication.* Nature, 2006. **444**(7119): p. 638-42.
27. Mallette, F.A., M.F. Gaumont-Leclerc, and G. Ferbeyre, *The DNA damage signaling pathway is a critical mediator of oncogene-induced senescence.* Genes Dev, 2007. **21**(1): p. 43-8.
28. Ceccaldi, R., P. Sarangi, and A.D. D'Andrea, *The Fanconi anaemia pathway: new players and new functions.* Nat Rev Mol Cell Biol, 2016. **17**(6): p. 337-49.
29. Tang, J., et al., *Acetylation limits 53BP1 association with damaged chromatin to promote homologous recombination.* Nat Struct Mol Biol, 2013. **20**(3): p. 317-25.
30. Shanbhag, N.M., et al., *ATM-dependent chromatin changes silence transcription in cis to DNA double-strand breaks.* Cell, 2010. **141**(6): p. 970-81.
31. Stark, J.M., et al., *Genetic steps of mammalian homologous repair with distinct mutagenic consequences.* Mol Cell Biol, 2004. **24**(21): p. 9305-16.

32. Bhargava, R., et al., *C-NHEJ without indels is robust and requires synergistic function of distinct XLF domains.* Nat Commun, 2018. **9**(1): p. 2484.
33. Olivieri, M., et al., *A Genetic Map of the Response to DNA Damage in Human Cells.* Cell, 2020. **182**(2): p. 481-496 e21.
34. Branon, T.C., et al., *Author Correction: Efficient proximity labeling in living cells and organisms with TurboID.* Nat Biotechnol, 2020. **38**(1): p. 108.
35. Biebricher, A., et al., *PICH: a DNA translocase specially adapted for processing anaphase bridge DNA.* Mol Cell, 2013. **51**(5): p. 691-701.
36. Dammermann, A. and A. Merdes, *Assembly of centrosomal proteins and microtubule organization depends on PCM-1.* J Cell Biol, 2002. **159**(2): p. 255-66.
37. Wang, G., et al., *PCM1 recruits Plk1 to the pericentriolar matrix to promote primary cilia disassembly before mitotic entry.* J Cell Sci, 2013. **126**(Pt 6): p. 1355-65.
38. Fernandes, J.B., et al., *FIGL1 and its novel partner FLIP form a conserved complex that regulates homologous recombination.* PLoS Genet, 2018. **14**(4): p. e1007317.
39. Hein, M.Y., et al., *A human interactome in three quantitative dimensions organized by stoichiometries and abundances.* Cell, 2015. **163**(3): p. 712-23.
40. Raschle, M., et al., *DNA repair. Proteomics reveals dynamic assembly of repair complexes during bypass of DNA cross-links.* Science, 2015. **348**(6234): p. 1253671.
41. Nakamura, K., et al., *Proteome dynamics at broken replication forks reveal a distinct ATM-directed repair response suppressing DNA double-strand break ubiquitination.* Mol Cell, 2021. **81**(5): p. 1084-1099 e6.
42. Wessel, S.R., et al., *Functional Analysis of the Replication Fork Proteome Identifies BET Proteins as PCNA Regulators.* Cell Rep, 2019. **28**(13): p. 3497-3509 e4.
43. Joukov, V., et al., *Functional communication between endogenous BRCA1 and its partner, BARD1, during Xenopus laevis development.* Proc Natl Acad Sci U S A, 2001. **98**(21): p. 12078-83.
44. Hashizume, R., et al., *The RING heterodimer BRCA1-BARD1 is a ubiquitin ligase inactivated by a breast cancer-derived mutation.* J Biol Chem, 2001. **276**(18): p. 14537-40.
45. Chun, J., E.S. Buechelmaier, and S.N. Powell, *Rad51 paralog complexes BCDX2 and CX3 act at different stages in the BRCA1-BRCA2-dependent homologous recombination pathway.* Mol Cell Biol, 2013. **33**(2): p. 387-95.
46. Bhowmick, R., et al., *RAD51 protects human cells from transcription-replication conflicts.* Mol Cell, 2022. **82**(18): p. 3366-3381 e9.

47. Wang, J.Y. and W. Edelmann, *Mismatch repair proteins as sensors of alkylation DNA damage.* Cancer Cell, 2006. **9**(6): p. 417-8.
48. Kumar, N., et al., *Global and transcription-coupled repair of 8-oxoG is initiated by nucleotide excision repair proteins.* Nat Commun, 2022. **13**(1): p. 974.
49. Kawanishi, S. and M. Murata, *Mechanism of DNA damage induced by bromate differs from general types of oxidative stress.* Toxicology, 2006. **221**(2-3): p. 172-8.
50. Clairmont, C.S. and A.D. D'Andrea, *REV7 directs DNA repair pathway choice.* Trends Cell Biol, 2021. **31**(12): p. 965-978.
51. Zhang, Z., et al., *High Expression of C1ORF112 Predicts a Poor Outcome: A Potential Target for the Treatment of Low-Grade Gliomas.* Front Genet, 2021. **12**: p. 710944.
52. Chen, J., et al., *Pan-Cancer Analysis Identified C1ORF112 as a Potential Biomarker for Multiple Tumor Types.* Front Mol Biosci, 2021. **8**: p. 693651.
53. Sanjana, N.E., O. Shalem, and F. Zhang, *Improved vectors and genome-wide libraries for CRISPR screening.* Nat Methods, 2014. **11**(8): p. 783-784.
54. Tzelepis, K., et al., *A CRISPR Dropout Screen Identifies Genetic Vulnerabilities and Therapeutic Targets in Acute Myeloid Leukemia.* Cell Rep, 2016. **17**(4): p. 1193-1205.
55. Kuleshov, M.V., et al., *Enrichr: a comprehensive gene set enrichment analysis web server 2016 update.* Nucleic Acids Res, 2016. **44**(W1): p. W90-7.
56. Chen, E.Y., et al., *Enrichr: interactive and collaborative HTML5 gene list enrichment analysis tool.* BMC Bioinformatics, 2013. **14**: p. 128.
57. Montojo, J., et al., *GeneMANIA Cytoscape plugin: fast gene function predictions on the desktop.* Bioinformatics, 2010. **26**(22): p. 2927-8.
58. Warde-Farley, D., et al., *The GeneMANIA prediction server: biological network integration for gene prioritization and predicting gene function.* Nucleic Acids Res, 2010. **38**(Web Server issue): p. W214-20.
59. Gu, Z., R. Eils, and M. Schlesner, *Complex heatmaps reveal patterns and correlations in multidimensional genomic data.* Bioinformatics, 2016. **32**(18): p. 2847-9.
60. Heath, J., et al., *POGZ promotes homology-directed DNA repair in an HP1-dependent manner.* EMBO Rep, 2022. **23**(1): p. e51041.
61. Neault, M., F.A. Mallette, and S. Richard, *miR-137 Modulates a Tumor Suppressor Network-Inducing Senescence in Pancreatic Cancer Cells.* Cell Rep, 2016. **14**(8): p. 1966-78.

62. Yang, W., et al., *Genomics of Drug Sensitivity in Cancer (GDSC): a resource for therapeutic biomarker discovery in cancer cells.* Nucleic Acids Res, 2013. **41**(Database issue): p. D955-61.
63. Vichai, V. and K. Kirtikara, *Sulforhodamine B colorimetric assay for cytotoxicity screening.* Nat Protoc, 2006. **1**(3): p. 1112-6.
64. Xu, Z.Y., et al., *Xrcc3 induces cisplatin resistance by stimulation of Rad51-related recombinational repair, S-phase checkpoint activation, and reduced apoptosis.* J Pharmacol Exp Ther, 2005. **314**(2): p. 495-505.
65. Lambert, J.P., et al., *Proximity biotinylation and affinity purification are complementary approaches for the interactome mapping of chromatin-associated protein complexes.* J Proteomics, 2015. **118**: p. 81-94.
66. Keller, A., et al., *Empirical statistical model to estimate the accuracy of peptide identifications made by MS/MS and database search.* Anal Chem, 2002. **74**(20): p. 5383-92.
67. Nesvizhskii, A.I., et al., *A statistical model for identifying proteins by tandem mass spectrometry.* Anal Chem, 2003. **75**(17): p. 4646-58.

Liaison between Chapter II and III

During the conduction of this research a total of 4 genome-wide screens were executed. Chapter II covers the intersection of the Namalwa and Raji screens and describes the uncovering of C1orf112 as novel factor involved in interstrand crosslink repair. In this chapter we employed an overlap between genome-wide scale datasets in order to choose C1orf112 for further characterization. In the design of the pipeline used for this functional genomics approach, we used pediatric Burkitt lymphoma cell lines that share common BL signatures such as p53 deficiency and the (8;14) translocation affecting c-myc. Nevertheless, and to uncover genetic vulnerabilities and synthetic lethal signatures common to BL regardless of a specific genetic background and aiming to boost our mapping of genetic vulnerabilities, we conducted two other genome-wide screens using the Ramos and DG75 cell lines. Chapter III covers the finding derived from the Ramos genome wide screen and results obtained in the DG75 screen will be covered in another publication which is not included in the present thesis. In Chapter III, instead of using the usual overlap between genome-wide datasets as employed in Chapter II, we used a different approach and to interrogate multiple poorly characterized hits of interest we employed CRISPR-based custom-made libraries and interrogated the effect of the genetic perturbation upon treatment with multiple DNA damaging agents: cisplatin, mitomycin-C, AZD6738(ATR inhibitor) and phleomycin. The results of this secondary validation using miniscreens is described in the following chapter and it highlights the complementary and useful targeted approach using tailored libraries. Altogether the two chapters covered in this thesis showed the power of CRISPR-based functional genomics in uncovering novel factors involved in DNA repair process such as interstrand crosslink repair.

Chapter III: Genome-wide CRISPR-based screening identifies C1orf27 as a novel regulator of DNA interstrand cross-link repair through its role in UFMylation.

Genome-wide CRISPR-based screening identifies C1orf27 as a novel regulator of DNA interstrand cross-link repair through its role in UFMylation.

Authors: Edgar Pinedo-Carpio, Abba Malina & Alexandre Orthwein

Running title: C1orf27 regulates interstrand crosslink DNA repair through its role in UFMylation.

Address correspondence to:

Alexandre Orthwein, M.Sc., Ph.D.

Lady Davis Institute, Segal Cancer Centre

Jewish General Hospital

Montreal, QC, H3T 1E2 Canada

e-mail: alexandre.orthwein@mcgill.ca

3.1 Abstract

DNA repair pathway play important roles in preserving genomic stability and preventing carcinogenesis. During the past two decades a unique network of proteins involved in DNA interstrand cross-link repair have been identified through the characterization of the Fanconi anemia (FA)/HR pathways. In bacteria and eukaryotes, the major ICL repair network encompasses the coordinated actions of FA, nucleotide excision (NER), homologous recombination (HR) and translesion synthesis (TLS) repair pathways, highlighting the complexity of this cellular response. Using a CRISPR-based genome wide screening approach, we identified C1orf27 as a novel factor involved in the modulation of ICL repair. Secondary validation and chemogenomic profiling of C1orf27 suggested of a potential role of this factor in UFMylation. Using miniturboID technology we interrogated the proximal interactome of C1orf27, UFSP2 and UFL1 in the context of ICL repair. This systemic proteomic analysis allowed us to identify a constitutive interaction between C1orf27 and UFSP2. In addition, we identified a novel constitutive interacting partner of C1orf27 such as TEX264 and TMEM263 as a potential novel factor involved in the UFM1 pathway. Altogether our study has uncovered a novel factor involved in UFMylation-dependent modulation of DNA interstrand cross-link repair.

3.2 Introduction

Cells are continuously challenged by endogenous and exogenous sources of DNA damage. Among these insults, DNA interstrand crosslink (ICL) are considered one of the most deleterious types of DNA lesion due to its role impairing replication and transcription [1-5], thereby representing a major threat for genome integrity. In that regard, ICL-inducing drugs, including platins or nitrogen-mustards, have an important role in chemotherapy regimens for the treatment of both solid and blood cancers. Cyclophosphamide and its analog mafosfamide are one of the oldest and more successful ICL agents used in oncology, composing the core component of the frontline combinatorial regimen used for the treatment of diffuse large B-cell and Burkitt lymphomas [6, 7]. Although a considerable number of patients respond well to these regimens, around 40 % of patients with high-grade B-cell lymphoma display refractory disease or relapse, and eventually perish from the disease [8-12]. Therefore, the identification of genomic vulnerabilities and sensitizing signatures using systemic approaches like functional genomics are of great importance.

The canonical pathway in charge of repairing ICLs is the FA/HR repair pathway. The FA/HR pathway is a complex DNA repair network that, along with FA core proteins, includes DNA repair factors involved in homologous recombination (HR), nucleotide excision repair (NER) and translesion synthesis (TLS) [3, 13]. Through decades of basic and clinical research the knowledge of these DNA repair response has been enriched and growth considerably. Recent efforts using functional genomics, among other approaches, have allowed researchers to uncover novel factors involved in ICL repair [14-23], highlighting that there are still important gaps in our knowledge of the molecular mechanism involved in this biological process. A key event in the activation of the FA/HR repair pathway is the monoubiquitination of the heterodimer ID2 by the FA core complex, which triggers the signaling cascade in this DNA repair response. Besides this ubiquitination and the deubiquitination of the ID2 heterodimer by the USP1 and UAF1 which down regulates this pathway

[3], it is very likely that other protein modifications are involved in the fine-tuning and regulation of this intricated response. A recently uncovered but still poorly understood ubiquitin-like protein modification with relevance to DNA repair is UFMylation [24, 25]. The pathway in charge of conjugating this protein modification is the UFM1 pathway and it modifies its protein targets following an E1-E2-E3 enzymatic reaction. UFM1 pathway has been linked to tissue homeostasis, endoplasmic reticulum (ER) stress response, and more recently to regulating ATM and MRN complex function upon DNA damage [25-30], however a potential specific role of UFM1 pathway in ICL response has not been explored yet.

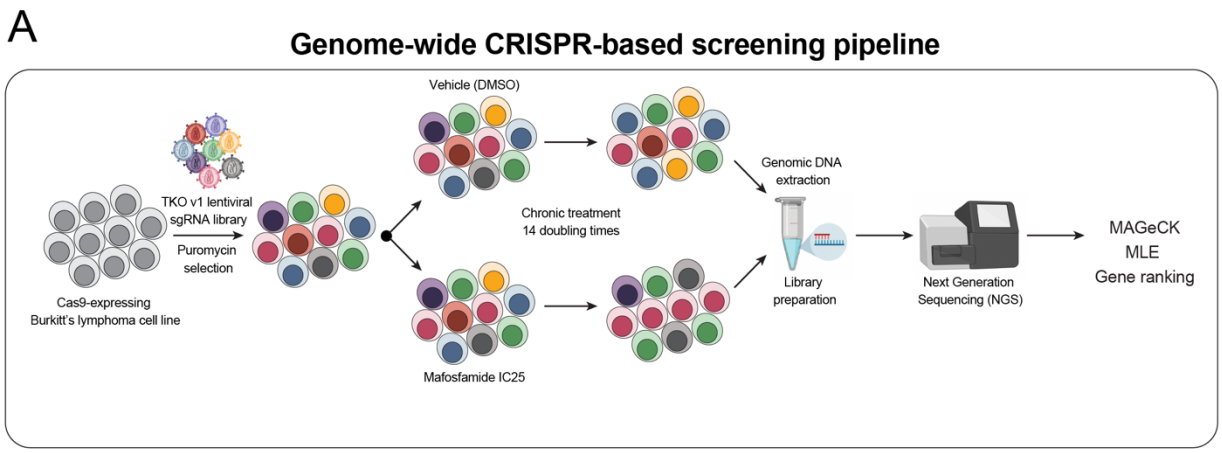
To better understand the genetic factors in the response to cyclophosphamide and its derivatives, we conducted a genome-wide screen in the Burkitt lymphoma Ramos cell line using mafosfamide as selective agent. As expected, our genome-wide synthetic lethal approach was significantly enriched with core components of the FA pathways, a series of HR factors along-side players in nucleotide excision repair (NER) and double-strand break (DSB) repair. Secondary validation of a series of poorly characterized genes (n=34 genes) allowed us to identify C1orf27 as potential novel regulator of the DNA damage response. Multi-omics data integration analysis and chemogenomic profiling identified a novel C1orf27-UFSP2 axis involved in a ubiquitin-like post-translation modification recently identified in the regulation of DDR: UFMylation [24, 25, 27, 28, 31, 32]. Critically, RNA expression levels of C1orf27 and canonical factors of the UFM1 pathway such as UFSP2 and UFL1 correlated with a poorer prognosis in a cohort of ovarian cancer patients. Collectively, our findings delineated C1orf27 as a novel player involved in the regulation of ICL repair through its role in the ubiquitin-like modification UFMylation.

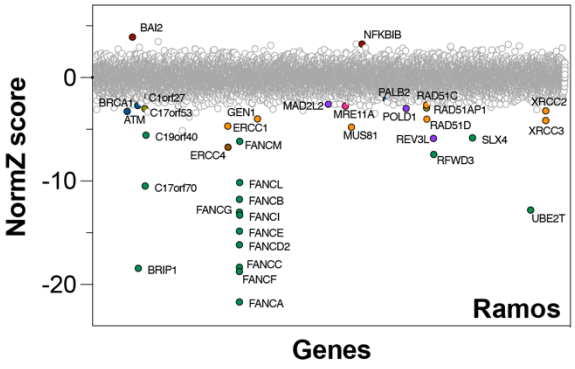
3.3 Results

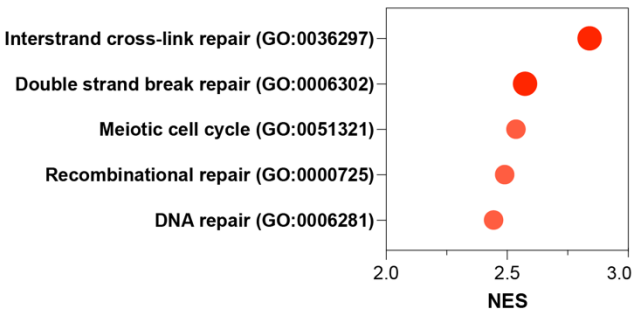
3.3.1 Genome-wide CRISPR screening identified open-reading frames as novel factors involved in the response to mafosfamide.

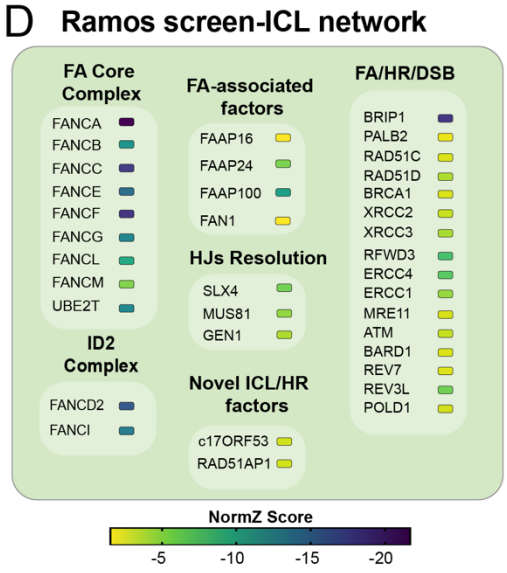
To identify novel factors involved in the response to ICL, we took advantage of the Ramos Burkitt lymphoma cells, which are cultured in suspension and display optimal genome-editing efficiency upon generation of stable Ramos-Cas9 BL cells(**Figure 3.S1A)** and editing assessment(**Figure 3.S1B**) throught the Fam83g assay as described previously [33], making them well suited for high-throughput screening upon ICL-treatment. Thus, we performed a genome-scale CRISPR-based screening (**Figure 3.1A**) in the Ramos Burkitt lymphoma cell line using the TKOv1 gRNA library [34]. We used the cyclophosphamide analog mafosfamide (MAF) as perturbagen, which is known to generate DNA interstrand crosslinks, and used an IC25 concentration(3.09uM) to uncover sensitizers. Quality control of our NGS data was assessed through FastQC and MAGeCK-Count command, overall, all our data displayed optimal coverage (above 0.9) (**Table 3.S1)** of our library in all our samples and adequate number of reads (**Table 3.S2, Figure 3.S1.1**) to assure further robust statistical analysis of our dropout screen. Bioinformatic analysis of our screen data using the MAGeCK [35, 36] and DrugZ [37] algorithms identified well established players in the ICL response (**Figure 3.1B**), including core Fanconi anemia (e.g., FANCA, FANCD2, FANCE, FANCI, FANCM, FANCL, FANCF, FANCB, FANCI, FANCG, UBE2T), HR (BRCA1, BRIP1, PALB2, BARD1) and NER (ERCC1 & ERCC4) factors. Gene ontology (GO) (**Figure 3.1C**) and Gene-set enrichment analyses (GSEA) (**Figure 3.S2 A**) revealed significant pathway enrichment in ICL (GO:0036297, NES=2.84); DSB repair (GO:0006302, NES=2.57), meiotic cell cycle (GO:0051321, NES=2.53), recombinational repair (GO:0000725, NES=2.489) and DNA repair (GO:0006281, NES=2.44). Furthermore, network analysis of genes enriched in GSEA analyses displayed great connectivity between the sensitizer hits involved in ICL and DNA repair processes (**Figure 3.S2 B and C**). Aside from identifying canonical FA proteins and their downstream interconnected repair modules (**Figure 3.1D**), our approach

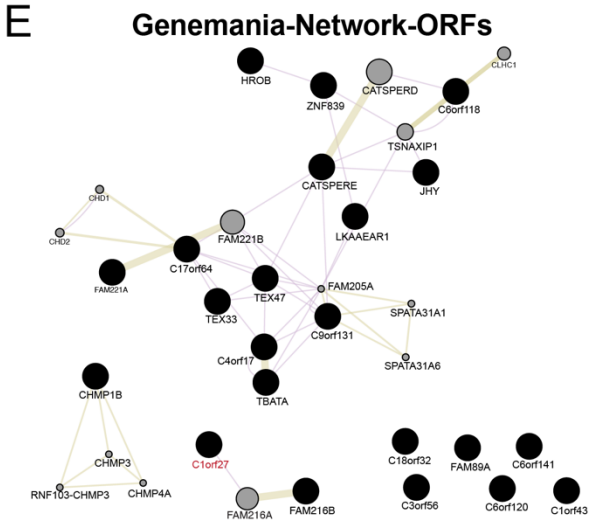
delineated recently described DNA repair factors involved in ICL and telomere maintenance by other groups [17-19, 23, 38-46], including HROB, SLX4IP and RAD51AP1 [17-19, 23, 38-46]. More interestingly, our systematic screening detected a series of open reading frames (**Figure 3.1E**) for which there is scarce or nil information about their ontology and cellular function. Consequently, we focused our attention on these 34 genes for secondary validation, aiming to identify novel genome stability factors.











Pinedo Carpio *et al.* Figure 3.1

Figure 3.1 Genome-wide CRISPR-based dropout screen identifies C1orf27 as a novel regulator of the response against mafosfamide.

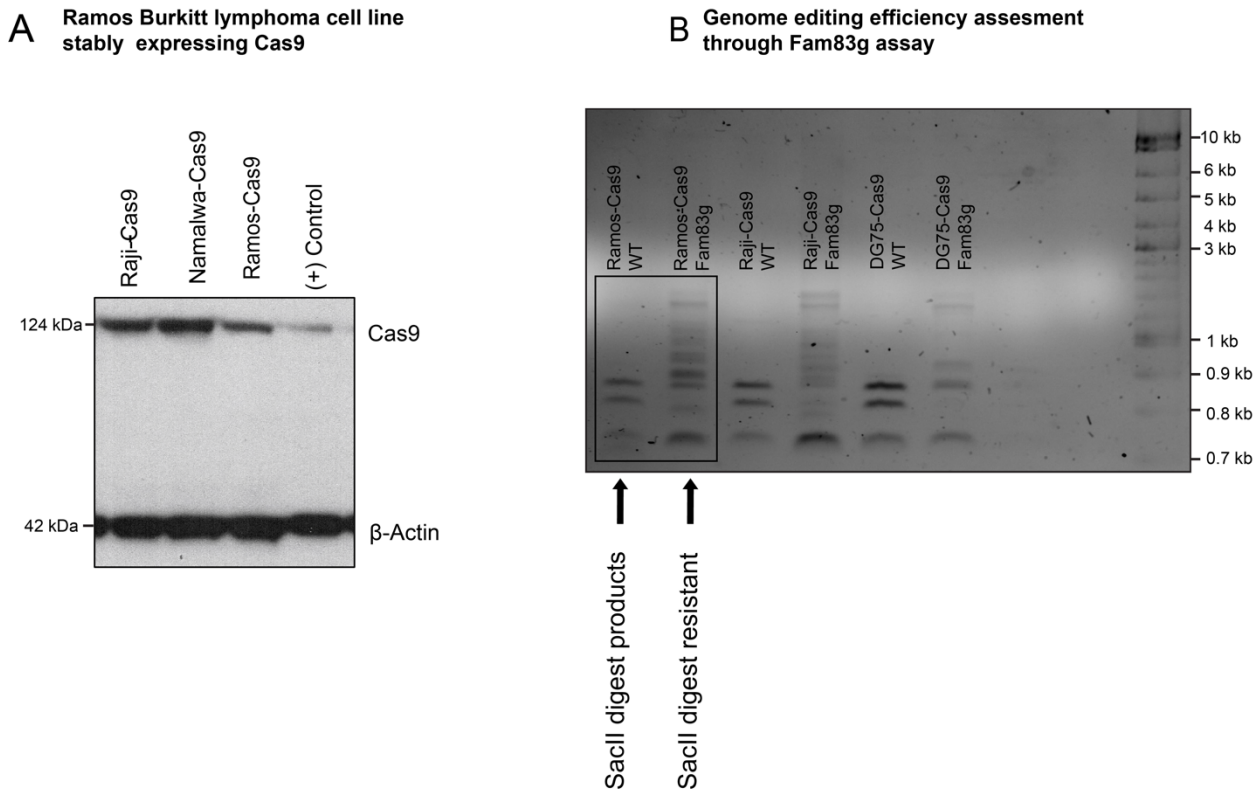
(A) Schematics describing genome-wide CRISPR-Cas9 pipeline and bioinformatic analysis used to obtain screen data and gene-ranking.

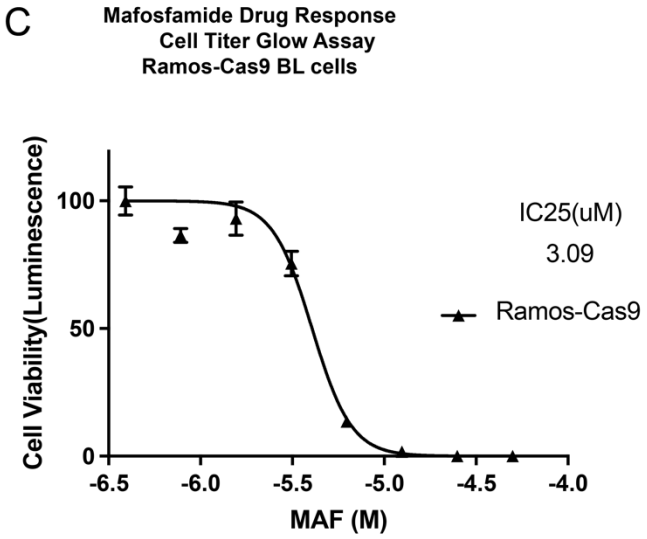
(B) Horizontal plot showing the gene-ranking obtained using the DrugZ algorithm and the positioning of different known and recently characterized hits in specific DNA repair pathways.

(C) GSEA analysis using the ranked gene list in the Ramos screen

(D) Bubble plot displaying FA ICL/HR repair factors identified in Ramos screen.

(E) Genemania-cytoscape network analysis displaying poorly characterized ORFs selected for secondary validation.





Pinedo Carpio *et al.* Figure 3.S1

Figure 3.S1 Additional information about screen parameters assessed for Ramos-Cas9 BL cells used in the Ramos-CRISPR screen related to Figure 3.1.

(A) WCE of Ramos-Cas9 cells analyzed by immunoblot with an anti-Cas9 antibody. Anti-β-actin was used as a loading control.

(B) Genome editing efficiency of Ramos-Cas9 BL cells assessed through Fam83g assay.

(C)Mafosfamide Drug response through Cell Titer Glow assay of Ramos-Cas9 BL cells.

Table 3S1 **Mapped read Statistics-Count Report Ramos Screen**

	Label	Reads	Mapped	Percentage
1	T01_Ram_EPC_90k_R1	29885775	27378198	0.92
2	T02_Ram_EPC_90k_R1	154881196	141786512	0.92
3	T03_Ram_EPC_90k_R1	100627989	92182178	0.92
4	T14M1_Ram_EPC_90k_R1	175869210	159836158	0.91
5	T14M2_Ram_EPC_90k_R1	98300561	89454553	0.91
6	T14M3_Ram_EPC_90k_R1	121024379	110349190	0.91
7	T14V1_Ram_EPC_90k_R1	86528599	78767669	0.91
8	T14V2_Ram_EPC_90k_R1	138603556	126315302	0.91
9	T14V3_Ram_EPC_90k_R1	104487624	95052703	0.91

Table 1: Summary of comparisons

Table 3S2 **Zero counts and Gini-Index Statistics-Count Report Ramos Screen**

	Label	TotalsgRNA	ZeroCounts	GiniIndex
1	T01_Ram_EPC_90k_R1	91320	1128	0.10
2	T02_Ram_EPC_90k_R1	91320	1022	0.08
3	T03_Ram_EPC_90k_R1	91320	1083	0.09
4	T14M1_Ram_EPC_90k_R1	91320	1809	0.10
5	T14M2_Ram_EPC_90k_R1	91320	1910	0.10
6	T14M3_Ram_EPC_90k_R1	91320	1844	0.10
7	T14V1_Ram_EPC_90k_R1	91320	1730	0.10
8	T14V2_Ram_EPC_90k_R1	91320	1736	0.10
9	T14V3_Ram_EPC_90k_R1	91320	1780	0.10

Table 2: Summary of comparisons

Figure 3S1.1 **Normalized read count distribution of all samples.**

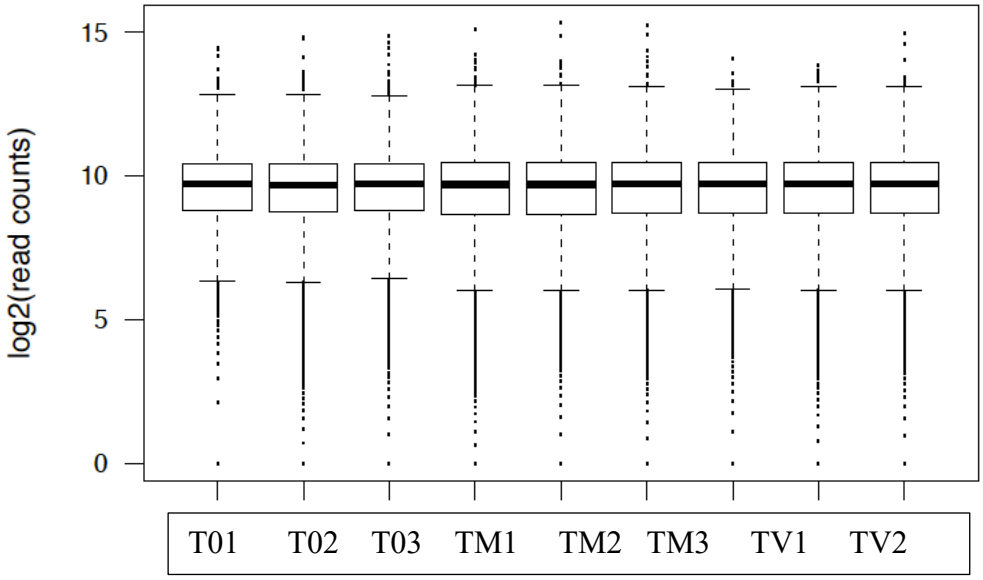


Table 3.S1 and Table 3.S2 Coverage assessment of Ramos CRISPR screen.

Tables were obtained using the MAGeCK count command and they display the number of reads obtained for each replicate for each condition and the number of reads mapped to the reference library. In addition, in Table 3.S2, the ZeroCounts and GiniIndex indicate the amount of sgRNA that were not mapped in the analysis.

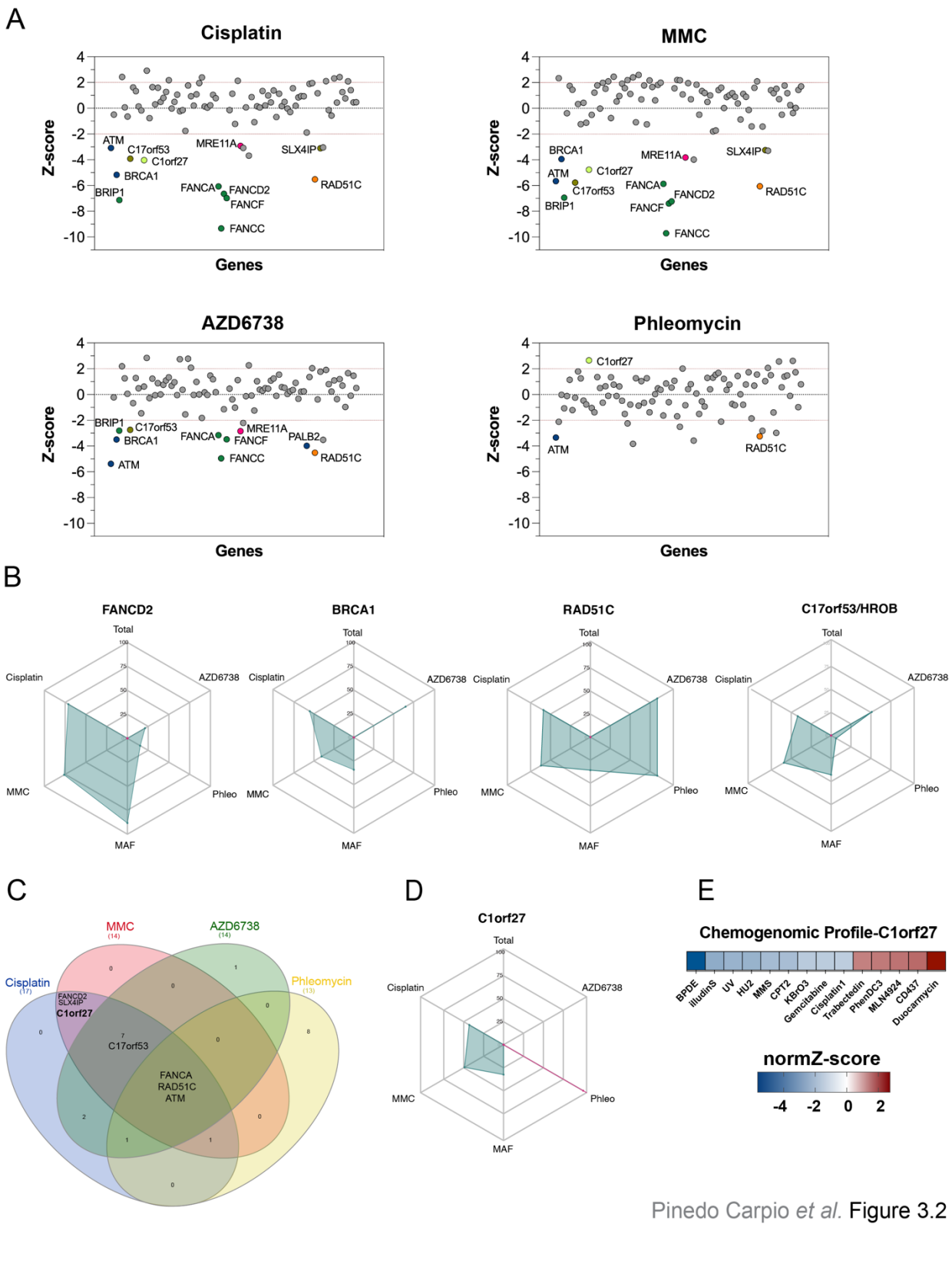
Figure 3.S1.1 Normalized read count distribution of all samples.

Figure was obtained using the MAGeCK count command and the box plot diagram displayed the normalized read count distribution obtained for all the samples for each condition. T01, T02, T03 represent the initial time point; TM1, TM2 and TM3 represent the treated (Mafosfamide IC25) conditions and TV1, TV2 and TV3 represent the vehicle control condition.

3.3.2 Secondary validation positioned C1orf27 as novel factor involved in the response to ICL.

To conduct our secondary validation, we designed a customized sgRNA library focused on our ORFs of interest with between 4 individual sgRNA for each gene tested, alongside positive (e.g., FANCA. FANCD2, RAD51C, BRCA1, MRE11 and ATM), negative (e.g., BAI2, PI3KCD & PAX5) and non-targeting sgRNAs as controls. Negative controls were chosen based on their original DrugZ normZ score obtained in the genome wide Ramos screen. To gain better insight into the contribution of these ORFs in the maintenance of genome stability, we employed a series of drugs that rely on distinct DNA repair pathways, including the intercalating agents mitomycin C (MMC) and cisplatin, the radiomimetic drug phleomycin and the ATR inhibitor AZD6738. We conducted these mini-screens using optimized IC25 concentrations (**Figure 3.S2.1**) of drugs (MMC IC25 = 0.24 uM; Cisplatin IC25 = 2.29 uM; Phleomycin IC25 = 8.4 uM; AZD6738 IC25 = 0.57uM) and using the Ramos-Cas9 Burkitt lymphoma cell line as cellular model, as previously described. As expected, bioinformatic analysis of our mini-screens using the MAGeCK algorithm showed that well established FA factors (e.g., FANCA, FANCD2, FANCC and FANCF) modulate the response to both MMC and cisplatin (**Figure 3.2 A-B).** Similarly, HR factors (e.g., BRCA1, MRE11, RAD51C and BRIP1) displayed a sensitizer profile in MMC, cisplatin and ATR-inhibitor miniscreens respectively, suggesting our targeted approach worked well. Interestingly, C1or27 emerged as a strong sensitizer in both MMC and cisplating mini-screens, suggesting a pan-ICL contribution of this ORF (**Figure 3.2 C**). Furthermore, we noticed that C1orf27 provided a striking resistance profile in our phleomycin mini-screen (**Figure 3.2 D**), suggesting a modulated role depending on the type of DNA damage used and the depletion of this factor. To cross validate our screen data, we took advantage of publicly available CRISPR screens conducted in presence of fourteen different genotoxic agents [47]. Chemogenomic profiling analysis showed that C1orf27 displayed a remarkable sensitizer profile in several screens conducted in the non-transformed RPE1-hTERT cell line (**Figure 3.2 E**). Targeting C1orf27 sensitized RPE1-

hTERT cells to benzo(a)pyrene diol epoxide (BPDE), IlludinS, ultraviolet light (UV), Hydroxyurea (HU) , Methyl Metanesulfonate (MMS), Camptothecin (CPT) and Cisplatin; drugs characterized for causing helix distorting lesions, replication stress and base alkylation . More interestingly, we noticed that loss of C1orf27 provided resistance to several alkylators and DNA synthesis inhibitors, such Duocarmycin SA, CD437, MLN4924, PhenDC3 and Trabectedin, in line with our phleomycin-based mini-screen data (**Figure 3.2 A)** in which C1orf27 display a resistance profile as well. This chemogenomic profile of C1orf27 suggests that this factor may play specific roles depending on type of lesions caused by different genotoxic agents. Altogether our findings suggest that C1orf27 may be a novel player involved in the response to DNA damage under different genotoxic conditions.



Pinedo Carpio *et al.* Figure 3.2

Figure 3.2 Secondary validation using targeted CRISPR-based screens and DNA damaging agents position C1orf27 as novel factor involved in ICL repair and replication stress.

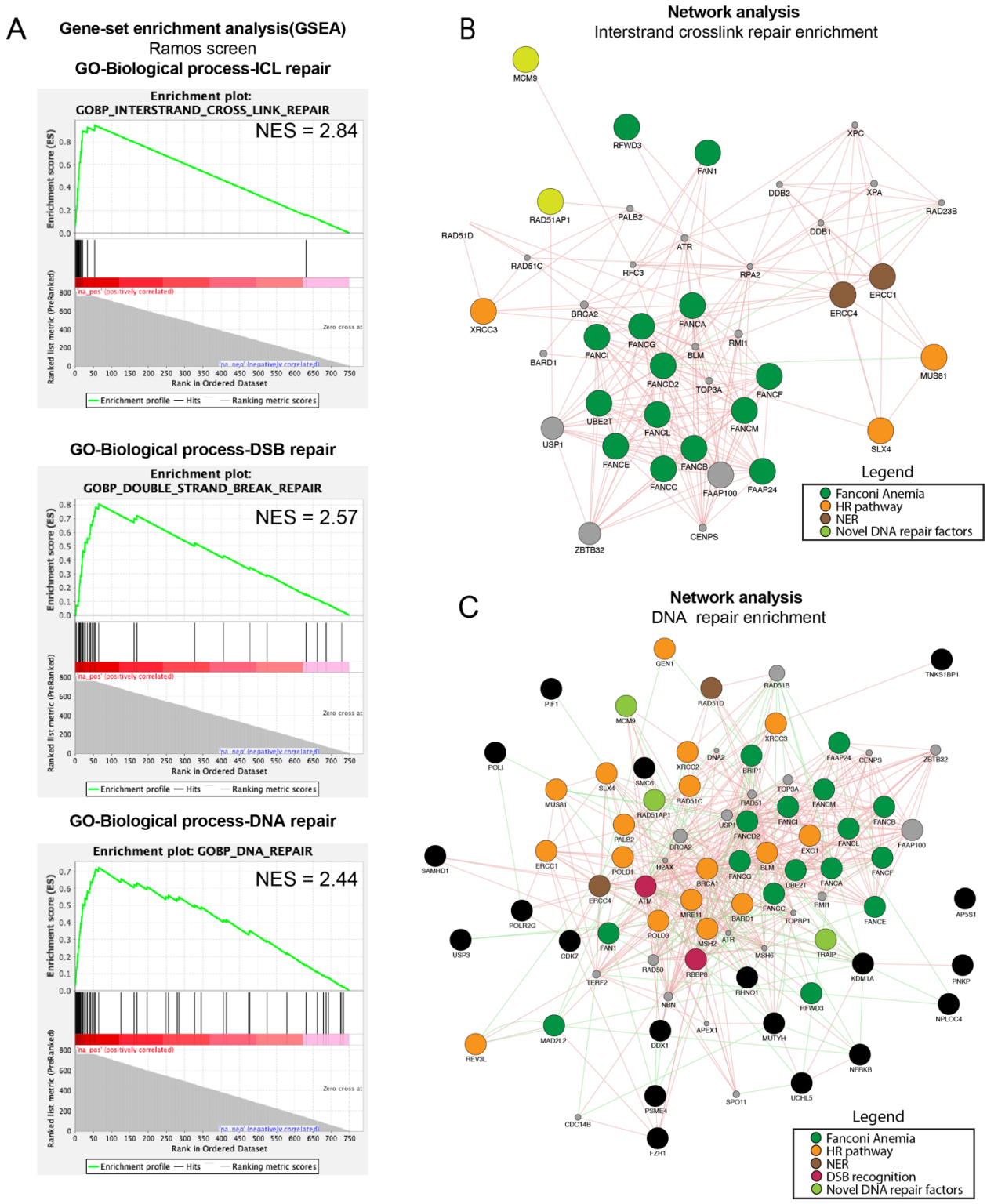
(A) Horizontal plots exhibiting the gene-ranking obtained in each mini-screen using MAGeCK MLE and displaying the sensitizers profile of our control genes and top assessed hits.

(B) Radar plots displaying sensitizer profile for different controls used in our screening strategy for all executed mini-screens and the genome-wide Ramos screen (MAF) respectively.

(C) Venetian plot displaying the intersection of hits among different mini screens.

(D) Radar plot displaying the pan- ICL sensitizer profile obtained for C1orf27 and its resistance profile under phleomycin treatment.

(E) Chemogenomic profiling of C1orf27 using the Durocher's genome-wide screens data in RPE1-htert cells which shows a sensitizer profile upon the usage of several agents targeting replication stress and ICL, along with an interesting resistance profile upon treatment with alkylators and DNA synthesis inhibitors.



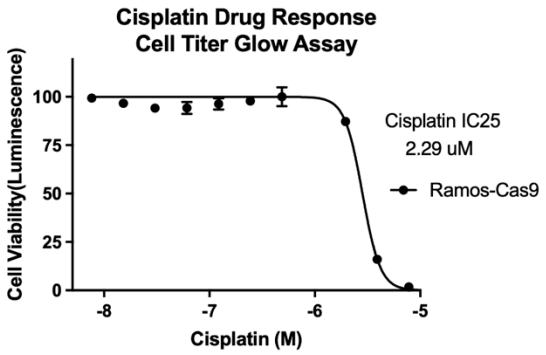
Pinedo Carpio *et al.* Figure 3.S2

Figure 3.S2 Gene-set enrichment Analysis (GSEA) and Network analysis of Ramos screen.

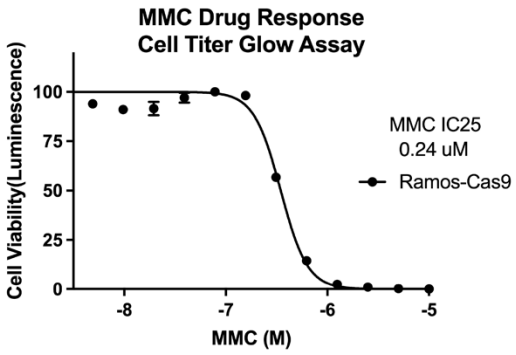
(A) Gene Set Enrichment Analysis (GSEA) analysis of the DrugZ normZ score obtained in the Ramos screen for ICL repair, DSB and DNA repair enrichments.

(B) & (C) Network analysis displaying protein physical and genetic interactions for genes enriched in Ramos GSEA analysis for ICL and DNA repair enrichment using Cytoscape and the GeneMANIA package.

A



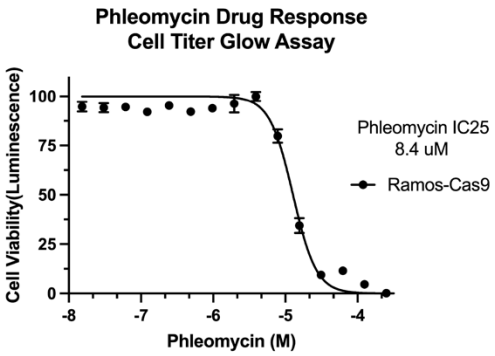
B



C



D



Pinedo Carpio *et al.* Figure 3.S2.1

Figure 3.S2.1 Additional information related to Ramos-Cas9 miniscreens parameters.

(A) Cisplatin Drug response through Cell Titer Glow assay of Ramos-Cas9 BL cells.

(B) Mitomycin-C Drug response through Cell Titer Glow assay of Ramos-Cas9 BL cells.

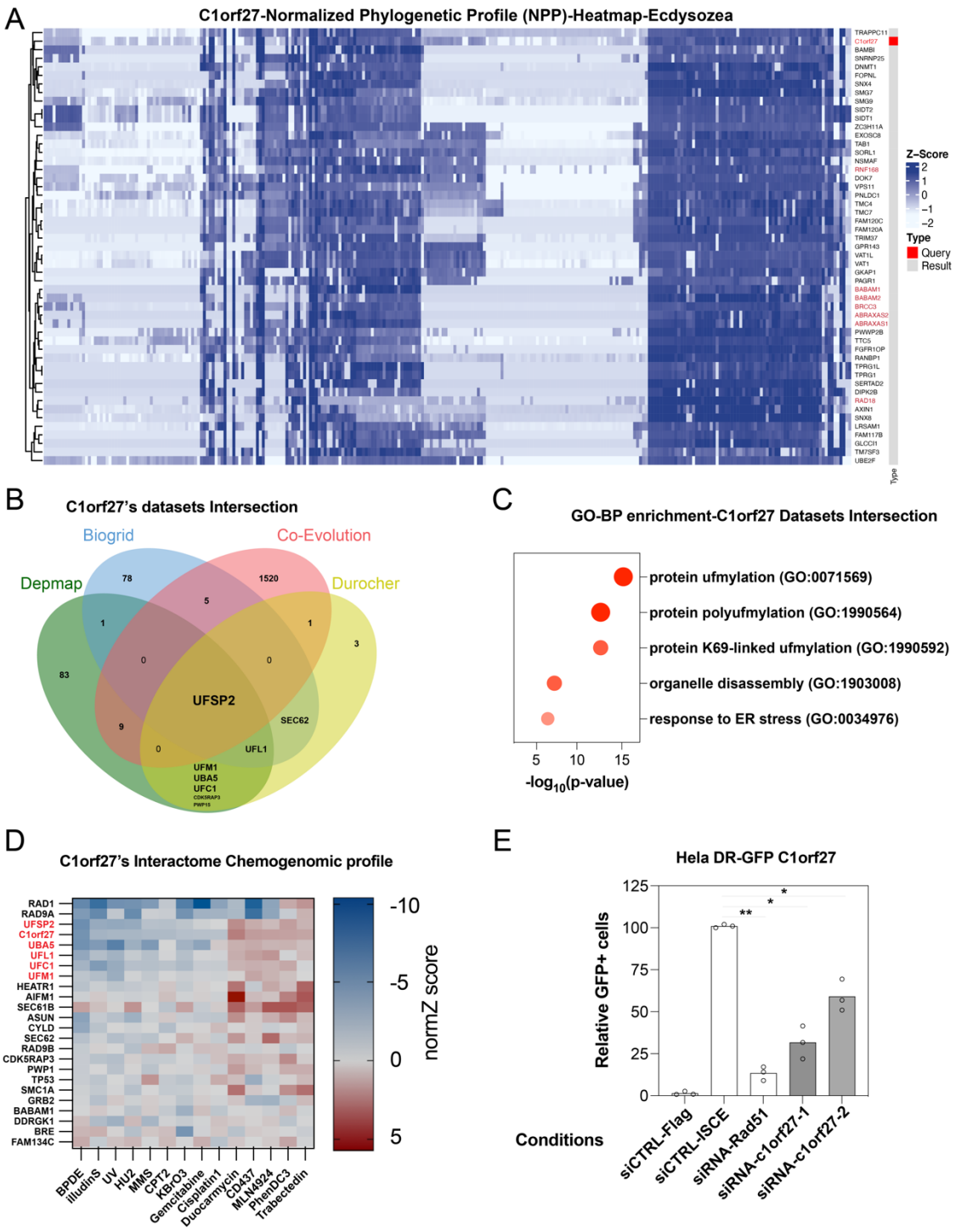
(C) AZD6738(ATR inhibitor) Drug response through Cell Titer Glow assay of Ramos-Cas9 BL cells.

(D) Phleomycin Drug response through Cell Titer Glow assay of Ramos-Cas9 BL cells.

3.3.3 Multiomics data integration analysis delineated C1orf27 as a novel factor involved in the UFM1 pathway.

To delineate the biological contribution of C1orf27, we used a clade-wise phylogenetic profiling (PP) tool CladeOScope, which has been previously shown to uncover functional interactions between genes and associated them with characterized pathways [48]. Interestingly, we observed that C1orf27 co-evolved with several factors involved in the regulation of the DNA damage response in the Ecdysozea (**Figure 3.3 A**), including the E3 Ubiquitin ligases RNF168 and RAD18 as well as several members of the BRISC complex (BABAM1-2, BRCC3, ABRAXAS1-2), indicative of a potential role of C1orf27 in this DNA repair cellular response. GO analysis of these gene set list revealed enrichment in protein K63-deubiquitination (GO:0070536, p=4.11E-04), regulation of DNA repair (GO:0006282, p=7.20E-04) and DSB repair via NHEJ (GO:0006303, p=0.001073701), among other DNA repair-related ontologies (**Figure 3.S3 A**). To further expand our understanding of C1or27, we performed an integrated analysis of publicly available genomic and proteomic datasets in which this factor was found as a hit of interest or prey respectively, along with CRISPR-based screen dependency data from the Depmap project and chemogenomic profiling information from drug-based synthetic lethal screening co-dependencies [47]. This integrated analysis allowed us to obtain a Venn plot displaying common proteins among these C1orf27-related datasets (**Figure 3.3 B**). GO analysis revealed a significant pathway enrichment in protein UFMylation (GO:0071569, p= 6.81E-16); protein poly-UFMylation (GO:1990564, p= 2.27E-13) and protein K69-linked UFMylation (GO:1990592, p= 2.27E-13) (**Figure 3.3 C**), suggestive of a potential link between C1orf27 and this poorly understood ubiquitin-like post-translational modification. Indeed, our multi-omics data integration analysis identified the cysteine protease UFSP2 as a common denominator between these different datasets (**Figure 3.3 B**). UFMylation is a ubiquitylation process regulated by ubiquitin-like proteins and controlled by the ubiquitin-fold modifier 1 (UFM1), the UFM1-activating enzyme UBA5,

the UFM1-conjugating enzyme UFC1 and the UFM1-specific ligase 1 (UFL1). UFM1 chains can be cleaved by UFM1-specific proteases, named UFSPs, making UFMylation a reversible process (UFM1 pathway described in detail in Figure II of Chapter 1). Chemogenomic profiling of the different players involved in UFMylation showed striking similarities with C1orf27**.** For instance, targeting UFSP2, UBA5, UFL1, UFC1 and UFM1 sensitized RPE1-hTERT cells to BPDE, IlludinS, UV, HU, MMS & CPT, which phenocopies C1orf27 profile and allows for a strong clustering of these factors in our chemogenomic profiling analysis (**Figure 3.3 D**). Our CRISPR-based screen data, along with our chemogenomic profiling and co-evolution assesment, suggest a potential role of C1orf27 in DNA repair. To assess this hypothesis, we used the Hela DR-GFP reporter cell line to measure DNA repair through homologous recombination (HR). Depletion of C1orf27 using two different siRNAs resulted in a significant impairment of HR potential (**Figure 3.3 E**), in particular siRNA 1, which effectively depletes C1orf27 protein levels, as determined by immunoblotting analysis (**Figure 3.S3 B**). These results indicate a potential role of C1orf27 in the normal functioning of homologous recombination independent of genotoxic stress caused by ICL agents. Like most of protein modification involved in DNA repair such as Ub or SUMO, we speculate that this role is probably linked to a UFM1-related regulatory function of this protein over a key factor directly involved in the repair of this type of lesion. Altogether, these data suggest that C1orf27 may be a novel player in the UFMylation protein modification, and its role in the regulation the DNA damage, in particular DNA interstrand crosslink repair, may be related to its regulatory function of homologous recombination downstream of the DSB originated during replication-related DNA damaging events such as ICL.



Pinedo Carpio *et al.* Figure 3.3

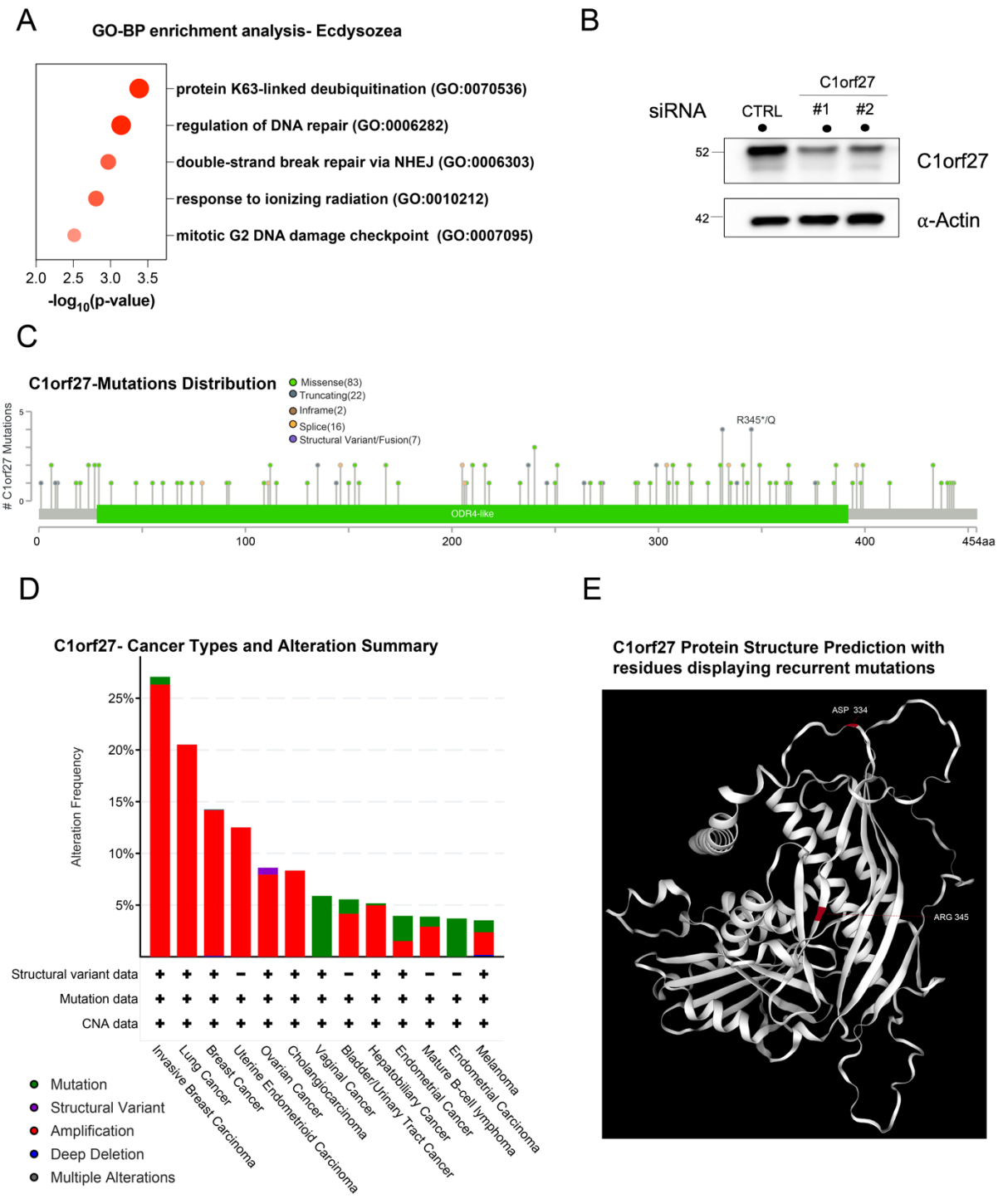
Figure 3.3 Multiomics analysis of C1orf27 and its potential role in Homologous recombination.

(A) Heatmap displaying the normalized phylogenetic profile (NPP) within the Ecdysozea clade obtained for C1orf27 using CladeOScope; co-evolved partners with a well described role in DNA repair are highlighted in red.

(B)Venn diagram displaying the factors that intersected between different omics C1orf27 datasets.

(D) Gene ontology analysis for biological processes performed in the gene set obtained after integrating multiple C1orf27 datasets, which revealed a significant enrichment for UFMylation ontologies for C1orf27 interactome partners.

(E)Quantification of GFP-positive HeLa cells depleted from Rad51or C1orf27. Cells were plated in 6-well plates at density of 100, 000 cells per well. Twenty-four hours later, cells were transfected with indicated siRNA. The following day, cells were transfected with the I-SceI expression plasmid or an empty vector. Data are representation of the means ± SEM; N= 3 Biological replicates. At least 30,000 cells were acquired and quantified per experiment in each condition. Statistical significance was obtained using a one-way Anova test and Dunnet's multiple comparison test.



Pinedo Carpio *et al.* Figure 3.S3

Figure 3.S3 Additional information of multiomics, mutational, DR-GFP assay and protein structure analysis of C1orf27.

(A) Gene ontology analysis for biological processes performed in C1orf27 and Ecdysozea-clade co-evolved factors, which displayed an enrichment for DNA repair ontologies.

(B)WCE of Hela DR-GFP cells depleted or not for C1orf27 were analyzed by immunoblotting with an anti-C1orf27 antibody. Anti-β-actin was used as a loading control.

(C)Lollipop schematics displaying frequency and type of mutations reported in cBioportal database for C1orf27 across its full-length protein structure. A total of 130 variants of uncertain significance (VUS) is reported.

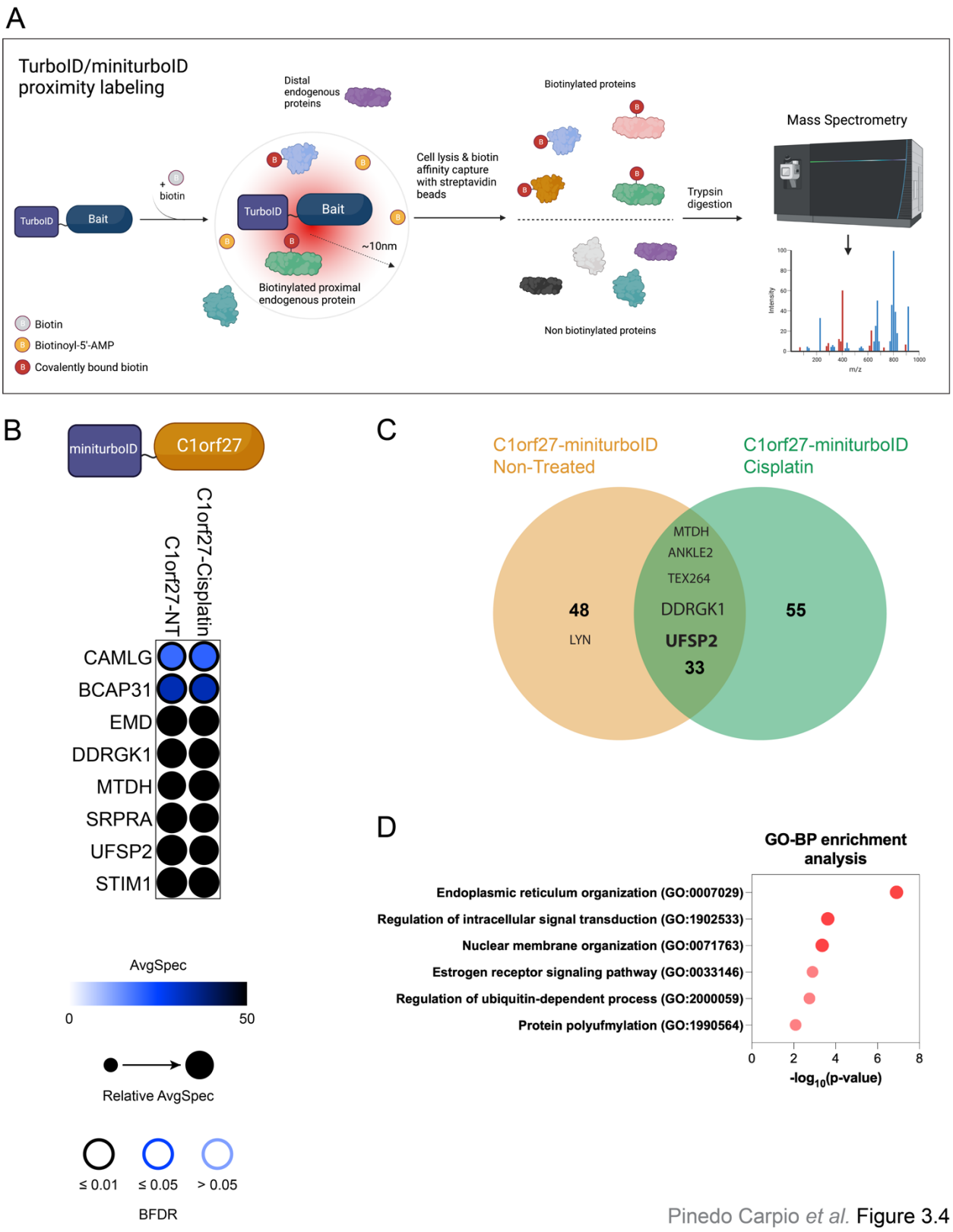
(D) Bar graph describing cancer types and C1orf27 mutations reported for each malignancy obtained from cBioportal mutation database with a minimum of 10 cases as threshold analysed.

(E)C1orf27 protein structure model prediction obtained through AlphaFold displaying residues with the most recurrent mutations reported in cBioportal: ARG 345(5 cases) and ASP 334(4 cases).

3.3.4 C1orf27 interacts with UFSP2, and they collaborative operate in the UFM1 pathway.

To elucidate the potential role of C1orf27 in the UFM1 pathway and DNA repair, we mapped its proximal interactome using the biotinylation-based proximity labeling technology miniturboID [49](**Figure 3.4 A& B**). Briefly, C1orf27 was tagged at its N-terminus with the biotin ligase miniturboID and stably expressed in HEK293 Flp-In^{TM}cells. The fused protein was assessed for its capacity to properly biotinylate proximal factors, this validation was conducted by immunoblotting analysis (**Figure 3.S4 A**). The proximal interacting networks of C1orf27 were generated in both cells left untreated (steady state) and cells treated with the ICL-agent Cisplatin at 2uM for 3 hours. A total of 81 high-confidence C1orf27 interacting factors obtained in 3 technical replicates were identified at steady conditions (AvgP score >0.5 &Fold-change >3.5), and 88 high-confidence factors upon ICL-induced DNA damage with Cisplatin (AvgP score >0.5 &Fold-change >3.5). To determine stable C1orf27 interacting factors identified in both conditions, we conducted an intersection of high-confidence preys and obtained a total of 33 shared factors (**Figure 3.4 C**). Using this approach, we identified key factors previously described in the UFM1 pathway such as the peptidase UFSP2 [50-54] and the substrate adapter for UFMylation DDRGK1 [29, 55]. In addition, we identified factors involved in cellular processes localized in the ER or important for its proper functioning, such as CAMLG [56], BCAP31 [57], STIM1 [58], which is in line with previous reports linking UFMylation to the ER cellular compartment [28, 51, 59-62]. Interestingly and aligning with our hypothesis that C1orf27 is involved in DNA repair and preservation of genome integrity, we also identified stable interacting factors involved in nuclear envelope integrity such as ANKLE2 [63], EMD [64] and TOR1AIP1 [65], along with TEX264, a novel factor recently described to conform a complex with p97 and SPRTN, which is reported to be involved in DNA-protein crosslink(DPC) and replication stress repair [66]. The interaction between C1orf27 and UFSP2 has been previously reported in an affinity-capture mass spectrometry study [67], a CRISPR-based functional genomics study [68], and a

report of C1orf27's ortholog (ODR4) in *C.elegans* [69], which strongly supports our findings. Gene ontology (GO) analysis (**Figure 3.4 D**) on the subset of stable 33 C1orf27's interacting partners revealed a significant pathway enrichment in Endoplasmic reticulum organization (GO:0007029, p= 1.24E-07), Nuclear membrane organization (GO:0071763, p=4.44E-04), regulation of Estrogen-receptor signaling (GO:0033146, p= 0.001269534) and protein poly-UFMylation (GO:1990564, p= 0.008223548). Altogether, our proteomic data strongly suggest that C1orf27 and UFSP2 are constitutive interacting partners, and they play a cooperating role in UFMylation under normal physiological conditions and their interaction is also important under genotoxic stress conditions such as ICL-induced DNA damage.



Pinedo Carpio *et al.* Figure 3.4

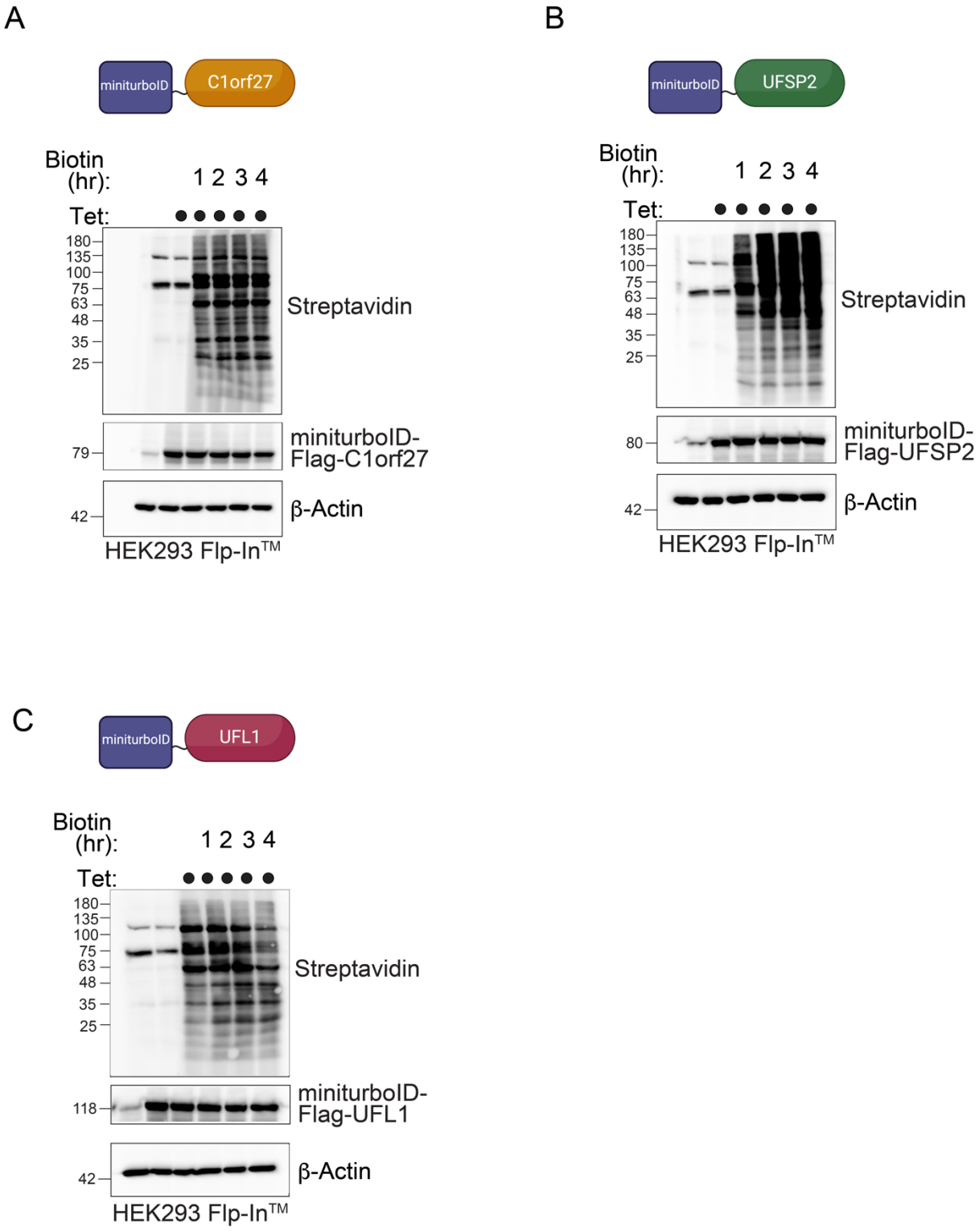
Figure 3.4 C1orf27 interacts with UFSP2, and they collaborative operate in the UFM1 pathway.

(A) Schematics describing the pipeline conducted using miniturboID proximity labeling.

(B) Dot plot analysis displaying high-confidence proximal interactors of C1orf27 identified by miniturboID, under steady conditions or in cells treated with the ICL-inducing agent Cisplatin. The spectral counts for each captured prey are shown as AvgSpec. The circle size represents the relative abundance of preys and the node edge color corresponds to the Bayesian False Discovery Rate (BFDR).

(C)Venn diagram displaying the intersection of high-confidence preys identified in treated and untreated cells. A total of 33 shared stable interacting partners of C1orf27 were identied including the peptidase UFSP2.

(D)Gene ontology for biological processes (GO-BP) diagram derived from the intersection proteomic datasets under treated and untreated conditions, which results in a dataset of 33 shared stable interacting factors of C1orf27. Size of the circle indicates the number of 33 common factors enriched withing a respective ontology.



Pinedo Carpio *et al.* Figure 3.S4

Figure 3.S4 Biotinylation and fusion-protein expression assessment of C1orf27-, UFSP2- and UFL1-miniturboID stable cells.

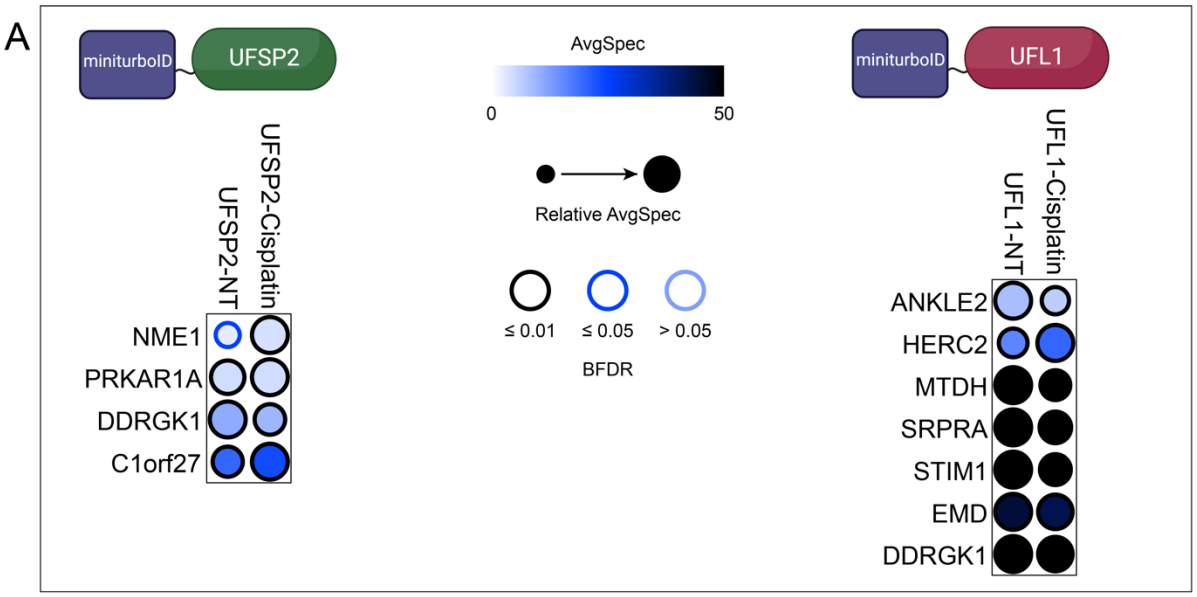
(A); (B) and (C) WCE of HEK293T Flp-In™ cells expressing fused protein with miniturboID, upon induction or not with 1uM tetracycline and supplemented with exogenous Biotin at 50uM. WCE were analyzed by immunoblotting with anti-streptavidin and anti-Flag antibodies. Anti-β-actin was used as a loading control.

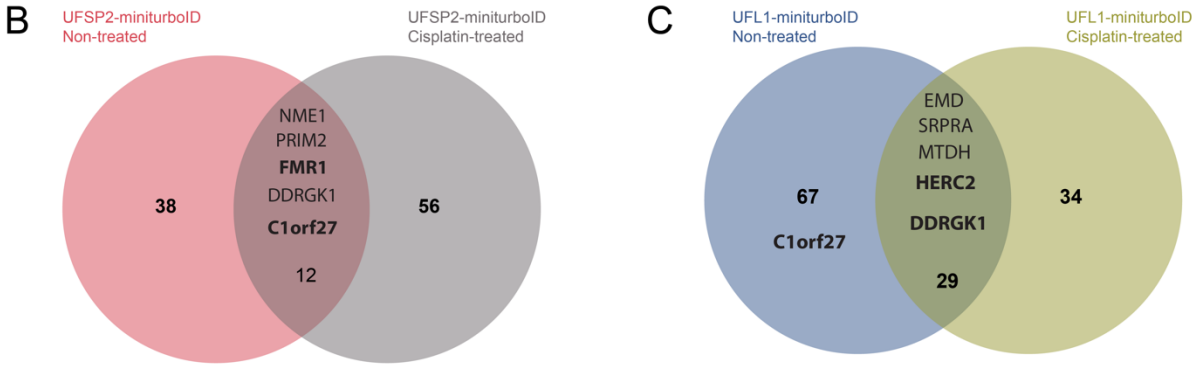
3.3.5 Probing the UFM1 protein network upon ICL damage through miniturboID proximity labeling.

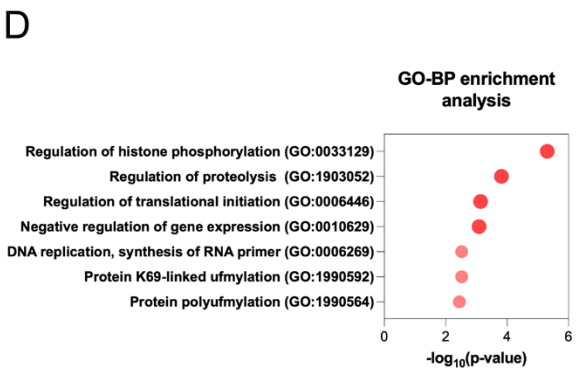
To further expand our knowledge of the protein network involved in the UFM1 pathway and further characterized the potential role of C1orf27 and its top interacting factor UFSP2, we conducted miniturboID proximity labeling proteomics in fused proteins of the peptidase UFSP2 and the E3-ligase involved in this pathway: UFL1. We decided to first target these two canonical UFM1-related factors to assessed both the positive and negative dynamics occurring in this pathway and its potential crosstalk with the role of C1orf27 and ICL repair. To preserve the same conditions under which C1orf27 proximity interactome was retrieved, we employed the same drug (Cisplatin) and biotinylating conditions. Briefly we generated stable HEK293 Flp-In^{TM}cells in which UFSP2 or UFL1 were tagged at their N-terminus with the biotin ligase miniturboID. The fused proteins were assessed for their capacity to properly biotinylate proximal factors, and these validations were conducted by immunoblotting analysis as previously described (**Figure 3.S4, B & C)**). The proximal interacting networks of UFSP2 and UFL1 were generated in both cells left untreated (steady state) and cells treated with the ICL-agent Cisplatin at 2uM for 3 hours. In the analysis of UFSP2 proximal interactome, a total of 50 high-confidence UFSP2 interacting factors obtained in 3 technical replicates were identified at steady conditions (AvgP score >0.5 & Fold-change >13), and 68 high-confidence factors upon ICL-induced DNA damage with Cisplatin (AvgP score >0.5 & Fold-change >6). Top high confidence interacting partners of UFSP2 are displayed in a dot plot analysis (**Figure 3.5 A**). To determine stable UFSP2 interacting factors identified in both conditions, we conducted an intersection of high-confidence preys and obtained a total of 12 common factors which are displayed in a Venn diagram (**Figure 3.5 B**). We reasoned that these 12 common stable factors are constitutive interacting parteners of UFSP2, among these preys we identified C1orf27, which reciprocally validated our previous results, and strengthens our dual proteomic findings. Moreover, is it plausible that these two

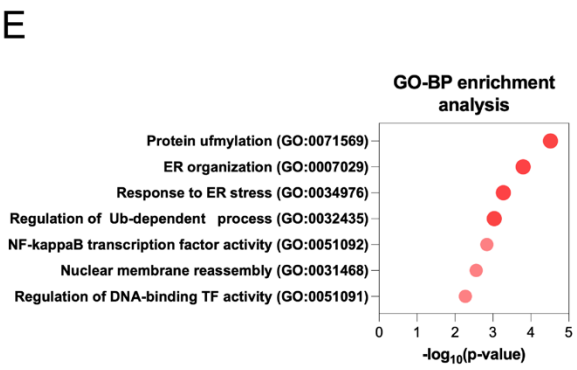
factors may conform a stable protein-complex which is stable at steady conditions and remains operative under ICL-induced DNA damaging conditions. In addition, we identified the adapter for UFMylation DDRGK1, which we previously captured as stable factor for C1orf27, this consistent result a potential cooperative role of these three factors in the UFM1 pathway. Moreover, we also identified NME1, as stable constitutive interacting partner of UFSP2. NME1(aka NM23-H1) is a endonuclease activated by Granzyme A(GzmA) [70] and is a core component of the SET complex involved in GzmA-mediated DNA damage. Interestingly, when GzmA is delivered into a target cell, the SET complex, which normalize reside in the ER compartment, is translocated into the nucleous, and participates in the oxidative stress response [71]. Altogether, this data regarding UFSP2 and NME1, points to a potential crosstalk between the UFMylation pathway and the oxidative stress response in which the SET complex is involved. Gene ontology (GO) analysis (**Figure 3.5 D**) on the subset of stable 12 UFSP2's interacting partners revealed a significant pathway enrichment in positive regulation of Histone phosphorylation (GO:0033129, p= 4.94E-06), regulation of proteolysis (GO:1903052, p=1.52E-04), Protein K69-linked UFMylation (GO:1990592, p= 0.002996653) and protein poly-UFMylation (GO:1990564, p= 0.002996653). In the analysis of the proximal interactome of the E3 ligase UFL1, we identified a total of 96 high-confidence UFL1 interacting factors obtained in 3 technical replicates were identified at steady conditions (AvgP score >0.5 & Fold-change >3), and 63 high-confidence factors upon ICL-induced DNA damage with Cisplatin (AvgP score >0.5 & Fold-change >13). Top high confidence interacting partners of UFL1 are displayed in a dot plot analysis (**Figure 3.5 A**). Following our previously employed methodology with C1orf27 and UFSP2, and ir order to determine stable UFL1 interacting factors identified in both conditions, we conducted an intersection of high-confidence preys and obtained a total of 29 common factors which are displayed in a Venn diagram (**Figure 3.5 C**). Among these 29 constitutive interacting factors of UFL1 we identified ANKLE2, MTDH and DDRGK1, which were previously identified in the C1orf27's

proteomic analysis. These consistent results using two different baits suggest that these factors are constitutive members of the same cellular process in which C1orf27 and UFL1 commonly participate, which we speculate is UFMylation. In addition, to these factors, we identified the E3 ubiquitin-protein ligase HERC2. Interestingly, HERC2 has been previously reported to be a key E3 ligase involved in excision repair upon Cisplatin-induced DNA damage [72], as a maintenance mediator of RNF168 levels [73, 74], negative regulator of BRCA1 [75], and key coordinator of ubiquitin-dependent assembly of DNA repair factors in damaged chromosomes [74]. Finally, we identified C1orf27 as a interacting factor of UFL1 at steady conditions but not upon Cisplatin-induced DNA damage, suggesting of a differential role of these factor under genotoxic stress. Gene ontology (GO) analysis (**Figure 3.5 E**) on the subset of stable 29 UFL1's interacting partners revealed a significant pathway enrichment in protein UFMylation(GO:0071569, p= 3.03E-05), ER organization (GO:0007029, p=1.592E-04), response to ER stress(GO:0034976, p= 5.32E-04) and regulation of proteasomal Ub-dependent protein catabolic process (GO:0032435, p= 9.19E-04). Altogether, out UFL1 proteomic data strongly suggest towards a link of the UFMylation pathway, and the oxidative stress response initiated in the ER compartment. The antagonistic crosstalk between the positive regulation of the UFM1 pathway through the activity of the E3 ligase UFL1 and the proposed negative regulation controlled by the C1orf27-UFSP2 axis remains to be further clarified though functional experiments.









Pinedo Carpio *et al.* Figure 3.5

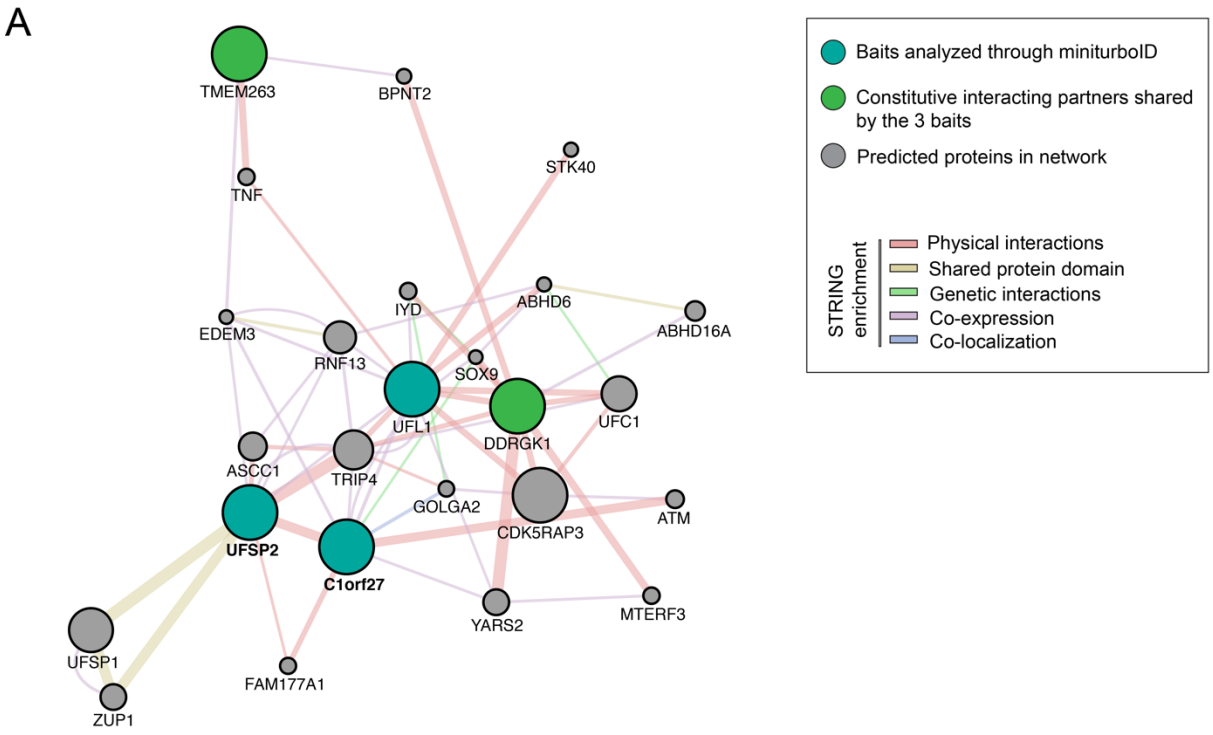
Figure 3.5 Probing the UFM1 protein network upon ICL damage through miniturboID proximity labeling.

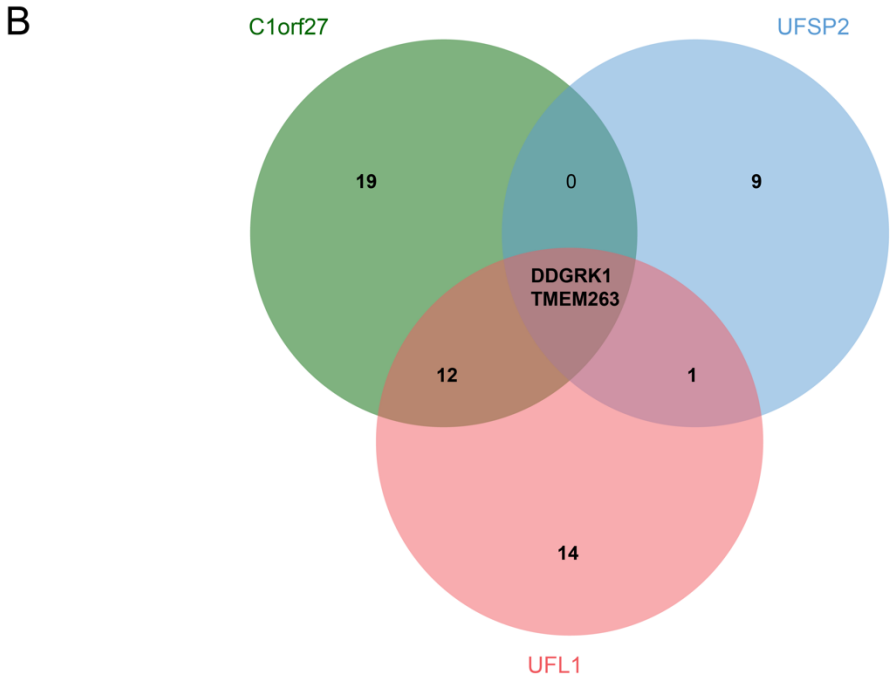
(A) Dot plot analysis of the top high-confidence proximal interactors of UFSP2 and UFL1 identified by miniturboID, under steady conditions or in cells treated with the ICL-inducing agent Cisplatin. The spectral counts for each captured prey are shown as AvgSpec. The circle size represents the relative abundance of preys and the node edge color corresponds to the Bayesian False Discovery Rate (BFDR).

(B)Venn diagram displaying the intersection of high-confidence preys identified in treated and untreated UFSP2-miniturboID cells. A total of 12 shared stable interacting partners of UFSP2 were identified including C1orf27.

(C)Venn diagram displaying the intersection of high-confidence preys identified in treated and untreated UFL1-miniturboID cells. A total of 29 shared stable interacting partners of UFL1 were identified. C1orf27 was identified as interacting factor only at steady conditions.

(D) and (E)Gene ontology for biological processes (GO-BP) diagram derived from the intersection proteomic datasets under treated and untreated conditions in both UFSP2- and UFL1-miniturboID cells.





Pinedo Carpio *et al.* Figure 3.S5

Figure 3.S5 Integrative analysis of the proximal interactomes of C1orf27, UFSP2 and UFL1.

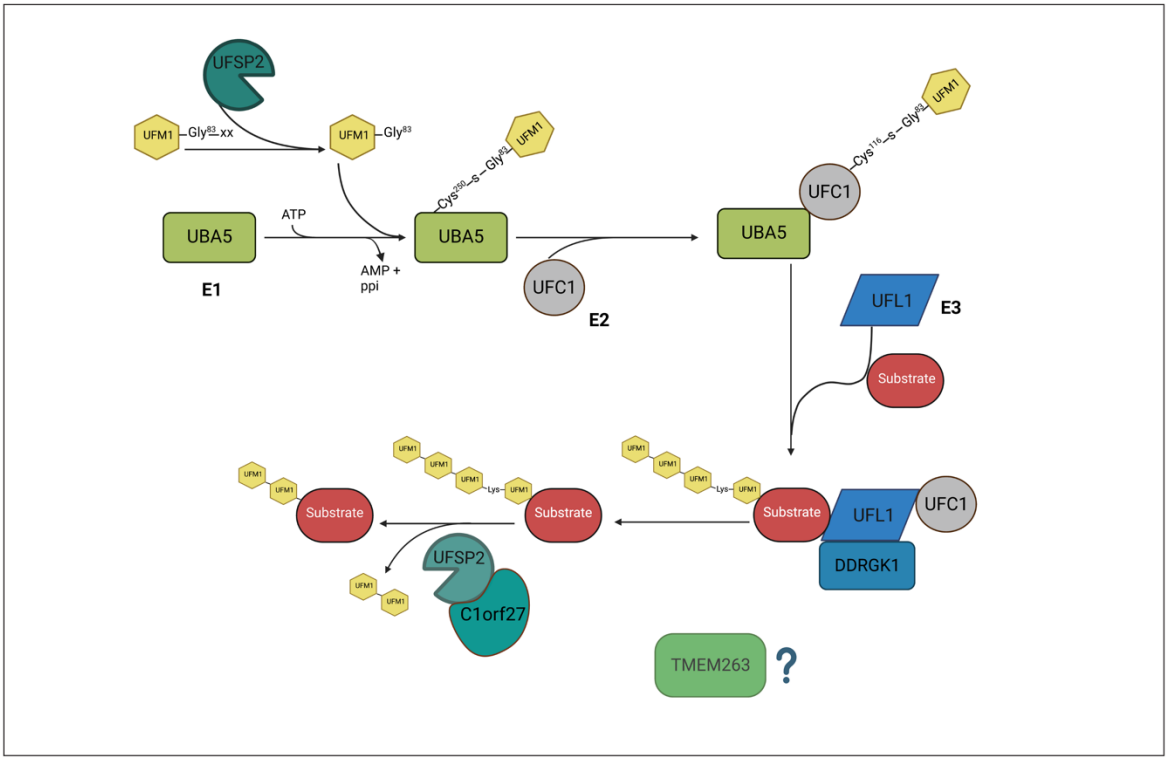
(A) Network analysis using Cytoscape and GeneMANIA package of the subset of shared stable interacting factors identified in the proteomic analysis conducted in C1orf27, the peptidase UFSP2 and the E3-ligase UFL1.

(B) Venn diagram describing the intersection of the three datasets of stable interacting factors obtained in treated and untreated conditions for C1orf27-, UFSP2- and UFL1-miniturboID cells.

3.3.6 Proposed model for C1orf27's role in the UFM1 pathway and its potential clinical relevance as a biomarker.

Based on our functional genomic and proteomic data, coupled with our multiomic analysis, which strongly suggest an important role of C1orf27 in the UFM1 pathway, we proposed a model (**Figure 3.6 A**) in which C1orf27 cooperates with the peptidase UFSP2 in the negative regulation of the pathway through deufmylation of targeted proteins. The exact mechanism in how C1orf27 regulates ICL repair through its role in the UFM1 pathway, remains to be clarified. Our preliminary analysis suggesting that C1orf27 plays a role in homologous recombination, points towards a potential regulation of factors involved in this portion of ICL repair, post-DSB generation. Our integrated proteomic data of our three datasets strongly suggest that C1orf27 forms an axis with UFSP2 involved in the UFM1 pathway. Moreover, the stable and consistent identification of DDRGK1 and TMEM263 in the 3 baits datasets is suggesting of a novel uncovered role for TMEM263 in the UFM1 pathway, which is beyond the scope of this present study and will be further analysed a posteriori. Finally, and to determine if the identification of C1orf27 could have clinical relevance we interrogated its RNA expression by RNA sequencing and how it correlates with clinical outcomes in publicly available ovarian cancer patient cohorts. Using a cohort of ovarian cancer patients (n=374) we found that C1orf27 expression correlated with a significant impact on the overall survival (OS) (**Figure 3.S6 A**, p=0.0043). When we assessed relapse-free survival (RFS, n=374), we also found a significant correlation between RNA expression and outcome (**Figure 3.S6 B**, p=0.00087). This suggest that C1orf27 expression correlates with outcomes of patients, and this goes in line with our results obtained in our screen and chemogenomic profiling data suggesting a role of C1orf27 in modulating the ICL response.

A

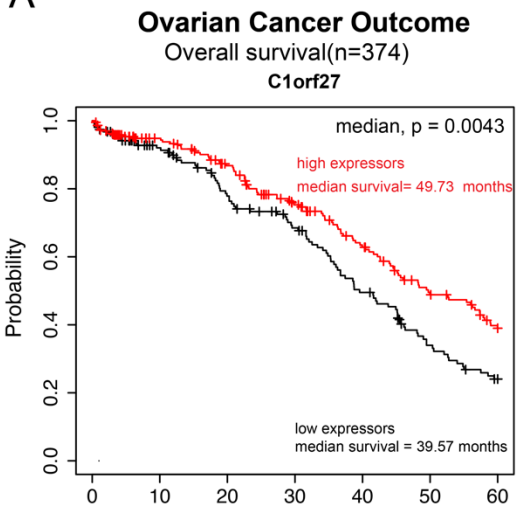


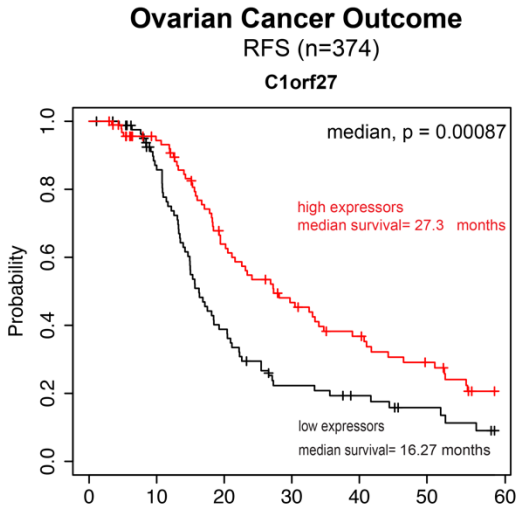
Pinedo Carpio *et al.* Figure 3.6

Figure 3.6 Proposed Model of C1orf27's role in the UFM1 pathway.

(A) Schematic describing the UFM1 pathway and the role of C1orf27 as constitutive interacting factor of the UFSP2 peptidase in the negative regulation step in which deUFMylation of targeted proteins occurs. The potential role in the UFM1 pathway of the novel constitutive factor TMEM263 identified in our three proteomic campaigns remains to be further elucidated.

A





Pinedo Carpio *et al.* Figure 3.S6

Figure 3.S6 C1orf27 expression correlates with poor survival in ovarian cancer.

(A) & (B) Overall and relapse-free survival analysis based on C1orf27 RNA-seq data in a cohort of ovarian cancer patients (n=374) using KMplot.

3.4 Discussion

In eukaryotes the FA pathway orchestrates the detection and removal of ICLs by the combined actions of homologous recombination (HR), nucleotide excision repair (NER) and Translesion DNA synthesis (TLS), with minor contributions from other DNA repair pathways [3, 13]. However, it remains largely unclear whether additional pathways contribute to the repair of ICLs. Due to the efficacy of ICL agents in cancer treatment there has been a considerable amount of research efforts focus on finding new ICL-inducing agents and increasing the sensitivity of current treatments. Based on their broad and successful usage in cancer therapeutics, the identification of factors involved in the modulation of sensitivity of tumor cells to ICL-inducing agents could have enormous therapeutic implications [19, 23-26].

Functional genomics as powerful approach to uncover genetic vulnerabilities and DDR factors. CRISPR-Cas9-based forward genetic screens have shown great efficacy in identifying cancer genetic vulnerabilities against specific compounds and gene essentiality for different types of cancer [10, 34, 68, 76-83]. Furthermore, these unbiased systemic approaches allow researchers to uncover oncogenic nodes and help to pinpoint synthetic lethal signatures that could contribute to a better stratification of cancer patients and the improvement of the efficacy of ICL-inducing agents in current chemotherapeutic regimens. Through the use of functional genomics and proteomics approaches several groups have recently uncovered novel factors involved in ICL DNA repair and HR, highlighting the complexity of this DNA repair pathway and that there are still considerable gaps in knowledge about this cellular response [14, 15, 17-22, 47, 84]. Here we report CRISPR-based genome-wide screening using a Burkitt lymphoma cell line and the use a of a pro-drug of cyclophosphamide(mafosfamide) as perturbagen. Our screening data analysis showed an exquisite dissection of the FA repair pathway along with well described factors involved in this DNA repair response. Furthermore, along with well described DNA factors we identified hits that have been

recently characterized as novel ICL factors by other research groups such as: HROB [17-19], RAD51AP1 [38, 41, 42], SLX4IP [23, 44-46] & TRAIP [85], highlighting the robustness of our screen data In addition, our secondary validation using CRISPR-based targeted miniscreening using tailored libraries allow us to identify C1orf27 as a novel factor involved in the modulation of ICL repair. Specifically, our functional validation using targeted screening have shown an important drug response profile and ranking for C1orf27 as sensitizer against two different ICL-inducing agents such as cisplatin and MMC, in addition of its sensitizer profile in our mafosfamide genome-wide screen, strongly suggesting that this uncharacterized protein plays a role as modulator of pan-ICL DNA repair response. In addition, our chemogenomic profiling using publicly available screen data from the Durocher group [47], revealed a strong sensitizer profile for C1orf27 and its interactome in several screens in which compounds that induce replication stress (HU, BPDE, IlludinS, MMS and Camptothecin) and crosslinking(cisplatin) were used. ICLs can be detected by different mechanisms depending on the DNA process taking place on the cross-linked DNA molecule. In active dividing cells the replication machinery encounters the adduct in S-phase of the cell cycle and the adduct will represent a physical barrier for the replisome. If this replication fork stalling and replication stress if left unrepaired this will lead to replication fork collapse and occurrence of DSBs [86]. FA proteins participate actively in the stabilization of the replication fork, the repair of the lesion blocking the replisome and the restart of replication after the adduct is removed, highlighting the great importance of FA proteins in the replication stress response.

UFMylation and its potential role in ICL repair. Ubiquitin and ubiquitin-like molecules (UBLs) represent the third most common post-translation modification after phosphorylation and glycosylation. The family of this small ubiquitin-like proteins can be conjugated to their targets following an E1-E2-E3 enzymatic reaction, which in turns could have an effect in protein structure, stability, and protein-protein interactions. Although the ubiquitin code and its related molecular

machinery has received lot of attention and has been extensively studied for decades, the biological role of many UBLs remains to be elucidated. One UBLs that have been discovered just 13 years ago is the ubiquitin-fold modifier 1(UFM1). Recent studies have revealed that the UFMylation pathway have profound implications in tissue homeostasis and the development of diseases such as cancer, heart failure, gut inflammation, and neurodevelopmental diseases [28]. Recently, a group found for the first time UFMylation activity in the nucleus. Specifically, they showed that UFL1 is recruited by the MRN complex and revealed that UFL1 activates ATM by UFMylating histone H4 at Lys31, in addition, they showed that this modification is antagonized by overexpression of UFM1-Specific peptidase 2(UFSP2) [26, 28]. A second study supporting the crosstalk between DNA damage response (DDR) and UFM1 pathway showed that UMFylation of the MRE11 subunit of the MRN complex increases ATM activity [28, 31]. Finally, more recently other two studies have showed that UMFylation is important for stability of TP53 and is critical for telomere lengthening and hematopoietic stem cell survival [24, 27, 28]. Our integrated screen and chemogenomic profiling analysis suggest that C1orf27 is novel modulator of DNA interstrand cross-link repair and replication stress response and that is important for UFMylation-related events involved in these cellular responses. Specifically, our analysis of the C1orf27 interactome network revealed a striking clustering profile with several factors involved in the novel ubiquitin-like UFM1 pathway. Interestingly, in a gene essentiality CRISPR-based screening study the Sabatini group showed that C1orf27(ODR4) cooperate and potentially formed a complex with UFSP2 [68], the critical peptidase important for the initiation and negative regulation of the UFM1 pathway. From the UFM1 pathway cluster of our chemogenomic profiling, UFSP2 phenocopied almost identically C1orf27 in sensitizing and resistance profile in fourteen different screens, supporting the coordinated role between these two factors.

Proximal interactome of C1orf27, UFSP2 and UFL1. Functional genomics efforts coupled with proteomics approaches have been shown to be effective in accelerating our understanding of novel DNA repair factors and biological processes in general [15, 16, 19, 87, 88]. TurboID and miniturboID technology have solved the problems found with BirA regarding the time of incubation needed for proper biotinylation while also reducing the levels of background signal. We took advantage of this novel technology in proximity labeling and used it to further expand our knowledge of the factors involved in UFMylation. Specifically, we interrogated the proximal interactomes of C1orf27, UFSP2 and UFL1, therefore addressing the gap in knowledge with respect to the protein network related to canonical UFM1-related factors (UFSP2 and UFL1) and at the same time, interrogating the proximal interactome of our hit of interest C1orf27. Our initial characterization of the C1orf27's interactome allowed us to identify a strong constitutive interaction of C1orf27 and UFSP2, which is in line with previous reports suggesting a cooperation between these two factors [52, 68, 69, 89]. The cooperation between these two factors was observed under steady conditions and under ICL-induced DNA damage, indicative of a stable role of these factors in UFMylation during ICL repair. In addition, the reciprocal analysis of UFSP2 proteomics identified C1orf27 and strongly validated their interaction. Furthermore, our mapping of the UFM1 pathway through our interrogation of UFSP2 and the E3 ligase UFL1, and the gene ontology analysis of the respective data, revealed a strong pathway enrichment related to the endoplasmic reticulum compartment and organization, the oxidative stress response, and nuclear membrane integrity. We identified the adapter protein DDGRK1 as a constitutive interactive partner of the three baits. Finally, we also identified the uncharacterized protein TMEM263(C12orf23) as a constitutive partner of the three baits. This factor has never been reported to participate in the UFM1 pathway, which highlights the novelty of our findings. Further characterization of the interacting partners of C1orf27 such as TEX264 and TMEM263, and its

cooperative function with the peptidase UFSP2, are necessary to further expand our understanding of these novel factors and the UFM1 pathway in ICL repair.

C1orf27 expression and Ovarian Cancer. Furthermore, when we assess if our screen and proteomic data obtained for C1orf27 could have clinical significance, we found that expression of C1orf27 correlates with patient outcome in a cohort of ovarian cancer patients. In addition, TCGA data revealed that several members of UFM1 pathway were mutated in different types of cancer [25], highlighting the potential role of UFMylation in genomic instability and carcinogenesis. Altogether, our data suggest that C1orf27 form a complex with UFSP2, the only deufmylation factor identified so far of the UFM1 pathway, and together play a coordinated role in the modulation of response against ICL agents. Further clarification and specific identification of the UFMylation-target in this pathway would clarify this novel DNA repair regulation.

3.5 Material and Methods

3.5.1 Cell Culture

Ramos Burkitt lymphoma cell line (a kind gift of Dr. Jerry Pelletier, McGill university) were culture in Roswell Park Memorial Institute (RPMI) 1640 medium (Wisent) and were supplemented with 10% fetal bovine serum (Sigma) and 1% Penicillin-Streptomycin (Wisent). Cells were tested for mycoplasma contamination and STR profiled. The following drugs were used in this study: mafosfamide (MAF, Toronto Research chemicals), puromycin dihydrochloride (Tocris) and blasticidin (InvivoGen).

3.5.2 CRISPR-Cas9 based genome-wide screening.

With minor modifications, Ramos genome-wide screen was conducted as previously described [90]. Briefly, 245 million Burkitt lymphoma Ramos cells stably expressing Cas9 were transduced with TKOv1 sgRNA lentiviral library at MOI (0.2), ensuring coverage of at least 500-fold for each individual sgRNA represented in the cell population. Two days post transduction, transduced cell populations were subjected to puromycin selection at a final concentration of 2 μg/ml during 7 days. After seven days of selection, media was replaced, and cells were allowed to recover without puromycin selection during 48h. Next, cells were counted to assure proper coverage and split into 2 groups, each in triplicate at a cell density of 45 million cells per replicate and treated with either mafosfamide at its IC25 dose (3.09 μM) or DMSO as a vehicle control population, in this point cell pellets corresponding to T0 replicates were collected. Cells were then cultured for up to 14 doubling times, which for Ramos cells was equivalent of 14 days. Cells were cultured with half-dose selection of puromycin at a concentration of 1 μg/ml during this period. Cells were counted every 3 days to preserve optimal cell density of 0.3 million cells per mL and to maintain fold coverage of at least 500 cells per sgRNA. At each time point of cellular passage, cell pellets were collected and snap frozen

with liquid nitrogen and stored at -80 degrees for subsequent genomic DNA isolation. Genomic DNA isolation was performed as described in [90]. For next-generation sequencing (NGS) libraries preparation, sgRNA integrated loci were amplified from genomic DNA using two rounds of nested PCR. The initial outer PCR consisted of 25 cycles of amplification with an annealing temperature of 65 °C using TaKaRa ExTaq® DNA Polymerase Hot-Start Version polymerase (Takara) and forward (FW) and reverse (RV) outer primers listed in **Table 3.S7**). Outer-PCR products were pooled, and ~2% of the input was amplified using Hot start Q5 polymerase to add Illumina HiSeq adapter sequences listed in (**Table 3.S7**). The resulting nested PCR product of around 200bp from each pooled sample was subsequently purified using separation and gel-extraction on an 8% 0.5× TBE polyacrylamide gel. Before loading each NGS library was quantified using qPCR and passed a quality control using a bioanalyzer kit (Agilent). NGS libraries were submitted for deep-sequencing on the HiSeq 2500 Illumina platform following the following protocol: standard Single-Read (SR) 50-cycle chemistry with dual-indexing with Rapid Run reagents. The first 20 cycles of sequencing were "dark cycles", or base additions without imaging. The actual 26-bp read begins after the dark cycles and contains two index reads, reading the i7 first, followed by i5 sequences. Once FASTQ files were retrieved, NGS read files were subjected to quality control using FastQC and RQC packages to assure proper uniformity and quality. As part of initial bioinformatic processing reads were trimmed of NGS adapter sequences using the Cutadapt tool. Reads were aligned to the sgRNA library index file using Bowtie2. BAM files were generated using samtools, and total read count tables were subsequently generated using the MAGeCK count command. DrugZ algorithm was used to identify gene knockouts which were depleted or enriched from T14 populations in comparison to T0 [37].

3.5.3 Secondary validation using miniscreens.

Generation of pooled libraries were conducted as previously described [80, 91, 92] and they were executed using the same protocol described above with their respective scaling down adjustments. Briefly, tailored minilibraries containing sgRNAs targeting ORFs of interest plus positive, negative and neutral controls, were designed and build through pool-cloning of sgRNAs into the lentiGuide-puro vector (Addgene, Plasmid # 52963). Coverage assessment after generation of the library was performed using NGS sequencing. Ramos-Cas9 cells were transduced with concentrated virus of lentiviral minilibrary and after two days of transduction, cells were subjected to puromycin selection for 7 days. Media was replaced and transduced puromycin selected cells were allowed to recover in fresh media without puromycin during 48h. Cells were counted, coverage assessed and cellular pools in triplicates were subjected to optimized concentrations of drugs (Mitomycin-C (Sigma), IC25 = 0.24 uM); (Cisplatin (Tocris), IC25 = 2.29 uM); (Phleomycin(Invivogen) IC25 = 8.4 uM); (AZD6738(Selleckchem), IC25 = 0.57uM)). Cells pellet were collected for T0 and T14 timepoints and genomic DNA isolation and NGS libraries preparation were conducted as described in [90].

3.5.4 Phylogenetic profiling of C1orf27 and Multiomics integrated analysis of C1orf27 and its interacting partners

The phylogenetic tool cladeOScope [48] was used to predict functional interactions between C1orf27 and selected factors that co-evolved with it in the Ecdysozea and Arthropoda clades respectively. Using CladeOScope, Biogrid, Depmap and the Durocher laboratory tool (https://durocher.shinyapps.io/GenotoxicScreens/) we generated an integrated intersected dataset for C1orf27 that allowed us to performed pathway enrichment analysis and identified factors participating in the same cellular process.

3.5.6 Proximity labeling using miniturboID.

HEK293 Flp-In^{tm} cells expressing miniturboID-tagged fused protein or miniturboID alone were seeded in 150 mm plates in technical triplicates. Induction of fusion protein and proximity biotinylation were conducted as previously described [90, 93, 94]. Briefly, induction of miniturboID-fused protein expression was conducted through addition of 1 μM tetracycline to culture media overnight. Next day, cells were treated or not with Cisplatin at a concentration of 2uM during 1h, after the 1h of incubation with cisplatin, the medium was supplemented with 50 μM biotin and left for additional 3hrs of incubation to induce biotinylation. After 4h of treatment with Cisplatin and 3h of biotinylation cells were harvested, washed twice with cold DPBS, and lysed in ice-cold RIPA buffer (50 mM Tris-HCl pH 7.4, 150 mM NaCl, 1% NP-40, 1 mM EDTA, 0.1% SDS and 0.5% sodium deoxycholate, 1 mM PMSF, 1 mM DTT) supplemented with 1:500 Sigma-Aldrich protease inhibitor cocktail P8340. Cellular pellets resuspended in lysis buffer were sonicated on ice for 30 secs at 30% amplitude (3 × 10 sec bursts with 2 seconds rest in between), while carefully avoiding formation of foam in the tube and overheating of the sample. After sonication, 250 units of benzonase (EMD) were added to easch sample. Samples were centrifuged for 30 minutes at 12,000 g at 4°C. Supernatants were transferred to pre-washed streptavidin-Sepharose high performance beads (GE, #17-5113-01) and incubated at 4°C on a rotator for 5 hrs. Beads were centrifuged at 400 g for 1 minute and sequentially washed twice with cold RIPA buffer and 3 times with of 50 mM ammonium bicarbonate buffer (ABC, pH 8.0). Beads were then resuspended in 100 μL of ABC, and digestion conducted by adding 10 μg of freshly prepared trypsin (Sigma) to the suspension for overnight digestion at 37°C with rotation. The next day, an additional 10 μg of trypsin was added to each sample, and further digestion was extended for another 3h. Beads were pelleted by centrifugation for 1 min at 400 g, and the supernatant-containing peptides were pooled with supernatants from two subsequent rinses with 100 μL of mass spectrometry grade H_2O. Formic acid was added to the pooled samples to a final

concentration of 5% to end digestion. Samples were centrifuged at 16,000 xg for 10 minutes at room temperature and supernatants were lyophilized using a Speedvac device during 3 hours at medium temperature settings. Dried peptides were kept at −80°C. Analysis of MS data was conducted as described before with minor modifications [93]. Briefly, samples were injected into an Orbitrap Fusion (Thermo Fisher), and raw files were analyzed with the Comet, XTandem! and Mascot search engines using the human RefSeq database. To estimate the interactions statistics, we used SAINTexpress version 3.6.1 on proteins with iProphet protein probability ≥ 0.9 and unique peptides ≥ 2. Each bait was compared against its respective negative control (treated or not with Cisplatin). These controls comprised of pulldowns from HEK cells expressing the empty vector (without the BirA*-Flag) in triple technical replicates. SAINT analyses were performed with the following compression settings: nControl:3, nCompressBaits:3. Interactions displaying an average probability (AvgP) ≥ 0.5 were considered as statistically significant (Supplementary Tables in Appendix 3S.6, 3.S7 and 3.S8). Unfiltered contaminants, such as Keratin, albumin, and artifact protein were discarded in every bioinformatics analyses. Using the ProHits-Viz online tool (prohits-viz.org), we generated a dot plot representing the relative AvgSpec of identified proteins for the three baits.

3.5.6 Kaplan Meier and differential gene expression analyses

Kaplan-Meier plotter (kmplot.com/analysis) was used to correlate the gene expression (RNA-seq, gene chip) of C1orf27 with ovarian cancer patient outcome. Only analysis showing a significant correlation (p-value<0.05) were represented.

3.5.7 Acknowledgments

We are grateful to members of the Orthwein's laboratory for critical reading of the manuscript, Jerry Pelletier for the Ramos cell line. EPC is a recipient of a doctoral fellowship from the Fonds de Recherche Santé Québec (FRQS). Work in the A.O. laboratory was supported by a CCSRI Innovation

Grant (#706389), a Transition Grant from the Cole Foundation and an internal Operating Fund from the Sir Mortimer B. Davis Foundation of the Jewish General Hospital.

3.5.8 Author Contributions

E.P.C and A.O. designed research; E.P.C and A.M performed research and analyzed data; E.P.C. wrote the original draft and E.P.C. and A.O edited the manuscript**.**

3.5.9 Conflict of interest

The authors declare that they have no conflict of interest.

3.5.10 References

1. Wang, A.T. and A. Smogorzewska, *SnapShot: Fanconi anemia and associated proteins.* Cell, 2015. **160**(1-2): p. 354-354 e1.
2. Kottemann, M.C. and A. Smogorzewska, *Fanconi anaemia and the repair of Watson and Crick DNA crosslinks.* Nature, 2013. **493**(7432): p. 356-63.
3. Niraj, J., A. Farkkila, and A.D. D'Andrea, *The Fanconi Anemia Pathway in Cancer.* Annu Rev Cancer Biol, 2019. **3**: p. 457-478.
4. Rodriguez, A. and A. D'Andrea, *Fanconi anemia pathway.* Curr Biol, 2017. **27**(18): p. R986-R988.
5. O'Rourke, J.J. and A.J. Deans, *The Fanca to Fancz of DNA Interstrand Crosslink Repair: Lessons from Fanconi Anemia.* DNA Repair in Cancer Therapy: Molecular Targets and Clinical Applications, 2nd Edition, 2016: p. 353-381.
6. Sehn, L.H. and R.D. Gascoyne, *Diffuse large B-cell lymphoma: optimizing outcome in the context of clinical and biologic heterogeneity.* Blood, 2015. **125**(1): p. 22-32.
7. Emadi, A., R.J. Jones, and R.A. Brodsky, *Cyclophosphamide and cancer: golden anniversary.* Nat Rev Clin Oncol, 2009. **6**(11): p. 638-47.
8. Johnson, N.A., et al., *Diffuse large B-cell lymphoma: reduced CD20 expression is associated with an inferior survival.* Blood, 2009. **113**(16): p. 3773-80.
9. Schmitz, R., et al., *Burkitt lymphoma pathogenesis and therapeutic targets from structural and functional genomics.* Nature, 2012. **490**(7418): p. 116-20.
10. Reddy, A., et al., *Genetic and Functional Drivers of Diffuse Large B Cell Lymphoma.* Cell, 2017. **171**(2): p. 481-494 e15.
11. Wever, C.M., et al., *The genomic landscape of two Burkitt lymphoma cases and derived cell lines: comparison between primary and relapse samples.* Leuk Lymphoma, 2018: p. 1-16.
12. Ryan D. Morin, S.A., Miguel Alcaide, et al., *Genetic Landscapes of Relapsed and Refractory Diffuse Large B-Cell Lymphomas.* Clinical Cancer Research, 2016. **22**(9): p. 2290-23000.
13. Nalepa, G. and D.W. Clapp, *Fanconi anaemia and cancer: an intricate relationship.* Nat Rev Cancer, 2018. **18**(3): p. 168-185.
14. Adeyemi, R.O., et al., *The Protexin complex counters resection on stalled forks to promote homologous recombination and crosslink repair.* Mol Cell, 2021. **81**(21): p. 4440-4456 e7.

15. Schubert, L., et al., *SCAI promotes error-free repair of DNA interstrand crosslinks via the Fanconi anemia pathway*. EMBO Rep, 2022. **23**(4): p. e53639.
16. Lemay, J.-F., et al., *A genome-wide screen identifies SCAI as a modulator of the UV-induced replicative stress response in human cells*. bioRxiv, 2022: p. 2022.01.17.476707.
17. Hustedt, N., et al., *Control of homologous recombination by the HROB-MCM8-MCM9 pathway*. Genes Dev, 2019. **33**(19-20): p. 1397-1415.
18. Wang, C., et al., *C17orf53 is identified as a novel gene involved in inter-strand crosslink repair*. DNA Repair (Amst), 2020. **95**: p. 102946.
19. Huang, J.W., et al., *MCM8IP activates the MCM8-9 helicase to promote DNA synthesis and homologous recombination upon DNA damage*. Nat Commun, 2020. **11**(1): p. 2948.
20. Shukla, V., et al., *HMCES Functions in the Alternative End-Joining Pathway of the DNA DSB Repair during Class Switch Recombination in B Cells*. Mol Cell, 2020. **77**(2): p. 384-394 e4.
21. Halabelian, L., et al., *Structural basis of HMCES interactions with abasic DNA and multivalent substrate recognition*. Nat Struct Mol Biol, 2019. **26**(7): p. 607-612.
22. Mohni, K.N., et al., *HMCES Maintains Genome Integrity by Shielding Abasic Sites in Single-Strand DNA*. Cell, 2019. **176**(1-2): p. 144-153 e13.
23. Zhang, H., et al., *SLX4IP acts with SLX4 and XPF-ERCC1 to promote interstrand crosslink repair*. Nucleic Acids Res, 2019. **47**(19): p. 10181-10201.
24. Liu, J., et al., *UFMylation maintains tumour suppressor p53 stability by antagonizing its ubiquitination*. Nat Cell Biol, 2020. **22**(9): p. 1056-1063.
25. Wei, Y. and X. Xu, *UFMylation: A Unique & Fashionable Modification for Life*. Genomics Proteomics Bioinformatics, 2016. **14**(3): p. 140-146.
26. Qin, B., et al., *UFL1 promotes histone H4 ufmylation and ATM activation*. Nat Commun, 2019. **10**(1): p. 1242.
27. Lee, L., et al., *UFMylation of MRE11 is essential for telomere length maintenance and hematopoietic stem cell survival*. Sci Adv, 2021. **7**(39): p. eabc7371.
28. Gerakis, Y., et al., *The UFMylation System in Proteostasis and Beyond*. Trends Cell Biol, 2019. **29**(12): p. 974-986.
29. Liu, J., et al., *A critical role of DDRGK1 in endoplasmic reticulum homoeostasis via regulation of IRE1alpha stability*. Nat Commun, 2017. **8**: p. 14186.
30. Zhang, M., et al., *RCAD/Ufl1, a Ufm1 E3 ligase, is essential for hematopoietic stem cell function and murine hematopoiesis*. Cell Death Differ, 2015. **22**(12): p. 1922-34.

31. Wang, Z., et al., *MRE11 UFMylation promotes ATM activation.* Nucleic Acids Res, 2019. **47**(8): p. 4124-4135.
32. Kulsuptrakul, J., et al., *A genome-wide CRISPR screen identifies UFMylation and TRAMP-like complexes as host factors required for hepatitis A virus infection.* Cell Rep, 2021. **34**(11): p. 108859.
33. Steinhart, Z., et al., *Genome-wide CRISPR screens reveal a Wnt-FZD5 signaling circuit as a druggable vulnerability of RNF43-mutant pancreatic tumors.* Nat Med, 2017. **23**(1): p. 60-68.
34. Hart, T., et al., *High-Resolution CRISPR Screens Reveal Fitness Genes and Genotype-Specific Cancer Liabilities.* Cell, 2015. **163**(6): p. 1515-26.
35. Li, W., et al., *MAGeCK enables robust identification of essential genes from genome-scale CRISPR/Cas9 knockout screens.* Genome Biol, 2014. **15**(12): p. 554.
36. Wang, B., et al., *Integrative analysis of pooled CRISPR genetic screens using MAGeCKFlute.* Nat Protoc, 2019. **14**(3): p. 756-780.
37. Colic, M., et al., *Identifying chemogenetic interactions from CRISPR screens with drugZ.* Genome Med, 2019. **11**(1): p. 52.
38. Barroso-Gonzalez, J., et al., *RAD51AP1 Is an Essential Mediator of Alternative Lengthening of Telomeres.* Mol Cell, 2020. **79**(2): p. 359.
39. Bridges, A.E., et al., *RAD51AP1 Deficiency Reduces Tumor Growth by Targeting Stem Cell Self-Renewal.* Cancer Res, 2020. **80**(18): p. 3855-3866.
40. Barroso-Gonzalez, J., et al., *RAD51AP1 Is an Essential Mediator of Alternative Lengthening of Telomeres.* Mol Cell, 2019. **76**(1): p. 217.
41. Liang, F., et al., *DNA requirement in FANCD2 deubiquitination by USP1-UAF1-RAD51AP1 in the Fanconi anemia DNA damage response.* Nat Commun, 2019. **10**(1): p. 2849.
42. Pires, E., P. Sung, and C. Wiese, *Role of RAD51AP1 in homologous recombination DNA repair and carcinogenesis.* DNA Repair (Amst), 2017. **59**: p. 76-81.
43. Dunlop, M.H., et al., *RAD51-associated protein 1 (RAD51AP1) interacts with the meiotic recombinase DMC1 through a conserved motif.* J Biol Chem, 2011. **286**(43): p. 37328-34.
44. Robinson, N.J., et al., *SLX4IP promotes RAP1 SUMOylation by PIAS1 to coordinate telomere maintenance through NF-kappaB and Notch signaling.* Sci Signal, 2021. **14**(689).
45. Mangosh, T.L., et al., *SLX4IP Promotes Telomere Maintenance in Androgen Receptor-Independent Castration-Resistant Prostate Cancer through ALT-like Telomeric PML Localization.* Mol Cancer Res, 2021. **19**(2): p. 301-316.

46. Panier, S., et al., *SLX4IP Antagonizes Promiscuous BLM Activity during ALT Maintenance.* Mol Cell, 2019. **76**(1): p. 27-43 e11.
47. Olivieri, M., et al., *A Genetic Map of the Response to DNA Damage in Human Cells.* Cell, 2020. **182**(2): p. 481-496 e21.
48. Tsaban, T., et al., *CladeOScope: functional interactions through the prism of clade-wise co-evolution.* NAR Genom Bioinform, 2021. **3**(2): p. lqab024.
49. Branon, T.C., et al., *Author Correction: Efficient proximity labeling in living cells and organisms with TurboID.* Nat Biotechnol, 2020. **38**(1): p. 108.
50. Zhou, J., et al., *Genomic profiling of the UFMylation family genes identifies UFSP2 as a potential tumour suppressor in colon cancer.* Clin Transl Med, 2021. **11**(12): p. e642.
51. Kang, S.H., et al., *Two novel ubiquitin-fold modifier 1 (Ufm1)-specific proteases, UfSP1 and UfSP2.* J Biol Chem, 2007. **282**(8): p. 5256-62.
52. Ha, B.H., et al., *Structure of ubiquitin-fold modifier 1-specific protease UfSP2.* J Biol Chem, 2011. **286**(12): p. 10248-57.
53. Di Rocco, M., et al., *Novel spondyloepimetaphyseal dysplasia due to UFSP2 gene mutation.* Clin Genet, 2018. **93**(3): p. 671-674.
54. Watson, C.M., et al., *Identification of a mutation in the ubiquitin-fold modifier 1-specific peptidase 2 gene, UFSP2, in an extended South African family with Beukes hip dysplasia.* S Afr Med J, 2015. **105**(7): p. 558-63.
55. Egunsola, A.T., et al., *Loss of DDRGK1 modulates SOX9 ubiquitination in spondyloepimetaphyseal dysplasia.* J Clin Invest, 2017. **127**(4): p. 1475-1484.
56. Yamamoto, Y. and T. Sakisaka, *Molecular machinery for insertion of tail-anchored membrane proteins into the endoplasmic reticulum membrane in mammalian cells.* Mol Cell, 2012. **48**(3): p. 387-97.
57. Annaert, W.G., et al., *Export of cellubrevin from the endoplasmic reticulum is controlled by BAP31.* J Cell Biol, 1997. **139**(6): p. 1397-410.
58. Zhang, S.L., et al., *STIM1 is a Ca2+ sensor that activates CRAC channels and migrates from the Ca2+ store to the plasma membrane.* Nature, 2005. **437**(7060): p. 902-5.
59. Banerjee, S., M. Kumar, and R. Wiener, *Decrypting UFMylation: How Proteins Are Modified with UFM1.* Biomolecules, 2020. **10**(10).
60. Komatsu, M., et al., *A novel protein-conjugating system for Ufm1, a ubiquitin-fold modifier.* EMBO J, 2004. **23**(9): p. 1977-86.

61. Yoo, H.M., et al., *Modification of ASC1 by UFM1 is crucial for ERalpha transactivation and breast cancer development.* Mol Cell, 2014. **56**(2): p. 261-274.
62. Liang, J.R., et al., *A Genome-wide ER-phagy Screen Highlights Key Roles of Mitochondrial Metabolism and ER-Resident UFMylation.* Cell, 2020. **180**(6): p. 1160-1177 e20.
63. Asencio, C., et al., *Coordination of kinase and phosphatase activities by Lem4 enables nuclear envelope reassembly during mitosis.* Cell, 2012. **150**(1): p. 122-35.
64. Tsatskis, Y., et al., *The NEMP family supports metazoan fertility and nuclear envelope stiffness.* Sci Adv, 2020. **6**(35): p. eabb4591.
65. Zhao, C., et al., *Regulation of Torsin ATPases by LAP1 and LULL1.* Proc Natl Acad Sci U S A, 2013. **110**(17): p. E1545-54.
66. Fielden, J., et al., *TEX264 coordinates p97- and SPRTN-mediated resolution of topoisomerase 1-DNA adducts.* Nat Commun, 2020. **11**(1): p. 1274.
67. Huttlin, E.L., et al., *Dual proteome-scale networks reveal cell-specific remodeling of the human interactome.* Cell, 2021. **184**(11): p. 3022-3040 e28.
68. Wang, T., et al., *Gene Essentiality Profiling Reveals Gene Networks and Synthetic Lethal Interactions with Oncogenic Ras.* Cell, 2017. **168**(5): p. 890-903 e15.
69. Chen, C., et al., *An ER complex of ODR-4 and ODR-8/Ufm1 specific protease 2 promotes GPCR maturation by a Ufm1-independent mechanism.* PLoS Genet, 2014. **10**(3): p. e1004082.
70. Martinvalet, D., P. Zhu, and J. Lieberman, *Granzyme A induces caspase-independent mitochondrial damage, a required first step for apoptosis.* Immunity, 2005. **22**(3): p. 355-70.
71. Chowdhury, D., et al., *The exonuclease TREX1 is in the SET complex and acts in concert with NM23-H1 to degrade DNA during granzyme A-mediated cell death.* Mol Cell, 2006. **23**(1): p. 133-42.
72. Kang, T.H., et al., *Circadian control of XPA and excision repair of cisplatin-DNA damage by cryptochrome and HERC2 ubiquitin ligase.* Proc Natl Acad Sci U S A, 2010. **107**(11): p. 4890-5.
73. Danielsen, J.R., et al., *DNA damage-inducible SUMOylation of HERC2 promotes RNF8 binding via a novel SUMO-binding Zinc finger.* J Cell Biol, 2012. **197**(2): p. 179-87.
74. Bekker-Jensen, S. and N. Mailand, *Assembly and function of DNA double-strand break repair foci in mammalian cells.* DNA Repair (Amst), 2010. **9**(12): p. 1219-28.
75. Wu, W., et al., *HERC2 is an E3 ligase that targets BRCA1 for degradation.* Cancer Res, 2010. **70**(15): p. 6384-92.

76. Koike-Yusa, H., et al., *Genome-wide recessive genetic screening in mammalian cells with a lentiviral CRISPR-guide RNA library.* Nat Biotechnol, 2014. **32**(3): p. 267-73.
77. Yu, J.S.L. and K. Yusa, *Genome-wide CRISPR-Cas9 screening in mammalian cells.* Methods, 2019. **164-165**: p. 29-35.
78. Chan, E.M., et al., *WRN helicase is a synthetic lethal target in microsatellite unstable cancers.* Nature, 2019. **568**(7753): p. 551-556.
79. Kategaya, L., et al., *Werner Syndrome Helicase Is Required for the Survival of Cancer Cells with Microsatellite Instability.* iScience, 2019. **13**: p. 488-497.
80. Shalem, O., et al., *Genome-scale CRISPR-Cas9 knockout screening in human cells.* Science, 2014. **343**(6166): p. 84-87.
81. Wang, T., et al., *Identification and characterization of essential genes in the human genome.* Science, 2015. **350**(6264): p. 1096-101.
82. Tzelepis, K., et al., *A CRISPR Dropout Screen Identifies Genetic Vulnerabilities and Therapeutic Targets in Acute Myeloid Leukemia.* Cell Rep, 2016. **17**(4): p. 1193-1205.
83. Parnas, O., et al., *A Genome-wide CRISPR Screen in Primary Immune Cells to Dissect Regulatory Networks.* Cell, 2015. **162**(3): p. 675-86.
84. He, Y.J., et al., *DYNLL1 binds to MRE11 to limit DNA end resection in BRCA1-deficient cells.* Nature, 2018. **563**(7732): p. 522-526.
85. Wu, R.A., et al., *TRAIP is a master regulator of DNA interstrand crosslink repair.* Nature, 2019. **567**(7747): p. 267-272.
86. Wang, L.C. and J. Gautier, *The Fanconi anemia pathway and ICL repair: implications for cancer therapy.* Crit Rev Biochem Mol Biol, 2010. **45**(5): p. 424-39.
87. Noordermeer, S.M., et al., *The shieldin complex mediates 53BP1-dependent DNA repair.* Nature, 2018. **560**(7716): p. 117-121.
88. Tkac, J., et al., *HELB Is a Feedback Inhibitor of DNA End Resection.* Mol Cell, 2016. **61**(3): p. 405-418.
89. Hein, M.Y., et al., *A human interactome in three quantitative dimensions organized by stoichiometries and abundances.* Cell, 2015. **163**(3): p. 712-23.
90. Findlay, S., et al., *SHLD2/FAM35A co-operates with REV7 to coordinate DNA double-strand break repair pathway choice.* EMBO J, 2018. **37**(18).
91. Hart, T., et al., *Evaluation and Design of Genome-Wide CRISPR/SpCas9 Knockout Screens.* G3 (Bethesda), 2017. **7**(8): p. 2719-2727.

92. Canver, M.C., et al., *Integrated design, execution, and analysis of arrayed and pooled CRISPR genome-editing experiments.* Nat Protoc, 2018. **13**(5): p. 946-986.
93. Heath, J., et al., *POGZ promotes homology-directed DNA repair in an HP1-dependent manner.* EMBO Rep, 2022. **23**(1): p. e51041.
94. Lambert, J.P., et al., *Proximity biotinylation and affinity purification are complementary approaches for the interactome mapping of chromatin-associated protein complexes.* J Proteomics, 2015. **118**: p. 81-94.

Chapter IV: General Discussion

4.1 C1orf112/FLIP is a novel regulator of interstrand crosslink repair that decreases FIGNL1-RAD51 interaction.

Power of CRISPR-based functional genomics to uncover DNA repair factors. In this thesis we carried out CRISPR-based genome wide screens using Burkitt lymphoma cell lines and used mafosfamide as ICL-inducing agent. Mafosfamide is a pro-drug of the widely used chemotherapeutic agent cyclophosphamide and it is expected to cause both interstrand and intrastrand crosslinks. Our systemic CRISPR-based approach probed the response against mafosfamide, and we were able to nicely dissect the entire FA core pathway and consequently obtained a remarkable pathway enrichment for ICL repair. Along with FA core proteins, we identified factors involved in downstream ICL repair events such as homologous recombination, TLS, excision repair and general DDR factors. In addition to canonical described DNA repair factors, we identified several novel ICL-related factors which have been recently characterized by other research groups such as HROB(C17orf53) [499, 539, 540], HMCES(C3orf37) [541-544], ZGRF1(C4orf21) [545], SLX4IP [546-548], RAD51AP1 [549-552], TRAIP [219] and SCAI [497, 498, 500]. This pathway enrichment and cross-validation of our hits prompted us to hypothesize with confidence that we could mine this screen dataset to uncover novel ICL repair factors. Accordingly, we identified C1orf112 as novel factor involved in ICL/HR DNA repair.

C1orf112 is a key player in the HR-mediated response to ICL. DNA interstrand crosslinks are one the most deleterious type of DNA damage, and the complexity of this cellular challenge requires the coordinated involvement of proteins from several DNA repair pathways including FA, HR, NER and TLS. To tackle this genetic insult while preserving genomic integrity, the FA/ICL repair pathway, in a still unclear pathway choice outcome, is channeled towards a faithful DNA repair through homologous recombination. A key upstream event in the activation of ICL-repair pathway is the

ubiquitination of the ID2 complex which triggers the full activation and signaling cascade of this response. Equally important and critical for the recombination-mediated repair, is the fine-tuned loading and unloading of RAD51, and its related filament formation. The mechanisms and players involved in mediating RAD51 loading and its positive regulation are well understood, however, the steps and factors involved in the negative regulation of RAD51 loading and the postsynaptic events following RAD51-mediated strand invasion are one of the least characterized and properly understood stages of ICL-induced homologous recombination [499]. Although in yeast the Srs2 DNA helicase have been described as the canonical negative regulator of Rad51, the human ortholog of Srs2 have not been yet identified. Still, several human helicases such as BLM, RECQ5, FANCJ and FBHI have been reported to be involved in RAD51-ssDNA filament dissociation [71, 126-130]. Nonetheless, the detailed molecular mechanism and factors involved in this regulation of RAD51-mediated recombination remains to be clarified. C1orf112 harbours a conserved domain of unknown function (DUF4487) and its cellular role has not yet been described in humans or mammals. Preliminary evolutionary studies suggest that C1orf112 and its DUF4487 domain are well conserved in vertebrates, and its homologues are present also in some invertebrates, plants and single-cell microorganisms [553]. Furthermore, seminal studies in plant orthologs such as *Arabidopsis thaliana* [554] and *Oryza sativa* [555] have described a common critical role of these orthologs in the regulation of meiotic recombination and crossover formation. Homologous recombination is important for the repair of DSBs in both mitotic and meiotic cells. During meiosis, HR is initiated by the generation of programmed DSBs mediated by SPO11 and recombinatorial-repair is mediated by DMC1 and RAD51 respectively [556, 557]. Similarly, to mitotic HR, the mechanisms involved in the prevention of aberrant recombination during meiosis such as non-allelic homologous recombination (NAHR) are poorly understood [555]. In addition, expression profiling has reported that C1orf112 is co-expressed with genes involved in FA/HR repair such as BRCA1, BRCA2, FANCD2, FANCI and RAD51 [558]. More recently, another

study using C1orf112 expression across multiple tumor types suggest a potential prognostic and oncogenic role for C1orf112 [559]. As part of our initial validation, we decided to use a different cellular background and a different ICL-inducing agent than the ones used in our two genome-wide screens. Instead of B-lymphocytes and mafosfamide, we use the non-transformed RPE1-htert cell line and another clinically relevant ICL-inducing agent: cisplatin. With this validation we ruled out that C1orf112 was not a malignant B-cell specific hit, and that its sensitizer ICL-related profile using a platin-derived agent such as cisplatin suggest that it is a pan-ICL factor. An interesting observation related to this validation relies on the fact that nitrogen-mustard agents (e.j. mafosfamide) and platin-derived agents (e.j. cisplatin) are reported to cause only around 5-10% of ICLs and that the rest of its cytotoxic activity is related to the generation of intrastrand crosslink, monoadducts and DNA-protein crosslinks(DPC) [341], which are repaired by pathways different than FA/ICL. Following up on our characterization of C1orf112 and its role in ICL/HR repair, we assessed through DNA repair and cellular fate assays if C1orf112 depletion could have consequences in genomic stability and DNA damage. Our results showed that C1orf112 depletion in U2OS cells triggers formation of micronuclei and that upon ICL-induction with cisplatin, there is an increase in γH2AX focus formation and intensity with respect to control cells. Micronuclei formation is a marker of genomic instability in cancer cells, and their generation is attributed to dysfunctional chromosome segregation, errors in DNA replication and repair. Moreover, recent reports suggest that micronuclei formation triggers genomic instability through an irreversible rupture of nuclear lamina causing substantial DSBs and chromothripisis [560-562]. Our observations are in line with these reports and suggest that C1orf112 is a key factor involved in preservation of genomic integrity and for tackling the repair of DSBs generated downstream of an ICL. Upon DNA damage gauging and activation of the DDR response, two potential cellular outcomes are triggered by the master DDR effector p53: Apoptosis and Senescence [563]. In C1orf112-deficient RPE1-htert cells treated with cisplatin we observed a

considerable increase of apoptotic cells with respect to control cells. These results suggest that in the absence of C1orf112 cells and upon cisplatin treatment, cells can not properly repair the ICL-induced DNA damage and cells undergo apoptosis. In order to recapitulate our results obtained in our screens using p53-deficient lymphoma cells, C1orf112 KO cells were generated in a p53-deficient RPE1-htert cellular background. Nevertheless, and being aware of the limitations of assessing a DNA repair phenotype in p53-deficient background, we decided to assess C1orf112 deficiency in an isogenic pair of cells with p53 WT and p53-deficient cells respectively. This assessment showed that in RPE1-htert p53 WT cells, C1orf112 deficiency triggered a senescence cellular response in a p53-regulated fashion. DNA damage sensing and DDR activation are key events in the cellular response leading to cellular senescence, and our results are consistent with our hypothesis that C1orf112 plays a role in preserving DNA damage and genomic instability. Recent reports [46, 346, 348] suggest that cellular metabolites such as formaldehydes and aldehydes represent an endogenous source of ICL-induced DNA damage. This physiological response to deal with by-products of regular metabolism requires a functional ICL-repair response, and our results in a p53-wt cellular background suggest that upon deficiency of C1orf112, there is an accumulation of DNA damage, likely linked to endogenous-ICLs, which lead to DDR activation and p53-controlled triggering of cellular senescence. We recapitulated these results using IMR90 cells, a commonly used non-transformed cellular model for senescence. Nevertheless, further characterization of our senescence phenotype will be necessary to fully understand this complex cellular response and assess the crosstalk between C1orf112 and p53-dependent DDR response. As part of our characterization of C1orf112 role in the FA/ICL signaling cascade, we observed that C1orf112 deficiency does not affect FANDC2 focus formation nor its ubiquitination upon induction of ICL with cisplatin treatment, which suggest that this factor plays a role downstream of FA core complex conformation and ID2 activation in the ICL response. Furthermore, our DR-GFP results, suggest that C1orf112 may play a role in DSB repair unrelated to ICL-repair and that this

is consistent with the results obtained for the C1orf112 orthologs in both *Arabidopsis thaliana* [554] and *Oryza sativa [555],* in which a role in DSB repair during meiotic homologous recombination is described. Factors involved in FA/ICL and HR repair display a consistent drug sensitivity to a different range of chemotherapeutic compounds, including ICL-agents and PARP inhibitors [37, 224, 319, 329]. Our analysis of C1orf112 expression and IC50 response in multiple cell lines using the GDSC datasets [564], along with our cytotoxicity assessment, displayed a striking sensitivity for ICL-drugs and PARP-inhibitors, which strongly points to an important role for C1orf112 in the repair of genetic insults using ICL-repair and HR. Chemogenomic profiling of C1orf112 in CRISPR-screens conducted in RPE1 hTERT p53-/- cells showed a striking sensitizer profile with different genotoxic drugs that induce replication roadblocks (Cisplatin), base alkylation-helix torsion(MNNG)and oxidative damage($KBrO_3$, H2O2). Altogether our drug-sensitivity and chemogenomic profiling supports a model in which C1orf112 plays a role in the repair of DNA lesions such as DSBs generated during replication stress caused by replication fork roadblocks.

C1orf112 forms a heterodimer with FIGNL1 to regulate RAD51 accumulation upon repair. Recent advances in proximity labeling and other proteomic approaches such as IPOND, have allowed the identification of multiple novel factors involved in DNA repair processes [461, 543, 565]. In particular, the incorporation of mutant versions of the ligase BirA with improved kinetics such as miniturboID and turboID [530, 566], allows now researchers to better map the interactome of target baits and improve the dynamic range while reducing at the same time the background signal and non-specific hits. In order to characterize the proximal partners of C1orf112, we have used miniturboID technology and mapped the proximal interactome of C1orf112. Specifically, we successfully identified FIGNL1 as a consistent interacting partner at steady conditions and upon DNA damage. Moreover, when performing the reciprocal analysis for FIGNL1, we identified C1orf112 in both treated and untreated conditions respectively, which suggested that these two factors may conform a complex

involved in a common cellular process. These results are consistent with a study in orthologs in which using a yeast two-hybrid approach [554], a French group found an interaction between the orthologs of FIGNL1 and C1orf112. Furthermore, in this study researchers found that C1orf112'ortholog (FLIP) limits meiotic crossover in cooperation with FIGNL1, and together they regulate strand invasion in homologous recombination. In parallel to the *A. thaliana* study, the Chinese group working on *Oryza sativa* described a role of the C1orf112 rice ortholog (MEICA1) [555] in prevention of aberrant meiotic recombination and they also reported an interaction of MEICA1 with TOP3α and MSH7. Altogether, these ortholog reports along with our data in human cells, suggest that this complex is highly conserved from plants to humans, and it may play similar and also distinctive functions in different organism belonging to very distant clades. The integration of our functional genomic and proteomic data suggests that our screens may have uncovered an entire novel axis involved in ICL-repair. We functionally validated our top interactor FIGNL1 and found a striking similarity in the sensitization phenotype against ICL treatment and a significant defect in HR repair, which remarkably phenocopy C1orf112 behaviour in these assays. Furthermore, we solidly validated the interaction between C1orf112 and FIGNL1 using the LacO/LacR assay. In addition, depletion of either protein in U2OS cells specifically reduced viability in the presence ICL-inducing agents such as cisplatin, mitomycin-C or folmaldehyde, chronic exposure to hydroxyurea (HU) and PARP inhibitors. Altogether, our data indicates that C1orf112 and FIGNL1 conform a complex that participates in the resolution of DNA lesions that are originated during replication stress events caused by different genotoxic sources. Interestingly, our proteomic analysis also identified ERCC6L as a constitutive interacting partner of C1orf112 at steady and under DNA damaging conditions. ERCC6L, also known as PICH is a factor previously reported to be important for preservation of genomic integrity through its role in the resolution of ultra-fine bridges [567], replication fork reversal [568] and centromere integrity in cooperation with Polo-like kinase 1(Plk1) [569]. Although we have focused our attention

on the cooperation of C1orf112 with FIGNL1 in ICL repair and homologous recombination, analysis of our proteomic data displayed a striking enrichment for centromeric proteins such as PCM1, CEP131 and CEP72, therefore it is plausible to speculate of a potential role of C1orf112 in the resolution of ultra-fine bridge resolution and the preservation of centromere integrity. Recent studies focused on centromere biology [570-572] have called the attention of the scientific community, as these poorly characterized regions in our chromosomes still represent unexplored regions of the human genome and their role in human disease and the mechanism involved in the preservation of their integrity remain poorly defined. The potential role of C1orf112 in centromere biology will require further characterization which is beyond the scope of this PhD research work.

C1orf112-FIGNL1 complex and other regulators of RAD51 activity. FIGNL1 is an AAA+ ATPase factor which was initially characterized by the Chen's group [573]. In this study FIGNL1 was reported to be required for an efficient HR repair and through MS/AP experiments was reported to interact with RAD51 and SPIDER(KIAA0146), noteworthy, in this study C1orf112 was listed as a weak (1 peptide count) interacting partner of FIGNL1. In follow up studies by the Shinohara's group [574] FIGNL1 was described as an interacting partner of SWSAP1, a key component of the newly described HR-related Shu complex. Specifically, Shinohara's group suggested that FIGNL1's interaction with SWSAP1 prevents its anti-recombinogenic activity over RAD51 filament. Additionally, recent reports by Berstein and Jasin's groups related to the Shu complex factors, suggest that this complex may play a positive mediator role in safeguarding RAD51-filament formation, and its crosstalk with FIGNL1 may be a conserved mechanism to prevent aberrant recombination-dependent repair, which could be analog to the antagonistic relationship between the yeast Shu complex and the antirecombinogenic factor Srs2 described initially by Rodney Rothstein group [575]. Phylogenetic analysis showed that C1orf112 is absent in alveolate, amoebozoa and fungi [553, 554]. Yet, in some organism such as *C.elegans or D. melanogaster* , in which C1orf112 is not present, FIGNL1

orthologs were detected, which led to suggest that C1orf112 may play a supporting scaffolding role for FIGNL1, and that the AAA+ ATPase activity of this factor could be the essential core of their cellular function in these organisms. Nevertheless, both C1orf112 and FIGNL1 are highly conserved in vertebrates and sequence identity among primates is extensive. Moreover, C1orf112 KO mouse is lethal [576-578], which indicates that although is a highly conserved factor, through evolution C1orf112 may have acquired great biological importance and that this factor is essential for normal physiology of advanced mammals. Indeed, our senescent phenotype is in line with the great importance for genomic stability proposed for C1orf112 observed in human cell lines. Interestingly and related to this senescent phenotype, a recent GWAS report focussed on the DDR mechanism governing human ovary aging found that, along with well characterized ICL/HR factors such as FANCA, FANCM, MCM8 and EXO1, C1orf112 was one of top genes linked to this process, which is consistent with the phenotype found in our study [579]. Our structure-function analysis of C1orf112 truncation and deletion mutants have demonstrated that the conserved DUF4487 domain and the tripeptide WCF motif within this DUF, are critical for the interaction of C1orf112 and FIGNL1. Interestingly, when assessing the interactions and dependency of these proteins, we observed a significant increase of RAD51 intensity in C1orf112 depleted U2OS 2-6-5 cells and ectopic expression of GFP-C1orf112 showed the opposite effect and resulted in a reduced signal of RAD51. Altogether these finding suggest that C1orf112 negatively regulates the interaction of FIGNL1 and RAD51 and points towards a model in which C1orf112-FIGNL1 complex controls RAD51 dynamics and prevents aberrant recombination events. This model is in line with previous reports for orthologs of C1orf112 and FIGNL1, and the ICL-dependent RAD51-persistence phenotype we found upon C1orf112 depletion suggest that in the absence of this complex, a BRCA2-mediated aberrant loading of RAD51 occurs which leads to recombination-dependent genomic instability and backlog of unrepair DNA damage. In a recent follow up study by the Mercier group [580], an antagonistic mechanism between

the positive mediator BRCA2 and FIGNL1 was described. Which suggest that this ancient mechanism involved in the fine-tuning of pro- and anti-recombinatorial events during HR is tightly controlled by antagonistic multiprotein complexes such as BRCA2-PALB2 and C1orf112-FIGNL1, and this is a highly conserved cellular process likely originated at the root of eukaryotes in the tree of life. The SWS1-SWSAP1-SPIDR complex have been reported [574, 581] as a positive regulator of RAD51 activity and our data suggest that the C1orf112-FIGNL1 complex here described, may counteract this function and play the opposite role negatively regulating RAD51 dynamics in response to replication stress events such as ICL-induced replisome collisions. Finally, expression analysis suggest that C1orf112 levels may modulate the response to different chemotherapeutic agents and could influence patient outcome. Altogether our study converging functional genomics, proximity-based proteomics and functional *in-cellulo* characterization of C1orf112, have allowed us to uncover a novel complex conformed by C1orf112 and FIGNL1 involved in ICL and DSBs repair. This study harbors profound implications related to ICL-repair and HR; however, further studies are required to fully understand the complex crosstalk between the C1orf112-FIGNL1 complex and positive mediators of RAD51 loading such as BRCA2-PALB2, the Shu complex and RAD51 orthologs.

4.2 CRISPR-based screening uncovers a novel factor involved in the modulation of the response against ICL-inducing agents.

In eukaryotes the FA pathway orchestrates the detection and removal of ICLs by the combined actions of homologous recombination (HR), nucleotide excision repair (NER) and Translesion DNA synthesis (TLS), with minor contributions from other DNA repair pathways [37, 222]. However, it remains largely unclear whether additional pathways contribute to the repair of ICLs. Due to the efficacy of ICL agents in cancer treatment there has been a considerable amount of research efforts focus on finding new ICL-inducing agents and increasing the sensitivity of current treatments. Based on their broad and successful usage in cancer therapeutics, the identification of factors involved in the

modulation of sensitivity of tumor cells to ICL-inducing agents could have enormous therapeutic implications [19, 23-26].

Uncovering novel regulators of ICL repair through CRISPR-based screening. CRISPR-Cas9-based forward genetic screens have shown great efficacy in identifying cancer genetic vulnerabilities against specific compounds and gene essentiality for different types of cancer [461, 465, 467, 472-475, 477, 582-586]. Furthermore, these unbiased systemic approaches allow researchers to uncover oncogenic nodes and help to pinpoint synthetic lethal signatures that could contribute to a better stratification of cancer patients and the improvement of the efficacy of ICL-inducing agents in current chemotherapeutic regimens. Through the use of functional genomics and proteomics approaches several groups have recently uncovered novel factors involved in ICL DNA repair and HR, highlighting the complexity of this DNA repair pathway and that there are still considerable gaps in knowledge about this cellular response [380, 492, 497-499, 539-543]. Here we report CRISPR-based genome-wide screening using a Burkitt lymphoma cell line and the ICL-inducing agent mafosfamide as perturbagen. Our screening data analysis showed an exquisite dissection of the FA repair pathway along with well described factors involved in this DNA repair response, which was supported by GSEA analysis displaying remarkable enrichment for ICL- and DSB repair. Furthermore, along with well described DNA factors we identified hits that have been recently characterized as novel ICL factors by other research groups such as: HROB [499, 539, 540], RAD51AP1 [549, 551, 552], SLX4IP [546-548, 587] & TRAIP [219], highlighting the robustness of our screen data. Altogether, the enrichment in DNA repair factors obtained in our genome-wide screening approach, allowed us to mine, with high confidence, the screen dataset aiming to uncover novel factors involved in ICL repair.

C1orf27 is a novel factor involved UFMylation. Additionally, our secondary validation using CRISPR-based targeted mini-screening using tailored libraries allow us to identify C1orf27 as a novel factor involved in the modulation of ICL repair. Specifically, our functional validation using targeted

screening have shown an important drug response profile and ranking for C1orf27 as sensitizer against two different ICL-inducing agents such as cisplatin and MMC. This screen results along with its sensitizer profile obtained in our mafosfamide genome-wide screen, strongly suggests that this uncharacterized protein plays a role as modulator of pan-ICL DNA repair response. Moreover, our chemogenomic profiling using publicly available screen data from the Durocher group [380], revealed a strong sensitizer profile for C1orf27 and its interactome in several screens in which compounds that induce replication stress (HU, BPDE, IlludinS, MMS and Camptothecin) and crosslinking(cisplatin) were used. This cross-validation of our hit with drug-based screen data from other research groups have allowed us to position C1orf27 as novel factor involved in replication stress-related events such as ICL repair. ICLs can be detected by different mechanisms depending on the DNA process taking place on the cross-linked DNA molecule. In active dividing cells the replication machinery encounters the adduct in S-phase of the cell cycle and the adduct will represent a physical barrier for the replisome. If this replication fork stalling and replication stress is left unrepaired, this will lead to replication fork collapse and occurrence of DSBs [588]. FA proteins participate actively in the stabilization of the replication fork, the repair of the lesion blocking the replisome and the restart of replication after the adduct is removed, highlighting the great importance of FA proteins in the replication stress response. Ubiquitin and ubiquitin-like molecules (UBLs) represent the third most common post-translation modification after phosphorylation and glycosylation. The family of this small ubiquitin-like proteins can be conjugated to their targets following an E1-E2-E3 enzymatic reaction, which in turns could have an effect in protein structure, stability, and protein-protein interactions. Although the ubiquitin code and its related molecular machinery has received lot of attention and has been extensively studied for decades, the biological role of many UBLs remains to be elucidated. One UBL that have been discovered just 13 years ago is the ubiquitin-fold modifier 1(UFM1). Recent studies have revealed that the UFMylation pathway have profound implications in tissue homeostasis and the development of

diseases such as cancer, heart failure, gut inflammation, and neurodevelopmental diseases [231]. Recently, a group found for the first time UFMylation activity in the nucleus. Specifically, they showed that UFL1 is recruited by the MRN complex and revealed that UFL1 activates ATM by UFMylating histone H4 at Lys31, and that this modification is antagonized by overexpression of UFM1-Specific peptidase 2(UFSP2) [231, 246]. A second study supporting the crosstalk between DNA damage response (DDR) and UFM1 pathway showed that UMFylation of the MRE11 subunit of the MRN complex increases ATM activity [231, 244]. Finally, more recently other two studies have showed that UMFylation is important for stability of TP53 and is critical for telomere lengthening and hematopoietic stem cell survival [231, 243, 245]. Our integrated screen and chemogenomic profiling analysis suggest that C1orf27 is novel modulator of DNA interstrand cross-link repair and that is important for UFMylation-related events involved in these cellular responses. Specifically, our analysis of the C1orf27 interactome network revealed a striking clustering profile with several factors involved in the novel ubiquitin-like UFM1 pathway. Interestingly, in a gene essentiality CRISPR-based screening study the Sabatini group showed that C1orf27(aka ODR4) cooperate and potentially formed a complex with UFSP2 [475], the critical peptidase important for the initiation and negative regulation of the UFM1 pathway. Clustering analysis of our chemogenomic profiling showed that UFSP2 phenocopied almost identically C1orf27 as sensitizer and resistance factor in fourteen different screens in RPE1 hTERT p53-/- cells [380], supporting the coordinated role between these two factors. **Proximal interactome mapping using miniturboID revealed a strong cooperation between C1orf27 and the peptidase UFSP2**. To further explore the proximal interactome of C1orf27, UFSP2 and UFL1, two key canonical factors involved in the UFM1 pathway, we conducted proximity labeling proteomic analysis with miniturboID technology, at steady and under ICL-induced DNA damaging conditions. The proteomic analysis of C1orf27's interactome revealed a stable interaction with the peptidase UFSP2 and other UFM1-relared factors such as DDRGK1, moreover, gene ontology

assessment of the stable interacting partners of C1orf27, revealed an striking enrichment in UFMylation These results strongly validated our hypothesis that C1orf27 cooperates and likely conforms a multiprotein complex with UFSP2 and DDRGK1, and points towards an important role of C1orf27 in the UFM1 pathway under normal physiological conditions and under genotoxic stress upon ICL damage. Furthermore, we identified TEX264 as a constitutive interacting partner of C1orf27. Although it was initially described to be a resident protein of the ER compartment involved in ER-phagy [589], a recent report [590] by the Ramadan's laboratory nicely showed that TEX264 along with the ATPase p97 and SPRTN conform a complex involved in DNA-protein crosslink repair. Furthermore, this study reported that TEX264 localised to the nuclear periphery and associates with replication forks. We initially identified C1orf27 as a sensitizer hit in our genome-wide Mafosfamide screen, and we nicely validated its pan-ICL sensitizer profile using Cisplatin and Mitomycin-C. Furthermore, in our proteomic approach we also interrogated the proximal interactome of C1orf27 in the context of ICL-induced DNA damage using Cisplatin. Although chemically different, all these compounds (mafosfamide, cisplatin and mitomycin-C) are ICL-agents, and they all trigger the formation of DNA intra- and interstrand crosslinks. Interestingly, and related to TEX264, as part of their mechanism of cytotoxicity, ICL agents such as Cisplatin, can also cause non enzymatic DNA-protein crosslinks (DPCs) by nonspecific crosslinking of chromatin-interacting proteins to DNA [591]. Therefore, our proteomic data and identification of TEX264 as constitutive interacting partner of C1orf27, suggest a potential role of UFMylation in ICL-induced non-enzymatic DNA-protein crosslink repair. The interaction between C1orf27 and TEX264 requires further characterization and research efforts aiming to elucidate the roles of these novel factors in the crosstalk between the UFM1 pathway and DPC repair would be of great importance.

The initial step in the signaling cascade activating the UFM1 pathway relies on the activity of two peptidases: UFSP1 and UFSP2. These two UFM1-specific cysteine proteases control the maturation

of the UFM1-precursor by cleaving the C-terminal dipeptide Ser-Cys and therefore exposing a single glycine residue in UFM1 [230, 232], allowing the subsequent E1-E2-E3 cascade. Although both UFSP1 and UFSP2 are highly specific for UFM1, due to a mutation in its catalytic N-terminal domain, UFSP1 is hypothetized to be inactive in humans [241, 592]. Nevertheless, studies showed that UFSP2 depletion strongly increases UFM1-conjugation [592], which suggest that even in the absence of UFSP2, there is still a compensatory protease activity in the initial maturation step, which allows the activation of the signaling cascade.Furthermore, this result also suggest that these two peptidases may have redundant functions in the initial maturation step, but de-UFMylation of targeted proteins, and the negative regulation of the pathway, is a function likely exclusive of UFSP2. Consequently, our multiomic and integrated proteomic showing a strong constitutive interaction between C1orf27 and UFSP2-but not with UFSP1- suggest that these two factors likely cooperate in the negative regulation of the pathway: de-UFMylation. Although more than six hundred E3 ligases involved in the Ubiquitination pathway have been identified, only one E3 ligase has been uncovered in the UFM1 pathway. The E3 UFM1-ligase 1(UFL1) is classified as a non-conventional scaffold-like E3, which is believed to bring its substrate and E2 in close proximity for protein-target conjugation [206, 230, 231, 246]. Furthermore, literature suggest that this type of E3 interact with adaptor proteins to modulate the levels of substrates and their conjugation. One reported adapter protein involved in this step is the adaptor DDRGK1(aka UFM1-binding protein 1; UFBP1) [237, 239]. The integration of our three proteomic campaigns concentrated on the proximal interactomes of C1orf27, UFSP2 and UFL1, showed that DDRGK1 is a constitutive interactor of these three factors under physiological conditions and under ICL-induced DNA damage, which is line with the literature and strongly validate the role of this adapter protein in the UFM1 pathway. Furthermore, this integrated analysis uncovered another factor shared among these three baits, which has not been previously reported to participated in the UFM1 pathway: TMEM263. Transmembrane protein 263(aka C12orf23) is a completely

uncharacterized factor predicted to be an integral component of the membrane. Strikingly, some genetic reports suggest a link between mutations in TMEM263 and skeletal dysplasia [593] and autosomal dwarfism [594], which are clinical pathological features commonly found in proteins involved in DNA repair, cell cycle and development. Furthermore, and strengthening our proteomic data linking TMEM263 with UFSP2, two genetic studies [250, 252] have reported mutations in UFSP2 in patients of a extended South African family-of Dutch origin- with spondyloepimetaphyseal and Beukes hip displasia, highlighting common clinical features of these two factors and a potential clinical role of UFMylation in these pathologies. Interestingly and related to ICL-repair, AP-MS proteomic data [595] reports an interaction of TMEM263 with C1orf112, the novel ICL-HR repair factor here characterized in Chapter II, and also an interaction with DNA specific DNA binging protein 1 (DDB1). Altogether these preliminary results coupled with our proteomic data suggest a potential crosstalk between the C1orf27-UFSP2-UFL1-TMEM263 axis and UFMylation-related ICL repair and prompts further molecular characterization of TMEM263 in DNA repair and UFMylation. Finally, when we assessed if our C1orf27 data could have clinical significance, we found that C1orf27 expression correlates with patient outcome in a cohort of ovarian cancer patients, and TCGA data revealed that several members of UFM1 pathway were mutated in different types of cancer [206]. Altogether, our data suggest that C1orf27 form a complex with UFSP2, the only deufmylation factor identified so far of the UFM1 pathway, and together play a coordinated role in the modulation of response in the ICL repair and replication stress. Further functional characterization of C1orf27 and its interacting partners UFSP2, TEX264 and TMEM263, along with a better understanding of this novel ubiquitin-like modification and its target proteins in ICL-repair would clarify this novel DNA repair regulation.

Future Directions

Chapter II

In this body of work, we have uncovered a novel regulatory role for the scaffolding protein C1orf112 over FIGNL1 anti-recombinogenic activity through the unloading of RAD51 during ICL and DSBs repair. However, both proteins are poorly characterized biochemically and structurally, consequently, it remains unclear what exact molecular function has the highly conserved but still uncharacterized domain DUF4487. We have uncovered that the tripeptide WCF within the DUF4487 domain is critical for the interaction of C1orf112 with FIGNL1, however we still do not know how these residues play a role in this interaction. Biochemical assays interrogating D-loop formation and strand invasion using recombinant proteins will contribute greatly with our understanding and better comprehension of the anti-recombinogenic role of the C1orf112-FIGNL1 complex here described and how this novel yet critical step in HR is regulated. Undergoing collaboration with the laboratory of Dr. Jean Yves-Masson from Laval university will fill-in this gap of biochemical knowledge about these proteins. In addition to C1orf112 and FIGNL1, our genome-wide and proteomics data suggest that we have uncovered other factors that may play a role in the C1orf112-FIGNL1 axis. One factor that displayed a strong sensitizer profile in both Namalwa and Raji screens and was a top proximal interactor for both C1orf112- and FIGNL1-miniturboID under steady and DNA damage conditions was pericentriolar material 1 protein (PCM1). Although previous studies have indicated a role for PCM1 as structural scaffold for centriolar satellite organization linked to centrosome function [596, 597] during cellular stress such as DNA damage. It remains unclear if a possible crosstalk between C1orf112-FIGNL1 and PCM1 may play a role in ICL and HR repair. Further epistatic analysis and protein-protein interaction under ICL damage would be necessary to clarify this potential link. In addition, and based on a previous study [580] by the Mercier laboratory in which double depletion of

BRCA2 and the FIGNL1 orthologue in Arabidopsis FIGL1 abrogates their respective phenotype, which suggest an additional backup pathway that fine-tune and regulate RAD51-mediated recombinatorial repair. Therefore, further characterization of the opposite and antagonistic roles between the canonical positive mediator of RAD51 function: BRCA2 and the here proposed negative mediator in human cells: C1orf112-FIGNL1 complex are necessary to fully understand this complex and tightly regulated cellular process.

A known adage in Biology states that "*structure determines function*", and nowadays we are fortunate to witness a major revolution in structure biology thanks to the improvements in AI-mediated modelling such as AlphaFold [598] and the advances in Cryo-EM technology as well. These technologies will allow us to better understand the structure and biological functions of these novel proteins and contribute greatly in the elucidation of their biological and clinical significance. In collaboration with the laboratory of Dr. Alba Guarné at McGill university, we have started the protein structure characterization of both proteins. Preliminary, we have uncovered that C1orf112 harbours a leucine zipper domain at its C-terminus and based on previous studies of DNA-binding proteins harboring these domains [599-601], we predicted that this leucine zipper structure allows homodimerization of C1orf112 monomers and enables its interaction with DNA. Full protein structure elucidation using cryogenic electron microscopy (Cryo-EM) and subsequent experimental validation of the AlphaFold protein structure prediction for C1orf112 and FIGNL1 is currently undergoing. Finally, aiming to further understand the role of C1orf112 in normal physiology and to move this research towards a translation application with clinical significance, we are currently acquiring an *in-vivo* conditional C1orf112 KO murine model in which we will assess the role of C1orf112 in mouse development, genome stability factor as part of the C1orf112-FIGNL1 complex in the negative regulation of RAD51-mediated HR repair and finally its function in chemotherapeutic response using ICL-inducing drugs such as cyclophosphamide.

Chapter III

The work presented in this chapter is part of an article under preparation. We have uncovered a novel role for C1orf27 in the regulation of ICL response. And our preliminary work suggest that this factor plays a role in the UFMylation pathway in a close cooperation with the protease UFSP2, and in a collaborative manner, they modulate the response against agents that cause replication stress such ICL agents and DNA alkylators. Although it is clear that post-translation modifications (PTMs) such as ubiquitylation and de-ubiquitylation of FA or HR proteins, are essential for a normal functioning of these DNA repair processes, it is still unclear if ubiquitin-like (UBL) modification such as UFMylation are also essential regulatory mechanisms to control positive and negative signaling during these cellular events. Consequently, further characterization of the UFM1 pathway and its potential role in ICL repair is of great importance. Our CRISPR-based functional genomic data suggest that C1orf27 and its interacting partners involved in this pathway play a role in the response to different genotoxic agents leading to replication stress and ICL formation. Preliminary work by the Sabatini group and previous work with orthologs, suggest that C1orf27 interacts and potentially collaborates with the peptidase UFSP2, however this protein interaction and its role in the context of ICL damage was not yet explored. Our integrative analysis of the proximal interactome of C1orf27, UFSP2 and UFL1 in the context of ICL repair, allowed us to: i) identify a constitutive interaction between C1orf27 and UFSP2; ii) identify a novel constitutive interacting partner of C1orf27 such as TEX264; iii) identified TMEM263 as a novel constitutive interacting factor of C1orf27, UFSP2 and UFL1, suggestive of a novel factor involved in UMFylation and potentially ICL repair. Nevertheless, further functional experiments assessing the role of the potential complex conformed by C1orf27 and UFSP2, along with their crosstalk and collaborative function with TEX264 and TMEM263 in cellular fate, DNA damage will be explored.

Final conclusion and summary

CRISPR-based screening represents a powerful approach that allows researchers to interrogated phenotypes and drug-based responses in an unbiased and genome-wide scale. Through this PhD work I have conducted a total of four genome-wide screens in Burkitt lymphoma cells and have interrogated in a genome-wide manner the response against the ICL-inducing agent mafosfamide. Throughout the body of work presented in this thesis I have demonstrated the power and robust efficacy of this approach to uncover novel factors involved in DNA repair processes such as FA/ICL repair. **In Chapter II**, we described the uncovering of C1orf112 as novel factor involved in the regulation of interstrand crosslink repair. More specifically, we have shown that C1orf112 controls cellular fate by regulating replicative stress-induced senescence and apoptosis. Furthermore, through proximity-labeling proteomics we have identified the anti-recombinase FIGNL1 as a constitutive partner of C1orf112, and our functional characterization of the C1orf112-FIGNL1 complex suggest that these two factors play an epistatic role in the repair of DNA lesions during replication stress events such as ICLs. We have identified that the tripeptide WCF motif within the DUF4487 domain in C1orf112 and the N-terminal region of FIGNL1 are critical for the interaction of these two factors. In addition, we found that levels of C1orf112 modulate the interaction of FIGNL1 and RAD51, thereby proposing a role for C1orf112 in the regulation of the FIGNL1 function in the unloading of RAD51 during homologous recombination repair. Altogether we conclude that C1orf112 is the previously unidentified regulator of the AAA+ ATPase FIGNL1 anti-recombinase involved in ICL and DSBs by homology-directed DNA repair pathways. **In Chapter III**, we described the execution of genome-wide and targeted CRISPR-based screening in Ramos Burkitt lymphoma cells and using also mafosfamide as perturbagen agent. This strategy has allowed us to uncover C1orf27 as a novel regulator of ICL response. More specifically, our mini-screening effort showed that C1orf27 depletion sensitized Ramos cells upon treatment with cisplatin and mitomycin C, highlighting the pan-ICL

sensitizer profile of this factor. Further chemogenomic profiling using CRISPR-based screening data showed that C1orf27 depletion sensitized RPE1-hTERT pp53-/- cells against multiple agents involved in replication stress and ICL repair. Multiomic integration of our screen data and proteomics and functional genomics publicly available resources allowed us to pinpoint interacting partners of C1orf27 and GO-analysis and network analysis have allowed us to identify UFMylation as the potential cellular process in which C1orf27 may play a role modulating ICL repair. Our chemogenomic analysis and proteomic efforts using miniturboID identified a consititutive collaborative function between C1orf27 and UFSP2. Furthermore, the reciprocal anaylysis, along with the previous reports about these factors, suggest of a potential conformation of a complex involved in the negative regulation step of deUFMylation. Finally, expression analysis of C1orf27 showed a correlation of gene expression levels and patient outcome in a cohort of ovarian cancer patients. Further functional characterization of C1orf27 and its interacting partners and their proposed role in UFMylation and ICL repair is necessary to shed light in this potential novel regulation of ICL repair and replication stress.

References

1. Costa, A. and J.F.X. Diffley, *The Initiation of Eukaryotic DNA Replication.* Annu Rev Biochem, 2022. **91**: p. 107-131.
2. Gaillard, H., T. Garcia-Muse, and A. Aguilera, *Replication stress and cancer.* Nat Rev Cancer, 2015. **15**(5): p. 276-89.
3. Techer, H. and P. Pasero, *The Replication Stress Response on a Narrow Path Between Genomic Instability and Inflammation.* Front Cell Dev Biol, 2021. **9**: p. 702584.
4. Berti, M. and A. Vindigni, *Replication stress: getting back on track.* Nat Struct Mol Biol, 2016. **23**(2): p. 103-9.
5. Saxena, S. and L. Zou, *Hallmarks of DNA replication stress.* Mol Cell, 2022. **82**(12): p. 2298-2314.
6. Ashour, M.E. and N. Mosammaparast, *Mechanisms of damage tolerance and repair during DNA replication.* Nucleic Acids Res, 2021. **49**(6): p. 3033-3047.
7. Ciccia, A. and S.J. Elledge, *The DNA damage response: making it safe to play with knives.* Mol Cell, 2010. **40**(2): p. 179-204.
8. Tubbs, A. and A. Nussenzweig, *Endogenous DNA Damage as a Source of Genomic Instability in Cancer.* Cell, 2017. **168**(4): p. 644-656.
9. Lehmann, A.R., et al., *Translesion synthesis: Y-family polymerases and the polymerase switch.* DNA Repair (Amst), 2007. **6**(7): p. 891-9.
10. Ide, H., et al., *Repair and biochemical effects of DNA-protein crosslinks.* Mutat Res, 2011. **711**(1-2): p. 113-22.
11. Vare, D., et al., *DNA interstrand crosslinks induce a potent replication block followed by formation and repair of double strand breaks in intact mammalian cells.* DNA Repair (Amst), 2012. **11**(12): p. 976-85.
12. Voulgaridou, G.P., et al., *DNA damage induced by endogenous aldehydes: current state of knowledge.* Mutat Res, 2011. **711**(1-2): p. 13-27.
13. Vrtis, K.B., et al., *Single-strand DNA breaks cause replisome disassembly.* Mol Cell, 2021. **81**(6): p. 1309-1318 e6.
14. Caldecott, K.W., *Single-strand break repair and genetic disease.* Nat Rev Genet, 2008. **9**(8): p. 619-31.

15. Kumar, C., et al., *The interplay of RNA:DNA hybrid structure and G-quadruplexes determines the outcome of R-loop-replisome collisions.* Elife, 2021. **10**.
16. Mirkin, E.V. and S.M. Mirkin, *Replication fork stalling at natural impediments.* Microbiol Mol Biol Rev, 2007. **71**(1): p. 13-35.
17. Voineagu, I., et al., *Replication stalling at unstable inverted repeats: interplay between DNA hairpins and fork stabilizing proteins.* Proc Natl Acad Sci U S A, 2008. **105**(29): p. 9936-41.
18. Crossley, M.P., M. Bocek, and K.A. Cimprich, *R-Loops as Cellular Regulators and Genomic Threats.* Mol Cell, 2019. **73**(3): p. 398-411.
19. Byun, T.S., et al., *Functional uncoupling of MCM helicase and DNA polymerase activities activates the ATR-dependent checkpoint.* Genes Dev, 2005. **19**(9): p. 1040-52.
20. Zou, L. and S.J. Elledge, *Sensing DNA damage through ATRIP recognition of RPA-ssDNA complexes.* Science, 2003. **300**(5625): p. 1542-8.
21. Saldivar, J.C., D. Cortez, and K.A. Cimprich, *The essential kinase ATR: ensuring faithful duplication of a challenging genome.* Nat Rev Mol Cell Biol, 2017. **18**(10): p. 622-636.
22. Quinet, A., D. Lemacon, and A. Vindigni, *Replication Fork Reversal: Players and Guardians.* Mol Cell, 2017. **68**(5): p. 830-833.
23. Neelsen, K.J. and M. Lopes, *Replication fork reversal in eukaryotes: from dead end to dynamic response.* Nat Rev Mol Cell Biol, 2015. **16**(4): p. 207-20.
24. Berti, M., D. Cortez, and M. Lopes, *The plasticity of DNA replication forks in response to clinically relevant genotoxic stress.* Nat Rev Mol Cell Biol, 2020. **21**(10): p. 633-651.
25. Cortez, D., *Replication-Coupled DNA Repair.* Mol Cell, 2019. **74**(5): p. 866-876.
26. Hakem, R., et al., *The tumor suppressor gene Brca1 is required for embryonic cellular proliferation in the mouse.* Cell, 1996. **85**(7): p. 1009-23.
27. Sharan, S.K., et al., *Embryonic lethality and radiation hypersensitivity mediated by Rad51 in mice lacking Brca2.* Nature, 1997. **386**(6627): p. 804-10.
28. Sonoda, E., et al., *Rad51-deficient vertebrate cells accumulate chromosomal breaks prior to cell death.* EMBO J, 1998. **17**(2): p. 598-608.
29. Tsuzuki, T., et al., *Targeted disruption of the Rad51 gene leads to lethality in embryonic mice.* Proc Natl Acad Sci U S A, 1996. **93**(13): p. 6236-40.
30. Hashimoto, Y., et al., *Rad51 protects nascent DNA from Mre11-dependent degradation and promotes continuous DNA synthesis.* Nat Struct Mol Biol, 2010. **17**(11): p. 1305-11.

31. Schlacher, K., et al., *Double-strand break repair-independent role for BRCA2 in blocking stalled replication fork degradation by MRE11.* Cell, 2011. **145**(4): p. 529-42.
32. Somyajit, K., et al., *Mammalian RAD51 paralogs protect nascent DNA at stalled forks and mediate replication restart.* Nucleic Acids Res, 2015. **43**(20): p. 9835-55.
33. Taylor, A.M.R., et al., *Chromosome instability syndromes.* Nat Rev Dis Primers, 2019. **5**(1): p. 64.
34. Oshima, J., J.M. Sidorova, and R.J. Monnat, Jr., *Werner syndrome: Clinical features, pathogenesis and potential therapeutic interventions.* Ageing Res Rev, 2017. **33**: p. 105-114.
35. Boerkoel, C.F., et al., *Mutant chromatin remodeling protein SMARCAL1 causes Schimke immuno-osseous dysplasia.* Nat Genet, 2002. **30**(2): p. 215-20.
36. Bellelli, R. and S.J. Boulton, *Spotlight on the Replisome: Aetiology of DNA Replication-Associated Genetic Diseases.* Trends Genet, 2021. **37**(4): p. 317-336.
37. Nalepa, G. and D.W. Clapp, *Fanconi anaemia and cancer: an intricate relationship.* Nat Rev Cancer, 2018. **18**(3): p. 168-185.
38. Lindahl, T. and B. Nyberg, *Rate of depurination of native deoxyribonucleic acid.* Biochemistry, 1972. **11**(19): p. 3610-8.
39. Lindahl, T. and A. Andersson, *Rate of chain breakage at apurinic sites in double-stranded deoxyribonucleic acid.* Biochemistry, 1972. **11**(19): p. 3618-23.
40. Lindahl, T., *Instability and decay of the primary structure of DNA.* Nature, 1993. **362**(6422): p. 709-15.
41. Tomasetti, C. and B. Vogelstein, *Cancer risk: role of environment-response.* Science, 2015. **347**(6223): p. 729-31.
42. Wu, S., et al., *Substantial contribution of extrinsic risk factors to cancer development.* Nature, 2016. **529**(7584): p. 43-7.
43. Lindahl, T. and D.E. Barnes, *Repair of endogenous DNA damage.* Cold Spring Harb Symp Quant Biol, 2000. **65**: p. 127-33.
44. Jackson, S.P. and J. Bartek, *The DNA-damage response in human biology and disease.* Nature, 2009. **461**(7267): p. 1071-8.
45. Polo, S.E. and S.P. Jackson, *Dynamics of DNA damage response proteins at DNA breaks: a focus on protein modifications.* Genes Dev, 2011. **25**(5): p. 409-33.
46. Garaycoechea, J.I., et al., *Alcohol and endogenous aldehydes damage chromosomes and mutate stem cells.* Nature, 2018. **553**(7687): p. 171-177.

47. Stinson, B.M. and J.J. Loparo, *Repair of DNA Double-Strand Breaks by the Nonhomologous End Joining Pathway.* Annu Rev Biochem, 2021. **90**: p. 137-164.
48. Karanam, K., et al., *Quantitative live cell imaging reveals a gradual shift between DNA repair mechanisms and a maximal use of HR in mid S phase.* Mol Cell, 2012. **47**(2): p. 320-9.
49. Lieber, M.R., *The mechanism of double-strand DNA break repair by the nonhomologous DNA end-joining pathway.* Annu Rev Biochem, 2010. **79**: p. 181-211.
50. Zhao, W., et al., *The BRCA Tumor Suppressor Network in Chromosome Damage Repair by Homologous Recombination.* Annu Rev Biochem, 2019. **88**: p. 221-245.
51. Scully, R., et al., *DNA double-strand break repair-pathway choice in somatic mammalian cells.* Nat Rev Mol Cell Biol, 2019. **20**(11): p. 698-714.
52. Gottlieb, T.M. and S.P. Jackson, *The DNA-dependent protein kinase: requirement for DNA ends and association with Ku antigen.* Cell, 1993. **72**(1): p. 131-42.
53. Nick McElhinny, S.A., et al., *Ku recruits the XRCC4-ligase IV complex to DNA ends.* Mol Cell Biol, 2000. **20**(9): p. 2996-3003.
54. Ahnesorg, P., P. Smith, and S.P. Jackson, *XLF interacts with the XRCC4-DNA ligase IV complex to promote DNA nonhomologous end-joining.* Cell, 2006. **124**(2): p. 301-13.
55. Buck, D., et al., *Cernunnos, a novel nonhomologous end-joining factor, is mutated in human immunodeficiency with microcephaly.* Cell, 2006. **124**(2): p. 287-99.
56. Ochi, T., et al., *DNA repair. PAXX, a paralog of XRCC4 and XLF, interacts with Ku to promote DNA double-strand break repair.* Science, 2015. **347**(6218): p. 185-188.
57. Graham, T.G., J.C. Walter, and J.J. Loparo, *Two-Stage Synapsis of DNA Ends during Non-homologous End Joining.* Mol Cell, 2016. **61**(6): p. 850-8.
58. Blackford, A.N. and S.P. Jackson, *ATM, ATR, and DNA-PK: The Trinity at the Heart of the DNA Damage Response.* Mol Cell, 2017. **66**(6): p. 801-817.
59. Vilenchik, M.M. and A.G. Knudson, *Endogenous DNA double-strand breaks: production, fidelity of repair, and induction of cancer.* Proc Natl Acad Sci U S A, 2003. **100**(22): p. 12871-6.
60. McVey, M. and S.E. Lee, *MMEJ repair of double-strand breaks (director's cut): deleted sequences and alternative endings.* Trends Genet, 2008. **24**(11): p. 529-38.
61. Chang, H.H.Y., et al., *Non-homologous DNA end joining and alternative pathways to double-strand break repair.* Nat Rev Mol Cell Biol, 2017. **18**(8): p. 495-506.

62. Robert, I., F. Dantzer, and B. Reina-San-Martin, *Parp1 facilitates alternative NHEJ, whereas Parp2 suppresses IgH/c-myc translocations during immunoglobulin class switch recombination.* J Exp Med, 2009. **206**(5): p. 1047-56.
63. Brown, M.S. and D.K. Bishop, *DNA strand exchange and RecA homologs in meiosis.* Cold Spring Harb Perspect Biol, 2014. **7**(1): p. a016659.
64. Panier, S. and S.J. Boulton, *Double-strand break repair: 53BP1 comes into focus.* Nat Rev Mol Cell Biol, 2014. **15**(1): p. 7-18.
65. Ceccaldi, R., B. Rondinelli, and A.D. D'Andrea, *Repair Pathway Choices and Consequences at the Double-Strand Break.* Trends Cell Biol, 2016. **26**(1): p. 52-64.
66. Bunting, S.F., et al., *53BP1 inhibits homologous recombination in Brca1-deficient cells by blocking resection of DNA breaks.* Cell, 2010. **141**(2): p. 243-54.
67. Bouwman, P., et al., *53BP1 loss rescues BRCA1 deficiency and is associated with triple-negative and BRCA-mutated breast cancers.* Nat Struct Mol Biol, 2010. **17**(6): p. 688-95.
68. Bothmer, A., et al., *53BP1 regulates DNA resection and the choice between classical and alternative end joining during class switch recombination.* J Exp Med, 2010. **207**(4): p. 855-65.
69. Adamo, A., et al., *Preventing nonhomologous end joining suppresses DNA repair defects of Fanconi anemia.* Mol Cell, 2010. **39**(1): p. 25-35.
70. Pace, P., et al., *Ku70 corrupts DNA repair in the absence of the Fanconi anemia pathway.* Science, 2010. **329**(5988): p. 219-23.
71. Kowalczykowski, S.C., *An Overview of the Molecular Mechanisms of Recombinational DNA Repair.* Cold Spring Harb Perspect Biol, 2015. **7**(11).
72. Mehta, A. and J.E. Haber, *Sources of DNA double-strand breaks and models of recombinational DNA repair.* Cold Spring Harb Perspect Biol, 2014. **6**(9): p. a016428.
73. Heyer, W.D., K.T. Ehmsen, and J. Liu, *Regulation of homologous recombination in eukaryotes.* Annu Rev Genet, 2010. **44**: p. 113-39.
74. Kuzminov, A., *Recombinational repair of DNA damage in Escherichia coli and bacteriophage lambda.* Microbiol Mol Biol Rev, 1999. **63**(4): p. 751-813, table of contents.
75. Kreuzer, K.N., *Recombination-dependent DNA replication in phage T4.* Trends Biochem Sci, 2000. **25**(4): p. 165-73.
76. Seitz, E.M., C.A. Haseltine, and S.C. Kowalczykowski, *DNA recombination and repair in the archaea.* Adv Appl Microbiol, 2001. **50**: p. 101-69.

77. Williams, R.S., J.S. Williams, and J.A. Tainer, *Mre11-Rad50-Nbs1 is a keystone complex connecting DNA repair machinery, double-strand break signaling, and the chromatin template.* Biochem Cell Biol, 2007. **85**(4): p. 509-20.
78. Limbo, O., et al., *Ctp1 is a cell-cycle-regulated protein that functions with Mre11 complex to control double-strand break repair by homologous recombination.* Mol Cell, 2007. **28**(1): p. 134-46.
79. Sartori, A.A., et al., *Human CtIP promotes DNA end resection.* Nature, 2007. **450**(7169): p. 509-14.
80. Lengsfeld, B.M., et al., *Sae2 is an endonuclease that processes hairpin DNA cooperatively with the Mre11/Rad50/Xrs2 complex.* Mol Cell, 2007. **28**(4): p. 638-51.
81. Cannavo, E. and P. Cejka, *Sae2 promotes dsDNA endonuclease activity within Mre11-Rad50-Xrs2 to resect DNA breaks.* Nature, 2014. **514**(7520): p. 122-5.
82. Reginato, G., E. Cannavo, and P. Cejka, *Physiological protein blocks direct the Mre11-Rad50-Xrs2 and Sae2 nuclease complex to initiate DNA end resection.* Genes Dev, 2017. **31**(23-24): p. 2325-2330.
83. Wang, W., et al., *Plasticity of the Mre11-Rad50-Xrs2-Sae2 nuclease ensemble in the processing of DNA-bound obstacles.* Genes Dev, 2017. **31**(23-24): p. 2331-2336.
84. Stafa, A., et al., *Template switching during break-induced replication is promoted by the Mph1 helicase in Saccharomyces cerevisiae.* Genetics, 2014. **196**(4): p. 1017-28.
85. Garcia, V., et al., *Bidirectional resection of DNA double-strand breaks by Mre11 and Exo1.* Nature, 2011. **479**(7372): p. 241-4.
86. Symington, L.S., *Mechanism and regulation of DNA end resection in eukaryotes.* Crit Rev Biochem Mol Biol, 2016. **51**(3): p. 195-212.
87. Nimonkar, A.V., et al., *BLM-DNA2-RPA-MRN and EXO1-BLM-RPA-MRN constitute two DNA end resection machineries for human DNA break repair.* Genes Dev, 2011. **25**(4): p. 350-62.
88. Cejka, P., *DNA End Resection: Nucleases Team Up with the Right Partners to Initiate Homologous Recombination.* J Biol Chem, 2015. **290**(38): p. 22931-8.
89. Cannavo, E., P. Cejka, and S.C. Kowalczykowski, *Relationship of DNA degradation by Saccharomyces cerevisiae exonuclease 1 and its stimulation by RPA and Mre11-Rad50-Xrs2 to DNA end resection.* Proc Natl Acad Sci U S A, 2013. **110**(18): p. E1661-8.
90. Sturzenegger, A., et al., *DNA2 cooperates with the WRN and BLM RecQ helicases to mediate long-range DNA end resection in human cells.* J Biol Chem, 2014. **289**(39): p. 27314-27326.

91. Pinto, C., et al., *Human DNA2 possesses a cryptic DNA unwinding activity that functionally integrates with BLM or WRN helicases.* Elife, 2016. **5**.

92. Wu, Y., et al., *EEPD1 Rescues Stressed Replication Forks and Maintains Genome Stability by Promoting End Resection and Homologous Recombination Repair.* PLoS Genet, 2015. **11**(12): p. e1005675.

93. Thangavel, S., et al., *DNA2 drives processing and restart of reversed replication forks in human cells.* J Cell Biol, 2015. **208**(5): p. 545-62.

94. Wold, M.S., *Replication protein A: a heterotrimeric, single-stranded DNA-binding protein required for eukaryotic DNA metabolism.* Annu Rev Biochem, 1997. **66**: p. 61-92.

95. Prakash, R., et al., *Homologous recombination and human health: the roles of BRCA1, BRCA2, and associated proteins.* Cold Spring Harb Perspect Biol, 2015. **7**(4): p. a016600.

96. Sigurdsson, S., et al., *Mediator function of the human Rad51B-Rad51C complex in Rad51/RPA-catalyzed DNA strand exchange.* Genes Dev, 2001. **15**(24): p. 3308-18.

97. Zhao, W., et al., *BRCA1-BARD1 promotes RAD51-mediated homologous DNA pairing.* Nature, 2017. **550**(7676): p. 360-365.

98. Chen, Z., H. Yang, and N.P. Pavletich, *Mechanism of homologous recombination from the RecA-ssDNA/dsDNA structures.* Nature, 2008. **453**(7194): p. 489-4.

99. van der Heijden, T., et al., *Homologous recombination in real time: DNA strand exchange by RecA.* Mol Cell, 2008. **30**(4): p. 530-8.

100. McVey, M., et al., *Eukaryotic DNA Polymerases in Homologous Recombination.* Annu Rev Genet, 2016. **50**: p. 393-421.

101. Kane, D.P., et al., *Competition between replicative and translesion polymerases during homologous recombination repair in Drosophila.* PLoS Genet, 2012. **8**(4): p. e1002659.

102. Hicks, W.M., M. Kim, and J.E. Haber, *Increased mutagenesis and unique mutation signature associated with mitotic gene conversion.* Science, 2010. **329**(5987): p. 82-5.

103. Barber, L.J., et al., *RTEL1 maintains genomic stability by suppressing homologous recombination.* Cell, 2008. **135**(2): p. 261-71.

104. Holliday, R., *The Induction of Mitotic Recombination by Mitomycin C in Ustilago and Saccharomyces.* Genetics, 1964. **50**: p. 323-35.

105. West, S.C., *Molecular views of recombination proteins and their control.* Nat Rev Mol Cell Biol, 2003. **4**(6): p. 435-45.

106. Wyatt, H.D. and S.C. West, *Holliday junction resolvases.* Cold Spring Harb Perspect Biol, 2014. **6**(9): p. a023192.

107. West, S.C., et al., *Resolution of Recombination Intermediates: Mechanisms and Regulation.* Cold Spring Harb Symp Quant Biol, 2015. **80**: p. 103-9.

108. Wu, L. and I.D. Hickson, *The Bloom's syndrome helicase suppresses crossing over during homologous recombination.* Nature, 2003. **426**(6968): p. 870-4.

109. Hickson, I.D., *RecQ helicases: caretakers of the genome.* Nat Rev Cancer, 2003. **3**(3): p. 169-78.

110. Ray, J.H. and J. German, *Bloom's syndrome and EM9 cells in BrdU-containing medium exhibit similarly elevated frequencies of sister chromatid exchange but dissimilar amounts of cellular proliferation and chromosome disruption.* Chromosoma, 1984. **90**(5): p. 383-8.

111. Andersen, S.L., et al., *Drosophila MUS312 and the vertebrate ortholog BTBD12 interact with DNA structure-specific endonucleases in DNA repair and recombination.* Mol Cell, 2009. **35**(1): p. 128-35.

112. Fekairi, S., et al., *Human SLX4 is a Holliday junction resolvase subunit that binds multiple DNA repair/recombination endonucleases.* Cell, 2009. **138**(1): p. 78-89.

113. Munoz, I.M., et al., *Coordination of structure-specific nucleases by human SLX4/BTBD12 is required for DNA repair.* Mol Cell, 2009. **35**(1): p. 116-27.

114. Svendsen, J.M., et al., *Mammalian BTBD12/SLX4 assembles a Holliday junction resolvase and is required for DNA repair.* Cell, 2009. **138**(1): p. 63-77.

115. Castor, D., et al., *Cooperative control of holliday junction resolution and DNA repair by the SLX1 and MUS81-EME1 nucleases.* Mol Cell, 2013. **52**(2): p. 221-33.

116. Garner, E., et al., *Human GEN1 and the SLX4-associated nucleases MUS81 and SLX1 are essential for the resolution of replication-induced Holliday junctions.* Cell Rep, 2013. **5**(1): p. 207-15.

117. Wyatt, H.D., et al., *Coordinated actions of SLX1-SLX4 and MUS81-EME1 for Holliday junction resolution in human cells.* Mol Cell, 2013. **52**(2): p. 234-47.

118. Ip, S.C., et al., *Identification of Holliday junction resolvases from humans and yeast.* Nature, 2008. **456**(7220): p. 357-61.

119. Rass, U., et al., *Mechanism of Holliday junction resolution by the human GEN1 protein.* Genes Dev, 2010. **24**(14): p. 1559-69.

120. Gari, K., et al., *The Fanconi anemia protein FANCM can promote branch migration of Holliday junctions and replication forks.* Mol Cell, 2008. **29**(1): p. 141-8.

121. Girard, C., et al., *FANCM-associated proteins MHF1 and MHF2, but not the other Fanconi anemia factors, limit meiotic crossovers.* Nucleic Acids Res, 2014. **42**(14): p. 9087-95.

122. Sun, W., et al., *The FANCM ortholog Fml1 promotes recombination at stalled replication forks and limits crossing over during DNA double-strand break repair.* Mol Cell, 2008. **32**(1): p. 118-28.
123. Prakash, R., et al., *Yeast Mph1 helicase dissociates Rad51-made D-loops: implications for crossover control in mitotic recombination.* Genes Dev, 2009. **23**(1): p. 67-79.
124. Krejci, L., et al., *DNA helicase Srs2 disrupts the Rad51 presynaptic filament.* Nature, 2003. **423**(6937): p. 305-9.
125. Chiolo, I., et al., *Srs2 and Sgs1 DNA helicases associate with Mre11 in different subcomplexes following checkpoint activation and CDK1-mediated Srs2 phosphorylation.* Mol Cell Biol, 2005. **25**(13): p. 5738-51.
126. Bugreev, D.V., et al., *Novel pro- and anti-recombination activities of the Bloom's syndrome helicase.* Genes Dev, 2007. **21**(23): p. 3085-94.
127. Hu, Y., et al., *RECQL5/Recql5 helicase regulates homologous recombination and suppresses tumor formation via disruption of Rad51 presynaptic filaments.* Genes Dev, 2007. **21**(23): p. 3073-84.
128. Fugger, K., et al., *Human Fbh1 helicase contributes to genome maintenance via pro- and anti-recombinase activities.* J Cell Biol, 2009. **186**(5): p. 655-63.
129. Sommers, J.A., et al., *FANCJ uses its motor ATPase to destabilize protein-DNA complexes, unwind triplexes, and inhibit RAD51 strand exchange.* J Biol Chem, 2009. **284**(12): p. 7505-17.
130. Simandlova, J., et al., *FBH1 helicase disrupts RAD51 filaments in vitro and modulates homologous recombination in mammalian cells.* J Biol Chem, 2013. **288**(47): p. 34168-34180.
131. Moldovan, G.L., et al., *Inhibition of homologous recombination by the PCNA-interacting protein PARI.* Mol Cell, 2012. **45**(1): p. 75-86.
132. Ceccaldi, R., et al., *Homologous-recombination-deficient tumours are dependent on Poltheta-mediated repair.* Nature, 2015. **518**(7538): p. 258-62.
133. Lee, K. and S.E. Lee, *Saccharomyces cerevisiae Sae2- and Tel1-dependent single-strand DNA formation at DNA break promotes microhomology-mediated end joining.* Genetics, 2007. **176**(4): p. 2003-14.
134. Li, F., et al., *Microarray-based genetic screen defines SAW1, a gene required for Rad1/Rad10-dependent processing of recombination intermediates.* Mol Cell, 2008. **30**(3): p. 325-35.
135. Yu, A.M. and M. McVey, *Synthesis-dependent microhomology-mediated end joining accounts for multiple types of repair junctions.* Nucleic Acids Res, 2010. **38**(17): p. 5706-17.
136. O'Connor, K.W., et al., *PARI overexpression promotes genomic instability and pancreatic tumorigenesis.* Cancer Res, 2013. **73**(8): p. 2529-39.

137. Bhargava, R., D.O. Onyango, and J.M. Stark, *Regulation of Single-Strand Annealing and its Role in Genome Maintenance.* Trends Genet, 2016. **32**(9): p. 566-575.
138. Paques, F. and J.E. Haber, *Two pathways for removal of nonhomologous DNA ends during double-strand break repair in Saccharomyces cerevisiae.* Mol Cell Biol, 1997. **17**(11): p. 6765-71.
139. Pannunzio, N.R., G.M. Manthey, and A.M. Bailis, *RAD59 is required for efficient repair of simultaneous double-strand breaks resulting in translocations in Saccharomyces cerevisiae.* DNA Repair (Amst), 2008. **7**(5): p. 788-800.
140. Ackerson, S.M., et al., *To Join or Not to Join: Decision Points Along the Pathway to Double-Strand Break Repair vs. Chromosome End Protection.* Front Cell Dev Biol, 2021. **9**: p. 708763.
141. Scharer, O.D., *Nucleotide excision repair in eukaryotes.* Cold Spring Harb Perspect Biol, 2013. **5**(10): p. a012609.
142. Boyce, R.P. and P. Howard-Flanders, *Release of Ultraviolet Light-Induced Thymine Dimers from DNA in E. Coli K-12.* Proc Natl Acad Sci U S A, 1964. **51**: p. 293-300.
143. Pettijohn, D. and P. Hanawalt, *Evidence for Repair-Replication of Ultraviolet Damaged DNA in Bacteria.* J Mol Biol, 1964. **9**: p. 395-410.
144. Rasmussen, R.E. and R.B. Painter, *Evidence for Repair of Ultra-Violet Damaged Deoxyribonucleic Acid in Cultured Mammalian Cells.* Nature, 1964. **203**: p. 1360-2.
145. Setlow, R.B. and W.L. Carrier, *The Disappearance of Thymine Dimers from DNA: An Error-Correcting Mechanism.* Proc Natl Acad Sci U S A, 1964. **51**: p. 226-31.
146. Cleaver, J.E., *Defective repair replication of DNA in xeroderma pigmentosum.* Nature, 1968. **218**(5142): p. 652-6.
147. DiGiovanna, J.J. and K.H. Kraemer, *Shining a light on xeroderma pigmentosum.* J Invest Dermatol, 2012. **132**(3 Pt 2): p. 785-96.
148. Lehmann, A.R., *DNA repair-deficient diseases, xeroderma pigmentosum, Cockayne syndrome and trichothiodystrophy.* Biochimie, 2003. **85**(11): p. 1101-11.
149. Marteijn, J.A., et al., *Understanding nucleotide excision repair and its roles in cancer and ageing.* Nat Rev Mol Cell Biol, 2014. **15**(7): p. 465-81.
150. Spivak, G., *Nucleotide excision repair in humans.* DNA Repair (Amst), 2015. **36**: p. 13-18.
151. Gillet, L.C. and O.D. Scharer, *Molecular mechanisms of mammalian global genome nucleotide excision repair.* Chem Rev, 2006. **106**(2): p. 253-76.
152. Hanawalt, P.C. and G. Spivak, *Transcription-coupled DNA repair: two decades of progress and surprises.* Nat Rev Mol Cell Biol, 2008. **9**(12): p. 958-70.

153. Sancar, A. and W.D. Rupp, *A novel repair enzyme: UVRABC excision nuclease of Escherichia coli cuts a DNA strand on both sides of the damaged region.* Cell, 1983. **33**(1): p. 249-60.
154. Sladek, F.M., et al., *In vitro repair of psoralen-DNA cross-links by RecA, UvrABC, and the 5'-exonuclease of DNA polymerase I.* J Biol Chem, 1989. **264**(12): p. 6755-65.
155. Zhao, J., et al., *Mismatch repair and nucleotide excision repair proteins cooperate in the recognition of DNA interstrand crosslinks.* Nucleic Acids Res, 2009. **37**(13): p. 4420-9.
156. Cole, R.S., *Repair of DNA containing interstrand crosslinks in Escherichia coli: sequential excision and recombination.* Proc Natl Acad Sci U S A, 1973. **70**(4): p. 1064-8.
157. Cheng, S., A. Sancar, and J.E. Hearst, *RecA-dependent incision of psoralen-crosslinked DNA by (A)BC excinuclease.* Nucleic Acids Res, 1991. **19**(3): p. 657-63.
158. Noll, D.M., T.M. Mason, and P.S. Miller, *Formation and repair of interstrand cross-links in DNA.* Chem Rev, 2006. **106**(2): p. 277-301.
159. Semlow, D.R. and J.C. Walter, *Mechanisms of Vertebrate DNA Interstrand Cross-Link Repair.* Annu Rev Biochem, 2021. **90**: p. 107-135.
160. Sugasawa, K., et al., *Xeroderma pigmentosum group C protein complex is the initiator of global genome nucleotide excision repair.* Mol Cell, 1998. **2**(2): p. 223-32.
161. Volker, M., et al., *Sequential assembly of the nucleotide excision repair factors in vivo.* Mol Cell, 2001. **8**(1): p. 213-24.
162. De Silva, I.U., et al., *Defining the roles of nucleotide excision repair and recombination in the repair of DNA interstrand cross-links in mammalian cells.* Mol Cell Biol, 2000. **20**(21): p. 7980-90.
163. Lehmann, A.R., *Replication of damaged DNA in mammalian cells: new solutions to an old problem.* Mutat Res, 2002. **509**(1-2): p. 23-34.
164. Ulrich, H.D., *Conservation of DNA damage tolerance pathways from yeast to humans.* Biochem Soc Trans, 2007. **35**(Pt 5): p. 1334-7.
165. Hoeijmakers, J.H., *Genome maintenance mechanisms for preventing cancer.* Nature, 2001. **411**(6835): p. 366-74.
166. Baynton, K. and R.P. Fuchs, *Lesions in DNA: hurdles for polymerases.* Trends Biochem Sci, 2000. **25**(2): p. 74-9.
167. Ler, A.A.L. and M.P. Carty, *DNA Damage Tolerance Pathways in Human Cells: A Potential Therapeutic Target.* Front Oncol, 2021. **11**: p. 822500.
168. Makarova, A.V. and P.M. Burgers, *Eukaryotic DNA polymerase zeta.* DNA Repair (Amst), 2015. **29**: p. 47-55.

169. Yang, W., *An overview of Y-Family DNA polymerases and a case study of human DNA polymerase eta.* Biochemistry, 2014. **53**(17): p. 2793-803.

170. Waters, L.S., et al., *Eukaryotic translesion polymerases and their roles and regulation in DNA damage tolerance.* Microbiol Mol Biol Rev, 2009. **73**(1): p. 134-54.

171. McCulloch, S.D. and T.A. Kunkel, *The fidelity of DNA synthesis by eukaryotic replicative and translesion synthesis polymerases.* Cell Res, 2008. **18**(1): p. 148-61.

172. Makridakis, N.M. and J.K. Reichardt, *Translesion DNA polymerases and cancer.* Front Genet, 2012. **3**: p. 174.

173. Knobel, P.A. and T.M. Marti, *Translesion DNA synthesis in the context of cancer research.* Cancer Cell Int, 2011. **11**: p. 39.

174. Basu, A., et al., *DNA damage, mutagenesis, and DNA repair.* J Nucleic Acids, 2010. **2010**: p. 182894.

175. Pilzecker, B., O.A. Buoninfante, and H. Jacobs, *DNA damage tolerance in stem cells, ageing, mutagenesis, disease and cancer therapy.* Nucleic Acids Res, 2019. **47**(14): p. 7163-7181.

176. Quinet, A., et al., *Filling gaps in translesion DNA synthesis in human cells.* Mutat Res Genet Toxicol Environ Mutagen, 2018. **836**(Pt B): p. 127-142.

177. Guo, C., et al., *Y-family DNA polymerases in mammalian cells.* Cell Mol Life Sci, 2009. **66**(14): p. 2363-81.

178. Friedberg, E.C., R. Wagner, and M. Radman, *Specialized DNA polymerases, cellular survival, and the genesis of mutations.* Science, 2002. **296**(5573): p. 1627-30.

179. Bridges, B.A. and R. Woodgate, *Mutagenic repair in Escherichia coli: products of the recA gene and of the umuD and umuC genes act at different steps in UV-induced mutagenesis.* Proc Natl Acad Sci U S A, 1985. **82**(12): p. 4193-7.

180. Bridges, B.A. and R. Woodgate, *The two-step model of bacterial UV mutagenesis.* Mutat Res, 1985. **150**(1-2): p. 133-9.

181. Goodman, M.F. and R. Woodgate, *Translesion DNA polymerases.* Cold Spring Harb Perspect Biol, 2013. **5**(10): p. a010363.

182. Murakumo, Y., et al., *A human REV7 homolog that interacts with the polymerase zeta catalytic subunit hREV3 and the spindle assembly checkpoint protein hMAD2.* J Biol Chem, 2000. **275**(6): p. 4391-7.

183. Nelson, J.R., C.W. Lawrence, and D.C. Hinkle, *Thymine-thymine dimer bypass by yeast DNA polymerase zeta.* Science, 1996. **272**(5268): p. 1646-9.

184. Clairmont, C.S. and A.D. D'Andrea, *REV7 directs DNA repair pathway choice.* Trends Cell Biol, 2021. **31**(12): p. 965-978.
185. de Krijger, I., V. Boersma, and J.J.L. Jacobs, *REV7: Jack of many trades.* Trends Cell Biol, 2021. **31**(8): p. 686-701.
186. Nair, D.T., et al., *Rev1 employs a novel mechanism of DNA synthesis using a protein template.* Science, 2005. **309**(5744): p. 2219-22.
187. Martin, S.K. and R.D. Wood, *DNA polymerase zeta in DNA replication and repair.* Nucleic Acids Res, 2019. **47**(16): p. 8348-8361.
188. Raschle, M., et al., *Mechanism of replication-coupled DNA interstrand crosslink repair.* Cell, 2008. **134**(6): p. 969-80.
189. Budzowska, M., et al., *Regulation of the Rev1-pol zeta complex during bypass of a DNA interstrand cross-link.* EMBO J, 2015. **34**(14): p. 1971-85.
190. Neal, J.A., et al., *The role of hRev7, the accessory subunit of hPolzeta, in translesion synthesis past DNA damage induced by benzo[a]pyrene diol epoxide (BPDE).* BMC Cell Biol, 2010. **11**: p. 97.
191. Sonoda, E., et al., *Multiple roles of Rev3, the catalytic subunit of polzeta in maintaining genome stability in vertebrates.* EMBO J, 2003. **22**(12): p. 3188-97.
192. Okada, T., et al., *Multiple roles of vertebrate REV genes in DNA repair and recombination.* Mol Cell Biol, 2005. **25**(14): p. 6103-11.
193. Hicks, J.K., et al., *Differential roles for DNA polymerases eta, zeta, and REV1 in lesion bypass of intrastrand versus interstrand DNA cross-links.* Mol Cell Biol, 2010. **30**(5): p. 1217-30.
194. Sharma, S., et al., *REV1 and polymerase zeta facilitate homologous recombination repair.* Nucleic Acids Res, 2012. **40**(2): p. 682-91.
195. Bluteau, D., et al., *Biallelic inactivation of REV7 is associated with Fanconi anemia.* J Clin Invest, 2016. **126**(9): p. 3580-4.
196. Khalaj, M., et al., *A missense mutation in Rev7 disrupts formation of Polzeta, impairing mouse development and repair of genotoxic agent-induced DNA lesions.* J Biol Chem, 2014. **289**(6): p. 3811-24.
197. Garaycoechea, J.I., C. Quinlan, and M.S. Luijsterburg, *Pathological consequences of DNA damage in the kidney.* Nat Rev Nephrol, 2023. **19**(4): p. 229-243.
198. Lord, C.J. and A. Ashworth, *The DNA damage response and cancer therapy.* Nature, 2012. **481**(7381): p. 287-94.

199. Bergink, S. and S. Jentsch, *Principles of ubiquitin and SUMO modifications in DNA repair.* Nature, 2009. **458**(7237): p. 461-7.
200. Komander, D. and M. Rape, *The ubiquitin code.* Annu Rev Biochem, 2012. **81**: p. 203-29.
201. Yates, M. and A. Marechal, *Ubiquitylation at the Fork: Making and Breaking Chains to Complete DNA Replication.* Int J Mol Sci, 2018. **19**(10).
202. Jackson, S.P. and D. Durocher, *Regulation of DNA damage responses by ubiquitin and SUMO.* Mol Cell, 2013. **49**(5): p. 795-807.
203. Schwertman, P., S. Bekker-Jensen, and N. Mailand, *Regulation of DNA double-strand break repair by ubiquitin and ubiquitin-like modifiers.* Nat Rev Mol Cell Biol, 2016. **17**(6): p. 379-94.
204. Kim, W., et al., *Systematic and quantitative assessment of the ubiquitin-modified proteome.* Mol Cell, 2011. **44**(2): p. 325-40.
205. Wagner, S.A., et al., *A proteome-wide, quantitative survey of in vivo ubiquitylation sites reveals widespread regulatory roles.* Mol Cell Proteomics, 2011. **10**(10): p. M111 013284.
206. Wei, Y. and X. Xu, *UFMylation: A Unique & Fashionable Modification for Life.* Genomics Proteomics Bioinformatics, 2016. **14**(3): p. 140-146.
207. Komander, D., M.J. Clague, and S. Urbe, *Breaking the chains: structure and function of the deubiquitinases.* Nat Rev Mol Cell Biol, 2009. **10**(8): p. 550-63.
208. Dikic, I., S. Wakatsuki, and K.J. Walters, *Ubiquitin-binding domains - from structures to functions.* Nat Rev Mol Cell Biol, 2009. **10**(10): p. 659-71.
209. Lukas, J., C. Lukas, and J. Bartek, *More than just a focus: The chromatin response to DNA damage and its role in genome integrity maintenance.* Nat Cell Biol, 2011. **13**(10): p. 1161-9.
210. Kinner, A., et al., *Gamma-H2AX in recognition and signaling of DNA double-strand breaks in the context of chromatin.* Nucleic Acids Res, 2008. **36**(17): p. 5678-94.
211. Stucki, M., et al., *MDC1 directly binds phosphorylated histone H2AX to regulate cellular responses to DNA double-strand breaks.* Cell, 2005. **123**(7): p. 1213-26.
212. Kolas, N.K., et al., *Orchestration of the DNA-damage response by the RNF8 ubiquitin ligase.* Science, 2007. **318**(5856): p. 1637-40.
213. Mailand, N., et al., *RNF8 ubiquitylates histones at DNA double-strand breaks and promotes assembly of repair proteins.* Cell, 2007. **131**(5): p. 887-900.
214. Huen, M.S., et al., *RNF8 transduces the DNA-damage signal via histone ubiquitylation and checkpoint protein assembly.* Cell, 2007. **131**(5): p. 901-14.

215. Panier, S., et al., *Tandem protein interaction modules organize the ubiquitin-dependent response to DNA double-strand breaks.* Mol Cell, 2012. **47**(3): p. 383-95.

216. Doil, C., et al., *RNF168 binds and amplifies ubiquitin conjugates on damaged chromosomes to allow accumulation of repair proteins.* Cell, 2009. **136**(3): p. 435-46.

217. Stewart, G.S., et al., *The RIDDLE syndrome protein mediates a ubiquitin-dependent signaling cascade at sites of DNA damage.* Cell, 2009. **136**(3): p. 420-34.

218. Lehmann, A.R., *Ubiquitin-family modifications in the replication of DNA damage.* FEBS Lett, 2011. **585**(18): p. 2772-9.

219. Wu, R.A., et al., *TRAIP is a master regulator of DNA interstrand crosslink repair.* Nature, 2019. **567**(7747): p. 267-272.

220. Tan, W. and A.J. Deans, *The ubiquitination machinery of the Fanconi Anemia DNA repair pathway.* Prog Biophys Mol Biol, 2021. **163**: p. 5-13.

221. Huang, Y., et al., *Modularized functions of the Fanconi anemia core complex.* Cell Rep, 2014. **7**(6): p. 1849-57.

222. Niraj, J., A. Farkkila, and A.D. D'Andrea, *The Fanconi Anemia Pathway in Cancer.* Annu Rev Cancer Biol, 2019. **3**: p. 457-478.

223. Kottemann, M.C. and A. Smogorzewska, *Fanconi anaemia and the repair of Watson and Crick DNA crosslinks.* Nature, 2013. **493**(7432): p. 356-63.

224. Ceccaldi, R., P. Sarangi, and A.D. D'Andrea, *The Fanconi anaemia pathway: new players and new functions.* Nat Rev Mol Cell Biol, 2016. **17**(6): p. 337-49.

225. Nijman, S.M., et al., *The deubiquitinating enzyme USP1 regulates the Fanconi anemia pathway.* Mol Cell, 2005. **17**(3): p. 331-9.

226. Tanaka, K., T. Suzuki, and T. Chiba, *The ligation systems for ubiquitin and ubiquitin-like proteins.* Mol Cells, 1998. **8**(5): p. 503-12.

227. Jentsch, S. and G. Pyrowolakis, *Ubiquitin and its kin: how close are the family ties?* Trends Cell Biol, 2000. **10**(8): p. 335-42.

228. Yeh, E.T., L. Gong, and T. Kamitani, *Ubiquitin-like proteins: new wines in new bottles.* Gene, 2000. **248**(1-2): p. 1-14.

229. Schwartz, D.C. and M. Hochstrasser, *A superfamily of protein tags: ubiquitin, SUMO and related modifiers.* Trends Biochem Sci, 2003. **28**(6): p. 321-8.

230. Komatsu, M., et al., *A novel protein-conjugating system for Ufm1, a ubiquitin-fold modifier.* EMBO J, 2004. **23**(9): p. 1977-86.

231. Gerakis, Y., et al., *The UFMylation System in Proteostasis and Beyond.* Trends Cell Biol, 2019. **29**(12): p. 974-986.
232. Kang, S.H., et al., *Two novel ubiquitin-fold modifier 1 (Ufm1)-specific proteases, UfSP1 and UfSP2.* J Biol Chem, 2007. **282**(8): p. 5256-62.
233. Ha, B.H., et al., *Structural basis for Ufm1 processing by UfSP1.* J Biol Chem, 2008. **283**(21): p. 14893-900.
234. Ha, B.H., et al., *Structure of ubiquitin-fold modifier 1-specific protease UfSP2.* J Biol Chem, 2011. **286**(12): p. 10248-57.
235. Liu, G., et al., *NMR and X-RAY structures of human E2-like ubiquitin-fold modifier conjugating enzyme 1 (UFC1) reveal structural and functional conservation in the metazoan UFM1-UBA5-UFC1 ubiquination pathway.* J Struct Funct Genomics, 2009. **10**(2): p. 127-36.
236. Zheng, M., et al., *UBE1DC1, an ubiquitin-activating enzyme, activates two different ubiquitin-like proteins.* J Cell Biochem, 2008. **104**(6): p. 2324-34.
237. Tatsumi, K., et al., *A novel type of E3 ligase for the Ufm1 conjugation system.* J Biol Chem, 2010. **285**(8): p. 5417-27.
238. Lemaire, K., et al., *Ubiquitin fold modifier 1 (UFM1) and its target UFBP1 protect pancreatic beta cells from ER stress-induced apoptosis.* PLoS One, 2011. **6**(4): p. e18517.
239. Cai, Y., et al., *UFBP1, a Key Component of the Ufm1 Conjugation System, Is Essential for Ufmylation-Mediated Regulation of Erythroid Development.* PLoS Genet, 2015. **11**(11): p. e1005643.
240. Liu, J., et al., *A critical role of DDRGK1 in endoplasmic reticulum homoeostasis via regulation of IRE1alpha stability.* Nat Commun, 2017. **8**: p. 14186.
241. Yoo, H.M., et al., *Modification of ASC1 by UFM1 is crucial for ERalpha transactivation and breast cancer development.* Mol Cell, 2014. **56**(2): p. 261-274.
242. Zhang, M., et al., *RCAD/Ufl1, a Ufm1 E3 ligase, is essential for hematopoietic stem cell function and murine hematopoiesis.* Cell Death Differ, 2015. **22**(12): p. 1922-34.
243. Liu, J., et al., *UFMylation maintains tumour suppressor p53 stability by antagonizing its ubiquitination.* Nat Cell Biol, 2020. **22**(9): p. 1056-1063.
244. Wang, Z., et al., *MRE11 UFMylation promotes ATM activation.* Nucleic Acids Res, 2019. **47**(8): p. 4124-4135.
245. Lee, L., et al., *UFMylation of MRE11 is essential for telomere length maintenance and hematopoietic stem cell survival.* Sci Adv, 2021. **7**(39): p. eabc7371.

246. Qin, B., et al., *UFL1 promotes histone H4 ufmylation and ATM activation.* Nat Commun, 2019. **10**(1): p. 1242.

247. Muona, M., et al., *Biallelic Variants in UBA5 Link Dysfunctional UFM1 Ubiquitin-like Modifier Pathway to Severe Infantile-Onset Encephalopathy.* Am J Hum Genet, 2016. **99**(3): p. 683-694.

248. Colin, E., et al., *Biallelic Variants in UBA5 Reveal that Disruption of the UFM1 Cascade Can Result in Early-Onset Encephalopathy.* Am J Hum Genet, 2016. **99**(3): p. 695-703.

249. Duan, R., et al., *UBA5 Mutations Cause a New Form of Autosomal Recessive Cerebellar Ataxia.* PLoS One, 2016. **11**(2): p. e0149039.

250. Di Rocco, M., et al., *Novel spondyloepimetaphyseal dysplasia due to UFSP2 gene mutation.* Clin Genet, 2018. **93**(3): p. 671-674.

251. Egunsola, A.T., et al., *Loss of DDRGK1 modulates SOX9 ubiquitination in spondyloepimetaphyseal dysplasia.* J Clin Invest, 2017. **127**(4): p. 1475-1484.

252. Watson, C.M., et al., *Identification of a mutation in the ubiquitin-fold modifier 1-specific peptidase 2 gene, UFSP2, in an extended South African family with Beukes hip dysplasia.* S Afr Med J, 2015. **105**(7): p. 558-63.

253. Sancar, A., et al., *Molecular mechanisms of mammalian DNA repair and the DNA damage checkpoints.* Annu Rev Biochem, 2004. **73**: p. 39-85.

254. Zhou, B.B. and S.J. Elledge, *The DNA damage response: putting checkpoints in perspective.* Nature, 2000. **408**(6811): p. 433-9.

255. Harrison, J.C. and J.E. Haber, *Surviving the breakup: the DNA damage checkpoint.* Annu Rev Genet, 2006. **40**: p. 209-35.

256. Waterman, D.P., J.E. Haber, and M.B. Smolka, *Checkpoint Responses to DNA Double-Strand Breaks.* Annu Rev Biochem, 2020. **89**: p. 103-133.

257. Giglia-Mari, G., A. Zotter, and W. Vermeulen, *DNA damage response.* Cold Spring Harb Perspect Biol, 2011. **3**(1): p. a000745.

258. Weinert, T.A. and L.H. Hartwell, *The RAD9 gene controls the cell cycle response to DNA damage in Saccharomyces cerevisiae.* Science, 1988. **241**(4863): p. 317-22.

259. Hartwell, L.H. and T.A. Weinert, *Checkpoints: controls that ensure the order of cell cycle events.* Science, 1989. **246**(4930): p. 629-34.

260. Kim, S.T., et al., *Substrate specificities and identification of putative substrates of ATM kinase family members.* J Biol Chem, 1999. **274**(53): p. 37538-43.

261. O'Neill, T., et al., *Utilization of oriented peptide libraries to identify substrate motifs selected by ATM.* J Biol Chem, 2000. **275**(30): p. 22719-27.

262. Kim, J.H., et al., *The Mre11-Nbs1 Interface Is Essential for Viability and Tumor Suppression.* Cell Rep, 2017. **18**(2): p. 496-507.

263. Shroff, R., et al., *Distribution and dynamics of chromatin modification induced by a defined DNA double-strand break.* Curr Biol, 2004. **14**(19): p. 1703-11.

264. Ira, G., et al., *DNA end resection, homologous recombination and DNA damage checkpoint activation require CDK1.* Nature, 2004. **431**(7011): p. 1011-7.

265. Mantiero, D., et al., *Dual role for Saccharomyces cerevisiae Tel1 in the checkpoint response to double-strand breaks.* EMBO Rep, 2007. **8**(4): p. 380-7.

266. Rogakou, E.P., et al., *DNA double-stranded breaks induce histone H2AX phosphorylation on serine 139.* J Biol Chem, 1998. **273**(10): p. 5858-68.

267. Savic, V., et al., *Formation of dynamic gamma-H2AX domains along broken DNA strands is distinctly regulated by ATM and MDC1 and dependent upon H2AX densities in chromatin.* Mol Cell, 2009. **34**(3): p. 298-310.

268. Fernandez-Capetillo, O., et al., *H2AX: the histone guardian of the genome.* DNA Repair (Amst), 2004. **3**(8-9): p. 959-67.

269. Stucki, M. and S.P. Jackson, *gammaH2AX and MDC1: anchoring the DNA-damage-response machinery to broken chromosomes.* DNA Repair (Amst), 2006. **5**(5): p. 534-43.

270. Bartek, J. and J. Lukas, *Mammalian G1- and S-phase checkpoints in response to DNA damage.* Curr Opin Cell Biol, 2001. **13**(6): p. 738-47.

271. Pardee, A.B., *Regulation, restriction, and reminiscences.* J Biol Chem, 2002. **277**(30): p. 26709-16.

272. Paulovich, A.G. and L.H. Hartwell, *A checkpoint regulates the rate of progression through S phase in S. cerevisiae in response to DNA damage.* Cell, 1995. **82**(5): p. 841-7.

273. Painter, R.B. and B.R. Young, *Radiosensitivity in ataxia-telangiectasia: a new explanation.* Proc Natl Acad Sci U S A, 1980. **77**(12): p. 7315-7.

274. Santocanale, C. and J.F. Diffley, *A Mec1- and Rad53-dependent checkpoint controls late-firing origins of DNA replication.* Nature, 1998. **395**(6702): p. 615-8.

275. Tercero, J.A. and J.F. Diffley, *Regulation of DNA replication fork progression through damaged DNA by the Mec1/Rad53 checkpoint.* Nature, 2001. **412**(6846): p. 553-7.

276. Costanzo, V., et al., *Reconstitution of an ATM-dependent checkpoint that inhibits chromosomal DNA replication following DNA damage.* Mol Cell, 2000. **6**(3): p. 649-59.

277. Kastan, M.B., et al., *A mammalian cell cycle checkpoint pathway utilizing p53 and GADD45 is defective in ataxia-telangiectasia.* Cell, 1992. **71**(4): p. 587-97.

278. Heffernan, T.P., et al., *An ATR- and Chk1-dependent S checkpoint inhibits replicon initiation following UVC-induced DNA damage.* Mol Cell Biol, 2002. **22**(24): p. 8552-61.

279. Howlett, N.G., et al., *Biallelic inactivation of BRCA2 in Fanconi anemia.* Science, 2002. **297**(5581): p. 606-9.

280. Abraham, R.T., *Cell cycle checkpoint signaling through the ATM and ATR kinases.* Genes Dev, 2001. **15**(17): p. 2177-96.

281. Cortez, D., et al., *ATR and ATRIP: partners in checkpoint signaling.* Science, 2001. **294**(5547): p. 1713-6.

282. Tibbetts, R.S., et al., *Functional interactions between BRCA1 and the checkpoint kinase ATR during genotoxic stress.* Genes Dev, 2000. **14**(23): p. 2989-3002.

283. Lee, J.S., et al., *hCds1-mediated phosphorylation of BRCA1 regulates the DNA damage response.* Nature, 2000. **404**(6774): p. 201-4.

284. Zhao, H. and H. Piwnica-Worms, *ATR-mediated checkpoint pathways regulate phosphorylation and activation of human Chk1.* Mol Cell Biol, 2001. **21**(13): p. 4129-39.

285. Xu, B., et al., *Two molecularly distinct G(2)/M checkpoints are induced by ionizing irradiation.* Mol Cell Biol, 2002. **22**(4): p. 1049-59.

286. Brown, E.J. and D. Baltimore, *Essential and dispensable roles of ATR in cell cycle arrest and genome maintenance.* Genes Dev, 2003. **17**(5): p. 615-28.

287. Gorgoulis, V., et al., *Cellular Senescence: Defining a Path Forward.* Cell, 2019. **179**(4): p. 813-827.

288. Hayflick, L. and P.S. Moorhead, *The serial cultivation of human diploid cell strains.* Exp Cell Res, 1961. **25**: p. 585-621.

289. Hernandez-Segura, A., J. Nehme, and M. Demaria, *Hallmarks of Cellular Senescence.* Trends Cell Biol, 2018. **28**(6): p. 436-453.

290. Rodier, F. and J. Campisi, *Four faces of cellular senescence.* J Cell Biol, 2011. **192**(4): p. 547-56.

291. d'Adda di Fagagna, F., *Living on a break: cellular senescence as a DNA-damage response.* Nat Rev Cancer, 2008. **8**(7): p. 512-22.

292. Halazonetis, T.D., V.G. Gorgoulis, and J. Bartek, *An oncogene-induced DNA damage model for cancer development.* Science, 2008. **319**(5868): p. 1352-5.

293. Hills, S.A. and J.F. Diffley, *DNA replication and oncogene-induced replicative stress.* Curr Biol, 2014. **24**(10): p. R435-44.

294. Passos, J.F. and T. Von Zglinicki, *Oxygen free radicals in cell senescence: are they signal transducers?* Free Radic Res, 2006. **40**(12): p. 1277-83.
295. Collin, G., et al., *Transcriptional repression of DNA repair genes is a hallmark and a cause of cellular senescence.* Cell Death Dis, 2018. **9**(3): p. 259.
296. Serrano, M., et al., *Oncogenic ras provokes premature cell senescence associated with accumulation of p53 and p16INK4a.* Cell, 1997. **88**(5): p. 593-602.
297. Sharpless, N.E. and C.J. Sherr, *Forging a signature of in vivo senescence.* Nat Rev Cancer, 2015. **15**(7): p. 397-408.
298. Yousefzadeh, M., et al., *DNA damage-how and why we age?* Elife, 2021. **10**.
299. Beausejour, C.M., et al., *Reversal of human cellular senescence: roles of the p53 and p16 pathways.* EMBO J, 2003. **22**(16): p. 4212-22.
300. Lanigan, F., J.G. Geraghty, and A.P. Bracken, *Transcriptional regulation of cellular senescence.* Oncogene, 2011. **30**(26): p. 2901-11.
301. McClintock, B., *The Stability of Broken Ends of Chromosomes in Zea Mays.* Genetics, 1941. **26**(2): p. 234-82.
302. McClintock, B., *The Behavior in Successive Nuclear Divisions of a Chromosome Broken at Meiosis.* Proc Natl Acad Sci U S A, 1939. **25**(8): p. 405-16.
303. McClintock, B., *Letter from Barbara McClintock to Elizabeth H. Blackburn.* The American Philosophical Society. Library. Barbara McClintock Papers, 1983.
304. Hayflick, L., *The Limited in Vitro Lifetime of Human Diploid Cell Strains.* Exp Cell Res, 1965. **37**: p. 614-36.
305. Olovnikov, A.M., *A theory of marginotomy. The incomplete copying of template margin in enzymic synthesis of polynucleotides and biological significance of the phenomenon.* J Theor Biol, 1973. **41**(1): p. 181-90.
306. Hanahan, D. and R.A. Weinberg, *The hallmarks of cancer.* Cell, 2000. **100**(1): p. 57-70.
307. Hanahan, D., *Hallmarks of Cancer: New Dimensions.* Cancer Discov, 2022. **12**(1): p. 31-46.
308. Prieur, A. and D.S. Peeper, *Cellular senescence in vivo: a barrier to tumorigenesis.* Curr Opin Cell Biol, 2008. **20**(2): p. 150-5.
309. Jones, C.J., et al., *Evidence for a telomere-independent "clock" limiting RAS oncogene-driven proliferation of human thyroid epithelial cells.* Mol Cell Biol, 2000. **20**(15): p. 5690-9.
310. Di Micco, R., M. Fumagalli, and F. d'Adda di Fagagna, *Breaking news: high-speed race ends in arrest--how oncogenes induce senescence.* Trends Cell Biol, 2007. **17**(11): p. 529-36.

311. Guido, F., *Familiäre infantile perniziosaartige Anämie (perniziöses Blutbild und Konstitution)/ [Familial infantile pernicious-like anemia (pernicious blood picture and constitution)]*. Jahrbuch for Kinderheilkunde, 1927. **117**: p. 257-280.

312. Auerbach, A.D., *Fanconi anemia and its diagnosis.* Mutat Res, 2009. **668**(1-2): p. 4-10.

313. Auerbach, A.D., A. Rogatko, and T.M. Schroeder-Kurth, *International Fanconi Anemia Registry: relation of clinical symptoms to diepoxybutane sensitivity.* Blood, 1989. **73**(2): p. 391-6.

314. Cervenka, J., D. Arthur, and C. Yasis, *Mitomycin C test for diagnostic differentiation of idiopathic aplastic anemia and Fanconi anemia.* Pediatrics, 1981. **67**(1): p. 119-27.

315. Rosenberg, P.S., H. Tamary, and B.P. Alter, *How high are carrier frequencies of rare recessive syndromes? Contemporary estimates for Fanconi Anemia in the United States and Israel.* Am J Med Genet A, 2011. **155A**(8): p. 1877-83.

316. Rosendorff, J., et al., *Fanconi anemia: another disease of unusually high prevalence in the Afrikaans population of South Africa.* Am J Med Genet, 1987. **27**(4): p. 793-7.

317. Tamary, H., et al., *Frequency and natural history of inherited bone marrow failure syndromes: the Israeli Inherited Bone Marrow Failure Registry.* Haematologica, 2010. **95**(8): p. 1300-7.

318. Callen, E., et al., *A common founder mutation in FANCA underlies the world's highest prevalence of Fanconi anemia in Gypsy families from Spain.* Blood, 2005. **105**(5): p. 1946-9.

319. O'Rourke, J.J. and A.J. Deans, *The Fanca to Fancz of DNA Interstrand Crosslink Repair: Lessons from Fanconi Anemia.* DNA Repair in Cancer Therapy: Molecular Targets and Clinical Applications, 2nd Edition, 2016: p. 353-381.

320. Kutler, D.I., et al., *A 20-year perspective on the International Fanconi Anemia Registry (IFAR).* Blood, 2003. **101**(4): p. 1249-56.

321. Giri, N., et al., *Endocrine abnormalities in patients with Fanconi anemia.* J Clin Endocrinol Metab, 2007. **92**(7): p. 2624-31.

322. D'Andrea, A.D., *Susceptibility Pathways in Fanconi's Anemia and Breast Cancer.* New England Journal of Medicine, 2010. **362**(20): p. 1909-1919.

323. Deans, A.J. and S.C. West, *DNA interstrand crosslink repair and cancer.* Nat Rev Cancer, 2011. **11**(7): p. 467-80.

324. Alter, B.P., *Cancer in Fanconi anemia, 1927-2001.* Cancer, 2003. **97**(2): p. 425-40.

325. Kutler, D.I., et al., *High incidence of head and neck squamous cell carcinoma in patients with Fanconi anemia.* Arch Otolaryngol Head Neck Surg, 2003. **129**(1): p. 106-12.

326. Rosenberg, P.S., M.H. Greene, and B.P. Alter, *Cancer incidence in persons with Fanconi anemia.* Blood, 2003. **101**(3): p. 822-6.

327. Alter, B.P., P.S. Rosenberg, and L.C. Brody, *Clinical and molecular features associated with biallelic mutations in FANCD1/BRCA2.* J Med Genet, 2007. **44**(1): p. 1-9.

328. Myers, K., et al., *The clinical phenotype of children with Fanconi anemia caused by biallelic FANCD1/BRCA2 mutations.* Pediatr Blood Cancer, 2012. **58**(3): p. 462-5.

329. Michl, J., J. Zimmer, and M. Tarsounas, *Interplay between Fanconi anemia and homologous recombination pathways in genome integrity.* EMBO J, 2016. **35**(9): p. 909-23.

330. D'Andrea, A.D., *The Fanconi road to cancer.* Genes Dev, 2003. **17**(16): p. 1933-6.

331. King, M.C., et al., *Breast and ovarian cancer risks due to inherited mutations in BRCA1 and BRCA2.* Science, 2003. **302**(5645): p. 643-6.

332. Southey, M.C., et al., *A PALB2 mutation associated with high risk of breast cancer.* Breast Cancer Res, 2010. **12**(6): p. R109.

333. Hofstatter, E.W., et al., *PALB2 mutations in familial breast and pancreatic cancer.* Fam Cancer, 2011. **10**(2): p. 225-31.

334. Tischkowitz, M.D., et al., *Analysis of the gene coding for the BRCA2-interacting protein PALB2 in familial and sporadic pancreatic cancer.* Gastroenterology, 2009. **137**(3): p. 1183-6.

335. Kiiski, J.I., et al., *Exome sequencing identifies FANCM as a susceptibility gene for triple-negative breast cancer.* Proc Natl Acad Sci U S A, 2014. **111**(42): p. 15172-7.

336. Solyom, S., et al., *Screening for large genomic rearrangements in the FANCA gene reveals extensive deletion in a Finnish breast cancer family.* Cancer Lett, 2011. **302**(2): p. 113-8.

337. Vaz, F., et al., *Mutation of the RAD51C gene in a Fanconi anemia-like disorder.* Nat Genet, 2010. **42**(5): p. 406-9.

338. van der Heijden, M.S., et al., *Fanconi anemia gene mutations in young-onset pancreatic cancer.* Cancer Res, 2003. **63**(10): p. 2585-8.

339. Virts, E.L., et al., *AluY-mediated germline deletion, duplication and somatic stem cell reversion in UBE2T defines a new subtype of Fanconi anemia.* Hum Mol Genet, 2015. **24**(18): p. 5093-108.

340. Ciccia, A., et al., *Identification of FAAP24, a Fanconi anemia core complex protein that interacts with FANCM.* Mol Cell, 2007. **25**(3): p. 331-43.

341. Clauson, C., O.D. Scharer, and L. Niedernhofer, *Advances in understanding the complex mechanisms of DNA interstrand cross-link repair.* Cold Spring Harb Perspect Biol, 2013. **5**(10): p. a012732.

342. Stone, M.P., et al., *Interstrand DNA cross-links induced by alpha,beta-unsaturated aldehydes derived from lipid peroxidation and environmental sources.* Acc Chem Res, 2008. **41**(7): p. 793-804.

343. Ridpath, J.R., et al., *Cells deficient in the FANC/BRCA pathway are hypersensitive to plasma levels of formaldehyde.* Cancer Res, 2007. **67**(23): p. 11117-22.

344. Kirchner, J.J., S.T. Sigurdsson, and P.B. Hopkins, *Interstrand cross-linking of duplex DNA by nitrous acid: covalent structure of the dG-to-dG cross-link at the sequence 5'-CG.* Journal of the American Chemical Society, 1992. **114**(11): p. 4021-4027.

345. Guainazzi, A. and O.D. Scharer, *Using synthetic DNA interstrand crosslinks to elucidate repair pathways and identify new therapeutic targets for cancer chemotherapy.* Cell Mol Life Sci, 2010. **67**(21): p. 3683-97.

346. Langevin, F., et al., *Fancd2 counteracts the toxic effects of naturally produced aldehydes in mice.* Nature, 2011. **475**(7354): p. 53-8.

347. Hira, A., et al., *Variant ALDH2 is associated with accelerated progression of bone marrow failure in Japanese Fanconi anemia patients.* Blood, 2013. **122**(18): p. 3206-9.

348. Dingler, F.A., et al., *Two Aldehyde Clearance Systems Are Essential to Prevent Lethal Formaldehyde Accumulation in Mice and Humans.* Mol Cell, 2020. **80**(6): p. 996-1012 e9.

349. Muniandy, P.A., et al., *DNA interstrand crosslink repair in mammalian cells: step by step.* Crit Rev Biochem Mol Biol, 2010. **45**(1): p. 23-49.

350. Niedzwiedz, W., et al., *The Fanconi anaemia gene FANCC promotes homologous recombination and error-prone DNA repair.* Mol Cell, 2004. **15**(4): p. 607-20.

351. Mirchandani, K.D., R.M. McCaffrey, and A.D. D'Andrea, *The Fanconi anemia core complex is required for efficient point mutagenesis and Rev1 foci assembly.* DNA Repair (Amst), 2008. **7**(6): p. 902-11.

352. Papadopoulo, D., et al., *Hypomutability in Fanconi anemia cells is associated with increased deletion frequency at the HPRT locus.* Proc Natl Acad Sci U S A, 1990. **87**(21): p. 8383-7.

353. Niedernhofer, L.J., A.S. Lalai, and J.H. Hoeijmakers, *Fanconi anemia (cross)linked to DNA repair.* Cell, 2005. **123**(7): p. 1191-8.

354. Fullbright, G., et al., *p97 Promotes a Conserved Mechanism of Helicase Unloading during DNA Cross-Link Repair.* Mol Cell Biol, 2016. **36**(23): p. 2983-2994.

355. Long, D.T., et al., *BRCA1 promotes unloading of the CMG helicase from a stalled DNA replication fork.* Mol Cell, 2014. **56**(1): p. 174-85.

356. Collis, S.J., et al., *FANCM and FAAP24 function in ATR-mediated checkpoint signaling independently of the Fanconi anemia core complex.* Mol Cell, 2008. **32**(3): p. 313-24.
357. Huang, M., et al., *The FANCM/FAAP24 complex is required for the DNA interstrand crosslink-induced checkpoint response.* Mol Cell, 2010. **39**(2): p. 259-68.
358. Alpi, A.F. and K.J. Patel, *Monoubiquitylation in the Fanconi anemia DNA damage response pathway.* DNA Repair (Amst), 2009. **8**(4): p. 430-5.
359. Walden, H. and A.J. Deans, *The Fanconi anemia DNA repair pathway: structural and functional insights into a complex disorder.* Annu Rev Biophys, 2014. **43**: p. 257-78.
360. Moldovan, G.L. and A.D. D'Andrea, *FANCD2 hurdles the DNA interstrand crosslink.* Cell, 2009. **139**(7): p. 1222-4.
361. Cohn, M.A., et al., *A UAF1-containing multisubunit protein complex regulates the Fanconi anemia pathway.* Mol Cell, 2007. **28**(5): p. 786-97.
362. Gibbs-Seymour, I., et al., *Ubiquitin-SUMO circuitry controls activated fanconi anemia ID complex dosage in response to DNA damage.* Mol Cell, 2015. **57**(1): p. 150-64.
363. Knipscheer, P., et al., *The Fanconi anemia pathway promotes replication-dependent DNA interstrand cross-link repair.* Science, 2009. **326**(5960): p. 1698-701.
364. Ho, T.V. and O.D. Scharer, *Translesion DNA synthesis polymerases in DNA interstrand crosslink repair.* Environ Mol Mutagen, 2010. **51**(6): p. 552-66.
365. Kim, Y., et al., *Mutations of the SLX4 gene in Fanconi anemia.* Nat Genet, 2011. **43**(2): p. 142-6.
366. Kratz, K., et al., *Deficiency of FANCD2-associated nuclease KIAA1018/FAN1 sensitizes cells to interstrand crosslinking agents.* Cell, 2010. **142**(1): p. 77-88.
367. Liu, T., et al., *FAN1 acts with FANCI-FANCD2 to promote DNA interstrand cross-link repair.* Science, 2010. **329**(5992): p. 693-6.
368. MacKay, C., et al., *Identification of KIAA1018/FAN1, a DNA repair nuclease recruited to DNA damage by monoubiquitinated FANCD2.* Cell, 2010. **142**(1): p. 65-76.
369. Smogorzewska, A., et al., *A genetic screen identifies FAN1, a Fanconi anemia-associated nuclease necessary for DNA interstrand crosslink repair.* Mol Cell, 2010. **39**(1): p. 36-47.
370. Stoepker, C., et al., *SLX4, a coordinator of structure-specific endonucleases, is mutated in a new Fanconi anemia subtype.* Nat Genet, 2011. **43**(2): p. 138-41.
371. Bhagwat, N., et al., *XPF-ERCC1 participates in the Fanconi anemia pathway of cross-link repair.* Mol Cell Biol, 2009. **29**(24): p. 6427-37.

372. Kim, Y., et al., *Regulation of multiple DNA repair pathways by the Fanconi anemia protein SLX4*. Blood, 2013. **121**(1): p. 54-63.

373. Wang, A.T., et al., *Human SNM1A and XPF-ERCC1 collaborate to initiate DNA interstrand cross-link repair*. Genes Dev, 2011. **25**(17): p. 1859-70.

374. Yamamoto, K.N., et al., *Involvement of SLX4 in interstrand cross-link repair is regulated by the Fanconi anemia pathway*. Proc Natl Acad Sci U S A, 2011. **108**(16): p. 6492-6.

375. Crossan, G.P., et al., *Disruption of mouse Slx4, a regulator of structure-specific nucleases, phenocopies Fanconi anemia*. Nat Genet, 2011. **43**(2): p. 147-52.

376. Bogliolo, M., et al., *Mutations in ERCC4, encoding the DNA-repair endonuclease XPF, cause Fanconi anemia*. Am J Hum Genet, 2013. **92**(5): p. 800-6.

377. Kashiyama, K., et al., *Malfunction of nuclease ERCC1-XPF results in diverse clinical manifestations and causes Cockayne syndrome, xeroderma pigmentosum, and Fanconi anemia*. Am J Hum Genet, 2013. **92**(5): p. 807-19.

378. Amunugama, R., et al., *Replication Fork Reversal during DNA Interstrand Crosslink Repair Requires CMG Unloading*. Cell Rep, 2018. **23**(12): p. 3419-3428.

379. Abdullah, U.B., et al., *RPA activates the XPF-ERCC1 endonuclease to initiate processing of DNA interstrand crosslinks*. EMBO J, 2017. **36**(14): p. 2047-2060.

380. Olivieri, M., et al., *A Genetic Map of the Response to DNA Damage in Human Cells*. Cell, 2020. **182**(2): p. 481-496 e21.

381. Kim, H., et al., *Regulation of Rev1 by the Fanconi anemia core complex*. Nat Struct Mol Biol, 2012. **19**(2): p. 164-70.

382. Lim, K., et al., *Biophysical characterization of the interaction between FAAP20-UBZ4 domain and Rev1-BRCT domain*. FEBS Lett, 2015. **589**(20 Pt B): p. 3037-43.

383. Roy, U. and O.D. Scharer, *Involvement of translesion synthesis DNA polymerases in DNA interstrand crosslink repair*. DNA Repair (Amst), 2016. **44**: p. 33-41.

384. Daley, J.M., et al., *Enhancement of BLM-DNA2-Mediated Long-Range DNA End Resection by CtIP*. Cell Rep, 2017. **21**(2): p. 324-332.

385. Mimitou, E.P. and L.S. Symington, *DNA end resection--unraveling the tail*. DNA Repair (Amst), 2011. **10**(3): p. 344-8.

386. Conant, J., *The Great Secret: The Classified World War II Disaster That Launched the War on Cancer*. Smithsonian Magazine, 2020.

387. Goodman, L.S., M.M. Wintrobe, and et al., *Nitrogen mustard therapy; use of methyl-bis (beta-chloroethyl) amine hydrochloride and tris (beta-chloroethyl) amine hydrochloride for Hodgkin's disease, lymphosarcoma, leukemia and certain allied and miscellaneous disorders.* J Am Med Assoc, 1946. **132**: p. 126-32.

388. Eastman, A., *Reevaluation of interaction of cis-dichloro(ethylenediamine)platinum(II) with DNA.* Biochemistry, 1986. **25**(13): p. 3912-5.

389. Gargiulo, D., et al., *Structural and function modification of DNA by mitomycin C. Mechanism of the DNA sequence specificity of mitomycins.* Nucleic Acids Symp Ser, 1995(34): p. 169-70.

390. Apps, M.G., E.H. Choi, and N.J. Wheate, *The state-of-play and future of platinum drugs.* Endocr Relat Cancer, 2015. **22**(4): p. R219-33.

391. Colleoni, M., et al., *Annual Hazard Rates of Recurrence for Breast Cancer During 24 Years of Follow-Up: Results From the International Breast Cancer Study Group Trials I to V.* J Clin Oncol, 2016. **34**(9): p. 927-35.

392. Emadi, A., R.J. Jones, and R.A. Brodsky, *Cyclophosphamide and cancer: golden anniversary.* Nat Rev Clin Oncol, 2009. **6**(11): p. 638-47.

393. Ushijima, K., *Treatment for recurrent ovarian cancer-at first relapse.* J Oncol, 2010. **2010**: p. 497429.

394. Schmitz, R., et al., *Oncogenic mechanisms in Burkitt lymphoma.* Cold Spring Harb Perspect Med, 2014. **4**(2).

395. Schmitz, R., et al., *Burkitt lymphoma pathogenesis and therapeutic targets from structural and functional genomics.* Nature, 2012. **490**(7418): p. 116-20.

396. Dunleavy, K., M. Roschewski, and W.H. Wilson, *Precision treatment of distinct molecular subtypes of diffuse large B-cell lymphoma: ascribing treatment based on the molecular phenotype.* Clin Cancer Res, 2014. **20**(20): p. 5182-93.

397. Schmitz, R., et al., *Genetics and Pathogenesis of Diffuse Large B-Cell Lymphoma.* N Engl J Med, 2018. **378**(15): p. 1396-1407.

398. Sehn, L.H. and R.D. Gascoyne, *Diffuse large B-cell lymphoma: optimizing outcome in the context of clinical and biologic heterogeneity.* Blood, 2015. **125**(1): p. 22-32.

399. Ferry, K.V., T.C. Hamilton, and S.W. Johnson, *Increased nucleotide excision repair in cisplatin-resistant ovarian cancer cells: role of ERCC1-XPF.* Biochem Pharmacol, 2000. **60**(9): p. 1305-13.

400. Takenaka, T., et al., *Combined evaluation of Rad51 and ERCC1 expressions for sensitivity to platinum agents in non-small cell lung cancer.* Int J Cancer, 2007. **121**(4): p. 895-900.

401. Taniguchi, T., et al., *Disruption of the Fanconi anemia-BRCA pathway in cisplatin-sensitive ovarian tumors.* Nat Med, 2003. **9**(5): p. 568-74.

402. Vaezi, A., et al., *XPF expression correlates with clinical outcome in squamous cell carcinoma of the head and neck.* Clin Cancer Res, 2011. **17**(16): p. 5513-22.

403. Friedman, O.M. and A.M. Seligman, *Preparation of N-Phosphorylated Derivatives of Bis-β-chloroethylamine1a.* Journal of the American Chemical Society, 1954. **76**(3): p. 655-658.

404. Arnold, H., F. Bourseaux, and N. Brock, *Chemotherapeutic action of a cyclic nitrogen mustard phosphamide ester (B 518-ASTA) in experimental tumours of the rat.* Nature, 1958. **181**(4613): p. 931.

405. Brock, N. and H. Wilmanns, *[Effect of a cyclic nitrogen mustard-phosphamidester on experimentally induced tumors in rats; chemotherapeutic effect and pharmacological properties of B 518 ASTA].* Dtsch Med Wochenschr, 1958. **83**(12): p. 453-8.

406. Ozuah, N.W., et al., *Five decades of low intensity and low survival: adapting intensified regimens to cure pediatric Burkitt lymphoma in Africa.* Blood Adv, 2020. **4**(16): p. 4007-4019.

407. Boddy, A.V. and S.M. Yule, *Metabolism and pharmacokinetics of oxazaphosphorines.* Clin Pharmacokinet, 2000. **38**(4): p. 291-304.

408. Mazur, L., et al., *Mafosfamide as a new anticancer agent: preclinical investigations and clinical trials.* Anticancer Res, 2012. **32**(7): p. 2783-9.

409. Mazur, L., M. Opydo-Chanek, and M. Stojak, *Glufosfamide as a new oxazaphosphorine anticancer agent.* Anticancer Drugs, 2011. **22**(6): p. 488-93.

410. Klein, H.O., et al., *Therapeutic effects of single-push or fractionated injections or continuous infusion of oxazaphosphorines (cyclophosphamide, ifosfamide, Asta Z 7557).* Cancer, 1984. **54**(6 Suppl): p. 1193-203.

411. Bruntsch, U., et al., *Phase-I study of mafosfamide-cyclohexylamine (ASTA-Z-7557, NSC 345 842) and limited phase-I data on mafosfamide-lysine.* Invest New Drugs, 1985. **3**(3): p. 293-6.

412. Abele, R., et al., *Phase I study of cyclohexylamine and lysine salt of mafosfamide.* Cancer Chemother Pharmacol, 1986. **16**(2): p. 182-3.

413. Mazur, L., et al., *Comparative effects of new generation oxazaphosphorines on the size and viability of human acute myeloblastic leukemia cells.* Folia Biol (Krakow), 2012. **60**(1-2): p. 35-40.

414. George B. Kauffman, R.P., Sandro Doldi & Matthew D. Hall, *Michele Peyrone (1813–1883), Discoverer of Cisplatin.* Platinum Metals Review, 2010. **54**(4): p. 250-256.

415. Kelland, L., *The resurgence of platinum-based cancer chemotherapy.* Nat Rev Cancer, 2007. **7**(8): p. 573-84.

416. Rottenberg, S., C. Disler, and P. Perego, *The rediscovery of platinum-based cancer therapy.* Nat Rev Cancer, 2021. **21**(1): p. 37-50.

417. Davies, M.S., S.J. Berners-Price, and T.W. Hambley, *Rates of platination of -AG- and -GA-containing double-stranded oligonucleotides: effect of chloride concentration.* J Inorg Biochem, 2000. **79**(1-4): p. 167-72.

418. Chaney, S.G., et al., *Protein interactions with platinum-DNA adducts: from structure to function.* J Inorg Biochem, 2004. **98**(10): p. 1551-9.

419. Luo, J., N.L. Solimini, and S.J. Elledge, *Principles of cancer therapy: oncogene and non-oncogene addiction.* Cell, 2009. **136**(5): p. 823-37.

420. Shalem, O., N.E. Sanjana, and F. Zhang, *High-throughput functional genomics using CRISPR-Cas9.* Nat Rev Genet, 2015. **16**(5): p. 299-311.

421. Hartwell, L.H., J. Culotti, and B. Reid, *Genetic control of the cell-division cycle in yeast. I. Detection of mutants.* Proc Natl Acad Sci U S A, 1970. **66**(2): p. 352-9.

422. Nurse, P., *Genetic control of cell size at cell division in yeast.* Nature, 1975. **256**(5518): p. 547-51.

423. Nusslein-Volhard, C. and E. Wieschaus, *Mutations affecting segment number and polarity in Drosophila.* Nature, 1980. **287**(5785): p. 795-801.

424. Nusslein-Volhard, C., H.G. Frohnhofer, and R. Lehmann, *Determination of anteroposterior polarity in Drosophila.* Science, 1987. **238**(4834): p. 1675-81.

425. Ellis, H.M. and H.R. Horvitz, *Genetic control of programmed cell death in the nematode C. elegans.* Cell, 1986. **44**(6): p. 817-29.

426. Najarro, E.H., et al., *Caenorhabditis elegans flamingo cadherin fmi-1 regulates GABAergic neuronal development.* J Neurosci, 2012. **32**(12): p. 4196-211.

427. Driever, W., et al., *A genetic screen for mutations affecting embryogenesis in zebrafish.* Development, 1996. **123**: p. 37-46.

428. Haffter, P., et al., *The identification of genes with unique and essential functions in the development of the zebrafish, Danio rerio.* Development, 1996. **123**: p. 1-36.

429. Sundaram, M.V., *The love-hate relationship between Ras and Notch.* Genes Dev, 2005. **19**(16): p. 1825-39.

430. Schneeberger, K., *Using next-generation sequencing to isolate mutant genes from forward genetic screens.* Nat Rev Genet, 2014. **15**(10): p. 662-76.

431. Fire, A., et al., *Potent and specific genetic interference by double-stranded RNA in Caenorhabditis elegans.* Nature, 1998. **391**(6669): p. 806-11.

432. Root, D.E., et al., *Genome-scale loss-of-function screening with a lentiviral RNAi library.* Nat Methods, 2006. **3**(9): p. 715-9.

433. Paddison, P.J., et al., *A resource for large-scale RNA-interference-based screens in mammals.* Nature, 2004. **428**(6981): p. 427-31.

434. Moffat, J. and D.M. Sabatini, *Building mammalian signalling pathways with RNAi screens.* Nat Rev Mol Cell Biol, 2006. **7**(3): p. 177-87.

435. Berns, K., et al., *A large-scale RNAi screen in human cells identifies new components of the p53 pathway.* Nature, 2004. **428**(6981): p. 431-7.

436. Boutros, M., et al., *Genome-wide RNAi analysis of growth and viability in Drosophila cells.* Science, 2004. **303**(5659): p. 832-5.

437. Jackson, A.L. and P.S. Linsley, *Recognizing and avoiding siRNA off-target effects for target identification and therapeutic application.* Nat Rev Drug Discov, 2010. **9**(1): p. 57-67.

438. Birmingham, A., et al., *3′ UTR seed matches, but not overall identity, are associated with RNAi off-targets.* Nat Methods, 2006. **3**(3): p. 199-204.

439. Jackson, A.L., et al., *Expression profiling reveals off-target gene regulation by RNAi.* Nat Biotechnol, 2003. **21**(6): p. 635-7.

440. Miller, J.C., et al., *A TALE nuclease architecture for efficient genome editing.* Nat Biotechnol, 2011. **29**(2): p. 143-8.

441. Reyon, D., et al., *FLASH assembly of TALENs for high-throughput genome editing.* Nat Biotechnol, 2012. **30**(5): p. 460-5.

442. Holkers, M., et al., *Differential integrity of TALE nuclease genes following adenoviral and lentiviral vector gene transfer into human cells.* Nucleic Acids Res, 2013. **41**(5): p. e63.

443. Hille, F., et al., *The Biology of CRISPR-Cas: Backward and Forward.* Cell, 2018. **172**(6): p. 1239-1259.

444. Jinek, M., et al., *A programmable dual-RNA-guided DNA endonuclease in adaptive bacterial immunity.* Science, 2012. **337**(6096): p. 816-21.

445. Mojica, F.J., G. Juez, and F. Rodriguez-Valera, *Transcription at different salinities of Haloferax mediterranei sequences adjacent to partially modified PstI sites.* Mol Microbiol, 1993. **9**(3): p. 613-21.

446. Mojica, F.J., et al., *Long stretches of short tandem repeats are present in the largest replicons of the Archaea Haloferax mediterranei and Haloferax volcanii and could be involved in replicon partitioning.* Mol Microbiol, 1995. **17**(1): p. 85-93.

447. Mojica, F.J., et al., *Biological significance of a family of regularly spaced repeats in the genomes of Archaea, Bacteria and mitochondria.* Mol Microbiol, 2000. **36**(1): p. 244-6.

448. Mojica, F.J., et al., *Intervening sequences of regularly spaced prokaryotic repeats derive from foreign genetic elements.* J Mol Evol, 2005. **60**(2): p. 174-82.

449. Bolotin, A., et al., *Clustered regularly interspaced short palindrome repeats (CRISPRs) have spacers of extrachromosomal origin.* Microbiology (Reading), 2005. **151**(Pt 8): p. 2551-2561.

450. Horvath, P., et al., *Diversity, activity, and evolution of CRISPR loci in Streptococcus thermophilus.* J Bacteriol, 2008. **190**(4): p. 1401-12.

451. Pourcel, C., G. Salvignol, and G. Vergnaud, *CRISPR elements in Yersinia pestis acquire new repeats by preferential uptake of bacteriophage DNA, and provide additional tools for evolutionary studies.* Microbiology (Reading), 2005. **151**(Pt 3): p. 653-663.

452. Barrangou, R., et al., *CRISPR provides acquired resistance against viruses in prokaryotes.* Science, 2007. **315**(5819): p. 1709-12.

453. Barrangou, R., *RNA-mediated programmable DNA cleavage.* Nat Biotechnol, 2012. **30**(9): p. 836-8.

454. Garneau, J.E., et al., *The CRISPR/Cas bacterial immune system cleaves bacteriophage and plasmid DNA.* Nature, 2010. **468**(7320): p. 67-71.

455. Marraffini, L.A. and E.J. Sontheimer, *CRISPR interference limits horizontal gene transfer in staphylococci by targeting DNA.* Science, 2008. **322**(5909): p. 1843-5.

456. Jiang, W., et al., *RNA-guided editing of bacterial genomes using CRISPR-Cas systems.* Nat Biotechnol, 2013. **31**(3): p. 233-9.

457. Sapranauskas, R., et al., *The Streptococcus thermophilus CRISPR/Cas system provides immunity in Escherichia coli.* Nucleic Acids Res, 2011. **39**(21): p. 9275-82.

458. Gasiunas, G., et al., *Cas9-crRNA ribonucleoprotein complex mediates specific DNA cleavage for adaptive immunity in bacteria.* Proc Natl Acad Sci U S A, 2012. **109**(39): p. E2579-86.

459. Deltcheva, E., et al., *CRISPR RNA maturation by trans-encoded small RNA and host factor RNase III.* Nature, 2011. **471**(7340): p. 602-7.

460. Cong, L., et al., *Multiplex genome engineering using CRISPR/Cas systems.* Science, 2013. **339**(6121): p. 819-23.

461. Shalem, O., et al., *Genome-scale CRISPR-Cas9 knockout screening in human cells.* Science, 2014. **343**(6166): p. 84-87.

462. Sanjana, N.E., O. Shalem, and F. Zhang, *Improved vectors and genome-wide libraries for CRISPR screening.* Nat Methods, 2014. **11**(8): p. 783-784.

463. Mali, P., et al., *RNA-guided human genome engineering via Cas9.* Science, 2013. **339**(6121): p. 823-6.

464. Yin, H., W. Xue, and D.G. Anderson, *CRISPR-Cas: a tool for cancer research and therapeutics.* Nat Rev Clin Oncol, 2019. **16**(5): p. 281-295.

465. Koike-Yusa, H., et al., *Genome-wide recessive genetic screening in mammalian cells with a lentiviral CRISPR-guide RNA library.* Nat Biotechnol, 2014. **32**(3): p. 267-73.

466. Wang, T., et al., *Genetic screens in human cells using the CRISPR-Cas9 system.* Science, 2014. **343**(6166): p. 80-4.

467. Hart, T., et al., *High-Resolution CRISPR Screens Reveal Fitness Genes and Genotype-Specific Cancer Liabilities.* Cell, 2015. **163**(6): p. 1515-26.

468. Colic, M. and T. Hart, *Common computational tools for analyzing CRISPR screens.* Emerg Top Life Sci, 2021. **5**(6): p. 779-788.

469. Lawson, K.A., et al., *Functional genomic landscape of cancer-intrinsic evasion of killing by T cells.* Nature, 2020. **586**(7827): p. 120-126.

470. Doench, J.G., et al., *Optimized sgRNA design to maximize activity and minimize off-target effects of CRISPR-Cas9.* Nat Biotechnol, 2016. **34**(2): p. 184-191.

471. Morgens, D.W., et al., *Genome-scale measurement of off-target activity using Cas9 toxicity in high-throughput screens.* Nat Commun, 2017. **8**: p. 15178.

472. Wang, T., et al., *Identification and characterization of essential genes in the human genome.* Science, 2015. **350**(6264): p. 1096-101.

473. Yu, J.S.L. and K. Yusa, *Genome-wide CRISPR-Cas9 screening in mammalian cells.* Methods, 2019. **164-165**: p. 29-35.

474. Tzelepis, K., et al., *A CRISPR Dropout Screen Identifies Genetic Vulnerabilities and Therapeutic Targets in Acute Myeloid Leukemia.* Cell Rep, 2016. **17**(4): p. 1193-1205.

475. Wang, T., et al., *Gene Essentiality Profiling Reveals Gene Networks and Synthetic Lethal Interactions with Oncogenic Ras.* Cell, 2017. **168**(5): p. 890-903 e15.

476. Tsherniak, A., et al., *Defining a Cancer Dependency Map.* Cell, 2017. **170**(3): p. 564-576 e16.

477. Reddy, A., et al., *Genetic and Functional Drivers of Diffuse Large B Cell Lymphoma.* Cell, 2017. **171**(2): p. 481-494 e15.
478. Behan, F.M., et al., *Prioritization of cancer therapeutic targets using CRISPR-Cas9 screens.* Nature, 2019. **568**(7753): p. 511-516.
479. Blomen, V.A., et al., *Gene essentiality and synthetic lethality in haploid human cells.* Science, 2015. **350**(6264): p. 1092-6.
480. Mair, B., et al., *Essential Gene Profiles for Human Pluripotent Stem Cells Identify Uncharacterized Genes and Substrate Dependencies.* Cell Rep, 2019. **27**(2): p. 599-615 e12.
481. Yilmaz, A., et al., *Defining essential genes for human pluripotent stem cells by CRISPR-Cas9 screening in haploid cells.* Nat Cell Biol, 2018. **20**(5): p. 610-619.
482. Institute, D.a.B., *DepMap. Cancer Dependency Map.* . 2018.
483. Institute, D.a.S., *Project Score , part of the Sanger Cancer Dependency Map. Sanger DepMap Portal* 2019.
484. Dempster, J.M., et al., *Agreement between two large pan-cancer CRISPR-Cas9 gene dependency data sets.* Nat Commun, 2019. **10**(1): p. 5817.
485. Boehm, J.S., et al., *Cancer research needs a better map.* Nature, 2021. **589**(7843): p. 514-516.
486. Bridges, C.B., *The origin of variations in sexual and sex-limited characters.* The American Naturalist, 1922. **56**(642): p. 51-63.
487. Setton, J., et al., *Synthetic Lethality in Cancer Therapeutics: The Next Generation.* Cancer Discov, 2021. **11**(7): p. 1626-1635.
488. Dobzhansky, T., *Genetics of natural populations. XIII. Recombination and variability in populations of Drosophila pseudoobscura.* Genetics, 1946. **31**(3): p. 269.
489. Nijman, S.M., *Synthetic lethality: general principles, utility and detection using genetic screens in human cells.* FEBS Lett, 2011. **585**(1): p. 1-6.
490. Zimmermann, M., et al., *CRISPR screens identify genomic ribonucleotides as a source of PARP-trapping lesions.* Nature, 2018. **559**(7713): p. 285-289.
491. Noordermeer, S.M., et al., *The shieldin complex mediates 53BP1-dependent DNA repair.* Nature, 2018. **560**(7716): p. 117-121.
492. He, Y.J., et al., *DYNLL1 binds to MRE11 to limit DNA end resection in BRCA1-deficient cells.* Nature, 2018. **563**(7732): p. 522-526.
493. Dev, H., et al., *Shieldin complex promotes DNA end-joining and counters homologous recombination in BRCA1-null cells.* Nat Cell Biol, 2018. **20**(8): p. 954-965.

494. Wang, C., et al., *Genome-wide CRISPR screens reveal synthetic lethality of RNASEH2 deficiency and ATR inhibition.* Oncogene, 2019. **38**(14): p. 2451-2463.

495. Alvarez-Quilon, A., et al., *Endogenous DNA 3' Blocks Are Vulnerabilities for BRCA1 and BRCA2 Deficiency and Are Reversed by the APE2 Nuclease.* Mol Cell, 2020. **78**(6): p. 1152-1165 e8.

496. Hustedt, N., et al., *A consensus set of genetic vulnerabilities to ATR inhibition.* Open Biol, 2019. **9**(9): p. 190156.

497. Adeyemi, R.O., et al., *The Protexin complex counters resection on stalled forks to promote homologous recombination and crosslink repair.* Mol Cell, 2021. **81**(21): p. 4440-4456 e7.

498. Schubert, L., et al., *SCAI promotes error-free repair of DNA interstrand crosslinks via the Fanconi anemia pathway.* EMBO Rep, 2022. **23**(4): p. e53639.

499. Hustedt, N., et al., *Control of homologous recombination by the HROB-MCM8-MCM9 pathway.* Genes Dev, 2019. **33**(19-20): p. 1397-1415.

500. Lemay, J.-F., et al., *A genome-wide screen identifies SCAI as a modulator of the UV-induced replicative stress response in human cells.* bioRxiv, 2022: p. 2022.01.17.476707.

501. Sapp, V., et al., *Genome-wide CRISPR/Cas9 screening in human iPS derived cardiomyocytes uncovers novel mediators of doxorubicin cardiotoxicity.* Sci Rep, 2021. **11**(1): p. 13866.

502. Du, M., et al., *Genome-wide CRISPR screen identified Rad18 as a determinant of doxorubicin sensitivity in osteosarcoma.* J Exp Clin Cancer Res, 2022. **41**(1): p. 154.

503. Jensen, T.I., et al., *Targeted regulation of transcription in primary cells using CRISPRa and CRISPRi.* Genome Res, 2021. **31**(11): p. 2120-2130.

504. Qi, L.S., et al., *Repurposing CRISPR as an RNA-guided platform for sequence-specific control of gene expression.* Cell, 2013. **152**(5): p. 1173-83.

505. Gilbert, L.A., et al., *Genome-Scale CRISPR-Mediated Control of Gene Repression and Activation.* Cell, 2014. **159**(3): p. 647-61.

506. Larson, M.H., et al., *CRISPR interference (CRISPRi) for sequence-specific control of gene expression.* Nat Protoc, 2013. **8**(11): p. 2180-96.

507. Yeo, N.C., et al., *An enhanced CRISPR repressor for targeted mammalian gene regulation.* Nat Methods, 2018. **15**(8): p. 611-616.

508. Abudayyeh, O.O., et al., *C2c2 is a single-component programmable RNA-guided RNA-targeting CRISPR effector.* Science, 2016. **353**(6299): p. aaf5573.

509. Xu, C., et al., *Programmable RNA editing with compact CRISPR-Cas13 systems from uncultivated microbes.* Nat Methods, 2021. **18**(5): p. 499-506.

510. Gaudelli, N.M., et al., *Programmable base editing of A*T to G*C in genomic DNA without DNA cleavage.* Nature, 2017. **551**(7681): p. 464-471.

511. Komor, A.C., et al., *Improved base excision repair inhibition and bacteriophage Mu Gam protein yields C:G-to-T:A base editors with higher efficiency and product purity.* Sci Adv, 2017. **3**(8): p. eaao4774.

512. Komor, A.C., et al., *Programmable editing of a target base in genomic DNA without double-stranded DNA cleavage.* Nature, 2016. **533**(7603): p. 420-4.

513. Rees, H.A., et al., *Improving the DNA specificity and applicability of base editing through protein engineering and protein delivery.* Nat Commun, 2017. **8**: p. 15790.

514. Kim, Y.B., et al., *Increasing the genome-targeting scope and precision of base editing with engineered Cas9-cytidine deaminase fusions.* Nat Biotechnol, 2017. **35**(4): p. 371-376.

515. Cuella-Martin, R., et al., *Functional interrogation of DNA damage response variants with base editing screens.* Cell, 2021. **184**(4): p. 1081-1097 e19.

516. Pusapati, G.V., et al., *CRISPR Screens Uncover Genes that Regulate Target Cell Sensitivity to the Morphogen Sonic Hedgehog.* Dev Cell, 2018. **44**(1): p. 113-129 e8.

517. Yu, J.S.L., et al., *CRISPR-Knockout Screen Identifies Dmap1 as a Regulator of Chemically Induced Reprogramming and Differentiation of Cardiac Progenitors.* Stem Cells, 2019. **37**(7): p. 958-972.

518. Li, M., et al., *Genome-wide CRISPR-KO Screen Uncovers mTORC1-Mediated Gsk3 Regulation in Naive Pluripotency Maintenance and Dissolution.* Cell Rep, 2018. **24**(2): p. 489-502.

519. Han, K., et al., *CRISPR screens in cancer spheroids identify 3D growth-specific vulnerabilities.* Nature, 2020. **580**(7801): p. 136-141.

520. Drost, J. and H. Clevers, *Organoids in cancer research.* Nat Rev Cancer, 2018. **18**(7): p. 407-418.

521. Haley, B. and F. Roudnicky, *Functional Genomics for Cancer Drug Target Discovery.* Cancer Cell, 2020. **38**(1): p. 31-43.

522. Li, W., et al., *MAGeCK enables robust identification of essential genes from genome-scale CRISPR/Cas9 knockout screens.* Genome Biol, 2014. **15**(12): p. 554.

523. Colic, M., et al., *Identifying chemogenetic interactions from CRISPR screens with drugZ.* Genome Med, 2019. **11**(1): p. 52.

524. Robinson, M.D., D.J. McCarthy, and G.K. Smyth, *edgeR: a Bioconductor package for differential expression analysis of digital gene expression data.* Bioinformatics, 2010. **26**(1): p. 139-40.

525. Luo, B., et al., *Highly parallel identification of essential genes in cancer cells.* Proc Natl Acad Sci U S A, 2008. **105**(51): p. 20380-5.

526. Rhee, H.W., et al., *Proteomic mapping of mitochondria in living cells via spatially restricted enzymatic tagging.* Science, 2013. **339**(6125): p. 1328-1331.

527. Lam, S.S., et al., *Directed evolution of APEX2 for electron microscopy and proximity labeling.* Nat Methods, 2015. **12**(1): p. 51-4.

528. Choi-Rhee, E., H. Schulman, and J.E. Cronan, *Promiscuous protein biotinylation by Escherichia coli biotin protein ligase.* Protein Sci, 2004. **13**(11): p. 3043-50.

529. Roux, K.J., et al., *A promiscuous biotin ligase fusion protein identifies proximal and interacting proteins in mammalian cells.* J Cell Biol, 2012. **196**(6): p. 801-10.

530. Branon, T.C., et al., *Author Correction: Efficient proximity labeling in living cells and organisms with TurboID.* Nat Biotechnol, 2020. **38**(1): p. 108.

531. Stoeger, T., et al., *Large-scale investigation of the reasons why potentially important genes are ignored.* PLoS Biol, 2018. **16**(9): p. e2006643.

532. Haynes, W.A., A. Tomczak, and P. Khatri, *Gene annotation bias impedes biomedical research.* Sci Rep, 2018. **8**(1): p. 1362.

533. Yang, X., et al., *A public genome-scale lentiviral expression library of human ORFs.* Nat Methods, 2011. **8**(8): p. 659-61.

534. Kong, S., et al., *Translatable circRNAs and lncRNAs: Driving mechanisms and functions of their translation products.* Cancer Lett, 2020. **483**: p. 59-65.

535. Lu, S., et al., *A hidden human proteome encoded by 'non-coding' genes.* Nucleic Acids Res, 2019. **47**(15): p. 8111-8125.

536. Ruiz-Orera, J., J.L. Villanueva-Canas, and M.M. Alba, *Evolution of new proteins from translated sORFs in long non-coding RNAs.* Exp Cell Res, 2020. **391**(1): p. 111940.

537. Mudge, J.M., et al., *Standardized annotation of translated open reading frames.* Nat Biotechnol, 2022. **40**(7): p. 994-999.

538. Broeils, L.A., et al., *Evolution and implications of de novo genes in humans.* Nat Ecol Evol, 2023.

539. Wang, C., et al., *C17orf53 is identified as a novel gene involved in inter-strand crosslink repair.* DNA Repair (Amst), 2020. **95**: p. 102946.

540. Huang, J.W., et al., *MCM8IP activates the MCM8-9 helicase to promote DNA synthesis and homologous recombination upon DNA damage.* Nat Commun, 2020. **11**(1): p. 2948.

541. Shukla, V., et al., *HMCES Functions in the Alternative End-Joining Pathway of the DNA DSB Repair during Class Switch Recombination in B Cells.* Mol Cell, 2020. **77**(2): p. 384-394 e4.

542. Halabelian, L., et al., *Structural basis of HMCES interactions with abasic DNA and multivalent substrate recognition.* Nat Struct Mol Biol, 2019. **26**(7): p. 607-612.

543. Mohni, K.N., et al., *HMCES Maintains Genome Integrity by Shielding Abasic Sites in Single-Strand DNA.* Cell, 2019. **176**(1-2): p. 144-153 e13.

544. Semlow, D.R., V.A. MacKrell, and J.C. Walter, *The HMCES DNA-protein cross-link functions as a constitutive DNA repair intermediate.* bioRxiv, 2021: p. 2021.07.29.454365.

545. Brannvoll, A., et al., *The ZGRF1 Helicase Promotes Recombinational Repair of Replication-Blocking DNA Damage in Human Cells.* Cell Rep, 2020. **32**(1): p. 107849.

546. Mangosh, T.L., et al., *SLX4IP Promotes Telomere Maintenance in Androgen Receptor-Independent Castration-Resistant Prostate Cancer through ALT-like Telomeric PML Localization.* Mol Cancer Res, 2021. **19**(2): p. 301-316.

547. Zhang, H., et al., *SLX4IP acts with SLX4 and XPF-ERCC1 to promote interstrand crosslink repair.* Nucleic Acids Res, 2019. **47**(19): p. 10181-10201.

548. Panier, S., et al., *SLX4IP Antagonizes Promiscuous BLM Activity during ALT Maintenance.* Mol Cell, 2019. **76**(1): p. 27-43 e11.

549. Barroso-Gonzalez, J., et al., *RAD51AP1 Is an Essential Mediator of Alternative Lengthening of Telomeres.* Mol Cell, 2020. **79**(2): p. 359.

550. Barroso-Gonzalez, J., et al., *RAD51AP1 Is an Essential Mediator of Alternative Lengthening of Telomeres.* Mol Cell, 2019. **76**(1): p. 217.

551. Liang, F., et al., *DNA requirement in FANCD2 deubiquitination by USP1-UAF1-RAD51AP1 in the Fanconi anemia DNA damage response.* Nat Commun, 2019. **10**(1): p. 2849.

552. Pires, E., P. Sung, and C. Wiese, *Role of RAD51AP1 in homologous recombination DNA repair and carcinogenesis.* DNA Repair (Amst), 2017. **59**: p. 76-81.

553. Edogbanya, J., et al., *Evolution, structure and emerging roles of C1ORF112 in DNA replication, DNA damage responses, and cancer.* Cell Mol Life Sci, 2021. **78**(9): p. 4365-4376.

554. Fernandes, J.B., et al., *FIGL1 and its novel partner FLIP form a conserved complex that regulates homologous recombination.* PLoS Genet, 2018. **14**(4): p. e1007317.

555. Hu, Q., et al., *Meiotic Chromosome Association 1 Interacts with TOP3alpha and Regulates Meiotic Recombination in Rice.* Plant Cell, 2017. **29**(7): p. 1697-1708.

556. Masson, J.Y. and S.C. West, *The Rad51 and Dmc1 recombinases: a non-identical twin relationship.* Trends Biochem Sci, 2001. **26**(2): p. 131-6.

557. Hinch, A.G., et al., *The Configuration of RPA, RAD51, and DMC1 Binding in Meiosis Reveals the Nature of Critical Recombination Intermediates.* Mol Cell, 2020. **79**(4): p. 689-701 e10.

558. van Dam, S., et al., *GeneFriends: an online co-expression analysis tool to identify novel gene targets for aging and complex diseases.* BMC Genomics, 2012. **13**: p. 535.

559. Chen, J., et al., *Pan-Cancer Analysis Identified C1ORF112 as a Potential Biomarker for Multiple Tumor Types.* Front Mol Biosci, 2021. **8**: p. 693651.

560. Shah, P., K. Wolf, and J. Lammerding, *Bursting the Bubble - Nuclear Envelope Rupture as a Path to Genomic Instability?* Trends Cell Biol, 2017. **27**(8): p. 546-555.

561. Zhang, C.Z., et al., *Chromothripsis from DNA damage in micronuclei.* Nature, 2015. **522**(7555): p. 179-84.

562. Hatch, E.M., et al., *Catastrophic nuclear envelope collapse in cancer cell micronuclei.* Cell, 2013. **154**(1): p. 47-60.

563. Jeggo, P.A., L.H. Pearl, and A.M. Carr, *DNA repair, genome stability and cancer: a historical perspective.* Nat Rev Cancer, 2016. **16**(1): p. 35-42.

564. Yang, W., et al., *Genomics of Drug Sensitivity in Cancer (GDSC): a resource for therapeutic biomarker discovery in cancer cells.* Nucleic Acids Res, 2013. **41**(Database issue): p. D955-61.

565. Gupta, R., et al., *DNA Repair Network Analysis Reveals Shieldin as a Key Regulator of NHEJ and PARP Inhibitor Sensitivity.* Cell, 2018. **173**(4): p. 972-988 e23.

566. Cho, K.F., et al., *Proximity labeling in mammalian cells with TurboID and split-TurboID.* Nat Protoc, 2020. **15**(12): p. 3971-3999.

567. Biebricher, A., et al., *PICH: a DNA translocase specially adapted for processing anaphase bridge DNA.* Mol Cell, 2013. **51**(5): p. 691-701.

568. Tian, T., et al., *The ZATT-TOP2A-PICH Axis Drives Extensive Replication Fork Reversal to Promote Genome Stability.* Mol Cell, 2021. **81**(1): p. 198-211 e6.

569. Lera, R.F., et al., *Plk1 protects kinetochore-centromere architecture against microtubule pulling forces.* EMBO Rep, 2019. **20**(10): p. e48711.

570. Mitrentsi, I., et al., *Heterochromatic repeat clustering imposes a physical barrier on homologous recombination to prevent chromosomal translocations.* Mol Cell, 2022. **82**(11): p. 2132-2147 e6.

571. Altemose, N., et al., *Complete genomic and epigenetic maps of human centromeres.* Science, 2022. **376**(6588): p. eabl4178.

572. Nurk, S., et al., *The complete sequence of a human genome.* Science, 2022. **376**(6588): p. 44-53.
573. Yuan, J. and J. Chen, *FIGNL1-containing protein complex is required for efficient homologous recombination repair.* Proc Natl Acad Sci U S A, 2013. **110**(26): p. 10640-5.
574. Matsuzaki, K., et al., *Human RAD51 paralogue SWSAP1 fosters RAD51 filament by regulating the anti-recombinase FIGNL1 AAA+ ATPase.* Nat Commun, 2019. **10**(1): p. 1407.
575. Bernstein, K.A., et al., *The Shu complex, which contains Rad51 paralogues, promotes DNA repair through inhibition of the Srs2 anti-recombinase.* Mol Biol Cell, 2011. **22**(9): p. 1599-607.
576. Consortium, T.I.M.P.; Available from: https://www.mousephenotype.org/data/genes/MGI:3590554.
577. Koscielny, G., et al., *The International Mouse Phenotyping Consortium Web Portal, a unified point of access for knockout mice and related phenotyping data.* Nucleic Acids Res, 2014. **42**(Database issue): p. D802-9.
578. Dickinson, M.E., et al., *High-throughput discovery of novel developmental phenotypes.* Nature, 2016. **537**(7621): p. 508-514.
579. Ruth, K.S., et al., *Genetic insights into biological mechanisms governing human ovarian ageing.* Nature, 2021. **596**(7872): p. 393-397.
580. Kumar, R., et al., *Antagonism between BRCA2 and FIGL1 regulates homologous recombination.* Nucleic Acids Res, 2019. **47**(10): p. 5170-5180.
581. Prakash, R., et al., *Distinct pathways of homologous recombination controlled by the SWS1-SWSAP1-SPIDR complex.* Nat Commun, 2021. **12**(1): p. 4255.
582. Chan, E.M., et al., *WRN helicase is a synthetic lethal target in microsatellite unstable cancers.* Nature, 2019. **568**(7753): p. 551-556.
583. Kategaya, L., et al., *Werner Syndrome Helicase Is Required for the Survival of Cancer Cells with Microsatellite Instability.* iScience, 2019. **13**: p. 488-497.
584. Parnas, O., et al., *A Genome-wide CRISPR Screen in Primary Immune Cells to Dissect Regulatory Networks.* Cell, 2015. **162**(3): p. 675-86.
585. Benslimane, Y., et al., *A novel p53 regulator, C16ORF72/TAPR1, buffers against telomerase inhibition.* Aging Cell, 2021. **20**(4): p. e13331.
586. Benslimane, Y., et al., *Genome-Wide Screens Reveal that Resveratrol Induces Replicative Stress in Human Cells.* Mol Cell, 2020. **79**(5): p. 846-856 e8.
587. Robinson, N.J., et al., *SLX4IP promotes RAP1 SUMOylation by PIAS1 to coordinate telomere maintenance through NF-kappaB and Notch signaling.* Sci Signal, 2021. **14**(689).

588. Wang, L.C. and J. Gautier, *The Fanconi anemia pathway and ICL repair: implications for cancer therapy.* Crit Rev Biochem Mol Biol, 2010. **45**(5): p. 424-39.

589. Chino, H., et al., *Intrinsically Disordered Protein TEX264 Mediates ER-phagy.* Mol Cell, 2019. **74**(5): p. 909-921 e6.

590. Fielden, J., et al., *TEX264 coordinates p97- and SPRTN-mediated resolution of topoisomerase 1-DNA adducts.* Nat Commun, 2020. **11**(1): p. 1274.

591. Stingele, J., R. Bellelli, and S.J. Boulton, *Mechanisms of DNA-protein crosslink repair.* Nat Rev Mol Cell Biol, 2017. **18**(9): p. 563-573.

592. Ishimura, R., et al., *A novel approach to assess the ubiquitin-fold modifier 1-system in cells.* FEBS Lett, 2017. **591**(1): p. 196-204.

593. Mohajeri, M.S.A., et al., *TMEM263: a novel candidate gene implicated in human autosomal recessive severe lethal skeletal dysplasia.* Hum Genomics, 2021. **15**(1): p. 42.

594. Wu, Z., et al., *A Novel Loss-of-Function Variant in Transmembrane Protein 263 (TMEM263) of Autosomal Dwarfism in Chicken.* Front Genet, 2018. **9**: p. 193.

595. Hein, M.Y., et al., *A human interactome in three quantitative dimensions organized by stoichiometries and abundances.* Cell, 2015. **163**(3): p. 712-23.

596. Dammermann, A. and A. Merdes, *Assembly of centrosomal proteins and microtubule organization depends on PCM-1.* J Cell Biol, 2002. **159**(2): p. 255-66.

597. Villumsen, B.H., et al., *A new cellular stress response that triggers centriolar satellite reorganization and ciliogenesis.* EMBO J, 2013. **32**(23): p. 3029-40.

598. Jumper, J., et al., *Highly accurate protein structure prediction with AlphaFold.* Nature, 2021. **596**(7873): p. 583-589.

599. Landschulz, W.H., P.F. Johnson, and S.L. McKnight, *The leucine zipper: a hypothetical structure common to a new class of DNA binding proteins.* Science, 1988. **240**(4860): p. 1759-64.

600. Manna, P.R., M.T. Dyson, and D.M. Stocco, *Role of basic leucine zipper proteins in transcriptional regulation of the steroidogenic acute regulatory protein gene.* Mol Cell Endocrinol, 2009. **302**(1): p. 1-11.

601. Cai, D.H., et al., *C/EBP alpha:AP-1 leucine zipper heterodimers bind novel DNA elements, activate the PU.1 promoter and direct monocyte lineage commitment more potently than C/EBP alpha homodimers or AP-1.* Oncogene, 2008. **27**(19): p. 2772-9.

Appendix

Chapter II

Table 2.S1 NormZ values for Namalwa and Raji CRISPR-screen, cut-off +/- 1.5 normZ score.

Namalwa_Sensitizers						
GENE	**sumZ**	**numObs**	**normZ**	**pval_synth**	**rank_synth**	**fdr_synth**
FANCA	-101.25	18	-19	9.06E-81	1	1.49E-76
FANCC	-96.46	18	-18.09	2.05E-73	2	1.69E-69
FANCD2	-88.01	18	-16.48	2.68E-61	3	1.47E-57
BRIP1	-74.31	18	-13.87	4.89E-44	4	2.01E-40
FANCI	-74.03	18	-13.81	1.04E-43	5	3.43E-40
UBE2T	-54.93	12	-12.53	2.64E-36	6	7.22E-33
MCM8	-63.48	18	-11.81	1.84E-32	7	4.32E-29
C19orf40	-62.73	18	-11.66	9.76E-32	8	2.01E-28
C3orf37	-61.16	18	-11.36	3.13E-30	9	5.71E-27
FANCB	-60.75	18	-11.29	7.68E-30	10	1.26E-26
FANCE	-60.54	18	-11.25	1.21E-29	11	1.81E-26
C17orf53	-59.84	18	-11.11	5.48E-29	12	7.5E-26
FANCM	-58.84	18	-10.92	4.52E-28	13	5.71E-25
FANCF	-52.04	15	-10.57	2E-26	14	2.34E-23
MUS81	-46.39	15	-9.4	2.84E-21	16	2.91E-18
C17orf70	-45.36	18	-8.36	3.25E-17	17	3.14E-14
FANCG	-41.6	18	-7.64	1.09E-14	18	9.97E-12
PTPRC	-41.42	18	-7.61	1.42E-14	19	1.23E-11
RNF168	-39.7	18	-7.28	1.68E-13	20	1.38E-10
RNF8	-37.52	18	-6.86	3.38E-12	21	2.65E-09
KIAA1524	-33.92	15	-6.79	5.44E-12	22	4.06E-09
MCM9	-36.65	18	-6.7	1.05E-11	23	7.53E-09
DCLRE1A	-33.34	15	-6.67	1.25E-11	24	8.58E-09
EME1	-35.88	18	-6.55	2.87E-11	25	1.88E-08
MEAF6	-28.09	12	-6.27	1.82E-10	26	1.15E-07
HELQ	-33.25	18	-6.05	7.27E-10	27	4.42E-07
RFWD3	-32.46	18	-5.9	1.81E-09	28	1.06E-06
MEN1	-32.01	18	-5.81	3.04E-09	29	1.72E-06
ZFAT	-31.44	18	-5.7	5.82E-09	30	3.19E-06
RAD51AP1	-25.51	12	-5.67	7.25E-09	31	3.84E-06
EXO1	-30.77	18	-5.58	1.22E-08	32	6.27E-06
NEIL3	-29.03	18	-5.25	7.78E-08	33	3.87E-05
SIRT1	-28.96	18	-5.23	8.34E-08	34	4.03E-05
SWI5	-28.69	18	-5.18	1.1E-07	35	5.15E-05
SLX4	-27.79	18	-5.01	2.71E-07	36	0.000124
APITD1	-15.8	6	-4.93	4.09E-07	37	0.000182
TSC2	-26.88	18	-4.84	6.56E-07	38	0.000284
TRAF3	-26.6	18	-4.78	8.62E-07	39	0.000363
SLX4IP	-26.27	18	-4.72	1.18E-06	40	0.000484
C4orf21	-26.2	18	-4.71	1.25E-06	41	0.0005

SCAI	-25.41	18	-4.56	2.58E-06	42	0.00101
DOT1L	-25.4	18	-4.56	2.62E-06	43	0.001
ERCC4	-25.38	18	-4.55	2.66E-06	44	0.000994
XRCC3	-25.3	18	-4.54	2.87E-06	45	0.00105
POLQ	-25.1	18	-4.5	3.43E-06	46	0.00123
CABIN1	-24.75	18	-4.43	4.66E-06	47	0.00163
EIF2AK3	-24.23	18	-4.33	7.35E-06	48	0.00252
RAD50	-24.16	18	-4.32	7.85E-06	49	0.00263
CPPED1	-24.1	18	-4.31	8.26E-06	50	0.00272
ANKRD32	-23.98	18	-4.29	9.12E-06	51	0.00294
PRUNE	-23.28	17	-4.28	9.36E-06	52	0.00296
GEN1	-19.34	12	-4.23	0.0000117	53	0.00362
SLC25A28	-23.66	18	-4.22	0.000012	54	0.00365
CCDC71L	-21.2	15	-4.14	0.0000172	55	0.00515
DAZAP1	-23.15	18	-4.13	0.0000184	56	0.00539
KHDRBS1	-22.68	18	-4.04	0.0000271	57	0.00781
ESCO1	-20.61	15	-4.02	0.0000293	58	0.0083
STRA13	-22.49	18	-4	0.0000314	59	0.00875
ING5	-22.37	18	-3.98	0.0000347	60	0.00949
PPME1	-22.19	18	-3.94	0.00004	61	0.0108
SIVA1	-22.06	18	-3.92	0.0000445	62	0.0118
RAD54L	-21.88	18	-3.89	0.0000509	63	0.0133
CCNT1	-21.88	18	-3.89	0.0000511	64	0.0131
PAXIP1	-21.85	18	-3.88	0.0000521	65	0.0132
IRF4	-21.62	18	-3.84	0.0000626	66	0.0156
STAG2	-21.57	18	-3.83	0.0000649	67	0.0159
PRKDC	-21.45	18	-3.8	0.0000711	68	0.0172
USP34	-21.26	18	-3.77	0.0000825	69	0.0196
TSC1	-21.02	18	-3.72	0.0000987	70	0.0232
DDX17	-20.88	18	-3.7	0.00011	71	0.0254
MND1	-14.76	9	-3.69	0.000111	72	0.0253
BRPF1	-20.83	18	-3.69	0.000114	73	0.0256
BRCA2	-20.75	18	-3.67	0.000121	74	0.0268
MDC1	-20.67	18	-3.65	0.000129	75	0.0282
WDTC1	-20.64	18	-3.65	0.000132	76	0.0284
LYN	-20.58	18	-3.64	0.000138	77	0.0294
ATM	-20.55	18	-3.63	0.000141	78	0.0297
TCEB3	-20.31	18	-3.59	0.000168	79	0.0349
FIGNL1	-18.52	15	-3.58	0.00017	80	0.0349
PSMC3IP	-20.18	18	-3.56	0.000185	81	0.0374
MSL1	-20.11	18	-3.55	0.000194	82	0.0389
MED16	-19.96	18	-3.52	0.000216	83	0.0428
MRE11A	-18.1	15	-3.49	0.000238	84	0.0466
UBE2A	-19.81	18	-3.49	0.00024	85	0.0464
RIF1	-19.74	18	-3.48	0.000253	86	0.0483
CNTROB	-19.69	18	-3.47	0.000262	87	0.0495
NFKBIB	-19.68	18	-3.47	0.000263	88	0.0491
RAD18	-11.35	6	-3.46	0.000267	89	0.0492

SLC7A11	-19.62	18	-3.45	0.000276	90	0.0503
CDC37	-19.49	18	-3.43	0.000302	91	0.0545
CUL3	-19.32	18	-3.4	0.000339	92	0.0605
MSL2	-19.21	18	-3.38	0.000367	93	0.0649
ERCC6	-19.11	18	-3.36	0.000394	94	0.0688
PDS5A	-19.08	18	-3.35	0.0004	95	0.0691
PFDN2	-19.06	18	-3.35	0.000407	96	0.0697
TRA2B	-18.73	18	-3.29	0.000508	97	0.0861
NCSTN	-18.58	18	-3.26	0.000563	98	0.0943
ACTR5	-18.31	18	-3.21	0.000672	99	0.112
BARD1	-18.23	18	-3.19	0.000709	100	0.116
BRD2	-18.23	18	-3.19	0.000709	101	0.115
EIF2AK1	-18.23	18	-3.19	0.000712	102	0.115
HNRNPU	-18.23	18	-3.19	0.000712	103	0.114
GIGYF2	-18.15	18	-3.17	0.00075	104	0.118
HNRNPA2B1	-18.09	18	-3.16	0.000779	105	0.122
ARHGEF2	-18.03	18	-3.15	0.000808	106	0.125
CSNK2B	-17.96	18	-3.14	0.000848	107	0.13
CHTF18	-17.94	18	-3.14	0.000858	108	0.131
BLM	-17.79	18	-3.11	0.000947	109	0.143
SNRNP70	-17.76	18	-3.1	0.000963	110	0.144
POLR2D	-10.23	6	-3.09	0.000993	111	0.147
HDAC3	-17.64	18	-3.08	0.00104	112	0.153
DSCC1	-16.06	15	-3.07	0.00108	113	0.157
APTX	-17.57	18	-3.07	0.00109	114	0.157
LIG4	-10.13	6	-3.06	0.00111	115	0.159
BIRC3	-10.05	6	-3.03	0.00121	116	0.171
H2AFX	-12.27	9	-3.02	0.00125	117	0.175
OAZ1	-15.83	15	-3.02	0.00126	118	0.176
SAMHD1	-17.32	18	-3.02	0.00128	119	0.176
RAD51C	-17.17	18	-2.99	0.0014	120	0.192
TGFBR1	-17.04	18	-2.96	0.00152	121	0.206
PDS5B	-16.77	18	-2.91	0.00179	122	0.241
RUNX1	-16.72	18	-2.9	0.00185	123	0.247
KLF16	-16.61	18	-2.88	0.00198	124	0.262
NELFA	-16.58	18	-2.88	0.00201	125	0.264
COPB2	-16.56	18	-2.87	0.00203	126	0.265
PSPN	-11.67	9	-2.86	0.0021	127	0.272
NFKBIA	-16.48	18	-2.86	0.00213	128	0.274
DDX5	-16.46	18	-2.85	0.00216	129	0.275
KDM5A	-16.46	18	-2.85	0.00216	130	0.273
SKA3	-15.02	15	-2.85	0.00217	131	0.273
ATRX	-16.43	18	-2.85	0.00221	132	0.274
NME1	-13.39	12	-2.84	0.00225	133	0.277
PAPOLA	-13.32	12	-2.83	0.00236	134	0.289
TGFBR2	-16.22	18	-2.81	0.0025	135	0.304
PPM1G	-16.17	18	-2.8	0.00257	136	0.31
MYCBP2	-16.17	18	-2.8	0.00257	137	0.308

MBNL1	-16.06	18	-2.78	0.00275	138	0.327
SRSF1	-15.53	17	-2.76	0.00287	139	0.339
MLX	-15.97	18	-2.76	0.00289	140	0.339
RASIP1	-15.92	18	-2.75	0.00298	141	0.347
CD80	-14.52	15	-2.75	0.00299	142	0.346
MAPKAPK2	-15.87	18	-2.74	0.00305	143	0.351
NBN	-12.95	12	-2.74	0.00307	144	0.35
KCTD5	-12.91	12	-2.73	0.00317	145	0.36
DHX35	-15.78	18	-2.72	0.00323	146	0.364
PPP6R3	-15.76	18	-2.72	0.00326	147	0.364
SKA1	-11.09	9	-2.71	0.0034	148	0.377
TXNDC17	-15.66	18	-2.7	0.00345	149	0.381
CD81	-15.49	18	-2.67	0.00381	150	0.417
TRAF2	-15.48	18	-2.67	0.00383	151	0.416
ELP5	-15.47	18	-2.66	0.00385	152	0.416
CARM1	-15.47	18	-2.66	0.00386	153	0.415
CENPE	-15.47	18	-2.66	0.00386	154	0.412
PDHA1	-15.46	18	-2.66	0.00388	155	0.411
KAT6A	-15.43	18	-2.66	0.00393	156	0.414
DDX49	-15.37	18	-2.65	0.00408	157	0.427
BRCA1	-15.31	18	-2.63	0.00421	158	0.438
C20orf173	-15.3	18	-2.63	0.00424	159	0.439
BCL6	-15.19	18	-2.61	0.0045	160	0.462
OSGIN2	-10.73	9	-2.61	0.00453	161	0.462
PAGR1	-15.16	18	-2.61	0.00458	162	0.464
CLASP2	-15.04	18	-2.58	0.0049	163	0.494
ERCC8	-15.04	18	-2.58	0.0049	164	0.491
RMI2	-13.71	15	-2.58	0.00496	165	0.494
REV3L	-15	18	-2.57	0.00502	166	0.497
TRNAU1AP	-14.99	18	-2.57	0.00502	167	0.494
PRPF39	-14.97	18	-2.57	0.00508	168	0.497
C15orf32	-14.95	18	-2.57	0.00514	169	0.5
CEP290	-14.89	18	-2.55	0.00532	170	0.514
SRRM1	-14.83	18	-2.54	0.00551	171	0.529
HEATR3	-14.79	18	-2.54	0.0056	172	0.535
DHX36	-14.78	18	-2.53	0.00564	173	0.535
PRPF38B	-14.77	18	-2.53	0.00566	174	0.535
SLC38A11	-14.76	18	-2.53	0.0057	175	0.535
WNT10A	-14.34	17	-2.53	0.00571	176	0.533
NUCB1	-14.75	18	-2.53	0.00573	177	0.532
XRCC1	-14.74	18	-2.53	0.00577	178	0.533
WDR48	-14.74	18	-2.53	0.00578	179	0.531
POLE4	-14.72	18	-2.52	0.00582	180	0.531
GAB4	-14.71	18	-2.52	0.00586	181	0.532
OR1M1	-11.98	12	-2.51	0.00598	182	0.54
PPM1D	-14.65	18	-2.51	0.00604	183	0.543
AP1M1	-14.63	18	-2.51	0.00611	184	0.546
HMGXB4	-14.63	18	-2.5	0.00614	185	0.545

CDT1	-14.61	18	-2.5	0.00618	186	0.546
CMIP	-14.59	18	-2.5	0.00627	187	0.551
TMEM101	-14.57	18	-2.49	0.00632	188	0.553
PAQR8	-14.56	18	-2.49	0.00636	189	0.553
HSPA9	-10.26	9	-2.48	0.00654	190	0.565
MED12	-14.48	18	-2.48	0.00663	191	0.57
DHX9	-11.81	12	-2.47	0.00667	192	0.571
SMC5	-14.46	18	-2.47	0.00669	193	0.57
GATAD2A	-14.45	18	-2.47	0.00674	194	0.571
OPA3	-14.35	18	-2.45	0.00711	195	0.599
TOPBP1	-14.33	18	-2.45	0.00718	196	0.602
PPP1R8	-14.27	18	-2.44	0.0074	197	0.617
WFDC8	-13.01	15	-2.43	0.00749	198	0.621
DNAJC9	-8.2	6	-2.42	0.00766	199	0.632
LCN8	-14.18	18	-2.42	0.00778	200	0.639
C1orf86	-14.05	18	-2.4	0.0083	201	0.679
STAG1	-14.04	18	-2.39	0.00837	202	0.681
INTS10	-13.99	18	-2.38	0.00857	203	0.693
BORA	-13.99	18	-2.38	0.00858	204	0.691
KIF7	-13.98	18	-2.38	0.00865	205	0.693
POU2AF1	-13.89	18	-2.36	0.00904	206	0.721
NRG3	-13.89	18	-2.36	0.00905	207	0.718
PARP1	-13.87	18	-2.36	0.00912	208	0.721
CNTF	-12.66	15	-2.36	0.00914	209	0.719
MYH9	-13.87	18	-2.36	0.00915	210	0.716
RIPK4	-13.85	18	-2.36	0.00921	211	0.717
OR2Z1	-13.79	18	-2.35	0.00951	212	0.737
IER2	-12.58	15	-2.34	0.00954	213	0.736
SPI1	-13.78	18	-2.34	0.00956	214	0.734
C1orf112	-13.77	18	-2.34	0.00963	215	0.736
RRP12	-13.75	18	-2.34	0.00972	216	0.74
RECQL5	-13.73	18	-2.33	0.00978	217	0.741
PCM1	-13.72	18	-2.33	0.00987	218	0.744
FAM178A	-13.68	18	-2.32	0.0101	219	0.754
DLD	-9.67	9	-2.32	0.0101	220	0.755
NHLRC2	-13.28	17	-2.32	0.0102	221	0.755
YLPM1	-13.66	18	-2.32	0.0102	222	0.752
ACR	-13.66	18	-2.32	0.0102	223	0.749
CD3D	-13.65	18	-2.32	0.0102	224	0.751
HIRA	-13.6	18	-2.31	0.0105	225	0.765
RBM26	-13.59	18	-2.31	0.0105	226	0.765
ILF2	-12.39	15	-2.3	0.0106	227	0.769
PNOC	-12.37	15	-2.3	0.0107	228	0.774
DEPDC5	-13.54	18	-2.3	0.0108	229	0.776
PWWP2A	-13.52	18	-2.29	0.0109	230	0.777
CAV3	-11.03	12	-2.29	0.011	231	0.779
USP9X	-13.5	18	-2.29	0.011	232	0.778
GAPT	-7.79	6	-2.29	0.011	233	0.777

PPHLN1	-13.48	18	-2.29	0.0111	234	0.781
STC1	-13.45	18	-2.28	0.0113	235	0.79
CDK12	-13.39	18	-2.27	0.0116	236	0.81
ZFR	-13.38	18	-2.27	0.0117	237	0.812
NXF1	-13.37	18	-2.27	0.0117	238	0.81
SS18	-13.34	18	-2.26	0.0119	239	0.819
PRR12	-13.33	18	-2.26	0.012	240	0.82
TLR6	-9.42	9	-2.26	0.012	241	0.82
SCN2B	-13.32	18	-2.26	0.0121	242	0.819
CEP97	-13.31	18	-2.25	0.0121	243	0.817
SENP5	-13.31	18	-2.25	0.0121	244	0.817
TRIM37	-13.24	18	-2.24	0.0125	245	0.839
PHKB	-13.22	18	-2.24	0.0126	246	0.844
KCNA1	-13.22	18	-2.24	0.0126	247	0.841
MLST8	-13.22	18	-2.24	0.0127	248	0.838
SPEN	-13.22	18	-2.24	0.0127	249	0.836
MDH1	-9.34	9	-2.24	0.0127	250	0.834
TICRR	-13.21	18	-2.23	0.0127	251	0.834
MED11	-13.2	18	-2.23	0.0128	252	0.832
RPAP1	-13.17	18	-2.23	0.013	253	0.843
SMC6	-13.17	18	-2.23	0.013	254	0.841
UBR4	-13.16	18	-2.22	0.013	255	0.84
NUDT2	-9.3	9	-2.22	0.0131	256	0.841
CEP57	-11.98	15	-2.22	0.0132	257	0.847
GAD1	-13.12	18	-2.22	0.0133	258	0.845
RAD51B	-13.12	18	-2.22	0.0133	259	0.844
DOLK	-13.1	18	-2.21	0.0134	260	0.848
GLOD4	-13.09	18	-2.21	0.0135	261	0.848
DCAF15	-13.09	18	-2.21	0.0135	262	0.847
XRCC2	-9.24	9	-2.21	0.0136	263	0.85
SIRT5	-13.06	18	-2.21	0.0137	264	0.853
DTYMK	-12.28	16	-2.2	0.0139	265	0.861
METTL6	-9.21	9	-2.2	0.0139	266	0.861
TKT	-13.01	18	-2.2	0.014	267	0.862
MPDZ	-13.01	18	-2.2	0.014	268	0.861
MTR	-13	18	-2.19	0.0141	269	0.861
KIAA1919	-7.5	6	-2.19	0.0141	270	0.86
HIPK1	-12.97	18	-2.19	0.0143	271	0.867
NFKBIE	-12.97	18	-2.19	0.0143	272	0.864
POLR2I	-12.93	18	-2.18	0.0146	273	0.877
RAD51D	-12.92	18	-2.18	0.0146	274	0.877
ULK4	-12.86	18	-2.17	0.0151	275	0.9
CDCA5	-12.86	18	-2.17	0.0151	276	0.898
DIAPH1	-12.85	18	-2.17	0.0152	277	0.899
NPTN	-12.85	18	-2.17	0.0152	278	0.897
AGO2	-12.84	18	-2.16	0.0152	279	0.896
KCNQ2	-12.81	18	-2.16	0.0155	280	0.907
MR1	-10.4	12	-2.15	0.016	281	0.933

MS4A15	-12.73	18	-2.14	0.016	282	0.933
CCT5	-11.59	15	-2.14	0.0163	283	0.945
ESCO2	-8.92	9	-2.12	0.017	284	0.983
PGBD3	-12.59	18	-2.12	0.0171	285	0.989
ACADVL	-12.56	18	-2.11	0.0174	286	0.998
FOXM1	-12.55	18	-2.11	0.0175	287	1
CCL21	-7.24	6	-2.11	0.0176	288	1.01
IMP4	-12.18	17	-2.11	0.0176	289	1
KRT15	-12.49	18	-2.1	0.018	290	1.02
CHD7	-12.49	18	-2.1	0.018	291	1.02
FCGRT	-12.43	18	-2.09	0.0185	292	1.04
TBC1D20	-12.4	18	-2.08	0.0187	293	1.05
SEMA6C	-12.4	18	-2.08	0.0187	294	1.05
GTF2E1	-12.39	18	-2.08	0.0188	295	1.05
MAGT1	-12.38	18	-2.08	0.0189	296	1.05
MPC2	-8.74	9	-2.07	0.0191	297	1.05
SOX6	-12.36	18	-2.07	0.0191	298	1.05
CREBBP	-12.35	18	-2.07	0.0191	299	1.05
SERTAD2	-12.32	18	-2.07	0.0194	300	1.06
ATF7IP	-12.29	18	-2.06	0.0197	301	1.08
ZC3H14	-11.21	15	-2.06	0.0198	302	1.08
ARL2	-12.28	18	-2.06	0.0199	303	1.08
MLLT1	-12.27	18	-2.06	0.0199	304	1.07
TMEM39A	-12.27	18	-2.06	0.0199	305	1.07
VIT	-12.25	18	-2.05	0.0201	306	1.08
FOXA3	-11.17	15	-2.05	0.0202	307	1.08
RUNDC3B	-12.24	18	-2.05	0.0202	308	1.08
BEND3	-12.23	18	-2.05	0.0203	309	1.08
DNALI1	-12.2	18	-2.04	0.0205	310	1.09
AUNIP	-11.13	15	-2.04	0.0207	311	1.09
TEP1	-12.18	18	-2.04	0.0207	312	1.09
RALGAPA2	-12.18	18	-2.04	0.0208	313	1.09
PCMT1	-12.16	18	-2.04	0.0209	314	1.09
MGMT	-12.16	18	-2.03	0.021	315	1.09
ATR	-11.09	15	-2.03	0.0211	316	1.1
C12orf66	-12.14	18	-2.03	0.0211	317	1.1
C1QTNF5	-11.07	15	-2.03	0.0213	318	1.1
FANCL	-8.58	9	-2.03	0.0213	319	1.1
TRIM25	-12.12	18	-2.03	0.0214	320	1.1
N4BP1	-12.12	18	-2.03	0.0214	321	1.09
ELP2	-12.11	18	-2.02	0.0214	322	1.09
ZNF3	-12.11	18	-2.02	0.0214	323	1.09
RNF146	-12.09	18	-2.02	0.0216	324	1.1
AQP7	-6.98	6	-2.02	0.0217	325	1.09
LRRC45	-12.08	18	-2.02	0.0217	326	1.09
RNF166	-12.05	18	-2.01	0.022	327	1.11
BCAT2	-12.05	18	-2.01	0.0221	328	1.11
FAM13A	-12.04	18	-2.01	0.0221	329	1.1

GCLM	-12.04	18	-2.01	0.0221	330	1.1
HUWE1	-12.04	18	-2.01	0.0222	331	1.1
ORC1	-12.01	18	-2.01	0.0225	332	1.11
RARS2	-8.95	10	-2.01	0.0225	333	1.11
TIPRL	-9.78	12	-2	0.0228	334	1.12
MAF	-10.91	15	-1.99	0.023	335	1.13
RAD52	-11.92	18	-1.99	0.0233	336	1.14
SPATA3	-8.43	9	-1.99	0.0233	337	1.14
USP21	-11.91	18	-1.99	0.0234	338	1.14
PPFIBP2	-11.91	18	-1.99	0.0235	339	1.14
SCARA5	-11.88	18	-1.98	0.0237	340	1.15
AGRN	-11.55	17	-1.98	0.0238	341	1.14
FARS2	-11.88	18	-1.98	0.0238	342	1.14
SYT13	-11.87	18	-1.98	0.0239	343	1.14
EIF5	-10.83	15	-1.98	0.0239	344	1.14
AASS	-11.87	18	-1.98	0.0239	345	1.14
XPO6	-11.86	18	-1.98	0.024	346	1.14
MED19	-11.86	18	-1.98	0.024	347	1.14
IREB2	-11.84	18	-1.97	0.0243	348	1.15
RBBP7	-11.81	18	-1.97	0.0246	349	1.16
BRD4	-11.8	18	-1.97	0.0247	350	1.16
VPS28	-11.79	18	-1.96	0.0247	351	1.16
DOCK9	-11.79	18	-1.96	0.0247	352	1.15
UBE2H	-9.62	12	-1.96	0.0249	353	1.16
TRIM59	-9.61	12	-1.96	0.0249	354	1.16
PSIP1	-6.79	6	-1.96	0.025	355	1.16
SNRPA	-11.76	18	-1.96	0.0251	356	1.16
IRF7	-11.75	18	-1.96	0.0252	357	1.16
NPRL2	-11.75	18	-1.96	0.0252	358	1.16
DCLRE1C	-10.72	15	-1.95	0.0253	359	1.16
NFKB2	-11.73	18	-1.95	0.0254	360	1.16
NEK1	-11.73	18	-1.95	0.0254	361	1.16
CRISPLD1	-11.7	18	-1.95	0.0257	362	1.17
SLC50A1	-11.67	18	-1.94	0.0262	363	1.18
ORC2	-10.63	15	-1.94	0.0264	364	1.19
ARL15	-11.64	18	-1.94	0.0264	365	1.19
ZNF467	-11.64	18	-1.94	0.0265	366	1.19
KRTAP16-1	-11.63	18	-1.93	0.0266	367	1.19
F10	-11.63	18	-1.93	0.0266	368	1.19
INTS9	-10.6	15	-1.93	0.0267	369	1.19
ABCC1	-11.61	18	-1.93	0.0268	370	1.19
TMEM165	-11.58	18	-1.92	0.0272	371	1.2
EPHA8	-11.58	18	-1.92	0.0272	372	1.2
HS6ST2	-11.57	18	-1.92	0.0273	373	1.2
NGLY1	-11.57	18	-1.92	0.0273	374	1.2
SLC30A3	-11.57	18	-1.92	0.0273	375	1.2
MLLT10	-11.56	18	-1.92	0.0274	376	1.2
ORC5	-10.55	15	-1.92	0.0275	377	1.2

KANK2	-11.56	18	-1.92	0.0275	378	1.19
ALMS1	-11.54	18	-1.92	0.0276	379	1.2
CDH19	-10.53	15	-1.92	0.0277	380	1.2
TRPS1	-11.53	18	-1.92	0.0277	381	1.19
BABAM1	-11.53	18	-1.92	0.0277	382	1.19
POU2F2	-11.52	18	-1.91	0.0278	383	1.19
TXK	-11.51	18	-1.91	0.028	384	1.2
C21orf2	-11.48	18	-1.9	0.0284	385	1.21
CHST1	-11.47	18	-1.9	0.0285	386	1.22
GLRX3	-10.47	15	-1.9	0.0286	387	1.21
SNTG2	-11.46	18	-1.9	0.0286	388	1.21
CLGN	-6.62	6	-1.9	0.0286	389	1.21
AHCYL1	-11.44	18	-1.9	0.0289	390	1.22
ELOVL1	-11.44	18	-1.9	0.0289	391	1.22
TXNL1	-9.33	12	-1.9	0.029	392	1.22
COX7A2L	-6.59	6	-1.89	0.0291	393	1.22
GPR75	-10.4	15	-1.89	0.0295	394	1.23
RBMXL3	-9.3	12	-1.89	0.0295	395	1.23
MED26	-11.38	18	-1.89	0.0297	396	1.23
MED25	-11.37	18	-1.89	0.0297	397	1.23
EAF1	-11.36	18	-1.88	0.0299	398	1.23
CPN1	-11.35	18	-1.88	0.03	399	1.23
TMEM107	-11.34	18	-1.88	0.0301	400	1.24
ZKSCAN1	-11.33	18	-1.88	0.0303	401	1.24
ATP1A1	-11.32	18	-1.88	0.0304	402	1.24
TMEM222	-11.32	18	-1.87	0.0304	403	1.24
WDR96	-11.32	18	-1.87	0.0305	404	1.24
SRPK1	-11.3	18	-1.87	0.0306	405	1.24
SLC44A2	-11.3	18	-1.87	0.0307	406	1.24
ELP3	-11.29	18	-1.87	0.0308	407	1.24
ARSA	-11.28	18	-1.87	0.0309	408	1.24
MAP1LC3C	-7.97	9	-1.86	0.0311	409	1.25
TMEM201	-11.25	18	-1.86	0.0313	410	1.26
MYO9A	-11.23	18	-1.86	0.0316	411	1.26
IBA57	-11.22	18	-1.86	0.0317	412	1.27
PRR7	-11.22	18	-1.86	0.0317	413	1.26
KIFAP3	-11.21	18	-1.85	0.0319	414	1.26
LYRM1	-10.23	15	-1.85	0.0319	415	1.26
RBM14	-11.19	18	-1.85	0.0321	416	1.27
ASB7	-10.21	15	-1.85	0.0322	417	1.27
VAC14	-11.18	18	-1.85	0.0323	418	1.27
OR1J2	-6.45	6	-1.85	0.0324	419	1.27
CSE1L	-11.17	18	-1.85	0.0324	420	1.27
NUDC	-7.9	9	-1.85	0.0325	421	1.27
HEATR5B	-11.16	18	-1.84	0.0326	422	1.27
C20orf202	-11.15	18	-1.84	0.0327	423	1.27
SLC3A1	-11.15	18	-1.84	0.0327	424	1.27
COX6B2	-9.1	12	-1.84	0.0328	425	1.27

MCM7	-11.12	18	-1.84	0.0332	426	1.28
RIPK2	-11.11	18	-1.84	0.0333	427	1.28
SP8	-10.14	15	-1.83	0.0333	428	1.28
NCF4	-11.1	18	-1.83	0.0334	429	1.28
PNMA3	-11.1	18	-1.83	0.0334	430	1.28
KLK11	-11.08	18	-1.83	0.0337	431	1.28
FBXO22	-11.08	18	-1.83	0.0337	432	1.28
PCGF5	-6.39	6	-1.83	0.0338	433	1.28
G3BP2	-11.07	18	-1.83	0.0338	434	1.28
SEC24B	-11.07	18	-1.83	0.0338	435	1.28
TNFRSF12A	-11.06	18	-1.82	0.034	436	1.28
TPK1	-11.04	18	-1.82	0.0342	437	1.29
ZBTB18	-11.04	18	-1.82	0.0343	438	1.29
MRGPRX2	-9.01	12	-1.82	0.0344	439	1.29
IGDCC3	-11.03	18	-1.82	0.0344	440	1.28
DZIP1L	-11.02	18	-1.82	0.0345	441	1.29
INPP1	-11.02	18	-1.82	0.0345	442	1.28
DDX1	-11.01	18	-1.82	0.0346	443	1.28
DAO	-11	18	-1.81	0.0348	444	1.29
CDH11	-10.99	18	-1.81	0.0351	445	1.29
PLAG1	-10.03	15	-1.81	0.0351	446	1.29
SMOX	-10.98	18	-1.81	0.0352	447	1.29
VPS9D1	-10.98	18	-1.81	0.0352	448	1.29
RFC1	-10.97	18	-1.81	0.0353	449	1.29
LINS	-10.96	18	-1.81	0.0354	450	1.29
IPPK	-10.96	18	-1.81	0.0355	451	1.29
CCDC90B	-10.95	18	-1.8	0.0357	452	1.3
LCN2	-10.94	18	-1.8	0.0357	453	1.3
RGS11	-10.94	18	-1.8	0.0358	454	1.3
MRGBP	-10.93	18	-1.8	0.0359	455	1.3
GPR161	-10.93	18	-1.8	0.0359	456	1.29
HNRNPR	-8.92	12	-1.8	0.036	457	1.29
DR1	-8.92	12	-1.8	0.036	458	1.29
NCOA4	-7.72	9	-1.8	0.036	459	1.29
DHODH	-10.61	17	-1.8	0.0361	460	1.29
KLK10	-10.9	18	-1.79	0.0364	461	1.3
SPINK8	-9.94	15	-1.79	0.0365	462	1.3
SENP7	-10.89	18	-1.79	0.0365	463	1.29
OCA2	-10.88	18	-1.79	0.0366	464	1.3
NOXO1	-10.87	18	-1.79	0.0368	465	1.3
DIDO1	-10.86	18	-1.79	0.037	466	1.3
ZCCHC8	-10.85	18	-1.79	0.0371	467	1.31
NCAPH2	-10.85	18	-1.78	0.0372	468	1.31
METTL11B	-10.84	18	-1.78	0.0373	469	1.31
FRAT1	-10.83	18	-1.78	0.0374	470	1.31
MYH15	-10.83	18	-1.78	0.0375	471	1.31
CCND1	-10.83	18	-1.78	0.0375	472	1.3
RFTN2	-10.82	18	-1.78	0.0376	473	1.3

RILPL1	-10.82	18	-1.78	0.0376	474	1.3
ENDOV	-10.82	18	-1.78	0.0376	475	1.3
SLC25A37	-10.81	18	-1.78	0.0378	476	1.31
SLC36A1	-10.81	18	-1.78	0.0378	477	1.3
PPP1R7	-10.8	18	-1.78	0.0378	478	1.3
CDAN1	-10.5	17	-1.78	0.0378	479	1.3
CHD4	-10.8	18	-1.78	0.0379	480	1.3
TAF3	-10.79	18	-1.77	0.038	481	1.3
CNPPD1	-10.79	18	-1.77	0.038	482	1.29
CRYGC	-10.79	18	-1.77	0.038	483	1.29
NTRK1	-10.78	18	-1.77	0.0381	484	1.29
GATA5	-10.78	18	-1.77	0.0382	485	1.29
KRT33A	-7.62	9	-1.77	0.0382	486	1.29
TOE1	-10.78	18	-1.77	0.0382	487	1.29
UNC50	-9.83	15	-1.77	0.0383	488	1.29
ATXN1L	-10.77	18	-1.77	0.0384	489	1.29
FAM49A	-10.76	18	-1.77	0.0385	490	1.29
OPHN1	-10.75	18	-1.77	0.0386	491	1.29
ATAD3C	-7.6	9	-1.77	0.0387	492	1.29
SLC16A5	-10.74	18	-1.77	0.0388	493	1.29
FIGN	-10.74	18	-1.76	0.0389	494	1.29
NDUFA13	-10.73	18	-1.76	0.039	495	1.29
SRFBP1	-6.2	6	-1.76	0.039	496	1.29
WRN	-10.73	18	-1.76	0.039	497	1.29
CARNS1	-10.73	18	-1.76	0.039	498	1.29
SNAI3	-10.72	18	-1.76	0.0391	499	1.29
TAF5	-10.72	18	-1.76	0.0392	500	1.29
ATRIP	-10.1	16	-1.76	0.0393	501	1.29
SLC6A1	-10.7	18	-1.76	0.0394	502	1.29
CDK2	-10.7	18	-1.76	0.0394	503	1.29
PALB2	-10.7	18	-1.76	0.0395	504	1.29
RPF1	-8.73	12	-1.75	0.0397	505	1.29
DLX2	-10.68	18	-1.75	0.0398	506	1.29
NR3C2	-10.67	18	-1.75	0.04	507	1.3
CD79A	-10.67	18	-1.75	0.04	508	1.29
PODN	-10.66	18	-1.75	0.0401	509	1.29
CA3	-10.66	18	-1.75	0.0402	510	1.29
EPHA7	-10.66	18	-1.75	0.0402	511	1.29
SLC4A8	-10.65	18	-1.75	0.0403	512	1.29
MTBP	-9.72	15	-1.75	0.0404	513	1.29
SSU72	-10.61	18	-1.74	0.0409	514	1.31
CCNY	-10.61	18	-1.74	0.041	515	1.31
UVSSA	-10.61	18	-1.74	0.041	516	1.31
MZB1	-10.57	18	-1.73	0.0416	517	1.32
XRCC4	-7.46	9	-1.73	0.0419	518	1.33
CCDC36	-10.55	18	-1.73	0.042	519	1.33
PRSS38	-10.55	18	-1.73	0.042	520	1.33
CLLU1	-6.09	6	-1.73	0.0421	521	1.33

ADCK2	-10.54	18	-1.73	0.0422	522	1.33
OR6K2	-8.6	12	-1.73	0.0422	523	1.33
GJC2	-9.62	15	-1.73	0.0422	524	1.32
KCNB1	-10.54	18	-1.73	0.0422	525	1.32
MAN2B1	-10.53	18	-1.72	0.0423	526	1.32
AS3MT	-9.61	15	-1.72	0.0424	527	1.32
MAML1	-9.92	16	-1.72	0.0425	528	1.32
ZNF548	-10.52	18	-1.72	0.0426	529	1.32
CASP12	-8.56	12	-1.72	0.0431	530	1.33
AKAP3	-9.57	15	-1.72	0.0431	531	1.33
LCN10	-10.48	18	-1.72	0.0431	532	1.33
JOSD1	-9.57	15	-1.72	0.0431	533	1.33
SLC4A3	-10.47	18	-1.71	0.0434	534	1.34
DLST	-10.45	18	-1.71	0.0437	535	1.34
PAX7	-10.45	18	-1.71	0.0438	536	1.34
EIF4E2	-9.53	15	-1.71	0.0438	537	1.34
SRMS	-10.44	18	-1.71	0.0438	538	1.34
SRCRB4D	-10.44	18	-1.71	0.0439	539	1.34
TCERG1	-10.44	18	-1.71	0.0439	540	1.34
USP39	-10.14	17	-1.71	0.0439	541	1.33
USP29	-8.52	12	-1.71	0.0441	542	1.34
HRAS	-10.43	18	-1.7	0.0441	543	1.33
ROGDI	-10.43	18	-1.7	0.0441	544	1.33
BPIFA2	-10.42	18	-1.7	0.0442	545	1.33
MED17	-10.42	18	-1.7	0.0443	546	1.33
SAMD1	-10.41	18	-1.7	0.0444	547	1.33
TPM3	-6.01	6	-1.7	0.0445	548	1.34
BPIFB6	-10.38	18	-1.7	0.045	549	1.35
RBM41	-10.38	18	-1.69	0.045	550	1.35
HAT1	-9.47	15	-1.69	0.0451	551	1.35
B3GNT6	-10.37	18	-1.69	0.0451	552	1.34
PPP1R9A	-10.37	18	-1.69	0.0451	553	1.34
MLXIP	-10.37	18	-1.69	0.0452	554	1.34
KRTCAP2	-9.46	15	-1.69	0.0452	555	1.34
CA9	-10.36	18	-1.69	0.0454	556	1.34
CCDC120	-10.35	18	-1.69	0.0454	557	1.34
OTP	-10.34	18	-1.69	0.0456	558	1.34
ABTB1	-10.34	18	-1.69	0.0456	559	1.34
RANBP2	-9.44	15	-1.69	0.0456	560	1.34
EARS2	-10.34	18	-1.69	0.0457	561	1.34
SOD1	-6.89	8	-1.69	0.0457	562	1.33
RAB3B	-9.44	15	-1.69	0.0457	563	1.33
ZSWIM4	-10.32	18	-1.69	0.046	564	1.34
FRMD6	-10.32	18	-1.68	0.0461	565	1.34
POSTN	-10.31	18	-1.68	0.0462	566	1.34
NCOA3	-10.31	18	-1.68	0.0462	567	1.34
GJA9	-9.41	15	-1.68	0.0462	568	1.34
NRTN	-10.3	18	-1.68	0.0464	569	1.34

RPA2	-10.3	18	-1.68	0.0464	570	1.34
ZNF511	-10.3	18	-1.68	0.0464	571	1.34
KNTC1	-10.3	18	-1.68	0.0465	572	1.34
MRM1	-10.3	18	-1.68	0.0465	573	1.33
STX8	-7.27	9	-1.68	0.0468	574	1.34
GCC2	-10.28	18	-1.68	0.0468	575	1.34
SCAF4	-10.28	18	-1.68	0.0469	576	1.34
LRRC4C	-9.38	15	-1.68	0.0469	577	1.33
FAM208B	-10.28	18	-1.68	0.0469	578	1.33
KRT81	-8.39	12	-1.68	0.0469	579	1.33
NUDCD3	-10.27	18	-1.67	0.047	580	1.33
KRT31	-7.26	9	-1.67	0.0471	581	1.33
ME2	-7.25	9	-1.67	0.0472	582	1.33
ART4	-9.36	15	-1.67	0.0474	583	1.34
MAF1	-10.24	18	-1.67	0.0476	584	1.34
SFT2D1	-9.34	15	-1.67	0.0476	585	1.34
STK11IP	-10.24	18	-1.67	0.0476	586	1.34
SLC6A12	-10.23	18	-1.67	0.0478	587	1.34
NUP88	-10.23	18	-1.67	0.0478	588	1.34
PXMP4	-10.22	18	-1.67	0.0478	589	1.33
EIF2B1	-9.33	15	-1.67	0.0479	590	1.33
PTPRA	-10.21	18	-1.66	0.0482	591	1.34
UBAP2L	-10.2	18	-1.66	0.0482	592	1.34
MLH1	-10.2	18	-1.66	0.0483	593	1.34
ERCC1	-10.2	18	-1.66	0.0483	594	1.34
HIAT1	-10.19	18	-1.66	0.0485	595	1.34
OTUD5	-10.16	18	-1.65	0.049	596	1.35
C2orf73	-10.16	18	-1.65	0.0491	597	1.35
BUB1B	-10.15	18	-1.65	0.0492	598	1.35
RGS10	-8.28	12	-1.65	0.0494	599	1.35
HMOX2	-10.14	18	-1.65	0.0494	600	1.35
CPVL	-9.26	15	-1.65	0.0494	601	1.35
NAB1	-7.17	9	-1.65	0.0495	602	1.35
ZNF747	-10.13	18	-1.65	0.0496	603	1.35
RIBC2	-10.13	18	-1.65	0.0497	604	1.35
COLEC12	-10.12	18	-1.65	0.0498	605	1.35
KDM8	-10.12	18	-1.65	0.0498	606	1.35
TRAM1L1	-8.26	12	-1.65	0.05	607	1.35
NIPBL	-10.11	18	-1.64	0.0501	608	1.35
MARCH10	-10.1	18	-1.64	0.0502	609	1.35
PENK	-10.09	18	-1.64	0.0504	610	1.36
VHL	-10.09	18	-1.64	0.0505	611	1.36
CLDN20	-8.23	12	-1.64	0.0506	612	1.36
TNFRSF8	-10.08	18	-1.64	0.0507	613	1.36
NARFL	-9.49	16	-1.64	0.0509	614	1.36
MYNN	-9.19	15	-1.64	0.0509	615	1.36
SCP2D1	-7.11	9	-1.64	0.051	616	1.36
ITGA2B	-10.06	18	-1.63	0.0511	617	1.36

FOXN2	-9.18	15	-1.63	0.0512	618	1.36
CCNF	-10.05	18	-1.63	0.0512	619	1.36
OR5I1	-7.11	9	-1.63	0.0513	620	1.36
R3HCC1L	-10.05	18	-1.63	0.0513	621	1.36
HERC1	-10.04	18	-1.63	0.0514	622	1.36
GABRB3	-10.04	18	-1.63	0.0514	623	1.35
KCNMA1	-10.04	18	-1.63	0.0514	624	1.35
TMEM169	-10.04	18	-1.63	0.0515	625	1.35
C8orf74	-10.03	18	-1.63	0.0516	626	1.35
CX3CR1	-10.03	18	-1.63	0.0516	627	1.35
TTLL5	-10.02	18	-1.63	0.0518	628	1.35
FOXK1	-10.02	18	-1.63	0.0518	629	1.35
C11orf82	-8.18	12	-1.63	0.052	630	1.36
GPR98	-10.01	18	-1.62	0.0521	631	1.36
TEF	-10	18	-1.62	0.0522	632	1.36
CNTN2	-9.98	18	-1.62	0.0527	633	1.37
SESN3	-9.98	18	-1.62	0.0527	634	1.37
LRRTM1	-9.1	15	-1.62	0.0528	635	1.37
MRPS18B	-9.96	18	-1.62	0.0531	636	1.37
C8A	-9.95	18	-1.61	0.0532	637	1.37
SLC19A3	-7.04	9	-1.61	0.0532	638	1.37
C5orf30	-8.12	12	-1.61	0.0533	639	1.37
PMPCB	-9.94	18	-1.61	0.0534	640	1.37
SAV1	-9.07	15	-1.61	0.0535	641	1.37
ERCC6L	-9.93	18	-1.61	0.0537	642	1.37
TERF2	-9.93	18	-1.61	0.0537	643	1.37
PDP2	-9.93	18	-1.61	0.0537	644	1.37
STAM	-9.92	18	-1.61	0.054	645	1.37
RPH3AL	-9.91	18	-1.61	0.054	646	1.37
SEC31A	-9.91	18	-1.61	0.054	647	1.37
STH	-8.09	12	-1.61	0.054	648	1.37
ACY3	-9.91	18	-1.61	0.0541	649	1.37
MRPS14	-9.91	18	-1.61	0.0541	650	1.37
PAMR1	-9.91	18	-1.61	0.0541	651	1.37
TJP3	-9.9	18	-1.61	0.0542	652	1.37
XPNPEP1	-9.9	18	-1.6	0.0544	653	1.37
OR6N1	-8.08	12	-1.6	0.0545	654	1.37
PRPF19	-9.61	17	-1.6	0.0546	655	1.37
NFKBIZ	-9.88	18	-1.6	0.0548	656	1.37
CTGF	-9.88	18	-1.6	0.0548	657	1.37
ARHGEF10	-9.87	18	-1.6	0.0549	658	1.37
PLA2G6	-9.87	18	-1.6	0.055	659	1.37
PTGS1	-9.86	18	-1.6	0.0551	660	1.37
ZFP36	-9.86	18	-1.6	0.0552	661	1.37
KIAA0947	-9.84	18	-1.59	0.0557	662	1.38
LUZP1	-9.83	18	-1.59	0.0558	663	1.38
MGEA5	-9.83	18	-1.59	0.0559	664	1.38
SLC9A3R1	-9.82	18	-1.59	0.0559	665	1.38

SCGB3A2	-8.02	12	-1.59	0.0561	666	1.38
NUDCD2	-5.67	6	-1.59	0.0561	667	1.38
PNPLA8	-9.81	18	-1.59	0.0562	668	1.38
CNTRL	-9.81	18	-1.59	0.0562	669	1.38
CCDC3	-9.8	18	-1.59	0.0563	670	1.38
SF3B3	-9.8	18	-1.59	0.0564	671	1.38
RPP25L	-9.8	18	-1.59	0.0564	672	1.38
KISS1R	-9.8	18	-1.58	0.0565	673	1.38
LRRC8E	-9.79	18	-1.58	0.0566	674	1.38
ADRA1A	-9.79	18	-1.58	0.0566	675	1.38
MRPS9	-9.78	18	-1.58	0.057	676	1.38
GPR133	-9.77	18	-1.58	0.0571	677	1.39
CRCT1	-6.9	9	-1.58	0.0573	678	1.39
SKP2	-9.75	18	-1.58	0.0576	679	1.39
SERPINB1	-9.74	18	-1.57	0.0577	680	1.39
PABPC1L	-9.72	18	-1.57	0.0582	681	1.4
RCC2	-5.61	6	-1.57	0.0582	682	1.4
COL9A2	-9.71	18	-1.57	0.0585	683	1.41
ZFPM1	-9.7	18	-1.57	0.0585	684	1.41
MRPL21	-9.7	18	-1.57	0.0587	685	1.41
TRPM1	-9.7	18	-1.57	0.0587	686	1.41
GTSE1	-9.69	18	-1.57	0.0588	687	1.41
TIMM22	-9.69	18	-1.56	0.0589	688	1.41
KLHL28	-9.68	18	-1.56	0.059	689	1.41
DKK1	-9.68	18	-1.56	0.0591	690	1.41
CHRD	-9.68	18	-1.56	0.0591	691	1.4
ARHGAP11A	-6.85	9	-1.56	0.0591	692	1.4
KIAA0319L	-9.68	18	-1.56	0.0591	693	1.4
ZNF594	-5.59	6	-1.56	0.0591	694	1.4
SLC24A3	-9.66	18	-1.56	0.0594	695	1.4
ELOF1	-9.66	18	-1.56	0.0596	696	1.41
STK32C	-9.65	18	-1.56	0.0598	697	1.41
MNDA	-7.87	12	-1.55	0.06	698	1.41
OCLN	-8.8	15	-1.55	0.06	699	1.41
TGS1	-9.63	18	-1.55	0.0602	700	1.41
TIAL1	-9.63	18	-1.55	0.0602	701	1.41
PIANP	-8.79	15	-1.55	0.0603	702	1.41
EDAR	-9.62	18	-1.55	0.0604	703	1.41
TK1	-9.62	18	-1.55	0.0604	704	1.41
MPPED2	-9.61	18	-1.55	0.0606	705	1.41
JAK1	-9.61	18	-1.55	0.0607	706	1.41
TONSL	-9.33	17	-1.55	0.0608	707	1.41
SAFB2	-9.59	18	-1.55	0.061	708	1.42
CRKL	-9.59	18	-1.55	0.0611	709	1.42
TMC2	-9.59	18	-1.54	0.0612	710	1.42
ADAT3	-7.83	12	-1.54	0.0612	711	1.41
SLC17A7	-9.59	18	-1.54	0.0612	712	1.41
TEAD3	-9.58	18	-1.54	0.0613	713	1.41

MSMB	-5.53	6	-1.54	0.0613	714	1.41
ATXN7L3	-9.57	18	-1.54	0.0617	715	1.42
ZNF232	-8.73	15	-1.54	0.0617	716	1.42
KIAA1432	-9.56	18	-1.54	0.0618	717	1.42
ACVRL1	-9.56	18	-1.54	0.0618	718	1.41
ISL1	-9.56	18	-1.54	0.0618	719	1.41
CYP4F11	-9.56	18	-1.54	0.0619	720	1.41
LAMB3	-9.56	18	-1.54	0.0619	721	1.41
TCF25	-9.55	18	-1.54	0.062	722	1.41
XRN2	-9.55	18	-1.54	0.0621	723	1.41
BTBD2	-9.55	18	-1.54	0.0621	724	1.41
RRAS	-9.54	18	-1.54	0.0623	725	1.41
TSPAN17	-9.54	18	-1.54	0.0623	726	1.41
PTPRS	-9.54	18	-1.54	0.0623	727	1.41
AIP	-9.53	18	-1.53	0.0625	728	1.41
PRR24	-5.5	6	-1.53	0.0626	729	1.41
C16orf62	-9.53	18	-1.53	0.0626	730	1.41
SLCO1A2	-7.78	12	-1.53	0.0627	731	1.41
C15orf43	-7.77	12	-1.53	0.0627	732	1.41
SPAG17	-9.52	18	-1.53	0.0627	733	1.41
VASH2	-9.51	18	-1.53	0.063	734	1.41
VSIG2	-9.51	18	-1.53	0.063	735	1.41
GJC3	-8.68	15	-1.53	0.0631	736	1.41
MCM2	-9.5	18	-1.53	0.0632	737	1.41
IL5RA	-5.48	6	-1.53	0.0632	738	1.41
KCTD20	-9.5	18	-1.53	0.0633	739	1.41
BTK	-9.5	18	-1.53	0.0633	740	1.41
CCDC154	-9.49	18	-1.53	0.0635	741	1.41
AFAP1	-9.49	18	-1.53	0.0636	742	1.41
RBM12	-8.65	15	-1.52	0.0637	743	1.41
ZNF74	-9.48	18	-1.52	0.0638	744	1.41
YTHDF1	-9.48	18	-1.52	0.0638	745	1.41
FKBP15	-9.47	18	-1.52	0.0638	746	1.41
TRAIP	-9.47	18	-1.52	0.0639	747	1.41
MYL7	-8.65	15	-1.52	0.0639	748	1.4
SNW1	-8.65	15	-1.52	0.0639	749	1.4
NMD3	-5.47	6	-1.52	0.064	750	1.4
GMPPB	-9.47	18	-1.52	0.064	751	1.4
CDCA2	-9.47	18	-1.52	0.064	752	1.4
SPARC	-9.47	18	-1.52	0.0641	753	1.4
CDK6	-9.47	18	-1.52	0.0641	754	1.4
PAX5	-9.46	18	-1.52	0.0641	755	1.4
ABCD4	-9.46	18	-1.52	0.0642	756	1.4
TEX29	-9.46	18	-1.52	0.0643	757	1.4
METTL21C	-9.46	18	-1.52	0.0643	758	1.39
GNRH1	-7.72	12	-1.52	0.0643	759	1.39
NDUFAF7	-9.45	18	-1.52	0.0644	760	1.39
CHORDC1	-8.63	15	-1.52	0.0644	761	1.39

OR4C15	-5.45	6	-1.52	0.0645	762	1.39
TMEM63B	-9.44	18	-1.52	0.0647	763	1.39
CCDC136	-9.44	18	-1.52	0.0647	764	1.39
PGPEP1	-9.44	18	-1.52	0.0648	765	1.39
LTB	-8.61	15	-1.52	0.0648	766	1.39
ACSM2B	-6.67	9	-1.52	0.0648	767	1.39
PGR	-9.43	18	-1.52	0.0649	768	1.39
MARS	-9.43	18	-1.51	0.065	769	1.39
TMEM17	-7.69	12	-1.51	0.0652	770	1.39
GUSB	-9.41	18	-1.51	0.0655	771	1.4
MTHFD1	-9.4	18	-1.51	0.0656	772	1.4
VPREB3	-8.58	15	-1.51	0.0656	773	1.39
ZNF251	-9.4	18	-1.51	0.0656	774	1.39
EBLN2	-5.43	6	-1.51	0.0656	775	1.39
SCN3B	-9.4	18	-1.51	0.0656	776	1.39
UBOX5	-9.4	18	-1.51	0.0657	777	1.39
ZRSR2	-6.64	9	-1.51	0.0658	778	1.39
CTIF	-9.39	18	-1.51	0.0658	779	1.39
DUS1L	-9.39	18	-1.51	0.0659	780	1.39
METTL7B	-9.39	18	-1.51	0.066	781	1.39
CPEB4	-9.39	18	-1.51	0.066	782	1.39
ACTA2	-9.38	18	-1.51	0.066	783	1.39
EVI5	-9.38	18	-1.51	0.066	784	1.38
VIMP	-9.38	18	-1.51	0.066	785	1.38
KARS	-9.38	18	-1.5	0.0662	786	1.38
RPP30	-8.56	15	-1.5	0.0662	787	1.38
SNX18	-9.37	18	-1.5	0.0662	788	1.38
PGAM2	-9.37	18	-1.5	0.0663	789	1.38
AP4E1	-9.37	18	-1.5	0.0665	790	1.38
H2AFJ	-8.55	15	-1.5	0.0665	791	1.38
ABCB4	-9.36	18	-1.5	0.0667	792	1.38
SDE2	-9.34	18	-1.5	0.067	793	1.39
HOXD11	-9.34	18	-1.5	0.0671	794	1.39
C1orf56	-7.62	12	-1.5	0.0672	795	1.39
ZBTB24	-9.33	18	-1.5	0.0674	796	1.39
CITED1	-8.52	15	-1.5	0.0674	797	1.39

Namalwa_Resistance						
GENE	**sumZ**	**numObs**	**normZ**	**pval_supp**	**rank_supp**	**fdr_supp**
TYMS	19.69	18	4.03	0.000028	1	0.46
KDELR2	16.18	18	3.36	0.000388	2	3.18
HTRA2	15.97	18	3.32	0.000447	3	2.45
PRDM8	15.71	18	3.27	0.000536	4	2.2
ING3	14.95	18	3.13	0.00088	5	2.89
SHMT2	14.92	18	3.12	0.000901	6	2.47
SPINK4	13.05	15	3	0.00134	7	3.14
AGPAT6	14.19	18	2.98	0.00143	8	2.93
IMPDH2	13.98	18	2.94	0.00163	9	2.97

HSPA14	13.59	18	2.87	0.00206	10	3.39
PDCL	13.52	18	2.85	0.00216	11	3.22
CEP120	13.42	18	2.84	0.00229	12	3.13
INPP5K	13.32	18	2.82	0.00242	13	3.06
ID3	12.12	15	2.81	0.00249	15	2.73
CHAF1B	9.41	9	2.81	0.00245	14	2.87
PDE12	10.8	12	2.8	0.00257	16	2.63
SUV39H1	13.18	18	2.79	0.00264	17	2.55
CELF1	12.97	18	2.75	0.00297	18	2.71
TMCO1	12.89	18	2.73	0.00312	19	2.7
SDF2	11.7	15	2.72	0.00325	20	2.67
RIC8A	12.56	18	2.67	0.00376	21	2.94
PATL1	12.42	18	2.65	0.00408	22	3.04
CC2D1A	12.26	18	2.62	0.00446	24	3.05
PIGW	11.2	15	2.62	0.00445	23	3.18
WDR17	12.22	18	2.61	0.00457	25	3
CCDC47	12.06	18	2.58	0.005	28	2.93
SLC6A11	12.07	18	2.58	0.00497	27	3.02
SKIV2L	12.08	18	2.58	0.00493	26	3.12
ACAT2	11.92	18	2.55	0.00538	30	2.95
PIGN	11.94	18	2.55	0.00531	29	3.01
INVS	11.88	18	2.54	0.0055	31	2.92
SCG3	10.72	15	2.52	0.00593	34	2.86
AMPD2	11.76	18	2.52	0.00589	33	2.93
ISCA1	9.61	12	2.52	0.00584	32	3
GTF3C2	11.62	18	2.49	0.00634	35	2.97
C12orf65	8.17	9	2.48	0.00658	38	2.84
PTRH2	8.17	9	2.48	0.00657	37	2.92
ING1	11.57	18	2.48	0.00649	36	2.96
C3orf18	10.4	15	2.45	0.00713	39	3
CENPJ	11.27	18	2.43	0.00763	41	3.06
BIRC6	11.3	18	2.43	0.00752	40	3.09
AIG1	11.25	18	2.42	0.00769	43	2.94
MSX2	7.96	9	2.42	0.00766	42	3
ALDH18A1	11.17	18	2.41	0.00806	46	2.88
ADPGK	11.18	18	2.41	0.008	45	2.92
ACTRT2	10.22	15	2.41	0.00794	44	2.96
FAM3A	11.12	18	2.4	0.00826	47	2.89
ZNF248	7.82	9	2.39	0.00848	49	2.84
ADAM17	11.08	18	2.39	0.00842	48	2.88
LARP1	11.04	18	2.38	0.00858	50	2.82
UBA6	8.95	12	2.37	0.00896	55	2.68
SERPINA6	10.98	18	2.37	0.00887	54	2.7
PIBF1	10.98	18	2.37	0.00886	53	2.75
PIGS	10.99	18	2.37	0.00882	52	2.79
VIP	6.35	6	2.37	0.00882	51	2.84
MYOM3	10.81	18	2.34	0.00967	57	2.79
PIGT	10.83	18	2.34	0.00959	56	2.81

SLC25A39	10.76	18	2.33	0.00991	58	2.81
HK2	8.75	12	2.32	0.0101	60	2.78
ZDHHC15	10.73	18	2.32	0.0101	59	2.81
MTFMT	10.67	18	2.31	0.0104	62	2.75
DUSP19	8.72	12	2.31	0.0103	61	2.78
KIF21B	10.53	18	2.29	0.0111	64	2.86
KBTBD11	10.54	18	2.29	0.0111	63	2.89
C15orf40	6.06	6	2.28	0.0114	65	2.88
TMEM2	10.43	18	2.27	0.0117	68	2.83
LYRM9	8.54	12	2.27	0.0115	67	2.82
ABP1	10.47	18	2.27	0.0115	66	2.86
COL4A6	10.38	18	2.26	0.012	72	2.74
TBL3	10.38	18	2.26	0.012	71	2.77
DAB1	10.39	18	2.26	0.0119	70	2.8
ALG3	10.42	18	2.26	0.0118	69	2.81
GLI1	10.33	18	2.25	0.0123	76	2.66
FUT2	7.31	9	2.25	0.0123	75	2.69
PRELP	10.34	18	2.25	0.0123	74	2.72
MOCS1	10.37	18	2.25	0.0121	73	2.72
PFKM	10.3	18	2.24	0.0125	77	2.66
SUCLA2	7.26	9	2.23	0.0127	78	2.68
PYGO1	10.18	18	2.22	0.0133	80	2.73
PKN2	10.2	18	2.22	0.0131	79	2.73
RNF4	7.15	9	2.21	0.0137	84	2.68
SPATC1L	10.11	18	2.21	0.0137	83	2.71
MAP6D1	10.12	18	2.21	0.0136	82	2.73
PELI2	10.16	18	2.21	0.0134	81	2.71
PRKAA2	10.06	18	2.2	0.014	88	2.62
LILRB4	10.07	18	2.2	0.014	87	2.65
SLC25A32	8.22	12	2.2	0.014	86	2.67
RANBP17	10.09	18	2.2	0.0138	85	2.67
TAF1C	10.01	18	2.19	0.0144	90	2.63
PRMT10	10.04	18	2.19	0.0142	89	2.62
MBTPS2	9.96	18	2.18	0.0147	92	2.63
TTC37	9.98	18	2.18	0.0146	91	2.64
TCEA2	9.9	18	2.17	0.0152	94	2.65
WEE2	9.93	18	2.17	0.015	93	2.64
PGLYRP3	9.86	18	2.16	0.0155	96	2.65
APOOL	5.69	6	2.16	0.0155	95	2.67
IGHMBP2	9.8	18	2.15	0.0159	100	2.62
PDCD7	9.8	18	2.15	0.0159	99	2.64
HHIP	9.81	18	2.15	0.0158	98	2.66
DCTD	9.82	18	2.15	0.0158	97	2.68
CENPO	9.75	18	2.14	0.0163	104	2.58
TMEM185A	6.89	9	2.14	0.0163	103	2.6
RNF186	8.9	15	2.14	0.0163	102	2.63
BAZ2B	9.79	18	2.14	0.016	101	2.61
PCNXL3	9.69	18	2.13	0.0168	109	2.53

AGRP	9.7	18	2.13	0.0167	108	2.54
ARHGAP26	9.72	18	2.13	0.0165	107	2.54
STAU1	9.72	18	2.13	0.0165	106	2.56
ACSL3	9.73	18	2.13	0.0165	105	2.58
ELOVL5	9.67	18	2.12	0.017	112	2.49
SYT2	9.67	18	2.12	0.0169	111	2.51
P2RY6	8.83	15	2.12	0.0169	110	2.53
CKB	9.59	18	2.11	0.0176	116	2.49
TRIAP1	6.79	9	2.11	0.0175	115	2.49
HGF	9.61	18	2.11	0.0174	114	2.51
NRD1	9.63	18	2.11	0.0172	113	2.5
TLE3	9.55	18	2.1	0.0179	118	2.5
LGR5	9.56	18	2.1	0.0178	117	2.51
COL4A5	9.51	18	2.09	0.0183	122	2.46
KRT36	9.52	18	2.09	0.0182	121	2.47
PLA2G3	9.52	18	2.09	0.0181	120	2.48
PIGB	9.53	18	2.09	0.0181	119	2.5
MEFV	9.43	18	2.08	0.0189	126	2.47
FZD5	9.44	18	2.08	0.0189	125	2.48
ZNF608	9.45	18	2.08	0.0188	124	2.49
LY6G6D	7.73	12	2.08	0.0186	123	2.49
ORMDL3	9.39	18	2.07	0.0193	129	2.46
ETFDH	9.41	18	2.07	0.0192	128	2.46
AAAS	9.41	18	2.07	0.0191	127	2.47
GML	7.64	12	2.06	0.0196	130	2.47
METAP1D	9.27	18	2.05	0.0204	134	2.5
STRIP1	9.27	18	2.05	0.0204	133	2.52
CACNA1B	9.28	18	2.05	0.0203	132	2.52
HSD17B12	7.58	12	2.05	0.0203	131	2.54
C8orf4	5.32	6	2.04	0.0209	140	2.45
RNF222	8.42	15	2.04	0.0208	139	2.46
ATXN10	9.24	18	2.04	0.0207	138	2.47
ILDR1	9.24	18	2.04	0.0207	137	2.48
RER1	9.25	18	2.04	0.0206	136	2.49
GXYLT2	9.25	18	2.04	0.0205	135	2.5
CCDC107	9.2	18	2.03	0.021	141	2.45
RNLS	9.11	18	2.02	0.0219	148	2.44
KLHL15	8.33	15	2.02	0.0218	147	2.43
HPDL	9.14	18	2.02	0.0217	146	2.44
CCDC149	9.14	18	2.02	0.0216	145	2.45
YWHAB	5.29	6	2.02	0.0215	144	2.45
TCHP	9.16	18	2.02	0.0215	143	2.47
NCR3LG1	9.16	18	2.02	0.0214	142	2.48
SNAI2	9.09	18	2.01	0.0222	154	2.36
CRADD	9.09	18	2.01	0.0221	153	2.38
TSC22D2	8.3	15	2.01	0.0221	152	2.39
TAZ	9.1	18	2.01	0.022	151	2.39
GIMAP5	7.44	12	2.01	0.022	150	2.41

MYO1A	9.11	18	2.01	0.022	149	2.42
DENND4A	9.01	18	2	0.0229	160	2.36
AGXT2	9.01	18	2	0.0229	159	2.37
FAM160A2	9.02	18	2	0.0229	158	2.38
FRY	9.02	18	2	0.0229	157	2.39
PNCK	9.04	18	2	0.0227	156	2.39
GPD1L	9.05	18	2	0.0225	155	2.39
EPHA10	8.96	18	1.99	0.0235	165	2.34
MX2	8.96	18	1.99	0.0235	164	2.35
SOX3	8.97	18	1.99	0.0233	163	2.35
OR14A16	5.19	6	1.99	0.0232	162	2.36
MACROD2	9	18	1.99	0.0231	161	2.35
RGR	8.91	18	1.98	0.024	172	2.3
LRRC8A	8.92	18	1.98	0.024	171	2.3
PRSS16	8.92	18	1.98	0.024	170	2.32
COPS7B	8.92	18	1.98	0.024	169	2.33
EPS15	8.94	18	1.98	0.0237	168	2.32
HSF5	8.95	18	1.98	0.0236	167	2.32
TRAF4	8.95	18	1.98	0.0236	166	2.34
COPS5	8.85	18	1.97	0.0246	176	2.3
GANAB	8.87	18	1.97	0.0245	175	2.3
MSR1	8.88	18	1.97	0.0243	174	2.3
IL19	8.89	18	1.97	0.0242	173	2.3
OTOP3	8.81	18	1.96	0.0251	181	2.28
C2orf74	6.23	9	1.96	0.025	180	2.29
MARK2	8.82	18	1.96	0.025	179	2.29
ANKRD26	8.83	18	1.96	0.0249	178	2.29
C17orf105	7.21	12	1.96	0.0248	177	2.31
JAGN1	8.75	18	1.95	0.0258	185	2.29
TIGD3	8.76	18	1.95	0.0257	184	2.29
CHCHD10	6.2	9	1.95	0.0256	183	2.3
LAX1	8.79	18	1.95	0.0253	182	2.29
F12	8.72	18	1.94	0.0261	190	2.26
SLC7A1	8.73	18	1.94	0.026	189	2.26
PLEKHF1	8.73	18	1.94	0.026	188	2.27
ZEB2	8.74	18	1.94	0.0259	187	2.28
PKNOX2	8.74	18	1.94	0.0259	186	2.29
KCNE3	7.89	15	1.93	0.0271	198	2.25
COPG1	8.64	18	1.93	0.027	197	2.25
SGSM3	8.64	18	1.93	0.027	196	2.27
SUSD3	8.65	18	1.93	0.027	195	2.28
PDCD10	7.06	12	1.93	0.027	194	2.28
FAM122B	8.67	18	1.93	0.0267	193	2.27
SYNE4	8.67	18	1.93	0.0267	192	2.28
FAM78A	8.69	18	1.93	0.0265	191	2.28
TTC34	8.61	18	1.92	0.0275	201	2.25
COPZ1	8.63	18	1.92	0.0272	200	2.24
C11orf96	8.63	18	1.92	0.0272	199	2.25

LRRC8B	6.03	9	1.91	0.0284	208	2.24
GPR179	8.53	18	1.91	0.0284	207	2.25
LRRC70	6.05	9	1.91	0.028	206	2.24
AQP5	8.56	18	1.91	0.028	205	2.25
DPM2	7	12	1.91	0.0279	204	2.25
PLD5	8.57	18	1.91	0.0279	203	2.26
RNF220	8.58	18	1.91	0.0279	202	2.27
PTDSS2	8.48	18	1.9	0.029	213	2.24
ARHGAP9	8.48	18	1.9	0.029	212	2.25
CENPM	7.76	15	1.9	0.0288	211	2.25
HCFC1	8.51	18	1.9	0.0286	210	2.24
POLR3D	8.52	18	1.9	0.0285	209	2.24
SUCLG1	8.44	18	1.89	0.0295	219	2.22
ATP11B	8.45	18	1.89	0.0295	218	2.22
HLA-DMA	8.45	18	1.89	0.0294	217	2.22
MFAP4	8.46	18	1.89	0.0293	216	2.23
OR8I2	6.9	12	1.89	0.0293	215	2.24
PRKAA1	6.91	12	1.89	0.0293	214	2.25
LETM1	8.38	18	1.88	0.0304	225	2.22
FANK1	8.39	18	1.88	0.0302	224	2.22
GTF2E2	6.85	12	1.88	0.0302	223	2.23
CCDC134	8.4	18	1.88	0.03	222	2.22
EXT1	8.41	18	1.88	0.0299	221	2.22
FOXN3	8.41	18	1.88	0.0299	220	2.23
ALPK3	8.33	18	1.87	0.031	229	2.22
PTER	8.34	18	1.87	0.0309	228	2.22
RASSF7	8.35	18	1.87	0.0308	227	2.23
CDH10	8.35	18	1.87	0.0307	226	2.23
RCE1	8.28	18	1.86	0.0317	233	2.23
TMEM167B	4.79	6	1.86	0.0313	232	2.22
LYPLAL1	5.88	9	1.86	0.0312	231	2.22
KCNC1	8.32	18	1.86	0.0311	230	2.22
PAWR	6.71	12	1.85	0.0325	239	2.23
PGM3	8.22	18	1.85	0.0325	238	2.24
MAGEH1	5.82	9	1.85	0.0324	237	2.25
CST11	6.72	12	1.85	0.0323	236	2.25
USP49	8.24	18	1.85	0.0323	235	2.26
IGIP	4.77	6	1.85	0.0319	234	2.24
ARID3A	8.17	18	1.84	0.0332	243	2.25
NICN1	8.18	18	1.84	0.033	242	2.24
KIAA0586	8.19	18	1.84	0.0329	241	2.25
C6orf132	8.21	18	1.84	0.0326	240	2.23
TNFRSF1B	8.12	18	1.83	0.0339	248	2.25
C19orf69	6.64	12	1.83	0.0338	247	2.25
ME3	8.14	18	1.83	0.0337	246	2.25
SLCO6A1	8.15	18	1.83	0.0335	245	2.25
PLA2G4F	8.15	18	1.83	0.0334	244	2.25
ICAM3	8.06	18	1.82	0.0347	257	2.22

PDZRN3	8.06	18	1.82	0.0347	256	2.23
SMG1	8.06	18	1.82	0.0347	255	2.24
MPP3	8.07	18	1.82	0.0346	254	2.24
AES	8.1	18	1.82	0.0342	253	2.22
PCDH15	8.1	18	1.82	0.0341	252	2.23
DDX47	7.4	15	1.82	0.0341	251	2.23
OR10X1	4.68	6	1.82	0.0341	250	2.24
KRT85	8.11	18	1.82	0.0341	249	2.25
TMEM178A	8.01	18	1.81	0.0355	265	2.2
TRIB3	8.01	18	1.81	0.0354	264	2.2
NCR1	8.02	18	1.81	0.0354	263	2.21
KDM5C	8.02	18	1.81	0.0353	262	2.22
SLC25A29	8.02	18	1.81	0.0353	261	2.22
FCHSD2	7.32	15	1.81	0.0353	260	2.23
C10orf137	8.05	18	1.81	0.0349	259	2.22
HIST1H2AK	4.65	6	1.81	0.0349	258	2.22
HKR1	7.27	15	1.8	0.0362	269	2.21
EXOG	7.28	15	1.8	0.036	268	2.21
MAGEA4	4.61	6	1.8	0.036	267	2.21
FAM3B	7.99	18	1.8	0.0358	266	2.21
SLC39A1	7.9	18	1.79	0.0371	279	2.18
RPS27	4.57	6	1.79	0.0369	278	2.18
SKIDA1	7.23	15	1.79	0.0368	277	2.19
ATP6V1G1	5.6	9	1.79	0.0368	276	2.19
GSTM4	4.58	6	1.79	0.0368	275	2.2
PASD1	7.93	18	1.79	0.0368	274	2.2
NFXL1	7.93	18	1.79	0.0367	273	2.21
DUSP1	7.94	18	1.79	0.0365	272	2.2
PHTF2	7.95	18	1.79	0.0364	271	2.21
SRRD	7.26	15	1.79	0.0364	270	2.21
CSK	7.63	17	1.78	0.0379	288	2.16
SLC39A11	7.86	18	1.78	0.0378	287	2.17
FAH	7.87	18	1.78	0.0376	286	2.16
GPI	7.87	18	1.78	0.0376	285	2.17
LGR4	7.89	18	1.78	0.0373	284	2.16
UQCR11	6.44	12	1.78	0.0373	283	2.17
TNFAIP1	7.89	18	1.78	0.0373	282	2.17
NPW	6.45	12	1.78	0.0372	281	2.18
CDC34	7.9	18	1.78	0.0372	280	2.18
DUS3L	7.8	18	1.77	0.0387	292	2.18
MARCH2	7.8	18	1.77	0.0386	291	2.18
THG1L	7.82	18	1.77	0.0384	290	2.18
ALOX15	7.84	18	1.77	0.0381	289	2.17
LY86	4.47	6	1.76	0.0396	298	2.18
GDPD5	7.75	18	1.76	0.0395	297	2.18
CCDC177	7.1	15	1.76	0.039	296	2.17
APOA5	7.79	18	1.76	0.039	295	2.17
EXOSC8	7.79	18	1.76	0.0389	294	2.18

FNIP2	7.79	18	1.76	0.0388	293	2.18
SST	6.29	12	1.75	0.0404	304	2.18
PVR	7.71	18	1.75	0.0403	303	2.18
ELF1	7.71	18	1.75	0.0401	302	2.18
ARAP1	7.73	18	1.75	0.0398	301	2.17
SFTPC	7.74	18	1.75	0.0398	300	2.18
ZP1	7.74	18	1.75	0.0397	299	2.18
VNN2	6.24	12	1.74	0.0412	307	2.21
F2RL3	7.65	18	1.74	0.0412	306	2.21
PTOV1	7.67	18	1.74	0.0409	305	2.2
APOC3	6.2	12	1.73	0.0422	316	2.19
SCUBE1	7.59	18	1.73	0.0421	315	2.2
RCBTB2	7.6	18	1.73	0.0421	314	2.2
TNFRSF10B	7.6	18	1.73	0.042	313	2.2
C8orf47	6.94	15	1.73	0.0419	312	2.21
NFATC1	7.61	18	1.73	0.0418	311	2.21
NDEL1	6.95	15	1.73	0.0417	310	2.21
YIPF6	6.96	15	1.73	0.0417	309	2.22
ANKRD37	6.96	15	1.73	0.0416	308	2.22
TM6SF2	7.53	18	1.72	0.0432	329	2.16
ENPP7	7.54	18	1.72	0.0432	328	2.16
PXDC1	7.54	18	1.72	0.0431	327	2.16
LGI4	7.54	18	1.72	0.043	326	2.17
ATP2B4	7.55	18	1.72	0.0429	325	2.17
GP2	7.55	18	1.72	0.0428	324	2.17
DCAF10	7.56	18	1.72	0.0428	323	2.18
MTCH2	6.9	15	1.72	0.0427	322	2.18
RBM10	7.56	18	1.72	0.0427	321	2.19
APH1B	7.56	18	1.72	0.0426	320	2.19
PPP2R2D	6.18	12	1.72	0.0426	319	2.19
ADAMTS5	7.57	18	1.72	0.0425	318	2.2
HMGXB3	7.59	18	1.72	0.0423	317	2.19
PRTN3	7.49	18	1.71	0.044	334	2.17
ACSM5	6.84	15	1.71	0.0439	333	2.17
CCDC85A	7.5	18	1.71	0.0438	332	2.17
MAPKBP1	7.52	18	1.71	0.0434	331	2.15
TMF1	7.53	18	1.71	0.0432	330	2.15
RASL10A	7.43	18	1.7	0.045	341	2.17
MAGIX	7.44	18	1.7	0.0449	340	2.17
JKAMP	5.26	9	1.7	0.0449	339	2.17
IGF2BP1	7.45	18	1.7	0.0447	338	2.17
ISL2	7.45	18	1.7	0.0447	337	2.18
SYN3	7.47	18	1.7	0.0443	336	2.17
PDE7B	7.48	18	1.7	0.0441	335	2.16
HTR4	7.38	18	1.69	0.0459	351	2.15
TAT	7.38	18	1.69	0.0459	350	2.16
C2CD3	7.38	18	1.69	0.0459	349	2.16
PAEP	7.38	18	1.69	0.0459	348	2.17

ATG14	7.38	18	1.69	0.0459	347	2.17
C4orf48	7.39	18	1.69	0.0457	346	2.17
PARD6A	7.4	18	1.69	0.0456	345	2.17
EEF2K	7.41	18	1.69	0.0454	344	2.17
PLSCR3	7.41	18	1.69	0.0453	343	2.17
PITRM1	7.42	18	1.69	0.0452	342	2.17
PCOLCE2	7.33	18	1.68	0.0469	357	2.16
COL11A2	7.33	18	1.68	0.0469	356	2.16
IRF2BPL	7.34	18	1.68	0.0467	355	2.16
TFEC	7.34	18	1.68	0.0467	354	2.17
RTN4RL2	7.35	18	1.68	0.0464	353	2.16
NLRP2	7.37	18	1.68	0.0461	352	2.15
C6orf62	6.64	15	1.67	0.0479	362	2.18
PXDNL	7.3	18	1.67	0.0475	361	2.16
PNLIPRP2	7.31	18	1.67	0.0472	360	2.15
PROM1	7.31	18	1.67	0.0472	359	2.16
PAPD4	5.18	9	1.67	0.047	358	2.16
TAB1	7.22	18	1.66	0.0489	382	2.1
SLC16A10	7.22	18	1.66	0.0488	381	2.11
NOB1	5.11	9	1.66	0.0488	380	2.11
PTRHD1	5.9	12	1.66	0.0488	379	2.12
TERF2IP	7.23	18	1.66	0.0488	378	2.12
PPM1M	7.23	18	1.66	0.0488	377	2.12
ATP6V1C2	7.24	18	1.66	0.0486	376	2.13
CAP1	5.91	12	1.66	0.0486	375	2.13
MBTPS1	7.24	18	1.66	0.0486	374	2.14
ERN1	7.24	18	1.66	0.0486	373	2.14
C4orf3	7.24	18	1.66	0.0485	372	2.14
EPB41L1	7.24	18	1.66	0.0485	371	2.15
NIN	7.25	18	1.66	0.0484	370	2.15
MYH10	7.25	18	1.66	0.0483	369	2.15
ANXA3	5.93	12	1.66	0.0482	368	2.15
ZNF667	6.63	15	1.66	0.0482	367	2.16
AKR1C3	4.19	6	1.66	0.0482	366	2.16
CH25H	6.63	15	1.66	0.0481	365	2.17
SIPA1L3	7.27	18	1.66	0.048	364	2.17
TGM5	7.27	18	1.66	0.048	363	2.17
EFCC1	7.17	18	1.65	0.0499	396	2.07
LDOC1	5.07	9	1.65	0.0499	395	2.08
GINS4	6.97	17	1.65	0.0499	394	2.08
INO80B	6.98	17	1.65	0.0498	393	2.08
CACNG7	7.19	18	1.65	0.0495	392	2.08
RFFL	7.19	18	1.65	0.0495	391	2.08
CLDN17	7.2	18	1.65	0.0494	390	2.08
DNAJC16	7.2	18	1.65	0.0494	389	2.09
C12orf42	7.2	18	1.65	0.0493	388	2.09
KAL1	7.2	18	1.65	0.0493	387	2.09
PSMB10	7.2	18	1.65	0.0493	386	2.1

NDUFA3	5.88	12	1.65	0.0493	385	2.1
NDUFS4	7.2	18	1.65	0.0493	384	2.11
LAMB1	7.2	18	1.65	0.0492	383	2.11
CORIN	7.12	18	1.64	0.0509	408	2.05
MAP9	6.5	15	1.64	0.0509	407	2.05
CMTM6	5.04	9	1.64	0.0507	406	2.05
PKD1	7.14	18	1.64	0.0506	405	2.05
MYO15A	7.14	18	1.64	0.0505	404	2.06
ZNF292	7.14	18	1.64	0.0505	403	2.06
HSD11B1	7.15	18	1.64	0.0504	402	2.06
LDLRAD1	7.15	18	1.64	0.0503	401	2.06
DNASE1L2	7.15	18	1.64	0.0502	400	2.06
ESM1	6.53	15	1.64	0.0502	399	2.07
PHF6	5.06	9	1.64	0.0501	398	2.07
HAUS3	5.07	9	1.64	0.05	397	2.07
IPO9	7.06	18	1.63	0.052	417	2.05
NRN1	7.08	18	1.63	0.0518	416	2.05
ELF3	7.08	18	1.63	0.0518	415	2.05
C11orf93	5	9	1.63	0.0518	414	2.05
MYRIP	7.09	18	1.63	0.0515	413	2.05
SCRG1	5.01	9	1.63	0.0515	412	2.05
SEC14L1	7.09	18	1.63	0.0515	411	2.06
C11orf72	5.02	9	1.63	0.0513	410	2.06
FRYL	7.11	18	1.63	0.051	409	2.05
PTPN23	6.81	17	1.62	0.0531	430	2.03
CCDC9	7.01	18	1.62	0.053	429	2.03
GYPC	6.4	15	1.62	0.053	428	2.03
MFRP	7.03	18	1.62	0.0528	427	2.03
PRR5	7.03	18	1.62	0.0528	426	2.03
MAATS1	7.04	18	1.62	0.0526	425	2.03
CCDC116	7.04	18	1.62	0.0525	424	2.04
TLX1NB	4.98	9	1.62	0.0525	423	2.04
SCLT1	4.07	6	1.62	0.0524	422	2.04
UBAC1	7.04	18	1.62	0.0524	421	2.05
WISP1	7.06	18	1.62	0.0522	420	2.04
EFR3B	7.06	18	1.62	0.0522	419	2.05
SKIL	7.06	18	1.62	0.0521	418	2.05
C16orf74	6.96	18	1.61	0.0542	440	2.02
STEAP2	6.97	18	1.61	0.054	439	2.02
UBE2K	5.69	12	1.61	0.0539	438	2.02
CNTLN	6.98	18	1.61	0.0537	437	2.02
ZNF311	6.99	18	1.61	0.0536	436	2.02
FBXO46	6.99	18	1.61	0.0536	435	2.02
PRKAB1	7	18	1.61	0.0534	434	2.02
OR9G4	5.72	12	1.61	0.0533	433	2.02
S1PR2	5.72	12	1.61	0.0532	432	2.02
FBXO8	4.96	9	1.61	0.0532	431	2.03
GPAM	6.91	18	1.6	0.0553	456	1.99

MPDU1	6.91	18	1.6	0.0552	455	1.99
TMEM243	5.64	12	1.6	0.0552	454	2
ACTR6	6.31	15	1.6	0.0551	453	2
ZNRF3	6.92	18	1.6	0.055	452	2
VWA5B2	6.93	18	1.6	0.0549	451	2
OR1J4	4.9	9	1.6	0.0548	450	2
OR8S1	6.93	18	1.6	0.0548	449	2.01
TM4SF5	6.93	18	1.6	0.0547	448	2.01
UFM1	4	6	1.6	0.0547	447	2.01
GFAP	6.93	18	1.6	0.0547	446	2.02
STXBP5	6.94	18	1.6	0.0547	445	2.02
LRRC26	6.94	18	1.6	0.0545	444	2.02
CHERP	6.94	18	1.6	0.0545	443	2.02
ACSM3	6.95	18	1.6	0.0545	442	2.02
C12orf55	6.95	18	1.6	0.0544	441	2.03
C3orf67	6.85	18	1.59	0.0564	466	1.99
FUCA1	6.85	18	1.59	0.0564	465	1.99
FAM71F2	6.86	18	1.59	0.0563	464	2
GIMAP2	5.61	12	1.59	0.0561	463	1.99
SLC30A2	6.87	18	1.59	0.056	462	1.99
TRMT2A	6.88	18	1.59	0.0558	461	1.99
SPC24	6.88	18	1.59	0.0558	460	1.99
C14orf80	6.89	18	1.59	0.0556	459	1.99
KATNAL1	6.89	18	1.59	0.0556	458	2
LHFP	6.3	15	1.59	0.0554	457	1.99
CADM1	6.8	18	1.58	0.0576	476	1.99
ATP7A	6.8	18	1.58	0.0576	475	1.99
CLPS	5.57	12	1.58	0.0571	474	1.98
GPR135	6.23	15	1.58	0.057	473	1.98
SLC25A41	6.83	18	1.58	0.057	472	1.98
DNAJC13	6.84	18	1.58	0.0568	471	1.98
TTC6	6.85	18	1.58	0.0566	470	1.98
INCA1	6.85	18	1.58	0.0565	469	1.98
ASNA1	6.85	18	1.58	0.0565	468	1.98
UTF1	6.85	18	1.58	0.0565	467	1.99
PLA1A	6.75	18	1.57	0.0587	485	1.99
SLC7A5	6.75	18	1.57	0.0586	484	1.99
PDE1B	6.76	18	1.57	0.0586	483	1.99
OR2G6	4.78	9	1.57	0.0585	482	1.99
GPRC5A	6.17	15	1.57	0.0584	481	1.99
DLL1	6.77	18	1.57	0.0582	480	1.99
PITX1	6.78	18	1.57	0.0579	479	1.99
ALG5	6.79	18	1.57	0.0578	478	1.99
CAMK2G	6.79	18	1.57	0.0578	477	1.99
FAM132B	6.69	18	1.56	0.06	507	1.94
ZBTB8OS	3.87	6	1.56	0.06	506	1.95
CRYAB	6.69	18	1.56	0.0599	505	1.95
CLEC4D	4.74	9	1.56	0.0599	504	1.95

ZNF549	6.12	15	1.56	0.0598	503	1.95
MANF	4.74	9	1.56	0.0597	502	1.96
RGMA	6.71	18	1.56	0.0597	501	1.96
MAFB	6.71	18	1.56	0.0596	500	1.96
SEC61B	3.87	6	1.56	0.0596	499	1.96
KIRREL3	6.71	18	1.56	0.0596	498	1.97
GRM6	6.71	18	1.56	0.0595	497	1.97
FXR2	6.71	18	1.56	0.0595	496	1.97
MYBL2	6.72	18	1.56	0.0595	495	1.97
RERE	6.72	18	1.56	0.0595	494	1.98
PTPRM	6.73	18	1.56	0.0592	493	1.97
FGD1	6.73	18	1.56	0.0592	492	1.98
SERTAD3	4.76	9	1.56	0.0591	491	1.98
GBA	5.5	12	1.56	0.059	490	1.98
IGDCC4	6.74	18	1.56	0.0589	489	1.98
TMEM67	6.74	18	1.56	0.0589	488	1.98
DMWD	6.74	18	1.56	0.0589	487	1.99
WNT2B	6.74	18	1.56	0.0588	486	1.99
RP1	6.64	18	1.55	0.0612	520	1.93
ADAMTS7	6.64	18	1.55	0.0611	519	1.93
MRPL27	6.65	18	1.55	0.0611	518	1.94
FLII	6.65	18	1.55	0.061	517	1.94
CEP41	6.65	18	1.55	0.061	516	1.94
LONP2	6.65	18	1.55	0.0609	515	1.94
POFUT2	6.66	18	1.55	0.0608	514	1.94
ST6GAL2	6.66	18	1.55	0.0608	513	1.95
CTNND2	6.66	18	1.55	0.0606	512	1.95
PTF1A	5.45	12	1.55	0.0605	511	1.94
SERPINI2	4.72	9	1.55	0.0604	510	1.95
DCAF4L2	6.09	15	1.55	0.0604	509	1.95
XRCC5	6.68	18	1.55	0.0603	508	1.95
RASSF2	6.59	18	1.54	0.0623	537	1.9
MGAM	6.6	18	1.54	0.0622	536	1.91
ACHE	6.6	18	1.54	0.0621	535	1.91
COL11A1	6.6	18	1.54	0.0621	534	1.91
PDE6D	5.39	12	1.54	0.0621	533	1.91
SMARCD2	6.6	18	1.54	0.062	532	1.92
ZNF598	6.61	18	1.54	0.062	531	1.92
MEF2D	6.61	18	1.54	0.0619	530	1.92
KDM3B	6.62	18	1.54	0.0617	529	1.92
NRAP	6.62	18	1.54	0.0617	528	1.92
MIEN1	6.04	15	1.54	0.0616	527	1.92
OR2C3	6.05	15	1.54	0.0616	526	1.92
VWCE	6.63	18	1.54	0.0614	525	1.92
USP33	6.63	18	1.54	0.0614	524	1.93
STPG1	6.64	18	1.54	0.0612	523	1.92
MRPS5	6.64	18	1.54	0.0612	522	1.93
FAM81A	6.64	18	1.54	0.0612	521	1.93

NOTCH3	6.54	18	1.53	0.0635	555	1.88
LYPD3	6.54	18	1.53	0.0635	554	1.88
WDR75	6.54	18	1.53	0.0634	553	1.88
TMEM51	6.55	18	1.53	0.0634	552	1.89
SMIM12	4.63	9	1.53	0.0634	551	1.89
DNLZ	6.55	18	1.53	0.0633	550	1.89
OR14I1	5.98	15	1.53	0.0633	549	1.89
SLC25A21	5.99	15	1.53	0.0631	548	1.89
DOK1	5.99	15	1.53	0.0631	547	1.89
AAK1	6.56	18	1.53	0.0631	546	1.9
MANEAL	6.56	18	1.53	0.063	545	1.9
GUCY1B3	6.56	18	1.53	0.063	544	1.9
NDUFA12	5.36	12	1.53	0.0628	543	1.9
PPIH	6.57	18	1.53	0.0628	542	1.9
ZCCHC16	6	15	1.53	0.0627	541	1.9
BPTF	6.58	18	1.53	0.0627	540	1.91
PBX4	6.58	18	1.53	0.0626	539	1.91
SCN2A	6.58	18	1.53	0.0625	538	1.91
MMP7	6.48	18	1.52	0.0649	575	1.85
NFASC	6.48	18	1.52	0.0649	574	1.86
LY6G5C	5.3	12	1.52	0.0648	573	1.86
CENPB	6.49	18	1.52	0.0648	572	1.86
CYP4Z1	3.75	6	1.52	0.0647	571	1.86
PHYHIPL	5.93	15	1.52	0.0647	570	1.86
C1orf61	5.93	15	1.52	0.0646	569	1.86
SLC25A46	5.93	15	1.52	0.0645	568	1.87
ATG16L1	6.51	18	1.52	0.0643	567	1.86
LY6G6C	3.76	6	1.52	0.0643	566	1.87
CHAT	6.51	18	1.52	0.0643	565	1.87
NCAM1	6.51	18	1.52	0.0642	564	1.87
SLMAP	6.51	18	1.52	0.0642	563	1.87
SPACA7	5.95	15	1.52	0.0641	562	1.87
OPRD1	6.52	18	1.52	0.0641	561	1.88
ARHGAP12	6.52	18	1.52	0.064	560	1.88
AGER	6.52	18	1.52	0.064	559	1.88
IL18BP	6.53	18	1.52	0.0639	558	1.88
SMIM7	3.77	6	1.52	0.0638	557	1.88
CLSTN3	6.53	18	1.52	0.0637	556	1.88
SLC25A44	6.43	18	1.51	0.0661	594	1.83
CDKAL1	6.44	18	1.51	0.066	593	1.83
PDK2	6.44	18	1.51	0.066	592	1.83
OR13A1	6.45	18	1.51	0.0657	591	1.83
RNF126	5.27	12	1.51	0.0657	590	1.83
KCNJ10	5.89	15	1.51	0.0656	589	1.83
NOL6	6.27	17	1.51	0.0656	588	1.83
NCOR2	6.46	18	1.51	0.0655	587	1.83
FBN2	6.46	18	1.51	0.0655	586	1.84
SLC4A7	6.46	18	1.51	0.0653	585	1.84

EDC4	6.46	18	1.51	0.0653	584	1.84
ZNRF1	6.47	18	1.51	0.0653	583	1.84
SEPT7	3.73	6	1.51	0.0652	582	1.84
STOX2	6.47	18	1.51	0.0652	581	1.84
CSDE1	6.47	18	1.51	0.0651	580	1.84
PPARGC1A	6.47	18	1.51	0.0651	579	1.85
MRPL34	6.48	18	1.51	0.065	578	1.85
CPA5	6.48	18	1.51	0.065	577	1.85
RIPPLY2	3.74	6	1.51	0.065	576	1.85
ST6GALNAC4	6.38	18	1.5	0.0674	612	1.81
IL12B	6.38	18	1.5	0.0673	611	1.81
CELSR2	6.39	18	1.5	0.0673	610	1.81
BTNL2	6.39	18	1.5	0.0673	609	1.81
SLC26A4	6.39	18	1.5	0.0673	608	1.82
RILP	6.39	18	1.5	0.0672	607	1.82
TGFBR3L	6.39	18	1.5	0.0671	606	1.82
MUM1	6.4	18	1.5	0.067	605	1.82
SLC28A1	6.4	18	1.5	0.0668	604	1.82
GLO1	3.7	6	1.5	0.0668	603	1.82
C3orf58	6.41	18	1.5	0.0667	602	1.82
ETFA	6.41	18	1.5	0.0667	601	1.82
ANGPTL2	6.41	18	1.5	0.0666	600	1.82
MMP27	5.24	12	1.5	0.0666	599	1.83
RWDD1	3.71	6	1.5	0.0665	598	1.83
RBM23	6.42	18	1.5	0.0664	597	1.83
PPIC	5.24	12	1.5	0.0664	596	1.83
CCNE1	6.25	17	1.5	0.0662	595	1.83

Raji_Sensitizers						
GENE	**sumZ**	**numObs**	**normZ**	**pval_synth**	**rank_synth**	**fdr_synth**
BRIP1	-89.08	18	-18.07	2.55E-73	1	4.19E-69
MUS81	-83.77	18	-16.98	5.38E-65	2	4.42E-61
FANCI	-81.58	18	-16.54	1E-61	3	5.49E-58
FANCA	-72.91	18	-14.76	1.35E-49	4	5.56E-46
UBE2T	-51.45	12	-12.73	1.99E-37	5	6.54E-34
FANCC	-60.3	18	-12.17	2.12E-34	6	5.81E-31
EME1	-55.43	18	-11.18	2.69E-29	7	6.3E-26
FANCE	-54.78	18	-11.04	1.18E-28	8	2.42E-25
C17orf53	-54.63	18	-11.01	1.66E-28	9	3.03E-25
RFWD3	-48.06	18	-9.67	2.09E-22	10	3.43E-19
FANCD2	-47.73	18	-9.6	4.11E-22	11	6.14E-19
FAN1	-47.47	18	-9.55	6.77E-22	12	9.27E-19
BARD1	-43.62	18	-8.76	1.01E-18	13	1.28E-15
C19orf40	-41.48	18	-8.32	4.55E-17	14	5.34E-14
C17orf70	-38.31	18	-7.67	8.83E-15	15	9.66E-12
FANCF	-34.65	15	-7.6	1.53E-14	16	1.57E-11
ERCC4	-35.79	18	-7.15	4.3E-13	17	4.16E-10
FANCM	-34.29	18	-6.84	3.88E-12	18	3.54E-09

MCM8	-31.77	18	-6.33	1.25E-10	19	1.08E-07
FANCB	-31.72	18	-6.32	1.35E-10	20	1.1E-07
ERCC1	-30.81	18	-6.13	4.43E-10	21	3.46E-07
ATM	-30.07	18	-5.98	1.13E-09	22	8.42E-07
DSCC1	-26.48	15	-5.76	4.22E-09	23	3.01E-06
FANCG	-28.89	18	-5.74	4.83E-09	24	3.31E-06
KIAA1524	-25.14	15	-5.46	2.38E-08	25	1.56E-05
FIGNL1	-24.48	15	-5.31	5.43E-08	26	3.43E-05
MCM9	-26.5	18	-5.25	7.75E-08	27	4.71E-05
NBN	-21.49	12	-5.21	9.48E-08	28	5.56E-05
ERCC8	-25.54	18	-5.05	2.22E-07	29	0.000126
BRCA1	-25.48	18	-5.04	2.36E-07	30	0.000129
GEN1	-20.51	12	-4.96	3.46E-07	31	0.000183
RMND1	-22.79	15	-4.93	4.09E-07	32	0.00021
C3orf37	-24.09	18	-4.75	0.000001	33	0.000498
RAD51AP1	-19.11	12	-4.61	1.98E-06	34	0.000958
GPX5	-23.12	18	-4.55	2.65E-06	35	0.00124
ENO1	-22.62	18	-4.45	4.28E-06	36	0.00195
PDHB	-22.56	18	-4.44	4.54E-06	37	0.00202
SLX4	-22.41	18	-4.41	0.0000052	38	0.00225
RMI2	-20.34	15	-4.38	5.87E-06	39	0.00247
NHLRC2	-21.81	18	-4.29	9.11E-06	40	0.00374
POLQ	-20.89	18	-4.1	0.000021	41	0.00843
XRCC3	-20.76	18	-4.07	0.0000235	42	0.00917
REV3L	-20.43	18	-4	0.0000313	43	0.0119
ERCC6	-20.42	18	-4	0.0000317	44	0.0118
BLM	-20.36	18	-3.99	0.0000334	45	0.0122
INTS6	-18.53	15	-3.98	0.000035	46	0.0125
C1orf112	-20.2	18	-3.95	0.0000384	47	0.0134
TIPRL	-16.42	12	-3.94	0.0000413	48	0.0141
NDUFB7	-16.36	12	-3.92	0.0000441	49	0.0148
ERCC5	-19.6	18	-3.83	0.0000635	50	0.0208
TRAIP	-19.38	18	-3.79	0.0000761	51	0.0245
DCLRE1A	-17.55	15	-3.75	0.0000869	52	0.0274
ESCO2	-13.54	9	-3.74	0.0000922	53	0.0286
RTN4IP1	-11.02	6	-3.73	0.0000973	54	0.0296
HELQ	-18.78	18	-3.66	0.000124	55	0.0371
QRICH1	-18.44	18	-3.6	0.000162	56	0.0475
HUS1	-18.2	18	-3.54	0.000196	57	0.0566
U2SURP	-16.98	16	-3.51	0.000227	58	0.0642
MAD2L2	-17.86	18	-3.48	0.000255	59	0.071
SLX4IP	-17.61	18	-3.42	0.000307	60	0.0842
CCAR1	-17.43	18	-3.39	0.000354	61	0.0953
FBXW7	-17.41	18	-3.38	0.000358	62	0.0949
APITD1	-9.81	6	-3.3	0.000486	63	0.127
FANCL	-11.97	9	-3.28	0.000512	64	0.131
RBBP8	-16.91	18	-3.28	0.000517	65	0.131
ATP1A1	-16.81	18	-3.26	0.000555	66	0.138

ADCY7	-16.74	18	-3.25	0.000585	67	0.143
XPR1	-16.45	18	-3.19	0.000719	68	0.174
MSR1	-16.24	18	-3.14	0.000834	69	0.198
SIVA1	-16.06	18	-3.11	0.000947	70	0.222
MRPL49	-16.03	18	-3.1	0.000965	71	0.223
POLD3	-15.89	18	-3.07	0.00107	72	0.243
FLVCR1	-15.88	18	-3.07	0.00107	73	0.241
PCM1	-15.85	18	-3.06	0.00109	74	0.243
NKD1	-15.83	18	-3.06	0.00111	75	0.243
LEMD2	-15.66	18	-3.02	0.00125	76	0.269
MRPS24	-14.18	15	-3	0.00136	77	0.29
NDUFS1	-15.38	18	-2.97	0.0015	78	0.316
YBEY	-15.34	18	-2.96	0.00154	79	0.32
MDC1	-15.34	18	-2.96	0.00155	80	0.317
JPH3	-15.26	18	-2.94	0.00163	81	0.33
PNPT1	-10.79	9	-2.94	0.00163	82	0.327
BAZ1B	-15.24	18	-2.94	0.00165	83	0.326
ARHGEF40	-15.04	18	-2.9	0.00189	84	0.369
NUBPL	-15.01	18	-2.89	0.00192	85	0.371
NDUFA9	-14.99	18	-2.89	0.00194	86	0.37
TRERF1	-14.72	18	-2.83	0.00232	87	0.437
NDUFV1	-14.7	18	-2.83	0.00235	88	0.439
FBXO11	-14.65	18	-2.82	0.00241	89	0.445
PDHA1	-14.65	18	-2.82	0.00242	90	0.441
ERCC6L	-14.64	18	-2.81	0.00244	91	0.441
CYSLTR1	-8.41	6	-2.8	0.00254	92	0.454
SHCBP1L	-14.53	18	-2.79	0.00261	93	0.46
CCDC77	-14.5	18	-2.79	0.00265	94	0.464
ELP2	-14.5	18	-2.79	0.00266	95	0.46
ELP5	-14.49	18	-2.78	0.00268	96	0.458
BAG1	-14.48	18	-2.78	0.0027	97	0.458
MADD	-14.47	18	-2.78	0.0027	98	0.453
HEMGN	-8.35	6	-2.78	0.00272	99	0.451
ATG9A	-14.38	18	-2.76	0.00286	100	0.47
DIAPH2	-14.38	18	-2.76	0.00287	101	0.467
FBXL5	-14.34	18	-2.75	0.00294	102	0.473
PDE12	-11.69	12	-2.75	0.00299	103	0.477
CHTF8	-12.98	15	-2.73	0.00318	104	0.502
SH3GL1	-14.17	18	-2.72	0.00327	105	0.511
TSSC1	-14.16	18	-2.72	0.00329	106	0.509
ATP6V1H	-14.13	18	-2.71	0.00336	107	0.516
ELP6	-14.11	18	-2.71	0.00339	108	0.516
NAA35	-14.09	18	-2.7	0.00343	109	0.517
RPUSD3	-14.09	18	-2.7	0.00345	110	0.514
NDUFA8	-14.06	18	-2.7	0.0035	111	0.517
FOXRED1	-14.06	18	-2.7	0.00351	112	0.515
KTI12	-12.79	15	-2.69	0.00362	113	0.526
GTPBP10	-13.95	18	-2.67	0.00374	114	0.538

CHAF1B	-9.86	9	-2.67	0.00374	115	0.535
SH3BP5L	-13.91	18	-2.66	0.00385	116	0.545
ME2	-9.81	9	-2.66	0.00393	117	0.552
NDUFB5	-13.86	18	-2.66	0.00396	118	0.552
TMEM161B	-7.98	6	-2.65	0.00407	119	0.561
SPICE1	-13.81	18	-2.64	0.00409	120	0.559
LDLR	-13.79	18	-2.64	0.00414	121	0.561
NDUFA13	-13.77	18	-2.64	0.00417	122	0.562
C9orf41	-9.68	9	-2.62	0.00439	123	0.587
PVR	-13.66	18	-2.61	0.00448	124	0.593
PDS5A	-13.65	18	-2.61	0.0045	125	0.592
SCAI	-13.64	18	-2.61	0.00451	126	0.588
PI4K2B	-11.09	12	-2.6	0.00469	127	0.606
REEP5	-13.56	18	-2.59	0.00474	128	0.609
C1orf64	-13.55	18	-2.59	0.00478	129	0.608
CSE1L	-12.77	16	-2.59	0.00478	130	0.604
TLR9	-13.51	18	-2.58	0.00489	131	0.613
RNF32	-13.49	18	-2.58	0.00494	132	0.614
MDH2	-13.47	18	-2.58	0.00501	133	0.618
C4orf21	-13.45	18	-2.57	0.00505	134	0.619
OPN1SW	-13.43	18	-2.57	0.00513	135	0.624
MTOR	-13.37	18	-2.55	0.00532	136	0.642
PPM1B	-13.32	18	-2.55	0.00545	137	0.654
ATP9B	-13.32	18	-2.54	0.00547	138	0.651
BOD1L1	-13.31	18	-2.54	0.00549	139	0.648
SQSTM1	-13.31	18	-2.54	0.00551	140	0.647
FAM210A	-10.85	12	-2.54	0.00557	141	0.649
C10orf12	-10.84	12	-2.54	0.0056	142	0.647
CCDC70	-10.81	12	-2.53	0.00573	143	0.658
NICN1	-13.24	18	-2.53	0.00573	144	0.654
PPP2R4	-13.22	18	-2.53	0.00578	145	0.655
QTRTD1	-13.22	18	-2.52	0.00579	146	0.651
SMTNL2	-13.21	18	-2.52	0.00582	147	0.65
OR51A7	-7.63	6	-2.52	0.00584	148	0.648
TNFRSF10A	-13.19	18	-2.52	0.00589	149	0.65
KCNH3	-13.13	18	-2.51	0.0061	150	0.668
STK4	-13.13	18	-2.51	0.00611	151	0.664
NLRP8	-13.11	18	-2.5	0.00619	152	0.669
SLC30A9	-13.1	18	-2.5	0.00621	153	0.666
PGAP3	-13.09	18	-2.5	0.00626	154	0.667
MFSD3	-13.07	18	-2.49	0.00633	155	0.671
ATP5B	-13.04	18	-2.49	0.00643	156	0.676
AMMECR1	-13.04	18	-2.49	0.00645	157	0.675
EXOSC8	-12.99	18	-2.48	0.0066	158	0.686
RYR1	-12.97	18	-2.47	0.00671	159	0.693
AGPAT1	-12.96	18	-2.47	0.00674	160	0.692
KANK4	-12.95	18	-2.47	0.00677	161	0.69
NDUFAF3	-12.95	18	-2.47	0.00679	162	0.688

TRIM4	-10.54	12	-2.46	0.00693	163	0.698
HNF1B	-12.9	18	-2.46	0.00695	164	0.696
XRCC1	-12.89	18	-2.46	0.00701	165	0.697
INSIG2	-11.77	15	-2.46	0.00701	166	0.693
ATR	-12.89	18	-2.46	0.00701	167	0.69
C1QBP	-10.46	12	-2.44	0.00733	168	0.717
FAM134A	-12.79	18	-2.44	0.00744	169	0.723
ARID4A	-10.4	12	-2.42	0.00767	170	0.741
GARS	-12.72	18	-2.42	0.00773	171	0.742
C19orf26	-12.71	18	-2.42	0.00776	172	0.741
MECR	-12.71	18	-2.42	0.00777	173	0.738
NDUFAF7	-12.71	18	-2.42	0.00778	174	0.734
LASP1	-12.7	18	-2.42	0.00781	175	0.733
C1QC	-12.69	18	-2.42	0.00783	176	0.731
BRD9	-12.68	18	-2.41	0.0079	177	0.733
GRAMD3	-12.67	18	-2.41	0.00795	178	0.733
GIGYF2	-12.67	18	-2.41	0.00795	179	0.729
DBX1	-12.63	18	-2.4	0.00811	180	0.74
MET	-12.61	18	-2.4	0.0082	181	0.744
ACAD9	-12.61	18	-2.4	0.00822	182	0.742
UBE2O	-12.6	18	-2.4	0.00827	183	0.742
ALAS1	-12.57	18	-2.39	0.00837	184	0.747
ANGPTL6	-12.53	18	-2.38	0.0086	185	0.763
NDUFA2	-10.22	12	-2.38	0.00863	186	0.762
EEPD1	-12.51	18	-2.38	0.00866	187	0.761
NDUFA6	-11.42	15	-2.38	0.00871	188	0.761
ECSIT	-12.5	18	-2.38	0.00873	189	0.758
SLC25A1	-12.5	18	-2.38	0.00873	190	0.754
MARK2	-12.49	18	-2.37	0.00879	191	0.756
DCC	-12.47	18	-2.37	0.00888	192	0.759
STRA13	-12.46	18	-2.37	0.00891	193	0.758
PNKP	-12.43	18	-2.36	0.00909	194	0.77
OR2C1	-11.31	15	-2.35	0.00931	195	0.784
MTMR1	-12.36	18	-2.35	0.00944	196	0.791
TACO1	-12.35	18	-2.35	0.00948	197	0.79
LRRC73	-12.32	18	-2.34	0.00965	198	0.8
AHNAK2	-12.32	18	-2.34	0.00966	199	0.797
KIF26B	-12.31	18	-2.34	0.00968	200	0.795
FRRS1	-12.31	18	-2.34	0.00969	201	0.792
HSPB6	-12.29	18	-2.33	0.00982	202	0.798
IGF2BP1	-12.29	18	-2.33	0.00983	203	0.795
H1F0	-11.21	15	-2.33	0.00985	204	0.793
ADM5	-12.26	18	-2.33	0.00999	205	0.8
TBC1D9B	-12.25	18	-2.32	0.01	206	0.8
TRIT1	-12.25	18	-2.32	0.01	207	0.797
TACR2	-12.22	18	-2.32	0.0102	208	0.802
VWA9	-12.22	18	-2.32	0.0102	209	0.799
IGSF9B	-12.16	18	-2.31	0.0105	210	0.823

TUFM	-12.15	18	-2.31	0.0106	211	0.822
OTUB1	-12.13	18	-2.3	0.0107	212	0.827
PDS5B	-12.1	18	-2.29	0.0109	213	0.838
NUDCD2	-6.98	6	-2.29	0.0109	214	0.836
CTSF	-12.1	18	-2.29	0.0109	215	0.832
CD1C	-12.09	18	-2.29	0.0109	216	0.829
NUP88	-12.06	18	-2.29	0.0111	217	0.84
RBFA	-12.06	18	-2.29	0.0111	218	0.836
IGFBP6	-12.05	18	-2.29	0.0111	219	0.836
KDM8	-12.05	18	-2.28	0.0112	220	0.835
TCF20	-12.04	18	-2.28	0.0112	221	0.834
NAA11	-8.49	9	-2.28	0.0114	222	0.846
MPC1	-9.78	12	-2.27	0.0116	223	0.855
UPK3A	-11.96	18	-2.27	0.0117	224	0.859
CLOCK	-11.94	18	-2.26	0.0118	225	0.863
CNDP1	-11.94	18	-2.26	0.0118	226	0.86
AGTR1	-8.44	9	-2.26	0.0119	227	0.86
CGRRF1	-11.92	18	-2.26	0.012	228	0.862
TTBK2	-11.9	18	-2.25	0.0121	229	0.867
SMIM12	-8.4	9	-2.25	0.0122	230	0.873
TMEM139	-11.87	18	-2.25	0.0123	231	0.874
LHX2	-11.86	18	-2.25	0.0123	232	0.873
EHMT1	-11.86	18	-2.25	0.0124	233	0.871
AWAT2	-11.84	18	-2.24	0.0125	234	0.879
HECTD4	-11.8	18	-2.23	0.0128	235	0.894
KCMF1	-11.77	18	-2.23	0.013	236	0.904
LUC7L2	-11.75	18	-2.22	0.0131	237	0.908
GGPS1	-6.78	6	-2.22	0.0132	238	0.908
DNTTIP2	-11.7	18	-2.21	0.0134	239	0.923
DENND6A	-11.7	18	-2.21	0.0134	240	0.919
USP34	-11.69	18	-2.21	0.0135	241	0.92
OR7C2	-8.23	9	-2.2	0.0139	242	0.94
PRKD1	-11.63	18	-2.2	0.0139	243	0.943
NR2C2AP	-11.6	18	-2.19	0.0141	244	0.952
HESX1	-6.68	6	-2.19	0.0144	245	0.962
MYO1G	-11.56	18	-2.18	0.0145	246	0.966
RAD51D	-11.56	18	-2.18	0.0145	247	0.962
RRNAD1	-11.54	18	-2.18	0.0146	248	0.969
NGLY1	-11.54	18	-2.18	0.0146	249	0.965
STX16	-10.51	15	-2.17	0.0149	250	0.976
TM9SF4	-11.5	18	-2.17	0.0149	251	0.976
SNAI2	-11.47	18	-2.17	0.0151	252	0.986
PRSS27	-11.14	17	-2.16	0.0152	253	0.986
MPL	-11.46	18	-2.16	0.0153	254	0.986
CPSF4L	-11.45	18	-2.16	0.0153	255	0.986
MARS	-11.45	18	-2.16	0.0153	256	0.984
PRPH2	-11.42	18	-2.16	0.0155	257	0.993
RB1CC1	-11.4	18	-2.15	0.0158	258	1

MRPL1	-9.3	12	-2.15	0.0158	259	1
ENPP7	-11.39	18	-2.15	0.0158	260	0.999
PPHLN1	-11.39	18	-2.15	0.0158	261	0.996
CEP57	-10.38	15	-2.15	0.0159	262	1
SH3D21	-11.35	18	-2.14	0.0161	263	1.01
POLD1	-11.34	18	-2.14	0.0162	264	1.01
LRRC36	-11.32	18	-2.13	0.0164	265	1.02
HTR3E	-11.31	18	-2.13	0.0164	266	1.01
PDIK1L	-7.99	9	-2.13	0.0165	267	1.02
VIPAS39	-11.3	18	-2.13	0.0165	268	1.01
NCDN	-11.28	18	-2.13	0.0168	269	1.02
SETD5	-11.26	18	-2.12	0.0169	270	1.03
RECQL5	-11.26	18	-2.12	0.0169	271	1.02
ADAM20	-9.19	12	-2.12	0.0169	272	1.02
SARS2	-11.25	18	-2.12	0.0169	273	1.02
FKBP6	-11.24	18	-2.12	0.017	274	1.02
FAM179A	-11.24	18	-2.12	0.0171	275	1.02
ZC3H7A	-11.23	18	-2.12	0.0171	276	1.02
FBXO47	-11.22	18	-2.12	0.0172	277	1.02
SIT1	-10.25	15	-2.12	0.0172	278	1.02
LIMK2	-11.22	18	-2.11	0.0172	279	1.01
IREB2	-11.22	18	-2.11	0.0173	280	1.01
GPD1	-11.21	18	-2.11	0.0173	281	1.01
UVSSA	-11.18	18	-2.11	0.0176	282	1.02
CLUH	-11.17	18	-2.1	0.0176	283	1.02
NRD1	-11.17	18	-2.1	0.0177	284	1.02
XRCC4	-7.89	9	-2.1	0.0178	285	1.02
HOXC10	-10.15	15	-2.09	0.0181	286	1.04
VARS	-10.79	17	-2.09	0.0182	287	1.04
C8orf86	-9.06	12	-2.09	0.0184	288	1.05
MPST	-10.11	15	-2.09	0.0185	289	1.05
KIAA2022	-10.1	15	-2.08	0.0186	290	1.05
PRRC2B	-11.06	18	-2.08	0.0187	291	1.05
IKBKAP	-11.06	18	-2.08	0.0187	292	1.05
LINS	-11.05	18	-2.08	0.0188	293	1.05
HSPA12B	-11.05	18	-2.08	0.0188	294	1.05
KIAA1549	-11.03	18	-2.08	0.0189	295	1.05
CCDC97	-11.02	18	-2.07	0.0191	296	1.06
OPTN	-11.02	18	-2.07	0.0191	297	1.06
RNASEL	-11.01	18	-2.07	0.0191	298	1.05
RPAIN	-9.98	15	-2.06	0.0199	299	1.09
C17orf103	-10.94	18	-2.06	0.0199	300	1.09
BIN3	-10.94	18	-2.06	0.0199	301	1.08
TBRG4	-10.92	18	-2.05	0.0201	302	1.09
MARCO	-10.92	18	-2.05	0.0201	303	1.09
NUDT2	-7.71	9	-2.05	0.0202	304	1.09
ACRBP	-10.9	18	-2.05	0.0202	305	1.09
ATP5A1	-8.9	12	-2.05	0.0203	306	1.09

MRPL13	-8.86	12	-2.04	0.0207	307	1.11
MOCS3	-8.86	12	-2.04	0.0208	308	1.11
EIF4G3	-10.84	18	-2.04	0.0209	309	1.11
NDUFC2	-8.83	12	-2.03	0.0211	310	1.12
SLITRK6	-9.87	15	-2.03	0.0211	311	1.12
RBM10	-10.8	18	-2.03	0.0212	312	1.12
PABPC4L	-9.85	15	-2.03	0.0213	313	1.12
PDK1	-10.79	18	-2.03	0.0214	314	1.12
OR1L3	-6.22	6	-2.02	0.0215	315	1.12
CRBN	-10.77	18	-2.02	0.0215	316	1.12
C17orf49	-10.77	18	-2.02	0.0216	317	1.12
ITGB1BP1	-7.6	9	-2.02	0.0218	318	1.13
NDUFAF5	-10.74	18	-2.02	0.0219	319	1.13
AMHR2	-10.74	18	-2.02	0.0219	320	1.12
CES5A	-10.71	18	-2.01	0.0222	321	1.14
CNTRL	-10.71	18	-2.01	0.0222	322	1.13
GPX1	-6.16	6	-2	0.0227	323	1.15
NFATC2IP	-10.67	18	-2	0.0227	324	1.15
SRSF2	-10.35	17	-2	0.0228	325	1.15
IWS1	-10.65	18	-2	0.0229	326	1.15
IGFALS	-9.7	15	-1.99	0.0231	327	1.16
ARHGAP39	-10.63	18	-1.99	0.0231	328	1.16
PIGF	-6.13	6	-1.99	0.0232	329	1.16
SPATA22	-8.67	12	-1.99	0.0232	330	1.16
PITX1	-10.61	18	-1.99	0.0233	331	1.16
PIBF1	-10.61	18	-1.99	0.0233	332	1.15
SHARPIN	-10.61	18	-1.99	0.0233	333	1.15
LCA5	-8.66	12	-1.99	0.0234	334	1.15
COMMD6	-7.49	9	-1.99	0.0235	335	1.15
PREPL	-10.59	18	-1.99	0.0236	336	1.15
SLC27A2	-10.59	18	-1.99	0.0236	337	1.15
METTL22	-10.58	18	-1.98	0.0237	338	1.15
ACACA	-10.57	18	-1.98	0.0238	339	1.15
TGFB1I1	-10.57	18	-1.98	0.0238	340	1.15
SPCS1	-10.57	18	-1.98	0.0238	341	1.15
ARPC5	-10.57	18	-1.98	0.0238	342	1.14
DCK	-10.55	18	-1.98	0.0241	343	1.15
NOA1	-10.53	18	-1.97	0.0243	344	1.16
TRIM24	-10.52	18	-1.97	0.0243	345	1.16
IGSF10	-10.5	18	-1.97	0.0246	346	1.17
SLAMF1	-10.49	18	-1.96	0.0248	347	1.17
C11orf54	-7.41	9	-1.96	0.0248	348	1.17
SPAG9	-10.48	18	-1.96	0.0249	349	1.17
HSD17B12	-8.54	12	-1.96	0.025	350	1.17
ATRIP	-10.46	18	-1.96	0.025	351	1.17
PLCZ1	-8.54	12	-1.96	0.0251	352	1.17
SPC24	-10.46	18	-1.96	0.0251	353	1.17
SULT1C2	-10.46	18	-1.96	0.0251	354	1.16

EHF	-10.46	18	-1.96	0.0251	355	1.16
CATSPERB	-10.45	18	-1.96	0.0252	356	1.16
RNASE6	-8.52	12	-1.95	0.0253	357	1.16
ATP5I	-7.38	9	-1.95	0.0254	358	1.17
LMAN1	-10.42	18	-1.95	0.0255	359	1.17
MAP3K4	-10.42	18	-1.95	0.0256	360	1.17
GRM6	-10.39	18	-1.95	0.0259	361	1.18
LRWD1	-10.38	18	-1.94	0.0261	362	1.18
CELF2	-10.37	18	-1.94	0.0262	363	1.18
TAAR2	-7.32	9	-1.94	0.0264	364	1.19
RXRG	-10.35	18	-1.94	0.0264	365	1.19
MTFMT	-10.33	18	-1.93	0.0267	366	1.2
IPPK	-10.31	18	-1.93	0.0269	367	1.2
RNASEH2A	-10.31	18	-1.93	0.0269	368	1.2
SMPD4	-8.41	12	-1.92	0.0271	369	1.21
SDR39U1	-10.29	18	-1.92	0.0272	370	1.21
BTN2A2	-5.94	6	-1.92	0.0273	371	1.21
MGA	-10.26	18	-1.92	0.0275	372	1.22
RLBP1	-10.24	18	-1.91	0.0278	373	1.22
AHSG	-10.24	18	-1.91	0.0279	374	1.22
DBNDD1	-10.23	18	-1.91	0.0279	375	1.22
THTPA	-9.34	15	-1.91	0.0279	376	1.22
GATAD2A	-10.23	18	-1.91	0.028	377	1.22
CTNS	-10.22	18	-1.91	0.028	378	1.22
IGSF9	-10.21	18	-1.91	0.0282	379	1.22
XPO6	-10.21	18	-1.91	0.0282	380	1.22
MRPL40	-5.89	6	-1.91	0.0283	381	1.22
GTPBP3	-10.19	18	-1.9	0.0284	382	1.22
MC2R	-8.31	12	-1.9	0.0286	383	1.23
OR52R1	-7.2	9	-1.9	0.0287	384	1.23
SPAG17	-10.17	18	-1.9	0.0288	385	1.23
PSMC3	-9.28	15	-1.9	0.0289	386	1.23
WDR11	-10.16	18	-1.9	0.0289	387	1.23
F2R	-10.16	18	-1.9	0.0289	388	1.22
HEXIM1	-8.29	12	-1.89	0.0291	389	1.23
GPR61	-10.15	18	-1.89	0.0291	390	1.23
PRR5L	-10.13	18	-1.89	0.0293	391	1.23
CHMP4A	-5.84	6	-1.89	0.0294	392	1.23
STK39	-10.12	18	-1.89	0.0295	393	1.23
GMPR	-10.11	18	-1.89	0.0296	394	1.23
IVNS1ABP	-10.11	18	-1.89	0.0296	395	1.23
BRCA2	-10.1	18	-1.88	0.0298	396	1.23
SCN10A	-10.09	18	-1.88	0.0299	397	1.23
C1S	-10.09	18	-1.88	0.0299	398	1.23
GPR18	-7.13	9	-1.88	0.0299	399	1.23
TFAP2D	-10.07	18	-1.88	0.0302	400	1.24
CABIN1	-10.07	18	-1.88	0.0302	401	1.24
OR52K1	-5.81	6	-1.88	0.0303	402	1.24

OSBPL6	-10.04	18	-1.87	0.0306	403	1.25
DLAT	-10.04	18	-1.87	0.0306	404	1.24
PTPRK	-10.04	18	-1.87	0.0306	405	1.24
GPR174	-8.2	12	-1.87	0.0306	406	1.24
KANSL2	-10.04	18	-1.87	0.0306	407	1.24
YIF1A	-10.03	18	-1.87	0.0307	408	1.24
GH2	-7.08	9	-1.87	0.031	409	1.24
UNC50	-9.14	15	-1.87	0.031	410	1.24
NPC2	-8.17	12	-1.87	0.031	411	1.24
MRPS34	-10.01	18	-1.87	0.031	412	1.24
ZNF142	-10.01	18	-1.87	0.0311	413	1.23
NGFR	-10.01	18	-1.87	0.0311	414	1.23
DYRK4	-10	18	-1.86	0.0311	415	1.23
COQ7	-9.99	18	-1.86	0.0312	416	1.23
CLYBL	-9.97	18	-1.86	0.0315	417	1.24
CARHSP1	-9.97	18	-1.86	0.0315	418	1.24
GADD45GIP1	-9.97	18	-1.86	0.0315	419	1.24
SAMD10	-9.96	18	-1.86	0.0317	420	1.24
KCTD3	-9.96	18	-1.86	0.0317	421	1.24
ECHS1	-9.96	18	-1.86	0.0318	422	1.24
CHERP	-9.95	18	-1.85	0.0318	423	1.24
ZDHHC6	-7.03	9	-1.85	0.0319	424	1.23
MYOCD	-9.94	18	-1.85	0.0319	425	1.23
SEC62	-7.03	9	-1.85	0.0319	426	1.23
RSPO4	-9.94	18	-1.85	0.032	427	1.23
DUSP3	-9.93	18	-1.85	0.0322	428	1.23
NHEJ1	-9.06	15	-1.85	0.0322	429	1.23
RND3	-9.93	18	-1.85	0.0322	430	1.23
AUNIP	-9.05	15	-1.85	0.0324	431	1.23
NPSR1	-9.91	18	-1.85	0.0325	432	1.23
PRR12	-9.9	18	-1.84	0.0326	433	1.24
BRD3	-9.89	18	-1.84	0.0327	434	1.24
MIB2	-9.89	18	-1.84	0.0328	435	1.24
MXRA5	-9.88	18	-1.84	0.0328	436	1.24
FAM122A	-9.02	15	-1.84	0.033	437	1.24
POLE3	-6.98	9	-1.84	0.033	438	1.24
PTRH1	-9.86	18	-1.84	0.0331	439	1.24
DCN	-9.86	18	-1.84	0.0332	440	1.24
TTC39A	-9.86	18	-1.84	0.0332	441	1.24
TLCD1	-9.86	18	-1.84	0.0332	442	1.23
PGBD3	-9.85	18	-1.83	0.0333	443	1.23
RMDN2	-9.85	18	-1.83	0.0334	444	1.23
EFNA2	-9.85	18	-1.83	0.0334	445	1.23
FAM174B	-9.85	18	-1.83	0.0334	446	1.23
ACSL1	-9.84	18	-1.83	0.0334	447	1.23
MRPL17	-9.84	18	-1.83	0.0335	448	1.23
KBTBD8	-9.83	18	-1.83	0.0337	449	1.23
TMEM150B	-9.83	18	-1.83	0.0337	450	1.23

XPA	-8.01	12	-1.83	0.0339	451	1.23
FAM160B1	-9.8	18	-1.82	0.0341	452	1.24
HERC4	-9.8	18	-1.82	0.0341	453	1.24
SMIM13	-8.95	15	-1.82	0.0341	454	1.23
MAST2	-9.8	18	-1.82	0.0342	455	1.23
PHACTR2	-9.79	18	-1.82	0.0342	456	1.23
ZNF583	-8	12	-1.82	0.0342	457	1.23
KCNG3	-9.79	18	-1.82	0.0343	458	1.23
POLK	-9.79	18	-1.82	0.0343	459	1.23
PPP1R8	-9.78	18	-1.82	0.0344	460	1.23
CXorf64	-8.93	15	-1.82	0.0345	461	1.23
CXCL10	-5.65	6	-1.82	0.0345	462	1.23
ADH4	-8.93	15	-1.82	0.0345	463	1.22
DMGDH	-9.76	18	-1.81	0.0348	464	1.23
EMC4	-9.76	18	-1.81	0.0348	465	1.23
CDK20	-9.75	18	-1.81	0.0349	466	1.23
ZNF155	-6.89	9	-1.81	0.0349	467	1.23
TXK	-9.75	18	-1.81	0.0349	468	1.23
STXBP6	-9.74	18	-1.81	0.0351	469	1.23
CCKAR	-9.74	18	-1.81	0.0351	470	1.23
STK3	-9.71	18	-1.8	0.0355	471	1.24
RETSAT	-9.7	18	-1.8	0.0357	472	1.24
CLIP3	-9.7	18	-1.8	0.0357	473	1.24
TRIP11	-9.7	18	-1.8	0.0358	474	1.24
PLK2	-9.69	18	-1.8	0.0358	475	1.24
BAP1	-9.68	18	-1.8	0.036	476	1.24
PLA2R1	-9.68	18	-1.8	0.036	477	1.24
ATRX	-9.68	18	-1.8	0.036	478	1.24
HVCN1	-9.67	18	-1.8	0.0361	479	1.24
ZSWIM3	-9.67	18	-1.8	0.0362	480	1.24
LRP1B	-9.67	18	-1.8	0.0362	481	1.24
ATP6V0E1	-5.58	6	-1.8	0.0363	482	1.24
ARHGAP42	-7.88	12	-1.79	0.0366	483	1.24
UNC13A	-9.64	18	-1.79	0.0366	484	1.24
RAD50	-9.64	18	-1.79	0.0367	485	1.24
HHLA1	-9.63	18	-1.79	0.0369	486	1.25
EIF1	-5.56	6	-1.79	0.0369	487	1.24
ELK4	-8.79	15	-1.79	0.0369	488	1.24
ADAM7	-9.63	18	-1.79	0.0369	489	1.24
RBM15	-9.61	18	-1.79	0.0371	490	1.24
SP5	-9.61	18	-1.78	0.0372	491	1.24
SMARCA1	-9.61	18	-1.78	0.0372	492	1.24
PLLP	-8.75	15	-1.78	0.0376	493	1.25
TRABD2A	-9.59	18	-1.78	0.0376	494	1.25
LRIG3	-9.58	18	-1.78	0.0376	495	1.25
GNG11	-5.53	6	-1.78	0.0377	496	1.25
SRPK3	-9.58	18	-1.78	0.0377	497	1.25
DCLK3	-9.58	18	-1.78	0.0377	498	1.24

OR10J3	-7.82	12	-1.78	0.0378	499	1.24
ALDH7A1	-9.57	18	-1.78	0.0378	500	1.24
AAMP	-9.56	18	-1.77	0.038	501	1.24
TECPR1	-9.55	18	-1.77	0.0382	502	1.25
C12orf40	-5.51	6	-1.77	0.0383	503	1.25
DIRAS1	-6.75	9	-1.77	0.0383	504	1.25
KCTD4	-8.71	15	-1.77	0.0384	505	1.25
PNN	-9.53	18	-1.77	0.0385	506	1.25
ATG14	-9.53	18	-1.77	0.0385	507	1.25
SNX4	-8.7	15	-1.77	0.0385	508	1.24
MMP19	-9.53	18	-1.77	0.0385	509	1.24
C15orf26	-9.53	18	-1.77	0.0386	510	1.24
ARL6	-6.73	9	-1.77	0.0386	511	1.24
EXOC3L4	-9.52	18	-1.77	0.0386	512	1.24
CGN	-9.52	18	-1.77	0.0387	513	1.24
AP2A1	-9.5	18	-1.76	0.039	514	1.25
RIPK1	-9.5	18	-1.76	0.039	515	1.24
TMEM38A	-9.5	18	-1.76	0.0391	516	1.24
KIAA1324L	-9.5	18	-1.76	0.0391	517	1.24
MSH2	-9.49	18	-1.76	0.0392	518	1.24
LRRTM4	-8.66	15	-1.76	0.0392	519	1.24
MUC12	-9.49	18	-1.76	0.0393	520	1.24
IL20	-6.7	9	-1.76	0.0395	521	1.24
ANKK1	-9.47	18	-1.76	0.0396	522	1.25
AES	-9.46	18	-1.75	0.0397	523	1.25
HRH4	-8.64	15	-1.75	0.0397	524	1.25
NEK9	-9.46	18	-1.75	0.0397	525	1.24
GREB1	-9.45	18	-1.75	0.0398	526	1.24
TCN2	-9.45	18	-1.75	0.0399	527	1.24
ADARB1	-9.44	18	-1.75	0.0401	528	1.25
MAP3K11	-9.44	18	-1.75	0.0401	529	1.25
MON2	-9.44	18	-1.75	0.0401	530	1.24
XPO1	-9.17	17	-1.75	0.0402	531	1.24
PET100	-6.67	9	-1.75	0.0402	532	1.24
TRO	-9.43	18	-1.75	0.0403	533	1.24
EDDM3A	-5.44	6	-1.75	0.0404	534	1.24
SNRNP200	-9.41	18	-1.74	0.0406	535	1.25
HIPK3	-9.39	18	-1.74	0.0409	536	1.25
EPB41L4A	-9.36	18	-1.73	0.0416	537	1.27
MAN2B1	-9.35	18	-1.73	0.0416	538	1.27
F3	-9.35	18	-1.73	0.0417	539	1.27
AKAP9	-9.35	18	-1.73	0.0418	540	1.27
BHLHE23	-8.53	15	-1.73	0.0418	541	1.27
PIGZ	-9.33	18	-1.73	0.0421	542	1.27
WDR96	-9.33	18	-1.73	0.0421	543	1.27
CD48	-8.51	15	-1.73	0.0422	544	1.27
SRGN	-9.32	18	-1.72	0.0423	545	1.27
MGST2	-7.61	12	-1.72	0.0423	546	1.27

KCNQ4	-9.31	18	-1.72	0.0424	547	1.27
METTL11B	-8.5	15	-1.72	0.0424	548	1.27
HIC2	-8.49	15	-1.72	0.0426	549	1.28
ZNF793	-7.59	12	-1.72	0.0428	550	1.28
CNNM1	-9.29	18	-1.72	0.0428	551	1.28
NOP58	-8.47	15	-1.72	0.043	552	1.28
PCNA	-7.58	12	-1.72	0.043	553	1.28
AFTPH	-9.28	18	-1.72	0.043	554	1.27
ZNF226	-7.58	12	-1.72	0.043	555	1.27
SCFD2	-9.28	18	-1.72	0.0431	556	1.27
SLC47A2	-9.27	18	-1.71	0.0432	557	1.27
WISP3	-9.26	18	-1.71	0.0434	558	1.28
DZIP3	-9.25	18	-1.71	0.0436	559	1.28
NDUFB8	-9.24	18	-1.71	0.0437	560	1.28
NDRG4	-9.24	18	-1.71	0.0438	561	1.28
PARN	-9.23	18	-1.71	0.0439	562	1.28
NDUFV3	-9.23	18	-1.71	0.044	563	1.28
SLC25A35	-9.22	18	-1.7	0.0442	564	1.29
RNF44	-9.21	18	-1.7	0.0443	565	1.29
HAUS4	-7.51	12	-1.7	0.0445	566	1.29
MMD	-8.4	15	-1.7	0.0445	567	1.29
DDX39A	-9.2	18	-1.7	0.0446	568	1.29
PODN	-9.18	18	-1.7	0.0449	569	1.29
NOS3	-9.18	18	-1.7	0.0449	570	1.29
PPOX	-9.17	18	-1.7	0.045	571	1.3
FLG2	-9.16	18	-1.69	0.0453	572	1.3
C2orf16	-9.16	18	-1.69	0.0454	573	1.3
SREBF2	-9.16	18	-1.69	0.0454	574	1.3
ERF	-9.15	18	-1.69	0.0456	575	1.3
ZDHHC24	-9.14	18	-1.69	0.0456	576	1.3
IL22RA2	-8.35	15	-1.69	0.0456	577	1.3
NFRKB	-9.14	18	-1.69	0.0457	578	1.3
PAK3	-9.14	18	-1.69	0.0457	579	1.3
SCRN2	-9.13	18	-1.69	0.0458	580	1.3
RALGAPA1	-7.46	12	-1.69	0.0459	581	1.3
RAD51AP2	-7.45	12	-1.69	0.0459	582	1.3
FBXW10	-6.45	9	-1.68	0.046	583	1.3
MLLT6	-9.12	18	-1.68	0.046	584	1.29
UBXN6	-9.12	18	-1.68	0.0461	585	1.29
CYB5RL	-9.11	18	-1.68	0.0462	586	1.3
ZNF862	-9.11	18	-1.68	0.0464	587	1.3
ITIH3	-9.1	18	-1.68	0.0464	588	1.3
OR1A1	-7.43	12	-1.68	0.0464	589	1.29
PRKRA	-7.43	12	-1.68	0.0465	590	1.29
AIM1L	-9.09	18	-1.68	0.0466	591	1.29
EFNA4	-9.08	18	-1.68	0.0469	592	1.3
SUSD4	-9.08	18	-1.68	0.0469	593	1.3
PIEZO1	-9.08	18	-1.68	0.047	594	1.3

SETD1A	-9.07	18	-1.67	0.047	595	1.3
HMOX2	-9.07	18	-1.67	0.047	596	1.3
FSCN2	-9.07	18	-1.67	0.047	597	1.29
IL1F10	-5.24	6	-1.67	0.0471	598	1.29
FKBP5	-9.07	18	-1.67	0.0471	599	1.29
OTUB2	-6.41	9	-1.67	0.0472	600	1.29
GUF1	-7.4	12	-1.67	0.0472	601	1.29
AIP	-9.06	18	-1.67	0.0472	602	1.29
FHDC1	-9.06	18	-1.67	0.0474	603	1.29
ZNF276	-9.05	18	-1.67	0.0474	604	1.29
PBXIP1	-9.05	18	-1.67	0.0474	605	1.29
SULT1C3	-6.4	9	-1.67	0.0475	606	1.29
CERKL	-9.05	18	-1.67	0.0475	607	1.29
PUS3	-9.04	18	-1.67	0.0477	608	1.29
GID8	-9.04	18	-1.67	0.0478	609	1.29
ABCA7	-9.03	18	-1.67	0.0478	610	1.29
TMEM200A	-7.37	12	-1.67	0.0479	611	1.29
ARNT	-9.02	18	-1.66	0.0482	612	1.29
CNOT2	-9.01	18	-1.66	0.0482	613	1.29
APOO	-5.2	6	-1.66	0.0482	614	1.29
CNTD2	-9	18	-1.66	0.0485	615	1.29
PER3	-9	18	-1.66	0.0485	616	1.29
MALSU1	-6.36	9	-1.66	0.0485	617	1.29
CDH23	-9	18	-1.66	0.0485	618	1.29
SMARCAL1	-8.99	18	-1.66	0.0487	619	1.29
TENM2	-8.99	18	-1.66	0.0487	620	1.29
PIGU	-8.98	18	-1.66	0.0489	621	1.29
KDM1A	-8.98	18	-1.66	0.0489	622	1.29
NOG	-7.33	12	-1.65	0.0491	623	1.29
WDFY3	-8.97	18	-1.65	0.0491	624	1.29
FAS	-5.18	6	-1.65	0.0492	625	1.29
HEPACAM	-8.96	18	-1.65	0.0493	626	1.29
MRPS30	-8.18	15	-1.65	0.0494	627	1.29
APOLD1	-8.18	15	-1.65	0.0494	628	1.29
CLPSL1	-8.96	18	-1.65	0.0494	629	1.29
VIM	-8.96	18	-1.65	0.0494	630	1.29
EXOG	-8.17	15	-1.65	0.0495	631	1.29
NKX2-3	-8.95	18	-1.65	0.0496	632	1.29
MSC	-8.95	18	-1.65	0.0496	633	1.29
NXT1	-6.33	9	-1.65	0.0496	634	1.29
PCMT1	-8.94	18	-1.65	0.0498	635	1.29
PHF6	-6.31	9	-1.65	0.05	636	1.29
COQ5	-8.93	18	-1.64	0.05	637	1.29
GANC	-8.93	18	-1.64	0.0501	638	1.29
PLA2G4F	-8.93	18	-1.64	0.0501	639	1.29
UBE2F	-6.31	9	-1.64	0.0501	640	1.29
C9orf171	-8.92	18	-1.64	0.0502	641	1.29
NDUFA11	-8.92	18	-1.64	0.0502	642	1.28

ALS2	-8.91	18	-1.64	0.0503	643	1.28
ST8SIA6	-8.13	15	-1.64	0.0506	644	1.29
PRKACG	-8.12	15	-1.64	0.0507	645	1.29
CANX	-8.9	18	-1.64	0.0507	646	1.29
IKZF4	-8.88	18	-1.63	0.0511	647	1.3
USP25	-8.88	18	-1.63	0.0511	648	1.3
C16orf46	-8.1	15	-1.63	0.0512	649	1.3
OR51G1	-8.1	15	-1.63	0.0512	650	1.29
PSMB9	-8.87	18	-1.63	0.0512	651	1.29
JPH2	-8.85	18	-1.63	0.0516	652	1.3
FAM73A	-8.85	18	-1.63	0.0517	653	1.3
MRE11A	-8.08	15	-1.63	0.0517	654	1.3
PALB2	-8.84	18	-1.63	0.0518	655	1.3
UIMC1	-8.84	18	-1.63	0.0519	656	1.3
PTPRA	-8.84	18	-1.63	0.052	657	1.3
NFX1	-8.84	18	-1.63	0.052	658	1.3
SCFD1	-8.84	18	-1.63	0.052	659	1.3
CD97	-8.81	18	-1.62	0.0525	660	1.31
MROH5	-8.81	18	-1.62	0.0526	661	1.31
TBC1D19	-8.81	18	-1.62	0.0526	662	1.3
PPP6R3	-8.81	18	-1.62	0.0526	663	1.3
MINK1	-8.8	18	-1.62	0.0528	664	1.31
PTPN9	-8.79	18	-1.62	0.0529	665	1.31
C9orf153	-5.07	6	-1.62	0.053	666	1.31
RAD51B	-8.78	18	-1.62	0.0531	667	1.31
CNN1	-8.78	18	-1.61	0.0532	668	1.31
MAGED1	-8.76	18	-1.61	0.0536	669	1.31
PQLC3	-8.76	18	-1.61	0.0536	670	1.31
ARFIP2	-8.76	18	-1.61	0.0536	671	1.31
BSDC1	-8.76	18	-1.61	0.0536	672	1.31
SKOR1	-8.76	18	-1.61	0.0536	673	1.31
LONRF3	-8.76	18	-1.61	0.0537	674	1.31
SMAD1	-8.75	18	-1.61	0.0539	675	1.31
ZNF619	-8.75	18	-1.61	0.0539	676	1.31
ZNF112	-7.98	15	-1.61	0.054	677	1.31
F13B	-8.74	18	-1.61	0.0541	678	1.31
TDRD1	-8.74	18	-1.61	0.0541	679	1.31
PPAPDC2	-8.74	18	-1.61	0.0542	680	1.31
KLHL14	-8.74	18	-1.61	0.0542	681	1.31
DUSP22	-7.13	12	-1.61	0.0542	682	1.31
C1orf116	-8.72	18	-1.6	0.0545	683	1.31
OR14K1	-6.17	9	-1.6	0.0545	684	1.31
USP46	-8.72	18	-1.6	0.0545	685	1.31
C10orf62	-8.72	18	-1.6	0.0547	686	1.31
CRYBB2	-8.71	18	-1.6	0.0548	687	1.31
ANKRD11	-8.71	18	-1.6	0.0549	688	1.31
ZBTB9	-7.67	14	-1.6	0.055	689	1.31
TNFSF9	-7.1	12	-1.6	0.055	690	1.31

USPL1	-7.94	15	-1.6	0.055	691	1.31
NECAB2	-8.7	18	-1.6	0.0551	692	1.31
UHMK1	-8.69	18	-1.6	0.0552	693	1.31
R3HCC1	-8.69	18	-1.6	0.0552	694	1.31
SRFBP1	-5.02	6	-1.6	0.0552	695	1.3
ZRANB1	-8.69	18	-1.6	0.0552	696	1.3
AATK	-7.93	15	-1.59	0.0554	697	1.3
TTC39B	-8.68	18	-1.59	0.0555	698	1.31
CASP14	-8.68	18	-1.59	0.0555	699	1.3
SPTBN1	-8.68	18	-1.59	0.0555	700	1.3
MYO9A	-8.68	18	-1.59	0.0555	701	1.3
MYRFL	-8.68	18	-1.59	0.0556	702	1.3
TMCO6	-8.67	18	-1.59	0.0556	703	1.3
PSCA	-8.67	18	-1.59	0.0557	704	1.3
RAD51C	-8.66	18	-1.59	0.0559	705	1.3
GPR37L1	-8.66	18	-1.59	0.056	706	1.3
XK	-8.66	18	-1.59	0.056	707	1.3
KSR2	-8.66	18	-1.59	0.056	708	1.3
RSPH4A	-8.66	18	-1.59	0.056	709	1.3
YY2	-8.66	18	-1.59	0.056	710	1.3
CTLA4	-8.65	18	-1.59	0.0562	711	1.3
KDM4C	-8.64	18	-1.59	0.0564	712	1.3
NDST2	-8.63	18	-1.58	0.0566	713	1.3
OR13H1	-7.04	12	-1.58	0.0568	714	1.31
CD244	-8.62	18	-1.58	0.0569	715	1.31
ZNF710	-8.62	18	-1.58	0.0569	716	1.3
C5orf27	-4.97	6	-1.58	0.057	717	1.3
SALL4	-8.62	18	-1.58	0.057	718	1.3
ARL13B	-8.61	18	-1.58	0.057	719	1.3
DARS	-8.61	18	-1.58	0.0572	720	1.3
OR9I1	-7.03	12	-1.58	0.0572	721	1.3
FAM193B	-8.6	18	-1.58	0.0573	722	1.3
TMEM219	-8.6	18	-1.58	0.0574	723	1.3
TTYH1	-8.59	18	-1.57	0.0576	724	1.31
FRAT1	-8.58	18	-1.57	0.0577	725	1.31
PHF7	-8.58	18	-1.57	0.0578	726	1.31
STAC3	-8.58	18	-1.57	0.0579	727	1.31
NOXRED1	-8.58	18	-1.57	0.0579	728	1.31
CCDC64B	-8.33	17	-1.57	0.058	729	1.31
GLRX5	-4.95	6	-1.57	0.0581	730	1.31
POLG2	-8.56	18	-1.57	0.0583	731	1.31
FOXO1	-8.56	18	-1.57	0.0584	732	1.31
ZNF256	-7.81	15	-1.57	0.0584	733	1.31
ALX4	-8.55	18	-1.57	0.0584	734	1.31
TRIM45	-8.55	18	-1.57	0.0584	735	1.31
SDC4	-8.55	18	-1.57	0.0584	736	1.3
ISOC2	-8.54	18	-1.57	0.0587	737	1.31
ARID4B	-8.53	18	-1.56	0.059	738	1.31

PRUNE	-8.53	18	-1.56	0.059	739	1.31
OR2L13	-6.96	12	-1.56	0.0591	740	1.31
NAE1	-8.04	16	-1.56	0.0591	741	1.31
BACH1	-8.52	18	-1.56	0.0592	742	1.31
PTPN6	-8.52	18	-1.56	0.0593	743	1.31
MORN1	-8.52	18	-1.56	0.0593	744	1.31
ECI1	-8.52	18	-1.56	0.0593	745	1.31
UBE3D	-7.77	15	-1.56	0.0595	746	1.31
DNAH17	-8.51	18	-1.56	0.0595	747	1.31
WTAP	-6.94	12	-1.56	0.0597	748	1.31
GRIN2A	-8.5	18	-1.56	0.0598	749	1.31
E2F6	-6.94	12	-1.56	0.0598	750	1.31
B3GALT4	-7.75	15	-1.56	0.0599	751	1.31
GRK7	-8.49	18	-1.55	0.06	752	1.31
SESTD1	-8.49	18	-1.55	0.0601	753	1.31
NLRC3	-8.49	18	-1.55	0.0601	754	1.31
PTCH2	-8.48	18	-1.55	0.0602	755	1.31
RER1	-8.48	18	-1.55	0.0604	756	1.31
SLC19A2	-8.47	18	-1.55	0.0604	757	1.31
DERL3	-8.47	18	-1.55	0.0604	758	1.31
CEACAM18	-8.47	18	-1.55	0.0604	759	1.31
SLC30A7	-8.45	18	-1.55	0.061	760	1.32
ALMS1	-8.45	18	-1.55	0.0611	761	1.32
SCN5A	-8.45	18	-1.55	0.0611	762	1.32
C15orf39	-8.44	18	-1.55	0.0611	763	1.32
FLOT2	-8.44	18	-1.54	0.0612	764	1.32
GPER	-7.7	15	-1.54	0.0614	765	1.32
SHCBP1	-8.43	18	-1.54	0.0615	766	1.32
MICAL3	-8.43	18	-1.54	0.0615	767	1.32
TBC1D9	-8.43	18	-1.54	0.0615	768	1.32
CA5B	-7.69	15	-1.54	0.0617	769	1.32
PDCD4	-8.42	18	-1.54	0.0617	770	1.32
CRYGC	-8.42	18	-1.54	0.0617	771	1.32
ZC4H2	-8.42	18	-1.54	0.0618	772	1.31
NEK4	-8.42	18	-1.54	0.0618	773	1.31
CERS4	-8.41	18	-1.54	0.0619	774	1.31
RNF138	-4.86	6	-1.54	0.0619	775	1.31
RELA	-8.41	18	-1.54	0.0619	776	1.31
NDUFA5	-4.86	6	-1.54	0.0619	777	1.31
FAM159A	-8.41	18	-1.54	0.062	778	1.31
GPBAR1	-8.41	18	-1.54	0.062	779	1.31
KIAA1737	-8.41	18	-1.54	0.0621	780	1.31
LPP	-8.4	18	-1.54	0.0622	781	1.31
HMGCL	-8.39	18	-1.53	0.0624	782	1.31
LAPTM4A	-8.39	18	-1.53	0.0624	783	1.31
EXO1	-8.39	18	-1.53	0.0625	784	1.31
MBOAT4	-8.38	18	-1.53	0.0628	785	1.31
YPEL4	-8.37	18	-1.53	0.063	786	1.32

ZNF394	-8.37	18	-1.53	0.063	787	1.31
ZNF512	-8.37	18	-1.53	0.0631	788	1.31
C3orf35	-4.83	6	-1.53	0.0632	789	1.32
DDO	-8.36	18	-1.53	0.0633	790	1.32
COL23A1	-8.36	18	-1.53	0.0633	791	1.31
MRPL14	-7.62	15	-1.53	0.0634	792	1.31
CMTM4	-8.35	18	-1.53	0.0635	793	1.31
HNRNPR	-6.82	12	-1.53	0.0635	794	1.31
GOLGA7B	-8.34	18	-1.52	0.0637	795	1.31
NPEPPS	-8.34	18	-1.52	0.0637	796	1.31
POU2F1	-8.34	18	-1.52	0.0638	797	1.31
SAMD5	-7.61	15	-1.52	0.0638	798	1.31
MTF1	-8.34	18	-1.52	0.0639	799	1.31
ILF2	-7.61	15	-1.52	0.0639	800	1.31
ZNF623	-5.89	9	-1.52	0.0641	801	1.31
LYAR	-8.32	18	-1.52	0.0642	802	1.31
TSPAN17	-8.32	18	-1.52	0.0642	803	1.31
RNF175	-8.31	18	-1.52	0.0644	804	1.32
ZNF836	-4.8	6	-1.52	0.0646	805	1.32
CAMTA1	-8.3	18	-1.52	0.0647	806	1.32
RBM46	-8.3	18	-1.52	0.0648	807	1.32
ZNF366	-8.29	18	-1.51	0.065	808	1.32
CLEC4E	-6.77	12	-1.51	0.0651	809	1.32
RAB40C	-8.29	18	-1.51	0.0651	810	1.32
NDUFS7	-8.28	18	-1.51	0.0652	811	1.32
LRRTM2	-6.76	12	-1.51	0.0652	812	1.32
HARBI1	-8.28	18	-1.51	0.0652	813	1.32
NDUFB11	-8.28	18	-1.51	0.0653	814	1.32
FAM168A	-8.28	18	-1.51	0.0654	815	1.32
SLC46A3	-5.85	9	-1.51	0.0654	816	1.32
MCM3AP	-8.28	18	-1.51	0.0654	817	1.31
ZNF774	-8.28	18	-1.51	0.0654	818	1.31
PASD1	-8.27	18	-1.51	0.0655	819	1.31
NECAB3	-8.27	18	-1.51	0.0655	820	1.31
SMAP1	-8.27	18	-1.51	0.0655	821	1.31
BRF2	-7.55	15	-1.51	0.0655	822	1.31
CCP110	-8.27	18	-1.51	0.0656	823	1.31
HECTD1	-8.27	18	-1.51	0.0657	824	1.31
RFTN2	-8.26	18	-1.51	0.0657	825	1.31
HIST1H3F	-5.84	9	-1.51	0.0659	826	1.31
WHSC1	-8.25	18	-1.51	0.066	827	1.31
FBXO30	-7.53	15	-1.51	0.066	828	1.31
MTMR6	-8.25	18	-1.51	0.066	829	1.31
HLA-DMA	-8.25	18	-1.51	0.066	830	1.31
STAB2	-8.25	18	-1.51	0.0661	831	1.31
THYN1	-4.76	6	-1.51	0.0661	832	1.3
IARS	-8.25	18	-1.51	0.0661	833	1.3
VAV2	-8.25	18	-1.51	0.0662	834	1.3

DCBLD1	-8.25	18	-1.5	0.0662	835	1.3
P2RX3	-8.24	18	-1.5	0.0662	836	1.3
BAZ1A	-8.24	18	-1.5	0.0664	837	1.3
YRDC	-7	13	-1.5	0.0664	838	1.3
FFAR4	-8.24	18	-1.5	0.0664	839	1.3
HDAC3	-8.23	18	-1.5	0.0667	840	1.3
CEACAM8	-7.51	15	-1.5	0.0667	841	1.3
LGALS4	-8.23	18	-1.5	0.0667	842	1.3
PPP1R37	-8.22	18	-1.5	0.0668	843	1.3
BMP5	-8.22	18	-1.5	0.0668	844	1.3
EMC9	-7.51	15	-1.5	0.0668	845	1.3
PDGFC	-8.21	18	-1.5	0.067	846	1.3
MDFIC	-7.5	15	-1.5	0.067	847	1.3
TOR2A	-8.21	18	-1.5	0.0671	848	1.3
THUMPD2	-8.21	18	-1.5	0.0672	849	1.3
SCG5	-5.8	9	-1.5	0.0672	850	1.3
NABP2	-7.49	15	-1.5	0.0672	851	1.3
TYSND1	-8.21	18	-1.5	0.0673	852	1.3
CCNG2	-5.8	9	-1.5	0.0673	853	1.3
TNFAIP2	-8.2	18	-1.5	0.0674	854	1.3
FITM1	-8.2	18	-1.5	0.0674	855	1.29

Raji_Resistance						
GENE	**sumZ**	**numObs**	**normZ**	**pval_supp**	**rank_supp**	**fdr_supp**
TYMS	20.74	18	4.44	4.56E-06	1	0.0749
CAD	17.99	18	3.87	0.000054	2	0.443
ASF1A	15.72	18	3.41	0.000328	3	1.79
SLC25A32	12.82	12	3.4	0.000333	4	1.37
C10orf91	13.91	15	3.31	0.000469	5	1.54
MTHFD1L	14.48	18	3.15	0.00081	6	2.22
SHMT2	14.42	18	3.14	0.00084	7	1.97
APC2	13.99	18	3.05	0.00113	8	2.32
TCN1	9.52	9	2.95	0.00161	9	2.94
MTHFD2	9.43	9	2.92	0.00176	10	2.89
BAHD1	13.14	18	2.88	0.002	11	2.98
SBF1	13.08	18	2.87	0.00207	12	2.83
C9orf66	11.9	15	2.86	0.00214	13	2.71
TMEM56	7.5	6	2.85	0.0022	15	2.41
CCNO	12.99	18	2.85	0.0022	14	2.57
UPF3B	12.94	18	2.84	0.00227	16	2.33
ICMT	12.81	18	2.81	0.00247	17	2.39
GPR45	12.76	18	2.8	0.00254	18	2.32
PLAC9	7.34	6	2.79	0.00262	19	2.27
C15orf56	11.49	15	2.77	0.00284	20	2.33
ID3	11.42	15	2.75	0.00299	21	2.34
DYNC1I1	12.46	18	2.74	0.00308	23	2.2
UMPS	12.46	18	2.74	0.00308	22	2.3
GIMAP1	11.3	15	2.72	0.00324	24	2.22

PHGDH	12.08	18	2.66	0.0039	25	2.56
EXOSC1	6.95	6	2.65	0.004	26	2.52
C9orf53	10.71	15	2.59	0.00481	27	2.92
PI4KB	11.62	18	2.57	0.00513	29	2.91
PDYN	11.65	18	2.57	0.00504	28	2.96
ZBTB41	11.58	18	2.56	0.00525	32	2.69
PSTPIP2	11.59	18	2.56	0.00521	31	2.76
MAMDC2	11.6	18	2.56	0.00518	30	2.83
GCN1L1	11.49	18	2.54	0.00552	34	2.67
ARRB2	11.5	18	2.54	0.0055	33	2.74
REM1	11.06	17	2.52	0.00591	37	2.62
ERN2	11.4	18	2.52	0.00582	36	2.65
PHOX2B	11.41	18	2.52	0.00579	35	2.71
SPARC	11.32	18	2.51	0.00612	39	2.58
EXD2	11.32	18	2.51	0.00611	38	2.64
TYK2	11.31	18	2.5	0.00615	40	2.52
ANHX	11.22	18	2.49	0.00647	42	2.53
HSF1	11.25	18	2.49	0.00636	41	2.55
GLIS1	11.18	18	2.48	0.00663	48	2.27
TMEM74B	10.21	15	2.48	0.00662	47	2.31
AZU1	11.19	18	2.48	0.00659	46	2.35
IRF9	11.2	18	2.48	0.00656	45	2.39
GPI	11.21	18	2.48	0.00652	44	2.43
MAK16	11.22	18	2.48	0.00648	43	2.47
CASKIN2	11.12	18	2.47	0.00684	50	2.25
FIGLA	10.17	15	2.47	0.00676	49	2.27
RGL3	11.08	18	2.46	0.00703	53	2.18
ZNF768	10.12	15	2.46	0.00701	52	2.21
PIK3CD	11.09	18	2.46	0.00699	51	2.25
ZDHHC18	10.98	18	2.44	0.00741	55	2.21
TNPO1	8.99	12	2.44	0.0073	54	2.22
TTC24	10.95	18	2.43	0.00756	58	2.14
HOXA5	10.96	18	2.43	0.00752	57	2.17
FKBP2	10.97	18	2.43	0.00748	56	2.19
RING1	10.88	18	2.42	0.00786	60	2.15
CREBRF	10.92	18	2.42	0.0077	59	2.14
LHFPL5	10.83	18	2.41	0.00807	62	2.14
T	10.87	18	2.41	0.00791	61	2.13
REM2	10.78	18	2.4	0.00829	66	2.06
ST6GALNAC4	10.8	18	2.4	0.00822	65	2.08
SCML2	10.81	18	2.4	0.0082	64	2.1
MFHAS1	9.87	15	2.4	0.00814	63	2.12
SENP3	10.74	18	2.39	0.00848	69	2.02
TSC2	10.76	18	2.39	0.0084	68	2.03
FH	10.47	17	2.39	0.00833	67	2.04
SNAPC2	10.7	18	2.38	0.00871	71	2.02
USP13	10.71	18	2.38	0.00866	70	2.03
ADK	10.67	18	2.37	0.00882	72	2.01

CHMP7	10.6	18	2.36	0.00919	73	2.07
KIF15	10.55	18	2.35	0.00947	74	2.1
NUP85	9.58	15	2.34	0.00972	75	2.13
ZAR1L	9.54	15	2.33	0.01	80	2.05
RUNDC3A	10.46	18	2.33	0.0099	79	2.06
ADAM2	10.47	18	2.33	0.00988	78	2.08
PELO	10.48	18	2.33	0.00982	77	2.09
UTRN	10.48	18	2.33	0.0098	76	2.12
PDCL	10.39	18	2.32	0.0103	83	2.03
ITGB2	10.41	18	2.32	0.0102	82	2.04
KLF16	10.43	18	2.32	0.0101	81	2.04
EXOSC7	10.36	18	2.31	0.0105	84	2.05
DLK1	10.3	18	2.3	0.0108	85	2.09
BBX	10.28	18	2.29	0.011	86	2.09
ACOT11	10.21	18	2.28	0.0114	89	2.1
ANKRD54	10.23	18	2.28	0.0112	88	2.1
RAD9A	10.23	18	2.28	0.0112	87	2.12
HPS6	10.15	18	2.27	0.0117	92	2.1
STAT2	10.16	18	2.27	0.0117	91	2.1
FRYL	10.18	18	2.27	0.0116	90	2.11
ACP1	5.85	6	2.26	0.0119	94	2.08
HSD17B14	10.14	18	2.26	0.0118	93	2.09
ABCC10	10.06	18	2.25	0.0123	96	2.11
XKR3	5.82	6	2.25	0.0122	95	2.11
DLGAP2	10.01	18	2.24	0.0126	99	2.1
SYNGR1	10.03	18	2.24	0.0125	98	2.1
SYTL4	10.04	18	2.24	0.0124	97	2.1
SYNPO	9.92	18	2.22	0.0133	102	2.14
EFCAB12	9.65	17	2.22	0.0132	101	2.14
ZC3H6	9.94	18	2.22	0.0131	100	2.16
HDAC2	9.86	18	2.21	0.0137	108	2.08
MFN2	9.02	15	2.21	0.0136	107	2.08
MFSD10	9.88	18	2.21	0.0135	106	2.09
NSUN5	9.89	18	2.21	0.0134	105	2.1
NDE1	9.9	18	2.21	0.0134	104	2.12
LRRC10	9.9	18	2.21	0.0134	103	2.14
AAED1	6.92	9	2.19	0.0142	109	2.14
MICALL1	9.74	18	2.18	0.0146	110	2.18
TUB	9.66	18	2.17	0.0152	115	2.17
RETNLB	6.83	9	2.17	0.0152	114	2.18
AFF2	9.67	18	2.17	0.0151	113	2.2
SH3BGRL3	5.59	6	2.17	0.0151	112	2.21
METTL3	9.7	18	2.17	0.0149	111	2.2
ACTR1A	8.78	15	2.16	0.0156	119	2.15
ACTR10	8.78	15	2.16	0.0155	118	2.16
ETFB	9.64	18	2.16	0.0154	117	2.16
KRT19	7.88	12	2.16	0.0153	116	2.16
DPYSL2	9.57	18	2.15	0.0159	126	2.07

ANKRD34A	9.57	18	2.15	0.0159	125	2.09
PROSC	9.58	18	2.15	0.0158	124	2.1
CACNG1	9.58	18	2.15	0.0158	123	2.11
ZNF44	5.53	6	2.15	0.0158	122	2.13
SLC1A7	9.6	18	2.15	0.0157	121	2.12
ADIPOR2	9.61	18	2.15	0.0156	120	2.13
REEP6	8.65	15	2.13	0.0166	128	2.14
PDXK	9.49	18	2.13	0.0165	127	2.14
LYN	9.42	18	2.12	0.0172	132	2.14
OR6K2	7.69	12	2.12	0.0172	131	2.16
VAV1	9.42	18	2.12	0.0172	130	2.17
NGF	8.62	15	2.12	0.017	129	2.16
CYP2C18	7.66	12	2.11	0.0175	135	2.12
C7orf43	9.39	18	2.11	0.0174	134	2.14
SYCE1L	7.68	12	2.11	0.0173	133	2.13
GRPEL1	9.35	18	2.1	0.0178	136	2.15
SDHD	5.35	6	2.09	0.0185	140	2.17
GABARAPL2	9.28	18	2.09	0.0184	139	2.18
CEP192	9.29	18	2.09	0.0183	138	2.18
VWA3A	9.3	18	2.09	0.0183	137	2.19
KIAA1958	9.24	18	2.08	0.0188	142	2.18
CSAD	9.25	18	2.08	0.0187	141	2.18
APBB1	9.17	18	2.07	0.0194	145	2.2
UROS	8.37	15	2.07	0.0194	144	2.22
KPTN	9.2	18	2.07	0.0192	143	2.2
AHCY	6.82	10	2.06	0.0197	147	2.2
MGAT3	8.36	15	2.06	0.0196	146	2.21
C14orf93	9.08	18	2.05	0.0203	150	2.23
FAM135A	9.09	18	2.05	0.0202	149	2.23
CCL5	8.31	15	2.05	0.0201	148	2.23
MUC2	9.03	18	2.04	0.0209	155	2.21
CD300E	9.03	18	2.04	0.0209	154	2.22
ARHGEF15	9.04	18	2.04	0.0208	153	2.23
FCRL3	9.07	18	2.04	0.0205	152	2.21
ZCCHC7	5.24	6	2.04	0.0204	151	2.22
PRKAB2	8.98	18	2.03	0.0214	163	2.16
SYPL2	8.98	18	2.03	0.0214	162	2.17
MS4A8	8.98	18	2.03	0.0214	161	2.18
PRDM4	8.99	18	2.03	0.0213	160	2.18
KLHDC8A	9	18	2.03	0.0212	159	2.19
HDAC8	9	18	2.03	0.0212	158	2.2
C4orf50	9	18	2.03	0.0212	157	2.21
HAP1	9.01	18	2.03	0.0211	156	2.22
CSNK1A1	7.29	12	2.02	0.0219	169	2.13
DHX15	8.94	18	2.02	0.0218	168	2.14
MYBL1	8.17	15	2.02	0.0218	167	2.14
USP22	8.96	18	2.02	0.0216	166	2.14
PAXIP1	8.96	18	2.02	0.0216	165	2.15

ATXN1L	8.96	18	2.02	0.0216	164	2.16
STAT1	8.88	18	2.01	0.0225	175	2.11
HORMAD2	7.25	12	2.01	0.0225	174	2.12
PRMT1	8.88	18	2.01	0.0224	173	2.13
PKP4	8.89	18	2.01	0.0224	172	2.14
FAM221B	8.89	18	2.01	0.0223	171	2.14
B4GALNT4	8.9	18	2.01	0.0223	170	2.15
PPP1R26	7.22	12	2	0.0229	183	2.06
LCP1	8.85	18	2	0.0228	182	2.05
KIAA0195	8.86	18	2	0.0227	181	2.06
KLHL32	8.86	18	2	0.0227	180	2.07
TUBGCP2	8.86	18	2	0.0226	179	2.08
SPATA20	8.87	18	2	0.0226	178	2.08
PARD6A	8.87	18	2	0.0225	177	2.09
CARNS1	8.88	18	2	0.0225	176	2.1
MUC22	8.79	18	1.99	0.0235	187	2.06
TMEM246	8.03	15	1.99	0.0234	186	2.07
FBXO41	8.8	18	1.99	0.0234	185	2.08
DBI	8.8	18	1.99	0.0233	184	2.08
TARS	8.25	16	1.98	0.0239	191	2.06
CLEC1A	8.76	18	1.98	0.0239	190	2.06
TSR3	8.76	18	1.98	0.0238	189	2.07
GALE	8.76	18	1.98	0.0238	188	2.08
GLO1	5.02	6	1.97	0.0246	201	2.01
NPM3	8.69	18	1.97	0.0246	200	2.02
TAF1A	8.7	18	1.97	0.0245	199	2.02
PJA1	8.71	18	1.97	0.0244	198	2.03
TNFSF13B	7.95	15	1.97	0.0244	197	2.03
BCAP31	7.95	15	1.97	0.0244	196	2.04
GAD2	8.71	18	1.97	0.0243	195	2.05
ASIC4	8.71	18	1.97	0.0243	194	2.06
C16orf58	8.72	18	1.97	0.0243	193	2.06
ZSWIM7	5.04	6	1.97	0.0242	192	2.07
C1orf210	7.05	12	1.96	0.0253	211	1.97
CPNE3	8.64	18	1.96	0.0252	210	1.97
C8orf17	7.9	15	1.96	0.025	209	1.97
CSMD2	8.66	18	1.96	0.025	208	1.98
TFF1	8.66	18	1.96	0.025	207	1.98
YEATS2	8.66	18	1.96	0.025	206	1.99
MUC17	8.66	18	1.96	0.0249	205	2
KRT79	8.67	18	1.96	0.0249	204	2
JAK1	8.68	18	1.96	0.0248	203	2.01
PTPRZ1	8.68	18	1.96	0.0248	202	2.01
KIAA1257	8.6	18	1.95	0.0258	214	1.98
GFRA2	8.6	18	1.95	0.0257	213	1.98
CDR1	6.09	9	1.95	0.0255	212	1.98
EIF2B2	7.81	15	1.94	0.0263	218	1.98
POLA1	7.82	15	1.94	0.0261	217	1.98

ZBTB39	7.83	15	1.94	0.026	216	1.98
TBXA2R	8.58	18	1.94	0.026	215	1.98
KIF21B	8.49	18	1.93	0.0271	227	1.96
NEURL4	8.49	18	1.93	0.0271	226	1.97
RNFT2	8.51	18	1.93	0.0268	225	1.95
IQCF6	6.95	12	1.93	0.0268	224	1.96
OLIG1	8.52	18	1.93	0.0267	223	1.97
HOXB5	8.52	18	1.93	0.0267	222	1.98
LRRC38	8.52	18	1.93	0.0267	221	1.98
OR6M1	6.03	9	1.93	0.0266	220	1.98
ATP6V1B1	8.53	18	1.93	0.0265	219	1.99
GDPD1	6.9	12	1.92	0.0276	236	1.92
DDX51	8.45	18	1.92	0.0276	235	1.93
HIPK1	8.45	18	1.92	0.0276	234	1.93
SLC6A4	8.46	18	1.92	0.0275	233	1.94
PLEKHG5	8.46	18	1.92	0.0275	232	1.95
UNC13D	8.46	18	1.92	0.0275	231	1.95
XIRP2	8.46	18	1.92	0.0275	230	1.96
GTSE1	8.48	18	1.92	0.0272	229	1.95
ICOSLG	8.48	18	1.92	0.0272	228	1.96
PSG5	4.85	6	1.91	0.0283	241	1.93
ITPRIPL2	7.67	15	1.91	0.0282	240	1.93
IL20RB	8.41	18	1.91	0.0282	239	1.94
NELL2	8.41	18	1.91	0.0281	238	1.94
HYAL4	7.69	15	1.91	0.0279	237	1.94
SPAG5	8.34	18	1.9	0.029	246	1.94
GPC3	8.34	18	1.9	0.029	245	1.94
RRAGC	7.63	15	1.9	0.0288	244	1.94
AIRE	8.38	18	1.9	0.0285	243	1.93
RFX7	8.39	18	1.9	0.0284	242	1.93
ANK2	8.29	18	1.89	0.0297	248	1.97
SERPINF1	8.34	18	1.89	0.0291	247	1.93
GUCA2B	6.73	12	1.88	0.0304	263	1.9
NDP	5.83	9	1.88	0.0304	262	1.9
COL4A3	8.24	18	1.88	0.0304	261	1.91
ITGBL1	8.25	18	1.88	0.0304	260	1.92
CST9L	5.84	9	1.88	0.0303	259	1.92
SLC45A3	8.25	18	1.88	0.0303	258	1.93
MFSD12	8.26	18	1.88	0.0302	257	1.93
LMTK2	8.26	18	1.88	0.0302	256	1.94
KEAP1	8.26	18	1.88	0.0302	255	1.94
KCNJ12	6.75	12	1.88	0.0301	254	1.95
TCF24	5.84	9	1.88	0.0301	253	1.95
POLR2L	7.03	13	1.88	0.0301	252	1.96
NPRL2	8.27	18	1.88	0.03	251	1.96
KIAA1967	8.28	18	1.88	0.0298	250	1.96
GART	8.29	18	1.88	0.0297	249	1.96
CYP26C1	8.2	18	1.87	0.031	270	1.89

HTRA2	8.21	18	1.87	0.0308	269	1.88
RANGAP1	8.21	18	1.87	0.0308	268	1.89
C1QL3	7.51	15	1.87	0.0307	267	1.89
EIF4B	5.82	9	1.87	0.0306	266	1.89
TACC1	8.24	18	1.87	0.0305	265	1.89
GSKIP	6.73	12	1.87	0.0304	264	1.89
DUS3L	8.15	18	1.86	0.0317	285	1.83
ATAD2	8.15	18	1.86	0.0317	284	1.83
CDIPT	8.16	18	1.86	0.0316	283	1.83
SOX9	8.16	18	1.86	0.0316	282	1.84
CNEP1R1	7.45	15	1.86	0.0315	281	1.84
NPPA	7.45	15	1.86	0.0315	280	1.85
ZNF449	7.94	17	1.86	0.0315	279	1.85
SELPLG	7.46	15	1.86	0.0315	278	1.86
PTPRC	8.18	18	1.86	0.0314	277	1.86
SURF4	8.18	18	1.86	0.0314	276	1.87
PRG3	7.47	15	1.86	0.0313	275	1.87
C9orf139	8.18	18	1.86	0.0313	274	1.87
DUSP27	8.18	18	1.86	0.0313	273	1.88
RTN4RL2	8.19	18	1.86	0.0312	272	1.88
ZSCAN30	8.19	18	1.86	0.0311	271	1.88
GCM2	8.1	18	1.85	0.0325	295	1.81
JPH1	8.1	18	1.85	0.0325	294	1.81
TTR	8.11	18	1.85	0.0324	293	1.81
GALR1	8.11	18	1.85	0.0324	292	1.82
PPP1R27	8.11	18	1.85	0.0324	291	1.83
KRTAP19-1	4.68	6	1.85	0.0323	290	1.83
PDE6B	8.13	18	1.85	0.032	289	1.82
ARHGEF1	8.14	18	1.85	0.0319	288	1.82
GTSF1	8.14	18	1.85	0.0319	287	1.82
CA9	8.14	18	1.85	0.0318	286	1.83
PROM1	8.05	18	1.84	0.0332	304	1.8
FGF11	8.06	18	1.84	0.0331	303	1.8
HDAC4	8.06	18	1.84	0.0331	302	1.8
FGF9	8.07	18	1.84	0.033	301	1.8
WRB	8.07	18	1.84	0.0329	300	1.8
DAZAP2	5.71	9	1.84	0.0329	299	1.81
ST3GAL4	8.08	18	1.84	0.0327	298	1.8
IPO8	8.09	18	1.84	0.0327	297	1.81
YAE1D1	6.61	12	1.84	0.0326	296	1.81
CXXC1	8.01	18	1.83	0.0338	316	1.75
MAPK1	8.02	18	1.83	0.0338	315	1.76
IKZF5	7.32	15	1.83	0.0337	314	1.76
DUSP8	7.33	15	1.83	0.0336	313	1.76
MMP17	8.03	18	1.83	0.0335	312	1.76
WNT3A	8.03	18	1.83	0.0335	311	1.77
PCSK9	8.03	18	1.83	0.0335	310	1.77
SUN1	8.04	18	1.83	0.0335	309	1.78

TIMP2	8.04	18	1.83	0.0334	308	1.78
ASB13	8.04	18	1.83	0.0334	307	1.78
SIGLEC1	8.04	18	1.83	0.0333	306	1.79
EOMES	8.05	18	1.83	0.0333	305	1.79
CHRM1	7.96	18	1.82	0.0346	321	1.77
YAP1	7.27	15	1.82	0.0345	320	1.77
TSSC4	7.27	15	1.82	0.0345	319	1.78
TRIM10	7.98	18	1.82	0.0344	318	1.77
PI4KA	8	18	1.82	0.0341	317	1.76
CPS1	7.9	18	1.81	0.0355	328	1.78
PIEZO2	7.91	18	1.81	0.0354	327	1.78
GLMN	5.6	9	1.81	0.0353	326	1.78
GPN1	7.47	16	1.81	0.0352	325	1.78
RGL2	7.94	18	1.81	0.035	324	1.77
HADH	7.95	18	1.81	0.0348	323	1.77
DHX29	7.95	18	1.81	0.0348	322	1.78
NUAK2	7.85	18	1.8	0.0363	335	1.78
GJD2	7.19	15	1.8	0.036	334	1.77
TTLL12	7.87	18	1.8	0.036	333	1.78
GPBP1	7.88	18	1.8	0.0359	332	1.78
HS3ST3B1	7.2	15	1.8	0.0358	331	1.78
ZNF259	6.71	13	1.8	0.0357	330	1.78
HERC6	7.9	18	1.8	0.0356	329	1.78
TM7SF2	7.81	18	1.79	0.037	348	1.75
C14orf166	4.51	6	1.79	0.037	347	1.75
DNAAF3	7.82	18	1.79	0.0369	346	1.75
CCDC37	7.82	18	1.79	0.0369	345	1.75
CCBP2	6.39	12	1.79	0.0368	344	1.76
RAE1	7.61	17	1.79	0.0368	343	1.76
SOX18	7.83	18	1.79	0.0367	342	1.76
BANP	7.83	18	1.79	0.0367	341	1.76
MX1	7.83	18	1.79	0.0366	340	1.77
GSG2	7.84	18	1.79	0.0366	339	1.77
B9D2	7.84	18	1.79	0.0366	338	1.78
NOB1	5.23	8	1.79	0.0365	337	1.78
RBBP4	5.54	9	1.79	0.0365	336	1.78
ALOXE3	7.76	18	1.78	0.0379	362	1.72
PRPF4B	7.55	17	1.78	0.0378	361	1.72
KCTD6	7.09	15	1.78	0.0377	360	1.72
PIWIL3	7.77	18	1.78	0.0377	359	1.72
CDH22	7.77	18	1.78	0.0377	358	1.73
C20orf196	5.5	9	1.78	0.0376	357	1.73
SAP18	4.49	6	1.78	0.0376	356	1.73
CHST3	7.1	15	1.78	0.0375	355	1.74
TSPO	7.78	18	1.78	0.0375	354	1.74
IFRD1	6.36	12	1.78	0.0374	353	1.74
OLFML2A	7.79	18	1.78	0.0374	352	1.74
TANGO6	7.79	18	1.78	0.0374	351	1.75

SPP1	7.11	15	1.78	0.0373	350	1.75
SFMBT2	7.8	18	1.78	0.0373	349	1.75
TCF4	7.71	18	1.77	0.0388	370	1.72
METTL21B	7.73	18	1.77	0.0384	369	1.71
SLC39A8	5.47	9	1.77	0.0383	368	1.71
LDLRAD3	7.74	18	1.77	0.0382	367	1.71
RRP1	7.74	18	1.77	0.0382	366	1.71
SCRG1	5.48	9	1.77	0.0381	365	1.72
TMEM99	5.48	9	1.77	0.0381	364	1.72
RNF146	7.76	18	1.77	0.038	363	1.72
LRRN4CL	6.99	15	1.76	0.0396	379	1.72
PCNXL3	7.66	18	1.76	0.0396	378	1.72
FXR2	7.67	18	1.76	0.0394	377	1.72
TUBAL3	7.67	18	1.76	0.0394	376	1.72
SLC44A3	7.68	18	1.76	0.0393	375	1.72
FLI1	7.68	18	1.76	0.0392	374	1.72
TK1	7.69	18	1.76	0.0391	373	1.72
RRP36	7.69	18	1.76	0.0391	372	1.72
MT2A	4.45	6	1.76	0.0388	371	1.72
SNCG	4.4	6	1.75	0.0404	394	1.68
MARVELD3	7.62	18	1.75	0.0404	393	1.69
GAST	5.39	9	1.75	0.0404	392	1.69
RPP30	6.96	15	1.75	0.0403	391	1.69
TAC4	4.4	6	1.75	0.0402	390	1.69
AIPL1	7.62	18	1.75	0.0402	389	1.7
MAGEB5	4.4	6	1.75	0.0402	388	1.7
TARBP2	7.63	18	1.75	0.0402	387	1.7
OR2AP1	4.41	6	1.75	0.0401	386	1.71
RSPRY1	7.63	18	1.75	0.0401	385	1.71
SMG5	7.63	18	1.75	0.0401	384	1.71
FAM71F2	7.64	18	1.75	0.04	383	1.72
ARHGAP15	6.25	12	1.75	0.0398	382	1.71
CHMP2A	7.65	18	1.75	0.0397	381	1.71
CASKIN1	7.65	18	1.75	0.0397	380	1.72
TCTE3	6.9	15	1.74	0.0413	405	1.68
SSFA2	7.57	18	1.74	0.0413	404	1.68
UNK	7.57	18	1.74	0.0413	403	1.68
SMO	7.57	18	1.74	0.0412	402	1.68
C1orf123	7.58	18	1.74	0.0411	401	1.68
ZDHHC12	7.58	18	1.74	0.041	400	1.68
SFXN1	6.93	15	1.74	0.0408	399	1.68
CDC42EP4	7.59	18	1.74	0.0408	398	1.68
POU3F4	7.6	18	1.74	0.0407	397	1.68
ALDH5A1	7.6	18	1.74	0.0406	396	1.68
RASSF2	7.61	18	1.74	0.0405	395	1.68
CLSTN2	7.52	18	1.73	0.0421	416	1.66
DDX54	6.88	15	1.73	0.0418	415	1.65
TBCCD1	6.88	15	1.73	0.0418	414	1.66

HGSNAT	7.54	18	1.73	0.0418	413	1.66
FCF1	4.35	6	1.73	0.0418	412	1.66
CATSPER1	7.54	18	1.73	0.0418	411	1.67
POU3F3	6.88	15	1.73	0.0417	410	1.67
C16orf74	7.54	18	1.73	0.0417	409	1.67
C12orf68	6.88	15	1.73	0.0417	408	1.68
NLRP10	7.55	18	1.73	0.0416	407	1.68
CALHM1	7.55	18	1.73	0.0415	406	1.68
ZNF500	7.48	18	1.72	0.0429	426	1.66
ARMC7	7.48	18	1.72	0.0429	425	1.66
PAM16	7.48	18	1.72	0.0428	424	1.66
INTS3	6.84	15	1.72	0.0427	423	1.66
ARHGEF17	7.49	18	1.72	0.0427	422	1.66
MYH7	7.49	18	1.72	0.0426	421	1.66
CORO1C	7.5	18	1.72	0.0424	420	1.66
ANAPC5	7.5	18	1.72	0.0424	419	1.66
CCDC120	7.51	18	1.72	0.0424	418	1.66
ALDH2	7.51	18	1.72	0.0423	417	1.67
MGAM	7.42	18	1.71	0.044	434	1.66
FARSB	7.01	16	1.71	0.0436	433	1.65
FBXO42	7.44	18	1.71	0.0436	432	1.66
THSD7B	6.79	15	1.71	0.0436	431	1.66
PCDH10	7.45	18	1.71	0.0434	430	1.66
DNAJB2	7.45	18	1.71	0.0434	429	1.66
DHX33	6.8	15	1.71	0.0434	428	1.67
FRMD4B	7.45	18	1.71	0.0434	427	1.67
MUL1	7.37	18	1.7	0.045	447	1.65
TSPAN5	6.02	12	1.7	0.0449	446	1.65
BTK	7.37	18	1.7	0.0449	445	1.66
SULF2	7.38	18	1.7	0.0448	444	1.66
SIAH1	6.74	15	1.7	0.0448	443	1.66
CDH7	7.38	18	1.7	0.0447	442	1.66
KRT13	7.39	18	1.7	0.0447	441	1.66
PIGW	6.75	15	1.7	0.0446	440	1.66
METAP1D	7.39	18	1.7	0.0445	439	1.66
PAN2	7.4	18	1.7	0.0443	438	1.66
PRKRIP1	7.41	18	1.7	0.0443	437	1.66
CSTB	6.76	15	1.7	0.0442	436	1.67
TADA3	7.41	18	1.7	0.0442	435	1.67
PIP5K1A	5.18	9	1.69	0.0459	457	1.65
HABP4	7.32	18	1.69	0.0459	456	1.65
TSPAN14	7.33	18	1.69	0.0458	455	1.65
KIAA1239	6.69	15	1.69	0.0458	454	1.66
PPIE	6.69	15	1.69	0.0458	453	1.66
C6orf89	7.34	18	1.69	0.0456	452	1.66
SNRNP25	7.35	18	1.69	0.0454	451	1.65
DNASE1L1	7.35	18	1.69	0.0453	450	1.65
TLR6	5.2	9	1.69	0.0453	449	1.66

PGAP2	7.35	18	1.69	0.0452	448	1.66
GDI1	7.27	18	1.68	0.0469	468	1.65
DEFB126	5.14	9	1.68	0.0469	467	1.65
TBC1D21	7.27	18	1.68	0.0469	466	1.65
CHADL	7.28	18	1.68	0.0468	465	1.65
ADAP1	7.28	18	1.68	0.0468	464	1.66
C1QTNF6	7.28	18	1.68	0.0467	463	1.66
KCNC1	7.29	18	1.68	0.0466	462	1.66
BRIX1	4.21	6	1.68	0.0465	461	1.66
PAMR1	7.3	18	1.68	0.0463	460	1.65
FGF8	7.31	18	1.68	0.0461	459	1.65
GNA15	7.31	18	1.68	0.0461	458	1.65
CYB5R1	7.22	18	1.67	0.0479	481	1.64
FADS3	7.23	18	1.67	0.0478	480	1.64
NSUN7	7.23	18	1.67	0.0478	479	1.64
SGOL1	4.17	6	1.67	0.0477	478	1.64
ZBTB38	7.23	18	1.67	0.0477	477	1.64
AIFM1	7.23	18	1.67	0.0477	476	1.65
ELF3	7.24	18	1.67	0.0476	475	1.64
SNAP23	7.25	18	1.67	0.0474	474	1.64
IRF8	7.25	18	1.67	0.0473	473	1.64
KCNK12	7.25	18	1.67	0.0473	472	1.64
APOL1	6.62	15	1.67	0.0472	471	1.65
UPF1	6.62	15	1.67	0.0472	470	1.65
EHD1	7.26	18	1.67	0.0471	469	1.65
BUB1B	7.17	18	1.66	0.0489	495	1.62
KISS1	4.15	6	1.66	0.0488	494	1.62
PLCG2	7.18	18	1.66	0.0488	493	1.62
NUP93	6.98	17	1.66	0.0487	492	1.63
HBEGF	7.18	18	1.66	0.0487	491	1.63
GALNT14	7.18	18	1.66	0.0487	490	1.63
SEC24C	7.2	18	1.66	0.0484	489	1.62
EIF1B	5.09	9	1.66	0.0483	488	1.63
AGO4	7.21	18	1.66	0.0482	487	1.62
SH3TC1	7.21	18	1.66	0.0482	486	1.63
FAM26E	7.21	18	1.66	0.0481	485	1.63
TSHZ1	7.21	18	1.66	0.0481	484	1.63
RAVER2	7.22	18	1.66	0.048	483	1.63
C17orf77	5.89	12	1.66	0.048	482	1.63
HDHD3	7.15	18	1.65	0.0494	500	1.62
MAG	7.15	18	1.65	0.0493	499	1.62
TMEM97	4.13	6	1.65	0.0493	498	1.63
MGST3	5.84	12	1.65	0.0492	497	1.63
REPIN1	7.16	18	1.65	0.0492	496	1.63
BEND3	7.08	18	1.64	0.0509	523	1.6
LCN10	7.08	18	1.64	0.0508	522	1.6
STYX	4.09	6	1.64	0.0508	521	1.6
HRAS	7.09	18	1.64	0.0507	520	1.6

NPC1	7.09	18	1.64	0.0507	519	1.6
KAL1	7.09	18	1.64	0.0506	518	1.61
SIGIRR	7.09	18	1.64	0.0506	517	1.61
TRPV1	7.09	18	1.64	0.0506	516	1.61
ENGASE	7.09	18	1.64	0.0506	515	1.61
FGFRL1	7.1	18	1.64	0.0505	514	1.61
MARCKSL1	5.79	12	1.64	0.0505	513	1.62
ECE2	7.1	18	1.64	0.0505	512	1.62
GNAT1	7.1	18	1.64	0.0504	511	1.62
CYP1B1	7.1	18	1.64	0.0504	510	1.62
PEG10	6.48	15	1.64	0.0504	509	1.63
FBXO43	6.49	15	1.64	0.0503	508	1.63
GPR12	7.11	18	1.64	0.0503	507	1.63
LMTK3	7.11	18	1.64	0.0503	506	1.63
CSMD1	7.11	18	1.64	0.0502	505	1.63
TRAPPC1	6.92	17	1.64	0.0501	504	1.63
ATP6AP1	7.12	18	1.64	0.0501	503	1.63
DNAJC21	7.12	18	1.64	0.0501	502	1.64
YIPF5	4.11	6	1.64	0.05	501	1.64
TAF2	6.63	16	1.63	0.052	532	1.6
PIK3IP1	7.03	18	1.63	0.0519	531	1.61
RELT	7.04	18	1.63	0.0518	530	1.6
ZNF180	7.04	18	1.63	0.0516	529	1.6
SUV39H2	4.07	6	1.63	0.0515	528	1.6
AZIN1	4.99	9	1.63	0.0515	527	1.6
GNAT3	5.76	12	1.63	0.0515	526	1.61
MRPS14	6.66	16	1.63	0.0511	525	1.6
ZNF592	7.07	18	1.63	0.0511	524	1.6
ELOVL3	5.71	12	1.62	0.0529	541	1.61
GJB1	5.71	12	1.62	0.0528	540	1.61
PMP22	6.99	18	1.62	0.0528	539	1.61
PTGIS	7	18	1.62	0.0526	538	1.6
GABRQ	7	18	1.62	0.0525	537	1.61
FIBCD1	7	18	1.62	0.0525	536	1.61
QPCT	7.01	18	1.62	0.0524	535	1.61
ZNF516	7.02	18	1.62	0.0522	534	1.61
TADA1	6.41	15	1.62	0.0522	533	1.61
C18orf8	6.93	18	1.61	0.0542	554	1.61
SMARCE1	4	6	1.61	0.0542	553	1.61
STK33	4	6	1.61	0.0542	552	1.61
CES4A	6.93	18	1.61	0.0542	551	1.61
KHSRP	6.93	18	1.61	0.0541	550	1.62
KRT16	4	6	1.61	0.0541	549	1.62
ZNF646	6.34	15	1.61	0.0539	548	1.61
CLTA	6.94	18	1.61	0.0538	547	1.62
FAM178B	6.96	18	1.61	0.0534	546	1.61
RPS2	4.02	6	1.61	0.0534	545	1.61
PLEKHG1	6.97	18	1.61	0.0533	544	1.61

MMP2	6.97	18	1.61	0.0532	543	1.61
DDX58	6.97	18	1.61	0.0532	542	1.61
UBP1	6.88	18	1.6	0.0553	567	1.6
PSMD6	6.88	18	1.6	0.0552	566	1.6
ZNF165	6.9	18	1.6	0.0548	565	1.59
UNKL	6.9	18	1.6	0.0548	564	1.59
MYOM1	6.9	18	1.6	0.0547	563	1.6
SELE	6.91	18	1.6	0.0547	562	1.6
CHST4	6.91	18	1.6	0.0547	561	1.6
EFTUD1	6.91	18	1.6	0.0546	560	1.6
ACTL7A	6.32	15	1.6	0.0544	559	1.6
SEC31B	6.92	18	1.6	0.0544	558	1.6
ARMC12	5.88	13	1.6	0.0544	557	1.6
CHUK	6.92	18	1.6	0.0544	556	1.61
PLOD3	6.92	18	1.6	0.0543	555	1.61
MBTPS2	6.84	18	1.59	0.0562	580	1.59
MAML3	6.85	18	1.59	0.0561	579	1.59
LCP2	6.85	18	1.59	0.056	578	1.59
ARHGAP8	6.85	18	1.59	0.0559	577	1.59
SLC26A11	6.85	18	1.59	0.0559	576	1.59
AMER2	6.86	18	1.59	0.0557	575	1.59
FBXO10	6.87	18	1.59	0.0556	574	1.59
ELMOD3	6.87	18	1.59	0.0555	573	1.59
BST2	6.27	15	1.59	0.0555	572	1.59
PDPK1	6.27	15	1.59	0.0555	571	1.6
ZNF677	4.86	9	1.59	0.0554	570	1.6
PAPSS1	6.87	18	1.59	0.0554	569	1.6
PCID2	6.68	17	1.59	0.0554	568	1.6
PSAP	6.78	18	1.58	0.0576	593	1.6
PDE7B	6.78	18	1.58	0.0575	592	1.6
MC5R	6.2	15	1.58	0.0574	591	1.6
FOXE3	4.8	9	1.58	0.0574	590	1.6
SCAMP4	6.79	18	1.58	0.0574	589	1.6
CCDC71L	6.2	15	1.58	0.0573	588	1.6
POLR3GL	6.8	18	1.58	0.0573	587	1.6
FRS3	6.8	18	1.58	0.0572	586	1.6
PDK2	6.81	18	1.58	0.057	585	1.6
TMC1	6.81	18	1.58	0.057	584	1.6
HERC5	6.81	18	1.58	0.0568	583	1.6
EFCAB4B	6.82	18	1.58	0.0566	582	1.6
DACT1	6.83	18	1.58	0.0565	581	1.6
DGKA	6.73	18	1.57	0.0587	609	1.58
NBR1	6.73	18	1.57	0.0587	608	1.59
ATAD5	6.74	18	1.57	0.0587	607	1.59
RAB39B	6.74	18	1.57	0.0586	606	1.59
GFER	5.94	14	1.57	0.0586	605	1.59
SMC3	6.74	18	1.57	0.0585	604	1.59
PIGL	6.74	18	1.57	0.0585	603	1.59

SRD5A1	4.77	9	1.57	0.0583	602	1.59
NUCB2	6.16	15	1.57	0.0583	601	1.59
COPS7B	6.77	18	1.57	0.0579	600	1.58
YPEL2	4.79	9	1.57	0.0579	599	1.59
DLX3	6.38	16	1.57	0.0578	598	1.59
MIOS	6.77	18	1.57	0.0578	597	1.59
LGALS12	6.77	18	1.57	0.0578	596	1.59
OARD1	3.91	6	1.57	0.0577	595	1.59
CDC45	6.78	18	1.57	0.0576	594	1.59
SGK2	6.68	18	1.56	0.0599	625	1.58
DENND4B	6.69	18	1.56	0.0598	624	1.57
HOXC12	6.69	18	1.56	0.0598	623	1.57
STAT4	6.69	18	1.56	0.0597	622	1.58
SLC39A13	6.69	18	1.56	0.0597	621	1.58
C1QTNF8	6.69	18	1.56	0.0597	620	1.58
CST3	6.11	15	1.56	0.0596	619	1.58
TMED4	6.71	18	1.56	0.0594	618	1.58
FAM5B	6.71	18	1.56	0.0594	617	1.58
C1orf95	6.71	18	1.56	0.0593	616	1.58
IL4I1	6.71	18	1.56	0.0592	615	1.58
KIAA0355	6.72	18	1.56	0.0592	614	1.58
FAM124B	6.72	18	1.56	0.0592	613	1.58
IL17RB	6.72	18	1.56	0.059	612	1.58
FAM149B1	6.72	18	1.56	0.059	611	1.58
OR10C1	4.76	9	1.56	0.0588	610	1.58
CDC42BPG	6.64	18	1.55	0.061	639	1.57
SLC22A1	6.64	18	1.55	0.061	638	1.57
RAPGEF5	6.65	18	1.55	0.0609	637	1.57
EAF2	4.7	9	1.55	0.0608	636	1.57
KCNE1	5.43	12	1.55	0.0606	635	1.57
MTSS1	6.66	18	1.55	0.0606	634	1.57
BAHCC1	6.66	18	1.55	0.0606	633	1.57
SUPT3H	4.71	9	1.55	0.0604	632	1.57
PLEKHF1	6.67	18	1.55	0.0602	631	1.57
TRAK1	6.68	18	1.55	0.0601	630	1.57
ORAOV1	4.98	10	1.55	0.0601	629	1.57
SLC12A3	6.68	18	1.55	0.0601	628	1.57
TGFBR3	6.68	18	1.55	0.0601	627	1.57
ASIC3	6.68	18	1.55	0.06	626	1.57
GJA3	6.01	15	1.54	0.0623	658	1.55
PRR19	6.02	15	1.54	0.0623	657	1.56
ABHD3	6.59	18	1.54	0.0623	656	1.56
ABHD17A	3.81	6	1.54	0.0622	655	1.56
ZNF518B	6.02	15	1.54	0.0621	654	1.56
CTCF	6.6	18	1.54	0.062	653	1.56
ELAVL2	6.6	18	1.54	0.0619	652	1.56
MBNL1	6.6	18	1.54	0.0619	651	1.56
GCH1	6.03	15	1.54	0.0618	650	1.56

C6orf170	6.62	18	1.54	0.0616	649	1.56
ERC2	6.62	18	1.54	0.0616	648	1.56
ANKRD6	6.62	18	1.54	0.0616	647	1.56
MOBP	6.05	15	1.54	0.0615	646	1.56
C2orf71	6.62	18	1.54	0.0614	645	1.56
APBA1	6.62	18	1.54	0.0614	644	1.57
RILPL1	6.62	18	1.54	0.0614	643	1.57
SOGA1	6.63	18	1.54	0.0613	642	1.57
ENG	6.05	15	1.54	0.0613	641	1.57
SORCS2	6.63	18	1.54	0.0613	640	1.57
LRRC3B	4.62	9	1.53	0.0635	672	1.55
GTF2A1	6.18	16	1.53	0.0632	671	1.55
TMEM109	6.56	18	1.53	0.0631	670	1.55
ASPHD2	6.56	18	1.53	0.0629	669	1.54
ADAMTSL2	6.57	18	1.53	0.0628	668	1.54
SLC7A13	6	15	1.53	0.0628	667	1.55
BMP6	6.57	18	1.53	0.0628	666	1.55
HOXC5	6.57	18	1.53	0.0628	665	1.55
LPIN1	6.57	18	1.53	0.0626	664	1.55
SUCLG2	4.65	9	1.53	0.0626	663	1.55
EDN1	5.37	12	1.53	0.0626	662	1.55
EFCAB13	3.8	6	1.53	0.0626	661	1.55
ZMYM3	6.58	18	1.53	0.0626	660	1.56
NTF4	6.58	18	1.53	0.0625	659	1.56
CTAG2	3.75	6	1.52	0.0648	685	1.55
GK	5.3	12	1.52	0.0648	684	1.55
KLHL29	6.5	18	1.52	0.0646	683	1.55
RNF10	6.51	18	1.52	0.0644	682	1.55
NEBL	6.51	18	1.52	0.0644	681	1.55
IL1R1	6.51	18	1.52	0.0642	680	1.55
CNTNAP1	6.52	18	1.52	0.0641	679	1.55
CHDH	6.52	18	1.52	0.064	678	1.55
DCST2	6.52	18	1.52	0.0639	677	1.55
C14orf142	5.33	12	1.52	0.0639	676	1.55
RAD54L	6.53	18	1.52	0.0638	675	1.55
MFSD2A	6.53	18	1.52	0.0637	674	1.55
HIST1H2BO	3.77	6	1.52	0.0636	673	1.55
PRODH2	6.44	18	1.51	0.0661	695	1.56
PPFIA3	6.45	18	1.51	0.0659	694	1.56
RCOR2	6.45	18	1.51	0.0659	693	1.56
ATP6V1E2	5.27	12	1.51	0.0657	692	1.56
CNTD1	6.46	18	1.51	0.0656	691	1.56
TEX101	6.46	18	1.51	0.0655	690	1.56
RNF113A	5.9	15	1.51	0.0655	689	1.56
BAG3	6.47	18	1.51	0.0654	688	1.56
LDB3	6.48	18	1.51	0.0651	687	1.56
LZTR1	6.48	18	1.51	0.065	686	1.56
GNAI1	5.64	14	1.5	0.0674	725	1.53

KNTC1	6.39	18	1.5	0.0673	724	1.53
ZDHHC1	6.4	18	1.5	0.0672	723	1.53
ZDHHC14	6.4	18	1.5	0.0672	722	1.53
CCNG1	3.69	6	1.5	0.0672	721	1.53
OR56B1	4.53	9	1.5	0.0672	720	1.53
TOMM40L	6.4	18	1.5	0.0672	719	1.53
CPT1B	6.4	18	1.5	0.0672	718	1.54
RAF1	6.4	18	1.5	0.0671	717	1.54
PSD3	6.41	18	1.5	0.067	716	1.54
GALNTL5	4.53	9	1.5	0.0669	715	1.54
LIPA	6.41	18	1.5	0.0669	714	1.54
CCL22	5.85	15	1.5	0.0669	713	1.54
LRP5L	6.41	18	1.5	0.0668	712	1.54
ISL2	6.41	18	1.5	0.0668	711	1.54
THNSL2	6.41	18	1.5	0.0668	710	1.54
AATF	6.42	18	1.5	0.0668	709	1.55
C10orf71	6.42	18	1.5	0.0667	708	1.55
IFNGR1	6.42	18	1.5	0.0666	707	1.55
PLK4	6.43	18	1.5	0.0665	706	1.55
KRTAP22-1	5.25	12	1.5	0.0665	705	1.55
RNF215	6.43	18	1.5	0.0665	704	1.55
DOCK2	6.43	18	1.5	0.0664	703	1.55
ADCY5	6.43	18	1.5	0.0664	702	1.55
ABHD8	6.43	18	1.5	0.0663	701	1.55
FAM46A	6.43	18	1.5	0.0663	700	1.56
KAT2A	6.44	18	1.5	0.0662	699	1.56
MAB21L1	6.44	18	1.5	0.0662	698	1.56
HMGCS1	5.26	12	1.5	0.0662	697	1.56
HBS1L	6.44	18	1.5	0.0662	696	1.56

Table 2.S2 Genes Ontology analysis, related to figure 2.1D.

Term	Overlap	P-value	Adjusted P-value	Odds Ratio	Combined Score
DNA repair (GO:0006281)	36/298	1.56E-48	7.11E-46	87.1898547	9597.98901
interstrand cross-link repair (GO:0036297)	22/55	8.87E-42	2.03E-39	294.814815	27867.62499
double-strand break repair (GO:0006302)	23/164	8.21E-32	1.25E-29	73.374597	5251.967328
double-strand break repair via homologous recombination (GO:0000724)	20/97	3.10E-31	3.55E-29	109.73197	7708.430856
cellular response to DNA damage stimulus (GO:0006974)	27/350	2.90E-30	2.65E-28	40.9806502	2787.260748
DNA metabolic process (GO:0006259)	25/277	1.14E-29	8.70E-28	46.4876228	3098.018363
recombinational repair (GO:0000725)	17/79	6.35E-27	4.14E-25	108.97	6573.297194
DNA replication (GO:0006260)	12/108	1.54E-15	8.77E-14	45.0840909	1537.809478
double-strand break repair via nonhomologous end joining (GO:0006303)	10/62	8.27E-15	4.20E-13	67.0748988	2174.981596
mitotic DNA damage checkpoint signaling (GO:0044773)	9/59	3.35E-13	1.53E-11	61.7058621	1772.556185
DNA double-strand break processing (GO:0000729)	6/19	2.95E-11	1.22E-09	150.718789	3654.650116
DNA-dependent DNA replication maintenance of fidelity (GO:0045005)	7/43	1.00E-10	3.83E-09	64.4810185	1484.436371
telomere maintenance (GO:0000723)	7/56	6.99E-10	2.46E-08	47.3428571	998.0712468
DNA damage checkpoint signaling (GO:0000077)	6/32	9.51E-10	3.10E-08	75.3102144	1564.46129
resolution of meiotic recombination intermediates (GO:0000712)	5/16	1.54E-09	4.69E-08	146.055718	2963.876267

replication fork processing (GO:0031297)	6/39	3.36E-09	9.04E-08	59.314456	1157.273927
DNA integrity checkpoint signaling (GO:0031570)	6/39	3.36E-09	9.04E-08	59.314456	1157.273927
response to ionizing radiation (GO:0010212)	7/72	4.26E-09	1.08E-07	35.6605128	687.3585591
cellular macromolecule biosynthetic process (GO:0034645)	11/314	7.05E-09	1.70E-07	12.725719	238.8635874
regulation of double-strand break repair via homologous recombination (GO:0010569)	6/46	9.48E-09	2.17E-07	48.9172131	903.7203409
telomere organization (GO:0032200)	6/47	1.08E-08	2.36E-07	47.7217113	875.2412321
signal transduction in response to DNA damage (GO:0042770)	6/52	2.03E-08	4.21E-07	42.5238774	753.2615726
formation of extrachromosomal circular DNA (GO:0001325)	4/11	3.73E-08	6.82E-07	180.734694	3091.420359
t-circle formation (GO:0090656)	4/11	3.73E-08	6.82E-07	180.734694	3091.420359
telomere maintenance via telomere trimming (GO:0090737)	4/11	3.73E-08	6.82E-07	180.734694	3091.420359
regulation of signal transduction by p53 class mediator (GO:1901796)	8/156	5.05E-08	8.88E-07	18.1264315	304.5385195
nucleotide-excision repair (GO:0006289)	7/105	6.03E-08	1.02E-06	23.6130952	392.5473067
mitotic intra-S DNA damage checkpoint signaling (GO:0031573)	4/15	1.53E-07	2.49E-06	114.989899	1804.765614
DNA recombination (GO:0006310)	5/39	1.91E-07	3.01E-06	47.1987666	730.2018668
negative regulation of telomere maintenance (GO:0032205)	4/16	2.03E-07	3.09E-06	105.402116	1624.228511
cellular response to ionizing radiation (GO:0071479)	5/48	5.55E-07	8.18E-06	37.3030758	537.3178241
response to DNA damage checkpoint signaling (GO:0072423)	3/6	7.13E-07	1.02E-05	311.40625	4407.379492

regulation of DNA replication (GO:0006275)	5/53	9.18E-07	1.27E-05	33.4089382	464.4064399
positive regulation of response to DNA damage stimulus (GO:2001022)	5/55	1.11E-06	1.49E-05	32.0693548	439.7784352
negative regulation of telomere capping (GO:1904354)	3/7	1.25E-06	1.63E-05	233.542969	3175.233779
DNA geometric change (GO:0032392)	4/26	1.63E-06	2.06E-05	57.4632035	765.9348156
protein K6-linked ubiquitination (GO:0085020)	3/9	2.98E-06	3.67E-05	155.679688	1981.063565
negative regulation of double-strand break repair (GO:2000780)	4/32	3.85E-06	4.63E-05	45.1360544	562.6907486
telomeric loop disassembly (GO:0090657)	3/10	4.24E-06	4.97E-05	133.433036	1650.69693
mitotic G2 DNA damage checkpoint signaling (GO:0007095)	4/33	4.37E-06	5.00E-05	43.5774494	537.7393197
telomere maintenance via recombination (GO:0000722)	3/11	5.82E-06	6.48E-05	116.748047	1407.388389
mitotic G2/M transition checkpoint (GO:0044818)	4/45	1.55E-05	1.65E-04	30.8044909	341.2448079
positive regulation of double-strand break repair via homologous recombination (GO:1905168)	3/15	1.59E-05	1.65E-04	77.8164063	859.8836823
mitotic recombination (GO:0006312)	3/15	1.59E-05	1.65E-04	77.8164063	859.8836823
mitotic sister chromatid cohesion (GO:0007064)	3/16	1.95E-05	1.98E-04	71.8269231	778.9570578
positive regulation of DNA repair (GO:0045739)	4/48	2.00E-05	1.99E-04	28.6998557	310.4859061
DNA duplex unwinding (GO:0032508)	4/51	2.55E-05	2.48E-04	26.8638973	284.1047217
regulation of telomere maintenance via telomere lengthening (GO:1904356)	3/18	2.83E-05	2.64E-04	62.24375	651.893413
negative regulation of double-strand break repair via homologous recombination (GO:2000042)	3/18	2.83E-05	2.64E-04	62.24375	651.893413

negative regulation of DNA recombination (GO:0045910)	4/57	3.97E-05	3.63E-04	23.8155136	241.321313
protein localization to chromatin (GO:0071168)	3/21	4.58E-05	4.10E-04	51.8619792	518.200027
positive regulation of DNA metabolic process (GO:0051054)	4/63	5.90E-05	5.19E-04	21.3871402	208.2521823
response to gamma radiation (GO:0010332)	3/24	6.92E-05	5.96E-04	44.4464286	425.7611668
regulation of intracellular signal transduction (GO:1902531)	8/437	1.03E-04	8.70E-04	6.16459247	56.60419067
transcription-coupled nucleotide-excision repair (GO:0006283)	4/73	1.05E-04	8.74E-04	18.2783529	167.4219337
double-strand break repair via synthesis-dependent strand annealing (GO:0045003)	2/5	1.10E-04	8.96E-04	204.410256	1863.514013
positive regulation of DNA recombination (GO:0045911)	3/30	1.37E-04	0.001096281	34.5590278	307.4876947
replication-born double-strand break repair via sister chromatid exchange (GO:1990414)	2/6	1.64E-04	0.001266256	153.3	1335.739374
double-strand break repair via classical nonhomologous end joining (GO:0097680)	2/6	1.64E-04	0.001266256	153.3	1335.739374
positive regulation of telomere maintenance (GO:0032206)	3/32	1.66E-04	0.001266256	32.1724138	279.9652994
protein localization to chromosome (GO:0034502)	3/34	2.00E-04	0.001495456	30.09375	256.3726848
positive regulation of mitotic cell cycle spindle assembly checkpoint (GO:0090267)	2/7	2.30E-04	0.001665914	122.633846	1027.540438
positive regulation of spindle checkpoint (GO:0090232)	2/7	2.30E-04	0.001665914	122.633846	1027.540438
single strand break repair (GO:0000012)	2/8	3.06E-04	0.002148218	102.189744	827.0637613
telomeric D-loop disassembly (GO:0061820)	2/8	3.06E-04	0.002148218	102.189744	827.0637613
positive regulation of double-strand break repair (GO:2000781)	3/40	3.25E-04	0.00224952	25.2060811	202.4569365

response to UV (GO:0009411)	4/99	3.41E-04	0.002325113	13.2584795	105.8554031
regulation of DNA recombination (GO:0000018)	3/42	3.76E-04	0.002524832	23.9110577	188.5806921
regulation of DNA repair (GO:0006282)	3/45	4.61E-04	0.003010015	22.1997768	170.5386485
cellular response to radiation (GO:0071478)	3/45	4.61E-04	0.003010015	22.1997768	170.5386485
base-excision repair (GO:0006284)	3/48	5.58E-04	0.003591349	20.7166667	155.1933322
replicative senescence (GO:0090399)	2/12	7.14E-04	0.004469879	61.3015385	444.1062283
regulation of DNA-dependent DNA replication (GO:0090329)	2/12	7.14E-04	0.004469879	61.3015385	444.1062283
regulation of mitotic cell cycle spindle assembly checkpoint (GO:0090266)	2/13	8.42E-04	0.005199938	55.7258741	394.5239726
DNA-dependent DNA replication (GO:0006261)	4/129	9.25E-04	0.005635004	10.0612063	70.28711134
response to X-ray (GO:0010165)	2/14	9.80E-04	0.005894186	51.0794872	353.8653505
positive regulation of DNA biosynthetic process (GO:2000573)	3/61	0.001126	0.006528587	16.0627694	109.0582661
response to light stimulus (GO:0009416)	3/61	0.001126	0.006528587	16.0627694	109.0582661
positive regulation of DNA damage response, signal transduction by p53 class mediator (GO:0043517)	2/15	0.001129	0.006528587	47.147929	319.9835777
negative regulation of DNA replication (GO:0008156)	2/16	0.001287	0.0072613	43.778022	291.3615902
DNA unwinding involved in DNA replication (GO:0006268)	2/16	0.001287	0.0072613	43.778022	291.3615902
protein autoubiquitination (GO:0051865)	3/65	0.001353	0.007540752	15.0234375	99.23577719
cellular response to gamma radiation (GO:0071480)	2/17	0.001455	0.008013833	40.8574359	266.8982937

telomere capping (GO:0016233)	2/19	0.001822	0.00991333	36.0470588	227.3755291
regulation of centrosome cycle (GO:0046605)	2/22	0.002446	0.012995792	30.6353846	184.2248373
positive regulation of signal transduction by p53 class mediator (GO:1901798)	2/22	0.002446	0.012995792	30.6353846	184.2248373
positive regulation of protein ubiquitination (GO:0031398)	3/82	0.002634	0.013838131	11.7804589	69.9653533
regulation of telomere capping (GO:1904353)	2/23	0.002673	0.013880005	29.1750916	172.85228
regulation of cell cycle (GO:0051726)	5/296	0.003136	0.016103077	5.44340982	31.38012502
regulation of telomere maintenance (GO:0032204)	2/26	0.003411	0.017131	25.524359	144.995957
negative regulation of telomere maintenance via telomere lengthening (GO:1904357)	2/26	0.003411	0.017131	25.524359	144.995957
regulation of DNA damage response, signal transduction by p53 class mediator (GO:0043516)	2/28	0.00395	0.019623288	23.5585799	130.3716041
cellular response to chemical stress (GO:0062197)	3/101	0.004738	0.02328474	9.48740434	50.77697658
protein acetylation (GO:0006473)	2/31	0.004828	0.023473893	21.1183024	112.6292925
regulation of centrosome duplication (GO:0010824)	2/32	0.005139	0.024721943	20.4133333	107.5960378
positive regulation of telomere maintenance via telomerase (GO:0032212)	2/33	0.005459	0.025986748	19.7538462	102.9274896
female gamete generation (GO:0007292)	2/34	0.005788	0.0272675	19.1355769	98.58710807
negative regulation of DNA metabolic process (GO:0051053)	2/36	0.006472	0.029873775	18.0081448	90.76713343
positive regulation of telomere maintenance via telomere lengthening (GO:1904358)	2/36	0.006472	0.029873775	18.0081448	90.76713343
positive regulation of protein-containing complex assembly (GO:0031334)	3/118	0.00729	0.033313447	8.07798913	39.75426723

protein monoubiquitination (GO:0006513)	2/39	0.007563	0.034219926	16.5455301	80.8168081 4
protein ubiquitination (GO:0016567)	6/525	0.008208	0.036775334	3.67933289	17.6705057 9
regulation of double-strand break repair (GO:2000779)	2/42	0.008731	0.038738933	15.3023077	72.5461683 9
regulation of telomerase activity (GO:0051972)	2/46	0.010406	0.045725436	13.9083916	63.4972741 9
cellular response to alcohol (GO:0097306)	2/48	0.011292	0.04914808	13.3023411	59.642916
intrinsic apoptotic signaling pathway in response to DNA damage (GO:0008630)	2/51	0.012682	0.054675986	12.4860283	54.5336644 6
regulation of telomere maintenance via telomerase (GO:0032210)	2/52	0.013161	0.056210963	12.2356923	52.9866414 6
cytoplasmic microtubule organization (GO:0031122)	2/54	0.014142	0.059843333	11.7639053	50.0975015 1
AMP biosynthetic process (GO:0006167)	1/5	0.01664	0.063901911	75.4886364	309.1988807
positive regulation of DNA ligation (GO:0051106)	1/5	0.01664	0.063901911	75.4886364	309.1988807
positive regulation of histone H3-K9 acetylation (GO:2000617)	1/5	0.01664	0.063901911	75.4886364	309.1988807
response to indole-3-methanol (GO:0071680)	1/5	0.01664	0.063901911	75.4886364	309.1988807
cellular response to indole-3-methanol (GO:0071681)	1/5	0.01664	0.063901911	75.4886364	309.1988807
regulation of histone H4-K16 acetylation (GO:2000618)	1/5	0.01664	0.063901911	75.4886364	309.1988807
positive regulation of protein monoubiquitination (GO:1902527)	1/5	0.01664	0.063901911	75.4886364	309.1988807
DNA double-strand break processing involved in repair via single-strand annealing (GO:0010792)	1/5	0.01664	0.063901911	75.4886364	309.1988807
DNA ligation involved in DNA repair (GO:0051103)	1/5	0.01664	0.063901911	75.4886364	309.1988807

double-strand break repair via single-strand annealing (GO:0045002)	1/5	0.01664	0.063901911	75.4886364	309.1988807
regulation of protein monoubiquitination (GO:1902525)	1/5	0.01664	0.063901911	75.4886364	309.1988807
acetyl-CoA biosynthetic process from pyruvate (GO:0006086)	1/6	0.019935	0.071129897	60.3878788	236.4361615
regulation of t-circle formation (GO:1904429)	1/6	0.019935	0.071129897	60.3878788	236.4361615
negative regulation of histone H3-K9 methylation (GO:0051573)	1/6	0.019935	0.071129897	60.3878788	236.4361615
regulation of cell cycle checkpoint (GO:1901976)	1/6	0.019935	0.071129897	60.3878788	236.4361615
regulation of DNA-dependent DNA replication initiation (GO:0030174)	1/6	0.019935	0.071129897	60.3878788	236.4361615
cellular response to X-ray (GO:0071481)	1/6	0.019935	0.071129897	60.3878788	236.4361615
maintenance of DNA repeat elements (GO:0043570)	1/6	0.019935	0.071129897	60.3878788	236.4361615
protein K27-linked ubiquitination (GO:0044314)	1/6	0.019935	0.071129897	60.3878788	236.4361615
protein K29-linked ubiquitination (GO:0035519)	1/6	0.019935	0.071129897	60.3878788	236.4361615
mitotic G1 DNA damage checkpoint signaling (GO:0031571)	2/65	0.020078	0.071129897	9.7045177	37.92640544
protein polyubiquitination (GO:0000209)	4/314	0.021081	0.074109541	4.0190462	15.51095138
cellular response to light stimulus (GO:0071482)	2/70	0.023064	0.077452905	8.9886878	33.88253531
negative regulation of centriole replication (GO:0046600)	1/7	0.023219	0.077452905	50.320771	189.3461363
G-quadruplex DNA unwinding (GO:0044806)	1/7	0.023219	0.077452905	50.320771	189.3461363
negative regulation of double-strand break repair via nonhomologous end joining (GO:2001033)	1/7	0.023219	0.077452905	50.320771	189.3461363

positive regulation of histone H4 acetylation (GO:0090240)	1/7	0.023219	0.077452905	50.3207071	189.3461363
pexophagy (GO:0000425)	1/7	0.023219	0.077452905	50.3207071	189.3461363
protection from non-homologous end joining at telomere (GO:0031848)	1/7	0.023219	0.077452905	50.3207071	189.3461363
DNA damage response, signal transduction by p53 class mediator (GO:0030330)	2/74	0.025577	0.082360333	8.487606 84	31.116188 28
nucleic acid phosphodiester bond hydrolysis (GO:0090305)	2/75	0.026221	0.082360333	8.370916 75	30.479983 17
negative regulation of chromosome organization (GO:2001251)	1/8	0.026492	0.082360333	43.1298701	156.6003384
replication fork protection (GO:0048478)	1/8	0.026492	0.082360333	43.1298701	156.6003384
response to hydroperoxide (GO:0033194)	1/8	0.026492	0.082360333	43.1298701	156.6003384
positive regulation of meiotic nuclear division (GO:0045836)	1/8	0.026492	0.082360333	43.1298701	156.6003384
somatic hypermutation of immunoglobulin genes (GO:0016446)	1/8	0.026492	0.082360333	43.1298701	156.6003384
DNA damage induced protein phosphorylation (GO:0006975)	1/8	0.026492	0.082360333	43.1298701	156.6003384
peptidyl-serine autophosphorylation (GO:0036289)	1/8	0.026492	0.082360333	43.1298701	156.6003384
regulation of protein ADP-ribosylation (GO:0010835)	1/8	0.026492	0.082360333	43.1298701	156.6003384
cellular response to UV (GO:0034644)	2/77	0.027531	0.084439891	8.14687179	29.26724936
positive regulation of protein modification by small protein conjugation or removal (GO:1903322)	2/77	0.027531	0.084439891	8.14687179	29.26724936
regulation of cellular response to heat (GO:1900034)	2/79	0.028866	0.087944791	7.93446553	28.12842718
positive regulation of DNA-directed DNA polymerase activity (GO:1900264)	1/9	0.029755	0.088298389	37.7367424	132.6357515

negative regulation of mRNA 3'-end processing (GO:0031441)	1/9	0.029755	0.088298389	37.7367424	132.6357515
positive regulation of ligase activity (GO:0051351)	1/9	0.029755	0.088298389	37.7367424	132.6357515
regulation of DNA-directed DNA polymerase activity (GO:1900262)	1/9	0.029755	0.088298389	37.7367424	132.6357515
regulation of gene expression, epigenetic (GO:0040029)	2/82	0.030916	0.091153575	7.63576923	26.54550611
acetyl-CoA biosynthetic process (GO:0006085)	1/10	0.033007	0.09202161	33.5420875	114.4136696
negative regulation of peptidyl-lysine acetylation (GO:2000757)	1/10	0.033007	0.09202161	33.5420875	114.4136696
regulation of DNA damage checkpoint (GO:2000001)	1/10	0.033007	0.09202161	33.5420875	114.4136696
cellular response to hydroxyurea (GO:0072711)	1/10	0.033007	0.09202161	33.5420875	114.4136696
negative regulation of telomerase activity (GO:0051974)	1/10	0.033007	0.09202161	33.5420875	114.4136696
telomere maintenance in response to DNA damage (GO:0043247)	1/10	0.033007	0.09202161	33.5420875	114.4136696
microtubule anchoring at centrosome (GO:0034454)	1/10	0.033007	0.09202161	33.5420875	114.4136696
dosage compensation (GO:0007549)	1/10	0.033007	0.09202161	33.5420875	114.4136696
regulation of cell cycle G2/M phase transition (GO:1902749)	2/85	0.033023	0.09202161	7.35866543	25.09708755
negative regulation of centrosome duplication (GO:0010826)	1/11	0.036248	0.096309113	30.1863636	100.1396768
positive regulation of DNA methylation-dependent heterochromatin assembly (GO:0090309)	1/11	0.036248	0.096309113	30.1863636	100.1396768
negative regulation of intracellular estrogen receptor signaling pathway (GO:0033147)	1/11	0.036248	0.096309113	30.1863636	100.1396768
response to hydroxyurea (GO:0072710)	1/11	0.036248	0.096309113	30.1863636	100.1396768

cell proliferation in forebrain (GO:0021846)	1/11	0.036248	0.096309113	30.1863636	100.1396768
insulin-like growth factor receptor signaling pathway (GO:0048009)	1/11	0.036248	0.096309113	30.1863636	100.1396768
regulation of histone H3-K9 acetylation (GO:2000615)	1/11	0.036248	0.096309113	30.1863636	100.1396768
regulation of mRNA 3'-end processing (GO:0031440)	1/11	0.036248	0.096309113	30.1863636	100.1396768
protein complex oligomerization (GO:0051259)	2/90	0.036655	0.096829588	6.93881119	22.9410591
negative regulation of B cell proliferation (GO:0030889)	1/12	0.039478	0.097521253	27.4407713	88.6889136
negative regulation of cell division (GO:0051782)	1/12	0.039478	0.097521253	27.4407713	88.6889136
negative regulation of fatty acid biosynthetic process (GO:0045717)	1/12	0.039478	0.097521253	27.4407713	88.6889136
autophagy of peroxisome (GO:0030242)	1/12	0.039478	0.097521253	27.4407713	88.6889136
negative regulation of histone acetylation (GO:0035067)	1/12	0.039478	0.097521253	27.4407713	88.6889136
negative regulation of transcription elongation from RNA polymerase II promoter (GO:0034244)	1/12	0.039478	0.097521253	27.4407713	88.6889136
regulation of histone H3-K9 methylation (GO:0051570)	1/12	0.039478	0.097521253	27.4407713	88.6889136
microtubule anchoring (GO:0034453)	1/12	0.039478	0.097521253	27.4407713	88.6889136
microtubule anchoring at microtubule organizing center (GO:0072393)	1/12	0.039478	0.097521253	27.4407713	88.6889136
mitotic G1/S transition checkpoint signaling (GO:0044819)	1/12	0.039478	0.097521253	27.4407713	88.6889136
dosage compensation by inactivation of X chromosome (GO:0009048)	1/12	0.039478	0.097521253	27.4407713	88.6889136
double-strand break repair via break-induced replication (GO:0000727)	1/12	0.039478	0.097521253	27.4407713	88.6889136

ciliary basal body-plasma membrane docking (GO:0097711)	2/95	0.040434	0.099346421	6.56410256	21.05815992
AMP metabolic process (GO:0046033)	1/13	0.042698	0.10162928	25.1527778	79.32209211
negative regulation of DNA-dependent DNA replication (GO:2000104)	1/13	0.042698	0.10162928	25.1527778	79.32209211
negative regulation of histone methylation (GO:0031061)	1/13	0.042698	0.10162928	25.1527778	79.32209211
positive regulation of heterochromatin assembly (GO:0031453)	1/13	0.042698	0.10162928	25.1527778	79.32209211
negative regulation of nucleocytoplasmic transport (GO:0046823)	1/13	0.042698	0.10162928	25.1527778	79.32209211
DNA catabolic process (GO:0006308)	1/13	0.042698	0.10162928	25.1527778	79.32209211
positive regulation of cell cycle process (GO:0090068)	2/101	0.045154	0.105545781	6.16441336	19.09534602
negative regulation of DNA-templated transcription, elongation (GO:0032785)	1/14	0.045907	0.105545781	23.2167832	71.53426659
regulation of DNA methylation-dependent heterochromatin assembly (GO:0090308)	1/14	0.045907	0.105545781	23.2167832	71.53426659
negative regulation of TORC1 signaling (GO:1904262)	1/14	0.045907	0.105545781	23.2167832	71.53426659
nuclear migration (GO:0007097)	1/14	0.045907	0.105545781	23.2167832	71.53426659
intrinsic apoptotic signaling pathway (GO:0097193)	2/102	0.04596	0.105545781	6.10246154	18.7955147
mitotic sister chromatid segregation (GO:0000070)	2/102	0.04596	0.105545781	6.10246154	18.7955147
protein modification by small protein conjugation (GO:0032446)	4/409	0.048284	0.109468497	3.06141485	9.278089199
positive regulation of chromosome organization (GO:2001252)	1/15	0.049105	0.109468497	21.5573593	64.96939441
positive regulation of histone H3-K4 methylation (GO:0051571)	1/15	0.049105	0.109468497	21.5573593	64.96939441

negative regulation of mRNA processing (GO:0050686)	1/15	0.049105	0.109468497	21.5573593	64.9693941
histone mRNA catabolic process (GO:0071044)	1/15	0.049105	0.109468497	21.5573593	64.9693941
protein localization to chromosome, telomeric region (GO:0070198)	1/15	0.049105	0.109468497	21.5573593	64.9693941
regulation of protein ubiquitination (GO:0031396)	2/109	0.051746	0.113799541	5.70122214	16.8836403
purine ribonucleoside monophosphate biosynthetic process (GO:0009168)	1/16	0.052293	0.113799541	20.1191919	59.3695759
negative regulation of histone modification (GO:0031057)	1/16	0.052293	0.113799541	20.1191919	59.3695759
regulation of phosphate metabolic process (GO:0019220)	1/16	0.052293	0.113799541	20.1191919	59.3695759
protein localization to microtubule organizing center (GO:1905508)	1/16	0.052293	0.113799541	20.1191919	59.3695759
protein-containing complex subunit organization (GO:0043933)	2/112	0.054302	0.117611313	5.5448951	16.1533624
regulation of transferase activity (GO:0051338)	1/17	0.05547	0.118457728	18.8607955	54.5436566
negative regulation of fatty acid metabolic process (GO:0045922)	1/17	0.05547	0.118457728	18.8607955	54.5436566
embryo development ending in birth or egg hatching (GO:0009792)	1/17	0.05547	0.118457728	18.8607955	54.5436566
regulation of chromosome segregation (GO:0051983)	1/17	0.058637	0.121805493	17.7504456	50.3471096
RNA destabilization (GO:0050779)	1/17	0.058637	0.121805493	17.7504456	50.3471096
cellular response to alkaloid (GO:0071312)	1/17	0.058637	0.121805493	17.7504456	50.3471096
negative regulation of Rho protein signal transduction (GO:0035024)	1/17	0.058637	0.121805493	17.7504456	50.3471096
DNA strand elongation (GO:0022616)	1/17	0.058637	0.121805493	17.7504456	50.3471096

protein localization to centrosome (GO:0071539)	1/17	0.058637	0.121805493	17.7504456	50.34710965
regulation of cellular response to stress (GO:0080135)	2/118	0.059545	0.123131278	5.25649867	14.82871354
protein-containing complex assembly (GO:0065003)	3/267	0.060421	0.123822803	3.49236506	9.80102694
protein deubiquitination (GO:0016579)	3/267	0.060421	0.123822803	3.49236506	9.80102694
regulation of centriole replication (GO:0046599)	1/19	0.061794	0.124954349	16.763468	46.66874408
negative regulation of nervous system development (GO:0051961)	1/19	0.061794	0.124954349	16.763468	46.66874408
regulation of histone H3-K4 methylation (GO:0051569)	1/19	0.061794	0.124954349	16.763468	46.66874408
protein homooligomerization (GO:0051260)	2/121	0.06223	0.12528177	5.12320621	14.22675066
cellular response to nitrogen compound (GO:1901699)	1/20	0.06494	0.129032142	15.8803828	43.42169605
positive regulation of peptidyl-lysine acetylation (GO:2000758)	1/20	0.06494	0.129032142	15.8803828	43.42169605
maintenance of protein location in nucleus (GO:0051457)	1/20	0.06494	0.129032142	15.8803828	43.42169605
protein modification by small protein removal (GO:0070646)	3/276	0.065387	0.129359013	3.37568681	9.20694736
cellular response to oxidative stress (GO:0034599)	2/125	0.065873	0.129757739	4.95559725	13.47938373
error-prone translesion synthesis (GO:0042276)	1/21	0.068075	0.130168843	15.0856061	40.53717648
cellular response to inorganic substance (GO:0071241)	1/21	0.068075	0.130168843	15.0856061	40.53717648
spindle assembly checkpoint signaling (GO:0071173)	1/21	0.068075	0.130168843	15.0856061	40.53717648
nucleotide-excision repair, DNA incision, 3'-to lesion (GO:0006295)	1/21	0.068075	0.130168843	15.0856061	40.53717648

nucleotide-excision repair, preincision complex stabilization (GO:0006293)	1/21	0.068075	0.130168843	15.0856061	40.5371764
mitotic spindle assembly checkpoint signaling (GO:0007094)	1/21	0.068075	0.130168843	15.0856061	40.5371764
mitotic spindle checkpoint signaling (GO:0071174)	1/21	0.068075	0.130168843	15.0856061	40.5371764
G2/M transition of mitotic cell cycle (GO:0000086)	2/130	0.070524	0.132229414	4.76081731	12.6247139
negative regulation of B cell activation (GO:0050869)	1/22	0.0712	0.132229414	14.3665224	37.9600403
negative regulation of lipid biosynthetic process (GO:0051055)	1/22	0.0712	0.132229414	14.3665224	37.9600403
negative regulation of mitotic metaphase/anaphase transition (GO:0045841)	1/22	0.0712	0.132229414	14.3665224	37.9600403
regulation of chromosome organization (GO:0033044)	1/22	0.0712	0.132229414	14.3665224	37.9600403
homologous chromosome segregation (GO:0045143)	1/22	0.0712	0.132229414	14.3665224	37.9600403
negative regulation of protein dephosphorylation (GO:0035308)	1/22	0.0712	0.132229414	14.3665224	37.9600403
cell cycle G2/M phase transition (GO:0044839)	2/131	0.071468	0.132229414	4.72367323	12.4634681
negative regulation of intracellular protein transport (GO:0090317)	1/23	0.074315	0.133709013	13.7128099	35.6456061
positive regulation of histone acetylation (GO:0035066)	1/23	0.074315	0.133709013	13.7128099	35.6456061
negative regulation of phosphoprotein phosphatase activity (GO:0032515)	1/23	0.074315	0.133709013	13.7128099	35.6456061
negative regulation of reactive oxygen species metabolic process (GO:2000378)	1/23	0.074315	0.133709013	13.7128099	35.6456061
positive regulation of protein autophosphorylation (GO:0031954)	1/23	0.074315	0.133709013	13.7128099	35.6456061
DNA catabolic process, endonucleolytic (GO:0000737)	1/23	0.074315	0.133709013	13.7128099	35.6456061

regulation of protein export from nucleus (GO:0046825)	1/23	0.074315	0.133709013	13.712809	35.64560615
nucleotide-excision repair, DNA gap filling (GO:0006297)	1/24	0.07742	0.138206622	13.115942	33.55728719
protein K48-linked deubiquitination (GO:0071108)	1/24	0.07742	0.138206622	13.115942	33.55728719
positive regulation of DNA-templated transcription, elongation (GO:0032786)	1/25	0.080514	0.142616332	12.568831	31.66487558
positive regulation of vascular endothelial growth factor production (GO:0010575)	1/25	0.080514	0.142616332	12.568831	31.66487558
regulation of regulatory T cell differentiation (GO:0045589)	1/26	0.083598	0.145264104	12.065445	29.9432143
negative regulation of cell development (GO:0010721)	1/26	0.083598	0.145264104	12.065445	29.9432143
global genome nucleotide-excision repair (GO:0070911)	1/26	0.083598	0.145264104	12.065445	29.9432143
positive regulation of histone methylation (GO:0031062)	1/26	0.083598	0.145264104	12.065445	29.9432143
TOR signaling (GO:0031929)	1/26	0.083598	0.145264104	12.065445	29.9432143
regulation of transcription elongation from RNA polymerase II promoter (GO:0034243)	1/27	0.086672	0.149468861	11.600815	28.37119608
regulation of vascular endothelial growth factor production (GO:0010574)	1/27	0.086672	0.149468861	11.600815	28.37119608
positive regulation of transferase activity (GO:0051347)	2/148	0.088104	0.15132618	4.1700737	10.13009686
regulation of G2/M transition of mitotic cell cycle (GO:0010389)	2/149	0.089116	0.15132618	4.1414966	10.01337046
histone mRNA metabolic process (GO:0008334)	1/28	0.089736	0.15132618	11.170594	26.93098833
negative regulation of phosphatase activity (GO:0010923)	1/28	0.089736	0.15132618	11.170594	26.93098833
regulation of DNA-templated transcription, elongation (GO:0032784)	1/28	0.089736	0.15132618	11.170594	26.93098833

regulation of phosphatase activity (GO:0010921)	1/28	0.089736	0.15132618	11.1705948	26.9309883
cellular response to organic cyclic compound (GO:0071407)	2/150	0.090132	0.151434675	4.11330561	9.898596984
homologous chromosome pairing at meiosis (GO:0007129)	1/29	0.09279	0.151988942	10.7711039	25.6074287
regulation of DNA biosynthetic process (GO:2000278)	1/29	0.09279	0.151988942	10.7711039	25.6074287
regulation of double-strand break repair via nonhomologous end joining (GO:2001032)	1/29	0.09279	0.151988942	10.7711039	25.6074287
regulation of fatty acid biosynthetic process (GO:0042304)	1/29	0.09279	0.151988942	10.7711039	25.6074287
negative regulation of transferase activity (GO:0051348)	1/29	0.09279	0.151988942	10.7711039	25.6074287
mismatch repair (GO:0006298)	1/29	0.09279	0.151988942	10.7711039	25.6074287
protein K11-linked ubiquitination (GO:0070979)	1/29	0.09279	0.151988942	10.7711039	25.6074287
negative regulation of gene expression, epigenetic (GO:0045814)	1/30	0.095833	0.15585702	10.3991641	24.3875408
non-motile cilium assembly (GO:1905515)	1/30	0.095833	0.15585702	10.3991641	24.3875408
peptidyl-serine phosphorylation (GO:0018105)	2/156	0.096297	0.156056142	3.95184815	9.248572552
protein autophosphorylation (GO:0046777)	2/159	0.099425	0.160554773	3.87574718	8.946606668
negative regulation of DNA biosynthetic process (GO:2000279)	1/32	0.10189	0.162243425	9.72727273	22.215157
negative regulation of intracellular steroid hormone receptor signaling pathway (GO:0033144)	1/32	0.10189	0.162243425	9.72727273	22.215157
regulation of intracellular estrogen receptor signaling pathway (GO:0033146)	1/32	0.10189	0.162243425	9.72727273	22.215157
regulation of intracellular protein transport (GO:0033157)	1/32	0.10189	0.162243425	9.72727273	22.215157

positive regulation of histone modification (GO:0031058)	1/33	0.104904	0.16531388	9.42282197	21.24574767
signal transduction by p53 class mediator (GO:0072331)	1/33	0.104904	0.16531388	9.42282197	21.24574767
regulation of histone acetylation (GO:0035065)	1/33	0.104904	0.16531388	9.42282197	21.24574767
negative regulation of extrinsic apoptotic signaling pathway via death domain receptors (GO:1902042)	1/34	0.107907	0.169040805	9.13682277	20.34297848
post-translational protein modification (GO:0043687)	3/345	0.1092	0.169040805	2.68516996	5.946517488
peptidyl-serine modification (GO:0018209)	2/169	0.11005	0.169040805	3.64182404	8.036849573
regulation of TORC1 signaling (GO:1903432)	1/35	0.110901	0.169040805	8.86764706	19.50100521
base-excision repair, gap-filling (GO:0006287)	1/35	0.110901	0.169040805	8.86764706	19.50100521
response to estrogen (GO:0043627)	1/35	0.110901	0.169040805	8.86764706	19.50100521
negative regulation of neurogenesis (GO:0050768)	1/35	0.110901	0.169040805	8.86764706	19.50100521
negative regulation of organelle assembly (GO:1902116)	1/35	0.110901	0.169040805	8.86764706	19.50100521
negative regulation of Ras protein signal transduction (GO:0046580)	1/35	0.110901	0.169040805	8.86764706	19.50100521
negative regulation of cellular macromolecule biosynthetic process (GO:2000113)	4/547	0.110968	0.169040805	2.26723962	4.984562701
nucleotide-excision repair, DNA incision, 5'-to lesion (GO:0006296)	1/37	0.116858	0.176835434	8.37415825	17.97757683
regulation of protein autophosphorylation (GO:0031952)	1/37	0.116858	0.176835434	8.37415825	17.97757683
negative regulation of G0 to G1 transition (GO:0070317)	1/38	0.119822	0.178367591	8.14742015	17.28674296
negative regulation of TOR signaling (GO:0032007)	1/38	0.119822	0.178367591	8.14742015	17.28674296

DNA replication initiation (GO:0006270)	1/38	0.119822	0.178367591	8.14742015	17.28674296
mRNA destabilization (GO:0061157)	1/38	0.119822	0.178367591	8.14742015	17.28674296
regulation of phosphoprotein phosphatase activity (GO:0043666)	1/38	0.119822	0.178367591	8.14742015	17.28674296
negative regulation of cellular metabolic process (GO:0031324)	1/39	0.122777	0.179836286	7.93261563	16.63777734
regulation of T cell differentiation (GO:0045580)	1/39	0.122777	0.179836286	7.93261563	16.63777734
negative regulation of lymphocyte proliferation (GO:0050672)	1/39	0.122777	0.179836286	7.93261563	16.63777734
positive regulation of intracellular transport (GO:0032388)	1/39	0.122777	0.179836286	7.93261563	16.63777734
nucleotide-excision repair, DNA incision (GO:0033683)	1/39	0.122777	0.179836286	7.93261563	16.63777734
intraciliary transport involved in cilium assembly (GO:0035735)	1/40	0.125721	0.183560793	7.72882673	16.02718738
regulation of response to DNA damage stimulus (GO:2001020)	1/41	0.128656	0.186062297	7.53522727	15.4518494
regulation of G0 to G1 transition (GO:0070316)	1/41	0.128656	0.186062297	7.53522727	15.4518494
regulation of protein dephosphorylation (GO:0035304)	1/41	0.128656	0.186062297	7.53522727	15.4518494
regulation of mitotic cell cycle phase transition (GO:1901990)	2/188	0.131001	0.187913776	3.26666667	6.639653261
ATP-dependent chromatin remodeling (GO:0043044)	1/42	0.131581	0.187913776	7.35107169	14.90896177
regulation of extrinsic apoptotic signaling pathway via death domain receptors (GO:1902041)	1/42	0.131581	0.187913776	7.35107169	14.90896177
translesion synthesis (GO:0019985)	1/42	0.131581	0.187913776	7.35107169	14.90896177
spermatid development (GO:0007286)	1/43	0.134496	0.190884195	7.17568543	14.39600499

cellular response to retinoic acid (GO:0071300)	1/43	0.134496	0.190884195	7.17568543	14.39600499
positive regulation of mRNA catabolic process (GO:0061014)	1/44	0.137402	0.193208021	7.00845666	13.91070752
neurogenesis (GO:0022008)	1/44	0.137402	0.193208021	7.00845666	13.91070752
protein K63-linked ubiquitination (GO:0070534)	1/44	0.137402	0.193208021	7.00845666	13.91070752
positive regulation of macromolecule metabolic process (GO:0010604)	3/384	0.137887	0.193294997	2.40551181	4.76609776
regulation of B cell proliferation (GO:0030888)	1/46	0.143184	0.198891302	6.69629663	13.01507191
regulation of DNA metabolic process (GO:0051052)	1/46	0.143184	0.198891302	6.69629663	13.01507191
postreplication repair (GO:0006301)	1/46	0.143184	0.198891302	6.69629663	13.01507191
purine ribonucleotide biosynthetic process (GO:0009152)	1/48	0.148929	0.206243689	6.41070277	12.20782173
mitotic cell cycle phase transition (GO:0044772)	2/209	0.155121	0.214170174	2.93214418	5.46419550 9
regulation of cell migration (GO:0030334)	3/408	0.156701	0.215700425	2.26018519	4.18905702
negative regulation of cellular biosynthetic process (GO:0031327)	1/52	0.160304	0.219996609	5.90671 42	10.81332745
regulation of cyclin-dependent protein kinase activity (GO:1904029)	1/54	0.165935	0.227043025	5.68324757	10.20801139
pyruvate metabolic process (GO:0006090)	1/55	0.168737	0.230187275	5.57772166	9.92508116
positive regulation of cell motility (GO:2000147)	2/221	0.169268	0.230224151	2.76979276	4.91991162
DNA damage response, signal transduction by p53 class mediator resulting in cell cycle arrest (GO:0006977)	1/56	0.171529	0.232607913	5.47603306	9.65425476
regulation of reactive oxygen species metabolic process (GO:2000377)	1/57	0.174312	0.234296393	5.37797619	9.39481921

positive regulation of gene expression, epigenetic (GO:0045815)	1/57	0.174312	0.234296393	5.37797619	9.394819421
protein K48-linked ubiquitination (GO:0070936)	1/57	0.174312	0.234296393	5.37797619	9.394819421
RNA modification (GO:0009451)	1/58	0.177086	0.236632957	5.28335991	9.146117856
chordate embryonic development (GO:0043009)	1/58	0.177086	0.236632957	5.28335991	9.146117856
selective autophagy (GO:0061912)	1/59	0.179851	0.239626744	5.19200627	8.907539662
response to retinoic acid (GO:0032526)	1/62	0.188091	0.249152006	4.93591654	8.247082746
regulation of neurogenesis (GO:0050767)	1/62	0.188091	0.249152006	4.93591654	8.247082746
negative regulation of cell cycle process (GO:0010948)	1/64	0.193538	0.254158123	4.77873978	7.848026791
tRNA processing (GO:0008033)	1/64	0.193538	0.254158123	4.77873978	7.848026791
pre-replicative complex assembly (GO:0036388)	1/64	0.193538	0.254158123	4.77873978	7.848026791
regulation of cellular catabolic process (GO:0031329)	1/65	0.196249	0.256244688	4.70383523	7.659596935
tRNA modification (GO:0006400)	1/65	0.196249	0.256244688	4.70383523	7.659596935
positive regulation of catabolic process (GO:0009896)	1/67	0.201642	0.261791422	4.56083563	7.303080956
transcription elongation from RNA polymerase II promoter (GO:0006368)	1/67	0.201642	0.261791422	4.56083563	7.303080956
positive regulation of protein transport (GO:0051222)	1/69	0.207	0.267229446	4.42624777	6.971491259
DNA-templated transcription, elongation (GO:0006354)	1/69	0.207	0.267229446	4.42624777	6.971491259
nucleic acid metabolic process (GO:0090304)	1/71	0.212323	0.273328668	4.29935065	6.662471093

extrinsic apoptotic signaling pathway (GO:0097191)	1/72	0.214971	0.275960296	4.23858301	6.515765712
regulation of Rho protein signal transduction (GO:0035023)	1/73	0.217611	0.277968617	4.17950337	6.373943403
cellular component assembly (GO:0022607)	2/261	0.217752	0.277968617	2.33727354	3.562933854
positive regulation of gene expression (GO:0010628)	3/482	0.219024	0.278813663	1.90377088	2.891014283
fibroblast growth factor receptor signaling pathway (GO:0008543)	1/75	0.222863	0.282912318	4.06613432	6.104071158
regulation of cell division (GO:0051302)	1/76	0.225476	0.285436756	4.01171717	5.975614112
positive regulation of cell migration (GO:0030335)	2/269	0.227616	0.287349571	2.26632094	3.354370222
positive regulation of cell adhesion (GO:0045785)	1/80	0.235843	0.296099383	3.80782509	5.500744718
negative regulation of extrinsic apoptotic signaling pathway (GO:2001237)	1/80	0.235843	0.296099383	3.80782509	5.500744718
negative regulation of protein modification process (GO:0031400)	1/81	0.238413	0.298506187	3.76003788	5.390956777
regulation of cyclin-dependent protein serine/threonine kinase activity (GO:0000079)	1/82	0.240975	0.300889206	3.7134306	5.284446531
positive regulation of protein catabolic process (GO:0045732)	1/85	0.248609	0.308819872	3.58026696	4.983280583
positive regulation of programmed cell death (GO:0043068)	2/286	0.248678	0.308819872	2.12881907	2.962459428
negative regulation of cellular amide metabolic process (GO:0034249)	1/86	0.251137	0.311028587	3.53796791	4.888612633
negative regulation of translation (GO:0017148)	1/90	0.261165	0.322574017	3.37827715	4.535685188
positive regulation of cellular component biogenesis (GO:0044089)	1/92	0.266129	0.32606188	3.3036963	4.373344197
cellular response to fibroblast growth factor stimulus (GO:0044344)	1/92	0.266129	0.32606188	3.3036963	4.373344197

Wnt signaling pathway (GO:0016055)	1/92	0.266129	0.32606188	3.303696	4.373344197
negative regulation of cellular protein metabolic process (GO:0032269)	1/94	0.271061	0.33033269	3.232323	4.219514652
regulation of kinase activity (GO:0043549)	1/94	0.271061	0.33033269	3.232323	4.219514652
positive regulation of apoptotic process (GO:0043065)	2/310	0.278518	0.338518042	1.960539	2.506102963
cilium assembly (GO:0060271)	2/314	0.283491	0.343648716	1.935009	2.439222193
positive regulation of vasculature development (GO:1904018)	1/102	0.290462	0.349901637	2.975097	3.678058656
regulation of protein catabolic process (GO:0042176)	1/102	0.290462	0.349901637	2.975097	3.678058656
transcription by RNA polymerase II (GO:0006366)	2/320	0.290947	0.349901637	1.897919	2.343200762
cellular response to organonitrogen compound (GO:0071417)	1/103	0.292851	0.350124173	2.945781	3.617684852
chromatin remodeling (GO:0006338)	1/103	0.292851	0.350124173	2.945781	3.617684852
negative regulation of gene expression (GO:0010629)	2/322	0.29343	0.350124173	1.885865	2.312289364
regulation of cell cycle process (GO:0010564)	1/106	0.299971	0.356069849	2.861183	3.445060405
chromosome organization (GO:0051276)	1/106	0.299971	0.356069849	2.861183	3.445060405
response to tumor necrosis factor (GO:0034612)	1/110	0.309355	0.366256894	2.755629	3.233087498
regulation of protein serine/threonine kinase activity (GO:0071900)	1/111	0.311681	0.368057753	2.730440	3.183077173
negative regulation of cell motility (GO:2000146)	1/114	0.318614	0.374310527	2.657548	3.039634287
positive regulation of kinase activity (GO:0033674)	1/114	0.318614	0.374310527	2.657548	3.039634287

positive regulation of protein metabolic process (GO:0051247)	1/115	0.32091	0.376040873	2.634102	2.9939076
positive regulation of angiogenesis (GO:0045766)	1/116	0.323198	0.377753463	2.61106719	2.949172564
supramolecular fiber organization (GO:0097435)	2/351	0.329283	0.38388303	1.72660348	1.9179783 7
regulation of phosphorylation (GO:0042325)	1/125	0.343452	0.398369905	2.42045455	2.586756178
platelet degranulation (GO:0002576)	1/125	0.343452	0.398369905	2.42045455	2.586756178
plasma membrane bounded cell projection organization (GO:0120036)	1/128	0.35007	0.405017876	2.36292054	2.480172679
positive regulation of canonical Wnt signaling pathway (GO:0090263)	1/130	0.354445	0.409044369	2.32605121	2.412582241
regulation of cell adhesion (GO:0030155)	1/133	0.360954	0.415506287	2.27284206	2.316036612
negative regulation of programmed cell death (GO:0043069)	2/381	0.365872	0.420109239	1.58749746	1.596184081
protein-DNA complex assembly (GO:0065004)	1/143	0.382186	0.43555856	2.11171575	2.031149545
neuron development (GO:0048666)	1/143	0.382186	0.43555856	2.11171575	2.031149545
monocarboxylic acid metabolic process (GO:0032787)	1/143	0.382186	0.43555856	2.11171575	2.031149545
negative regulation of cell migration (GO:0030336)	1/144	0.384271	0.436844863	2.09684255	2.005437943
regulation of mRNA stability (GO:0043488)	1/146	0.388419	0.440465136	2.0677116	1.955374505
positive regulation of intracellular protein transport (GO:0090316)	1/148	0.39254	0.443943203	2.03937333	1.907053451
transmembrane receptor protein tyrosine kinase signaling pathway (GO:0007169)	2/404	0.393429	0.443943203	1.49491007	1.394534282
positive regulation of Wnt signaling pathway (GO:0030177)	1/153	0.402723	0.453310952	1.97179027	1.793357432

rRNA metabolic process (GO:0016072)	1/162	0.42063	0.472304202	1.86071899	1.611386759
neuron projection development (GO:0031175)	1/171	0.438008	0.48941216	1.7614082	1.454075085
nuclear-transcribed mRNA catabolic process (GO:0000956)	1/171	0.438008	0.48941216	1.7614082	1.454075085
rRNA processing (GO:0006364)	1/173	0.441799	0.492444596	1.74075053	1.422018325
neuron differentiation (GO:0030182)	1/174	0.443686	0.493343836	1.73060081	1.406353861
mitochondrion organization (GO:0007005)	1/175	0.445566	0.494231745	1.72056775	1.390925536
regulation of translation (GO:0006417)	1/178	0.451168	0.499234486	1.69114878	1.346010983
protein stabilization (GO:0050821)	1/179	0.453023	0.499916399	1.68156282	1.331481375
regulated exocytosis (GO:0045055)	1/180	0.454872	0.499916399	1.67208397	1.317165548
regulation of apoptotic process (GO:0042981)	3/742	0.455066	0.499916399	1.21748139	0.958538353
regulation of cellular macromolecule biosynthetic process (GO:2000112)	2/468	0.467103	0.511909358	1.28537471	0.978433495
ribosome biogenesis (GO:0042254)	1/192	0.476585	0.521050675	1.56607964	1.160637184
cellular response to tumor necrosis factor (GO:0071356)	1/194	0.48012	0.522415863	1.54969383	1.137041379
regulation of programmed cell death (GO:0043067)	1/194	0.48012	0.522415863	1.54969383	1.137041379
negative regulation of apoptotic process (GO:0043066)	2/485	0.485807	0.527348221	1.2390508	0.894526216
ncRNA processing (GO:0034470)	1/201	0.492308	0.533139003	1.49492424	1.059379816
generation of neurons (GO:0048699)	1/202	0.494026	0.533734751	1.48741143	1.048874192

regulation of angiogenesis (GO:0045765)	1/203	0.495738	0.534321515	1.479973	1.038508105
protein phosphorylation (GO:0006468)	2/496	0.497696	0.535170052	1.210775	0.844836679
proteasomal protein catabolic process (GO:0010498)	1/205	0.499146	0.535468428	1.465314	1.018184901
positive regulation of nucleic acid-templated transcription (GO:1903508)	2/511	0.513633	0.549719684	1.174187	0.782298062
cellular response to lipid (GO:0071396)	1/219	0.522371	0.557765538	1.370239	0.889801452
transcription, DNA-templated (GO:0006351)	1/221	0.525601	0.559906345	1.357644	0.873253617
cilium organization (GO:0044782)	1/228	0.536738	0.570440454	1.315311	0.818445703
apoptotic process (GO:0006915)	1/231	0.541432	0.572764907	1.297957	0.796346111
regulation of autophagy (GO:0010506)	1/231	0.541432	0.572764907	1.297957	0.796346111
positive regulation of transcription, DNA-templated (GO:0045893)	4/1183	0.565388	0.596725872	1.009949	0.575916598
negative regulation of cellular process (GO:0048523)	2/566	0.569224	0.599390523	1.056683	0.595420593
regulation of canonical Wnt signaling pathway (GO:0060828)	1/253	0.574451	0.602119048	1.183321	0.655963809
positive regulation of phosphorylation (GO:0042327)	1/253	0.574451	0.602119048	1.183321	0.655963809
plasma membrane bounded cell projection assembly (GO:0120031)	1/278	0.609135	0.637012963	1.075155	0.532971406
proteasome-mediated ubiquitin-dependent protein catabolic process (GO:0043161)	1/321	0.662395	0.691128736	0.928645	0.382503321
cellular response to oxygen-containing compound (GO:1901701)	1/323	0.66469	0.691943498	0.922783	0.376897134
positive regulation of cytokine production (GO:0001819)	1/335	0.67814	0.704341272	0.889085	0.345321634

ubiquitin-dependent protein catabolic process (GO:0006511)	1/354	0.698358	0.723695166	0.84041549	0.301728937
positive regulation of protein phosphorylation (GO:0001934)	1/371	0.715384	0.739661276	0.80110565	0.268319476
negative regulation of cell population proliferation (GO:0008285)	1/379	0.723065	0.74591534	0.78383037	0.25416232
phosphorylation (GO:0016310)	1/400	0.742269	0.764002058	0.74177869	0.221082409
organelle organization (GO:0006996)	1/420	0.759337	0.779813103	0.70564837	0.194272129
organelle assembly (GO:0070925)	1/425	0.763426	0.782255402	0.69714837	0.188187136
nervous system development (GO:0007399)	1/447	0.780623	0.798087074	0.6620125	0.163955584
negative regulation of nucleic acid-templated transcription (GO:1903507)	1/464	0.793063	0.808995124	0.63714903	0.147724625
cellular response to cytokine stimulus (GO:0071345)	1/482	0.805477	0.81982869	0.61273861	0.132547849
positive regulation of transcription by RNA polymerase II (GO:0045944)	2/908	0.814329	0.826996616	0.64618781	0.132720827
cellular protein modification process (GO:0006464)	2/1025	0.864377	0.87587691	0.56876457	0.082895026
positive regulation of cellular process (GO:0048522)	1/625	0.881249	0.890169317	0.46884713	0.059269388
regulation of gene expression (GO:0010468)	2/1079	0.883097	0.890169317	0.53870438	0.066972054
regulation of transcription, DNA-templated (GO:0006355)	5/2244	0.884326	0.890169317	0.63730928	0.078344292
regulation of cell population proliferation (GO:0042127)	1/764	0.926755	0.930828678	0.38067437	0.028956381
regulation of transcription by RNA polymerase II (GO:0006357)	4/2206	0.946788	0.948863994	0.5112524	0.027955479
negative regulation of transcription, DNA-templated (GO:0045892)	1/948	0.961573	0.961573154	0.30376628	0.011902971

Table 2.S3 NormZ values figure 2.5, 2.S3F and 2.6.

	Cisplatin1	CPT1	Etoposide	HU	IR	Doxorubicir	H2O2	MMS	Pyridostatin	UV
AIP	-0.66	-1.01	-0.65	-1.51	-1.53	-4.33	-2.55	-4.01	-2.34	-2.46
ATG9A	0.29	1.04	-0.51	1.99	1.1	-2.98	-0.38	-2.18	-1.58	-1.82
C1orf112	-1.12	-0.76	-0.76	-1.08	-1.1	-2.1	-2.39	-1.97	-1.6	-1.69
CUL5	-1.7	-3.51	-0.61	-1.01	-2.27	-2.46	-1.03	0.12	-0.42	-1.62
FIGNL1	-2.68	-0.42	-0.51	-0.74	-1.97	-0.11	1.2	-0.77	-0.63	0.41
GLRX3	-0.91	-0.76	-2.03	0.12	-1.23	-1.66	-0.92	-2.9	-2.8	-2.5
HIRA	0.09	-0.6	0	1.63	2.42	-3.58	0.93	-3.72	-2.32	-0.3
MCM9	-0.17	0.53	0.29	1.5	0.98	-1.1	0.43	-2.5	0.1	0.41
MORF4L1	-0.77	-2.62	-1.89	-1.64	-1.5	-1.7	0.12	-2.02	-0.25	-1.85
NAE1	-1.22	-1.41	-0.98	1.17	1.43	-6.27	0.9	-5.78	-3.93	-8.48
NF2	1.27	0.19	-2.2	-1.46	-0.37	-5.03	-1.14	1.89	9.86	-2.78
PAXIP1	-0.61	-3.3	-1.47	0.16	-1.77	-5.18	2.31	-3.25	0.36	-3.96
PPIL2	0.24	-0.82	-1.92	1.05	0.47	-2.59	0.52	-2.49	-1.41	-2.36
PPP2R4	-7.2	-9.35	-2.9	-1.09	-2.2	-4.86	-3.33	-5.67	-6.27	-4.56
VCPIP1	-0.52	-1.22	-1.49	-1.03	-0.59	-0.77	-0.04	-1.98	0.08	-1.65
XRCC3	-6.76	-4.03	-6.72	-2.23	-0.46	-3.75	-0.18	-2.37	-3.17	-3.29
	Bleomycin	Olaparib	AZD6738	Cisplatin2	Cisplatin3	ICRF	Formaldehy	PhenDC3	Duocarmyc	Trabectedin
AIP	2.92	-0.14	1.53	-0.8	-0.39	1.38	2.96	-2.13	-3.6	-1.67
ATG9A	0.12	-0.01	-7.06	-1.83	-2.21	-2.05	-0.88	-6.52	-3.15	-1.68
C1orf112	0.77	-0.49	-2.33	-3.69	-4.5	0.74	-0.28	0.01	0.12	0.64
CUL5	1.45	1.16	0.41	-0.8	-1.89	-2.87	-0.61	-2.07	-2.97	-1.98
FIGNL1	0.64	-0.6	-1.97	-2.57	-2.5	0.67	-1.14	-1.39	-0.46	-1.12
GLRX3	-1.05	-0.43	-1.54	-2.14	-2.71	-0.64	-1.22	-1.88	1.12	0.23
HIRA	1.82	-1.59	-7.17	-2.9	-0.67	0.08	1.1	4.07	0.6	0.11
MCM9	0.82	-0.38	-3.67	-5.51	-6.27	1.12	-1.42	-0.51	-0.85	-1.7
MORF4L1	-0.21	-0.2	-2.72	-1.21	-1.39	-1.8	-1.88	0.31	-2.16	-1.53
NAE1	0.65	0.78	-1.76	-4.84	-6.98	-5.71	4.07	0.48	-1.24	3.56
NF2	-0.37	-0.03	0.97	0.57	-0.86	-14.98	0.61	-0.33	-4.14	-1.26
PAXIP1	-0.59	-2.89	0.58	-4.37	-4.4	-5.75	0.47	3.38	-0.31	-1.35
PPIL2	1.3	-0.38	0.25	-1.89	-2.08	-0.35	0.17	-2.59	-0.78	-1.64
PPP2R4	0.62	-0.59	-1.75	-13.64	-10.59	0.01	-3.41	-0.74	1.87	-1.07
VCPIP1	0.46	0.94	-0.38	-1.95	0.48	0.72	-1.31	-1.34	0.44	0.43
XRCC3	-1.38	-5.25	1.82	-1.91	-3.27	0.05	-0.03	1.26	2.04	1.61

Table 2.S4 Hits from mTurboID Figure 2.4 and 2.5

C1orf112_NT									
Bait	**Treatment**	**PreyGene**	**Spec**	**SpecSum**	**AvgSpec**	**SAF**	**ctrlCounts**	**AvgP**	**Crapome_Freq.**
C1orf112	NT	RPL19	54|34|54	142	47.33	0.24147959	15|14|21	1	0.639664804
C1orf112	NT	CEP131	112|99|126	337	112.33	0.10400926	0|0|0	1	0.018156425
C1orf112	NT	ACTBL2	38|32|46	116	38.67	0.10284574	0|0|0	1	0.877094972
C1orf112	NT	PCM1	160|146|165	471	157	0.07756917	49|40|41	1	0.177374302
C1orf112	NT	UBR5	195|178|196	569	189.67	0.06776349	60|54|51	1	0.061452514
C1orf112	NT	DCXR	15|15|15	45	15	0.06198347	0|0|0	1	0.068435754
C1orf112	NT	CCDC138	38|36|45	119	39.67	0.05965414	1|5|4	1	0.039106145
C1orf112	NT	FIGNL1	32|41|44	117	39	0.0578635	0|0|0	1	0.01396648
C1orf112	NT	FLOT1	27|20|23	70	23.33	0.054637	5|5|7	1	0.062849162
C1orf112	NT	OFD1	50|51|56	157	52.33	0.05170949	4|1|4	1	0.089385475
C1orf112	NT	H2AFZ	6|7|6	19	6.33	0.04945313	0|0|0	1	0.68575419
C1orf112	NT	CYB5R3	13|16|11	40	13.33	0.04794964	0|0|2	1	0.089385475
C1orf112	NT	RAP1B	8|6|6	20	6.67	0.04042424	0|0|0	1	0.163407821
C1orf112	NT	ERCC6L	49|47|47	143	47.67	0.038136	9|13|9	1	0.086592179
C1orf112	NT	MTCH2	13|13|8	34	11.33	0.03739274	0|0|0	1	0.118715084
C1orf112	NT	NUDT19	14|14|14	42	14	0.03733333	0|1|3	1	0.023743017
C1orf112	NT	HMGN2	0|5|5	10	3.33	0.037	0|0|0	1	0.269553073
C1orf112	NT	NARS	19|16|18	53	17.67	0.03224453	3|0|6	1	0.089385475
C1orf112	NT	LYZ	4|7|3	14	4.67	0.03176871	0|0|0	1	0.058659218
C1orf112	NT	HADHA	20|27|21	68	22.67	0.02971166	0|0|3	1	0.215083799
C1orf112	NT	RPL29	5|5|4	14	4.67	0.02937107	0|0|0	1	0.55726257
C1orf112	NT	YKT6	7|8|2	17	5.67	0.02863636	0|0|0	1	0.093575419

C1orf112	NT	AKR1A1	9|9|9	27	9	0.02769231	0|0|0	1	0.069832402
C1orf112	NT	PDHA1	13|11|10	34	11.33	0.02647196	0|0|0	1	0.175977654
C1orf112	NT	SAR1B	6|9|0	15	5	0.02525253	0|0|0	1	0.069832402
C1orf112	NT	PITPNB	6|10|3	19	6.33	0.02335793	0|0|1	1	0.085195531
C1orf112	NT	CYP51A1	8|11|9	28	9.33	0.02309406	0|0|1	1	0.022346369
C1orf112	NT	PRPSAP1	9|8|8	25	8.33	0.02163636	0|0|0	1	0.122905028
C1orf112	NT	KRT5	20|17|0	37	12.33	0.02089831	0|0|0	1	0.709497207
C1orf112	NT	MAPK1	7|6|9	22	7.33	0.02036111	0|0|1	1	0.065642458
C1orf112	NT	CEP72	8|13|18	39	13	0.02009274	0|0|0	1	0.005586592
C1orf112	NT	PIBF1	11|14|19	44	14.67	0.01937913	3|3|2	1	0.002793296
C1orf112	NT	PPIC	2|4|6	12	4	0.01886792	0|0|0	1	0.008379888
C1orf112	NT	ACTN1	19|14|18	51	17	0.01859956	0|0|0	1	0.438547486
C1orf112	NT	SERPINB6	9|6|4	19	6.33	0.01683511	0|0|0	1	0.101955307
C1orf112	NT	RRAS2	2|4|4	10	3.33	0.01632353	0|0|0	1	0.027932961
C1orf112	NT	BIRC6	64|67|87	218	72.67	0.01496191	20|17|11	1	0.05027933
C1orf112	NT	KRT14	10|0|11	21	7	0.01483051	0|0|0	1	0.730446927
C1orf112	NT	GNB4	7|0|8	15	5	0.01470588	0|0|0	1	0.201117318
C1orf112	NT	CHID1	6|4|7	17	5.67	0.01442748	0|0|0	1	0.026536313
C1orf112	NT	FAM193A	13|19|20	52	17.33	0.0136996	4|5|3	1	0.033519553
C1orf112	NT	PTPA	2|7|4	13	4.33	0.01340557	0|0|0	1	0.018156425
C1orf112	NT	GPS2	3|6|4	13	4.33	0.01324159	0|0|0	1	0.004189944
C1orf112	NT	CDK4	3|4|5	12	4	0.01320132	0|0|0	1	0.227653631
C1orf112	NT	GPI	8|7|7	22	7.33	0.0131362	0|0|0	1	0.196927374
C1orf112	NT	PMPCA	7|10|3	20	6.67	0.01270476	0|0|0	1	0.087988827
C1orf112	NT	ADSS	3|8|6	17	5.67	0.01243421	0|0|0	1	0.107541899
C1orf112	NT	RRP8	5|5|4	14	4.67	0.01024123	0|0|0	1	0.069832402
C1orf112	NT	DNAJC7	4|6|3	13	4.33	0.00988584	0|0|0	1	0.209497207
C1orf112	NT	SATB2	6|5|10	21	7	0.0095498	0|0|0	1	0.039106145
C1orf112	NT	LTA4H	10|4|2	16	5.33	0.00908007	0|0|0	1	0.092178771

C1orf112	NT	COX15	4|4|3	11	3.67	0.00895122	0|0|0	1	0.00698324
C1orf112	NT	FYN	7|0|7	14	4.67	0.00869646	0|0|0	1	0.244413408
C1orf112	NT	CSPP1	13|7|9	29	9.67	0.00791974	0|0|0	1	0.002793296
C1orf112	NT	SRC	6|6|0	12	4	0.00746269	0|0|0	1	0.043296089
C1orf112	NT	PDE12	2|4|5	11	3.67	0.00602627	0|0|0	1	0.099162011
C1orf112	NT	SSX2IP	4|3|4	11	3.67	0.0059772	0|0|0	1	0.009776536
C1orf112	NT	ALDH7A1	5|4|0	9	3	0.00587084	0|0|0	1	0.12150838
C1orf112	NT	SRPK2	5|3|4	12	4	0.00581395	0|0|0	1	0.170391061
C1orf112	NT	ALDH9A1	5|4|0	9	3	0.00579151	0|0|0	1	0.145251397
C1orf112	NT	PREP	2|5|4	11	3.67	0.00516901	0|0|0	1	0.011173184
C1orf112	NT	CAMK2B	5|0|4	9	3	0.0045045	0|0|0	1	0.046089385
C1orf112	NT	VCPIP1	6|3|5	14	4.67	0.0038216	0|0|0	1	0.148044693
C1orf112	NT	KRBA1	2|4|5	11	3.67	0.00356311	0|0|0	1	0
C1orf112	NT	NCKAP5L	3|4|6	13	4.33	0.00324588	0|0|0	1	0
C1orf112	NT	LOC101060252	8|6|6	20	6.67	0.04388158	0|0|1	0.99	
C1orf112	NT	CS	12|13|11	36	12	0.02575107	0|0|2	0.99	0.270949721
C1orf112	NT	PCMT1	7|6|6	19	6.33	0.02221053	0|0|1	0.99	0.417597765
C1orf112	NT	SPCS3	3|5|2	10	3.33	0.0185	0|0|0	0.99	0.027932961
C1orf112	NT	SNX12	4|0|3	7	2.33	0.01438272	0|0|0	0.99	0.015363128
C1orf112	NT	DEGS1	7|3|3	13	4.33	0.01340557	0|0|0	0.99	0.001396648
C1orf112	NT	TST	2|5|3	10	3.33	0.01121212	0|0|0	0.99	0.029329609
C1orf112	NT	NANS	6|3|2	11	3.67	0.01022284	0|0|0	0.99	0.053072626
C1orf112	NT	IDH3G	4|2|3	9	3	0.00763359	0|0|0	0.99	0.016759777
C1orf112	NT	ALDH2	3|3|5	11	3.67	0.00709865	0|0|0	0.99	0.111731844
C1orf112	NT	AGPS	6|3|3	12	4	0.00607903	0|0|0	0.99	0.078212291
C1orf112	NT	MIPEP	6|3|3	12	4	0.0056101	0|0|0	0.99	0.005586592
C1orf112	NT	UAP1L1	0|3|4	7	2.33	0.00459566	0|0|0	0.99	0.009776536
C1orf112	NT	CCDC14	7|1|3	11	3.67	0.00402412	0|0|0	0.99	0.002793296

C1orf112	NT	SRRT	2|4|3	9	3	0.00342857	0|0|0	0.99	0.238826816
C1orf112	NT	PBRM1	3|4|3	10	3.33	0.00210493	0|0|0	0.99	0.068435754
C1orf112	NT	HRNR	2|3|7	12	4	0.00140351	0|0|0	0.99	0.311452514
C1orf112	NT	RPL36	2|3|3	8	2.67	0.02542857	0|0|0	0.98	0.308659218
C1orf112	NT	RHOA	3|5|6	14	4.67	0.02419689	1|0|0	0.98	0.12150838
C1orf112	NT	FAIM	3|3|0	6	2	0.01117318	0|0|0	0.98	0.008379888
C1orf112	NT	NUDT4	3|0|3	6	2	0.01111111	0|0|0	0.98	0.01396648
C1orf112	NT	FH	5|6|3	14	4.67	0.00915686	0|0|1	0.98	0.101955307
C1orf112	NT	CRKL	3|3|1	7	2.33	0.00768977	0|0|0	0.98	0.304469274
C1orf112	NT	ALDOA	3|3|2	8	2.67	0.00733516	0|0|0	0.98	0.420391061
C1orf112	NT	SMU1	3|1|3	7	2.33	0.00454191	0|0|0	0.98	0.101955307
C1orf112	NT	DIP2B	0|3|3	6	2	0.00126904	0|0|0	0.98	0.016759777
C1orf112	NT	HERC2	3|0|3	6	2	0.00041374	0|0|0	0.98	0.015363128
C1orf112	NT	IFI16	5|8|11	24	8	0.01097394	0|2|1	0.97	0.023743017
C1orf112	NT	PLPBP	5|2|1	8	2.67	0.00970909	0|0|0	0.94	0.117318436
C1orf112	NT	SCO2	2|1|4	7	2.33	0.0087594	0|0|0	0.94	0.078212291
C1orf112	NT	MAP2K3	2|5|0	7	2.33	0.00732704	0|0|0	0.94	0.030726257
C1orf112	NT	MBNL1	4|2|1	7	2.33	0.00600515	0|0|0	0.94	0.011173184
C1orf112	NT	MORF4L1	0|4|2	6	2	0.00552486	0|0|0	0.94	0.036312849
C1orf112	NT	LUC7L2	2|4|0	6	2	0.00510204	0|0|0	0.94	0.463687151
C1orf112	NT	GPR180	4|0|2	6	2	0.00454545	0|0|0	0.94	0.001396648
C1orf112	NT	ACBD3	5|0|2	7	2.33	0.00441288	0|0|0	0.94	0.149441341
C1orf112	NT	ARIH1	4|0|2	6	2	0.00359066	0|0|0	0.94	0.00698324
C1orf112	NT	C2CD3	4|1|2	7	2.33	0.00118696	0|0|0	0.94	0
C1orf112	NT	KMT2D	0|2|4	6	2	0.00036121	0|0|0	0.94	0.05726257
C1orf112	NT	UFM1	2|3|0	5	1.67	0.01964706	0|0|0	0.93	0.025139665
C1orf112	NT	MGST1	2|3|1	6	2	0.01290323	0|0|0	0.93	0.001396648
C1orf112	NT	YBEY	2|3|1	6	2	0.01197605	0|0|0	0.93	0.009776536
C1orf112	NT	CSN2	2|3|0	5	1.67	0.00745536	0|0|0	0.93	0.184357542

C1orf112	NT	SDR39U1	2|0|3	5	1.67	0.00569966	0|0|0	0.93	0.002793296
C1orf112	NT	PPP2R2A	3|2|2	7	2.33	0.00509847	0|0|0	0.93	0.424581006
C1orf112	NT	MAPK12	2|0|3	5	1.67	0.00467787	0|0|0	0.93	0.005586592
C1orf112	NT	MAPK14	0|2|3	5	1.67	0.00463889	0|0|0	0.93	0.00698324
C1orf112	NT	PTPN9	3|1|2	6	2	0.00337268	0|0|0	0.93	0.00698324
C1orf112	NT	CARM1	3|2|1	6	2	0.00328947	0|0|0	0.93	0.113128492
C1orf112	NT	GALNT2	2|0|3	5	1.67	0.00292469	0|0|0	0.93	0.019553073
C1orf112	NT	TRAFD1	2|0|3	5	1.67	0.00286942	0|0|0	0.93	0.026536313
C1orf112	NT	DHX33	2|0|3	5	1.67	0.00236209	0|0|0	0.93	0.027932961
C1orf112	NT	NEDD4L	3|0|2	5	1.67	0.00174869	0|0|0	0.93	0.004189944
C1orf112	NT	RPL35	9|8|5	22	7.33	0.0595935	0|0|2	0.92	0.421787709
C1orf112	NT	PABPN1	4|5|4	13	4.33	0.01415033	0|0|1	0.91	0.287709497
C1orf112	NT	AGO2	12|7|8	27	9	0.01090909	1|0|3	0.91	0.12849162
C1orf112	NT	LDHA	11|11|9	31	10.33	0.03770073	3|2|3	0.9	0.424581006
C1orf112	NT	UQCR10	2|2|1	5	1.67	0.02650794	0|0|0	0.89	0.011173184
C1orf112	NT	UBL5	0|2|2	4	1.33	0.01821918	0|0|0	0.89	0.030726257
C1orf112	NT	MTPN	2|2|2	6	2	0.01694915	0|0|0	0.89	0.173184358
C1orf112	NT	CUL2	12|13|8	33	11	0.0147651	5|1|2	0.89	0.048882682
C1orf112	NT	SRP19	2|1|2	5	1.67	0.01391667	0|0|0	0.89	0.00698324
C1orf112	NT	SRP14	2|1|2	5	1.67	0.01227941	0|0|0	0.89	0.472067039
C1orf112	NT	TMEM256	2|2|0	4	1.33	0.01176991	0|0|0	0.89	0.008379888
C1orf112	NT	GLRX5	0|2|2	4	1.33	0.00847134	0|0|0	0.89	0.027932961
C1orf112	NT	ANP32B	2|2|2	6	2	0.00796813	0|0|0	0.89	0.159217877
C1orf112	NT	MRPL9	2|2|2	6	2	0.00749064	0|0|0	0.89	0.061452514
C1orf112	NT	GCLM	2|2|2	6	2	0.00729927	0|0|0	0.89	0.040502793
C1orf112	NT	BPNT1	2|2|2	6	2	0.00649351	0|0|0	0.89	0.043296089
C1orf112	NT	UCHL5	2|2|2	6	2	0.00609756	0|0|0	0.89	0.082402235
C1orf112	NT	EMC2	2|2|1	5	1.67	0.0056229	0|0|0	0.89	0.011173184
C1orf112	NT	TRABD	2|2|2	6	2	0.00531915	0|0|0	0.89	0.018156425

C1orf112	NT	TSPYL1	2|2|2	6	2	0.00457666	0|0|0	0.89	0.030726257
C1orf112	NT	ADPGK	2|2|2	6	2	0.00403226	0|0|0	0.89	0.01396648
C1orf112	NT	SCCPDH	0|2|2	4	1.33	0.00310023	0|0|0	0.89	0.016759777
C1orf112	NT	DGKE	2|1|2	5	1.67	0.00294533	0|0|0	0.89	0.004189944
C1orf112	NT	SLC19A1	2|2|0	4	1.33	0.00241379	0|0|0	0.89	0.008379888
C1orf112	NT	CNOT6L	0|2|2	4	1.33	0.0023964	0|0|0	0.89	0.001396648
C1orf112	NT	RFTN1	2|0|2	4	1.33	0.00230104	0|0|0	0.89	0.01396648
C1orf112	NT	WDR46	2|0|2	4	1.33	0.00218033	0|0|0	0.89	0.011173184
C1orf112	NT	BRAT1	2|1|2	5	1.67	0.0020341	0|0|0	0.89	0.005586592
C1orf112	NT	TCF25	2|0|2	4	1.33	0.00196746	0|0|0	0.89	0.001396648
C1orf112	NT	PPP4R1	2|0|2	4	1.33	0.0014	0|0|0	0.89	0.011173184
C1orf112	NT	SLTM	2|0|2	4	1.33	0.00130906	0|0|0	0.89	0.11452514
C1orf112	NT	IDE	2|2|0	4	1.33	0.0013052	0|0|0	0.89	0.061452514
C1orf112	NT	VPS13C	2|0|2	4	1.33	0.00035849	0|0|0	0.89	0.016759777
C1orf112	NT	CKB	61|45|47	153	51	0.13385827	0|2|18	0.88	0.430167598
C1orf112	NT	RAB2A	14|13|15	42	14	0.07446809	0|0|4	0.88	0.113128492
C1orf112	NT	LMAN2	8|6|7	21	7	0.01966292	0|0|2	0.87	0.030726257
C1orf112	NT	PHF5A	4|4|2	10	3.33	0.03027273	0|0|1	0.85	0.18575419
C1orf112	NT	HNRNPUL2	18|15|13	46	15.33	0.02052209	2|4|6	0.85	0.188547486
C1orf112	NT	POR	4|4|4	12	4	0.00588235	0|0|1	0.85	0.043296089
C1orf112	NT	LAP3	15|9|12	36	12	0.02312139	0|0|4	0.84	0.083798883
C1orf112	NT	RPS10-NUDT3	22|20|20	62	20.67	0.07103093	7|7|0	0.83	0.430167598
C1orf112	NT	CDC42	8|6|8	22	7.33	0.03837696	2|2|2	0.83	0.230446927
C1orf112	NT	GSTP1	7|7|7	21	7	0.03333333	0|0|2	0.83	0.229050279
C1orf112	NT	MAD2L1	7|6|7	20	6.67	0.03253659	2|0|0	0.83	0.101955307
C1orf112	NT	NT5DC1	7|7|4	18	6	0.01318681	0|0|2	0.83	0.055865922
C1orf112	NT	GLRX3	9|10|6	25	8.33	0.02486567	0|0|3	0.79	0.155027933
C1orf112	NT	RPS10	22|18|20	60	20	0.12121212	0|0|8	0.77	0.469273743

C1orf112	NT	MRPL15	5|6|7	18	6	0.02027027	0|0|2	0.77	0.078212291
C1orf112	NT	CORO1B	4|3|3	10	3.33	0.00680982	1|0|0	0.72	0.219273743
C1orf112_NCS									
C1orf112	NCS	HIST1H2BB	107|91|116	314	104.67	0.83071429	0|0|0	1	0.716480447
C1orf112	NCS	SLC25A4	30|33|33	96	32	0.10738255	0|0|0	1	0.667597765
C1orf112	NCS	CEP131	107|103|107	317	105.67	0.09784259	0|0|0	1	0.018156425
C1orf112	NCS	PCM1	155|158|158	471	157	0.07756917	23|27|28	1	0.177374302
C1orf112	NCS	UBR5	198|206|190	594	198	0.07073955	11|31|41	1	0.061452514
C1orf112	NCS	KRT2	49|34|41	124	41.33	0.06467919	0|0|0	1	0.877094972
C1orf112	NCS	FIGNL1	38|44|44	126	42	0.06231454	3|0|0	1	0.01396648
C1orf112	NCS	CCDC138	30|38|41	109	36.33	0.05463158	0|0|4	1	0.039106145
C1orf112	NCS	LYZ	8|7|7	22	7.33	0.04986395	0|0|0	1	0.058659218
C1orf112	NCS	TNRC6B	79|90|87	256	85.33	0.04952409	22|18|30	1	0.226256983
C1orf112	NCS	SUMO1	4|5|6	15	5	0.04950495	0|0|0	1	0.201117318
C1orf112	NCS	OFD1	45|53|49	147	49	0.04841897	0|0|0	1	0.089385475
C1orf112	NCS	TNRC6A	77|92|78	247	82.33	0.04196228	12|12|23	1	0.173184358
C1orf112	NCS	ERCC6L	54|47|44	145	48.33	0.038664	4|6|6	1	0.086592179
C1orf112	NCS	NCOR1	65|88|81	234	78	0.03196721	28|15|22	1	0.141061453
C1orf112	NCS	BCOR	49|51|50	150	50	0.02905288	7|10|11	1	0.131284916
C1orf112	NCS	NSA2	7|6|9	22	7.33	0.02819231	0|0|0	1	0.05027933
C1orf112	NCS	PIBF1	20|15|16	51	17	0.02245707	2|3|2	1	0.002793296
C1orf112	NCS	GNB4	6|7|8	21	7	0.02058824	0|0|0	1	0.201117318
C1orf112	NCS	SNX12	0|5|4	9	3	0.01851852	0|0|0	1	0.015363128
C1orf112	NCS	CEP72	10|11|12	33	11	0.01700155	0|0|0	1	0.005586592
C1orf112	NCS	MTA3	9|8|9	26	8.67	0.01683495	0|0|0	1	0.231843575

C1orf112	NCS	BIRC6	76|74|63	213	71	0.01461808	0|0|5	1	0.05027933
C1orf112	NCS	CLTCL1	0|30|40	70	23.33	0.01422561	0|0|0	1	0.391061453
C1orf112	NCS	TAMM41	5|3|5	13	4.33	0.01370253	0|0|0	1	0.012569832
C1orf112	NCS	FAM193A	16|18|18	52	17.33	0.0136996	5|3|3	1	0.033519553
C1orf112	NCS	DERL1	5|1|4	10	3.33	0.01326693	0|0|0	1	0.008379888
C1orf112	NCS	IFI16	8|9|10	27	9	0.01234568	0|0|0	1	0.023743017
C1orf112	NCS	ORC5	4|5|2	11	3.67	0.01132716	0|0|0	1	0.037709497
C1orf112	NCS	AGO2	6|10|10	26	8.67	0.01050909	0|0|0	1	0.12849162
C1orf112	NCS	CSPP1	13|12|11	36	12	0.00982801	0|0|0	1	0.002793296
C1orf112	NCS	SATB2	6|7|8	21	7	0.0095498	0|0|0	1	0.039106145
C1orf112	NCS	SSX2IP	2|4|7	13	4.33	0.00705212	0|0|0	1	0.009776536
C1orf112	NCS	GPSM1	4|6|4	14	4.67	0.00691852	0|0|0	1	0.005586592
C1orf112	NCS	CHM	9|4|0	13	4.33	0.00663093	0|0|0	1	0
C1orf112	NCS	CCDC14	4|4|5	13	4.33	0.00474781	0|0|0	1	0.002793296
C1orf112	NCS	CUL5	5|4|2	11	3.67	0.00470513	0|0|0	1	0.048882682
C1orf112	NCS	DDX31	2|5|5	12	4	0.00470035	0|0|0	1	0.055865922
C1orf112	NCS	ANAPC1	8|7|7	22	7.33	0.00377058	0|0|0	1	0.120111732
C1orf112	NCS	PIK3C2A	6|3|7	16	5.33	0.00316133	0|0|0	1	0.011173184
C1orf112	NCS	SCD	4|3|4	11	3.67	0.01022284	0|0|0	0.99	0.019553073
C1orf112	NCS	MRPL9	0|4|4	8	2.67	0.01	0|0|0	0.99	0.061452514
C1orf112	NCS	SARM1	4|4|4	12	4	0.00552486	0|0|0	0.99	0.001396648
C1orf112	NCS	FASTKD5	4|4|4	12	4	0.0052356	0|0|0	0.99	0.019553073
C1orf112	NCS	NCKAP5L	3|4|4	11	3.67	0.00275112	0|0|0	0.99	0
C1orf112	NCS	AUP1	3|2|4	9	3	0.00731707	0|0|0	0.98	0.012569832
C1orf112	NCS	ARIH1	3|2|4	9	3	0.005386	0|0|0	0.98	0.00698324
C1orf112	NCS	LMF2	1|3|6	10	3.33	0.00471004	0|0|0	0.98	0.030726257
C1orf112	NCS	ZNF512	0|3|4	7	2.33	0.00410935	0|0|0	0.98	0.12150838
C1orf112	NCS	UBE4A	3|3|4	10	3.33	0.00312383	0|0|0	0.98	0.011173184
C1orf112	NCS	WDR11	6|3|2	11	3.67	0.00299837	0|0|0	0.98	0.060055866

C1orf112	NCS	TSHZ3	4|0|3	7	2.33	0.00215541	0|0|0	0.98	0.053072626
C1orf112	NCS	PBRM1	4|0|3	7	2.33	0.00147282	0|0|0	0.98	0.068435754
C1orf112	NCS	RDH11	10|10|8	28	9.33	0.02933962	2|2|2	0.96	0.039106145
C1orf112	NCS	SALL2	11|13|12	36	12	0.01191658	0|3|3	0.96	0.041899441
C1orf112	NCS	TBL2	3|3|2	8	2.67	0.00597315	0|0|0	0.96	0.065642458
C1orf112	NCS	ERCC3	3|2|3	8	2.67	0.00341432	0|0|0	0.96	0.002793296
C1orf112	NCS	SLFN11	2|3|3	8	2.67	0.00296337	0|0|0	0.96	0.061452514
C1orf112	NCS	ATP13A1	3|2|3	8	2.67	0.00221761	0|0|0	0.96	0.037709497
C1orf112	NCS	ITPR3	0|3|3	6	2	0.00074878	0|0|0	0.96	0.029329609
C1orf112	NCS	LOC100996852	2|4|0	6	2	0.01886792	0|0|0	0.9	
C1orf112	NCS	RHOG	2|4|0	6	2	0.0104712	0|0|0	0.9	0.019553073
C1orf112	NCS	CSN2	0|2|5	7	2.33	0.01040179	0|0|0	0.9	0.184357542
C1orf112	NCS	GPS2	0|4|2	6	2	0.00611621	0|0|0	0.9	0.004189944
C1orf112	NCS	SLC35B2	4|2|1	7	2.33	0.00539352	0|0|0	0.9	0.005586592
C1orf112	NCS	ARAF	2|0|4	6	2	0.00330033	0|0|0	0.9	0.058659218
C1orf112	NCS	KRBA1	4|1|2	7	2.33	0.00226214	0|0|0	0.9	0
C1orf112	NCS	XRN1	0|4|2	6	2	0.00118133	0|0|0	0.9	0.146648045
C1orf112	NCS	MGST1	2|3|2	7	2.33	0.01503226	0|0|0	0.88	0.001396648
C1orf112	NCS	NUDT4	2|0|3	5	1.67	0.00927778	0|0|0	0.88	0.01396648
C1orf112	NCS	SCO2	3|2|0	5	1.67	0.0062782	0|0|0	0.88	0.078212291
C1orf112	NCS	DHCR7	2|3|2	7	2.33	0.00490526	0|0|0	0.88	0.083798883
C1orf112	NCS	CDC25C	3|2|0	5	1.67	0.004175	0|0|0	0.88	0.005586592
C1orf112	NCS	OTUD5	2|2|3	7	2.33	0.00411661	0|0|0	0.88	0.005586592
C1orf112	NCS	NRIP1	2|2|3	7	2.33	0.00201209	0|0|0	0.88	0.001396648
C1orf112	NCS	ANKRD52	3|1|2	6	2	0.00185874	0|0|0	0.88	0.01396648
C1orf112	NCS	INTS5	3|2|0	5	1.67	0.00163886	0|0|0	0.88	0
C1orf112	NCS	PHKA1	2|3|0	5	1.67	0.00136549	0|0|0	0.88	0.044692737
C1orf112	NCS	RESF1	1|3|2	6	2	0.00114482	0|0|0	0.88	

C1orf112	NCS	SPATA2	6|2|4	12	4	0.00769231	0|0|1	0.87	0
C1orf112	NCS	TAB2	1|4|7	12	4	0.00577201	1|0|0	0.87	0.060055866
C1orf112	NCS	NDC1	8|12|5	25	8.33	0.01235905	0|3|1	0.86	0.025139665
C1orf112	NCS	DAD1	5|4|3	12	4	0.03539823	1|0|0	0.84	0.037709497
C1orf112	NCS	SPCS3	2|2|2	6	2	0.01111111	0|0|0	0.8	0.027932961
C1orf112	NCS	ELMOD2	1|2|2	5	1.67	0.00569966	0|0|0	0.8	0.004189944
C1orf112	NCS	DOLPP1	2|2|0	4	1.33	0.00558824	0|0|0	0.8	0.041899441
C1orf112	NCS	MPDU1	2|0|2	4	1.33	0.00538462	0|0|0	0.8	0.061452514
C1orf112	NCS	COX3	0|2|2	4	1.33	0.00511538	0|0|0	0.8	
C1orf112	NCS	NR2F2	2|2|2	6	2	0.00483092	0|0|0	0.8	0.005586592
C1orf112	NCS	GLA	0|2|2	4	1.33	0.00310023	0|0|0	0.8	0.113128492
C1orf112	NCS	RNF44	2|2|0	4	1.33	0.0030787	0|0|0	0.8	0.001396648
C1orf112	NCS	GPR180	0|2|2	4	1.33	0.00302273	0|0|0	0.8	0.001396648
C1orf112	NCS	NF2	2|1|2	5	1.67	0.00283051	0|0|0	0.8	0.011173184
C1orf112	NCS	PPIL2	2|0|2	4	1.33	0.00255769	0|0|0	0.8	0.06424581
C1orf112	NCS	RFTN1	2|2|0	4	1.33	0.00230104	0|0|0	0.8	0.01396648
C1orf112	NCS	TONSL	2|1|2	5	1.67	0.0012119	0|0|0	0.8	0.008379888
C1orf112	NCS	TEX2	0|2|2	4	1.33	0.00117284	0|0|0	0.8	0.051675978
C1orf112	NCS	SMG7	0|2|2	4	1.33	0.00116157	0|0|0	0.8	0.054469274
C1orf112	NCS	WDR33	2|0|2	4	1.33	0.00099551	0|0|0	0.8	0.163407821
C1orf112	NCS	MRPS2	8|14|10	32	10.67	0.0360473	3|3|3	0.79	0.090782123
C1orf112	NCS	CAMK2D	10|12|8	30	10	0.0203252	0|0|3	0.78	0.072625698
C1orf112	NCS	MRPS9	5|8|5	18	6	0.01515152	1|0|1	0.78	0.100558659
C1orf112	NCS	PATL1	7|7|3	17	5.67	0.00736364	2|0|1	0.77	0.034916201
C1orf112	NCS	DCAF7	3|4|4	11	3.67	0.01073099	0|0|1	0.75	0.188547486
C1orf112	NCS	NUP160	11|11|4	26	8.67	0.0060376	0|4|1	0.75	0.115921788
C1orf112	NCS	DHCR24	3|3|6	12	4	0.00775194	0|0|1	0.71	0.012569832
FIGNL1-NT									

Bait	Treatment	PreyGene	Spec	SpecSum	AvgSpec	SAF	ctrlCounts	AvgP	Crapome_Frequency
FIGNL1	NT	CCT2	502|591|627	1720	573.33	1.07164486	133|140|138	1	0.597765363
FIGNL1	NT	TCP1	274|346|381	1001	333.67	0.6001259	123|126|120	1	0.603351955
FIGNL1	NT	CCT7	197|242|276	715	238.33	0.43891344	93|92|92	1	0.502793296
FIGNL1	NT	RPAP3	88|73|61	222	74	0.1112782	27|21|24	1	0.159217877
FIGNL1	NT	PCM1	127|126|117	370	123.33	0.06093379	34|38|34	1	0.177374302
FIGNL1	NT	PFDN6	4|10|9	23	7.67	0.05945736	1|1|0	1	0.061452514
FIGNL1	NT	PDCL3	8|15|14	37	12.33	0.05158996	1|0|0	1	0.012569832
FIGNL1	NT	TNRC6A	96|95|95	286	95.33	0.04858818	22|21|12	1	0.173184358
FIGNL1	NT	TNRC6B	69|77|73	219	73	0.04236796	25|26|15	1	0.226256983
FIGNL1	NT	NUDCD2	5|7|7	19	6.33	0.04031847	0|0|0	1	0.019553073
FIGNL1	NT	AIP	12|15|12	39	13	0.03939394	0|0|1	1	0.054469274
FIGNL1	NT	SIRT2	14|13|17	44	14.67	0.03771208	0|0|0	1	0.00698324
FIGNL1	NT	CEP85	29|27|28	84	28	0.03674541	4|3|2	1	0.012569832
FIGNL1	NT	NUDCD3	14|10|13	37	12.33	0.03415512	0|0|0	1	0.029329609
FIGNL1	NT	NDUFS1	26|19|25	70	23.33	0.03376266	1|5|3	1	0.075418994
FIGNL1	NT	VCPIP1	36|42|30	108	36	0.0294599	0|0|0	1	0.148044693
FIGNL1	NT	FAM193A	36|38|32	106	35.33	0.02792885	5|8|3	1	0.033519553
FIGNL1	NT	C1orf112	27|22|22	71	23.67	0.02774912	1|3|0	1	0.001396648
FIGNL1	NT	NDUFV2	4|6|5	15	5	0.02008032	0|0|0	1	0.018156425
FIGNL1	NT	SMG7	19|17|18	54	18	0.01572052	0|1|3	1	0.054469274
FIGNL1	NT	HELZ	35|29|23	87	29	0.01493306	8|5|2	1	0.067039106
FIGNL1	NT	GNA13	3|8|5	16	5.33	0.01413793	0|0|0	1	0.203910615
FIGNL1	NT	AGO2	13|13|8	34	11.33	0.01373333	1|1|0	1	0.12849162
FIGNL1	NT	PIK3C2A	23|19|25	67	22.33	0.01324437	5|6|5	1	0.011173184

FIGNL1	NT	YEATS2	19|18|19	56	18.67	0.0131294	3|2|2	1	0.13547486
FIGNL1	NT	SLC25A12	11|6|8	25	8.33	0.01228614	0|0|0	1	0.092178771
FIGNL1	NT	MBOAT7	6|4|4	14	4.67	0.01170426	0|0|0	1	0.004189944
FIGNL1	NT	ITCH	6|12|11	29	9.67	0.0112181	0|2|1	1	0.009776536
FIGNL1	NT	WDR92	6|4|2	12	4	0.01120448	0|0|0	1	0.009776536
FIGNL1	NT	ALMS1	42|45|43	130	43.33	0.01039338	9|8|3	1	0.094972067
FIGNL1	NT	NDUFV3	7|4|0	11	3.67	0.00775899	0|0|0	1	0.025139665
FIGNL1	NT	AGO3	8|4|5	17	5.67	0.00659302	0|0|0	1	0.092178771
FIGNL1	NT	PAXIP1	7|4|7	18	6	0.00561272	0|0|0	1	0.023743017
FIGNL1	NT	TCF25	1|4|5	10	3.33	0.00492604	0|0|0	1	0.001396648
FIGNL1	NT	CEP192	10|9|7	26	8.67	0.00341742	0|0|0	1	0.061452514
FIGNL1	NT	UBR3	1|5|5	11	3.67	0.00194386	0|0|0	1	0.004189944
FIGNL1	NT	MUC19	0|4|5	9	3	0.00039567	0|0|0	1	0.004189944
FIGNL1	NT	GLS	53|46|52	151	50.33	0.08416388	11|14|21	0.99	0.075418994
FIGNL1	NT	NME4	12|6|8	26	8.67	0.04636364	1|0|1	0.99	0.039106145
FIGNL1	NT	HSPE1	0|8|6	14	4.67	0.04578431	0|0|1	0.99	0.233240223
FIGNL1	NT	NDUFAF7	13|16|12	41	13.67	0.03985423	2|3|3	0.99	0.018156425
FIGNL1	NT	PFDN1	3|4|4	11	3.67	0.03008197	0|0|0	0.99	0.078212291
FIGNL1	NT	NEK7	4|3|4	11	3.67	0.01215232	0|0|0	0.99	0.00698324
FIGNL1	NT	CDK5RAP2	16|13|13	42	14	0.00841852	0|2|0	0.99	0.015363128
FIGNL1	NT	CRTAP	2|4|4	10	3.33	0.00830424	0|0|0	0.99	0.015363128
FIGNL1	NT	ZC3H7A	6|7|3	16	5.33	0.00548919	1|0|0	0.99	0.033519553
FIGNL1	NT	PPP2R1B	4|0|4	8	2.67	0.00480216	0|0|0	0.99	0.189944134
FIGNL1	NT	TRANK1	4|4|0	8	2.67	0.00091282	0|0|0	0.99	0
FIGNL1	NT	STAT1	26|29|32	87	29	0.04073034	10|9|9	0.98	0.152234637
FIGNL1	NT	NDUFS2	15|10|10	35	11.67	0.02553611	1|3|0	0.98	0.060055866
FIGNL1	NT	DNAJC10	22|20|17	59	19.67	0.02480454	7|5|4	0.98	0.182960894
FIGNL1	NT	YBEY	3|4|0	7	2.33	0.0139521	0|0|0	0.98	0.009776536

FIGNL1	NT	HSPE1-MOB4	3|0|6	9	3	0.01149425	0|0|0	0.98	0.220670391
FIGNL1	NT	PON2	6|3|2	11	3.67	0.01036723	0|0|0	0.98	0.020949721
FIGNL1	NT	TTC4	5|3|2	10	3.33	0.00860465	0|0|0	0.98	0.004189944
FIGNL1	NT	SLC25A15	4|3|0	7	2.33	0.00774086	0|0|0	0.98	0.002793296
FIGNL1	NT	ECI2	0|3|5	8	2.67	0.00677665	0|0|0	0.98	0.034916201
FIGNL1	NT	FBRS	4|0|3	7	2.33	0.00506522	0|0|0	0.98	0.00698324
FIGNL1	NT	ATG9A	3|0|5	8	2.67	0.00318236	0|0|0	0.98	0.001396648
FIGNL1	NT	JAK1	5|2|3	10	3.33	0.00288562	0|0|0	0.98	0.019553073
FIGNL1	NT	GIGYF1	0|5|3	8	2.67	0.00257971	0|0|0	0.98	0.00698324
FIGNL1	NT	HERC2	4|3|3	10	3.33	0.00068887	0|0|0	0.98	0.015363128
FIGNL1	NT	PDRG1	3|2|3	8	2.67	0.02007519	0|0|0	0.96	0.016759777
FIGNL1	NT	BCS1L	8|7|6	21	7	0.01670644	0|1|1	0.96	0.019553073
FIGNL1	NT	C11orf49	3|3|3	9	3	0.00906344	0|0|0	0.96	0.131284916
FIGNL1	NT	URI1	2|3|3	8	2.67	0.00499065	0|0|0	0.96	0.032122905
FIGNL1	NT	FOXRED1	3|1|3	7	2.33	0.00479424	0|0|0	0.96	0.009776536
FIGNL1	NT	NEFH	0|3|3	6	2	0.00196078	0|0|0	0.96	0.365921788
FIGNL1	NT	KIF21A	3|3|3	9	3	0.00183262	0|0|0	0.96	0.030726257
FIGNL1	NT	C3	3|3|0	6	2	0.00120409	0|0|0	0.96	0.062849162
FIGNL1	NT	CRYBG3	12|13|8	33	11	0.0037037	4|2|0	0.95	0.053072626
FIGNL1	NT	DENND4A	5|5|3	13	4.33	0.00232421	0|1|0	0.93	0.043296089
FIGNL1	NT	NDUFA10	22|17|20	59	19.67	0.05540845	5|7|6	0.91	0.093575419
FIGNL1	NT	LRBA	13|25|24	62	20.67	0.0072197	10|6|2	0.91	0.125698324
FIGNL1	NT	MRPL14	4|0|2	6	2	0.0137931	0|0|0	0.9	0.103351955
FIGNL1	NT	RCN2	9|2|2	13	4.33	0.01292537	0|0|0	0.9	0.290502793
FIGNL1	NT	SCD	5|1|2	8	2.67	0.00743733	0|0|0	0.9	0.019553073
FIGNL1	NT	NEMP1	4|2|2	8	2.67	0.00719677	0|0|0	0.9	0.023743017
FIGNL1	NT	DNAJC7	0|2|4	6	2	0.00456621	0|0|0	0.9	0.209497207
FIGNL1	NT	SPATS2L	0|2|5	7	2.33	0.00417563	0|0|0	0.9	0.047486034

FIGNL1	NT	CEP76	0|4|2	6	2	0.0030349	0|0|0	0.9	0
FIGNL1	NT	SMG1	0|2|4	6	2	0.0005463	0|0|0	0.9	0.019553073
FIGNL1	NT	LYRM7	2|2|3	7	2.33	0.02240385	0|0|0	0.88	0.004189944
FIGNL1	NT	CNOT10	5|7|6	18	6	0.00806452	1|1|1	0.88	0.05027933
FIGNL1	NT	STX4	0|2|3	5	1.67	0.0056229	0|0|0	0.88	0.001396648
FIGNL1	NT	KATNA1	2|2|3	7	2.33	0.00474542	0|0|0	0.88	0.008379888
FIGNL1	NT	SSX2IP	3|1|2	6	2	0.00325733	0|0|0	0.88	0.009776536
FIGNL1	NT	QRSL1	0|2|3	5	1.67	0.00316288	0|0|0	0.88	0.002793296
FIGNL1	NT	RAPH1	3|2|1	6	2	0.00310559	0|0|0	0.88	0.104748603
FIGNL1	NT	GTF2H1	2|0|3	5	1.67	0.00304745	0|0|0	0.88	0.011173184
FIGNL1	NT	CDC7	3|2|0	5	1.67	0.00290941	0|0|0	0.88	0.004189944
FIGNL1	NT	USP33	2|3|2	7	2.33	0.00281401	0|0|0	0.88	0
FIGNL1	NT	WDR81	3|7|6	16	5.33	0.00274601	0|1|1	0.88	0.011173184
FIGNL1	NT	SMC6	3|2|2	7	2.33	0.00213566	0|0|0	0.88	0.008379888
FIGNL1	NT	MAP3K4	1|2|3	6	2	0.0012837	0|0|0	0.88	0.001396648
FIGNL1	NT	SOGA1	1|3|2	6	2	0.00120409	0|0|0	0.88	0.009776536
FIGNL1	NT	DOCK11	2|2|3	7	2.33	0.00112397	0|0|0	0.88	0.008379888
FIGNL1	NT	TMEM131	1|2|3	6	2	0.00106213	0|0|0	0.88	0
FIGNL1	NT	CCDC180	0|2|3	5	1.67	0.00098178	0|0|0	0.88	0.001396648
FIGNL1	NT	AGRN	0|3|2	5	1.67	0.00081663	0|0|0	0.88	0.00698324
FIGNL1	NT	DNA2	5|7|9	21	7	0.00660377	0|2|1	0.87	0.004189944
FIGNL1	NT	ITPR3	8|8|13	29	9.67	0.00362037	2|0|2	0.86	0.029329609
FIGNL1	NT	NDUFA12	4|2|5	11	3.67	0.02531034	1|0|0	0.84	0.008379888
FIGNL1	NT	NCDN	4|3|5	12	4	0.00548697	0|0|1	0.84	0.00698324
FIGNL1	NT	KIAA0355	7|9|14	30	10	0.00934579	2|3|2	0.82	0.00698324
FIGNL1	NT	NDUFA2	2|1|2	5	1.67	0.01686869	0|0|0	0.8	0.015363128
FIGNL1	NT	MRPL40	2|2|1	5	1.67	0.0081068	0|0|0	0.8	0.047486034
FIGNL1	NT	GEMIN6	2|2|0	4	1.33	0.00796407	0|0|0	0.8	0.036312849
FIGNL1	NT	UXT	0|2|2	4	1.33	0.00786982	0|0|0	0.8	0.005586592

FIGNL1	NT	RNF114	0|2|2	4	1.33	0.00583333	0|0|0	0.8	0.027932961
FIGNL1	NT	SCO2	0|2|2	4	1.33	0.005	0|0|0	0.8	0.078212291
FIGNL1	NT	ALG1	2|2|2	6	2	0.00431034	0|0|0	0.8	0.002793296
FIGNL1	NT	FYTTD1	2|0|2	4	1.33	0.00418239	0|0|0	0.8	0.033519553
FIGNL1	NT	KCTD12	2|0|2	4	1.33	0.00409231	0|0|0	0.8	0.103351955
FIGNL1	NT	XRCC3	0|2|2	4	1.33	0.00384393	0|0|0	0.8	0.001396648
FIGNL1	NT	SPG7	2|2|1	5	1.67	0.00341513	0|0|0	0.8	0
FIGNL1	NT	SMAD9	2|0|2	4	1.33	0.00284797	0|0|0	0.8	0.012569832
FIGNL1	NT	VAV2	2|2|2	6	2	0.0022779	0|0|0	0.8	0.004189944
FIGNL1	NT	TP73	2|2|0	4	1.33	0.00226576	0|0|0	0.8	0.005586592
FIGNL1	NT	CNTROB	2|2|2	6	2	0.00221484	0|0|0	0.8	0.005586592
FIGNL1	NT	ASCC2	1|2|2	5	1.67	0.00220608	0|0|0	0.8	0.026536313
FIGNL1	NT	MEN1	0|2|2	4	1.33	0.0021626	0|0|0	0.8	0.054469274
FIGNL1	NT	HIRA	2|2|2	6	2	0.00196657	0|0|0	0.8	0.023743017
FIGNL1	NT	NOA1	2|0|2	4	1.33	0.00190544	0|0|0	0.8	0.004189944
FIGNL1	NT	ERCC2	0|2|2	4	1.33	0.00175	0|0|0	0.8	0.001396648
FIGNL1	NT	PARG	1|2|2	5	1.67	0.00171107	0|0|0	0.8	0.065642458
FIGNL1	NT	DDB1	2|1|2	5	1.67	0.00146491	0|0|0	0.8	0.296089385
FIGNL1	NT	PASK	2|1|2	5	1.67	0.00126228	0|0|0	0.8	0.067039106
FIGNL1	NT	KDM4B	0|2|2	4	1.33	0.0012135	0|0|0	0.8	0.001396648
FIGNL1	NT	CCDC158	0|2|2	4	1.33	0.00119497	0|0|0	0.8	0
FIGNL1	NT	DHX34	2|2|0	4	1.33	0.0011636	0|0|0	0.8	0.002793296
FIGNL1	NT	CAMSAP3	0|2|2	4	1.33	0.00106485	0|0|0	0.8	0.124301676
FIGNL1	NT	SIPA1L3	1|2|2	5	1.67	0.00093768	0|0|0	0.8	0.025139665
FIGNL1	NT	COL7A1	0|2|2	4	1.33	0.00045177	0|0|0	0.8	0.001396648
FIGNL1	NT	EIF4ENIF1	8|10|16	34	11.33	0.01150254	2|3|3	0.79	0.115921788
FIGNL1	NT	TTC9C	5|8|3	16	5.33	0.03116959	1|1|1	0.78	0.001396648
FIGNL1	NT	ERAL1	7|8|7	22	7.33	0.01677346	2|0|0	0.77	0.055865922
FIGNL1	NT	POLDIP2	7|8|3	18	6	0.01630435	0|0|2	0.77	0.115921788

FIGNL1	NT	PFDN5	10|9|9	28	9.33	0.06058442	3|2|0	0.75	0.115921788
FIGNL1	NT	MAGED1	10|11|7	28	9.33	0.01199229	0|0|3	0.75	0.125698324
FIGNL1	NT	MYO9B	4|4|0	8	2.67	0.00132047	0|0|1	0.75	0.047486034
FIGNL1	NT	DHX37	8|10|11	29	9.67	0.00835782	4|2|2	0.7	0.090782123
FIGNL1	NT	HLA-A	0|3|6	9	3	0.00821918	0|0|1	0.7	0.159217877
FIGNL1	NT	NAE1	2|6|5	13	4.33	0.00810861	1|1|0	0.7	0.05027933
FIGNL1-NCS									
Bait	**Treatment**	**PreyGene**	**Spec**	**SpecSum**	**AvgSpec**	**SAF**	**ctrlCounts**	**AvgP**	**Crapome_Frequency**
FIGNL1	NCS	CCT2	443|342|434	1219	406.33	0.75949533	95|117|118	1	0.597765363
FIGNL1	NCS	RPAP3	58|59|52	169	56.33	0.08470677	18|20|18	1	0.159217877
FIGNL1	NCS	ACOT1	19|24|25	68	22.67	0.05384798	0|0|0	1	0.117318436
FIGNL1	NCS	PCM1	105|112|103	320	106.67	0.05270257	19|32|31	1	0.177374302
FIGNL1	NCS	PFDN6	8|6|6	20	6.67	0.05170543	0|0|0	1	0.061452514
FIGNL1	NCS	NUDCD2	6|8|8	22	7.33	0.0466879	0|0|0	1	0.019553073
FIGNL1	NCS	CCT6B	26|23|20	69	23	0.04339623	0|0|0	1	0.308659218
FIGNL1	NCS	TNRC6A	75|86|90	251	83.67	0.04264526	25|27|24	1	0.173184358
FIGNL1	NCS	NUDCD3	12|11|10	33	11	0.03047091	0|1|0	1	0.029329609
FIGNL1	NCS	CEP85	21|20|24	65	21.67	0.02843832	1|4|0	1	0.012569832
FIGNL1	NCS	C1orf112	26|22|23	71	23.67	0.02774912	2|3|2	1	0.001396648
FIGNL1	NCS	PDCL3	9|3|7	19	6.33	0.02648536	0|0|0	1	0.012569832
FIGNL1	NCS	NME4	3|7|4	14	4.67	0.02497326	0|0|0	1	0.039106145
FIGNL1	NCS	NDUFS1	14|16|20	50	16.67	0.02412446	0|2|4	1	0.075418994
FIGNL1	NCS	FAM193A	29|31|31	91	30.33	0.02397628	2|5|3	1	0.033519553
FIGNL1	NCS	AIP	8|7|6	21	7	0.02121212	0|0|0	1	0.054469274
FIGNL1	NCS	SIRT2	7|9|6	22	7.33	0.01884319	0|0|0	1	0.00698324
FIGNL1	NCS	VCPIP1	16|20|22	58	19.33	0.01581833	0|0|0	1	0.148044693

FIGNL1	NCS	BCS1L	6|7|6	19	6.33	0.0151074	0|0|0	1	0.019553073
FIGNL1	NCS	BCKDHA	9|8|2	19	6.33	0.01422472	0|0|1	1	0.090782123
FIGNL1	NCS	CNDP2	2|6|8	16	5.33	0.01122105	0|0|0	1	0.025139665
FIGNL1	NCS	AGO2	8|10|9	27	9	0.01090909	0|0|0	1	0.12849162
FIGNL1	NCS	POLDIP2	2|5|5	12	4	0.01086957	0|0|0	1	0.115921788
FIGNL1	NCS	MAGED1	6|10|9	25	8.33	0.01070694	0|0|1	1	0.125698324
FIGNL1	NCS	DNAJC7	6|3|5	14	4.67	0.0106621	0|0|0	1	0.209497207
FIGNL1	NCS	HDAC3	0|7|6	13	4.33	0.01011682	0|0|0	1	0.044692737
FIGNL1	NCS	CEP97	6|10|7	23	7.67	0.00886705	1|0|0	1	0.032122905
FIGNL1	NCS	AHCYL2	8|0|8	16	5.33	0.0087377	0|0|0	1	0.094972067
FIGNL1	NCS	SLC25A12	0|9|8	17	5.67	0.00836283	0|0|0	1	0.092178771
FIGNL1	NCS	TCF25	6|6|4	16	5.33	0.00788462	0|0|0	1	0.001396648
FIGNL1	NCS	NDUFS3	12|16|12	40	13.33	0.05049242	3|2|2	0.99	0.093575419
FIGNL1	NCS	HSPE1	0|4|4	8	2.67	0.02617647	0|0|0	0.99	0.233240223
FIGNL1	NCS	PRDX3	4|4|4	12	4	0.01680672	0|0|0	0.99	0.439944134
FIGNL1	NCS	NDUFV2	4|3|5	12	4	0.01606426	0|0|0	0.99	0.018156425
FIGNL1	NCS	PJA2	4|4|4	12	4	0.00564972	0|0|0	0.99	0
FIGNL1	NCS	SPATS2L	0|4|5	9	3	0.00537634	0|0|0	0.99	0.047486034
FIGNL1	NCS	ATG9A	4|1|4	9	3	0.00357569	0|0|0	0.99	0.001396648
FIGNL1	NCS	AGO3	4|0|5	9	3	0.00348837	0|0|0	0.99	0.092178771
FIGNL1	NCS	CLASP1	0|4|5	9	3	0.0020284	0|0|0	0.99	0.074022346
FIGNL1	NCS	COPS7B	0|3|4	7	2.33	0.00882576	0|0|0	0.97	0.033519553
FIGNL1	NCS	GPS2	0|3|4	7	2.33	0.00712538	0|0|0	0.97	0.004189944
FIGNL1	NCS	STXBP1	2|4|3	9	3	0.00497512	0|0|0	0.97	0.002793296
FIGNL1	NCS	RAVER2	4|3|1	8	2.67	0.00393805	0|0|0	0.97	0.002793296
FIGNL1	NCS	DOCK4	2|4|3	9	3	0.00152594	0|0|0	0.97	0.055865922
FIGNL1	NCS	CRYBG3	3|11|10	24	8	0.0026936	2|2|0	0.96	0.053072626
FIGNL1	NCS	MRPS12	2|3|3	8	2.67	0.01934783	0|0|0	0.95	0.026536313
FIGNL1	NCS	DTYMK	2|3|3	8	2.67	0.01420213	0|0|0	0.95	0.020949721

FIGNL1	NCS	NDUFS2	4|7|8	19	6.33	0.0138512	1|0|1	0.95	0.060055866
FIGNL1	NCS	CLIC4	3|3|3	9	3	0.01185771	0|0|0	0.95	0.06424581
FIGNL1	NCS	ARHGDIA	3|3|0	6	2	0.00980392	0|0|0	0.95	0.136871508
FIGNL1	NCS	SMG1	3|3|0	6	2	0.0005463	0|0|0	0.95	0.019553073
FIGNL1	NCS	STAT2	3|5|6	14	4.67	0.00551358	0|1|0	0.94	0.043296089
FIGNL1	NCS	AFG3L2	18|18|19	55	18.33	0.02299875	3|6|5	0.92	0.104748603
FIGNL1	NCS	DNAJA1	5|9|12	26	8.67	0.02183879	0|2|2	0.92	0.339385475
FIGNL1	NCS	ALMS1	25|23|31	79	26.33	0.00631566	4|5|10	0.91	0.094972067
FIGNL1	NCS	ACOT2	0|24|25	49	16.33	0.03380952	7|8|8	0.89	0.117318436
FIGNL1	NCS	CEP192	3|8|14	25	8.33	0.00328341	0|0|2	0.89	0.061452514
FIGNL1	NCS	NDUFB4	2|0|4	6	2	0.01666667	0|0|0	0.87	0.00698324
FIGNL1	NCS	REEP5	4|0|2	6	2	0.01058201	0|0|0	0.87	0.033519553
FIGNL1	NCS	PSMB4	0|2|4	6	2	0.00757576	0|0|0	0.87	0.208100559
FIGNL1	NCS	ACSF3	2|4|0	6	2	0.00347222	0|0|0	0.87	0.005586592
FIGNL1	NCS	GBE1	0|2|4	6	2	0.002849	0|0|0	0.87	0.025139665
FIGNL1	NCS	KDM6A	0|2|5	7	2.33	0.0016631	0|0|0	0.87	0.020949721
FIGNL1	NCS	CPS1	2|0|5	7	2.33	0.00154714	0|0|0	0.87	0.11452514
FIGNL1	NCS	NCOR2	0|4|2	6	2	0.00081367	0|0|0	0.87	0.078212291
FIGNL1	NCS	PIH1D1	16|20|21	57	19	0.06551724	7|6|5	0.86	0.111731844
FIGNL1	NCS	AK3	3|2|2	7	2.33	0.01026432	0|0|0	0.85	0.008379888
FIGNL1	NCS	ISOC2	3|2|1	6	2	0.00904977	0|0|0	0.85	0.125698324
FIGNL1	NCS	UBE2E3	0|3|2	5	1.67	0.00806763	0|0|0	0.85	0.029329609
FIGNL1	NCS	NEMP1	3|2|2	7	2.33	0.00628032	0|0|0	0.85	0.023743017
FIGNL1	NCS	CTU1	1|2|3	6	2	0.00574713	0|0|0	0.85	0.001396648
FIGNL1	NCS	FYTTD1	3|2|0	5	1.67	0.00525157	0|0|0	0.85	0.033519553
FIGNL1	NCS	C11orf49	0|2|3	5	1.67	0.00504532	0|0|0	0.85	0.131284916
FIGNL1	NCS	SPG7	0|3|2	5	1.67	0.00341513	0|0|0	0.85	0
FIGNL1	NCS	ISYNA1	0|2|3	5	1.67	0.00331349	0|0|0	0.85	0.152234637
FIGNL1	NCS	SLC16A10	3|2|0	5	1.67	0.00324272	0|0|0	0.85	0

FIGNL1	NCS	LRCH2	3|2|2	7	2.33	0.00304575	0|0|0	0.85	0.011173184
FIGNL1	NCS	GYS1	3|2|1	6	2	0.00297177	0|0|0	0.85	0.099162011
FIGNL1	NCS	FAM117B	0|2|3	5	1.67	0.00283531	0|0|0	0.85	0.008379888
FIGNL1	NCS	DSG2	2|3|2	7	2.33	0.00208408	0|0|0	0.85	0.157821229
FIGNL1	NCS	MCM9	2|3|2	7	2.33	0.0020385	0|0|0	0.85	0
FIGNL1	NCS	ZNF507	2|0|3	5	1.67	0.00175236	0|0|0	0.85	0.022346369
FIGNL1	NCS	FASTKD2	4|7|4	15	5	0.00704225	0|1|0	0.84	0.018156425
FIGNL1	NCS	MAIP1	6|4|4	14	4.67	0.01604811	0|0|1	0.83	0.034916201
FIGNL1	NCS	LYRM7	0|2|2	4	1.33	0.01278846	0|0|0	0.75	0.004189944
FIGNL1	NCS	PFDN1	2|0|2	4	1.33	0.01090164	0|0|0	0.75	0.078212291
FIGNL1	NCS	TRMT112	2|0|2	4	1.33	0.01064	0|0|0	0.75	0.068435754
FIGNL1	NCS	MAP1LC3B	0|2|2	4	1.33	0.01064	0|0|0	0.75	0.008379888
FIGNL1	NCS	MOB1A	1|2|2	5	1.67	0.00773148	0|0|0	0.75	0.094972067
FIGNL1	NCS	SDF2	2|2|0	4	1.33	0.00630332	0|0|0	0.75	0.005586592
FIGNL1	NCS	RCN2	2|2|2	6	2	0.00597015	0|0|0	0.75	0.290502793
FIGNL1	NCS	DNAJB11	0|2|2	4	1.33	0.00371508	0|0|0	0.75	0.163407821
FIGNL1	NCS	FAM53C	0|2|2	4	1.33	0.00339286	0|0|0	0.75	0
FIGNL1	NCS	FBRS	0|2|2	4	1.33	0.0028913	0|0|0	0.75	0.00698324
FIGNL1	NCS	C16orf58	0|2|2	4	1.33	0.00284188	0|0|0	0.75	0.002793296
FIGNL1	NCS	P4HA2	2|2|0	4	1.33	0.00249531	0|0|0	0.75	0.023743017
FIGNL1	NCS	CEP95	0|2|2	4	1.33	0.00161998	0|0|0	0.75	0.001396648
FIGNL1	NCS	CHD1L	2|0|2	4	1.33	0.00148272	0|0|0	0.75	0.005586592
FIGNL1	NCS	POLR1B	0|2|2	4	1.33	0.00123262	0|0|0	0.75	0.032122905
FIGNL1	NCS	EGFR	2|2|0	4	1.33	0.00109917	0|0|0	0.75	0.044692737
FIGNL1	NCS	GLI3	0|2|2	4	1.33	0.00084177	0|0|0	0.75	0.002793296
FIGNL1	NCS	DNAJC10	20|27|17	64	21.33	0.02689786	3|8|6	0.73	0.182960894
FIGNL1	NCS	EARS2	6|2|10	18	6	0.01147228	0|2|1	0.71	0.015363128
FIGNL1	NCS	MOCS3	7|3|5	15	5	0.01086957	1|1|0	0.71	0.001396648

Table 2.S5. Primers, sgRNAs, shRNAs and siRNAs sequences used in this study.

Name	Sequence 5'-3'	Used for[a]
sgCtrl (LacZ)	CCCGAATCTCTATCGTGCGG	KO in RPE1-hTERT Cas9 $p53^{-/-}$
sgC1orf112-1 Exon 13	TCCCTCACTGTTTGCTGAAC	KO in RPE1-hTERT Cas9 $p53^{-/-}$
sgC1orf112-2 Exon 5	TTATATGAAGGACTGAGGAG	KO in RPE1-hTERT Cas9 $p53^{-/-}$
sgFANCA	CCACAGCATGCATGTCGGGA	KO in RPE1-hTERT Cas9 $p53^{-/-}$
sgMRE11	GCAATCATGACGATCCCACA	KO in RPE1-hTERT Cas9 $p53^{-/-}$
sgFIGNL1-1	GAAGACCCTGATGCACGCTG	KO in RPE1-hTERT Cas9 $p53^{-/-}$
sgFIGNL1-2	TTCTAAATGGGTAGGTGAGG	KO in RPE1-hTERT Cas9 $p53^{-/-}$
shCtrl (scramble) (Addgene #1864)	CCTAAGGTTAAGTCGCCCTCG CTCGAGCGAGGGCGACTTAAC CTTAGG	KD in RPE1-hTERT WT and $p53^{-/-}$, and in IMR90
shC1orf112-1 (TRCN0000163284)	GCTTCCTGACTATGTTCGTTT	KD in RPE1-hTERT WT and $p53^{-/-}$, and in IMR90
shC1orf112-2 (TRCN0000165342)	GCAAGTTTCCTCCAAGCCTTT	KD in RPE1-hTERT WT and $p53^{-/-}$, and in IMR90
siC1orf112-1 (D-020930-01)	CAUAGUGGCUCAUCUGAUA	KD in U2OS, HeLa DR-GFP, U2OS DR-GFP, U2OS SA-GFP & RPE1-hTERT $p53^{-/-}$

siC1orf112-2 (D-020930-02)	AGACCUCGCUACUUAAAUU	KD in U2OS, U2OS DR-GFP, U2OS SA-GFP, HeLa DR-GFP & RPE1-hTERT $p53^{-/-}$
siC1orf112-3 (D-020930-03)	GAAACGACAACCAGGAUAU	KD in U2OS, U2OS DR-GFP, U2OS SA-GFP, HeLa DR-GFP & RPE1-hTERT $p53^{-/-}$
siC1orf112-4 (D-020930-04)	AGAGAUAGUUCCACAGUGU	KD in U2OS, U2OS 2-6-5, U2OS DR-GFP, U2OS SA-GFP, HeLa DR-GFP & RPE1-hTERT $p53^{-/-}$
siFIGNL1-1 (D-019091-03)	GAGCAUGAAUCUUCUAGAA	KD in HeLa DR-GFP
siFIGNL1-2 (D-019091-17)	GCACAGAUAUUACGCAUUC	KD in U2OS, U2OS DR-GFP & HeLa DR-GFP
siCtIP (M-011376-00)	Smart pool D-011376-01: GAGCAGACCUUUCUCAGUA D-011376-02: GAAGUGAACAAGAUCAUUA D-011376-03: CAACCAAGAUGUAUCCUUU D-011376-04: GAAUAGGACUGAGUACGGU	KD in U2OS DR-GFP, HeLa DR-GFP & U2OS SA-GFP
siRAD51 (M-003530-04)	Smart pool: D-003530-02: GAAGCUAUGUUCGCCAUUA D-003530-05: GCAGUGAUGUCCUGGAUAA D-003530-07: CCAACGAUGUGAAGAAAUU D-003530-08: AAGCUAUGUUCGCCAUUAA	KD in U2OS, U2OS 2-6-5, U2OS DR-GFP & HeLa DR-GFP
siFANCA (custom)	GGACAGAUCUGCACGGCUC	KD in U2OS
siCtrl-1 (custom)	UGGUUUACAUGUCGACUAA	KD in U2OS and U2OS 2-6-5

siCtrl-2 (D-001210-03)	UGGUUUACAUGUUUUCUGA	KD in U2OS and U2OS 2-6-5
GAPDH FW	CAACGTGTCAGTGGTGGACC	RT, qPCR
GAPDH RV	TCGTTGAGGGCAATGCCAGC	RT, qPCR
FIGNL1 FW	ACCAGCCGCAGGTGAAAAC	qPCR
FIGNL1 RV	ACAATGCTCCTTGATGCTGC	qPCR
TKO library outer-PCR primer FW	AGGGCCTATTTCCCATGATTCCTT	PCR
TKO library outer-PCR primer RV	TCAAAAAAGCACCGACTCGG	PCR
TKO library inner-PCR primer trueseq i5 1	AATGATACGGCGACCACCGAGATC TACACTATAGCCTACACTCTTTCCC TACACGACGCTCTTCCGATCTTGTG GAAAGGACGAGGTACCG	PCR
TKO library inner-PCR primer trueseq i5 2	AATGATACGGCGACCACCGAGATC TACACATAGAGGCACACTCTTTCC CTACACGACGCTCTTCCGATCTTGT GGAAAGGACGAGGTACCG	PCR
TKO library inner-PCR primer trueseq i5 3	AATGATACGGCGACCACCGAGATCT ACACCCTATCCTACACTCTTTCCCTA CACGACGCTCTTCCGATCTTGTGGAA AGGACGAGGTACCG	PCR
TKO library inner-PCR primer trueseq i5 4	AATGATACGGCGACCACCGAGATCTA CACGGCTCTGAACACTCTTTCCCTACA CGACGCTCTTCCGATCTTGTGGAAAG GACGAGGTACCG	PCR
TKO library inner-PCR primer trueseq i7 1	CAAGCAGAAGACGGCATACGAGATC GAGTAATGTGACTGGAGTTCAGACGT GTGCTCTTCCGATCTATTTTAACTTGC TATTTCTAGCTCTAAAAC	PCR

TKO library inner-PCR primer trueseq i7 2	CAAGCAGAAGACGGCATACGAGATTC TCCGGAGTGACTGGAGTTCAGACGTG TGCTCTTCCGATCTATTTTAACTTGCTA TTTCTAGCTCTAAAAC	PCR
TKO library inner-PCR primer trueseq i7 3	CAAGCAGAAGACGGCATACGAGATAA TGAGCGGTGACTGGAGTTCAGACGTGT GCTCTTCCGATCTATTTTAACTTGCTAT TTCTAGCTCTAAAAC	PCR
TKO library inner-PCR primer trueseq i7 4	CAAGCAGAAGACGGCATACGAGATGG AATCTCGTGACTGGAGTTCAGACGTGT GCTCTTCCGATCTATTTTAACTTGCTAT TTCTAGCTCTAAAAC	PCR
TKO library inner-PCR primer trueseq i7 5	CAAGCAGAAGACGGCATACGAGATTTC TGAATGTGACTGGAGTTCAGACGTGTG CTCTTCCGATCTATTTTAACTTGCTATTT CTAGCTCTAAAAC	PCR
TKO library inner-PCR primer trueseq i7 6	CAAGCAGAAGACGGCATACGAGATAC GAATTCGTGACTGGAGTTCAGACGTGT GCTCTTCCGATCTATTTTAACTTGCTAT TTCTAGCTCTAAAAC	PCR
C1orf112 FL attb1 cloning FW	GGGGACAAGTTTGTACAAAAAAGCAG GCTTCATGTTTTTACCTCATATGAACCA CC	PCR
C1orf112 FL attb1 cloning RV	GGGGACCACTTTGTACAAGAAAGCTGG GTTTCACCCTAGAGTATGTATGTAACGT	PCR

C1orf112 NTD quickchange oligo FW	GGGGACAAGTTTGTACAAAAAAGCAGG CTTCATG CATGCATTTCATGCCAATACT TGGA	PCR
C1orf112 NTD quickchange oligo RV	GGGGACCACTTTGTACAAGAAAGCTGG GTTTCACCCTAGAGTATGTATGTAACGT	PCR
C1orf112 ΔCTD quickchange oligo FW	GTTCGCTGAGGGAACAAATCATGAAGA GATATAGCCATAGTGTCTCAGTTCTGA	PCR
C1orf112 ΔCTD quickchange oligo RV	TCAGAACTGAGACACTATGGCTATATC TCTTCATGATTTGTTCCCTCAGCGAAC	PCR
C1orf112 ΔWCF quickchange oligo FW	TTTGTTAGCTATGGATGCACTTGCTCGA TATGGGACTG	PCR
C1orf112 ΔWCF quickchange oligo RV	CAGTCCCATATCGAGCAAGTGCATCCAT AGCTAACAAA	PCR
FIGNL1 1-120 & 1-360 oligo FW	GGGGACAAGTTTGTACAAAAAAGCAGG CTCCATGCAGACCTCCAGCTCTA	PCR
FIGNL1 1-120 oligo RV	GGGGACCACTTTGTACAAGAAAGCTGGG TCCTATTGCATCATCTTCTGTACACTACTC	PCR
FIGNL1 1-360 oligo RV	GGGGACCACTTTGTACAAGAAAGCTGGG TCCTAAGGCTTACATTGCATTCCT	PCR
FIGNL1 361-674 oligo FW	GGGGACCACTTTGTACAAGAAAGCTGGG TCCTATTGCATCATCTTCTGTACACTACTC	PCR
FIGNL1 121-674 oligo FW	GGGGACAAGTTTGTACAAAAAAGCAGGC TCCATGGCTGGCAAAAAATTCAAAGA	PCR
FIGNL1 361-674 & 121-674 oligo RV	GGGGACCACTTTGTACAAGAAAGCTGGG TCTTACTTTCCACAACCAAAAGTTTT	PCR
FIGNL1 FRBD (aa) oligo FW	GGGGACAAGTTTGTACAAAAAAGCAGGC TCCATGTTTAAAACTGCAAAAGAACAATT AT	PCR

FIGNL1 FRBD oligo RV	GGGGACCACTTTGTACAAGAAAGCTGGG TCCTATATAGGAGGAACAAACTTTCC	PCR
FIGNL1 ΔFRBD oligo FW	CCCAAGCAAGATGGGGGGAGA	PCR
FIGNL1 ΔFRBD oligo RV	TGTAGGCAGGCTGCTATCCTCC	PCR
FIGNL1 F295E oligo FW	CCTACAGAGAAAACTGCAAAAGAAC	PCR
FIGNL1 F295E oligo RV	CAGGCTGCTATCCTCCTTTG	PCR
FIGNL1 K447A oligo FW	GGTGCAACTCTAATTGGCAAG	PCR
FIGNL1 K447A oligo RV	AGTCCCAGGAGGACCAAAG	PCR
FIGNL1 D500A oligo FW	ATTGCCGAAATTGATTCCTTG	PCR
FIGNL1 D500A oligo RV	AAATATCACAGCTGGTTGCTG	PCR

[a] KD: knockdown

Table 2.S6. Antibodies used in this study

Primary antibodies		
Target	**Catalog number**	**Used for**
Rabbit anti-53BP1	NB100-304 (Novus)	IF
Rabbit anti-BRCA1	07-434 (Millipore)	IF
Mouse anti-BRCA2	OP95 (Calbiochem, Millipore)	IF
Mouse anti-Cas9	14697 (Cell signaling)	
Human anti-centromere (CREST)	HCT-0100 (Immunovision)	IF
Rabbit anti-mCherry	NBP2-25157 (Novus)	WB
Mouse anti-Cyclin A1	611269 (BD Bioscience)	IF
Rabbit anti-C1orf112	ab121774 (Abcam)	WB
Rabbit anti-FANCA	A301-980A-M (Bethyl)	WB
Rabbit anti-FANCD2	NB100-182 (Novus)	IF
Mouse anti-FLAG	M2 (Sigma)	WB
Mouse anti-GFP IgG1κ (clones 7.1 and 13.1)	11814460001 (Sigma)	WB
Mouse anti-phospho-Histone H2A.X (Ser139) (γ-H2AX)	05-636 (Millipore)	IF
Rabbit anti-Lamin-B	Ab16048 (Abcam	IF
Rabbit anti-RAD51	70-001 (Bio Academia)	IF
Anti-Streptavidin HRP conjugated	RPN1231V (GE Healthcare)	WB
Mouse anti-a-Tubulin	CP06 (Sigma)	WB
Secondary antibodies		
Target	**Catalog number**	**Used for**
Alexa Fluor 488 goat anti-rabbit	A-11034 (Thermo Fisher Scientific)	IF
Alexa Fluor 555 goat anti-rabbit	A-21428 (Thermo Fisher Scientific)	IF
Alexa Fluor 647 goat anti-rabbit	A-21244 (Thermo Fisher Scientific)	IF
Alexa Fluor 488 goat anti-mouse	A-11029 (Thermo Fisher Scientific)	IF
Alexa Fluor 555 goat anti-mouse	A-21424 (Thermo Fisher Scientific)	IF
Alexa Fluor 647 goat anti-mouse	A-21236 (Thermo Fisher Scientific)	IF
Alexa Fluor 647 donkey anti-human	A-21445 (Thermo Fisher Scientific)	IF
Goat anti-rabbit HRP	7074 (Cell Signaling)	WB

Sheep anti-mouse-HRP	A-9044	WB

Table 2.S7. Plasmids used in this study

Plasmid	Source
lentiCas9-Blast	Addgene #52962
Toronto KnockOut (TKO) CRISPR library – v1	Addgene #1000000069
pKLV2-U6gRNA5(BbsI)-PGKpuro2AmCherry	Addgene #67977
pKLV2-U6gRNA5(BbsI)-PGKpuro2ABFP	Addgene #67991
pOG44	Invitrogen™ V600520
pDEST-pcDNA5-FLAG-miniturbo	This study
FLAG-miniturbo-C1orf112	This study
pDEST-pcDNA5-FRT-TO-mCherry-LacRnls	Described in (Orthwein *et al*, 2015)
mCherry-LacRnls C1orf112 FL (1-854)	This study
mCherry-LacRnls FIGNL1 1-674	This study
mCherry-LacRnls FIGNL1 1-120	This study
mCherry-LacRnls FIGNL1 121-674	This study
mCherry-LacRnls FIGNL1 1-360	This study
mCherry-LacRnls FIGNL1 361-674	This study
mCherry-LacRnls FIGNL1 FRBD (295-344)	This study
mCherry-LacRnls FIGNL1 ΔFRBD (Δ295-344)	This study
mCherry-LacRnls FIGNL1 F295E	This study
mCherry-LacRnls FIGNL1 K447A	This study
mCherry-LacRnls FIGNL1 D500A	This study
mCherry-LacRnls FIGNL1 KDm (K447A/D500A)	This study
pDEST-pcDNA5-FRT-TO-eGFP	Described in (Escribano-Díaz *et al*, 2013)
GFP-C1orf112 FL (1-854)	This study
GFP-C1orf112 NTD (1-175)	This study
GFP-C1orf112 ΔCTD (1-735)	This study
GFP-C1orf112 ΔWCF (461-463)	This study
GFP-FIGNL1 FL (1-674)	This study
pCBASceI	Addgene #26477

Table 2.S8 Bioinformatic packages and algorithms used in this study.

Tool name	Reference	Source
MAGecK 0.5.9.5	https://sourceforge.net/p/mageck/wiki/Home/	(Li *et al*, 2014)
DrugZ	https://github.com/hart-lab/drugz	(Colic *et al*, 2019)
R-Studio 22.07.1	https://www.r-project.org/	R software
GSEA 4.3.0	https://www.gsea-msigdb.org/gsea/index.jsp	(Subramanian *et al*, 2005; Mootha *et al*, 2003)
Graphpad-Prism 9.3.1	https://www.graphpad.com/scientific-software/prism/	GraphPad
Snapgene 6.0.6	https://www.snapgene.com	Dotmatics
FlowJo 10.7.2	https://www.flowjo.com	FlowJo LLC
Fiji – ImageJ 2.3.0	https://imagej.net/Fiji	(Schneider *et al*, 2012)
Adobe Photoshop 22.1.0	https://www.adobe.com/products/illustrator.html	Adobe
Adobe Illustrator 25.0.1	https://www.adobe.com/products/photoshop.html	Adobe

Table 3.S3 NormZ values for Ramos CRISPR-screen related to figure 3.1 B.

Ramos Sensitizers						
GENE	**sumZ**	**numObs**	**normZ**	**pval_synth**	**rank_synth**	**fdr_synth**
FANCA	-105.9	18	-21.7	9.7E-105	1	1.6E-100
FANCF	-83.57	15	-18.74	1.14E-78	2	9.33E-75
BRIP1	-90.02	18	-18.43	4.13E-76	3	2.26E-72
FANCC	-89.5	18	-18.32	2.95E-75	4	1.21E-71
FANCD2	-78.98	18	-16.15	5.91E-59	5	1.94E-55
FANCE	-72.59	18	-14.83	4.87E-50	6	1.33E-46
FANCI	-65.15	18	-13.29	1.29E-40	7	3.03E-37
FANCG	-58.2	15	-13	5.87E-39	8	1.2E-35
UBE2T	-51.23	12	-12.8	8.68E-38	9	1.58E-34
FANCB	-57.78	18	-11.77	2.79E-32	10	4.57E-29
C17orf70	-51.46	18	-10.47	6.17E-26	11	9.2E-23
FANCL	-35.29	9	-10.15	1.71E-24	12	2.34E-21
RFWD3	-36.75	18	-7.43	5.38E-14	13	6.8E-11
ERCC4	-33.4	18	-6.74	7.97E-12	14	9.34E-09
FANCM	-30.64	18	-6.17	3.44E-10	15	3.77E-07
REV3L	-29.28	18	-5.89	1.94E-09	16	1.99E-06
SLX4	-28.93	18	-5.82	3.02E-09	17	2.91E-06
C19orf40	-27.71	18	-5.56	1.31E-08	18	0.000012
CLEC2A	-14.82	6	-5.14	1.35E-07	19	0.000117
MUS81	-21.91	15	-4.8	8.01E-07	20	0.000658
ERCC1	-23.53	18	-4.7	1.29E-06	21	0.00101
XRCC3	-20.8	18	-4.14	1.75E-05	22	0.013

RAD51D	-20.16	18	-4.01	0.000031	23	0.0221
GEN1	-16.44	12	-4	3.15E-05	24	0.0216
COQ2	-19.14	18	-3.8	7.37E-05	25	0.0484
OFD1	-17.62	18	-3.48	0.00025	26	0.158
CTF1	-14.09	12	-3.41	0.00033	27	0.201
C1orf43	-16.87	18	-3.33	0.000438	28	0.257
ATM	-16.56	18	-3.26	0.000549	29	0.311
XRCC2	-11.58	9	-3.23	0.000627	30	0.343
KCTD5	-13.2	12	-3.18	0.000729	31	0.386
VAPB	-14.35	15	-3.09	0.001	32	0.515
A4GNT	-11.09	9	-3.08	0.00102	33	0.509
H1FX	-14.23	15	-3.06	0.0011	34	0.529
C17orf53	-15.34	18	-3.01	0.0013	35	0.61
DZIP3	-15.23	18	-2.99	0.0014	36	0.639
POLD1	-15.22	18	-2.99	0.00141	37	0.627
RAD51AP1	-12.2	12	-2.93	0.0017	38	0.734
ANKRD10	-14.81	18	-2.9	0.00185	39	0.78
FAM64A	-14.73	18	-2.88	0.00196	40	0.804
SYN1	-14.65	18	-2.87	0.00206	41	0.825
NMRAL1	-14.51	18	-2.84	0.00225	42	0.879
CYP4V2	-14.38	18	-2.81	0.00245	43	0.936
MRE11A	-12.91	15	-2.76	0.00286	44	1.07
CHMP1B	-12.87	15	-2.76	0.00293	45	1.07
DDX1	-12.71	15	-2.72	0.00328	46	1.17
BRCA1	-13.85	18	-2.7	0.00344	47	1.2
CHRAC1	-11.29	12	-2.7	0.00347	48	1.19
NRARP	-11.27	12	-2.69	0.00353	49	1.18
NECAP2	-13.66	18	-2.66	0.00386	50	1.27

PEBP4	-13.65	18	-2.66	0.00388	51	1.25
CXCR7	-9.64	9	-2.66	0.00392	52	1.24
RAD51C	-13.63	18	-2.66	0.00393	53	1.22
GSC	-13.56	18	-2.64	0.00411	54	1.25
S100A13	-11.03	12	-2.63	0.00423	55	1.26
BARD1	-12.67	16	-2.62	0.00442	56	1.29
TEX36	-13.37	18	-2.6	0.0046	57	1.33
ATP6V1C2	-13.35	18	-2.6	0.00465	58	1.32
MCM9	-13.32	18	-2.6	0.00473	59	1.31
JAKMIP2	-13.27	18	-2.58	0.00487	60	1.33
MAD2L2	-13.27	18	-2.58	0.00489	61	1.32
TM9SF1	-13.25	18	-2.58	0.00495	62	1.31
SYNJ1	-13.16	18	-2.56	0.00522	63	1.36
CLUH	-11.98	15	-2.55	0.00533	64	1.37
EPM2AIP1	-10.71	12	-2.55	0.00536	65	1.35
FZD5	-13.06	18	-2.54	0.00553	66	1.37
MGEA5	-13.05	18	-2.54	0.00555	67	1.36
KCNJ2	-13.05	18	-2.54	0.00558	68	1.35
TBATA	-13.02	18	-2.53	0.00567	69	1.35
SCRN2	-11.86	15	-2.53	0.00575	70	1.35
SAMHD1	-12.98	18	-2.52	0.0058	71	1.34
DHX40	-9.16	9	-2.52	0.0059	72	1.34
IGFL2	-9.15	9	-2.52	0.00592	73	1.33
CLEC12B	-12.91	18	-2.51	0.00603	74	1.34
CTBP1	-12.88	18	-2.5	0.00614	75	1.34
SBSN	-12.86	18	-2.5	0.00622	76	1.34
DNAJC5G	-11.74	15	-2.5	0.00622	77	1.32
GPRIN3	-11.74	15	-2.5	0.00624	78	1.31

ITM2B	-10.45	12	-2.49	0.00645	79	1.34
EVC2	-12.74	18	-2.47	0.00668	80	1.37
REXO2	-9	9	-2.47	0.0067	81	1.36
ITK	-12.69	18	-2.46	0.00685	82	1.37
IRAK2	-12.67	18	-2.46	0.00693	83	1.37
G0S2	-10.33	12	-2.46	0.007	84	1.37
ARRDC2	-12.65	18	-2.46	0.00704	85	1.36
STT3A	-12.64	18	-2.45	0.00706	86	1.35
PIN4	-8.93	9	-2.45	0.00711	87	1.34
RTN4RL1	-12.57	18	-2.44	0.00736	88	1.37
HDHD1	-11.47	15	-2.44	0.0074	89	1.36
GPR61	-12.56	18	-2.44	0.0074	90	1.35
CCDC79	-12.51	18	-2.43	0.00762	91	1.37
RPSA	-10.21	12	-2.43	0.00764	92	1.36
CAP2	-12.49	18	-2.42	0.00771	93	1.36
SHISA5	-12.43	18	-2.41	0.00794	94	1.39
C11orf63	-12.41	18	-2.41	0.00806	95	1.39
IGSF10	-12.4	18	-2.41	0.00808	96	1.38
PKD2	-12.38	18	-2.4	0.00818	97	1.38
UHRF2	-11.27	15	-2.39	0.00837	98	1.4
LSM4	-11.26	15	-2.39	0.00838	99	1.39
FXR1	-11.26	15	-2.39	0.00838	100	1.38
LIPH	-12.33	18	-2.39	0.00842	101	1.37
SPATA17	-12.3	18	-2.38	0.00857	102	1.38
PAQR9	-11.19	15	-2.38	0.00876	103	1.4
SLC30A5	-12.25	18	-2.37	0.0088	104	1.39
MUC15	-9.99	12	-2.37	0.00886	105	1.39
TMPRSS11F	-8.65	9	-2.37	0.00888	106	1.38

PLOD2	-9.99	12	-2.37	0.00891	107	1.37
RBM26	-12.2	18	-2.36	0.00905	108	1.37
FOXP1	-12.16	18	-2.35	0.00929	109	1.4
ZNF229	-11.07	15	-2.35	0.00946	110	1.41
MXD3	-12.05	18	-2.33	0.00982	111	1.45
RND3	-12.04	18	-2.33	0.00992	112	1.45
MSL1	-12.01	18	-2.32	0.0101	113	1.46
PPP2R4	-10.96	15	-2.32	0.0101	114	1.45
CDH18	-12	18	-2.32	0.0101	115	1.44
SLC6A5	-11.99	18	-2.32	0.0102	116	1.44
C10orf90	-11.99	18	-2.32	0.0102	117	1.43
CLEC9A	-11.98	18	-2.32	0.0102	118	1.42
PSMB8	-11.97	18	-2.32	0.0103	119	1.42
HADHB	-10.87	15	-2.3	0.0106	120	1.45
CHST9	-8.42	9	-2.3	0.0106	121	1.44
DPYD	-11.91	18	-2.3	0.0107	122	1.43
ARL14EPL	-9.71	12	-2.3	0.0107	123	1.43
HLA-E	-10.84	15	-2.3	0.0108	124	1.44
RRP12	-11.82	18	-2.28	0.0112	125	1.47
ZDHHC6	-8.29	9	-2.27	0.0117	126	1.53
WDR78	-11.7	18	-2.26	0.0119	127	1.54
TNFSF14	-11.67	18	-2.25	0.0121	128	1.55
NXPE3	-10.64	15	-2.25	0.0122	129	1.55
CTSH	-10.64	15	-2.25	0.0122	130	1.54
ZMAT1	-10.63	15	-2.25	0.0123	131	1.54
CNOT2	-11.64	18	-2.25	0.0123	132	1.53
COIL	-9.5	12	-2.25	0.0123	133	1.52
NAALAD2	-11.61	18	-2.24	0.0125	134	1.53

TMEM40	-11.61	18	-2.24	0.0125	135	1.52
MUTYH	-10.58	15	-2.24	0.0127	136	1.53
EPB41L2	-11.58	18	-2.23	0.0127	137	1.53
C19orf69	-9.42	12	-2.23	0.013	138	1.55
KLK12	-11.53	18	-2.23	0.013	139	1.54
AADAT	-10.52	15	-2.22	0.0131	140	1.53
PIR	-11.51	18	-2.22	0.0132	141	1.54
PPARGC1B	-11.51	18	-2.22	0.0132	142	1.53
TMTC2	-11.5	18	-2.22	0.0133	143	1.52
CCBL2	-9.38	12	-2.21	0.0134	144	1.53
GLIS2	-11.48	18	-2.21	0.0134	145	1.52
LAMC2	-11.45	18	-2.21	0.0136	146	1.53
C9orf139	-11.44	18	-2.21	0.0137	147	1.53
WDR35	-11.44	18	-2.21	0.0137	148	1.52
STAP1	-8.09	9	-2.21	0.0137	149	1.51
EMC10	-11.11	17	-2.2	0.0138	150	1.51
TECPR2	-11.42	18	-2.2	0.0138	151	1.5
C1orf137	-6.59	6	-2.2	0.0139	152	1.5
ARGLU1	-11.41	18	-2.2	0.0139	153	1.49
SHB	-11.38	18	-2.19	0.0141	154	1.5
OR1G1	-8.04	9	-2.19	0.0141	155	1.5
FAM89A	-11.37	18	-2.19	0.0142	156	1.49
CTSA	-11.34	18	-2.18	0.0145	157	1.51
HSD17B3	-11.33	18	-2.18	0.0145	158	1.51
CCBP2	-8.01	9	-2.18	0.0145	159	1.5
EXOC6B	-11.31	18	-2.18	0.0147	160	1.51
SMYD1	-11.29	18	-2.18	0.0148	161	1.51
CUZD1	-11.24	18	-2.16	0.0152	162	1.54

ODF3B	-10.25	15	-2.16	0.0153	163	1.54
TLR10	-7.93	9	-2.16	0.0154	164	1.54
CLECL1	-6.47	6	-2.16	0.0155	165	1.54
GNS	-11.2	18	-2.16	0.0155	166	1.54
RNF145	-10.22	15	-2.16	0.0156	167	1.53
C1orf101	-11.17	18	-2.15	0.0158	168	1.54
EAF2	-7.89	9	-2.15	0.0159	169	1.54
TP53TG5	-11.15	18	-2.15	0.0159	170	1.53
TNFSF13	-6.43	6	-2.14	0.016	171	1.54
CASR	-11.13	18	-2.14	0.0161	172	1.54
NKG7	-11.1	18	-2.14	0.0163	173	1.55
ADAMTS5	-11.1	18	-2.14	0.0164	174	1.54
TKT	-11.09	18	-2.13	0.0165	175	1.54
KIAA1683	-11.09	18	-2.13	0.0165	176	1.53
FOXB1	-10.11	15	-2.13	0.0166	177	1.54
PNKP	-10.11	15	-2.13	0.0166	178	1.53
ZNFX1	-11.06	18	-2.13	0.0167	179	1.53
PRRT1	-11.06	18	-2.13	0.0167	180	1.52
CCS	-11.05	18	-2.13	0.0168	181	1.52
TMEM30A	-10.05	15	-2.12	0.0171	182	1.54
ACTR1B	-11	18	-2.12	0.0172	183	1.54
GNE	-10.99	18	-2.11	0.0173	184	1.55
PALB2	-10.98	18	-2.11	0.0174	185	1.54
PRUNE2	-10.98	18	-2.11	0.0174	186	1.53
TLK1	-8.96	12	-2.11	0.0174	187	1.53
HTR2C	-10.98	18	-2.11	0.0174	188	1.52
PRKD3	-10.97	18	-2.11	0.0175	189	1.52
NDUFB7	-8.93	12	-2.1	0.0178	190	1.54

ZNF235	-7.73	9	-2.1	0.0178	191	1.53
SERAC1	-9.97	15	-2.1	0.0179	192	1.53
TYSND1	-10.92	18	-2.1	0.0179	193	1.52
SNAI1	-9.96	15	-2.1	0.018	194	1.52
TAS2R8	-6.3	6	-2.1	0.018	195	1.52
RCSD1	-10.9	18	-2.09	0.0181	196	1.52
CLCF1	-10.89	18	-2.09	0.0182	197	1.52
ZNF226	-8.89	12	-2.09	0.0183	198	1.51
MPP5	-10.86	18	-2.09	0.0185	199	1.52
SNX24	-7.68	9	-2.09	0.0185	200	1.52
LRRC8A	-10.85	18	-2.08	0.0186	201	1.52
CCDC129	-10.85	18	-2.08	0.0186	202	1.51
ARL6IP1	-7.67	9	-2.08	0.0186	203	1.5
DNAJC27	-8.84	12	-2.08	0.0188	204	1.51
KIAA1731	-10.82	18	-2.08	0.0188	205	1.51
CRYBG3	-10.78	18	-2.07	0.0193	206	1.54
GALR3	-9.83	15	-2.07	0.0193	207	1.53
NBR1	-10.75	18	-2.06	0.0195	208	1.54
RAB11FIP2	-10.74	18	-2.06	0.0196	209	1.54
SH2D1A	-6.2	6	-2.06	0.0197	210	1.54
ST8SIA1	-10.73	18	-2.06	0.0197	211	1.53
CYP8B1	-9.79	15	-2.06	0.0197	212	1.53
GOLIM4	-10.71	18	-2.06	0.0199	213	1.53
ZNF35	-9.78	15	-2.06	0.0199	214	1.53
CHTF18	-10.7	18	-2.05	0.02	215	1.53
CDK7	-6.17	6	-2.05	0.0201	216	1.52
MTMR14	-10.65	18	-2.04	0.0205	217	1.55
TCF25	-10.64	18	-2.04	0.0207	218	1.56

ADRB2	-10.63	18	-2.04	0.0207	219	1.55
RAP2A	-8.68	12	-2.04	0.0207	220	1.54
SLX4IP	-10.63	18	-2.04	0.0207	221	1.54
NUP62	-10.32	17	-2.04	0.0208	222	1.54
TAF3	-10.62	18	-2.04	0.0209	223	1.53
UBR4	-10.61	18	-2.03	0.021	224	1.53
VRK3	-10.61	18	-2.03	0.021	225	1.53
PGAP1	-10.58	18	-2.03	0.0213	226	1.54
EBP	-10.55	18	-2.02	0.0216	227	1.56
UBE4A	-10.53	18	-2.02	0.0218	228	1.57
ARNTL	-10.53	18	-2.02	0.0218	229	1.56
NAA40	-10.52	18	-2.02	0.0219	230	1.56
PRR22	-10.52	18	-2.02	0.0219	231	1.56
ARIH2OS	-9.6	15	-2.02	0.0219	232	1.55
RPGRIP1L	-10.5	18	-2.01	0.0221	233	1.56
GRSF1	-10.5	18	-2.01	0.0222	234	1.55
BICC1	-10.49	18	-2.01	0.0222	235	1.55
SMAD4	-10.49	18	-2.01	0.0222	236	1.55
MYBPC2	-10.48	18	-2.01	0.0224	237	1.55
BCL2L1	-8.55	12	-2.01	0.0224	238	1.54
WWOX	-10.45	18	-2	0.0226	239	1.55
TEX2	-10.45	18	-2	0.0227	240	1.55
SMTN	-10.43	18	-2	0.0229	241	1.56
TNFSF8	-7.37	9	-2	0.0229	242	1.55
C3orf56	-9.51	15	-2	0.023	243	1.55
ANKRD13A	-10.41	18	-1.99	0.0231	244	1.55
C12orf77	-10.41	18	-1.99	0.0231	245	1.55
RPRD1B	-10.41	18	-1.99	0.0231	246	1.54

POC5	-10.4	18	-1.99	0.0232	247	1.54
ZFPM2	-10.4	18	-1.99	0.0232	248	1.54
BLOC1S6	-8.49	12	-1.99	0.0233	249	1.53
USP37	-10.38	18	-1.99	0.0235	250	1.54
RASA2	-10.38	18	-1.99	0.0235	251	1.54
IFNAR2	-10.37	18	-1.99	0.0235	252	1.53
ACVR2A	-10.37	18	-1.99	0.0235	253	1.52
CYP4X1	-10.37	18	-1.99	0.0235	254	1.52
TMEM107	-10.37	18	-1.99	0.0235	255	1.51
VPS33A	-10.37	18	-1.98	0.0236	256	1.51
PRSS48	-10.36	18	-1.98	0.0236	257	1.51
SHMT1	-10.36	18	-1.98	0.0236	258	1.5
RGL2	-10.35	18	-1.98	0.0238	259	1.51
ZNF841	-7.31	9	-1.98	0.024	260	1.51
TMEM38A	-10.33	18	-1.98	0.024	261	1.51
BEND7	-10.32	18	-1.97	0.0241	262	1.51
PKD2L2	-9.42	15	-1.97	0.0241	263	1.51
KTN1	-10.31	18	-1.97	0.0242	264	1.51
HSPBAP1	-10.31	18	-1.97	0.0243	265	1.5
HTR2B	-9.41	15	-1.97	0.0243	266	1.5
ATP8A2	-10.31	18	-1.97	0.0243	267	1.49
ASH2L	-10.3	18	-1.97	0.0243	268	1.49
KCTD3	-10.3	18	-1.97	0.0244	269	1.49
POLI	-9.39	15	-1.97	0.0245	270	1.49
MIER2	-10.29	18	-1.97	0.0245	271	1.49
RSRC2	-10.27	18	-1.97	0.0247	272	1.49
CYP1A2	-10.24	18	-1.96	0.0251	273	1.51
MYLK	-10.24	18	-1.96	0.0251	274	1.5

CLMN	-10.22	18	-1.96	0.0253	275	1.51
DESI2	-9.33	15	-1.95	0.0253	276	1.5
NPLOC4	-9.33	15	-1.95	0.0253	277	1.5
CALCR	-10.21	18	-1.95	0.0255	278	1.5
CEP170B	-10.2	18	-1.95	0.0256	279	1.5
SYNGR2	-8.33	12	-1.95	0.0256	280	1.5
SLC26A3	-10.19	18	-1.95	0.0257	281	1.5
ITGAX	-10.18	18	-1.95	0.0258	282	1.5
CLK1	-10.18	18	-1.95	0.0258	283	1.5
SFT2D1	-9.27	15	-1.94	0.0261	284	1.51
BNIP3L	-10.14	18	-1.94	0.0263	285	1.51
CLN5	-10.14	18	-1.94	0.0264	286	1.51
GPRC5B	-10.14	18	-1.94	0.0264	287	1.51
MSL2	-10.13	18	-1.94	0.0265	288	1.51
CD101	-10.12	18	-1.93	0.0266	289	1.51
MAFG	-5.84	6	-1.93	0.0266	290	1.51
PDPN	-8.26	12	-1.93	0.0267	291	1.51
CHRNG	-10.11	18	-1.93	0.0267	292	1.5
TOP1MT	-10.07	18	-1.92	0.0272	293	1.53
CISD3	-9.17	15	-1.92	0.0275	294	1.54
PPP1R9A	-10.05	18	-1.92	0.0275	295	1.53
PCYT1B	-10.04	18	-1.92	0.0276	296	1.53
GRK7	-10.04	18	-1.92	0.0277	297	1.53
GRIA3	-10.03	18	-1.91	0.0278	298	1.53
CCDC117	-10.02	18	-1.91	0.0279	299	1.53
TRAIP	-10.01	18	-1.91	0.0279	300	1.53
ERMP1	-10.01	18	-1.91	0.028	301	1.52
TCEANC2	-10.01	18	-1.91	0.028	302	1.52

TEX33	-10.01	18	-1.91	0.028	303	1.52
MUC4	-10.01	18	-1.91	0.028	304	1.51
POLR2G	-8.16	12	-1.91	0.0281	305	1.51
BHLHE22	-8.16	12	-1.91	0.0282	306	1.51
DAOA	-9.12	15	-1.91	0.0282	307	1.51
ANKS1A	-9.99	18	-1.91	0.0282	308	1.5
C17orf64	-9.12	15	-1.91	0.0283	309	1.5
FAM221A	-9.98	18	-1.91	0.0283	310	1.5
MEOX2	-9.11	15	-1.91	0.0284	311	1.5
CDC42BPA	-9.98	18	-1.9	0.0284	312	1.49
STRN3	-9.11	15	-1.9	0.0284	313	1.49
OR6F1	-9.1	15	-1.9	0.0285	314	1.49
COL3A1	-9.97	18	-1.9	0.0285	315	1.49
KLF3	-9.1	15	-1.9	0.0285	316	1.48
GINS1	-7.05	9	-1.9	0.0285	317	1.48
CLEC4D	-7.05	9	-1.9	0.0286	318	1.47
OR4K1	-7.04	9	-1.9	0.0287	319	1.47
SLC37A1	-9.96	18	-1.9	0.0287	320	1.47
CAT	-9.96	18	-1.9	0.0287	321	1.47
IDO2	-9.95	18	-1.9	0.0288	322	1.47
SAT1	-7.04	9	-1.9	0.0288	323	1.46
ZDHHC1	-9.94	18	-1.9	0.0289	324	1.46
GZMA	-9.07	15	-1.9	0.0289	325	1.46
ACAD11	-9.92	18	-1.89	0.0292	326	1.47
KCTD19	-9.92	18	-1.89	0.0292	327	1.47
SLC5A11	-9.92	18	-1.89	0.0292	328	1.46
NKD2	-9.91	18	-1.89	0.0294	329	1.47
TRPM4	-9.91	18	-1.89	0.0294	330	1.46

C20orf201	-9.02	15	-1.88	0.0298	331	1.48
SIDT1	-9.88	18	-1.88	0.0298	332	1.47
AMTN	-9.88	18	-1.88	0.0298	333	1.47
PLAC8L1	-9.87	18	-1.88	0.0299	334	1.47
KIAA1586	-5.7	6	-1.88	0.0299	335	1.46
ADAM18	-9.86	18	-1.88	0.0301	336	1.47
GATSL3	-9.86	18	-1.88	0.0301	337	1.46
C12orf5	-9.86	18	-1.88	0.0301	338	1.46
OR2AK2	-8.99	15	-1.88	0.0302	339	1.46
CRYGN	-9.85	18	-1.88	0.0302	340	1.46
DMXL1	-9.85	18	-1.88	0.0302	341	1.45
MTO1	-9.84	18	-1.88	0.0304	342	1.46
DAGLA	-9.83	18	-1.87	0.0305	343	1.46
EVI5	-9.82	18	-1.87	0.0306	344	1.46
OR10C1	-6.94	9	-1.87	0.0306	345	1.46
HSPB7	-9.82	18	-1.87	0.0306	346	1.45
SHQ1	-6.94	9	-1.87	0.0307	347	1.45
EFCAB4B	-9.81	18	-1.87	0.0308	348	1.45
ISPD	-8.95	15	-1.87	0.0309	349	1.45
F10	-9.8	18	-1.87	0.0309	350	1.45
TEX35	-9.8	18	-1.87	0.0309	351	1.45
TPD52	-9.8	18	-1.87	0.0309	352	1.44
BLM	-8.94	15	-1.87	0.031	353	1.44
ZNF689	-9.79	18	-1.87	0.031	354	1.44
GRHL2	-9.78	18	-1.86	0.0311	355	1.44
HSPA14	-9.78	18	-1.86	0.0312	356	1.44
SLC41A2	-7.98	12	-1.86	0.0314	357	1.44
H1FNT	-8.92	15	-1.86	0.0314	358	1.44

CNR2	-8.91	15	-1.86	0.0315	359	1.44
REEP6	-8.9	15	-1.86	0.0316	360	1.44
SP4	-9.75	18	-1.86	0.0316	361	1.44
DEPTOR	-9.74	18	-1.85	0.0318	362	1.44
CTSK	-9.73	18	-1.85	0.032	363	1.45
MAP7D3	-9.72	18	-1.85	0.0321	364	1.45
RCC1	-8.87	15	-1.85	0.0322	365	1.45
FOXRED1	-9.71	18	-1.85	0.0322	366	1.44
DSCR4	-7.93	12	-1.85	0.0323	367	1.44
CXCL9	-7.93	12	-1.85	0.0323	368	1.44
HMGCS1	-7.58	11	-1.85	0.0325	369	1.45
ADHFE1	-9.68	18	-1.84	0.0326	370	1.45
SAGE1	-7.9	12	-1.84	0.0327	371	1.45
IKZF5	-8.83	15	-1.84	0.0328	372	1.45
EXO1	-9.67	18	-1.84	0.0329	373	1.45
ZFYVE20	-9.65	18	-1.84	0.0331	374	1.45
LRRC4B	-9.65	18	-1.84	0.0331	375	1.45
PAGE3	-6.82	9	-1.84	0.0331	376	1.45
MPDU1	-9.63	18	-1.83	0.0334	377	1.45
IL1RAPL1	-9.63	18	-1.83	0.0335	378	1.45
FAIM2	-9.63	18	-1.83	0.0335	379	1.45
HELZ	-9.62	18	-1.83	0.0335	380	1.45
MTR	-9.62	18	-1.83	0.0335	381	1.44
FBXO47	-9.62	18	-1.83	0.0336	382	1.44
FIP1L1	-9.61	18	-1.83	0.0337	383	1.44
MIDN	-9.6	18	-1.83	0.0338	384	1.45
MRGPRG	-8.77	15	-1.83	0.0339	385	1.44
DEPDC1B	-9.59	18	-1.82	0.0341	386	1.45

MED13L	-9.59	18	-1.82	0.0341	387	1.45
ICA1	-9.59	18	-1.82	0.0341	388	1.44
C6orf120	-8.75	15	-1.82	0.0342	389	1.44
GABBR1	-9.57	18	-1.82	0.0343	390	1.44
JMJD6	-9.57	18	-1.82	0.0343	391	1.44
HCST	-6.77	9	-1.82	0.0344	392	1.44
ZNF45	-6.76	9	-1.82	0.0345	393	1.44
STK4	-9.56	18	-1.82	0.0346	394	1.44
RAB8A	-9.55	18	-1.82	0.0346	395	1.44
CREB3L3	-9.55	18	-1.82	0.0346	396	1.44
LTF	-9.55	18	-1.82	0.0347	397	1.43
LMAN2L	-9.54	18	-1.81	0.0349	398	1.44
SECISBP2	-9.54	18	-1.81	0.0349	399	1.44
C4orf17	-7.79	12	-1.81	0.0349	400	1.43
PDZD8	-9.52	18	-1.81	0.0352	401	1.44
CDIPT	-8.69	15	-1.81	0.0352	402	1.44
STAMBPL1	-9.5	18	-1.81	0.0355	403	1.44
ILF3	-9.5	18	-1.81	0.0355	404	1.44
ADAMTSL4	-9.5	18	-1.81	0.0355	405	1.44
IQCF3	-8.67	15	-1.81	0.0355	406	1.43
SYT11	-9.49	18	-1.8	0.0356	407	1.43
AGO3	-9.49	18	-1.8	0.0357	408	1.43
DACT3	-8.65	15	-1.8	0.0358	409	1.44
MICAL2	-9.47	18	-1.8	0.0359	410	1.44
GTF2F1	-8.64	15	-1.8	0.036	411	1.44
TSPO2	-9.46	18	-1.8	0.0361	412	1.44
MTUS2	-8.64	15	-1.8	0.0361	413	1.43
ELTD1	-9.46	18	-1.8	0.0362	414	1.43

KAT6B	-9.44	18	-1.79	0.0364	415	1.44
FAM216B	-6.68	9	-1.79	0.0364	416	1.44
NR1H4	-8.61	15	-1.79	0.0365	417	1.44
STAU2	-6.67	9	-1.79	0.0366	418	1.44
GOLGA4	-9.42	18	-1.79	0.0367	419	1.44
CXCL17	-5.44	6	-1.79	0.0367	420	1.44
TRMT2B	-9.41	18	-1.79	0.0369	421	1.44
AICDA	-9.4	18	-1.79	0.0371	422	1.44
CYP2J2	-9.4	18	-1.78	0.0371	423	1.44
GPR115	-8.58	15	-1.78	0.0372	424	1.44
BTN3A2	-5.42	6	-1.78	0.0374	425	1.44
ABRA	-9.38	18	-1.78	0.0375	426	1.44
GAST	-6.63	9	-1.78	0.0376	427	1.44
RPN2	-9.37	18	-1.78	0.0377	428	1.44
KIF27	-7.65	12	-1.78	0.0377	429	1.44
POU6F2	-9.37	18	-1.78	0.0377	430	1.44
RNF38	-9.36	18	-1.78	0.0377	431	1.44
ZKSCAN8	-9.36	18	-1.78	0.0378	432	1.44
CYP1A1	-8.82	16	-1.78	0.0378	433	1.43
ERF	-9.36	18	-1.78	0.0378	434	1.43
MYL4	-8.54	15	-1.78	0.0378	435	1.43
RAPGEF1	-9.35	18	-1.77	0.038	436	1.43
RBBP8	-9.33	18	-1.77	0.0382	437	1.44
MDGA2	-9.33	18	-1.77	0.0383	438	1.43
ADAL	-9.32	18	-1.77	0.0384	439	1.44
MALT1	-7.61	12	-1.77	0.0384	440	1.43
PGC	-9.31	18	-1.77	0.0386	441	1.44
HOXD9	-9.31	18	-1.77	0.0387	442	1.44

SMAD2	-9.31	18	-1.77	0.0387	443	1.43
CORO2B	-9.3	18	-1.76	0.0388	444	1.43
PIF1	-9.3	18	-1.76	0.0389	445	1.43
SYNGAP1	-9.3	18	-1.76	0.0389	446	1.43
SAMD9	-8.48	15	-1.76	0.039	447	1.43
LRTM1	-9.28	18	-1.76	0.0392	448	1.43
SLC17A8	-8.47	15	-1.76	0.0392	449	1.43
DDX39B	-9.27	18	-1.76	0.0393	450	1.43
ZNF792	-9.27	18	-1.76	0.0394	451	1.43
PBXIP1	-9.26	18	-1.76	0.0396	452	1.44
C1orf27	-7.56	12	-1.76	0.0396	453	1.43
ACTRT3	-9.26	18	-1.76	0.0396	454	1.43
CCDC81	-9.25	18	-1.75	0.0397	455	1.43
MLF1	-9.25	18	-1.75	0.0398	456	1.43
INPP4A	-9.25	18	-1.75	0.0398	457	1.43
CALD1	-9.25	18	-1.75	0.0398	458	1.42
WAPAL	-9.23	18	-1.75	0.0401	459	1.43
PDCD5	-6.52	9	-1.75	0.0401	460	1.43
RAX	-9.22	18	-1.75	0.0402	461	1.43
STAT5B	-9.22	18	-1.75	0.0402	462	1.43
OR2B11	-8.42	15	-1.75	0.0402	463	1.43
KLHL33	-9.22	18	-1.75	0.0403	464	1.42
AGER	-8.41	15	-1.75	0.0403	465	1.42
EPHX3	-9.21	18	-1.75	0.0405	466	1.42
TBC1D15	-9.2	18	-1.74	0.0406	467	1.43
COL4A6	-9.18	18	-1.74	0.041	468	1.44
PDHA1	-9.17	18	-1.74	0.0411	469	1.44
ARHGAP19	-9.17	18	-1.74	0.0411	470	1.44

AQP9	-9.17	18	-1.74	0.0412	471	1.43
MMGT1	-8.36	15	-1.73	0.0414	472	1.44
FIBIN	-9.15	18	-1.73	0.0415	473	1.44
OR51D1	-8.35	15	-1.73	0.0415	474	1.44
CALCOCO1	-9.14	18	-1.73	0.0416	475	1.44
FOXK1	-9.13	18	-1.73	0.0418	476	1.44
CCDC137	-8.34	15	-1.73	0.0418	477	1.44
DMD	-9.13	18	-1.73	0.0419	478	1.44
RERG	-8.33	15	-1.73	0.042	479	1.44
NKTR	-9.11	18	-1.73	0.0422	480	1.44
SYNJ2BP	-6.44	9	-1.73	0.0422	481	1.44
KRTAP13-1	-6.44	9	-1.73	0.0422	482	1.44
IDH3G	-9.11	18	-1.73	0.0422	483	1.43
ADCY9	-9.11	18	-1.73	0.0422	484	1.43
RGAG4	-8.32	15	-1.73	0.0423	485	1.43
RPP14	-6.44	9	-1.72	0.0423	486	1.43
SRPX2	-9.11	18	-1.72	0.0423	487	1.43
ISM1	-9.1	18	-1.72	0.0424	488	1.43
SYTL2	-9.1	18	-1.72	0.0425	489	1.42
TTC9C	-9.09	18	-1.72	0.0427	490	1.43
PHC3	-9.09	18	-1.72	0.0427	491	1.43
TLE3	-9.08	18	-1.72	0.0427	492	1.43
MMP19	-9.08	18	-1.72	0.0428	493	1.42
TCTA	-8.28	15	-1.72	0.043	494	1.43
TTC9B	-9.07	18	-1.72	0.043	495	1.43
LTB	-8.28	15	-1.72	0.0431	496	1.43
LDHA	-5.23	6	-1.72	0.0431	497	1.42
C9orf131	-9.06	18	-1.71	0.0432	498	1.42

CAPRIN1	-9.06	18	-1.71	0.0433	499	1.42
ATP11A	-9.05	18	-1.71	0.0434	500	1.42
NXPE1	-9.05	18	-1.71	0.0435	501	1.42
LIPK	-9.04	18	-1.71	0.0436	502	1.43
H1F0	-8.24	15	-1.71	0.0437	503	1.43
RNF10	-9.03	18	-1.71	0.0438	504	1.42
GRIA2	-9.02	18	-1.71	0.0439	505	1.43
SOGA3	-9.02	18	-1.71	0.0439	506	1.42
EPS8	-9.02	18	-1.71	0.0439	507	1.42
CCNB3	-9.02	18	-1.71	0.0439	508	1.42
F9	-7.35	12	-1.7	0.0442	509	1.42
FZR1	-9	18	-1.7	0.0442	510	1.42
NFRKB	-8.22	15	-1.7	0.0443	511	1.42
DCUN1D3	-7.35	12	-1.7	0.0443	512	1.42
KDM1A	-9	18	-1.7	0.0443	513	1.42
PRPH2	-9	18	-1.7	0.0443	514	1.42
NPAS3	-9	18	-1.7	0.0444	515	1.41
TMIGD1	-6.36	9	-1.7	0.0444	516	1.41
APOBEC3H	-8.99	18	-1.7	0.0445	517	1.41
SENP1	-8.99	18	-1.7	0.0446	518	1.41
GFRA3	-8.98	18	-1.7	0.0447	519	1.41
PECR	-8.97	18	-1.7	0.045	520	1.42
CDKN3	-7.32	12	-1.7	0.045	521	1.42
OR2G3	-8.18	15	-1.69	0.0451	522	1.42
FAM120B	-8.96	18	-1.69	0.0452	523	1.42
CENPC1	-8.17	15	-1.69	0.0454	524	1.42
MICALCL	-8.16	15	-1.69	0.0454	525	1.42
PLCXD3	-8.94	18	-1.69	0.0455	526	1.42

KLHL40	-8.94	18	-1.69	0.0456	527	1.42
CLEC7A	-6.31	9	-1.69	0.0457	528	1.42
AP2B1	-8.93	18	-1.69	0.0458	529	1.42
LRP2BP	-8.92	18	-1.69	0.0459	530	1.42
SMOX	-8.92	18	-1.69	0.0459	531	1.42
APOB	-8.92	18	-1.69	0.0459	532	1.42
OR2AT4	-7.28	12	-1.68	0.046	533	1.42
OR6B3	-6.3	9	-1.68	0.0461	534	1.42
TSPO	-8.91	18	-1.68	0.0461	535	1.41
NDUFB5	-8.9	18	-1.68	0.0463	536	1.42
ZNF22	-6.29	9	-1.68	0.0464	537	1.42
RAB28	-8.89	18	-1.68	0.0464	538	1.42
CCDC89	-8.12	15	-1.68	0.0464	539	1.41
ANKRD52	-8.89	18	-1.68	0.0465	540	1.41
CCDC43	-8.89	18	-1.68	0.0465	541	1.41
UGGT1	-8.89	18	-1.68	0.0466	542	1.41
ATMIN	-6.28	9	-1.68	0.0466	543	1.41
CDH12	-8.89	18	-1.68	0.0466	544	1.41
ST3GAL6	-7.25	12	-1.68	0.0466	545	1.4
LMOD3	-8.88	18	-1.68	0.0467	546	1.4
ATP6V0D1	-8.87	18	-1.68	0.0468	547	1.4
GLP2R	-8.87	18	-1.68	0.0469	548	1.4
NPAT	-8.1	15	-1.68	0.0469	549	1.4
C19orf10	-8.87	18	-1.68	0.0469	550	1.4
MTMR8	-8.87	18	-1.68	0.047	551	1.4
FCN3	-8.86	18	-1.67	0.047	552	1.4
OXR1	-8.86	18	-1.67	0.047	553	1.4
TRAPPC11	-8.86	18	-1.67	0.0471	554	1.4

CLSTN2	-8.85	18	-1.67	0.0472	555	1.4
CST9L	-6.26	9	-1.67	0.0473	556	1.4
HNRNPUL1	-8.85	18	-1.67	0.0474	557	1.4
MRPL41	-6.25	9	-1.67	0.0475	558	1.4
CCDC147	-8.84	18	-1.67	0.0476	559	1.4
EIF4G3	-8.84	18	-1.67	0.0476	560	1.39
LHX3	-8.84	18	-1.67	0.0476	561	1.39
RANBP3L	-7.21	12	-1.67	0.0476	562	1.39
C1S	-8.83	18	-1.67	0.0478	563	1.39
RAB20	-8.83	18	-1.67	0.0478	564	1.39
KAL1	-8.82	18	-1.67	0.0479	565	1.39
SMC6	-8.82	18	-1.67	0.0479	566	1.39
CCDC177	-8.05	15	-1.67	0.0479	567	1.39
CAPNS2	-7.18	12	-1.66	0.0484	568	1.4
GTPBP1	-8.79	18	-1.66	0.0485	569	1.4
DUS1L	-8.79	18	-1.66	0.0485	570	1.4
GSTZ1	-8.79	18	-1.66	0.0485	571	1.39
ADAM28	-8.79	18	-1.66	0.0485	572	1.39
S100A6	-8.01	15	-1.66	0.0488	573	1.4
MED20	-8.77	18	-1.66	0.0489	574	1.4
IRF2BP2	-8.77	18	-1.66	0.0489	575	1.4
IMPACT	-5.06	6	-1.65	0.049	576	1.4
CDC25C	-8.76	18	-1.65	0.0491	577	1.4
TBC1D9	-8.76	18	-1.65	0.0492	578	1.4
HTT	-8.75	18	-1.65	0.0493	579	1.4
HK3	-8.75	18	-1.65	0.0493	580	1.4
SMURF2	-8.75	18	-1.65	0.0495	581	1.4
ANKRD1	-8.75	18	-1.65	0.0495	582	1.4

STARD7	-8.74	18	-1.65	0.0495	583	1.39
PLA2G12B	-8.74	18	-1.65	0.0495	584	1.39
HTR3D	-8.74	18	-1.65	0.0495	585	1.39
WBP2	-8.74	18	-1.65	0.0496	586	1.39
SYT5	-8.72	18	-1.65	0.05	587	1.4
MRPL16	-8.47	17	-1.64	0.05	588	1.4
LMAN1	-8.72	18	-1.64	0.0501	589	1.4
GIPR	-8.71	18	-1.64	0.0502	590	1.4
WDR74	-7.95	15	-1.64	0.0502	591	1.39
SCARA5	-8.7	18	-1.64	0.0503	592	1.4
TACR1	-8.7	18	-1.64	0.0504	593	1.39
WFDC8	-7.94	15	-1.64	0.0506	594	1.4
ATRAID	-8.68	18	-1.64	0.0508	595	1.4
HSPB6	-8.68	18	-1.64	0.0508	596	1.4
ALS2	-8.68	18	-1.64	0.0508	597	1.4
C10orf118	-8.68	18	-1.64	0.0509	598	1.4
SENP7	-8.68	18	-1.64	0.0509	599	1.39
RFX6	-8.68	18	-1.64	0.0509	600	1.39
ZBTB24	-8.68	18	-1.64	0.0509	601	1.39
OST4	-5	6	-1.63	0.0511	602	1.39
CCDC73	-6.12	9	-1.63	0.0513	603	1.4
STAC2	-8.66	18	-1.63	0.0514	604	1.4
SRL	-8.65	18	-1.63	0.0514	605	1.39
VPS39	-8.65	18	-1.63	0.0514	606	1.39
AP3B2	-8.65	18	-1.63	0.0514	607	1.39
DHPS	-8.41	17	-1.63	0.0515	608	1.39
MOB2	-8.65	18	-1.63	0.0515	609	1.39
SHC3	-8.65	18	-1.63	0.0516	610	1.39

VDAC3	-6.11	9	-1.63	0.0516	611	1.39
EFCAB7	-7.06	12	-1.63	0.0517	612	1.39
HCAR1	-7.89	15	-1.63	0.0518	613	1.39
NRK	-8.64	18	-1.63	0.0518	614	1.39
GCC2	-7.87	15	-1.62	0.0521	615	1.39
PNMAL1	-8.62	18	-1.62	0.0522	616	1.39
ANO10	-8.62	18	-1.62	0.0523	617	1.39
CXCR6	-6.09	9	-1.62	0.0523	618	1.39
EAPP	-8.61	18	-1.62	0.0523	619	1.39
TRIM21	-8.61	18	-1.62	0.0523	620	1.39
CYB5A	-6.09	9	-1.62	0.0524	621	1.38
POLD3	-8.6	18	-1.62	0.0525	622	1.39
CCDC64	-8.6	18	-1.62	0.0526	623	1.39
ZNF556	-7.85	15	-1.62	0.0527	624	1.39
ACP5	-8.6	18	-1.62	0.0527	625	1.38
MAP6	-8.59	18	-1.62	0.0527	626	1.38
FPR1	-7.02	12	-1.62	0.0528	627	1.38
PPIL6	-6.07	9	-1.62	0.0529	628	1.38
JOSD2	-8.59	18	-1.62	0.0529	629	1.38
C18orf32	-6.07	9	-1.62	0.053	630	1.38
UBXN2B	-4.95	6	-1.62	0.0531	631	1.38
CBLN2	-8.57	18	-1.61	0.0532	632	1.38
GPR50	-8.56	18	-1.61	0.0535	633	1.39
FNBP1L	-8.56	18	-1.61	0.0536	634	1.39
TNNI3K	-8.55	18	-1.61	0.0537	635	1.39
VPS45	-8.55	18	-1.61	0.0537	636	1.39
C5orf55	-8.54	18	-1.61	0.054	637	1.39
ASRGL1	-8.54	18	-1.61	0.054	638	1.39

DOCK7	-8.53	18	-1.61	0.0541	639	1.39
LYPD1	-8.53	18	-1.61	0.0541	640	1.39
KCND1	-8.53	18	-1.61	0.0541	641	1.38
SLC4A1AP	-7.79	15	-1.61	0.0542	642	1.39
SBK2	-8.53	18	-1.61	0.0542	643	1.38
STH	-6.95	12	-1.6	0.0545	644	1.39
NHLRC2	-8.51	18	-1.6	0.0546	645	1.39
AP2A2	-8.51	18	-1.6	0.0546	646	1.39
ATF3	-7.76	15	-1.6	0.0548	647	1.39
PRAC	-6.93	12	-1.6	0.055	648	1.39
NQO1	-8.48	18	-1.59	0.0554	649	1.4
SNAPC3	-5.99	9	-1.59	0.0556	650	1.4
ZNF711	-8.47	18	-1.59	0.0556	651	1.4
DOCK11	-7.19	13	-1.59	0.0557	652	1.4
CPSF3L	-8.46	18	-1.59	0.0558	653	1.4
DNAJC5B	-5.98	9	-1.59	0.0558	654	1.4
CACHD1	-8.46	18	-1.59	0.0559	655	1.4
LRRC58	-7.71	15	-1.59	0.056	656	1.4
FBXL7	-8.45	18	-1.59	0.056	657	1.4
TACR3	-8.45	18	-1.59	0.0561	658	1.4
GALC	-8.44	18	-1.59	0.0564	659	1.4
C6orf141	-8.43	18	-1.59	0.0564	660	1.4
MCM10	-7.43	14	-1.58	0.0565	661	1.4
SNCAIP	-8.42	18	-1.58	0.0567	662	1.41
RACGAP1	-5.95	9	-1.58	0.0567	663	1.4
UBAP1	-8.41	18	-1.58	0.0569	664	1.41
CYP26A1	-8.41	18	-1.58	0.0569	665	1.41
KIAA1109	-8.41	18	-1.58	0.057	666	1.4

GRIPAP1	-7.67	15	-1.58	0.057	667	1.4
ATHL1	-8.4	18	-1.58	0.0572	668	1.41
CCDC160	-4.85	6	-1.58	0.0572	669	1.4
ANK1	-8.39	18	-1.58	0.0573	670	1.4
OLFML2A	-8.38	18	-1.58	0.0576	671	1.41
DUOXA1	-8.38	18	-1.57	0.0577	672	1.41
SIGLECL1	-8.38	18	-1.57	0.0578	673	1.41
MALL	-4.83	6	-1.57	0.0578	674	1.41
TTPAL	-7.64	15	-1.57	0.0579	675	1.41
TRIM40	-7.63	15	-1.57	0.0581	676	1.41
RIBC2	-7.63	15	-1.57	0.0582	677	1.41
FAN1	-8.36	18	-1.57	0.0582	678	1.41
PSMD5	-8.35	18	-1.57	0.0583	679	1.41
TMEM255A	-8.35	18	-1.57	0.0584	680	1.41
FAM105A	-8.35	18	-1.57	0.0584	681	1.41
SEMA5B	-8.34	18	-1.57	0.0586	682	1.41
AP1G1	-8.34	18	-1.57	0.0587	683	1.41
C7orf62	-7.61	15	-1.57	0.0588	684	1.41
SLC46A1	-8.33	18	-1.56	0.0588	685	1.41
SFXN4	-8.33	18	-1.56	0.0589	686	1.41
ZNF200	-8.32	18	-1.56	0.0592	687	1.41
VPS16	-8.32	18	-1.56	0.0592	688	1.41
ANO9	-8.32	18	-1.56	0.0592	689	1.41
TRIML2	-5.88	9	-1.56	0.0593	690	1.41
INCENP	-7.59	15	-1.56	0.0593	691	1.41
ATP13A5	-8.31	18	-1.56	0.0594	692	1.41
TNFSF18	-4.79	6	-1.56	0.0596	693	1.41
RGS22	-8.3	18	-1.56	0.0596	694	1.41

KIAA1524	-7.58	15	-1.56	0.0597	695	1.41
TCL1A	-4.79	6	-1.56	0.0597	696	1.41
CCDC50	-8.29	18	-1.56	0.0597	697	1.41
HOXD13	-8.29	18	-1.56	0.0599	698	1.41
SQRDL	-7.56	15	-1.55	0.0601	699	1.41
NR0B2	-8.28	18	-1.55	0.0602	700	1.41
S100PBP	-8.28	18	-1.55	0.0602	701	1.41
TTLL7	-8.27	18	-1.55	0.0603	702	1.41
ABTB1	-8.27	18	-1.55	0.0603	703	1.41
TRA2B	-8.27	18	-1.55	0.0604	704	1.41
CDH10	-8.26	18	-1.55	0.0606	705	1.41
CLN6	-8.26	18	-1.55	0.0607	706	1.41
CABP7	-7.54	15	-1.55	0.0607	707	1.41
CCDC176	-6.74	12	-1.55	0.0607	708	1.41
FBXO16	-8.25	18	-1.55	0.0608	709	1.41
MMAA	-8.25	18	-1.55	0.0608	710	1.4
CBX6	-8.25	18	-1.55	0.0608	711	1.4
APITD1	-4.76	6	-1.55	0.0608	712	1.4
CUL5	-8.25	18	-1.55	0.0609	713	1.4
ECT2L	-8.25	18	-1.55	0.0609	714	1.4
AP5S1	-8.25	18	-1.55	0.0609	715	1.4
SUPT5H	-8.24	18	-1.55	0.061	716	1.4
MRPL55	-8.24	18	-1.55	0.0611	717	1.4
SOCS7	-8.24	18	-1.55	0.0611	718	1.4
PIK3R1	-8.24	18	-1.55	0.0611	719	1.4
PDZD2	-8.23	18	-1.54	0.0612	720	1.4
C6orf118	-8.23	18	-1.54	0.0613	721	1.39
CORO7	-7.25	14	-1.54	0.0615	722	1.4

MRPL50	-5.81	9	-1.54	0.0615	723	1.4
CSPP1	-8.22	18	-1.54	0.0616	724	1.4
ZMYND12	-7.5	15	-1.54	0.0617	725	1.4
FAM211B	-8.22	18	-1.54	0.0617	726	1.39
LARP1	-8.22	18	-1.54	0.0617	727	1.39
KCNQ3	-8.22	18	-1.54	0.0617	728	1.39
ZNF839	-8.21	18	-1.54	0.0617	729	1.39
KIF13A	-8.21	18	-1.54	0.0618	730	1.39
CCDC62	-8.21	18	-1.54	0.062	731	1.39
GARS	-7.73	16	-1.54	0.0621	732	1.39
OR1J2	-4.73	6	-1.54	0.0621	733	1.39
PSME4	-8.19	18	-1.54	0.0622	734	1.39
KIAA1324	-8.19	18	-1.54	0.0623	735	1.39
KLRB1	-6.68	12	-1.53	0.0624	736	1.39
NME5	-4.73	6	-1.53	0.0624	737	1.39
ZNF436	-7.47	15	-1.53	0.0625	738	1.39
ANKRD32	-8.18	18	-1.53	0.0626	739	1.39
ZNF534	-5.79	9	-1.53	0.0626	740	1.39
NR0B1	-8.18	18	-1.53	0.0626	741	1.39
TEX13A	-7.46	15	-1.53	0.0627	742	1.39
MSH2	-8.18	18	-1.53	0.0627	743	1.38
KLHL23	-7.46	15	-1.53	0.0628	744	1.39
SCARF1	-8.17	18	-1.53	0.0628	745	1.38
TOR2A	-8.17	18	-1.53	0.0628	746	1.38
OTUD5	-8.17	18	-1.53	0.0629	747	1.38
SLC27A2	-8.16	18	-1.53	0.0631	748	1.38
LMBRD1	-7.45	15	-1.53	0.0632	749	1.38
UCHL5	-6.66	12	-1.53	0.0633	750	1.38

SLC36A3	-8.15	18	-1.53	0.0635	751	1.39
MBL2	-7.43	15	-1.53	0.0635	752	1.39
LBH	-6.65	12	-1.53	0.0636	753	1.38
HIPK3	-8.14	18	-1.53	0.0636	754	1.38
SLC9A3R1	-8.14	18	-1.53	0.0636	755	1.38
PKNOX1	-8.14	18	-1.52	0.0637	756	1.38
LRRC38	-8.13	18	-1.52	0.0638	757	1.38
TMEM38B	-7.42	15	-1.52	0.0639	758	1.38
FUT8	-8.13	18	-1.52	0.0639	759	1.38
CACNA1B	-8.13	18	-1.52	0.064	760	1.38
NARS2	-6.63	12	-1.52	0.064	761	1.38
EXTL2	-4.69	6	-1.52	0.064	762	1.38
SPATA25	-8.12	18	-1.52	0.0643	763	1.38
KCNG1	-8.11	18	-1.52	0.0643	764	1.38
MOG	-8.11	18	-1.52	0.0644	765	1.38
PCYOX1L	-8.11	18	-1.52	0.0645	766	1.38
NLGN2	-8.1	18	-1.52	0.0645	767	1.38
PCOLCE	-8.1	18	-1.52	0.0645	768	1.38
ITFG2	-8.1	18	-1.52	0.0645	769	1.38
CLPSL2	-7.4	15	-1.52	0.0646	770	1.38
MMP16	-8.1	18	-1.52	0.0646	771	1.38
C14orf166B	-7.39	15	-1.52	0.0647	772	1.38
CFDP1	-8.09	18	-1.52	0.0648	773	1.38
MDFIC	-7.39	15	-1.52	0.0649	774	1.38
OR9G1	-5.72	9	-1.51	0.0649	775	1.37
OR6N1	-6.6	12	-1.51	0.065	776	1.37
SUPV3L1	-8.09	18	-1.51	0.065	777	1.37
ERAS	-7.36	15	-1.51	0.0657	778	1.39

NLRP14	-7.36	15	-1.51	0.0657	779	1.38
NDUFB11	-8.06	18	-1.51	0.0658	780	1.38
ENO1	-8.06	18	-1.51	0.0658	781	1.38
PHLDA3	-7.35	15	-1.51	0.0659	782	1.38
TMEM161B	-4.65	6	-1.51	0.0659	783	1.38
USP3	-8.05	18	-1.51	0.0659	784	1.38
ZC3HAV1L	-8.05	18	-1.51	0.066	785	1.38
PTRH1	-8.05	18	-1.51	0.0661	786	1.38
TNKS1BP1	-8.04	18	-1.51	0.0661	787	1.38
HIST1H4D	-4.64	6	-1.5	0.0663	788	1.38
NCAPG2	-8.04	18	-1.5	0.0663	789	1.38
CCDC64B	-7.58	16	-1.5	0.0663	790	1.38
HECA	-8.04	18	-1.5	0.0664	791	1.38
AK9	-8.03	18	-1.5	0.0664	792	1.38
UBN2	-8.03	18	-1.5	0.0665	793	1.38
RHNO1	-4.64	6	-1.5	0.0665	794	1.38
TNFRSF12A	-8.02	18	-1.5	0.0666	795	1.38
LPIN1	-8.02	18	-1.5	0.0666	796	1.37
KIF14	-8.02	18	-1.5	0.0666	797	1.37
ARRDC4	-8.02	18	-1.5	0.0666	798	1.37
C9orf169	-8.02	18	-1.5	0.0667	799	1.37
MYNN	-7.32	15	-1.5	0.0669	800	1.37
CD70	-8.02	18	-1.5	0.0669	801	1.37
ASB5	-8.02	18	-1.5	0.0669	802	1.37
MYBPC3	-8.01	18	-1.5	0.067	803	1.37
ARL1	-6.54	12	-1.5	0.067	804	1.37
SH2B2	-8.01	18	-1.5	0.067	805	1.37
ZC3H13	-8.01	18	-1.5	0.0671	806	1.37

OR10AD1	-8.01	18	-1.5	0.0671	807	1.36
ACOT9	-8	18	-1.5	0.0673	808	1.37
ACIN1	-8	18	-1.5	0.0673	809	1.37
GSPT1	-7.54	16	-1.5	0.0674	810	1.37

Ramos Resistance						
GENE	**sumZ**	**numObs**	**normZ**	**pval_supp**	**rank_supp**	**fdr_supp**
BAI2	18.21	18	3.91	4.55E-05	1	0.747
CAMK1D	16.04	18	3.47	0.000264	2	2.17
NAP1L5	12.25	12	3.25	0.000575	3	3.15
NFKBIB	14.96	18	3.24	0.000592	4	2.43
TMEM151A	13.55	15	3.22	0.000643	5	2.11
GSTM4	8.28	6	3.12	0.000919	6	2.51
TRAPPC2L	14.06	18	3.06	0.00111	7	2.61
SDHA	9.76	9	3	0.00133	8	2.73
SDF2	12.38	15	2.96	0.00156	9	2.85
BTF3	7.74	6	2.92	0.00173	10	2.85
NMNAT1	7.65	6	2.89	0.00192	11	2.87
PLEKHG1	13.1	18	2.86	0.00213	12	2.91
ZNF783	13.06	18	2.85	0.00218	13	2.75
TGM7	12.79	18	2.8	0.00259	14	3.04
GAS6	12.74	18	2.78	0.00268	15	2.94
CST3	11.62	15	2.78	0.0027	16	2.77
APOA1	11.48	15	2.75	0.00298	17	2.87
CSTF2	12.53	18	2.74	0.00306	18	2.79
LRRC55	12.33	18	2.7	0.00346	19	2.99
DPP10	12.31	18	2.7	0.00351	20	2.88
TEAD4	12.27	18	2.69	0.0036	21	2.82

SLC16A8	12.22	18	2.68	0.00371	22	2.77
SPIRE2	12.16	18	2.66	0.00386	23	2.75
SYPL1	11.09	15	2.66	0.00388	24	2.66
SPTBN4	12.13	18	2.66	0.00391	25	2.57
PAX5	12.05	18	2.64	0.00412	26	2.6
CNGB1	11.95	18	2.62	0.00438	27	2.66
SNRNP70	11.93	18	2.62	0.00443	28	2.6
CCDC6	11.89	18	2.61	0.00455	29	2.57
SLC18A3	10.85	15	2.61	0.00455	30	2.49
DOC2B	11.88	18	2.61	0.00456	31	2.41
PNPLA5	11.86	18	2.6	0.00461	32	2.36
GOT2	6.83	6	2.6	0.0047	33	2.34
PIK3CD	11.74	18	2.58	0.00496	34	2.4
DAAM2	11.7	18	2.57	0.00508	35	2.38
KATNAL2	11.69	18	2.57	0.00511	36	2.33
LOXL2	11.68	18	2.57	0.00514	37	2.28
ZNF367	11.56	18	2.54	0.00553	38	2.39
TNFRSF25	11.53	18	2.53	0.00563	39	2.37
CDH16	11.49	18	2.53	0.00577	40	2.37
LONRF2	11.43	18	2.51	0.00597	41	2.39
INTS9	11.37	18	2.5	0.00616	42	2.41
ELN	11.28	18	2.48	0.00651	43	2.49
EIF3L	6.45	6	2.46	0.0069	44	2.57
CLDN14	11.15	18	2.46	0.00701	45	2.56
WDR55	11.12	18	2.45	0.00713	46	2.54
FAM124A	11.11	18	2.45	0.00716	47	2.5
RNF141	10.14	15	2.45	0.00718	48	2.45
MROH2A	11.08	18	2.44	0.00729	49	2.44

NADK	11.08	18	2.44	0.0073	50	2.4
CEACAM16	11.07	18	2.44	0.00735	51	2.36
FAM162A	6.38	6	2.44	0.0074	52	2.34
FAM107B	10.06	15	2.43	0.00755	53	2.34
PSPH	8.96	12	2.42	0.00773	54	2.35
EPDR1	10.97	18	2.42	0.00776	55	2.32
MAGEB4	7.73	9	2.41	0.00795	56	2.33
DNTTIP2	10.9	18	2.4	0.0081	57	2.33
UNC5D	10.87	18	2.4	0.00822	58	2.33
RCVRN	9.92	15	2.4	0.00826	59	2.3
EMX2	10.83	18	2.39	0.0084	60	2.3
PRRT3	10.78	18	2.38	0.00866	61	2.33
MEFV	9.81	15	2.37	0.00882	62	2.33
SEPT1	10.75	18	2.37	0.00882	63	2.3
ACP1	6.2	6	2.37	0.00886	64	2.27
CD38	10.71	18	2.36	0.00902	65	2.28
EFNA2	10.66	18	2.35	0.00928	66	2.31
KAZN	10.32	17	2.35	0.00949	67	2.32
C10orf25	9.68	15	2.34	0.00954	68	2.3
ARL11	9.68	15	2.34	0.00955	69	2.27
C6orf106	6.12	6	2.34	0.0096	70	2.25
SLC8A1	10.57	18	2.34	0.00972	71	2.25
SLC44A1	10.51	18	2.32	0.01	72	2.29
ADRM1	10.49	18	2.32	0.0101	73	2.28
IFT27	10.48	18	2.32	0.0102	74	2.27
PLAT	10.45	18	2.31	0.0104	75	2.27
MRPL23	10.43	18	2.31	0.0105	76	2.27
BEST2	10.43	18	2.31	0.0105	77	2.24

RNF222	9.51	15	2.3	0.0106	78	2.23
ZNF335	10.41	18	2.3	0.0106	79	2.21
FHIT	6.01	6	2.3	0.0106	80	2.18
CDC37	10.33	18	2.29	0.0111	81	2.24
SLC25A27	10.31	18	2.28	0.0112	82	2.24
CYGB	10.31	18	2.28	0.0112	83	2.22
NOS2	10.3	18	2.28	0.0113	84	2.2
PYY	5.94	6	2.28	0.0113	85	2.18
CXorf30	5.94	6	2.28	0.0114	86	2.17
C2orf61	10.26	18	2.27	0.0115	87	2.17
OSTF1	9.36	15	2.27	0.0116	88	2.16
C2CD2L	10.23	18	2.27	0.0117	89	2.16
SNRPD3	9.32	15	2.26	0.0118	90	2.15
REM1	9.92	17	2.26	0.0118	91	2.13
FAM107A	10.21	18	2.26	0.0118	92	2.11
ACER1	10.19	18	2.26	0.0119	93	2.11
BIRC6	10.11	18	2.24	0.0125	94	2.18
IGHMBP2	10.08	18	2.24	0.0127	95	2.19
BOLA1	9.19	15	2.23	0.0128	96	2.18
OR5M11	9.19	15	2.23	0.0128	97	2.16
AAR2	10.05	18	2.23	0.0129	98	2.15
PSMA1	5.8	6	2.23	0.0129	99	2.15
ICMT	9.99	18	2.22	0.0133	100	2.18
ATXN3	9.09	15	2.21	0.0135	101	2.2
NAA60	9.92	18	2.2	0.0138	102	2.23
UEVLD	9.9	18	2.2	0.0139	103	2.22
RASAL1	9.9	18	2.2	0.014	104	2.2
NCAM2	9.89	18	2.2	0.014	105	2.19

SIGLEC9	8.07	12	2.2	0.014	106	2.17
ADAMTS19	9.89	18	2.2	0.0141	107	2.16
SLITRK1	9.02	15	2.19	0.0141	108	2.14
PABPC4L	9.02	15	2.19	0.0141	109	2.12
BNIP2	9.02	15	2.19	0.0141	110	2.1
ZEB1	9.88	18	2.19	0.0141	111	2.09
PTPRN	9.88	18	2.19	0.0141	112	2.07
NABP1	9.87	18	2.19	0.0142	113	2.06
FTO	9.87	18	2.19	0.0142	114	2.04
IDS	9.82	18	2.18	0.0146	115	2.08
FAM217B	6.94	9	2.18	0.0146	116	2.07
OXA1L	9.79	18	2.18	0.0148	117	2.07
JAM3	9.79	18	2.18	0.0148	118	2.06
SIX1	9.78	18	2.17	0.0148	119	2.05
KCNMB3	6.92	9	2.17	0.0149	120	2.03
NLRP10	9.76	18	2.17	0.015	121	2.03
GPR78	9.76	18	2.17	0.015	122	2.02
RSPH6A	9.76	18	2.17	0.015	123	2.01
PSG5	5.63	6	2.17	0.0151	124	1.99
INPP5E	9.75	18	2.17	0.0151	125	1.98
LURAP1	8.9	15	2.17	0.0151	126	1.97
CLDN8	7.94	12	2.16	0.0153	127	1.98
SLC26A10	9.16	16	2.16	0.0154	128	1.97
MBD3L1	6.86	9	2.16	0.0155	129	1.97
TBX21	9.7	18	2.16	0.0155	130	1.96
PDE8B	9.68	18	2.15	0.0157	131	1.96
ABCA3	9.68	18	2.15	0.0157	132	1.95
GPR162	9.67	18	2.15	0.0158	133	1.94

LIMA1	9.66	18	2.15	0.0158	134	1.94
MUC22	9.65	18	2.15	0.0159	135	1.93
ALAS2	9.64	18	2.14	0.016	136	1.93
DCTPP1	9.61	18	2.14	0.0162	137	1.94
ADAMTS9	9.61	18	2.14	0.0163	138	1.93
VEGFA	9.61	18	2.14	0.0163	139	1.92
RTP4	9.61	18	2.14	0.0163	140	1.91
NPAS1	9.31	17	2.13	0.0165	141	1.92
PRPF40B	8.74	15	2.13	0.0166	142	1.91
HCRTR1	9.54	18	2.12	0.0169	143	1.93
C19orf44	9.54	18	2.12	0.0169	144	1.92
SNX3	8.67	15	2.11	0.0172	145	1.95
COX5B	9.45	18	2.1	0.0177	146	1.99
EPS15L1	9.44	18	2.1	0.0177	147	1.98
EPCAM	9.43	18	2.1	0.0178	148	1.97
DBR1	9.43	18	2.1	0.0178	149	1.96
LGALS2	8.6	15	2.1	0.0179	150	1.96
INSRR	9.42	18	2.1	0.0179	151	1.95
SYAP1	9.41	18	2.1	0.0179	152	1.94
CYTH2	9.4	18	2.1	0.0181	153	1.94
APH1A	9.4	18	2.09	0.0181	154	1.93
ZBTB10	9.39	18	2.09	0.0182	155	1.92
CEBPA	8.57	15	2.09	0.0182	156	1.91
TTC7B	9.37	18	2.09	0.0184	157	1.92
C10orf2	7.61	12	2.08	0.0188	158	1.95
EVI5L	9.31	18	2.08	0.019	159	1.96
CAPN14	9.3	18	2.07	0.0191	160	1.95
ETV3	8.48	15	2.07	0.0191	161	1.95

FOXRED2	9.29	18	2.07	0.0191	162	1.94
CHRNB1	9.28	18	2.07	0.0192	163	1.93
BIK	7.58	12	2.07	0.0192	164	1.92
HOXC5	9.27	18	2.07	0.0193	165	1.92
SPRY2	9.26	18	2.07	0.0194	166	1.92
ZFYVE16	9.25	18	2.06	0.0195	167	1.92
CR1	9.24	18	2.06	0.0196	168	1.91
AGBL2	9.23	18	2.06	0.0197	169	1.91
FAM102A	9.21	18	2.06	0.0199	170	1.92
ZMAT3	9.21	18	2.06	0.0199	171	1.91
SCAF8	9.2	18	2.05	0.0199	172	1.9
NCR2	9.19	18	2.05	0.02	173	1.9
IRAK1BP1	8.38	15	2.05	0.0202	174	1.91
TMCC3	9.17	18	2.05	0.0203	175	1.91
IL37	5.29	6	2.05	0.0204	176	1.9
FFAR2	9.15	18	2.04	0.0205	177	1.9
RIC8A	9.13	18	2.04	0.0207	178	1.91
KRBA1	9.13	18	2.04	0.0207	179	1.9
PTPRN2	9.12	18	2.04	0.0208	180	1.89
EPB42	8.32	15	2.04	0.0208	181	1.89
C17orf47	8.32	15	2.04	0.0209	182	1.88
C12orf68	8.31	15	2.03	0.021	183	1.88
RAB30	5.25	6	2.03	0.0211	184	1.88
ID4	8.3	15	2.03	0.0211	185	1.88
ATE1	9.08	18	2.03	0.0212	186	1.87
PLEKHA4	9.08	18	2.03	0.0213	187	1.87
SPATA16	8.27	15	2.03	0.0214	188	1.87
PRSS46	8.27	15	2.02	0.0214	189	1.86

RPP38	7.38	12	2.02	0.0216	190	1.87
RGMB	9.04	18	2.02	0.0217	191	1.86
PHLPP2	9.03	18	2.02	0.0217	192	1.86
CCR2	5.21	6	2.02	0.0217	193	1.85
IRF3	9.02	18	2.02	0.0218	194	1.85
PTMA	8.22	15	2.01	0.022	195	1.85
NR6A1	8.75	17	2.01	0.022	196	1.84
ZNF16	9.01	18	2.01	0.022	197	1.83
DNAJC3	7.35	12	2.01	0.022	198	1.83
SNRPN	7.03	11	2.01	0.0222	199	1.83
C4orf3	8.99	18	2.01	0.0222	200	1.82
SPATA22	7.33	12	2.01	0.0223	201	1.82
HOXC11	8.97	18	2.01	0.0224	202	1.82
SCNN1A	8.95	18	2	0.0227	203	1.83
PLCG2	8.94	18	2	0.0227	204	1.82
ARC	8.94	18	2	0.0227	205	1.82
KIF6	8.93	18	2	0.0228	206	1.82
SF3A1	8.93	18	2	0.0228	207	1.81
WBP1L	8.15	15	2	0.0229	208	1.81
ZBTB9	7.28	12	2	0.023	209	1.81
EVC	8.91	18	1.99	0.023	210	1.8
DHX58	8.89	18	1.99	0.0233	211	1.81
CORO6	8.88	18	1.99	0.0234	212	1.81
ZNF189	8.1	15	1.99	0.0235	213	1.81
UBTD1	8.87	18	1.99	0.0235	214	1.8
GPT2	8.86	18	1.98	0.0237	215	1.81
C17orf82	8.04	15	1.97	0.0242	216	1.84
HS3ST6	8.78	18	1.97	0.0246	217	1.86

EIF4E3	8.01	15	1.97	0.0247	218	1.86
CCDC91	5.06	6	1.97	0.0247	219	1.85
RNPEP	8.76	18	1.96	0.0248	220	1.85
C9orf173	8.75	18	1.96	0.0249	221	1.85
ZNF581	7.99	15	1.96	0.0249	222	1.84
CHMP1A	8.74	18	1.96	0.0251	223	1.84
PLSCR1	7.13	12	1.96	0.0251	224	1.84
GALNT15	8.73	18	1.96	0.0252	225	1.84
DNAJC15	7.12	12	1.96	0.0252	226	1.83
CCM2L	8.72	18	1.95	0.0253	227	1.83
RFXANK	8.72	18	1.95	0.0253	228	1.82
PQLC2	8.7	18	1.95	0.0255	229	1.83
ELF2	7.94	15	1.95	0.0256	230	1.83
CSNK1D	8.69	18	1.95	0.0257	231	1.82
MED9	7.09	12	1.95	0.0258	232	1.82
STK33	5	6	1.94	0.026	233	1.83
KLHL36	8.65	18	1.94	0.0262	234	1.84
GNMT	8.65	18	1.94	0.0262	235	1.83
USF2	8.63	18	1.94	0.0264	236	1.83
QPCT	8.63	18	1.94	0.0264	237	1.83
GNRH2	7.04	12	1.93	0.0265	238	1.83
RASSF1	8.62	18	1.93	0.0266	239	1.82
ZBTB2	7.86	15	1.93	0.0266	240	1.82
TBC1D10A	8.61	18	1.93	0.0266	241	1.81
ARHGAP8	8.61	18	1.93	0.0267	242	1.81
VRTN	7.86	15	1.93	0.0267	243	1.8
HSPA12B	8.6	18	1.93	0.0268	244	1.8
ITGBL1	8.6	18	1.93	0.0268	245	1.79

SLC2A2	8.6	18	1.93	0.0269	246	1.79
PDE5A	8.59	18	1.93	0.0269	247	1.79
UNCX	8.58	18	1.93	0.027	248	1.79
BCR	8.58	18	1.93	0.0271	249	1.79
TTC7A	8.57	18	1.92	0.0272	250	1.79
MUC20	6.05	9	1.92	0.0273	251	1.78
ELOVL3	6.99	12	1.92	0.0273	252	1.78
MAG	8.56	18	1.92	0.0273	253	1.77
NPC1L1	8.55	18	1.92	0.0274	254	1.77
IL20RA	8.54	18	1.92	0.0276	255	1.78
RSAD1	8.53	18	1.92	0.0277	256	1.77
KLF1	8.52	18	1.91	0.0279	257	1.78
EPHX4	7.77	15	1.91	0.028	258	1.78
WFDC3	8.51	18	1.91	0.028	259	1.78
ZCCHC13	6.94	12	1.91	0.028	260	1.77
NR1I3	8.49	18	1.91	0.0282	261	1.77
FAM135B	8.49	18	1.91	0.0282	262	1.77
CKAP5	8.25	17	1.91	0.0283	263	1.76
RABGGTA	8.49	18	1.91	0.0283	264	1.76
GPRC5C	8.48	18	1.91	0.0283	265	1.75
MBLAC2	8.47	18	1.9	0.0285	266	1.76
RGS19	8.47	18	1.9	0.0285	267	1.75
OR13J1	7.72	15	1.9	0.0286	268	1.75
ZHX2	8.46	18	1.9	0.0287	269	1.75
GPSM3	8.46	18	1.9	0.0287	270	1.74
MYO3B	8.46	18	1.9	0.0287	271	1.74
ZNF548	8.45	18	1.9	0.0288	272	1.74
BSND	8.45	18	1.9	0.0288	273	1.73

HOOK2	8.43	18	1.9	0.029	274	1.74
PASD1	8.43	18	1.89	0.0291	275	1.73
AOAH	8.42	18	1.89	0.0291	276	1.73
RHOH	7.69	15	1.89	0.0292	277	1.73
OLIG1	8.42	18	1.89	0.0292	278	1.73
ISL1	8.41	18	1.89	0.0293	279	1.72
HSF1	8.41	18	1.89	0.0294	280	1.72
TRIM35	8.4	18	1.89	0.0295	281	1.72
PCGF1	8.4	18	1.89	0.0295	282	1.71
COL15A1	8.39	18	1.89	0.0295	283	1.71
TGDS	6.85	12	1.89	0.0296	284	1.71
MIF	7.64	15	1.88	0.0298	285	1.72
PLEKHH3	8.36	18	1.88	0.03	286	1.72
KIFC1	8.36	18	1.88	0.03	287	1.71
PCSK4	8.35	18	1.88	0.0301	288	1.72
PTPRB	8.35	18	1.88	0.0302	289	1.71
LRR1	7.62	15	1.88	0.0302	290	1.71
SPRY4	7.62	15	1.88	0.0302	291	1.7
KAT2B	8.34	18	1.88	0.0304	292	1.71
IGFL4	6.8	12	1.88	0.0304	293	1.7
JHDM1D	8.33	18	1.87	0.0305	294	1.7
C2orf16	8.32	18	1.87	0.0305	295	1.7
NDNF	8.32	18	1.87	0.0306	296	1.69
SURF4	8.09	17	1.87	0.0306	297	1.69
CABS1	4.8	6	1.87	0.0306	298	1.69
FBXO41	8.3	18	1.87	0.0308	299	1.69
MYL10	8.3	18	1.87	0.0308	300	1.69
RGS11	6.78	12	1.87	0.0308	301	1.68

CD2AP	8.3	18	1.87	0.0309	302	1.68
ZDHHC16	8.3	18	1.87	0.0309	303	1.67
ROS1	8.3	18	1.87	0.0309	304	1.67
IMMP2L	8.29	18	1.87	0.031	305	1.67
ULK2	8.29	18	1.87	0.031	306	1.66
NLK	7.56	15	1.87	0.0311	307	1.66
ATP1A3	8.28	18	1.87	0.0311	308	1.66
COL6A1	7.56	15	1.86	0.0311	309	1.65
OR10R2	6.76	12	1.86	0.0312	310	1.65
SLC26A11	7.55	15	1.86	0.0313	311	1.65
CHRDL2	8.27	18	1.86	0.0314	312	1.65
CRYM	8.26	18	1.86	0.0315	313	1.65
LLGL2	8.25	18	1.86	0.0315	314	1.65
TUBA8	6.74	12	1.86	0.0316	315	1.65
HTATIP2	8.25	18	1.86	0.0316	316	1.64
RPS24	7.52	15	1.86	0.0317	317	1.64
SIRT3	8.24	18	1.86	0.0317	318	1.64
SOX1	8.24	18	1.86	0.0317	319	1.63
DNMT3A	7.52	15	1.85	0.0318	320	1.63
GK5	8.22	18	1.85	0.032	321	1.64
PRSS53	8.22	18	1.85	0.0321	322	1.63
AMPD3	8.21	18	1.85	0.0322	323	1.64
KNOP1	4.74	6	1.85	0.0323	324	1.63
ZNF451	8.2	18	1.85	0.0323	325	1.63
PROM2	8.19	18	1.85	0.0324	326	1.63
PSMB11	6.69	12	1.85	0.0325	327	1.63
TRPV3	8.19	18	1.85	0.0325	328	1.63
SOHLH1	8.19	18	1.84	0.0326	329	1.62

PTGES3L	8.18	18	1.84	0.0326	330	1.62
PROK1	7.47	15	1.84	0.0326	331	1.62
HES2	7.47	15	1.84	0.0326	332	1.61
CATSPER4	8.18	18	1.84	0.0327	333	1.61
CALHM3	8.16	18	1.84	0.0329	334	1.62
LUZP2	8.16	18	1.84	0.0329	335	1.61
INSM1	7.44	15	1.84	0.033	336	1.61
ZNF350	4.7	6	1.83	0.0333	337	1.62
TMEM132B	8.14	18	1.83	0.0333	338	1.62
TMEM56	4.7	6	1.83	0.0333	339	1.61
SPTLC2	8.13	18	1.83	0.0334	340	1.61
MRGPRD	8.12	18	1.83	0.0335	341	1.61
CD1D	8.11	18	1.83	0.0336	342	1.61
MC2R	6.61	12	1.83	0.0339	343	1.62
PACS2	8.1	18	1.83	0.0339	344	1.62
SLC22A16	8.09	18	1.83	0.0339	345	1.61
XIRP2	8.09	18	1.82	0.0341	346	1.62
EMR1	7.37	15	1.82	0.0342	347	1.62
CD2	7.36	15	1.82	0.0344	348	1.62
TCTE1	8.06	18	1.82	0.0344	349	1.62
IQSEC1	8.06	18	1.82	0.0345	350	1.62
TNFRSF18	8.05	18	1.82	0.0346	351	1.62
SF3A2	7.83	17	1.82	0.0346	352	1.61
MED29	8.04	18	1.81	0.0349	353	1.62
COG1	7.33	15	1.81	0.0349	354	1.62
PSMD13	8.03	18	1.81	0.035	355	1.62
C8orf82	8.02	18	1.81	0.0351	356	1.62
GPR148	6.54	12	1.81	0.0352	357	1.62

HTR4	8.02	18	1.81	0.0352	358	1.61
VARS	7.55	16	1.81	0.0352	359	1.61
CELF5	7.06	14	1.81	0.0354	360	1.61
NES	7.99	18	1.81	0.0355	361	1.62
SURF2	7.99	18	1.81	0.0355	362	1.61
TIMM17B	4.61	6	1.8	0.0356	363	1.61
CTNND2	7.98	18	1.8	0.0357	364	1.61
UBAP2L	7.98	18	1.8	0.0357	365	1.61
GP5	7.97	18	1.8	0.0359	366	1.61
PLA2G4F	7.96	18	1.8	0.036	367	1.61
DHX57	7.96	18	1.8	0.0361	368	1.61
ZNF7	7.96	18	1.8	0.0361	369	1.61
STUB1	7.96	18	1.8	0.0362	370	1.6
SLC41A1	7.95	18	1.8	0.0362	371	1.6
WARS	7.95	18	1.8	0.0362	372	1.6
LIPN	7.26	15	1.8	0.0363	373	1.6
CAMK2G	7.95	18	1.8	0.0363	374	1.59
DIABLO	7.94	18	1.79	0.0365	375	1.6
IQCK	7.93	18	1.79	0.0365	376	1.59
CUL4B	7.93	18	1.79	0.0366	377	1.59
C10orf54	7.93	18	1.79	0.0366	378	1.59
IZUMO4	7.92	18	1.79	0.0368	379	1.59
PGAM5	7.91	18	1.79	0.0369	380	1.59
ADAT3	6.46	12	1.79	0.0369	381	1.59
ANKRD13C	7.91	18	1.79	0.037	382	1.59
RTP3	7.22	15	1.79	0.037	383	1.58
PRDM13	7.9	18	1.79	0.037	384	1.58
RAF1	7.9	18	1.79	0.0371	385	1.58

DNAH12	7.9	18	1.79	0.0371	386	1.58
C10orf88	7.89	18	1.78	0.0372	387	1.58
NAPRT1	7.89	18	1.78	0.0372	388	1.57
PITX3	7.89	18	1.78	0.0372	389	1.57
SRRM3	7.89	18	1.78	0.0373	390	1.57
GDE1	7.88	18	1.78	0.0374	391	1.57
PON1	7.87	18	1.78	0.0376	392	1.57
SPSB2	7.87	18	1.78	0.0376	393	1.57
KHDRBS1	7.85	18	1.78	0.0379	394	1.58
HAUS4	6.41	12	1.78	0.0379	395	1.58
OR6M1	5.55	9	1.77	0.038	396	1.58
RASSF5	7.84	18	1.77	0.0381	397	1.58
FIBP	7.84	18	1.77	0.0381	398	1.57
TSHZ3	7.15	15	1.77	0.0382	399	1.57
ZNF618	7.83	18	1.77	0.0383	400	1.57
GPR111	7.15	15	1.77	0.0383	401	1.57
ANKRD30B	5.53	9	1.77	0.0385	402	1.57
PURB	7.13	15	1.77	0.0385	403	1.57
VAX2	7.81	18	1.77	0.0386	404	1.57
OR5A2	5.52	9	1.77	0.0388	405	1.57
LDLRAD1	7.8	18	1.76	0.0388	406	1.57
GTF2A1L	7.79	18	1.76	0.039	407	1.57
THRA	7.79	18	1.76	0.039	408	1.57
OPCML	7.79	18	1.76	0.039	409	1.57
OR10W1	6.36	12	1.76	0.039	410	1.56
IQCF1	5.5	9	1.76	0.0391	411	1.56
TRAPPC5	7.1	15	1.76	0.0392	412	1.56
BEAN1	7.77	18	1.76	0.0393	413	1.56

DHRS11	7.77	18	1.76	0.0393	414	1.56
MMD	7.09	15	1.76	0.0394	415	1.56
SMAP1	7.76	18	1.76	0.0394	416	1.55
MLLT1	7.76	18	1.76	0.0394	417	1.55
KIF2B	6.33	12	1.76	0.0395	418	1.55
FAM160A2	7.75	18	1.76	0.0396	419	1.55
SLC23A1	7.74	18	1.75	0.0398	420	1.55
HS3ST1	7.06	15	1.75	0.0399	421	1.55
THSD7B	7.74	18	1.75	0.0399	422	1.55
NEU3	7.73	18	1.75	0.0399	423	1.55
HNRNPA0	7.06	15	1.75	0.04	424	1.55
SLC2A6	7.72	18	1.75	0.0402	425	1.55
WASL	7.72	18	1.75	0.0402	426	1.55
CIB3	7.71	18	1.75	0.0403	427	1.55
ZNF419	4.45	6	1.75	0.0404	428	1.55
HSD17B14	7.7	18	1.74	0.0405	429	1.55
CPED1	7.7	18	1.74	0.0405	430	1.55
SDF2L1	7.7	18	1.74	0.0406	431	1.55
LHFP	7.02	15	1.74	0.0407	432	1.55
NHSL2	7.69	18	1.74	0.0408	433	1.55
RAPGEF6	7.68	18	1.74	0.0408	434	1.54
CECR6	7.01	15	1.74	0.0409	435	1.54
DLGAP3	7.67	18	1.74	0.041	436	1.54
HDAC10	7.67	18	1.74	0.0411	437	1.54
LRRC46	7.67	18	1.74	0.0411	438	1.54
SLC28A3	7.67	18	1.74	0.0411	439	1.54
TTC24	7.66	18	1.74	0.0412	440	1.54
MET	7.65	18	1.73	0.0415	441	1.54

CD226	7.63	18	1.73	0.0418	442	1.55
ZNF142	7.63	18	1.73	0.0418	443	1.55
DTX2	6.96	15	1.73	0.0418	444	1.55
KIR3DL3	6.23	12	1.73	0.0419	445	1.54
AXL	7.62	18	1.73	0.0419	446	1.54
PIH1D2	6.95	15	1.73	0.042	447	1.54
FNTB	7.4	17	1.73	0.0421	448	1.54
COL5A2	7.61	18	1.73	0.0422	449	1.54
MAP2K1	5.38	9	1.72	0.0423	450	1.54
SURF1	7.6	18	1.72	0.0423	451	1.54
CEBPE	7.6	18	1.72	0.0424	452	1.54
SLC18B1	6.2	12	1.72	0.0424	453	1.54
OR10G3	6.2	12	1.72	0.0425	454	1.54
ZNF540	5.37	9	1.72	0.0425	455	1.53
PAEP	6.92	15	1.72	0.0428	456	1.54
BPNT1	6.19	12	1.72	0.0428	457	1.54
EIF3H	7.58	18	1.72	0.0428	458	1.53
C11orf83	7.58	18	1.72	0.0428	459	1.53
KSR1	7.57	18	1.72	0.0429	460	1.53
PHKB	7.57	18	1.72	0.0429	461	1.53
EIF4E2	6.9	15	1.72	0.0432	462	1.53
TMEM179	7.55	18	1.71	0.0432	463	1.53
PACSIN1	7.55	18	1.71	0.0433	464	1.53
RBM20	7.55	18	1.71	0.0433	465	1.53
ZNF274	7.54	18	1.71	0.0435	466	1.53
EBF3	7.54	18	1.71	0.0436	467	1.53
GFI1B	7.53	18	1.71	0.0437	468	1.53
THAP9	7.52	18	1.71	0.0439	469	1.54

MIPOL1	5.31	9	1.71	0.0441	470	1.54
TTC6	7.5	18	1.7	0.0442	471	1.54
AMER2	7.5	18	1.7	0.0443	472	1.54
FBXW8	7.5	18	1.7	0.0443	473	1.54
PKIG	7.5	18	1.7	0.0443	474	1.53
VENTX	6.84	15	1.7	0.0443	475	1.53
LHFPL1	7.49	18	1.7	0.0444	476	1.53
UTP6	7.49	18	1.7	0.0446	477	1.53
SRD5A3	6.83	15	1.7	0.0446	478	1.53
GLOD4	7.48	18	1.7	0.0447	479	1.53
PLA2G3	7.47	18	1.7	0.0448	480	1.53
TRDMT1	7.47	18	1.7	0.0448	481	1.53
PDP2	7.47	18	1.7	0.0449	482	1.53
LAMC3	7.46	18	1.7	0.045	483	1.53
FAM222B	7.46	18	1.7	0.045	484	1.53
C5orf34	6.09	12	1.69	0.0451	485	1.53
IKZF1	7.46	18	1.69	0.0451	486	1.52
AURKB	6.81	15	1.69	0.0451	487	1.52
PRTN3	7.45	18	1.69	0.0452	488	1.52
EVA1B	7.45	18	1.69	0.0452	489	1.52
CHPF2	7.45	18	1.69	0.0452	490	1.51
PLCD3	7.44	18	1.69	0.0454	491	1.52
MYRF	7.01	16	1.69	0.0455	492	1.52
TNFAIP8L1	6.78	15	1.69	0.0456	493	1.52
TEKT5	6.77	15	1.69	0.0459	494	1.52
ZNF517	6.77	15	1.68	0.046	495	1.53
OR14I1	6.76	15	1.68	0.0462	496	1.53
RSG1	7.4	18	1.68	0.0463	497	1.53

OR51E2	6.04	12	1.68	0.0463	498	1.53
FERMT1	7.39	18	1.68	0.0463	499	1.52
NBAS	7.38	18	1.68	0.0466	500	1.53
CLPP	7.38	18	1.68	0.0466	501	1.53
PLAC9	4.26	6	1.68	0.0466	502	1.52
GOLGA2	7.36	18	1.67	0.047	503	1.53
RAE1	6.01	12	1.67	0.047	504	1.53
SRM	7.36	18	1.67	0.047	505	1.53
FREM3	7.36	18	1.67	0.0471	506	1.53
HRAS	7.35	18	1.67	0.0472	507	1.53
KIAA2026	6.71	15	1.67	0.0472	508	1.53
SOAT1	6.71	15	1.67	0.0472	509	1.52
GAK	7.35	18	1.67	0.0473	510	1.52
TRIP6	7.35	18	1.67	0.0473	511	1.52
VANGL1	7.35	18	1.67	0.0473	512	1.52
IDNK	7.33	18	1.67	0.0476	513	1.52
MON2	7.33	18	1.67	0.0477	514	1.52
VOPP1	4.23	6	1.67	0.0477	515	1.52
ST8SIA6	6.68	15	1.67	0.0478	516	1.52
KLHL38	7.32	18	1.67	0.0479	517	1.52
IL1RAPL2	7.31	18	1.66	0.048	518	1.52
SAMSN1	7.31	18	1.66	0.048	519	1.52
ZNF551	5.97	12	1.66	0.048	520	1.51
SREBF1	7.31	18	1.66	0.0481	521	1.51
CD5	7.3	18	1.66	0.0482	522	1.51
ERH	4.21	6	1.66	0.0483	523	1.51
SRGAP1	7.3	18	1.66	0.0483	524	1.51
ELL2	7.3	18	1.66	0.0483	525	1.51

SIK3	7.29	18	1.66	0.0485	526	1.51
DAZAP2	5.15	9	1.66	0.0486	527	1.51
PIM1	7.28	18	1.66	0.0487	528	1.51
MAEL	7.28	18	1.66	0.0488	529	1.51
COA1	7.27	18	1.66	0.0488	530	1.51
PDIA5	7.27	18	1.66	0.0489	531	1.51
HERC3	7.27	18	1.65	0.049	532	1.51
TMEM189	7.26	18	1.65	0.049	533	1.51
SLC4A4	7.26	18	1.65	0.0491	534	1.51
GAL3ST2	6.63	15	1.65	0.0491	535	1.51
ZNF793	5.93	12	1.65	0.0492	536	1.51
OR4D1	5.92	12	1.65	0.0493	537	1.51
NAALADL1	7.25	18	1.65	0.0494	538	1.51
SETD1A	7.24	18	1.65	0.0496	539	1.51
RPH3A	7.24	18	1.65	0.0496	540	1.51
MYLK3	7.24	18	1.65	0.0496	541	1.5
PIK3AP1	7.23	18	1.65	0.0497	542	1.51
C19orf59	7.22	18	1.65	0.0499	543	1.51
LGALS1	7.22	18	1.64	0.05	544	1.51
CAPN11	7.22	18	1.64	0.05	545	1.51
HOXC9	7	17	1.64	0.0503	546	1.51
D2HGDH	7.2	18	1.64	0.0504	547	1.51
ZNF358	7.2	18	1.64	0.0504	548	1.51
MAP3K12	7.19	18	1.64	0.0506	549	1.51
PRKAB1	7.18	18	1.64	0.0508	550	1.52
PITPNM3	7.17	18	1.64	0.051	551	1.52
PEX2	4.14	6	1.64	0.051	552	1.52
CCL24	4.14	6	1.63	0.0511	553	1.52

TMEM8A	7.16	18	1.63	0.0512	554	1.52
PCDH8	7.16	18	1.63	0.0512	555	1.52
YARS2	7.15	18	1.63	0.0514	556	1.52
RASGEF1A	7.15	18	1.63	0.0514	557	1.52
WHAMM	7.15	18	1.63	0.0515	558	1.51
NANOS3	6.52	15	1.63	0.0515	559	1.51
PSMD8	7.14	18	1.63	0.0516	560	1.51
KCNB2	7.14	18	1.63	0.0517	561	1.51
EDEM1	7.14	18	1.63	0.0518	562	1.51
C12orf42	7.13	18	1.63	0.0518	563	1.51
FMO3	7.13	18	1.63	0.0519	564	1.51
TMEM41B	5.82	12	1.63	0.052	565	1.51
DBX2	7.11	18	1.62	0.0523	566	1.52
NDST3	7.11	18	1.62	0.0524	567	1.52
ZNF195	5.03	9	1.62	0.0524	568	1.51
DROSHA	7.11	18	1.62	0.0524	569	1.51
TCEB3B	6.49	15	1.62	0.0525	570	1.51
EGFLAM	7.09	18	1.62	0.0528	571	1.52
FAM221B	7.09	18	1.62	0.0528	572	1.51
FKBP9	4.09	6	1.62	0.0528	573	1.51
C1orf94	7.09	18	1.62	0.0528	574	1.51
UBE2J1	7.09	18	1.62	0.0529	575	1.51
HLA-DOA	7.08	18	1.62	0.0529	576	1.51
DPYSL2	7.08	18	1.62	0.053	577	1.51
CCNJL	7.08	18	1.62	0.0531	578	1.51
SDE2	7.07	18	1.62	0.0531	579	1.51
PSMC5	7.07	18	1.62	0.0532	580	1.5
GPR107	7.06	18	1.61	0.0534	581	1.51

ZNF474	4.99	9	1.61	0.0536	582	1.51
ACER3	5.76	12	1.61	0.0536	583	1.51
SPRR2G	4.07	6	1.61	0.0537	584	1.51
YIPF3	7.05	18	1.61	0.0537	585	1.51
ZNF263	7.04	18	1.61	0.0539	586	1.51
BPIFA3	6.43	15	1.61	0.0539	587	1.51
R3HDM4	7.04	18	1.61	0.054	588	1.51
ODF3L1	7.03	18	1.61	0.054	589	1.51
TANGO6	7.03	18	1.61	0.054	590	1.5
MX1	6.42	15	1.61	0.0541	591	1.5
CLDN12	6.42	15	1.61	0.0541	592	1.5
DCSTAMP	7.03	18	1.61	0.0541	593	1.5
FRAT1	7.03	18	1.61	0.0542	594	1.5
EFR3B	7.03	18	1.61	0.0542	595	1.49
GBA2	7.03	18	1.61	0.0542	596	1.49
DYNLT3	4.06	6	1.61	0.0542	597	1.49
TBX1	7.02	18	1.6	0.0543	598	1.49
GADL1	7.02	18	1.6	0.0544	599	1.49
LYPD5	7.02	18	1.6	0.0544	600	1.49
CYLC1	4.05	6	1.6	0.0545	601	1.49
HMGCL	7.01	18	1.6	0.0547	602	1.49
OTUD3	7	18	1.6	0.0548	603	1.49
TTBK1	6.99	18	1.6	0.0549	604	1.49
CUBN	6.99	18	1.6	0.055	605	1.49
MYCBPAP	6.98	18	1.6	0.0552	606	1.5
MYOM1	6.98	18	1.6	0.0553	607	1.49
TRAPPC1	6.98	18	1.6	0.0553	608	1.49
PMPCA	6.37	15	1.59	0.0554	609	1.49

ZDHHC2	6.37	15	1.59	0.0554	610	1.49
MAST1	6.97	18	1.59	0.0555	611	1.49
ANXA4	6.97	18	1.59	0.0555	612	1.49
C12orf45	4.93	9	1.59	0.0555	613	1.48
C1orf192	6.36	15	1.59	0.0555	614	1.48
NFXL1	6.96	18	1.59	0.0556	615	1.48
FPGT	4.02	6	1.59	0.0557	616	1.48
IDI1	6.35	15	1.59	0.0558	617	1.49
SLC6A14	4.92	9	1.59	0.0559	618	1.48
SIPA1L3	6.95	18	1.59	0.0559	619	1.48
TBC1D1	6.95	18	1.59	0.056	620	1.48
SEC31B	6.34	15	1.59	0.056	621	1.48
PAPSS2	6.95	18	1.59	0.056	622	1.48
C1orf172	6.95	18	1.59	0.056	623	1.48
SFRP5	6.95	18	1.59	0.056	624	1.47
DGKG	6.94	18	1.59	0.0561	625	1.47
HOXD12	6.33	15	1.59	0.0562	626	1.47
HTR5A	6.33	15	1.59	0.0562	627	1.47
TOLLIP	6.94	18	1.59	0.0563	628	1.47
ARHGAP12	6.93	18	1.59	0.0563	629	1.47
KRTAP11-1	5.66	12	1.59	0.0564	630	1.47
PTRH2	4.9	9	1.59	0.0564	631	1.47
KANSL2	6.93	18	1.59	0.0564	632	1.47
NKX6-1	6.93	18	1.59	0.0564	633	1.46
AMDHD2	6.93	18	1.59	0.0565	634	1.46
SERPIND1	6.93	18	1.58	0.0565	635	1.46
NEK7	4.89	9	1.58	0.0566	636	1.46
IGIP	3.99	6	1.58	0.0567	637	1.46

HUS1	6.91	18	1.58	0.0569	638	1.46
INPP5F	6.3	15	1.58	0.057	639	1.46
ENTPD2	6.9	18	1.58	0.057	640	1.46
C12orf40	3.99	6	1.58	0.0571	641	1.46
KCNMB1	6.9	18	1.58	0.0572	642	1.46
ZFR2	6.89	18	1.58	0.0573	643	1.46
TRIM68	6.89	18	1.58	0.0574	644	1.46
ATG2A	6.89	18	1.58	0.0574	645	1.46
CPVL	6.29	15	1.58	0.0574	646	1.46
MRPS15	6.29	15	1.58	0.0574	647	1.46
PCDH19	6.89	18	1.58	0.0574	648	1.45
ZKSCAN2	6.88	18	1.58	0.0576	649	1.46
BECN1	6.28	15	1.57	0.0576	650	1.45
KIAA0368	6.28	15	1.57	0.0577	651	1.45
UCHL3	5.62	12	1.57	0.0577	652	1.45
TIMM44	6.87	18	1.57	0.0578	653	1.45
B3GNT7	6.87	18	1.57	0.0578	654	1.45
PLEKHO2	6.87	18	1.57	0.0579	655	1.45
SRPK3	6.87	18	1.57	0.0579	656	1.45
GPN1	6.27	15	1.57	0.058	657	1.45
ARHGAP15	5.6	12	1.57	0.058	658	1.45
IL20	4.85	9	1.57	0.058	659	1.45
CMTM8	6.86	18	1.57	0.0581	660	1.44
NANS	6.86	18	1.57	0.0581	661	1.44
SRSF7	6.85	18	1.57	0.0584	662	1.45
DMP1	6.25	15	1.57	0.0584	663	1.45
GPR88	6.25	15	1.57	0.0584	664	1.44
TP53I3	6.84	18	1.57	0.0585	665	1.44

SMAD6	6.84	18	1.57	0.0586	666	1.44
MTCH2	6.24	15	1.57	0.0586	667	1.44
SLC9A2	6.83	18	1.57	0.0587	668	1.44
NUBP2	6.83	18	1.57	0.0587	669	1.44
RCAN3	6.24	15	1.57	0.0587	670	1.44
HAUS5	6.83	18	1.56	0.0589	671	1.44
KANK4	6.23	15	1.56	0.059	672	1.44
CRK	6.82	18	1.56	0.059	673	1.44
ENTPD8	6.82	18	1.56	0.059	674	1.44
SPEF1	6.81	18	1.56	0.0594	675	1.44
UBR1	6.79	18	1.56	0.0597	676	1.45
CCDC70	5.54	12	1.56	0.0598	677	1.45
LGI4	6.79	18	1.56	0.0599	678	1.45
CPEB1	6.79	18	1.56	0.0599	679	1.45
PSMD2	6.78	18	1.55	0.0601	680	1.45
SMAD7	6.78	18	1.55	0.0602	681	1.45
MAOB	6.18	15	1.55	0.0602	682	1.45
TAB2	6.18	15	1.55	0.0603	683	1.45
HOXA6	6.76	18	1.55	0.0605	684	1.45
TNRC18	6.76	18	1.55	0.0605	685	1.45
CHCHD10	4.78	9	1.55	0.0605	686	1.45
BMP4	6.76	18	1.55	0.0605	687	1.45
SLC29A4	6.17	15	1.55	0.0606	688	1.44
TRIM60	4.78	9	1.55	0.0606	689	1.44
RBM38	6.76	18	1.55	0.0606	690	1.44
GPR123	6.75	18	1.55	0.0609	691	1.45
ACAP1	6.74	18	1.55	0.061	692	1.45
C1orf233	6.15	15	1.55	0.0611	693	1.45

C17orf77	5.5	12	1.54	0.0612	694	1.45
LELP1	5.49	12	1.54	0.0613	695	1.45
CCDC96	6.72	18	1.54	0.0615	696	1.45
GUK1	6.13	15	1.54	0.0616	697	1.45
MARCH5	6.72	18	1.54	0.0616	698	1.45
SRMS	6.71	18	1.54	0.0617	699	1.45
MUC2	6.71	18	1.54	0.0619	700	1.45
MYOG	6.12	15	1.54	0.0619	701	1.45
VPS18	6.7	18	1.54	0.0619	702	1.45
RASD1	6.7	18	1.54	0.062	703	1.45
C9orf3	6.7	18	1.54	0.0621	704	1.45
GPR68	6.11	15	1.54	0.0623	705	1.45
SAMD14	6.69	18	1.54	0.0623	706	1.45
RCL1	6.1	15	1.53	0.0625	707	1.45
ASB7	6.1	15	1.53	0.0626	708	1.45
HYI	6.68	18	1.53	0.0626	709	1.45
LRRC70	4.72	9	1.53	0.0627	710	1.45
GLIPR1L1	6.09	15	1.53	0.0628	711	1.45
ZCWPW1	6.67	18	1.53	0.0628	712	1.45
AKAP5	3.85	6	1.53	0.0629	713	1.45
NCKAP1L	6.67	18	1.53	0.0629	714	1.45
LGI2	6.66	18	1.53	0.0629	715	1.44
CDC42EP4	6.08	15	1.53	0.063	716	1.44
CHCHD1	6.08	15	1.53	0.0632	717	1.45
PINX1	6.07	15	1.53	0.0632	718	1.44
COL18A1	6.65	18	1.53	0.0633	719	1.44
NAA50	3.84	6	1.53	0.0634	720	1.44
ZNF787	6.65	18	1.53	0.0634	721	1.44

EHF	6.64	18	1.53	0.0635	722	1.44
C6orf132	6.64	18	1.53	0.0636	723	1.44
WDR90	6.64	18	1.52	0.0637	724	1.44
CDC42BPB	6.63	18	1.52	0.0639	725	1.45
TRAK1	6.63	18	1.52	0.0639	726	1.44
TDRD12	6.62	18	1.52	0.0641	727	1.45
RFWD2	3.82	6	1.52	0.0641	728	1.44
POLRMT	6.62	18	1.52	0.0641	729	1.44
PARVA	6.61	18	1.52	0.0642	730	1.44
EBNA1BP2	6.03	15	1.52	0.0645	731	1.45
C10orf85	4.67	9	1.52	0.0645	732	1.45
TMEM115	6.6	18	1.52	0.0646	733	1.45
DDX53	3.81	6	1.52	0.0646	734	1.44
FRK	6.59	18	1.52	0.0648	735	1.45
WDR85	6.59	18	1.51	0.0649	736	1.45
POR	6.58	18	1.51	0.0651	737	1.45
VSIG2	6.58	18	1.51	0.0651	738	1.45
HOXB4	6.57	18	1.51	0.0653	739	1.45
RALGDS	6.57	18	1.51	0.0653	740	1.45
CLCN4	6.57	18	1.51	0.0654	741	1.45
S100A9	5.36	12	1.51	0.0654	742	1.45
MRPL27	6.57	18	1.51	0.0654	743	1.45
HMX1	6.57	18	1.51	0.0655	744	1.44
TADA1	5.99	15	1.51	0.0655	745	1.44
PARP3	5.99	15	1.51	0.0655	746	1.44
ZNF266	5.36	12	1.51	0.0656	747	1.44
SHOC2	6.56	18	1.51	0.0656	748	1.44
MLPH	6.56	18	1.51	0.0657	749	1.44

CNNM4	6.56	18	1.51	0.0657	750	1.44
PIBF1	6.55	18	1.51	0.0658	751	1.44
PIH1D3	4.63	9	1.51	0.0659	752	1.44
ESRRB	6.55	18	1.51	0.0659	753	1.44
COMMD6	4.63	9	1.51	0.0659	754	1.43
ST8SIA3	6.55	18	1.51	0.066	755	1.43
BANP	6.55	18	1.51	0.066	756	1.43
MRPS9	6.54	18	1.5	0.0662	757	1.43
GGA3	6.53	18	1.5	0.0663	758	1.44
LY6G6D	5.33	12	1.5	0.0665	759	1.44
ZSCAN21	6.52	18	1.5	0.0666	760	1.44
TBKBP1	6.52	18	1.5	0.0668	761	1.44
GPR146	6.52	18	1.5	0.0668	762	1.44
GPR183	3.76	6	1.5	0.0669	763	1.44
NEUROD1	6.51	18	1.5	0.0669	764	1.44
ADNP	5.94	15	1.5	0.067	765	1.44
ART4	5.94	15	1.5	0.067	766	1.44
TTR	6.51	18	1.5	0.067	767	1.43
NALCN	6.51	18	1.5	0.0671	768	1.43
NRG4	5.3	12	1.5	0.0674	769	1.44
ZNF510	4.59	9	1.5	0.0675	770	1.44

Table 3.S4 GSEA-Gene Ontology analysis related to figure 3.1 C and 3.S2 A

NAME	SIZE	ES	NES	NOM p-val	FDR q-val	FWER p-val
GOBP_INTERSTRAND_CROSS_LINK_REPAIR	22	0.945399	2.840668	0	0	0
GOBP_DOUBLE_STRAND_BREAK_REPAIR	34	0.805053	2.57407	0	0	0
GOBP_MEIOTIC_CELL_CYCLE_PROCESS	16	0.890945	2.535938	0	0	0
GOBP_NUCLEAR_CHROMOSOME_SEGREGATION	18	0.859324	2.503383	0	0	0
GOBP_RECOMBINATIONAL_REPAIR	27	0.803204	2.489281	0	0	0
GOBP_DNA_REPAIR	59	0.721306	2.443671	0	0	0
GOBP_ORGANELLE_FISSION	27	0.784403	2.437494	0	0	0
GOBP_MEIOTIC_CELL_CYCLE	20	0.813892	2.411553	0	0	0
GOBP_DNA_RECOMBINATION	38	0.721228	2.33956	0	0	0
GOBP_CHROMOSOME_SEGREGATION	22	0.773191	2.327074	0	0	0
GOBP_DNA_METABOLIC_PROCESS	75	0.609662	2.10529	0	4.52E-05	5.00E-04
GOBP_CELLULAR_RESPONSE_TO_DNA_DAMAGE_STIMULUS	74	0.603258	2.087503	0	4.97E-05	6.00E-04
GOBP_NEGATIVE_REGULATION_OF_MITOTIC_CELL_CYCLE	23	0.660498	2.00639	0	2.53E-04	0.0033
GOBP_MITOTIC_CELL_CYCLE_CHECKPOINT	15	0.710218	2.004017	0	2.70E-04	0.0038
GOBP_CELL_CYCLE_CHECKPOINT	19	0.678529	1.99426	0	3.12E-04	0.0047
GOBP_TELOMERE_ORGANIZATION	16	0.694972	1.983919	0	3.98E-04	0.0063
GOBP_REGULATION_OF_CELL_CYCLE_PHASE_TRANSITION	23	0.639782	1.934424	0	7.85E-04	0.0133
GOBP_REGULATION_OF_CHROMOSOME_ORGANIZATION	16	0.67553	1.932504	1.02E-04	7.63E-04	0.0137
GOBP_NEGATIVE_REGULATION_OF_CELL_CYCLE_PHASE_TRANSITION	18	0.663148	1.920184	0	9.12E-04	0.0173
GOBP_DNA_INTEGRITY_CHECKPOINT	15	0.669952	1.890133	3.10E-04	0.001379	0.0272
GOBP_POSITIVE_REGULATION_OF_CELL_CYCLE_PROCESS	18	0.646042	1.88434	3.05E-04	0.001441	0.0299

GOBP_CELL_CYCLE_PROCESS	67	0.545653	1.869046	0	0.001815	0.0394
GOBP_POSITIVE_REGULATION_OF_DNA_METABOLIC_PROCESS	15	0.656006	1.852081	3.10E-04	0.002377	0.0536
GOBP_NUCLEIC_ACID_PHOSPHODIESTER_BOND_HYDROLYSIS	20	0.614107	1.814301	3.04E-04	0.00415	0.0953
GOBP_NEGATIVE_REGULATION_OF_CELL_CYCLE_PROCESS	20	0.605387	1.794663	2.02E-04	0.005318	0.1247
GOBP_NEGATIVE_REGULATION_OF_CELL_CYCLE	34	0.556794	1.779714	1.00E-04	0.006499	0.1573
GOBP_REGULATION_OF_RESPONSE_TO_DNA_DAMAGE_STIMULUS	15	0.626603	1.764004	0.001447	0.008026	0.1965
GOBP_REGULATION_OF_MITOTIC_CELL_CYCLE	32	0.552556	1.756775	3.01E-04	0.008507	0.214
GOBP_POSITIVE_REGULATION_OF_ORGANELLE_ORGANIZATION	24	0.571864	1.746885	6.05E-04	0.009419	0.2418
GOBP_CHROMOSOME_ORGANIZATION	57	0.505577	1.707926	0	0.015397	0.3757
GOBP_DNA_REPLICATION	28	0.545177	1.70064	6.03E-04	0.016311	0.4028
GOBP_CELL_CYCLE	85	0.485303	1.69922	0	0.016107	0.4084
GOBP_REGULATION_OF_CELLULAR_RESPONSE_TO_STRESS	32	0.532839	1.696494	7.02E-04	0.016234	0.4189
GOBP_POSITIVE_REGULATION_OF_CELL_CYCLE	21	0.567981	1.695356	0.002334	0.015996	0.4241
GOBP_REGULATION_OF_CELL_CYCLE	56	0.500933	1.689712	1.00E-04	0.016874	0.4502
GOBP_REGULATION_OF_CELL_CYCLE_PROCESS	40	0.506568	1.652633	5.00E-04	0.026207	0.617
GOBP_MITOTIC_NUCLEAR_DIVISION	15	0.580782	1.636194	0.007004	0.031413	0.691
GOBP_NEGATIVE_REGULATION_OF_ORGANELLE_ORGANIZATION	18	0.559864	1.634674	0.005411	0.031155	0.6966
GOBP_GAMETE_GENERATION	30	0.516706	1.626911	0.001405	0.033251	0.7313
GOBP_DNA_DEPENDENT_DNA_REPLICATION	16	0.565804	1.611064	0.008189	0.039269	0.798
GOBP_REGIONALIZATION	20	0.539788	1.609527	0.00508	0.03902	0.8056
GOBP_SEXUAL_REPRODUCTION	31	0.502115	1.59716	0.003206	0.044139	0.8458
GOBP_REPRODUCTION	60	0.467432	1.588185	6.00E-04	0.047968	0.8749
GOBP_RESPONSE_TO_RADIATION	29	0.505139	1.582014	0.003615	0.050392	0.8936

GOBP_ANATOMICAL_STRUCTURE_HOMEOSTASIS	24	0.518245	1.577395	0.005035	0.051974	0.9067
GOBP_REGULATION_OF_LYMPHOCYTE_ACTIVATION	19	0.534699	1.573192	0.009454	0.053351	0.9164
GOBP_MICROTUBULE_CYTOSKELETON_ORGANIZATION	19	0.528721	1.558548	0.01017	0.061745	0.9467
GOBP_REGULATION_OF_DNA_METABOLIC_PROCESS	21	0.524905	1.557655	0.009211	0.061094	0.9491
GOBP_MULTICELLULAR_ORGANISM_REPRODUCTION	32	0.488619	1.551946	0.005015	0.063879	0.9585
GOBP_CELL_CYCLE_PHASE_TRANSITION	32	0.486221	1.545691	0.005617	0.067196	0.9675
GOBP_T_CELL_ACTIVATION	18	0.52941	1.543314	0.014335	0.067678	0.9708
GOBP_PATTERN_SPECIFICATION_PROCESS	26	0.497698	1.540815	0.009455	0.068348	0.9745
GOBP_MITOTIC_CELL_CYCLE	50	0.452058	1.509585	0.003702	0.093501	0.9945
GOBP_LYMPHOCYTE_ACTIVATION	32	0.472262	1.502816	0.009521	0.098523	0.9963
GOBP_MALE_GAMETE_GENERATION	24	0.488331	1.493505	0.017904	0.106635	0.9979
GOBP_REGULATION_OF_ORGANELLE_ORGANIZATION	50	0.447026	1.492361	0.0036	0.105908	0.998
GOBP_CELL_CYCLE_G2_M_PHASE_TRANSITION	15	0.525757	1.478974	0.028996	0.119212	0.9988
GOBP_MULTI_ORGANISM_PROCESS	36	0.448789	1.448901	0.014125	0.157897	1
GOBP_CELLULAR_RESPONSE_TO_ABIOTIC_STIMULUS	20	0.482746	1.428366	0.035251	0.188981	1
GOBP_SIGNAL_TRANSDUCTION_BY_P53_CLASS_MEDIATOR	20	0.477028	1.41524	0.040791	0.21068	1
GOBP_LYMPHOCYTE_MEDIATED_IMMUNITY	21	0.459646	1.375882	0.056455	0.2968	1
GOBP_NEGATIVE_REGULATION_OF_CELLULAR_COMPONENT_ORGANIZATION	29	0.430504	1.355331	0.052917	0.349374	1
GOBP_DNA_BIOSYNTHETIC_PROCESS	16	0.473651	1.354781	0.078651	0.345466	1
GOBP_DEVELOPMENT_OF_PRIMARY_SEXUAL_CHARACTERISTICS	15	0.478604	1.350481	0.081639	0.352864	1
GOBP_REGULATION_OF_LEUKOCYTE_MEDIATED_IMMUNITY	15	0.478151	1.348376	0.084389	0.353818	1

GOBP_RNA_CATABOLIC_PROCESS	18	0.459549	1.335445	0.085037	0.388829	1
GOBP_MORPHOGENESIS_OF_AN_EPITHELIUM	24	0.439387	1.335075	0.067769	0.384258	1
GOBP_CHROMATIN_ORGANIZATION	25	0.434153	1.334892	0.063873	0.379176	1
GOBP_TISSUE_MORPHOGENESIS	29	0.420232	1.324076	0.069177	0.40853	1
GOBP_RESPONSE_TO_ABIOTIC_STIMULUS	64	0.386164	1.318463	0.0282	0.421737	1
GOBP_SMALL_MOLECULE_BIOSYNTHETIC_PROCESS	25	0.430598	1.317859	0.078186	0.417984	1
GOBP_ANIMAL_ORGAN_MORPHOGENESIS	40	0.402708	1.316867	0.05496	0.41559	1
GOBP_CYTOKINE_MEDIATED_SIGNALING_PATHWAY	29	0.420179	1.31677	0.074003	0.410215	1
GOBP_MONONUCLEAR_CELL_DIFFERENTIATION	24	0.430989	1.315597	0.087338	0.408563	1
GOBP_EMBRYO_DEVELOPMENT_ENDING_IN_BIRTH_OR_EGG_HATCHING	33	0.409166	1.310332	0.070699	0.420765	1
GOBP_EMBRYO_DEVELOPMENT	44	0.394691	1.302166	0.060018	0.44314	1
GOBP_REGULATION_OF_RESPONSE_TO_STRESS	65	0.380035	1.300639	0.0374	0.442721	1
GOBP_DNA_CONFORMATION_CHANGE	17	0.450325	1.293761	0.116878	0.461649	1
GOBP_REGULATION_OF_CELL_ACTIVATION	24	0.42334	1.289501	0.103598	0.471407	1
GOBP_LIPID_BIOSYNTHETIC_PROCESS	33	0.403746	1.286807	0.087074	0.475413	1
GOBP_MICROTUBULE_BASED_PROCESS	32	0.403797	1.284628	0.089029	0.477558	1
GOBP_POSITIVE_REGULATION_OF_CELL_POPULATION_PROLIFERATION	36	0.398018	1.282456	0.082374	0.479567	1
GOBP_POSITIVE_REGULATION_OF_CELL_ACTIVATION	16	0.449252	1.281844	0.122131	0.476014	1
GOBP_EMBRYONIC_MORPHOGENESIS	19	0.43365	1.277652	0.119439	0.48573	1
GOBP_ORGANELLE_LOCALIZATION	31	0.40256	1.274714	0.095878	0.490808	1
GOBP_POSITIVE_REGULATION_OF_PROTEIN_MODIFICATION_PROCESS	49	0.38181	1.272381	0.069521	0.493691	1
GOBP_DEVELOPMENTAL_PROCESS_INVOLVED_IN_REPRODUCTION	39	0.391763	1.271081	0.085886	0.49278	1
GOBP_ADAPTIVE_IMMUNE_RESPONSE	19	0.432267	1.269725	0.125013	0.492252	1

GOBP_REGULATION_OF_RESPONSE_TO_EXTERNAL_STIMULUS	39	0.390125	1.268974	0.089053	0.489544	1
GOBP_CELL_ACTIVATION	55	0.374815	1.264559	0.0691	0.5004	1
GOBP_REGULATION_OF_DEFENSE_RESPONSE	33	0.394234	1.259871	0.106065	0.512461	1
GOBP_CELLULAR_RESPONSE_TO_CHEMICAL_STRESS	18	0.431499	1.257525	0.140224	0.515857	1
GOBP_SEX_DIFFERENTIATION	17	0.434712	1.254046	0.147777	0.523247	1
GOBP_PROTEIN_COMPLEX_OLIGOMERIZATION	16	0.436964	1.252077	0.15058	0.525206	1
GOBP_REPRODUCTIVE_SYSTEM_DEVELOPMENT	23	0.409643	1.240005	0.144486	0.567094	1
GOBP_IMMUNE_RESPONSE_REGULATING_SIGNALING_PATHWAY	19	0.422357	1.23751	0.157718	0.571211	1
GOBP_POSITIVE_REGULATION_OF_IMMUNE_RESPONSE	29	0.393591	1.237481	0.132551	0.565444	1
GOBP_ADAPTIVE_IMMUNE_RESPONSE_BASED_ON_SOMATIC_RECOMBINATION_OF_IMMUNE_RECEPTORS_BUILT_FROM_IMMUNOGLOBULIN_SUPERFAMILY_DOMAINS	16	0.433848	1.236329	0.164953	0.56421	1
GOBP_REGULATION_OF_IMMUNE_SYSTEM_PROCESS	63	0.360966	1.234987	0.0869	0.563866	1
GOBP_POSITIVE_REGULATION_OF_PHOSPHORUS_METABOLIC_PROCESS	41	0.37754	1.23299	0.113957	0.566084	1
GOBP_PROTEIN_MODIFICATION_BY_SMALL_PROTEIN_CONJUGATION	41	0.374365	1.225967	0.121649	0.588432	1
GOBP_LEUKOCYTE_MEDIATED_IMMUNITY	39	0.376121	1.224343	0.124137	0.589165	1
GOBP_REGULATION_OF_CELL_ADHESION	15	0.435557	1.224219	0.175222	0.583918	1
GOBP_ORGANIC_CYCLIC_COMPOUND_CATABOLIC_PROCESS	31	0.38727	1.223764	0.139262	0.580168	1
GOBP_EMBRYONIC_ORGAN_DEVELOPMENT	16	0.428225	1.220146	0.179854	0.589313	1
GOBP_OSSIFICATION	16	0.428044	1.218584	0.186018	0.590173	1
GOBP_CELL_POPULATION_PROLIFERATION	84	0.348311	1.21693	0.0775	0.591209	1
GOBP_POSITIVE_REGULATION_OF_PROTEIN_PHOSPHORYLATION	37	0.375668	1.216155	0.138694	0.588839	1

GOBP_MAPK_CASCADE	35	0.374787	1.209224	0.15024	0.6112	1
GOBP_MYELOID_LEUKOCYTE_MEDIATED_IMMUNITY	19	0.411016	1.207497	0.18708	0.612743	1
GOBP_IMMUNE_SYSTEM_DEVELOPMENT	49	0.361067	1.203702	0.131926	0.622754	1
GOBP_MACROMOLECULE_CATABOLIC_PROCESS	54	0.358374	1.203248	0.126138	0.619017	1
GOBP_REGULATION_OF_INNATE_IMMUNE_RESPONSE	15	0.42775	1.201592	0.203388	0.620397	1
GOBP_REGULATION_OF_INFLAMMATORY_RESPONSE	17	0.415623	1.197555	0.210731	0.631511	1
GOBP_NEGATIVE_REGULATION_OF_IMMUNE_SYSTEM_PROCESS	15	0.424451	1.196702	0.210184	0.629547	1
GOBP_MYELOID_LEUKOCYTE_ACTIVATION	24	0.391167	1.195051	0.194066	0.630807	1
GOBP_GLYCOPROTEIN_BIOSYNTHETIC_PROCESS	16	0.41861	1.193978	0.20826	0.62971	1
GOBP_GLYCOPROTEIN_METABOLIC_PROCESS	16	0.41861	1.191595	0.216501	0.634051	1
GOBP_REGULATION_OF_MAPK_CASCADE	27	0.382224	1.188005	0.196122	0.643591	1
GOBP_LEUKOCYTE_DIFFERENTIATION	28	0.380531	1.18666	0.191269	0.643878	1
GOBP_HEART_DEVELOPMENT	21	0.397153	1.185169	0.21373	0.644714	1
GOBP_COVALENT_CHROMATIN_MODIFICATION	18	0.404882	1.181106	0.223151	0.656222	1
GOBP_MRNA_METABOLIC_PROCESS	37	0.364195	1.178955	0.184803	0.659899	1
GOBP_NEGATIVE_REGULATION_OF_RESPONSE_TO_STIMULUS	71	0.342242	1.178574	0.1323	0.656118	1
GOBP_CELLULAR_RESPONSE_TO_LIPID	23	0.388925	1.176398	0.215914	0.659861	1
GOBP_RESPONSE_TO_OXIDATIVE_STRESS	19	0.398938	1.175631	0.223985	0.657755	1
GOBP_CARBOHYDRATE_DERIVATIVE_METABOLIC_PROCESS	42	0.358913	1.175332	0.175605	0.65384	1
GOBP_PRODUCTION_OF_MOLECULAR_MEDIATOR_OF_IMMUNE_RESPONSE	15	0.414017	1.169855	0.242781	0.671124	1
GOBP_CARBOHYDRATE_METABOLIC_PROCESS	22	0.387811	1.169087	0.227957	0.669049	1
GOBP_PROTEIN_LOCALIZATION_TO_ORGANELLE	36	0.362495	1.168636	0.193471	0.66574	1
GOBP_ORGANELLE_ASSEMBLY	30	0.371468	1.166319	0.214408	0.670128	1

GOBP_RESPONSE_TO_CYTOKINE	40	0.357111	1.163392	0.194556	0.676887	1
GOBP_NEGATIVE_REGULATION_OF_GENE_EXPRESSION	37	0.359532	1.161392	0.20747	0.679986	1
GOBP_ANATOMICAL_STRUCTURE_FORMATION_INVOLVED_IN_MORPHOGENESIS	43	0.35333	1.159441	0.19908	0.682884	1
GOBP_CYTOSKELETON_ORGANIZATION	44	0.350613	1.156822	0.19996	0.688578	1
GOBP_CELL_DIVISION	27	0.371631	1.155712	0.234904	0.687954	1
GOBP_POSITIVE_REGULATION_OF_IMMUNE_SYSTEM_PROCESS	39	0.35432	1.151178	0.219476	0.701564	1
GOBP_HOMEOSTATIC_PROCESS	92	0.326703	1.149552	0.1571	0.703088	1
GOBP_NEGATIVE_REGULATION_OF_SIGNALING	63	0.336146	1.148631	0.1826	0.701858	1
GOBP_IMMUNE_EFFECTOR_PROCESS	58	0.338773	1.148061	0.1908	0.699237	1
GOBP_TUBE_DEVELOPMENT	43	0.348511	1.146403	0.21941	0.701157	1
GOBP_DEPHOSPHORYLATION	15	0.405843	1.144513	0.269207	0.703859	1
GOBP_GLYCEROPHOSPHOLIPID_METABOLIC_PROCESS	17	0.394062	1.139312	0.271025	0.720273	1
GOBP_SKELETAL_SYSTEM_DEVELOPMENT	17	0.394216	1.139141	0.274283	0.716007	1
GOBP_POSITIVE_REGULATION_OF_RESPONSE_TO_EXTERNAL_STIMULUS	20	0.382987	1.138687	0.27419	0.712907	1
GOBP_REGULATION_OF_RESPONSE_TO_BIOTIC_STIMULUS	21	0.380035	1.138475	0.265856	0.7089	1
GOBP_CIRCULATORY_SYSTEM_DEVELOPMENT	43	0.345862	1.136997	0.230069	0.710034	1
GOBP_PEPTIDYL_AMINO_ACID_MODIFICATION	53	0.338774	1.136687	0.218109	0.706492	1
GOBP_POSITIVE_REGULATION_OF_IMMUNE_EFFECTOR_PROCESS	15	0.403943	1.136331	0.28595	0.703171	1
GOBP_CARBOHYDRATE_DERIVATIVE_BIOSYNTHETIC_PROCESS	26	0.366531	1.133154	0.270536	0.711164	1
GOBP_RESPONSE_TO_BACTERIUM	23	0.373451	1.132737	0.271106	0.70816	1
GOBP_ESTABLISHMENT_OF_ORGANELLE_LOCALIZATION	18	0.387218	1.132253	0.286122	0.705408	1

GOBP_CENTRAL_NERVOUS_SYSTEM_DEVELOPMENT	35	0.351957	1.131923	0.253407	0.702083	1
GOBP_MULTICELLULAR_ORGANISMAL_HOMEOSTASIS	17	0.394115	1.131869	0.287809	0.697722	1
GOBP_CELL_ACTIVATION_INVOLVED_IN_IMMUNE_RESPONSE	29	0.358581	1.125886	0.276094	0.716693	1
GOBP_NEGATIVE_REGULATION_OF_CELL_DEATH	45	0.338911	1.119745	0.254825	0.7368	1
GOBP_EXOCYTOSIS	36	0.345727	1.115703	0.279764	0.748456	1
GOBP_TUBE_MORPHOGENESIS	32	0.351175	1.115585	0.282277	0.744209	1
GOBP_REGULATION_OF_WNT_SIGNALING_PATHWAY	21	0.373127	1.115376	0.303903	0.740391	1
GOBP_POSITIVE_REGULATION_OF_PROTEIN_METABOLIC_PROCESS	65	0.326007	1.113889	0.2423	0.741654	1
GOBP_BIOLOGICAL_ADHESION	46	0.334701	1.105091	0.278984	0.772559	1
GOBP_REGULATION_OF_IMMUNE_RESPONSE	39	0.34015	1.104158	0.293305	0.771553	1
GOBP_DEFENSE_RESPONSE	57	0.325516	1.102098	0.276055	0.775205	1
GOBP_CELL_SURFACE_RECEPTOR_SIGNALING_PATHWAY_INVOLVED_IN_CELL_CELL_SIGNALING	31	0.348245	1.09992	0.308894	0.779394	1
GOBP_POSITIVE_REGULATION_OF_DEFENSE_RESPONSE	16	0.386098	1.099313	0.329463	0.777126	1
GOBP_DEVELOPMENTAL_GROWTH	20	0.367633	1.096054	0.327382	0.785599	1
GOBP_EPITHELIUM_DEVELOPMENT	48	0.329919	1.095437	0.296	0.783423	1
GOBP_INFLAMMATORY_RESPONSE	25	0.35585	1.091381	0.336419	0.795024	1
GOBP_POSITIVE_REGULATION_OF_SIGNALING	72	0.31718	1.0911	0.2732	0.791434	1
GOBP_CELLULAR_MACROMOLECULE_CATABOLIC_PROCESS	46	0.32931	1.08958	0.308131	0.792901	1
GOBP_REGULATION_OF_DNA_BINDING_TRANSCRIPTION_FACTOR_ACTIVITY	21	0.36331	1.086958	0.344019	0.798707	1
GOBP_METAL_ION_TRANSPORT	22	0.361189	1.085998	0.343238	0.79797	1
GOBP_REGULATION_OF_HEMOPOIESIS	17	0.375089	1.0845	0.356236	0.799321	1

GOBP_HEAD_DEVELOPMENT	26	0.350747	1.083595	0.341544	0.798291	1
GOBP_PEPTIDYL_LYSINE_MODIFICATION	19	0.368334	1.081066	0.354313	0.803875	1
GOBP_VIRAL_LIFE_CYCLE	16	0.378723	1.080457	0.357048	0.801736	1
GOBP_PROTEIN_PHOSPHORYLATION	64	0.314765	1.077952	0.309931	0.80712	1
GOBP_POSITIVE_REGULATION_OF_NUCLEOBASE_CONTAINING_COMPOUND_METABOLIC_PROCESS	84	0.309243	1.077204	0.2992	0.805524	1
GOBP_CELLULAR_RESPONSE_TO_HORMONE_STIMULUS	23	0.35396	1.077035	0.35653	0.80167	1
GOBP_REGULATION_OF_CATION_TRANSMEMBRANE_TRANSPORT	18	0.368496	1.073188	0.370155	0.812356	1
GOBP_B_CELL_ACTIVATION	17	0.371477	1.069824	0.375574	0.821181	1
GOBP_CYTOKINE_PRODUCTION	30	0.339933	1.068931	0.357236	0.820133	1
GOBP_REGULATION_OF_IMMUNE_EFFECTOR_PROCESS	21	0.356655	1.061661	0.38548	0.844473	1
GOBP_MYELOID_CELL_DIFFERENTIATION	17	0.366058	1.061236	0.382239	0.841544	1
GOBP_RESPONSE_TO_TUMOR_NECROSIS_FACTOR	16	0.370716	1.061014	0.388883	0.837861	1
GOBP_REGULATION_OF_INTRACELLULAR_TRANSPORT	16	0.371448	1.057061	0.398176	0.848821	1
GOBP_RESPONSE_TO_OXYGEN_LEVELS	17	0.365826	1.055672	0.394219	0.849685	1
GOBP_POSITIVE_REGULATION_OF_MAPK_CASCADE	16	0.369468	1.055266	0.397741	0.846754	1
GOBP_POSITIVE_REGULATION_OF_INTRACELLULAR_SIGNAL_TRANSDUCTION	42	0.319994	1.050581	0.386955	0.860518	1
GOBP_APOPTOTIC_PROCESS	75	0.30283	1.048474	0.3716	0.864274	1
GOBP_BLOOD_VESSEL_MORPHOGENESIS	24	0.342771	1.046505	0.400805	0.867411	1
GOBP_CELLULAR_ION_HOMEOSTASIS	34	0.32483	1.042455	0.411641	0.878524	1
GOBP_CELLULAR_LIPID_METABOLIC_PROCESS	45	0.314792	1.042348	0.403281	0.874395	1
GOBP_REGULATION_OF_MEMBRANE_POTENTIAL	18	0.359211	1.042276	0.415697	0.870164	1
GOBP_PROTEIN_CATABOLIC_PROCESS	38	0.319868	1.040632	0.41233	0.872011	1

GOBP_REGULATION_OF_INTRACELLULAR_SIGNAL_TRANSDUCTION	78	0.300183	1.04056	0.388	0.867839	1
GOBP_CELLULAR_PROTEIN_CONTAINING_COMPLEX_ASSEMBLY	28	0.332933	1.039682	0.420561	0.866768	1
GOBP_PROTEIN_CONTAINING_COMPLEX_SUBUNIT_ORGANIZATION	70	0.30161	1.039057	0.3926	0.864763	1
GOBP_MRNA_PROCESSING	22	0.345925	1.037638	0.418713	0.865787	1
GOBP_NEGATIVE_REGULATION_OF_NUCLEOBASE_CONTAINING_COMPOUND_METABOLIC_PROCESS	66	0.301856	1.035316	0.405081	0.870134	1
GOBP_NEGATIVE_REGULATION_OF_MOLECULAR_FUNCTION	40	0.317394	1.034171	0.417734	0.870052	1
GOBP_REGULATION_OF_PROTEIN_MODIFICATION_PROCESS	65	0.302256	1.033709	0.4155	0.867465	1
GOBP_REGULATION_OF_TRANSMEMBRANE_TRANSPORT	24	0.338634	1.033362	0.423422	0.864534	1
GOBP_NEGATIVE_REGULATION_OF_TRANSCRIPTION_BY_RNA_POLYMERASE_II	35	0.320301	1.032059	0.425251	0.865158	1
GOBP_REGULATION_OF_CELLULAR_PROTEIN_LOCALIZATION	26	0.333202	1.030551	0.429678	0.866502	1
GOBP_CELL_PROJECTION_ASSEMBLY	22	0.341389	1.028886	0.434405	0.868378	1
GOBP_CELLULAR_AMINO_ACID_METABOLIC_PROCESS	16	0.35815	1.026752	0.438859	0.871974	1
GOBP_POSITIVE_REGULATION_OF_CELLULAR_COMPONENT_BIOGENESIS	22	0.339808	1.026331	0.44215	0.869324	1
GOBP_ION_HOMEOSTASIS	36	0.317938	1.025578	0.442887	0.867923	1
GOBP_PROCESS_UTILIZING_AUTOPHAGIC_MECHANISM	30	0.325164	1.024723	0.444444	0.866903	1
GOBP_CANONICAL_WNT_SIGNALING_PATHWAY	17	0.355406	1.024719	0.439251	0.862808	1
GOBP_CELL_CELL_SIGNALING_BY_WNT	27	0.329765	1.022639	0.452316	0.866205	1
GOBP_REGULATION_OF_CELLULAR_COMPONENT_MOVEMENT	33	0.319871	1.021118	0.447764	0.867648	1

GOBP_PROTEIN_MODIFICATION_BY_SMALL_PROTEIN_CONJUGATION_OR_REMOVAL	54	0.302264	1.019179	0.45089	0.870526	1
GOBP_RESPONSE_TO_GROWTH_FACTOR	16	0.356755	1.016572	0.463195	0.875762	1
GOBP_FOREBRAIN_DEVELOPMENT	15	0.358968	1.011296	0.464112	0.890443	1
GOBP_SIGNAL_RELEASE	20	0.339829	1.010601	0.465064	0.888845	1
GOBP_VASCULATURE_DEVELOPMENT	27	0.325142	1.009284	0.475003	0.889463	1
GOBP_DEFENSE_RESPONSE_TO_OTHER_ORGANISM	41	0.309506	1.008399	0.468988	0.888522	1
GOBP_RNA_PROCESSING	37	0.31171	1.007991	0.470559	0.885919	1
GOBP_RESPONSE_TO_BIOTIC_STIMULUS	59	0.296756	1.005228	0.481548	0.891651	1
GOBP_PHOSPHOLIPID_BIOSYNTHETIC_PROCESS	17	0.349256	1.005069	0.478132	0.888193	1
GOBP_NEGATIVE_REGULATION_OF_MULTICELLULAR_ORGANISMAL_PROCESS	29	0.320403	1.004749	0.479012	0.885338	1
GOBP_FATTY_ACID_METABOLIC_PROCESS	15	0.356377	1.002447	0.478825	0.88928	1
GOBP_REGULATION_OF_CATABOLIC_PROCESS	41	0.305797	1.001565	0.491346	0.888373	1
GOBP_GLYCEROLIPID_METABOLIC_PROCESS	20	0.337389	0.999769	0.485946	0.89057	1
GOBP_LIPID_METABOLIC_PROCESS	61	0.292974	0.998666	0.4921	0.890491	1
GOBP_NEGATIVE_REGULATION_OF_CELL_POPULATION_PROLIFERATION	22	0.331162	0.998231	0.483372	0.888055	1
GOBP_POSITIVE_REGULATION_OF_GENE_EXPRESSION	41	0.304819	0.997944	0.4996	0.885138	1
GOBP_CELL_CYCLE_G1_S_PHASE_TRANSITION	17	0.347213	0.997358	0.487944	0.883296	1
GOBP_IN_UTERO_EMBRYONIC_DEVELOPMENT	23	0.328506	0.992924	0.497983	0.894346	1
GOBP_REGULATION_OF_APOPTOTIC_SIGNALING_PATHWAY	15	0.352438	0.992726	0.490403	0.891169	1
GOBP_BIOLOGICAL_PROCESS_INVOLVED_IN_SYMBIOTIC_INTERACTION	42	0.302277	0.99038	0.508056	0.895223	1
GOBP_POSITIVE_REGULATION_OF_CELLULAR_COMPONENT_ORGANIZATION	50	0.29601	0.990365	0.5134	0.891459	1
GOBP_MUSCLE_ORGAN_DEVELOPMENT	19	0.335878	0.986565	0.50387	0.900157	1
GOBP_DETECTION_OF_STIMULUS	29	0.312868	0.984275	0.522237	0.90386	1

GOBP_REGULATION_OF_ANATOMICAL_STRUCTURE_MORPHOGENESIS	32	0.310282	0.982235	0.524827	0.906703	1
GOBP_ORGANONITROGEN_COMPOUND_CATABOLIC_PROCESS	53	0.293189	0.98221	0.5323	0.902971	1
GOBP_CELL_MIGRATION	45	0.297438	0.981993	0.529912	0.899879	1
GOBP_REGULATION_OF_SMALL_MOLECULE_METABOLIC_PROCESS	16	0.345465	0.980744	0.512198	0.900146	1
GOBP_RESPONSE_TO_MOLECULE_OF_BACTERIAL_ORIGIN	16	0.342203	0.980321	0.516516	0.897793	1
GOBP_CILIUM_ORGANIZATION	15	0.346395	0.976457	0.521623	0.906443	1
GOBP_CELL_CELL_SIGNALING	75	0.280633	0.970382	0.569	0.922146	1
GOBP_PHOSPHOLIPID_METABOLIC_PROCESS	20	0.327042	0.969669	0.539826	0.920642	1
GOBP_DIVALENT_INORGANIC_CATION_HOMEOSTASIS	20	0.326439	0.969553	0.538814	0.91727	1
GOBP_POSITIVE_REGULATION_OF_MULTICELLULAR_ORGANISMAL_PROCESS	60	0.285067	0.967624	0.572957	0.91957	1
GOBP_NEGATIVE_REGULATION_OF_INTRACELLULAR_SIGNAL_TRANSDUCTION	23	0.317486	0.96522	0.547446	0.923271	1
GOBP_REGULATION_OF_PROTEIN_PHOSPHORYLATION	49	0.289356	0.963458	0.569371	0.925079	1
GOBP_CELLULAR_MACROMOLECULE_LOCALIZATION	81	0.276846	0.962532	0.593059	0.92429	1
GOBP_ORGANOPHOSPHATE_METABOLIC_PROCESS	39	0.295056	0.959466	0.573518	0.930008	1
GOBP_APOPTOTIC_SIGNALING_PATHWAY	26	0.310939	0.958369	0.567709	0.929687	1
GOBP_NERVOUS_SYSTEM_PROCESS	45	0.289064	0.955927	0.593978	0.933438	1
GOBP_ACTIN_FILAMENT_BASED_PROCESS	29	0.304596	0.955526	0.575118	0.930954	1
GOBP_MODIFICATION_DEPENDENT_MACROMOLECULE_CATABOLIC_PROCESS	21	0.319971	0.95456	0.565614	0.930203	1
GOBP_REGULATION_OF_AUTOPHAGY	19	0.32496	0.953197	0.557305	0.930679	1
GOBP_MITOCHONDRION_ORGANIZATION	18	0.327	0.952919	0.559382	0.927872	1
GOBP_RESPONSE_TO_ENDOGENOUS_STIMULUS	66	0.278192	0.952864	0.605082	0.92442	1

GOBP_MUSCLE_CONTRACTION	23	0.31299	0.952032	0.569457	0.923343	1
GOBP_METAL_ION_HOMEOSTASIS	26	0.309247	0.951966	0.577438	0.919991	1
GOBP_RESPONSE_TO_LIPID	41	0.290525	0.951378	0.588936	0.918177	1
GOBP_REGULATION_OF_CELLULAR_LOCALIZATION	40	0.291399	0.948862	0.597378	0.922	1
GOBP_POSTTRANSCRIPTIONAL_REGULATION_OF_GENE_EXPRESSION	21	0.316229	0.946547	0.57801	0.925342	1
GOBP_GROWTH	32	0.298158	0.946096	0.59146	0.923126	1
GOBP_SECRETION	58	0.279441	0.945969	0.6172	0.920014	1
GOBP_REGULATION_OF_CELLULAR_COMPONENT_BIOGENESIS	41	0.287867	0.944674	0.603825	0.920316	1
GOBP_ORGANONITROGEN_COMPOUND_BIOSYNTHETIC_PROCESS	65	0.276012	0.944197	0.6282	0.91825	1
GOBP_CALCIUM_ION_TRANSPORT	17	0.327242	0.943628	0.577494	0.916426	1
GOBP_POSITIVE_REGULATION_OF_TRANSPORT	35	0.293818	0.943283	0.608953	0.914011	1
GOBP_CELL_CELL_ADHESION	22	0.312355	0.943164	0.585563	0.910934	1
GOBP_POSITIVE_REGULATION_OF_TRANSCRIPTION_BY_RNA_POLYMERASE_II	53	0.280349	0.942957	0.619286	0.908161	1
GOBP_REGULATION_OF_PHOSPHORUS_METABOLIC_PROCESS	61	0.275921	0.941934	0.6236	0.907713	1
GOBP_NEUROGENESIS	59	0.276967	0.941907	0.6256	0.904445	1
GOBP_SMALL_MOLECULE_METABOLIC_PROCESS	78	0.27045	0.937932	0.6505	0.912121	1
GOBP_REGULATION_OF_MULTICELLULAR_ORGANISMAL_DEVELOPMENT	56	0.277299	0.936044	0.6422	0.913982	1
GOBP_CIRCULATORY_SYSTEM_PROCESS	19	0.318913	0.93597	0.593191	0.910862	1
GOBP_NEGATIVE_REGULATION_OF_DEVELOPMENTAL_PROCESS	26	0.30171	0.9318	0.610776	0.919106	1
GOBP_MUSCLE_SYSTEM_PROCESS	25	0.3034	0.926105	0.623388	0.931256	1
GOBP_CELLULAR_HOMEOSTASIS	47	0.278815	0.924935	0.651596	0.931066	1
GOBP_GLYCOSYLATION	15	0.328432	0.923489	0.602449	0.931532	1

GOBP_NEGATIVE_REGULATION_OF_CATALYTIC_ACTIVITY	20	0.310216	0.922735	0.616969	0.930186	1
GOBP_SENSORY_ORGAN_DEVELOPMENT	15	0.326678	0.921916	0.612192	0.929061	1
GOBP_GLAND_DEVELOPMENT	17	0.320111	0.920392	0.611879	0.929864	1
GOBP_POSITIVE_REGULATION_OF_LOCOMOTION	22	0.304694	0.920276	0.622332	0.926867	1
GOBP_POSITIVE_REGULATION_OF_ION_TRANSPORT	28	0.294208	0.91673	0.64394	0.932795	1
GOBP_REGULATION_OF_TRANSPORT	67	0.266665	0.916508	0.6871	0.930095	1
GOBP_RESPONSE_TO_PEPTIDE	19	0.30828	0.90709	0.640122	0.950867	1
GOBP_DETECTION_OF_CHEMICAL_STIMULUS	17	0.313334	0.903868	0.637832	0.955688	1
GOBP_RESPONSE_TO_VIRUS	17	0.314054	0.903538	0.641996	0.953188	1
GOBP_RESPONSE_TO_HORMONE	33	0.283256	0.903532	0.66523	0.949907	1
GOBP_RNA_SPLICING	18	0.309321	0.902745	0.647412	0.948567	1
GOBP_NEGATIVE_REGULATION_OF_BIOSYNTHETIC_PROCESS	63	0.264344	0.901902	0.716772	0.947427	1
GOBP_G_PROTEIN_COUPLED_RECEPTOR_SIGNALING_PATHWAY	44	0.273262	0.900102	0.702281	0.948647	1
GOBP_SENSORY_PERCEPTION	31	0.283774	0.899312	0.68289	0.947341	1
GOBP_VESICLE_ORGANIZATION	15	0.319495	0.899275	0.644922	0.944198	1
GOBP_POSITIVE_REGULATION_OF_BIOSYNTHETIC_PROCESS	79	0.259004	0.898591	0.7402	0.942645	1
GOBP_REGULATION_OF_HORMONE_LEVELS	22	0.297915	0.898409	0.656225	0.939886	1
GOBP_ACTIVATION_OF_IMMUNE_RESPONSE	20	0.303688	0.898145	0.655606	0.937369	1
GOBP_EPITHELIAL_CELL_DIFFERENTIATION	21	0.30047	0.89758	0.661175	0.935585	1
GOBP_RESPONSE_TO_LIGHT_STIMULUS	18	0.307708	0.897356	0.650907	0.932988	1
GOBP_ORGANOPHOSPHATE_BIOSYNTHETIC_PROCESS	25	0.292222	0.896675	0.668915	0.931455	1
GOBP_REGULATION_OF_CELLULAR_CATABOLIC_PROCESS	35	0.278022	0.893666	0.691738	0.935439	1
GOBP_REGULATION_OF_SECRETION	21	0.299508	0.893486	0.669501	0.932758	1

GOBP_INORGANIC_ION_TRANSMEMBRANE_TRANSPORT	34	0.279139	0.892516	0.692978	0.931941	1
GOBP_REGULATION_OF_CELL_DEATH	65	0.260251	0.891371	0.7393	0.931535	1
GOBP_TRANSMEMBRANE_TRANSPORT	58	0.262387	0.890145	0.737574	0.931285	1
GOBP_MICROTUBULE_BASED_MOVEMENT	16	0.312128	0.889743	0.659819	0.929161	1
GOBP_REGULATION_OF_ION_TRANSPORT	53	0.26418	0.885704	0.740174	0.935387	1
GOBP_ORGANIC_ACID_METABOLIC_PROCESS	44	0.269223	0.884817	0.729156	0.934376	1
GOBP_ENDOMEMBRANE_SYSTEM_ORGANIZATION	25	0.288065	0.884551	0.689916	0.931932	1
GOBP_POSITIVE_REGULATION_OF_TRANSFERASE_ACTIVITY	32	0.278521	0.884539	0.700782	0.928952	1
GOBP_PROTEIN_LOCALIZATION_TO_MEMBRANE	27	0.285813	0.884423	0.690637	0.926219	1
GOBP_ESTABLISHMENT_OF_PROTEIN_LOCALIZATION	87	0.251683	0.88305	0.7774	0.926293	1
GOBP_CATION_TRANSMEMBRANE_TRANSPORT	36	0.274048	0.88222	0.715101	0.925127	1
GOBP_REGULATION_OF_CELL_DIFFERENTIATION	60	0.258898	0.878031	0.7593	0.931391	1
GOBP_CELLULAR_RESPONSE_TO_ORGANIC_CYCLIC_COMPOUND	29	0.278159	0.875037	0.711776	0.934797	1
GOBP_ENDOCYTOSIS	26	0.282506	0.873749	0.704726	0.934577	1
GOBP_SENSORY_PERCEPTION_OF_CHEMICAL_STIMULUS	15	0.307429	0.870053	0.684819	0.939505	1
GOBP_NEGATIVE_REGULATION_OF_PROTEIN_METABOLIC_PROCESS	31	0.274755	0.869368	0.732003	0.938007	1
GOBP_REGULATION_OF_PEPTIDASE_ACTIVITY	16	0.304416	0.86661	0.691349	0.940807	1
GOBP_POSITIVE_REGULATION_OF_DEVELOPMENTAL_PROCESS	57	0.256166	0.865402	0.775578	0.940381	1
GOBP_POSITIVE_REGULATION_OF_CATALYTIC_ACTIVITY	61	0.255011	0.865022	0.7861	0.938235	1
GOBP_PROTEIN_LOCALIZATION_TO_CELL_PERIPHERY	15	0.305434	0.861243	0.692736	0.943125	1
GOBP_REGULATION_OF_GROWTH	21	0.286408	0.855888	0.723775	0.950996	1

GOBP_ANION_TRANSMEMBRANE_TRANSPORT	17	0.297878	0.855566	0.716692	0.948682	1
GOBP_NEURON_DIFFERENTIATION	50	0.255964	0.85235	0.793259	0.952012	1
GOBP_CELL_JUNCTION_ASSEMBLY	18	0.293768	0.852095	0.718922	0.949583	1
GOBP_INNATE_IMMUNE_RESPONSE	30	0.27098	0.851443	0.760261	0.94795	1
GOBP_CELLULAR_RESPONSE_TO_PEPTIDE	15	0.301467	0.849476	0.721597	0.94886	1
GOBP_MEMBRANE_ORGANIZATION	33	0.266247	0.84799	0.768398	0.948843	1
GOBP_DETECTION_OF_STIMULUS_INVOLVED_IN_SENSORY_PERCEPTION	18	0.291837	0.847983	0.727115	0.945978	1
GOBP_CELLULAR_PROTEIN_CATABOLIC_PROCESS	29	0.270559	0.846439	0.759414	0.946022	1
GOBP_CHEMICAL_HOMEOSTASIS	52	0.252873	0.845873	0.806861	0.944223	1
GOBP_POSITIVE_REGULATION_OF_PROTEIN_KINASE_ACTIVITY	24	0.275504	0.841291	0.757163	0.949882	1
GOBP_RAS_PROTEIN_SIGNAL_TRANSDUCTION	16	0.294638	0.840619	0.730152	0.948271	1
GOBP_LOCOMOTION	54	0.248665	0.839609	0.8148	0.947289	1
GOBP_NEGATIVE_REGULATION_OF_CELL_DIFFERENTIATION	20	0.284305	0.839475	0.748809	0.94471	1
GOBP_RESPONSE_TO_METAL_ION	16	0.294693	0.838363	0.73332	0.943881	1
GOBP_RESPONSE_TO_NITROGEN_COMPOUND	47	0.250702	0.835426	0.811744	0.946309	1
GOBP_ENZYME_LINKED_RECEPTOR_PROTEIN_SIGNALING_PATHWAY	29	0.265816	0.833513	0.781592	0.946855	1
GOBP_ALCOHOL_METABOLIC_PROCESS	15	0.295012	0.833173	0.739198	0.94467	1
GOBP_MUSCLE_TISSUE_DEVELOPMENT	15	0.294809	0.832404	0.737412	0.943256	1
GOBP_POSITIVE_REGULATION_OF_CATABOLIC_PROCESS	18	0.28576	0.831911	0.748417	0.941369	1
GOBP_CELL_JUNCTION_ORGANIZATION	24	0.271776	0.82993	0.772878	0.94207	1
GOBP_NEGATIVE_REGULATION_OF_PROTEIN_MODIFICATION_PROCESS	15	0.293621	0.829616	0.740649	0.939873	1
GOBP_CELLULAR_RESPONSE_TO_OXYGEN_CONTAINING_COMPOUND	52	0.24695	0.82954	0.832867	0.937276	1
GOBP_NCRNA_METABOLIC_PROCESS	15	0.29342	0.82897	0.743833	0.935531	1

GOBP_REGULATION_OF_ANION_TRANSPORT	32	0.260908	0.828521	0.79535	0.933582	1
GOBP_POSITIVE_REGULATION_OF_ANION_TRANSPORT	16	0.289015	0.82546	0.756629	0.936096	1
GOBP_POSITIVE_REGULATION_OF_CELL_DIFFERENTIATION	35	0.256863	0.824932	0.809977	0.934294	1
GOBP_MONOCARBOXYLIC_ACID_METABOLIC_PROCESS	24	0.268406	0.821378	0.780483	0.937391	1
GOBP_MUSCLE_STRUCTURE_DEVELOPMENT	23	0.268112	0.813392	0.789973	0.947473	1
GOBP_LIPID_LOCALIZATION	20	0.272872	0.810765	0.788824	0.948881	1
GOBP_CELL_PROJECTION_ORGANIZATION	55	0.237936	0.803325	0.867087	0.957539	1
GOBP_NUCLEOBASE_CONTAINING_SMALL_MOLECULE_METABOLIC_PROCESS	27	0.258034	0.801472	0.813505	0.957654	1
GOBP_REGULATION_OF_PEPTIDE_TRANSPORT	25	0.26086	0.800872	0.815299	0.955833	1
GOBP_CELLULAR_RESPONSE_TO_NITROGEN_COMPOUND	32	0.252252	0.797348	0.829992	0.958341	1
GOBP_PROTEOLYSIS	74	0.230275	0.797257	0.9014	0.955781	1
GOBP_PROTEIN_MODIFICATION_BY_SMALL_PROTEIN_REMOVAL	21	0.266813	0.79612	0.809413	0.954752	1
GOBP_BEHAVIOR	19	0.270107	0.790314	0.813382	0.96032	1
GOBP_STEROID_METABOLIC_PROCESS	19	0.265727	0.786024	0.809043	0.963499	1
GOBP_REGULATION_OF_CELLULAR_AMIDE_METABOLIC_PROCESS	16	0.275366	0.785323	0.802795	0.961764	1
GOBP_REGULATION_OF_BODY_FLUID_LEVELS	18	0.267941	0.784192	0.817709	0.960598	1
GOBP_POSITIVE_REGULATION_OF_PROTEIN_SERINE_THREONINE_KINASE_ACTIVITY	15	0.276881	0.78289	0.805544	0.959712	1
GOBP_REGULATION_OF_TRANSFERASE_ACTIVITY	48	0.234665	0.781872	0.885366	0.958449	1
GOBP_POSITIVE_REGULATION_OF_MOLECULAR_FUNCTION	71	0.227458	0.781633	0.9156	0.95614	1
GOBP_RESPONSE_TO_OXYGEN_CONTAINING_COMPOUND	77	0.225337	0.781048	0.9224	0.95431	1

GOBP_POSITIVE_REGULATION_OF_HYDROLASE_ACTIVITY	32	0.244865	0.778409	0.861824	0.955127	1
GOBP_SUPRAMOLECULAR_FIBER_ORGANIZATION	15	0.276063	0.775396	0.816476	0.956445	1
GOBP_PURINE_CONTAINING_COMPOUND_METABOLIC_PROCESS	19	0.262454	0.771368	0.831485	0.958898	1
GOBP_REGULATION_OF_PROTEIN_LOCALIZATION	41	0.234852	0.767593	0.887366	0.960977	1
GOBP_SYNAPTIC_SIGNALING	30	0.243333	0.76533	0.86563	0.961103	1
GOBP_NEURON_DEVELOPMENT	44	0.232225	0.764526	0.895648	0.959465	1
GOBP_CATION_TRANSPORT	46	0.230359	0.763656	0.90199	0.957882	1
GOBP_ORGANIC_HYDROXY_COMPOUND_METABOLIC_PROCESS	26	0.247426	0.76227	0.858321	0.956949	1
GOBP_ORGANIC_ACID_TRANSPORT	16	0.267211	0.76181	0.83275	0.95495	1
GOBP_REGULATION_OF_HYDROLASE_ACTIVITY	44	0.231241	0.761164	0.90106	0.953169	1
GOBP_RESPONSE_TO_INORGANIC_SUBSTANCE	24	0.249585	0.758067	0.86235	0.95424	1
GOBP_SMALL_GTPASE_MEDIATED_SIGNAL_TRANSDUCTION	22	0.252081	0.75747	0.856927	0.952376	1
GOBP_RESPONSE_TO_ORGANIC_CYCLIC_COMPOUND	44	0.230098	0.755768	0.905681	0.95178	1
GOBP_REGULATION_OF_SYSTEM_PROCESS	26	0.244936	0.755185	0.869797	0.949915	1
GOBP_PROTEASOMAL_PROTEIN_CATABOLIC_PROCESS	17	0.256537	0.739316	0.864813	0.964215	1
GOBP_POSITIVE_REGULATION_OF_CELL_DEATH	24	0.242135	0.736219	0.880962	0.964717	1
GOBP_REGULATION_OF_NEURON_PROJECTION_DEVELOPMENT	15	0.258029	0.72849	0.86547	0.969722	1
GOBP_CELLULAR_COMPONENT_DISASSEMBLY	26	0.234954	0.724651	0.895997	0.970764	1
GOBP_ESTABLISHMENT_OF_PROTEIN_LOCALIZATION_TO_ORGANELLE	18	0.249534	0.723688	0.882155	0.969146	1
GOBP_TRANSMEMBRANE_RECEPTOR_PROTEIN_TYROSINE_KINASE_SIGNALING_PATHWAY	21	0.239447	0.714807	0.89576	0.974509	1
GOBP_WOUND_HEALING	19	0.243451	0.714781	0.894528	0.972015	1

GOBP_REGULATION_OF_CELL_DEVELOPMENT	18	0.245609	0.71399	0.887598	0.970192	1
GOBP_AGING	16	0.249417	0.710885	0.88567	0.97035	1
GOBP_AMIDE_BIOSYNTHETIC_PROCESS	27	0.226667	0.703753	0.918639	0.973626	1
GOBP_INTRACELLULAR_PROTEIN_TRANSPORT	48	0.211017	0.700148	0.956383	0.973963	1
GOBP_RESPONSE_TO_WOUNDING	25	0.225544	0.697363	0.917683	0.973601	1
GOBP_CELL_MORPHOGENESIS_INVOLVED_IN_DIFFERENTIATION	25	0.226274	0.694971	0.918394	0.972893	1
GOBP_SMALL_MOLECULE_CATABOLIC_PROCESS	25	0.221249	0.680062	0.933259	0.980845	1
GOBP_CELLULAR_AMIDE_METABOLIC_PROCESS	37	0.209662	0.677871	0.954919	0.979819	1
GOBP_TAXIS	18	0.232199	0.674448	0.921982	0.979559	1
GOBP_INTRACELLULAR_TRANSPORT	75	0.194136	0.673353	0.9845	0.977774	1
GOBP_CELL_MORPHOGENESIS	38	0.205541	0.667377	0.960849	0.978959	1
GOBP_PEPTIDE_METABOLIC_PROCESS	27	0.21342	0.661127	0.948267	0.980138	1
GOBP_REGULATION_OF_PROTEOLYSIS	22	0.213035	0.639852	0.948858	0.988867	1
GOBP_REGULATION_OF_PROTEIN_KINASE_ACTIVITY	35	0.195597	0.626788	0.974148	0.99235	1
GOBP_REGULATION_OF_PROTEIN_SERINE_THREONINE_KINASE_ACTIVITY	23	0.206333	0.626324	0.957166	0.990071	1
GOBP_RESPONSE_TO_CARBOHYDRATE	17	0.215387	0.618839	0.9538	0.990648	1
GOBP_LIPID_CATABOLIC_PROCESS	18	0.210965	0.614679	0.9589	0.989785	1
GOBP_GENERATION_OF_PRECURSOR_METABOLITES_AND_ENERGY	18	0.210098	0.611993	0.958953	0.988347	1
GOBP_REGULATION_OF_NERVOUS_SYSTEM_DEVELOPMENT	20	0.201876	0.598959	0.966545	0.990439	1
GOBP_PEPTIDE_BIOSYNTHETIC_PROCESS	24	0.195653	0.596545	0.973708	0.988784	1
GOBP_RESPONSE_TO_EXTRACELLULAR_STIMULUS	21	0.198046	0.591958	0.969028	0.987796	1
GOBP_CELL_GROWTH	15	0.199167	0.560766	0.975673	0.993289	1
GOBP_REGULATION_OF_CELL_PROJECTION_ORGANIZATION	25	0.169372	0.520487	0.991944	0.997678	1

GOBP_GOLGI_VESICLE_TRANSPORT	18	0.177556	0.518027	0.989798	0.995579	1
GOBP_AXON_DEVELOPMENT	20	0.169834	0.503651	0.992901	0.99477	1

Table 3.S5 MAGeCK MLE Z-scores values for Ramos miniscreens related to figure 3.2 A.

Gene	Cisplatin|z		Gene	MMC|z		Gene	AZD6738|z		Gene	Phleomycin|z
FANCC	-9.3339		FANCC	-9.7053		ATM	-5.3751		CHMP1B	-3.8311
BRIP1	-7.13		FANCD2	-7.3934		FANCC	-4.9544		NFKBIB	-3.5785
FANCF	-6.9808		FANCF	-7.2296		RAD51C	-4.5171		ATM	-3.347
FANCD2	-6.6465		BRIP1	-6.9388		PALB2	-3.9758		RAD51C	-3.2459
FANCA	-6.07		RAD51C	-6.0501		SMARCC1	-3.5208		TEKT4	-2.9848
RAD51C	-5.5132		FANCA	-5.8703		BRCA1	-3.4937		RHOA	-2.8146
BRCA1	-5.1659		C17orf53	-5.7681		FANCF	-3.4755		LKAAEAR1	-2.5041
C1orf27	-4.0271		ATM	-5.6553		FANCA	-3.1526		CD38	-2.2483
C17orf53	-3.9166		C1orf27	-4.7672		MRE11A	-2.8431		BAI2	-2.1153
NFKBIB	-3.6795		NFKBIB	-3.9774		BRIP1	-2.8112		NT_22	-2.1039
SLX4IP	-3.1069		BRCA1	-3.9392		C17orf53	-2.7442		PALB2	-1.8586
MYDGF	-3.0862		MRE11A	-3.8167		MYDGF	-2.2012		HPS6	-1.6926
ATM	-3.083		SMARCC1	-3.2962		DNAJC21	-1.8201		FANCA	-1.6255
SMARCC1	-3.045		SLX4IP	-3.2414		CDK2AP1	-1.544		NT_14	-1.5092
MRE11A	-2.9169		NT_19	-1.795		C1orf137	-1.4621		CCDC186	-1.5026
PALB2	-1.8867		NT_20	-1.7249		NT_14	-1.2418		TBATA	-1.3963
CDK2AP1	-1.7607		RHOA	-1.4226		FANCD2	-1.1462		ERICH4	-1.3834
LKAAEAR1	-1.2159		PALB2	-1.4043		LKAAEAR1	-1.0246		C3orf56	-1.3777
NT_14	-1.0868		DNAJC21	-1.2409		WDSUB1	-0.97097		C12orf77	-1.2029
C3orf56	-0.7692		C18orf32	-1.2252		C17orf64	-0.67031		BRIP1	-1.0637
NT_22	-0.67837		C1orf137	-1.1232		HPS6	-0.38674		C1orf43	-1.0487
C12orf77	-0.63938		chr10Promis	-1.0828		RHOA	-0.38632		ZNF835	-0.9831
TEKT4	-0.56961		NT_29	-0.865		TP53TG5	-0.35497		NT_16	-0.93623
BAI2	-0.48983		C7orf62	-0.76171		NT_30	-0.33481		chr10Ran	-0.86871
NT_27	-0.29652		C1orf43	-0.50151		C3orf56	-0.27841		NT_27	-0.83686

CCDC186	-0.22749		TP53TG5	-0.49907		BAI2	-0.22263		MRE11A	-0.83554
C1orf137	-0.16685		NT_14	-0.49002		NAP1L5	-0.13048		NT_30	-0.79618
CD38	-0.14609		BRPF1	-0.38251		NT_22	-0.10507		CDK2AP1	-0.77533
TBATA	-0.14377		ZNF233	-0.36399		ZNF79	-0.098778		C1orf137	-0.77478
GAS6	-0.14047		NT_32	-0.13593		NT_13	-0.084864		NT_26	-0.72841
NT_26	-0.022487		C6orf118	-0.013401		C6orf118	-0.05814		CYSRT1	-0.64871
C9orf139	-0.015965		NT_23	0.024661		CARD9	-0.038558		C6orf120	-0.63365
EXOC3-AS1	0.038053		ZNF79	0.030994		EXOC3-AS1	-0.031783		FANCD2	-0.5965
NT_16	0.062142		WDSUB1	0.25138		chr10Ran	-0.031616		NT_15	-0.53368
C11orf63	0.070848		C17orf64	0.33136		CYSRT1	0.0054577		EXOC3-AS1	-0.52742
NAP1L5	0.072131		NT_28	0.37532		C6orf141	0.0075039		CARD9	-0.48412
ERICH4	0.14198		C1orf101	0.43634		NT_26	0.044017		C1orf101	-0.46462
C1orf101	0.14697		NT_17	0.49136		C12orf77	0.061305		C17orf53	-0.24179
NT_15	0.15095		C9orf139	0.53463		ERICH4	0.1674		C9orf139	-0.12378
NT_24	0.1637		FAM216B	0.61455		FAM89A	0.18102		BRPF1	-0.11606
NT_29	0.19166		CYP4F11	0.69027		NT_31	0.22492		WDSUB1	-0.10966
chr10Ran	0.20551		NAP1L5	0.70354		TEKT4	0.22921		C7orf50	-0.10636
NT_18	0.22364		TEX33	0.7207		NT_32	0.24404		BRCA1	-0.01883
FAM216B	0.23394		NT_24	0.88635		NT_27	0.2545		NT_29	0.018208
C6orf118	0.30133		NT_31	0.89205		NT_17	0.29302		FAM216B	0.033508
TP53TG5	0.44422		NT_27	0.89463		NT_28	0.36205		NT_13	0.081632
NT_20	0.46105		CAMK1D	0.96211		CD38	0.37123		NT_24	0.35167
ZNF835	0.46193		NT_18	1.0121		NT_16	0.38578		FAM89A	0.36315
ZNF839	0.46968		NT_25	1.0142		GAS6	0.45594		NT_18	0.40489
CAMK1D	0.48862		LRRC74A	1.0813		NT_19	0.46117		MYDGF	0.41669
C6orf141	0.49023		CDK2AP1	1.118		C1orf101	0.48728		FAM221A	0.48597
NT_25	0.49591		NT_30	1.1203		NT_18	0.48912		C6orf118	0.50873
WDSUB1	0.76479		USP39	1.1761		ZNF839	0.50362		FANCF	0.54671

FAM89A	0.78628		NT_26	1.1777		NT_25	0.51512		TP53TG5	0.56375
C7orf50	0.80978		TBATA	1.1854		NT_24	0.58305		CAMK1D	0.62793
NT_30	0.84856		NT_16	1.188		C1orf27	0.62		C6orf141	0.63765
NT_13	0.87155		C3orf56	1.2155		C9orf139	0.68195		PAX5	0.69337
NT_32	0.92687		NT_15	1.3428		USP39	0.69199		NT_25	0.76457
chr10Promis	0.92846		SUMO3	1.4019		C7orf50	0.7517		C9orf131	0.7715
NT_31	0.94768		NT_21	1.4185		TBATA	0.80124		NT_31	0.77686
NT_19	0.98979		ZNF835	1.431		C6orf120	0.87531		ZNF839	0.79221
FAM221A	1.0489		C12orf77	1.4481		NT_29	0.90669		NAP1L5	0.80341
CARD9	1.0556		C6orf141	1.513		CAMK1D	0.96246		FANCC	0.8593
CYP4F11	1.0846		TEKT4	1.5176		CYP4F11	0.9862		CYP4F11	1.0411
HPS6	1.125		GAS6	1.5557		NT_15	1.0283		SLX4IP	1.0456
NT_23	1.1286		CCDC186	1.5694		NT_20	1.0851		GAS6	1.0658
RHOA	1.1717		PAX5	1.5965		C7orf62	1.0918		C11orf63	1.1423
USP39	1.2602		NT_22	1.6121		TEX33	1.094		NT_23	1.2221
C7orf62	1.271		EXOC3-AS1	1.6519		LRRC74A	1.1186		C18orf32	1.2563
C18orf32	1.332		ZNF839	1.7117		FAM221A	1.1816		DNAJC21	1.2629
NT_17	1.3469		C11orf63	1.7429		USP35	1.1915		chr10Promis	1.2671
NT_21	1.3875		USP35	1.7663		C4orf17	1.2297		NT_17	1.2879
ZNF79	1.4111		CYSRT1	1.7828		NT_21	1.2407		NT_19	1.3057
NT_28	1.5608		C4orf17	1.7855		C11orf63	1.257		C7orf62	1.3397
C6orf120	1.5998		FAM221A	1.8246		C18orf32	1.2776		C4orf17	1.3613
C17orf64	1.6226		NT_13	1.8337		C9orf131	1.3305		USP35	1.3959
C4orf17	1.6495		CARD9	1.9176		PAX5	1.3569		NT_28	1.4494
CHMP1B	1.7677		MYDGF	1.9581		ZNF835	1.4582		USP39	1.4838
PAX5	1.8943		C6orf120	1.9791		FAM216B	1.4641		SUMO3	1.5022
CYSRT1	1.9535		FAM89A	1.9985		NT_23	1.5468		NT_20	1.5488
PIK3CD	1.9575		C7orf50	2.0923		ZNF233	1.6529		PIK3CD	1.5617

ZNF233	2.0979		PIK3CD	2.0965		SLX4IP	1.7694		NT_21	1.6874
SUMO3	2.1058		ERICH4	2.1632		SUMO3	1.9025		ZNF79	1.7308
LRRC74A	2.1293		LKAAEAR1	2.1854		PIK3CD	2.0403		NT_32	1.7357
C9orf131	2.1782		CD38	2.1913		chr10Promis	2.0775		C17orf64	1.7984
TEX33	2.313		HPS6	2.2043		BRPF1	2.1966		LRRC74A	2.0189
DNAJC21	2.3957		BAI2	2.3495		NFKBIB	2.2716		SMARCC1	2.0687
USP35	2.4163		CHMP1B	2.4109		CCDC186	2.7412		TEX33	2.5675
BRPF1	2.432		C9orf131	2.4619		CHMP1B	2.7871		ZNF233	2.6139
C1orf43	2.9201		chr10Ran	2.5955		C1orf43	2.844		C1orf27	2.6533

Table 3.S6 Gene Ontology analysis related to figure 3.3 C & 3.S3 A

GO-BP -Ecdysozea			
Term	**P-value**	**Adj. P-value**	**Comb.Score**
protein K63-linked deubiquitination (GO:0070536)	9.99E-07	4.11E-04	893.7491801
regulation of DNA repair (GO:0006282)	4.05E-06	7.20E-04	548.2189532
positive regulation of DNA repair (GO:0045739)	5.26E-06	7.20E-04	500.0009572
positive regulation of response to DNA damage stimulus (GO:2001022)	9.10E-06	9.35E-04	411.7502118
double-strand break repair via nonhomologous end joining (GO:0006303)	1.47E-05	0.001073701	346.9699826
positive regulation of DNA metabolic process (GO:0051054)	1.57E-05	0.001073701	339.115199
response to ionizing radiation (GO:0010212)	2.66E-05	0.001564556	279.9932047
regulation of intracellular estrogen receptor signaling pathway (GO:0033146)	6.13E-05	0.003072852	444.2665633
mitotic G2 DNA damage checkpoint signaling (GO:0007095)	6.73E-05	0.003072852	425.2912191
mitotic G2/M transition checkpoint (GO:0044818)	1.72E-04	0.007048805	274.0281342
nucleic acid transport (GO:0050657)	2.51E-04	0.009367398	898.6959133
positive regulation of cytoplasmic transport (GO:1903651)	3.06E-04	0.010478898	779.6150655
mitotic DNA damage checkpoint signaling (GO:0044773)	3.84E-04	0.011655502	186.2995821
positive regulation of insulin receptor signaling pathway (GO:0046628)	4.33E-04	0.011655502	610.5071105
protein deubiquitination (GO:0016579)	4.38E-04	0.011655502	67.58788458
positive regulation of cellular response to insulin stimulus (GO:1900078)	5.04E-04	0.011655502	548.5772314
protein modification by small protein removal (GO:0070646)	5.09E-04	0.011655502	64.03906304
protein autoubiquitination (GO:0051865)	5.10E-04	0.011655502	162.1184372
double-strand break repair (GO:0006302)	6.40E-04	0.013395415	82.69462951
DNA repair (GO:0006281)	7.20E-04	0.013395415	56.45845053
nuclear-transcribed mRNA catabolic process (GO:0000956)	7.49E-04	0.013395415	77.51540154
histone H2A monoubiquitination (GO:0035518)	7.50E-04	0.013395415	415.842006
histone H2A ubiquitination (GO:0033522)	7.50E-04	0.013395415	415.842006
RNA transport (GO:0050658)	8.07E-04	0.013811382	129.309748
positive regulation of protein catabolic process (GO:0045732)	0.00111613	0.018349101	109.8163544

negative regulation of cell death (GO:0060548)	0.00149203	0.022910782	94.68706467
histone monoubiquitination (GO:0010390)	0.00150509	0.022910782	255.9746186
regulation of insulin receptor signaling pathway (GO:0046626)	0.00522835	0.076744658	105.7584641
negative regulation of BMP signaling pathway (GO:0030514)	0.00692853	0.098194064	86.04771438
nuclear-transcribed mRNA catabolic process, (GO:0000288)	0.00799787	0.109570844	77.35835803
protein ubiquitination (GO:0016567)	0.00826915	0.109632938	20.83648966
positive regulation of catabolic process (GO:0009896)	0.01129223	0.111705268	59.642916
protein retention in Golgi apparatus (GO:0045053)	0.01194361	0.111705268	469.7922321
aggresome assembly (GO:0070842)	0.01194361	0.111705268	469.7922321
beta-catenin destruction complex assembly (GO:1904885)	0.01194361	0.111705268	469.7922321
negative regulation of smooth muscle cell apoptotic process (GO:0034392)	0.01194361	0.111705268	469.7922321
constitutive secretory pathway (GO:0045054)	0.01194361	0.111705268	469.7922321
regulation of adipose tissue development (GO:1904177)	0.01431553	0.111705268	360.4389302
negative regulation of histone H3-K9 methylation (GO:0051573)	0.01431553	0.111705268	360.4389302
inclusion body assembly (GO:0070841)	0.01431553	0.111705268	360.4389302
negative regulation of triglyceride metabolic process (GO:0090209)	0.01431553	0.111705268	360.4389302
maintenance of DNA methylation (GO:0010216)	0.01431553	0.111705268	360.4389302
nuclear polyadenylation-dependent ncRNA catabolic process (GO:0071046)	0.01431553	0.111705268	360.4389302
nuclear polyadenylation-dependent rRNA catabolic process (GO:0071035)	0.01431553	0.111705268	360.4389302
nuclear polyadenylation-dependent tRNA catabolic process (GO:0071038)	0.01431553	0.111705268	360.4389302
tRNA surveillance (GO:0106354)	0.01431553	0.111705268	360.4389302
vacuole organization (GO:0007033)	0.01431553	0.111705268	360.4389302
regulation of BMP signaling pathway (GO:0030510)	0.0143583	0.111705268	49.55983889
negative regulation of cellular component organization (GO:0051129)	0.01582381	0.111705268	45.93219538
negative regulation of cellular response to growth factor stimulus (GO:0090288)	0.01582381	0.111705268	45.93219538
protein modification by small protein conjugation (GO:0032446)	0.01652167	0.111705268	18.00290634
negative regulation of centriole replication (GO:0046600)	0.01668187	0.111705268	289.5305338
regulation of vascular associated smooth muscle cell apoptotic process (GO:1905459)	0.01668187	0.111705268	289.5305338
positive regulation of intracellular estrogen receptor signaling pathway (GO:0033148)	0.01668187	0.111705268	289.5305338

regulation of histamine secretion by mast cell (GO:1903593)	0.01668187	0.111705268	289.5305338
positive regulation of chromosome segregation (GO:0051984)	0.01904265	0.111705268	240.1325946
positive regulation of early endosome to late endosome transport (GO:2000643)	0.01904265	0.111705268	240.1325946
positive regulation of endocytic recycling (GO:2001137)	0.01904265	0.111705268	240.1325946
negative regulation of mitochondrial fusion (GO:0010637)	0.01904265	0.111705268	240.1325946
histone H2A-K119 monoubiquitination (GO:0036353)	0.01904265	0.111705268	240.1325946
positive regulation of intracellular steroid hormone receptor signaling pathway	0.01904265	0.111705268	240.1325946
negative regulation of vascular associated smooth muscle cell differentiation	0.01904265	0.111705268	240.1325946
positive regulation of protein localization to early endosome (GO:1902966)	0.01904265	0.111705268	240.1325946
positive regulation of protein localization to endosome (GO:1905668)	0.01904265	0.111705268	240.1325946
U4 snRNA 3'-end processing (GO:0034475)	0.01904265	0.111705268	240.1325946
endosomal vesicle fusion (GO:0034058)	0.01904265	0.111705268	240.1325946
regulation of protein localization to early endosome (GO:1902965)	0.01904265	0.111705268	240.1325946
negative regulation of protein kinase activity (GO:0006469)	0.01975373	0.111705268	38.51508981
positive regulation of autophagosome assembly (GO:2000786)	0.02139788	0.111705268	203.9201587
exonucleolytic trimming involved in rRNA processing (GO:0000459)	0.02139788	0.111705268	203.9201587
exonucleolytic trimming to generate mature 3'-end of 5.8S rRNA from tricistronic	0.02139788	0.111705268	203.9201587
regulation of aspartic-type endopeptidase activity involved in amyloid precursor	0.02139788	0.111705268	203.9201587
positive regulation of mast cell degranulation (GO:0043306)	0.02139788	0.111705268	203.9201587
regulation of ER to Golgi vesicle-mediated transport (GO:0060628)	0.02139788	0.111705268	203.9201587
somatic recombination of immunoglobulin genes involved in immune response	0.02139788	0.111705268	203.9201587
nuclear RNA surveillance (GO:0071027)	0.02139788	0.111705268	203.9201587
regulation of mitotic centrosome separation (GO:0046602)	0.02139788	0.111705268	203.9201587
mRNA-containing ribonucleoprotein complex export from nucleus (GO:0071427)	0.023603	0.111705268	33.34128392
receptor recycling (GO:0001881)	0.02374757	0.111705268	176.341144
regulation of tau-protein kinase activity (GO:1902947)	0.02374757	0.111705268	176.341144
negative regulation of inclusion body assembly (GO:0090084)	0.02374757	0.111705268	176.341144
rRNA 3'-end processing (GO:0031125)	0.02374757	0.111705268	176.341144
nuclear mRNA surveillance (GO:0071028)	0.02374757	0.111705268	176.341144

nuclear-transcribed mRNA catabolic process, exonucleolytic, 3'-5' (GO:0034427)	0.02374757	0.111705268	176.341144
regulation of protein catabolic process (GO:0042176)	0.02494935	0.111705268	31.85734648
mRNA transport (GO:0051028)	0.02586405	0.111705268	30.92488814
negative regulation of centrosome duplication (GO:0010826)	0.02609174	0.111705268	154.7047932
positive regulation of ceramide biosynthetic process (GO:2000304)	0.02609174	0.111705268	154.7047932
positive regulation of DNA methylation-dependent heterochromatin assembly	0.02609174	0.111705268	154.7047932
negative regulation of intracellular estrogen receptor signaling pathway (GO:0033147)	0.02609174	0.111705268	154.7047932
regulation of endocytic recycling (GO:2001135)	0.02609174	0.111705268	154.7047932
isotype switching (GO:0045190)	0.02609174	0.111705268	154.7047932
chromatin-mediated maintenance of transcription (GO:0048096)	0.02609174	0.111705268	154.7047932
positive regulation of sphingolipid biosynthetic process (GO:0090154)	0.02609174	0.111705268	154.7047932
regulation of mitochondrial fusion (GO:0010635)	0.02609174	0.111705268	154.7047932
positive regulation of vacuole organization (GO:0044090)	0.02609174	0.111705268	154.7047932
RNA export from nucleus (GO:0006405)	0.0267923	0.113445574	30.03454384
mRNA export from nucleus (GO:0006406)	0.02726146	0.113445574	29.60433926
negative regulation of transmembrane receptor protein serine/threonine kinase	0.02773394	0.113445574	29.1836995
regulation of triglyceride catabolic process (GO:0010896)	0.0284304	0.113445574	137.3227634
negative regulation of transcription elongation from RNA polymerase II promoter	0.0284304	0.113445574	137.3227634
regulation of histone H3-K9 methylation (GO:0051570)	0.0284304	0.113445574	137.3227634
early endosome to Golgi transport (GO:0034498)	0.0284304	0.113445574	137.3227634
nuclear-transcribed mRNA catabolic process, nonsense-mediated decay	0.03014571	0.114943841	27.21405339
protein neddylation (GO:0045116)	0.03076356	0.114943841	123.0844037
negative regulation of histone methylation (GO:0031061)	0.03076356	0.114943841	123.0844037
positive regulation of heterochromatin assembly (GO:0031453)	0.03076356	0.114943841	123.0844037
positive regulation of protein exit from endoplasmic reticulum (GO:0070863)	0.03076356	0.114943841	123.0844037
chromatin organization involved in regulation of transcription (GO:0034401)	0.03076356	0.114943841	123.0844037
regulation of protein exit from endoplasmic reticulum (GO:0070861)	0.03076356	0.114943841	123.0844037
positive regulation of protein metabolic process (GO:0051247)	0.03113311	0.115276667	26.48367768
regulation of protein binding (GO:0043393)	0.03263809	0.118265184	25.44387289

negative regulation of DNA-templated transcription, elongation (GO:0032785)	0.03309123	0.118265184	111.2304765
response to X-ray (GO:0010165)	0.03309123	0.118265184	111.2304765
regulation of DNA methylation-dependent heterochromatin assembly (GO:0090308)	0.03309123	0.118265184	111.2304765
positive regulation of histone H3-K4 methylation (GO:0051571)	0.03541343	0.124401027	101.2251692
regulation of dephosphorylation (GO:0035303)	0.03541343	0.124401027	101.2251692
B cell activation involved in immune response (GO:0002312)	0.03773017	0.129225831	92.68005026
regulation of ceramide biosynthetic process (GO:2000303)	0.03773017	0.129225831	92.68005026
regulation of phosphate metabolic process (GO:0019220)	0.03773017	0.129225831	92.68005026
positive regulation of canonical Wnt signaling pathway (GO:0090263)	0.03893567	0.132015993	21.85652806
negative regulation of amyloid-beta formation (GO:1902430)	0.04004146	0.132015993	85.30698892
positive regulation of cell cycle phase transition (GO:1901989)	0.04234731	0.132015993	78.88796683
negative regulation of lipid catabolic process (GO:0050995)	0.04234731	0.132015993	78.88796683
regulation of cellular protein catabolic process (GO:1903362)	0.04234731	0.132015993	78.88796683
regulation of chromosome segregation (GO:0051983)	0.04234731	0.132015993	78.88796683
regulation of early endosome to late endosome transport (GO:2000641)	0.04234731	0.132015993	78.88796683
rRNA catabolic process (GO:0016075)	0.04234731	0.132015993	78.88796683
melanosome transport (GO:0032402)	0.04234731	0.132015993	78.88796683
pigment granule transport (GO:0051904)	0.04234731	0.132015993	78.88796683
establishment of melanosome localization (GO:0032401)	0.04464774	0.132015993	73.25512876
positive regulation of cellular protein catabolic process (GO:1903364)	0.04464774	0.132015993	73.25512876
regulation of centriole replication (GO:0046599)	0.04464774	0.132015993	73.25512876
histone deubiquitination (GO:0016578)	0.04464774	0.132015993	73.25512876
negative regulation of nervous system development (GO:0051961)	0.04464774	0.132015993	73.25512876
regulation of histone H3-K4 methylation (GO:0051569)	0.04464774	0.132015993	73.25512876
DNA alkylation (GO:0006305)	0.04464774	0.132015993	73.25512876
DNA methylation or demethylation (GO:0044728)	0.04464774	0.132015993	73.25512876
negative regulation of amyloid precursor protein catabolic process (GO:1902992)	0.04464774	0.132015993	73.25512876
protein targeting to lysosome (GO:0006622)	0.04694276	0.134896737	68.27724817
regulation of smooth muscle cell migration (GO:0014910)	0.04694276	0.134896737	68.27724817

positive regulation of hormone secretion (GO:0046887)	0.04694276	0.134896737	68.27724817
positive regulation of intracellular protein transport (GO:0090316)	0.04916547	0.134896737	17.76856353
positive regulation of transferase activity (GO:0051347)	0.04916547	0.134896737	17.76856353
beta-catenin destruction complex disassembly (GO:1904886)	0.04923239	0.134896737	63.85033052
calcium-mediated signaling using intracellular calcium source (GO:0035584)	0.04923239	0.134896737	63.85033052
melanosome localization (GO:0032400)	0.04923239	0.134896737	63.85033052
nuclear-transcribed mRNA poly(A) tail shortening (GO:0000289)	0.04923239	0.134896737	63.85033052
positive regulation of vascular associated smooth muscle cell proliferation	0.04923239	0.134896737	63.85033052
poly(A)+ mRNA export from nucleus (GO:0016973)	0.04923239	0.134896737	63.85033052
positive regulation of multicellular organismal process (GO:0051240)	0.04978716	0.135513389	11.46782941
maturation of 5.8S rRNA from tricistronic rRNA transcript (SSU-rRNA, 5.8S rRNA,	0.05151662	0.137618593	59.89095446
organelle fusion (GO:0048284)	0.05151662	0.137618593	59.89095446
cellular response to DNA damage stimulus (GO:0006974)	0.05156512	0.137618593	11.1675423
positive regulation of Wnt signaling pathway (GO:0030177)	0.05216309	0.138316313	16.83843396
positive regulation of protein kinase activity (GO:0045860)	0.05277037	0.139029638	16.66125458
positive regulation of NF-kappaB transcription factor activity (GO:0051092)	0.05338021	0.139056247	16.48687399
gene expression (GO:0010467)	0.05373934	0.139056247	10.82149771
DNA methylation (GO:0006306)	0.05379548	0.139056247	56.33146627
neuromuscular junction development (GO:0007528)	0.05606898	0.14313262	53.11645428
nucleotide-binding domain, leucine rich repeat containing receptor signaling pathway	0.05606898	0.14313262	53.11645428
negative regulation of endocytosis (GO:0045806)	0.05833713	0.146858951	50.20012391
positive regulation of peptidyl-threonine phosphorylation (GO:0010800)	0.05833713	0.146858951	50.20012391
protein transport (GO:0015031)	0.05860065	0.146858951	10.12125087
negative regulation of cell development (GO:0010721)	0.06059995	0.15003963	47.54431676
positive regulation of histone methylation (GO:0031062)	0.06059995	0.15003963	47.54431676
regulation of transcription elongation from RNA polymerase II promoter	0.06285744	0.1519671	45.11699716
cellular response to unfolded protein (GO:0034620)	0.06285744	0.1519671	45.11699716
melanosome organization (GO:0032438)	0.06285744	0.1519671	45.11699716
cytoplasmic pattern recognition receptor signaling pathway (GO:0002753)	0.06285744	0.1519671	45.11699716

regulation of calcium-mediated signaling (GO:0050848)	0.06510962	0.152914584	42.89108305
macromolecule catabolic process (GO:0009057)	0.06510962	0.152914584	42.89108305
nucleotide-binding oligomerization domain containing signaling pathway	0.06510962	0.152914584	42.89108305
protein localization to Golgi apparatus (GO:0034067)	0.06510962	0.152914584	42.89108305
protein localization to lysosome (GO:0061462)	0.06510962	0.152914584	42.89108305
regulation of ubiquitin-protein transferase activity (GO:0051438)	0.06735649	0.156404062	40.84353327
MyD88-dependent toll-like receptor signaling pathway (GO:0002755)	0.06735649	0.156404062	40.84353327
negative regulation of gene expression, epigenetic (GO:0045814)	0.06959808	0.158037638	38.95462833
histone H3-K4 methylation (GO:0051568)	0.06959808	0.158037638	38.95462833
snRNA 3'-end processing (GO:0034472)	0.06959808	0.158037638	38.95462833
ncRNA catabolic process (GO:0034661)	0.06959808	0.158037638	38.95462833
negative regulation of osteoblast differentiation (GO:0045668)	0.0718344	0.159588853	37.20739859
positive regulation of protein targeting to mitochondrion (GO:1903955)	0.0718344	0.159588853	37.20739859
positive regulation of proteolysis involved in cellular protein catabolic process	0.0718344	0.159588853	37.20739859
positive regulation of ubiquitin-protein transferase activity (GO:0051443)	0.0718344	0.159588853	37.20739859
negative regulation of intracellular steroid hormone receptor signaling pathway	0.07406545	0.162785561	35.5871659
cellular response to topologically incorrect protein (GO:0035967)	0.07406545	0.162785561	35.5871659
exonucleolytic catabolism of deadenylated mRNA (GO:0043928)	0.07629125	0.166785658	34.08117343
regulation of amyloid-beta formation (GO:1902003)	0.07851181	0.168944262	32.67828452
negative regulation of mitochondrion organization (GO:0010823)	0.07851181	0.168944262	32.67828452
histone lysine methylation (GO:0034968)	0.07851181	0.168944262	32.67828452
positive regulation of cell cycle G1/S phase transition (GO:1902808)	0.08072714	0.169279878	31.3687361
regulation of autophagosome assembly (GO:2000785)	0.08072714	0.169279878	31.3687361
negative regulation of neurogenesis (GO:0050768)	0.08072714	0.169279878	31.3687361
negative regulation of organelle assembly (GO:1902116)	0.08072714	0.169279878	31.3687361
nuclear-transcribed mRNA catabolic process, exonucleolytic (GO:0000291)	0.08072714	0.169279878	31.3687361
endomembrane system organization (GO:0010256)	0.08251861	0.172157651	10.87694077
regulation of cell cycle G1/S phase transition (GO:1902806)	0.08293726	0.172157651	30.14393553
regulation of vascular associated smooth muscle cell proliferation (GO:1904705)	0.08514218	0.174967175	28.99629222

regulation of intracellular steroid hormone receptor signaling pathway (GO:0033143)	0.08514218	0.174967175	28.99629222
positive regulation of insulin secretion (GO:0032024)	0.0873419	0.177775265	27.9190773
regulation of protein targeting to mitochondrion (GO:1903214)	0.08953645	0.177775265	26.90630608
regulation of protein tyrosine kinase activity (GO:0061097)	0.08953645	0.177775265	26.90630608
protein monoubiquitination (GO:0006513)	0.08953645	0.177775265	26.90630608
regulation of cellular component biogenesis (GO:0044087)	0.08953645	0.177775265	26.90630608
positive regulation of intracellular transport (GO:0032388)	0.08953645	0.177775265	26.90630608
regulation of peptidyl-threonine phosphorylation (GO:0010799)	0.08953645	0.177775265	26.90630608
import into cell (GO:0098657)	0.09391005	0.182061461	25.05329844
JNK cascade (GO:0007254)	0.09391005	0.182061461	25.05329844
nucleobase-containing compound catabolic process (GO:0034655)	0.09391005	0.182061461	25.05329844
visual system development (GO:0150063)	0.09391005	0.182061461	25.05329844
endosome organization (GO:0007032)	0.09391005	0.182061461	25.05329844
regulation of ubiquitin-dependent protein catabolic process (GO:2000058)	0.09608913	0.183686657	24.20399666
positive regulation of epithelial to mesenchymal transition (GO:0010718)	0.09608913	0.183686657	24.20399666
positive regulation of protein tyrosine kinase activity (GO:0061098)	0.09608913	0.183686657	24.20399666
positive regulation of peptide hormone secretion (GO:0090277)	0.09826307	0.186972795	23.40087617
mitotic spindle assembly (GO:0090307)	0.1004319	0.189346386	22.64045732
protein K63-linked ubiquitination (GO:0070534)	0.1004319	0.189346386	22.64045732
regulation of synaptic transmission, glutamatergic (GO:0051966)	0.10475425	0.193067244	21.23543393
positive regulation of organelle assembly (GO:1902117)	0.10475425	0.193067244	21.23543393
positive regulation of smooth muscle cell proliferation (GO:0048661)	0.10475425	0.193067244	21.23543393
postreplication repair (GO:0006301)	0.10475425	0.193067244	21.23543393
vesicle organization (GO:0016050)	0.10475425	0.193067244	21.23543393
negative regulation of MAP kinase activity (GO:0043407)	0.10905625	0.20009875	19.96709792
response to unfolded protein (GO:0006986)	0.11119966	0.202225928	19.37841413
RNA catabolic process (GO:0006401)	0.11119966	0.202225928	19.37841413
positive regulation of ion transport (GO:0043270)	0.11333801	0.205206714	18.81737167
inositol lipid-mediated signaling (GO:0048017)	0.11547133	0.20724331	18.28217177

negative regulation of transport (GO:0051051)	0.11547133	0.20724331	18.28217177
negative regulation of protein-containing complex assembly (GO:0031333)	0.11759963	0.208591541	17.77116479
endocytic recycling (GO:0032456)	0.11759963	0.208591541	17.77116479
positive regulation of DNA-binding transcription factor activity (GO:0051091)	0.1177451	0.208591541	7.512474433
positive regulation of macroautophagy (GO:0016239)	0.1197229	0.210282537	17.2828352
cellular macromolecule catabolic process (GO:0044265)	0.1197229	0.210282537	17.2828352
positive regulation of signal transduction (GO:0009967)	0.12248422	0.214055816	7.19473547
regulation of canonical Wnt signaling pathway (GO:0060828)	0.1232787	0.214055816	7.143643366
interstrand cross-link repair (GO:0036297)	0.12395446	0.214055816	16.36873936
ceramide metabolic process (GO:0006672)	0.12395446	0.214055816	16.36873936
protein-containing complex disassembly (GO:0032984)	0.12606277	0.21498671	15.94050153
positive regulation of establishment of protein localization to mitochondrion	0.12606277	0.21498671	15.94050153
sensory organ development (GO:0007423)	0.12606277	0.21498671	15.94050153
positive regulation of gene expression, epigenetic (GO:0045815)	0.1281661	0.217670529	15.52997838
eye development (GO:0001654)	0.13026448	0.219420908	15.13615481
positive regulation of protein binding (GO:0032092)	0.13026448	0.219420908	15.13615481
regulation of endocytosis (GO:0030100)	0.13652999	0.227639662	14.0458046
pattern recognition receptor signaling pathway (GO:0002221)	0.13652999	0.227639662	14.0458046
negative regulation of kinase activity (GO:0033673)	0.13860865	0.227639662	13.71001749
I-kappaB kinase/NF-kappaB signaling (GO:0007249)	0.13860865	0.227639662	13.71001749
stress-activated MAPK cascade (GO:0051403)	0.13860865	0.227639662	13.71001749
regulation of neurogenesis (GO:0050767)	0.13860865	0.227639662	13.71001749
amyloid fibril formation (GO:1990000)	0.14068242	0.227639662	13.38684559
negative regulation of endopeptidase activity (GO:0010951)	0.14068242	0.227639662	13.38684559
neuropeptide signaling pathway (GO:0007218)	0.14068242	0.227639662	13.38684559
organonitrogen compound catabolic process (GO:1901565)	0.14068242	0.227639662	13.38684559
DNA metabolic process (GO:0006259)	0.14271118	0.229182743	6.056883679
protein catabolic process (GO:0030163)	0.14275129	0.229182743	13.07563286
canonical Wnt signaling pathway (GO:0060070)	0.15097814	0.240511683	11.93870546

negative regulation of transforming growth factor beta receptor signaling pathway	0.15097814	0.240511683	11.93870546
negative regulation of cellular catabolic process (GO:0031330)	0.15302274	0.241893636	11.67885591
RNA 3'-end processing (GO:0031123)	0.15302274	0.241893636	11.67885591
phosphatidylinositol-mediated signaling (GO:0048015)	0.15709749	0.247383399	11.18521876
positive regulation of protein secretion (GO:0050714)	0.15912766	0.24962392	10.95062711
positive regulation of JNK cascade (GO:0046330)	0.16115304	0.251839921	10.72369034
mRNA processing (GO:0006397)	0.16190692	0.252059642	5.220994937
negative regulation of protein binding (GO:0032091)	0.16317364	0.252121684	10.50406327
mitotic nuclear division (GO:0140014)	0.16317364	0.252121684	10.50406327
establishment of protein localization to organelle (GO:0072594)	0.16720057	0.256415795	10.08545552
regulation of epithelial to mesenchymal transition (GO:0010717)	0.16720057	0.256415795	10.08545552
negative regulation of developmental process (GO:0051093)	0.16920691	0.256620069	9.885878423
positive regulation of protein modification by small protein conjugation or removal	0.16920691	0.256620069	9.885878423
regulation of organelle assembly (GO:1902115)	0.16920691	0.256620069	9.885878423
negative regulation of protein serine/threonine kinase activity (GO:0071901)	0.17120851	0.2587011	9.692415749
negative regulation of NF-kappaB transcription factor activity (GO:0032088)	0.1732054	0.258836889	9.50480889
positive regulation of ubiquitin-dependent protein catabolic process (GO:2000060)	0.1732054	0.258836889	9.50480889
mRNA 3'-end processing (GO:0031124)	0.1732054	0.258836889	9.50480889
protein polyubiquitination (GO:0000209)	0.17381747	0.258836889	4.78889087
regulation of organelle organization (GO:0033043)	0.17519757	0.259950187	9.322813204
positive regulation of cellular amide metabolic process (GO:0034250)	0.17718504	0.261953429	9.146197104
regulation of gene expression, epigenetic (GO:0040029)	0.17916783	0.262992776	8.974741207
positive regulation of protein ubiquitination (GO:0031398)	0.17916783	0.262992776	8.974741207
regulation of osteoblast differentiation (GO:0045667)	0.18114593	0.2649501	8.808237552
spindle assembly (GO:0051225)	0.18311937	0.265943677	8.646488886
nuclear export (GO:0051168)	0.18311937	0.265943677	8.646488886
negative regulation of cellular amide metabolic process (GO:0034249)	0.18705228	0.26974908	8.336517035
regulation of neuron death (GO:1901214)	0.18705228	0.26974908	8.336517035
negative regulation of binding (GO:0051100)	0.19096665	0.272470276	8.043437426

retrograde transport, endosome to Golgi (GO:0042147)	0.19096665	0.272470276	8.043437426
intracellular protein transport (GO:0006886)	0.1928141	0.272470276	4.203565719
positive regulation of inflammatory response (GO:0050729)	0.19291691	0.272470276	7.902835242
transforming growth factor beta receptor signaling pathway (GO:0007179)	0.19291691	0.272470276	7.902835242
post-Golgi vesicle-mediated transport (GO:0006892)	0.19291691	0.272470276	7.902835242
positive regulation of binding (GO:0051099)	0.19486257	0.274275734	7.76599501
toll-like receptor signaling pathway (GO:0002224)	0.19680363	0.276062426	7.632778142
Wnt signaling pathway (GO:0016055)	0.19874011	0.277830557	7.503052567
positive regulation of peptidyl-serine phosphorylation (GO:0033138)	0.20067201	0.278635804	7.376692362
visual perception (GO:0007601)	0.20067201	0.278635804	7.376692362
negative regulation of MAPK cascade (GO:0043409)	0.20259936	0.279423951	7.253577403
interleukin-1-mediated signaling pathway (GO:0070498)	0.20259936	0.279423951	7.253577403
sensory perception of light stimulus (GO:0050953)	0.20452216	0.281132463	7.133593038
protein maturation (GO:0051604)	0.20835414	0.283338476	6.902583071
regulation of MAP kinase activity (GO:0043405)	0.20835414	0.283338476	6.902583071
positive regulation of defense response (GO:0031349)	0.21026335	0.283338476	6.79135291
negative regulation of neuron death (GO:1901215)	0.21026335	0.283338476	6.79135291
RNA splicing (GO:0008380)	0.21026335	0.283338476	6.79135291
regulation of peptidyl-serine phosphorylation (GO:0033135)	0.21026335	0.283338476	6.79135291
positive regulation of stress-activated MAPK cascade (GO:0032874)	0.21216804	0.284970804	6.682843716
regulation of transforming growth factor beta receptor signaling pathway	0.21406824	0.286586477	6.576964037
positive regulation of cell cycle process (GO:0090068)	0.21596396	0.287905091	6.473626345
positive regulation of cellular protein metabolic process (GO:0032270)	0.21785519	0.287905091	6.372746834
regulation of cell death (GO:0010941)	0.21785519	0.287905091	6.372746834
calcium-mediated signaling (GO:0019722)	0.21785519	0.287905091	6.372746834
regulation of insulin secretion (GO:0050796)	0.22162427	0.291947354	6.178044569
regulation of JNK cascade (GO:0046328)	0.22350213	0.293480436	6.084071124
small GTPase mediated signal transduction (GO:0007264)	0.22537556	0.294997947	5.992254146
regulation of protein ubiquitination (GO:0031396)	0.23096933	0.30040631	5.729076782

modulation of chemical synaptic transmission (GO:0050804)	0.23096933	0.30040631	5.729076782
negative regulation of programmed cell death (GO:0043069)	0.23242796	0.300915476	3.276406056
regulation of protein kinase activity (GO:0045859)	0.23282511	0.300915476	5.645233549
Fc-epsilon receptor signaling pathway (GO:0038095)	0.23467651	0.301412646	5.563233389
regulation of Wnt signaling pathway (GO:0030111)	0.23467651	0.301412646	5.563233389
Fc receptor signaling pathway (GO:0038093)	0.23652354	0.302838548	5.483020803
activation of protein kinase activity (GO:0032147)	0.2402045	0.30514665	5.327746925
cellular response to transforming growth factor beta stimulus (GO:0071560)	0.2402045	0.30514665	5.327746925
cellular amide metabolic process (GO:0043603)	0.24203846	0.30514665	5.252584903
cellular response to lectin (GO:1990858)	0.24203846	0.30514665	5.252584903
stimulatory C-type lectin receptor signaling pathway (GO:0002223)	0.24203846	0.30514665	5.252584903
regulation of protein-containing complex assembly (GO:0043254)	0.24386809	0.30557861	5.179008816
sphingolipid metabolic process (GO:0006665)	0.24386809	0.30557861	5.179008816
innate immune response activating cell surface receptor signaling pathway	0.24933106	0.311474358	4.967346711
regulation of mRNA catabolic process (GO:0061013)	0.25475537	0.317286234	4.768407103
protein targeting (GO:0006605)	0.2601413	0.321350627	4.581160506
negative regulation of cell growth (GO:0030308)	0.26192813	0.321350627	4.521180811
negative regulation of growth (GO:0045926)	0.26192813	0.321350627	4.521180811
synapse organization (GO:0050808)	0.26192813	0.321350627	4.521180811
circulatory system development (GO:0072359)	0.26192813	0.321350627	4.521180811
organelle organization (GO:0006996)	0.26719518	0.326836955	2.681558387
Golgi organization (GO:0007030)	0.26903327	0.328108826	4.292597324
RNA metabolic process (GO:0016070)	0.27431814	0.332580394	4.132255213
transmembrane receptor protein serine/threonine kinase signaling pathway	0.27431814	0.332580394	4.132255213
positive regulation of peptidyl-tyrosine phosphorylation (GO:0050731)	0.27607143	0.333721639	4.080778857
organic substance transport (GO:0071702)	0.27956558	0.33695441	3.980635256
regulation of intracellular signal transduction (GO:1902531)	0.28238279	0.339354756	2.466675149
positive regulation of response to external stimulus (GO:0032103)	0.28477587	0.340240933	3.837100064
protein dephosphorylation (GO:0006470)	0.28477587	0.340240933	3.837100064

positive regulation of cellular catabolic process (GO:0031331)	0.28822887	0.342498694	3.745613412
Ras protein signal transduction (GO:0007265)	0.28994925	0.342498694	3.701070788
protein localization to organelle (GO:0033365)	0.28994925	0.342498694	3.701070788
receptor-mediated endocytosis (GO:0006898)	0.29166555	0.342498694	3.657303244
negative regulation of DNA-binding transcription factor activity (GO:0043433)	0.29166555	0.342498694	3.657303244
nitrogen compound transport (GO:0071705)	0.29166555	0.342498694	3.657303244
regulation of mRNA stability (GO:0043488)	0.29679013	0.347523489	3.530470633
brain development (GO:0007420)	0.30356647	0.354448348	3.371160821
negative regulation of protein phosphorylation (GO:0001933)	0.30693062	0.357361144	3.295424203
dephosphorylation (GO:0016311)	0.30860672	0.358297633	3.258484568
cellular response to interleukin-1 (GO:0071347)	0.31194703	0.361155571	3.186394535
regulation of signal transduction by p53 class mediator (GO:1901796)	0.31361125	0.362062425	3.151218039
mitotic spindle organization (GO:0007052)	0.31527153	0.362265589	3.116603764
positive regulation of transcription, DNA-templated (GO:0045893)	0.31555008	0.362265589	1.669634478
rRNA metabolic process (GO:0016072)	0.32351413	0.370374111	2.95155159
heart development (GO:0007507)	0.32678389	0.373078276	2.889065386
negative regulation of canonical Wnt signaling pathway (GO:0090090)	0.32841297	0.373899526	2.858537872
cellular protein-containing complex assembly (GO:0034622)	0.33327706	0.378389153	2.769701144
rRNA processing (GO:0006364)	0.34130734	0.386438895	2.630250401
positive regulation of developmental process (GO:0051094)	0.34766331	0.391884501	2.525840738
positive regulation of nucleic acid-templated transcription (GO:1903508)	0.34802395	0.391884501	1.752949101
RNA processing (GO:0006396)	0.35081874	0.393952187	2.475852314
endoplasmic reticulum to Golgi vesicle-mediated transport (GO:0006888)	0.36019561	0.40337982	2.334096192
negative regulation of cell differentiation (GO:0045596)	0.36943982	0.411489875	2.203623295
negative regulation of Wnt signaling pathway (GO:0030178)	0.36943982	0.411489875	2.203623295
ribosome biogenesis (GO:0042254)	0.37096775	0.412074986	2.18288972
negative regulation of macromolecule metabolic process (GO:0010605)	0.37401275	0.413223762	2.142243719
regulation of programmed cell death (GO:0043067)	0.37401275	0.413223762	2.142243719
regulation of signal transduction (GO:0009966)	0.38005951	0.418778709	2.064102922

modification-dependent protein catabolic process (GO:0019941)	0.38455701	0.421474485	2.008112768
ncRNA processing (GO:0034470)	0.38455701	0.421474485	2.008112768
negative regulation of cellular process (GO:0048523)	0.3956514	0.432480658	1.385829111
positive regulation of protein modification process (GO:0031401)	0.40367979	0.440085927	1.788622954
regulation of cell growth (GO:0001558)	0.40800943	0.443629296	1.742773179
positive regulation of cellular process (GO:0048522)	0.44501888	0.482593029	1.092156054
RNA splicing, via transesterification reactions with bulged adenosine as nucleophile	0.45497781	0.492094419	1.320464317
positive regulation of phosphorylation (GO:0042327)	0.45762401	0.493657392	1.300205623
positive regulation of cell differentiation (GO:0045597)	0.46418458	0.499423728	1.251376824
regulation of protein phosphorylation (GO:0001932)	0.47452022	0.509210993	1.178297454
protein-containing complex assembly (GO:0065003)	0.47579837	0.509252941	1.169572487
central nervous system development (GO:0007417)	0.47707347	0.509291421	1.160934633
mRNA splicing, via spliceosome (GO:0000398)	0.48466056	0.516050494	1.11087427
negative regulation of gene expression (GO:0010629)	0.54159922	0.575186771	0.797925258
cellular protein localization (GO:0034613)	0.54937048	0.581936259	0.762482312
positive regulation of cytokine production (GO:0001819)	0.55592877	0.587369474	0.733725572
post-translational protein modification (GO:0043687)	0.56665215	0.59716419	0.688862772
supramolecular fiber organization (GO:0097435)	0.57296403	0.602271655	0.663646665
ubiquitin-dependent protein catabolic process (GO:0006511)	0.57608613	0.604008668	0.651486431
positive regulation of protein phosphorylation (GO:0001934)	0.59336033	0.620537135	0.587745377
positive regulation of macromolecule metabolic process (GO:0010604)	0.6061031	0.632254759	0.544319733
regulation of cell migration (GO:0030334)	0.62860904	0.654071684	0.474341767
positive regulation of cell population proliferation (GO:0008284)	0.68420623	0.710123129	0.33251769
neutrophil degranulation (GO:0043312)	0.68960124	0.711691168	0.32077165
positive regulation of gene expression (GO:0010628)	0.69036455	0.711691168	0.31913551
negative regulation of apoptotic process (GO:0043066)	0.69264347	0.711691168	0.314288114
neutrophil activation involved in immune response (GO:0002283)	0.69264347	0.711691168	0.314288114
neutrophil mediated immunity (GO:0002446)	0.69490597	0.712235296	0.30953061
cellular protein modification process (GO:0006464)	0.71280069	0.728758916	0.272365078

cytokine-mediated signaling pathway (GO:0019221)	0.78037512	0.795866437	0.164514757
negative regulation of transcription by RNA polymerase II (GO:0000122)	0.81218966	0.826262251	0.124867272
regulation of apoptotic process (GO:0042981)	0.83746201	0.849868854	0.097844639
regulation of cell population proliferation (GO:0042127)	0.84614978	0.856570343	0.089392183
positive regulation of transcription by RNA polymerase II (GO:0045944)	0.89278207	0.901556343	0.050668469
negative regulation of transcription, DNA-templated (GO:0045892)	0.90306217	0.909702332	0.043537791
regulation of gene expression (GO:0010468)	0.93041959	0.934969323	0.02686586
regulation of transcription by RNA polymerase II (GO:0006357)	0.97466586	0.976759506	0.008984138
regulation of transcription, DNA-templated (GO:0006355)	0.97675951	0.976759506	0.008076006
GO-BP C1orf27's datasets			
Term	**P-value**	**Adjusted P-**	**Combined**
protein ufmylation (GO:0071569)	1.99E-18	6.81E-16	4884755.969
protein polyufmylation (GO:1990564)	1.99E-15	2.27E-13	3380718.344
protein K69-linked ufmylation (GO:1990592)	1.99E-15	2.27E-13	3380718.344
reticulophagy (GO:0061709)	2.55E-12	2.18E-10	16657.402
regulation of intracellular estrogen receptor signaling pathway (GO:0033146)	3.92E-10	2.68E-08	4000.454075
organelle disassembly (GO:1903008)	5.41E-10	3.09E-08	3668.870529
regulation of intracellular steroid hormone receptor signaling pathway (GO:0033143)	8.46E-10	4.13E-08	3254.867248
response to endoplasmic reticulum stress (GO:0034976)	3.92E-09	1.68E-07	1167.917623
selective autophagy (GO:0061912)	9.54E-09	3.62E-07	1703.240001
positive regulation of transcription by RNA polymerase I (GO:0045943)	3.01E-06	1.03E-04	1729.986067
protein modification by small protein conjugation (GO:0032446)	8.98E-06	2.79E-04	178.2177365
negative regulation of IRE1-mediated unfolded protein response (GO:1903895)	1.50E-05	4.27E-04	6431.42993
erythrocyte differentiation (GO:0030218)	2.53E-05	6.65E-04	669.1142369
positive regulation of transcription of nucleolar large rRNA by RNA polymerase I	6.71E-05	0.001638853	2085.577517
negative regulation of endoplasmic reticulum unfolded protein response	1.16E-04	0.002569776	1430.110648
negative regulation of NF-kappaB transcription factor activity (GO:0032088)	1.28E-04	0.002569776	319.9939258

regulation of IRE1-mediated unfolded protein response (GO:1903894)	1.35E-04	0.002569776	1288.680448
regulation of transcription of nucleolar large rRNA by RNA polymerase I	1.35E-04	0.002569776	1288.680448
positive regulation of proteolysis involved in cellular protein catabolic process	6.82E-04	0.012279329	436.0135628
negative regulation of DNA-binding transcription factor activity (GO:0043433)	7.34E-04	0.012542884	139.444177
brain development (GO:0007420)	8.43E-04	0.01372147	130.2078239
regulation of signal transduction by p53 class mediator (GO:1901796)	9.44E-04	0.014672011	123.0586129
regulation of ubiquitin-dependent protein catabolic process (GO:2000058)	0.00125256	0.01862496	289.6022105
regulation of mitotic cell cycle (GO:0007346)	0.00138023	0.01966824	101.604966
myeloid cell differentiation (GO:0030099)	0.00191433	0.02599309	216.8667908
regulation of intracellular signal transduction (GO:1902531)	0.00197608	0.02599309	53.52731729
regulation of proteasomal protein catabolic process (GO:0061136)	0.00206276	0.02612826	206.0168682
organonitrogen compound catabolic process (GO:1901565)	0.00279591	0.034150057	166.9084811
negative regulation of cellular catabolic process (GO:0031330)	0.00334317	0.03942634	147.296878
positive regulation of cellular protein localization (GO:1903829)	0.00353585	0.04030864	141.6073654
positive regulation of ubiquitin-dependent protein catabolic process (GO:2000060)	0.00435718	0.047022717	122.1503505
central nervous system development (GO:0007417)	0.00439979	0.047022717	55.03450503
regulation of defense response (GO:0031347)	0.00479789	0.049723532	114.0371527
regulation of cell cycle (GO:0051726)	0.00579932	0.057340666	47.17464903
positive regulation of metallopeptidase activity (GO:1905050)	0.00623494	0.057340666	1056.296661
regulation of proteasomal ubiquitin-dependent protein catabolic process	0.00715789	0.057340666	85.36813977
heparan sulfate proteoglycan biosynthetic process, enzymatic modification	0.00747745	0.057340666	814.7533475
positive regulation of I-kappaB phosphorylation (GO:1903721)	0.00747745	0.057340666	814.7533475
N-acetylneuraminate catabolic process (GO:0019262)	0.00747745	0.057340666	814.7533475
regulation of protein ubiquitination (GO:0031396)	0.00813573	0.057340666	77.68767334
regulation of cytoskeleton organization (GO:0051493)	0.00857224	0.057340666	74.73677741
amino sugar catabolic process (GO:0046348)	0.00871846	0.057340666	657.633561
regulation of I-kappaB phosphorylation (GO:1903719)	0.00871846	0.057340666	657.633561
regulation of metallopeptidase activity (GO:1905048)	0.00871846	0.057340666	657.633561
definitive hemopoiesis (GO:0060216)	0.00871846	0.057340666	657.633561

tRNA threonylcarbamoyladenosine metabolic process (GO:0070525)	0.00871846	0.057340666	657.633561
posttranslational protein targeting to membrane, translocation (GO:0031204)	0.00871846	0.057340666	657.633561
catecholamine catabolic process (GO:0042424)	0.00871846	0.057340666	657.633561
negative regulation of p38MAPK cascade (GO:1903753)	0.00871846	0.057340666	657.633561
negative regulation of protein import (GO:1904590)	0.00871846	0.057340666	657.633561
negative regulation of protein import into nucleus (GO:0042308)	0.00871846	0.057340666	657.633561
negative regulation of protein kinase activity by regulation of protein phosphorylation	0.00871846	0.057340666	657.633561
TORC1 signaling (GO:0038202)	0.00995799	0.058717813	547.857721
regulation of wound healing, spreading of epidermal cells (GO:1903689)	0.00995799	0.058717813	547.857721
positive regulation of execution phase of apoptosis (GO:1900119)	0.00995799	0.058717813	547.857721
regulation of mitochondrial gene expression (GO:0062125)	0.00995799	0.058717813	547.857721
regulation of myeloid leukocyte differentiation (GO:0002761)	0.00995799	0.058717813	547.857721
heparan sulfate proteoglycan biosynthetic process, polysaccharide chain biosynthetic	0.00995799	0.058717813	547.857721
regulation of RNA polymerase II regulatory region sequence-specific DNA binding	0.01119603	0.059886543	467.164971
anoikis (GO:0043276)	0.01119603	0.059886543	467.164971
regulation of response to external stimulus (GO:0032101)	0.01140601	0.059886543	60.31782697
cellular response to leucine (GO:0071233)	0.01243259	0.059886543	405.5533029
cellular response to leucine starvation (GO:1990253)	0.01243259	0.059886543	405.5533029
negative regulation of cellular protein catabolic process (GO:1903363)	0.01243259	0.059886543	405.5533029
positive regulation of rRNA processing (GO:2000234)	0.01243259	0.059886543	405.5533029
positive regulation of transcription by RNA polymerase III (GO:0045945)	0.01243259	0.059886543	405.5533029
hematopoietic stem cell differentiation (GO:0060218)	0.01243259	0.059886543	405.5533029
response to leucine (GO:0043201)	0.01243259	0.059886543	405.5533029
positive regulation of keratinocyte migration (GO:0051549)	0.01243259	0.059886543	405.5533029
cellular biogenic amine catabolic process (GO:0042402)	0.01243259	0.059886543	405.5533029
N-acetylneuraminate metabolic process (GO:0006054)	0.01243259	0.059886543	405.5533029
telomere maintenance via recombination (GO:0000722)	0.01366766	0.064032036	357.1008996
nucleus localization (GO:0051647)	0.01366766	0.064032036	357.1008996
regulation of keratinocyte migration (GO:0051547)	0.01490124	0.066184748	318.0863027

megakaryocyte differentiation (GO:0030219)	0.01490124	0.066184748	318.0863027
carboxylic acid catabolic process (GO:0046395)	0.01490124	0.066184748	318.0863027
posttranslational protein targeting to endoplasmic reticulum membrane	0.01490124	0.066184748	318.0863027
peptidyl-serine phosphorylation (GO:0018105)	0.01612389	0.069843115	46.1943807
negative regulation of nucleocytoplasmic transport (GO:0046823)	0.01613335	0.069843115	286.0577742
protein modification by small protein conjugation or removal (GO:0070647)	0.01736398	0.073314576	259.3369253
covalent chromatin modification (GO:0016569)	0.01736398	0.073314576	259.3369253
Arp2/3 complex-mediated actin nucleation (GO:0034314)	0.01859313	0.074550234	236.73765
mitotic recombination (GO:0006312)	0.01859313	0.074550234	236.73765
catecholamine metabolic process (GO:0006584)	0.01859313	0.074550234	236.73765
regulation of dephosphorylation (GO:0035303)	0.01859313	0.074550234	236.73765
peptidyl-serine modification (GO:0018209)	0.01874655	0.074550234	41.01607693
regulation of rRNA processing (GO:2000232)	0.0198208	0.076165331	217.398956
necroptotic process (GO:0070266)	0.0198208	0.076165331	217.398956
protein localization to endoplasmic reticulum (GO:0070972)	0.0198208	0.076165331	217.398956
regulation of translation (GO:0006417)	0.02066103	0.078511908	37.94977273
positive regulation of phosphoprotein phosphatase activity (GO:0032516)	0.02227173	0.080178228	186.1003826
positive regulation of cell cycle phase transition (GO:1901989)	0.02227173	0.080178228	186.1003826
regulation of transcription by RNA polymerase I (GO:0006356)	0.02227173	0.080178228	186.1003826
regulation of cellular protein catabolic process (GO:1903362)	0.02227173	0.080178228	186.1003826
programmed necrotic cell death (GO:0097300)	0.02227173	0.080178228	186.1003826
neuromuscular process (GO:0050905)	0.02349499	0.081164498	173.2825761
heparan sulfate proteoglycan biosynthetic process (GO:0015012)	0.02349499	0.081164498	173.2825761
dopamine metabolic process (GO:0042417)	0.02349499	0.081164498	173.2825761
negative regulation of protein localization to nucleus (GO:1900181)	0.02349499	0.081164498	173.2825761
ribosome biogenesis (GO:0042254)	0.02379479	0.081378165	33.84990604
hepaticobiliary system development (GO:0061008)	0.02471677	0.08213413	161.9356388
regulation of programmed necrotic cell death (GO:0062098)	0.02471677	0.08213413	161.9356388
actin nucleation (GO:0045010)	0.02593709	0.08213413	151.8276652

positive regulation of phosphatase activity (GO:0010922)	0.02593709	0.08213413	151.8276652
regulation of transcription by RNA polymerase III (GO:0006359)	0.02593709	0.08213413	151.8276652
regulation of mitochondrial translation (GO:0070129)	0.02593709	0.08213413	151.8276652
positive regulation of transcription regulatory region DNA binding (GO:2000679)	0.02593709	0.08213413	151.8276652
heparan sulfate proteoglycan metabolic process (GO:0030201)	0.02593709	0.08213413	151.8276652
regulation of inflammatory response (GO:0050727)	0.02711196	0.082188798	30.40469878
positive regulation of peptidase activity (GO:0010952)	0.02715595	0.082188798	142.7724214
positive regulation of signal transduction by p53 class mediator (GO:1901798)	0.02715595	0.082188798	142.7724214
positive regulation of translational initiation (GO:0045948)	0.02715595	0.082188798	142.7724214
regulation of execution phase of apoptosis (GO:1900117)	0.02715595	0.082188798	142.7724214
negative regulation of intracellular protein transport (GO:0090317)	0.02837334	0.082937449	134.6187109
mitotic cell cycle checkpoint signaling (GO:0007093)	0.02837334	0.082937449	134.6187109
regulation of necroptotic process (GO:0060544)	0.02837334	0.082937449	134.6187109
response to nutrient levels (GO:0031667)	0.02837334	0.082937449	134.6187109
apoptotic nuclear changes (GO:0030262)	0.02958927	0.083632469	127.2425658
nucleotide-binding domain, leucine rich repeat containing receptor signaling pathway	0.02958927	0.083632469	127.2425658
regulation of cell size (GO:0008361)	0.02958927	0.083632469	127.2425658
negative regulation of NIK/NF-kappaB signaling (GO:1901223)	0.02958927	0.083632469	127.2425658
positive regulation of lipid metabolic process (GO:0045834)	0.03080373	0.085544727	120.5414282
cellular polysaccharide biosynthetic process (GO:0033692)	0.03080373	0.085544727	120.5414282
regulation of I-kappaB kinase/NF-kappaB signaling (GO:0043122)	0.03163554	0.085544727	26.72012408
positive regulation of protein insertion into mitochondrial membrane involved in	0.03201674	0.085544727	114.4297551
TOR signaling (GO:0031929)	0.03201674	0.085544727	114.4297551
negative regulation of macroautophagy (GO:0016242)	0.03201674	0.085544727	114.4297551
regulation of protein insertion into mitochondrial membrane involved in apoptotic	0.03201674	0.085544727	114.4297551
cytoplasmic pattern recognition receptor signaling pathway (GO:0002753)	0.03322829	0.086602408	108.8356587
positive regulation of mitotic cell cycle (GO:0045931)	0.03322829	0.086602408	108.8356587
regulation of autophagy (GO:0010506)	0.03347054	0.086602408	25.47139968
macromolecule catabolic process (GO:0009057)	0.03443839	0.086602408	103.6983082

nucleotide-binding oligomerization domain containing signaling pathway	0.03443839	0.086602408	103.6983082
regulation of phosphatase activity (GO:0010921)	0.03443839	0.086602408	103.6983082
regulation of DNA-templated transcription, elongation (GO:0032784)	0.03443839	0.086602408	103.6983082
cellular response to acid chemical (GO:0071229)	0.03443839	0.086602408	103.6983082
positive regulation of extrinsic apoptotic signaling pathway (GO:2001238)	0.03564703	0.088342628	98.96590014
positive regulation of viral genome replication (GO:0045070)	0.03564703	0.088342628	98.96590014
maturation of SSU-rRNA from tricistronic rRNA transcript (SSU-rRNA, 5.8S rRNA,	0.03685421	0.090677273	94.59405782
activation of protein kinase B activity (GO:0032148)	0.03805995	0.091665515	90.54455793
regulation of cellular component size (GO:0032535)	0.03805995	0.091665515	90.54455793
negative regulation of proteasomal ubiquitin-dependent protein catabolic process	0.03805995	0.091665515	90.54455793
liver development (GO:0001889)	0.03926424	0.091845052	86.7843089
response to amino acid (GO:0043200)	0.03926424	0.091845052	86.7843089
hematopoietic progenitor cell differentiation (GO:0002244)	0.03926424	0.091845052	86.7843089
protein K63-linked deubiquitination (GO:0070536)	0.03926424	0.091845052	86.7843089
signal transduction by p53 class mediator (GO:0072331)	0.04046708	0.091845052	83.28452527
lytic vacuole organization (GO:0080171)	0.04046708	0.091845052	83.28452527
negative regulation of JNK cascade (GO:0046329)	0.04046708	0.091845052	83.28452527
mitotic G2 DNA damage checkpoint signaling (GO:0007095)	0.04046708	0.091845052	83.28452527
positive regulation of protein dephosphorylation (GO:0035307)	0.04166848	0.091845052	80.0200556
cellular response to amino acid stimulus (GO:0071230)	0.04166848	0.091845052	80.0200556
positive regulation of mitochondrial outer membrane permeabilization involved in	0.04166848	0.091845052	80.0200556
positive regulation of cell cycle G1/S phase transition (GO:1902808)	0.04286843	0.091845052	76.96883173
maturation of SSU-rRNA (GO:0030490)	0.04286843	0.091845052	76.96883173
regulation of lipid biosynthetic process (GO:0046890)	0.04286843	0.091845052	76.96883173
positive regulation of lipid biosynthetic process (GO:0046889)	0.04286843	0.091845052	76.96883173
intrinsic apoptotic signaling pathway by p53 class mediator (GO:0072332)	0.04406694	0.091845052	74.11141474
regulation of microtubule-based process (GO:0032886)	0.04406694	0.091845052	74.11141474
regulation of cell cycle G1/S phase transition (GO:1902806)	0.04406694	0.091845052	74.11141474
regulation of osteoclast differentiation (GO:0045670)	0.04406694	0.091845052	74.11141474

regulation of protein import into nucleus (GO:0042306)	0.04406694	0.091845052	74.11141474
positive regulation of cell migration (GO:0030335)	0.04413124	0.091845052	20.02948517
negative regulation of stress-activated MAPK cascade (GO:0032873)	0.045264	0.091845052	71.43061834
positive regulation of cytokinesis (GO:0032467)	0.045264	0.091845052	71.43061834
regulation of microtubule cytoskeleton organization (GO:0070507)	0.045264	0.091845052	71.43061834
regulation of p38MAPK cascade (GO:1900744)	0.045264	0.091845052	71.43061834
negative regulation of ubiquitin-dependent protein catabolic process (GO:2000059)	0.04645963	0.091845052	68.91119481
lysosome organization (GO:0007040)	0.04645963	0.091845052	68.91119481
regulation of apoptotic signaling pathway (GO:2001233)	0.04645963	0.091845052	68.91119481
connective tissue development (GO:0061448)	0.04645963	0.091845052	68.91119481
regulation of phosphoprotein phosphatase activity (GO:0043666)	0.04645963	0.091845052	68.91119481
negative regulation of proteasomal protein catabolic process (GO:1901799)	0.04645963	0.091845052	68.91119481
stem cell differentiation (GO:0048863)	0.04884658	0.094381525	64.30363063
positive regulation of wound healing (GO:0090303)	0.04884658	0.094381525	64.30363063
response to organonitrogen compound (GO:0010243)	0.04884658	0.094381525	64.30363063
ribosomal small subunit biogenesis (GO:0042274)	0.04884658	0.094381525	64.30363063
epithelial cell migration (GO:0010631)	0.0500379	0.096140235	62.19251854
nucleic acid-templated transcription (GO:0097659)	0.05122779	0.096795049	60.19648932
positive regulation of epithelial to mesenchymal transition (GO:0010718)	0.05122779	0.096795049	60.19648932
negative regulation of protein catabolic process (GO:0042177)	0.05122779	0.096795049	60.19648932
negative regulation of type I interferon production (GO:0032480)	0.05241625	0.098496465	58.30676718
positive regulation of biosynthetic process (GO:0009891)	0.05360328	0.099093625	56.51543007
positive regulation of cell division (GO:0051781)	0.05360328	0.099093625	56.51543007
intracellular protein transmembrane transport (GO:0065002)	0.05360328	0.099093625	56.51543007
positive regulation of RNA metabolic process (GO:0051254)	0.05478888	0.100202119	54.81530943
mitotic G2/M transition checkpoint (GO:0044818)	0.05478888	0.100202119	54.81530943
regulation of protein localization to nucleus (GO:1900180)	0.05715581	0.103974922	51.66330276
cellular macromolecule biosynthetic process (GO:0034645)	0.05815866	0.105006841	15.5889034
negative regulation of MAP kinase activity (GO:0043407)	0.05833713	0.105006841	50.20012391

aminoglycan biosynthetic process (GO:0006023)	0.05951704	0.10601473	48.80545398
positive regulation of actin filament polymerization (GO:0030838)	0.05951704	0.10601473	48.80545398
regulation of cellular component movement (GO:0051270)	0.06069553	0.107553737	47.4748002
negative regulation of protein ubiquitination (GO:0031397)	0.0618726	0.109074378	46.2040466
ameboidal-type cell migration (GO:0001667)	0.06304826	0.109454331	44.9894157
regulation of intrinsic apoptotic signaling pathway (GO:2001242)	0.06304826	0.109454331	44.9894157
cartilage development (GO:0051216)	0.06304826	0.109454331	44.9894157
regulation of apoptotic process (GO:0042981)	0.0638483	0.110283423	9.765584153
glycosaminoglycan metabolic process (GO:0030203)	0.06539532	0.111826002	42.71490646
regulation of cyclin-dependent protein kinase activity (GO:1904029)	0.06539532	0.111826002	42.71490646
negative regulation of protein modification by small protein conjugation or removal	0.06656674	0.11326281	41.6488814
telomere maintenance (GO:0000723)	0.06773675	0.114118064	40.62663584
positive regulation of establishment of protein localization to mitochondrion	0.06773675	0.114118064	40.62663584
regulation of tumor necrosis factor-mediated signaling pathway (GO:0010803)	0.07007254	0.117474548	38.70359077
negative regulation of autophagy (GO:0010507)	0.07123833	0.117698102	37.79829279
positive regulation of apoptotic signaling pathway (GO:2001235)	0.07123833	0.117698102	37.79829279
mitotic DNA damage checkpoint signaling (GO:0044773)	0.07123833	0.117698102	37.79829279
apical junction assembly (GO:0043297)	0.07240271	0.118477161	36.92774584
ribonucleoprotein complex biogenesis (GO:0022613)	0.07240271	0.118477161	36.92774584
positive regulation of viral process (GO:0048524)	0.07588746	0.123588152	34.50654989
regulation of extrinsic apoptotic signaling pathway (GO:2001236)	0.07704625	0.123708064	33.75754823
regulation of cilium assembly (GO:1902017)	0.07704625	0.123708064	33.75754823
protein catabolic process (GO:0030163)	0.07704625	0.123708064	33.75754823
tRNA modification (GO:0006400)	0.07820364	0.123931499	33.03513646
cellular response to nutrient levels (GO:0031669)	0.07935964	0.123931499	32.33799172
positive regulation of cell cycle (GO:0045787)	0.07935964	0.123931499	32.33799172
negative regulation of G2/M transition of mitotic cell cycle (GO:0010972)	0.07935964	0.123931499	32.33799172
cell-cell junction assembly (GO:0007043)	0.07935964	0.123931499	32.33799172
regulation of protein localization (GO:0032880)	0.07935964	0.123931499	32.33799172

regulation of viral genome replication (GO:0045069)	0.08051425	0.125163066	31.66487558
negative regulation of programmed cell death (GO:0043069)	0.08147401	0.12581205	11.27369654
positive regulation of protein localization to nucleus (GO:1900182)	0.08166747	0.12581205	31.01462747
positive regulation of macromolecule metabolic process (GO:0010604)	0.08257821	0.126447326	11.12340712
cellular response to decreased oxygen levels (GO:0036294)	0.0828193	0.126447326	30.38615875
regulation of plasma membrane bounded cell projection assembly (GO:0120032)	0.08396974	0.12763401	29.77844728
Fc-gamma receptor signaling pathway involved in phagocytosis (GO:0038096)	0.0851188	0.128240661	29.19053247
gland development (GO:0048732)	0.0851188	0.128240661	29.19053247
Fc-gamma receptor signaling pathway (GO:0038094)	0.08626648	0.129399712	28.6215108
regulation of hydrolase activity (GO:0051336)	0.08741277	0.129430451	28.07053167
regulation of actin filament-based process (GO:0032970)	0.08741277	0.129430451	28.07053167
phosphorylation (GO:0016310)	0.08854654	0.129430451	10.36903918
Fc receptor mediated stimulatory signaling pathway (GO:0002431)	0.08855768	0.129430451	27.53679363
regulation of cytokine-mediated signaling pathway (GO:0001959)	0.08855768	0.129430451	27.53679363
cellular response to amino acid starvation (GO:0034198)	0.08855768	0.129430451	27.53679363
response to amino acid starvation (GO:1990928)	0.08970121	0.130543888	27.01954096
regulation of epithelial to mesenchymal transition (GO:0010717)	0.09084336	0.131645892	26.51806044
positive regulation of protein modification by small protein conjugation or removal	0.09198414	0.132178894	26.03167848
regulation of organelle assembly (GO:1902115)	0.09198414	0.132178894	26.03167848
negative regulation of protein serine/threonine kinase activity (GO:0071901)	0.09312355	0.133212645	25.55975844
positive regulation of proteasomal ubiquitin-dependent protein catabolic process	0.09426158	0.133212645	25.10169813
regulation of neuron differentiation (GO:0045664)	0.09426158	0.133212645	25.10169813
regulation of cellular response to heat (GO:1900034)	0.09426158	0.133212645	25.10169813
negative regulation of cell cycle (GO:0045786)	0.09539824	0.133713927	24.65692758
regulation of NIK/NF-kappaB signaling (GO:1901222)	0.09539824	0.133713927	24.65692758
positive regulation of cellular amide metabolic process (GO:0034250)	0.09653353	0.134145661	24.22490692
negative regulation of protein modification process (GO:0031400)	0.09653353	0.134145661	24.22490692
positive regulation of protein ubiquitination (GO:0031398)	0.09766746	0.134145661	23.80512445
regulation of cyclin-dependent protein serine/threonine kinase activity (GO:0000079)	0.09766746	0.134145661	23.80512445

ephrin receptor signaling pathway (GO:0048013)	0.09766746	0.134145661	23.80512445
regulation of cytokinesis (GO:0032465)	0.09993121	0.136705888	23.00035749
positive regulation of proteasomal protein catabolic process (GO:1901800)	0.1021895	0.138685753	22.23903168
negative regulation of phosphorylation (GO:0042326)	0.1021895	0.138685753	22.23903168
protein targeting to membrane (GO:0006612)	0.10331661	0.139661188	21.87363238
regulation of type I interferon production (GO:0032479)	0.10556675	0.141583644	21.17147993
mitochondrial translational elongation (GO:0070125)	0.10556675	0.141583644	21.17147993
positive regulation of autophagy (GO:0010508)	0.10668979	0.141976295	20.83402802
negative regulation of protein kinase activity (GO:0006469)	0.10668979	0.141976295	20.83402802
regulation of actin cytoskeleton organization (GO:0032956)	0.10781147	0.142912882	20.50522053
negative regulation of cellular protein metabolic process (GO:0032269)	0.11116842	0.145112971	19.56763781
cotranslational protein targeting to membrane (GO:0006613)	0.11116842	0.145112971	19.56763781
positive regulation of epithelial cell migration (GO:0010634)	0.11116842	0.145112971	19.56763781
negative regulation of MAPK cascade (GO:0043409)	0.11116842	0.145112971	19.56763781
regulation of MAP kinase activity (GO:0043405)	0.11451323	0.148346688	18.69751865
glycosaminoglycan biosynthetic process (GO:0006024)	0.11451323	0.148346688	18.69751865
positive regulation of cell population proliferation (GO:0008284)	0.11771219	0.151516239	7.687346326
positive regulation of translation (GO:0045727)	0.11784596	0.151516239	17.88820673
positive regulation of cell cycle process (GO:0090068)	0.1189542	0.15179119	17.6309201
positive regulation of protein localization to membrane (GO:1905477)	0.1189542	0.15179119	17.6309201
intrinsic apoptotic signaling pathway (GO:0097193)	0.12006109	0.15179119	17.37953892
positive regulation of cellular protein metabolic process (GO:0032270)	0.12006109	0.15179119	17.37953892
positive regulation of gene expression (GO:0010628)	0.12100184	0.15179119	7.458778243
protein targeting to ER (GO:0045047)	0.12116665	0.15179119	17.13387384
cellular response to organonitrogen compound (GO:0071417)	0.12116665	0.15179119	17.13387384
negative regulation of apoptotic process (GO:0043066)	0.12224161	0.152060511	7.375537535
translational elongation (GO:0006414)	0.12227088	0.152060511	16.89374333
regulation of JNK cascade (GO:0046328)	0.12337377	0.152324298	16.65897326
mitochondrial translation (GO:0032543)	0.12337377	0.152324298	16.65897326

protein phosphorylation (GO:0006468)	0.12681534	0.156010233	7.081274237
regulation of protein serine/threonine kinase activity (GO:0071900)	0.12996326	0.159309798	15.35401603
regulation of macroautophagy (GO:0016241)	0.13105687	0.160076605	15.15244359
activation of protein kinase activity (GO:0032147)	0.13324014	0.161589106	14.7617593
histone modification (GO:0016570)	0.13324014	0.161589106	14.7617593
cellular protein modification process (GO:0006464)	0.13404482	0.161990558	5.081959176
regulation of cellular response to stress (GO:0080135)	0.13759089	0.165690441	14.02697939
positive regulation of intracellular signal transduction (GO:1902533)	0.14811129	0.17773355	5.931770318
positive regulation of macromolecule biosynthetic process (GO:0010557)	0.14944763	0.178710101	12.28039109
cellular response to hypoxia (GO:0071456)	0.15158652	0.180636199	11.99985643
regulation of cell motility (GO:2000145)	0.15372024	0.182542789	11.72929835
regulation of cellular component organization (GO:0051128)	0.16009055	0.189449722	10.97273388
positive regulation of cellular catabolic process (GO:0031331)	0.16220374	0.191288552	10.7374769
protein localization to organelle (GO:0033365)	0.16325842	0.191870723	10.6228004
positive regulation of intracellular protein transport (GO:0090316)	0.16955978	0.198593991	9.973291337
actin filament organization (GO:0007015)	0.17373535	0.202100307	9.574062632
negative regulation of protein phosphorylation (GO:0001933)	0.17373535	0.202100307	9.574062632
positive regulation of NF-kappaB transcription factor activity (GO:0051092)	0.1768538	0.205030501	9.290728574
regulation of cell differentiation (GO:0045595)	0.17789076	0.205535949	9.199173872
skeletal system development (GO:0001501)	0.17996094	0.206532351	9.020216702
cellular response to starvation (GO:0009267)	0.17996094	0.206532351	9.020216702
protein autophosphorylation (GO:0046777)	0.18099415	0.207023405	8.932756208
positive regulation of transcription, DNA-templated (GO:0045893)	0.18162393	0.207051278	3.705026765
positive regulation of cellular process (GO:0048522)	0.18313632	0.208081795	4.5851761
rRNA metabolic process (GO:0016072)	0.18408628	0.208468572	8.678115112
negative regulation of canonical Wnt signaling pathway (GO:0090090)	0.18716721	0.21125804	8.43453772
positive regulation of I-kappaB kinase/NF-kappaB signaling (GO:0043123)	0.19329559	0.217457543	7.977991301
rRNA processing (GO:0006364)	0.19532851	0.219024103	7.834237857
positive regulation of cellular biosynthetic process (GO:0031328)	0.20240507	0.226217432	7.361219511

negative regulation of cytokine production (GO:0001818)	0.20441595	0.227720695	7.234098293
negative regulation of Wnt signaling pathway (GO:0030178)	0.21340481	0.236962485	6.701580386
negative regulation of macromolecule metabolic process (GO:0010605)	0.21637937	0.238715309	6.537293537
regulation of programmed cell death (GO:0043067)	0.21637937	0.238715309	6.537293537
negative regulation of intracellular signal transduction (GO:1902532)	0.22032866	0.242290684	6.327600165
ncRNA processing (GO:0034470)	0.22327808	0.244747129	6.176957217
phosphate-containing compound metabolic process (GO:0006796)	0.23400125	0.255681881	5.668602472
translation (GO:0006412)	0.23593559	0.256974433	5.582983159
regulation of cell growth (GO:0001558)	0.23882831	0.259299303	5.458158359
positive regulation of cell motility (GO:2000147)	0.24266891	0.261806835	5.298146134
transcription, DNA-templated (GO:0006351)	0.24266891	0.261806835	5.298146134
regulation of cell population proliferation (GO:0042127)	0.24729816	0.265962171	3.063294031
apoptotic process (GO:0006915)	0.2521892	0.27037212	4.927578234
membrane organization (GO:0061024)	0.2625288	0.28057766	4.562956866
positive regulation of DNA-binding transcription factor activity (GO:0051091)	0.26625452	0.283673043	4.440265277
regulation of canonical Wnt signaling pathway (GO:0060828)	0.27273109	0.289670911	4.237017552
positive regulation of cell differentiation (GO:0045597)	0.27732357	0.293636725	4.100149408
regulation of protein phosphorylation (GO:0001932)	0.28461369	0.300425562	3.894344225
protein deubiquitination (GO:0016579)	0.28551998	0.300454867	3.869691995
protein modification by small protein removal (GO:0070646)	0.29362709	0.30803824	3.657766766
proteolysis (GO:0006508)	0.30341591	0.317334066	3.421052074
innate immune response (GO:0045087)	0.31655462	0.330066101	3.132641853
positive regulation of apoptotic process (GO:0043065)	0.32346433	0.33624559	2.993035924
negative regulation of gene expression (GO:0010629)	0.33370328	0.345667743	2.799886475
cellular response to oxygen-containing compound (GO:1901701)	0.33454978	0.345667743	2.784606323
positive regulation of multicellular organismal process (GO:0051240)	0.35291365	0.363543574	2.476539776
cellular response to DNA damage stimulus (GO:0006974)	0.35701888	0.366668037	2.41333869
gene expression (GO:0010467)	0.36191216	0.370580713	2.340476601
positive regulation of protein phosphorylation (GO:0001934)	0.37398945	0.381804158	2.171403176

regulation of gene expression (GO:0010468)	0.39377223	0.400803874	1.422034472
transmembrane receptor protein tyrosine kinase signaling pathway (GO:0007169)	0.39979185	0.405723478	1.855234669
regulation of cell migration (GO:0030334)	0.40284913	0.407616577	1.821364821
negative regulation of cellular process (GO:0048523)	0.5123415	0.516875498	0.95727927
positive regulation of transcription by RNA polymerase II (GO:0045944)	0.6872287	0.69127122	0.328563984
regulation of transcription by RNA polymerase II (GO:0006357)	0.94626041	0.94903537	0.018548183
regulation of transcription, DNA-templated (GO:0006355)	0.94905891	0.949058906	0.017222231

Table 3.S7. High confidence hits obtained in C1orf27-miniturboID proteomics related to Figure 3.4

Bait	Condition	Prey	Spec	SpecSum	AvgSpec	AvgP	SaintScore	FoldChange	BFDR
C1orf27	NT	UFSP2	86|83|95	264	88	**1**	1	**880**	0
C1orf27	NT	MTDH	58|64|49	171	57	**1**	1	**570**	0
C1orf27	NT	DDRGK1	52|51|54	157	52.33	**1**	1	**523.33**	0
C1orf27	NT	CAMLG	18|20|20	58	19.33	**1**	1	**193.33**	0
C1orf27	NT	KTN1	13|10|11	34	11.33	**1**	1	**113.33**	0
C1orf27	NT	TK1	10|10|10	30	10	**1**	1	**100**	0
C1orf27	NT	ANKLE2	11|9|8	28	9.33	**1**	1	**93.33**	0
C1orf27	NT	VEZT	7|8|8	23	7.67	**1**	1	**76.67**	0
C1orf27	NT	MAVS	7|7|8	22	7.33	**1**	1	**73.33**	0
C1orf27	NT	VAPB	6|7|8	21	7	**1**	1	**70**	0
C1orf27	NT	TACC1	5|7|8	20	6.67	**1**	1	**66.67**	0
C1orf27	NT	BCAP31	34|35|32	101	33.67	**1**	1	**33.67**	0
C1orf27	NT	STIM1	101|91|93	285	95	**1**	1	**11.88**	0
C1orf27	NT	EMD	61|60|66	187	62.33	**1**	1	**6.45**	0
C1orf27	NT	SRPRA	92|95|101	288	96	**1**	1	**4.72**	0
C1orf27	NT	RRM1	6|5|3	14	4.67	**0.99**	0.99	**46.67**	0
C1orf27	NT	CAMK2D	3|6|4	13	4.33	**0.99**	0.99	**43.33**	0
C1orf27	NT	CLCC1	3|5|4	12	4	**0.99**	0.99	**40**	0
C1orf27	NT	CDKAL1	4|4|3	11	3.67	**0.99**	0.99	**36.67**	0
C1orf27	NT	RTN4	13|9|12	34	11.33	**0.99**	0.99	**17**	0
C1orf27	NT	TMEM263	3|3|5	11	3.67	**0.98**	0.98	**36.67**	0
C1orf27	NT	SNUPN	3|3|4	10	3.33	**0.98**	0.98	**33.33**	0
C1orf27	NT	PSMA4	4|2|4	10	3.33	**0.94**	0.94	**33.33**	0.01
C1orf27	NT	LEMD3	11|10|6	27	9	**0.94**	0.94	**6.75**	0.01
C1orf27	NT	SYAP1	16|16|17	49	16.33	**0.94**	0.94	**3.5**	0.01

C1orf27	NT	SRPRB	25|23|25	73	24.33	**0.94**	0.94	**3.04**	0.01
C1orf27	NT	AKAP1	3|3|2	8	2.67	**0.92**	0.92	**26.67**	0.01
C1orf27	NT	VAPA	3|2|3	8	2.67	**0.92**	0.92	**26.67**	0.01
C1orf27	NT	RANBP1	3|3|2	8	2.67	**0.92**	0.92	**26.67**	0.01
C1orf27	NT	TOR1AIP1	10|11|12	33	11	**0.9**	0.9	**11**	0.02
C1orf27	NT	DAP3	2|2|4	8	2.67	**0.88**	0.88	**26.67**	0.02
C1orf27	NT	FKBP8	11|10|10	31	10.33	**0.69**	0.69	**3.44**	0.03
C1orf27	NT	HIST2H2AA4	33|26|0	59	19.67	**0.67**	0.67	**196.67**	0.04
C1orf27	NT	RDX	15|14|0	29	9.67	**0.67**	0.67	**96.67**	0.04
C1orf27	NT	MTCL1	0|11|12	23	7.67	**0.67**	0.67	**76.67**	0.05
C1orf27	NT	AP3B2	8|0|10	18	6	**0.67**	0.67	**60**	0.06
C1orf27	NT	LYN	8|0|8	16	5.33	**0.67**	0.67	**53.33**	0.07
C1orf27	NT	SYNE2	6|0|10	16	5.33	**0.67**	0.67	**53.33**	0.08
C1orf27	NT	MAPK1	6|5|0	11	3.67	**0.67**	0.67	**36.67**	0.08
C1orf27	NT	CDC123	5|5|0	10	3.33	**0.67**	0.67	**33.33**	0.09
C1orf27	NT	STX18	4|4|0	8	2.67	**0.66**	0.66	**26.67**	0.09
C1orf27	NT	CDK5RAP3	4|4|0	8	2.67	**0.66**	0.66	**26.67**	0.09
C1orf27	NT	ITPR2	4|0|4	8	2.67	**0.66**	0.66	**26.67**	0.09
C1orf27	NT	STIM2	3|0|5	8	2.67	**0.66**	0.66	**26.67**	0.12
C1orf27	NT	TEX264	0|4|4	8	2.67	**0.66**	0.66	**26.67**	0.09
C1orf27	NT	PPP1R15B	3|0|4	7	2.33	**0.65**	0.65	**23.33**	0.12
C1orf27	NT	TMEM214	3|0|4	7	2.33	**0.65**	0.65	**23.33**	0.12
C1orf27	NT	ADGRV1	4|0|3	7	2.33	**0.65**	0.65	**23.33**	0.12
C1orf27	NT	NRDC	4|3|0	7	2.33	**0.65**	0.65	**23.33**	0.12
C1orf27	NT	LOC107986255	3|4|0	7	2.33	**0.65**	0.65	**23.33**	0.12
C1orf27	NT	HLA-A	3|0|3	6	2	**0.64**	0.64	**20**	0.14
C1orf27	NT	HLTF	3|3|0	6	2	**0.64**	0.64	**20**	0.14

C1orf27	NT	BLNK	0|3|3	6	2	**0.64**	0.64	**20**	0.14
C1orf27	NT	BIRC2	2|0|5	7	2.33	**0.61**	0.61	**23.33**	0.16
C1orf27	NT	FADS2	4|0|2	6	2	**0.61**	0.61	**20**	0.16
C1orf27	NT	TOR1AIP2	4|0|2	6	2	**0.61**	0.61	**20**	0.16
C1orf27	NT	PTGES3L-AARSD1	3|2|0	5	1.67	**0.6**	0.6	**16.67**	0.17
C1orf27	NT	MOSPD2	2|0|3	5	1.67	**0.6**	0.6	**16.67**	0.17
C1orf27	NT	SCD	3|2|0	5	1.67	**0.6**	0.6	**16.67**	0.17
C1orf27	NT	MRPL27	3|2|0	5	1.67	**0.6**	0.6	**16.67**	0.17
C1orf27	NT	LSG1	3|0|2	5	1.67	**0.6**	0.6	**16.67**	0.17
C1orf27	NT	MAPK8	2|0|3	5	1.67	**0.6**	0.6	**16.67**	0.17
C1orf27	NT	ABHD14B	0|2|3	5	1.67	**0.6**	0.6	**16.67**	0.17
C1orf27	NT	SPTLC1	0|2|3	5	1.67	**0.6**	0.6	**16.67**	0.17
C1orf27	NT	UQCR10	0|2|3	5	1.67	**0.6**	0.6	**16.67**	0.17
C1orf27	NT	KIF4B	2|2|0	4	1.33	**0.55**	0.55	**13.33**	0.2
C1orf27	NT	ADSS	2|2|0	4	1.33	**0.55**	0.55	**13.33**	0.2
C1orf27	NT	JPH1	2|2|0	4	1.33	**0.55**	0.55	**13.33**	0.2
C1orf27	NT	CNP	2|2|0	4	1.33	**0.55**	0.55	**13.33**	0.2
C1orf27	NT	RRAGB	2|2|0	4	1.33	**0.55**	0.55	**13.33**	0.2
C1orf27	NT	RRP7A	2|0|2	4	1.33	**0.55**	0.55	**13.33**	0.2
C1orf27	NT	MRPS30	2|0|2	4	1.33	**0.55**	0.55	**13.33**	0.2
C1orf27	NT	FOXP2	2|2|0	4	1.33	**0.55**	0.55	**13.33**	0.2
C1orf27	NT	IDE	2|2|0	4	1.33	**0.55**	0.55	**13.33**	0.2
C1orf27	NT	VPS26C	2|0|2	4	1.33	**0.55**	0.55	**13.33**	0.2
C1orf27	NT	APBB1	2|0|2	4	1.33	**0.55**	0.55	**13.33**	0.2
C1orf27	NT	ND4	2|2|0	4	1.33	**0.55**	0.55	**13.33**	0.2
C1orf27	NT	AK4	2|0|2	4	1.33	**0.55**	0.55	**13.33**	0.2
C1orf27	NT	DNAJA2	2|2|0	4	1.33	**0.55**	0.55	**13.33**	0.2

C1orf27	NT	TARS2	4|3|7	14	4.67	**0.54**	0.54	**7**	0.25
C1orf27	NT	IDI1	5|6|4	15	5	**0.51**	0.51	**3.75**	0.25
Bait	**Condition**	**Prey**	**Spec**	**SpecSum**	**AvgSpec**	**AvgP**	**SaintScore**	**FoldChange**	**BFDR**
C1orf27	Cisplatin	UFSP2	86|94|73	253	84.33	**1**	1	**843.33**	0
C1orf27	Cisplatin	HDC	50|75|62	187	62.33	**1**	1	**623.33**	0
C1orf27	Cisplatin	MTDH	67|59|59	185	61.67	**1**	1	**616.67**	0
C1orf27	Cisplatin	DDRGK1	56|57|49	162	54	**1**	1	**540**	0
C1orf27	Cisplatin	KTN1	16|26|17	59	19.67	**1**	1	**196.67**	0
C1orf27	Cisplatin	GNB2	9|12|11	32	10.67	**1**	1	**106.67**	0
C1orf27	Cisplatin	RTN4	8|13|10	31	10.33	**1**	1	**103.33**	0
C1orf27	Cisplatin	ANKLE2	13|11|7	31	10.33	**1**	1	**103.33**	0
C1orf27	Cisplatin	VAPB	9|9|7	25	8.33	**1**	1	**83.33**	0
C1orf27	Cisplatin	MAVS	8|7|8	23	7.67	**1**	1	**76.67**	0
C1orf27	Cisplatin	CCDC88C	5|9|5	19	6.33	**1**	1	**63.33**	0
C1orf27	Cisplatin	TACC1	8|4|5	17	5.67	**1**	1	**56.67**	0
C1orf27	Cisplatin	CDKAL1	7|4|4	15	5	**1**	1	**50**	0
C1orf27	Cisplatin	POTEA	5|4|4	13	4.33	**1**	1	**43.33**	0
C1orf27	Cisplatin	CAMLG	23|21|20	64	21.33	**1**	1	**21.33**	0
C1orf27	Cisplatin	BCAP31	35|32|36	103	34.33	**1**	1	**17.17**	0
C1orf27	Cisplatin	STIM1	102|95|87	284	94.67	**1**	1	**12.91**	0
C1orf27	Cisplatin	EMD	63|62|56	181	60.33	**1**	1	**7.54**	0
C1orf27	Cisplatin	SRPRA	95|96|87	278	92.67	**1**	1	**4.63**	0
C1orf27	Cisplatin	TMPO	109|108|104	321	107	**1**	1	**2.87**	0
C1orf27	Cisplatin	MORC3	3|5|5	13	4.33	**0.99**	0.99	**43.33**	0
C1orf27	Cisplatin	SPCS2	4|4|4	12	4	**0.99**	0.99	**40**	0
C1orf27	Cisplatin	SNAP47	4|5|3	12	4	**0.99**	0.99	**40**	0

C1orf27	Cisplatin	TMEM263	3|4|4	11	3.67	**0.99**	0.99	**36.67**	0
C1orf27	Cisplatin	VAPA	4|4|3	11	3.67	**0.99**	0.99	**36.67**	0
C1orf27	Cisplatin	SEC16A	56|49|50	155	51.67	**0.99**	0.99	**2.98**	0
C1orf27	Cisplatin	ERGIC1	3|3|4	10	3.33	**0.98**	0.98	**33.33**	0
C1orf27	Cisplatin	SRP54	18|17|20	55	18.33	**0.98**	0.98	**3.67**	0
C1orf27	Cisplatin	PSMA4	4|4|2	10	3.33	**0.94**	0.94	**33.33**	0
C1orf27	Cisplatin	TEX264	4|4|2	10	3.33	**0.94**	0.94	**33.33**	0
C1orf27	Cisplatin	SBF1	2|3|3	8	2.67	**0.93**	0.93	**26.67**	0.01
C1orf27	Cisplatin	SYAP1	21|18|16	55	18.33	**0.9**	0.9	**6.11**	0.01
C1orf27	Cisplatin	TOR1AIP2	2|5|2	9	3	**0.89**	0.89	**30**	0.01
C1orf27	Cisplatin	JPH1	3|2|2	7	2.33	**0.88**	0.88	**23.33**	0.02
C1orf27	Cisplatin	MTFP1	2|2|3	7	2.33	**0.88**	0.88	**23.33**	0.02
C1orf27	Cisplatin	LRRC59	3|2|2	7	2.33	**0.88**	0.88	**23.33**	0.02
C1orf27	Cisplatin	TMEM214	2|3|2	7	2.33	**0.88**	0.88	**23.33**	0.02
C1orf27	Cisplatin	POLDIP2	2|2|2	6	2	**0.84**	0.84	**20**	0.03
C1orf27	Cisplatin	TRABD	2|2|2	6	2	**0.84**	0.84	**20**	0.03
C1orf27	Cisplatin	GRAMD1A	6|8|5	19	6.33	**0.81**	0.81	**9.5**	0.03
C1orf27	Cisplatin	TOR1AIP1	11|11|9	31	10.33	**0.76**	0.76	**7.75**	0.04
C1orf27	Cisplatin	SYNE2	11|8|11	30	10	**0.74**	0.74	**7.5**	0.04
C1orf27	Cisplatin	VEZT	10|14|11	35	11.67	**0.72**	0.72	**7**	0.05
C1orf27	Cisplatin	RAB5B	0|12|10	22	7.33	**0.67**	0.67	**73.33**	0.05
C1orf27	Cisplatin	NAV2	0|12|8	20	6.67	**0.67**	0.67	**66.67**	0.06
C1orf27	Cisplatin	RPS6KA4	0|7|5	12	4	**0.67**	0.67	**40**	0.07
C1orf27	Cisplatin	SYNE1	5|0|6	11	3.67	**0.67**	0.67	**36.67**	0.07
C1orf27	Cisplatin	ABHD11	5|4|0	9	3	**0.66**	0.66	**30**	0.08
C1orf27	Cisplatin	DTNB	5|0|4	9	3	**0.66**	0.66	**30**	0.08
C1orf27	Cisplatin	PSMD10	5|3|0	8	2.67	**0.66**	0.66	**26.67**	0.1
C1orf27	Cisplatin	EXPH5	4|0|4	8	2.67	**0.66**	0.66	**26.67**	0.09

C1orf27	Cisplatin	NRDC	0|4|4	8	2.67	**0.66**	0.66	**26.67**	0.09
C1orf27	Cisplatin	DNAJA2	4|0|3	7	2.33	**0.66**	0.66	**23.33**	0.1
C1orf27	Cisplatin	SHPK	0|3|4	7	2.33	**0.66**	0.66	**23.33**	0.1
C1orf27	Cisplatin	POLR2H	3|0|3	6	2	**0.65**	0.65	**20**	0.11
C1orf27	Cisplatin	TMED5	3|3|0	6	2	**0.65**	0.65	**20**	0.11
C1orf27	Cisplatin	RNF121	3|3|0	6	2	**0.65**	0.65	**20**	0.11
C1orf27	Cisplatin	RRAGB	3|0|3	6	2	**0.65**	0.65	**20**	0.11
C1orf27	Cisplatin	MOSPD2	0|3|3	6	2	**0.65**	0.65	**20**	0.11
C1orf27	Cisplatin	SHMT2	10|13|10	33	11	**0.64**	0.64	**4.71**	0.13
C1orf27	Cisplatin	TKT	7|0|2	9	3	**0.61**	0.61	**30**	0.14
C1orf27	Cisplatin	TRUB1	5|2|0	7	2.33	**0.61**	0.61	**23.33**	0.14
C1orf27	Cisplatin	ELAVL2	2|4|0	6	2	**0.61**	0.61	**20**	0.14
C1orf27	Cisplatin	UTP11	2|4|0	6	2	**0.61**	0.61	**20**	0.14
C1orf27	Cisplatin	TRMT2A	0|4|2	6	2	**0.61**	0.61	**20**	0.14
C1orf27	Cisplatin	DCAF13	2|3|0	5	1.67	**0.6**	0.6	**16.67**	0.15
C1orf27	Cisplatin	RPAP1	2|3|0	5	1.67	**0.6**	0.6	**16.67**	0.15
C1orf27	Cisplatin	CLN6	2|0|3	5	1.67	**0.6**	0.6	**16.67**	0.15
C1orf27	Cisplatin	MRPS10	2|3|0	5	1.67	**0.6**	0.6	**16.67**	0.15
C1orf27	Cisplatin	ABHD12	3|2|0	5	1.67	**0.6**	0.6	**16.67**	0.15
C1orf27	Cisplatin	MRPS28	2|0|3	5	1.67	**0.6**	0.6	**16.67**	0.15
C1orf27	Cisplatin	RNASEH2B	2|0|3	5	1.67	**0.6**	0.6	**16.67**	0.15
C1orf27	Cisplatin	TMEM165	3|2|0	5	1.67	**0.6**	0.6	**16.67**	0.15
C1orf27	Cisplatin	OSBP	2|0|3	5	1.67	**0.6**	0.6	**16.67**	0.15
C1orf27	Cisplatin	AKAP1	0|2|3	5	1.67	**0.6**	0.6	**16.67**	0.15
C1orf27	Cisplatin	UQCRQ	0|3|2	5	1.67	**0.6**	0.6	**16.67**	0.15
C1orf27	Cisplatin	CPD	0|3|2	5	1.67	**0.6**	0.6	**16.67**	0.15
C1orf27	Cisplatin	TENM3	0|2|3	5	1.67	**0.6**	0.6	**16.67**	0.15
C1orf27	Cisplatin	ORMDL1	0|3|2	5	1.67	**0.6**	0.6	**16.67**	0.15

C1orf27	Cisplatin	SCD	2|2|0	4	1.33	**0.56**	0.56	**13.33**	0.2
C1orf27	Cisplatin	REEP5	2|2|0	4	1.33	**0.56**	0.56	**13.33**	0.2
C1orf27	Cisplatin	TMEM41B	2|2|0	4	1.33	**0.56**	0.56	**13.33**	0.2
C1orf27	Cisplatin	UTP6	2|2|0	4	1.33	**0.56**	0.56	**13.33**	0.2
C1orf27	Cisplatin	FADS2	0|2|2	4	1.33	**0.56**	0.56	**13.33**	0.2
C1orf27	Cisplatin	NPM3	0|2|2	4	1.33	**0.56**	0.56	**13.33**	0.2
C1orf27	Cisplatin	PIK3R4	0|2|2	4	1.33	**0.56**	0.56	**13.33**	0.2
C1orf27	Cisplatin	WDR41	0|2|2	4	1.33	**0.56**	0.56	**13.33**	0.2
C1orf27	Cisplatin	RAB3GAP2	24|17|13	54	18	**0.56**	0.56	**4.15**	0.22

Table 3.S8. High confidence hits obtained in UFSP2-miniturboID proteomics.

Bait	Condition	Prey	Spec	SpecSum	AvgSpec	AvgP	SaintScore	FoldChange	BFDR
UFSP2	NT	C1orf27	24|20|16	60	20	**1**	1	**200**	0
UFSP2	NT	DDRGK1	8|13|12	33	11	**1**	1	**110**	0
UFSP2	NT	CAMK2D	8|4|3	15	5	**0.98**	0.98	**50**	0.01
UFSP2	NT	PRKAR1A	3|5|5	13	4.33	**0.98**	0.98	**43.33**	0
UFSP2	NT	CHID1	4|5|3	12	4	**0.98**	0.98	**40**	0.01
UFSP2	NT	NR2F2	3|4|4	11	3.67	**0.98**	0.98	**36.67**	0.01
UFSP2	NT	EXOC1	3|3|6	12	4	**0.97**	0.97	**40**	0.01
UFSP2	NT	PAPSS2	3|3|3	9	3	**0.96**	0.96	**30**	0.01
UFSP2	NT	DAP3	3|3|3	9	3	**0.96**	0.96	**30**	0.01
UFSP2	NT	MB21D2	3|3|3	9	3	**0.96**	0.96	**30**	0.01
UFSP2	NT	RRAGB	3|2|4	9	3	**0.91**	0.91	**30**	0.02
UFSP2	NT	TMEM263	3|3|2	8	2.67	**0.9**	0.9	**26.67**	0.03
UFSP2	NT	NME1	3|3|2	8	2.67	**0.9**	0.9	**26.67**	0.03
UFSP2	NT	HLA-A	2|3|2	7	2.33	**0.83**	0.83	**23.33**	0.04
UFSP2	NT	USP5	2|2|2	6	2	**0.77**	0.77	**20**	0.05
UFSP2	NT	PSIP1	7|0|4	11	3.67	**0.66**	0.66	**36.67**	0.06
UFSP2	NT	RAB2B	5|4|0	9	3	**0.66**	0.66	**30**	0.08
UFSP2	NT	FMR1	5|4|0	9	3	**0.66**	0.66	**30**	0.08
UFSP2	NT	CYTB	4|5|0	9	3	**0.66**	0.66	**30**	0.08
UFSP2	NT	FAR1	4|4|0	8	2.67	**0.66**	0.66	**26.67**	0.12
UFSP2	NT	STK11IP	3|4|0	7	2.33	**0.65**	0.65	**23.33**	0.13
UFSP2	NT	UQCR10	0|4|3	7	2.33	**0.65**	0.65	**23.33**	0.13
UFSP2	NT	TSC1	3|3|0	6	2	**0.64**	0.64	**20**	0.15
UFSP2	NT	PSMA4	3|0|3	6	2	**0.64**	0.64	**20**	0.15
UFSP2	NT	INTS2	3|0|3	6	2	**0.64**	0.64	**20**	0.15

UFSP2	NT	OBSCN	3|0|3	6	2	**0.64**	0.64	**20**	0.15
UFSP2	NT	SETD5	3|0|3	6	2	**0.64**	0.64	**20**	0.15
UFSP2	NT	TENM3	5|0|2	7	2.33	**0.59**	0.59	**23.33**	0.19
UFSP2	NT	MRPS16	2|0|5	7	2.33	**0.59**	0.59	**23.33**	0.19
UFSP2	NT	RPS6KA4	2|5|0	7	2.33	**0.59**	0.59	**23.33**	0.19
UFSP2	NT	ZFP42	2|0|4	6	2	**0.59**	0.59	**20**	0.21
UFSP2	NT	ARHGAP10	4|0|2	6	2	**0.59**	0.59	**20**	0.21
UFSP2	NT	PM20D2	0|2|4	6	2	**0.59**	0.59	**20**	0.21
UFSP2	NT	GOLPH3	0|4|2	6	2	**0.59**	0.59	**20**	0.21
UFSP2	NT	SPNS1	3|0|2	5	1.67	**0.58**	0.58	**16.67**	0.24
UFSP2	NT	PRIM2	2|3|0	5	1.67	**0.58**	0.58	**16.67**	0.24
UFSP2	NT	MED14	2|3|0	5	1.67	**0.58**	0.58	**16.67**	0.24
UFSP2	NT	SNX3	2|0|3	5	1.67	**0.58**	0.58	**16.67**	0.24
UFSP2	NT	EIF5	0|2|3	5	1.67	**0.58**	0.58	**16.67**	0.24
UFSP2	NT	CYB5R1	0|2|3	5	1.67	**0.58**	0.58	**16.67**	0.24
UFSP2	NT	POLDIP2	0|3|2	5	1.67	**0.58**	0.58	**16.67**	0.24
UFSP2	NT	RANBP1	0|3|2	5	1.67	**0.58**	0.58	**16.67**	0.24
UFSP2	NT	AKT1	2|2|0	4	1.33	**0.52**	0.52	**13.33**	0.27
UFSP2	NT	ATPAF1	2|2|0	4	1.33	**0.52**	0.52	**13.33**	0.27
UFSP2	NT	EED	2|2|0	4	1.33	**0.52**	0.52	**13.33**	0.27
UFSP2	NT	PRKCA	2|0|2	4	1.33	**0.52**	0.52	**13.33**	0.27
UFSP2	NT	WASHC2A	2|2|0	4	1.33	**0.52**	0.52	**13.33**	0.27
UFSP2	NT	SHKBP1	2|2|0	4	1.33	**0.52**	0.52	**13.33**	0.27
UFSP2	NT	ALG6	0|2|2	4	1.33	**0.52**	0.52	**13.33**	0.27
UFSP2	NT	MTDH	0|2|2	4	1.33	**0.52**	0.52	**13.33**	0.27
Bait	**Condition**	**Prey**	**Spec**	**SpecSum**	**AvgSpec**	**AvgP**	**SaintScore**	**FoldChange**	**BFDR**
UFSP2	Cisplatin	C1orf27	28|24|19	71	23.67	**1**	1	**236.67**	0

UFSP2	Cisplatin	PTBP3	17|16|15	48	16	**1**	1	**160**	0
UFSP2	Cisplatin	GNB2	11|12|13	36	12	**1**	1	**120**	0
UFSP2	Cisplatin	RNF20	8|9|10	27	9	**1**	1	**90**	0
UFSP2	Cisplatin	DDRGK1	11|10|7	28	9.33	**1**	1	**93.33**	0
UFSP2	Cisplatin	ATP2B4	4|5|7	16	5.33	**1**	1	**53.33**	0
UFSP2	Cisplatin	CCDC88C	5|4|7	16	5.33	**1**	1	**53.33**	0
UFSP2	Cisplatin	FMR1	5|4|6	15	5	**1**	1	**50**	0
UFSP2	Cisplatin	PRIM2	4|4|4	12	4	**0.99**	0.99	**40**	0
UFSP2	Cisplatin	PRKAR1A	3|5|6	14	4.67	**0.99**	0.99	**46.67**	0
UFSP2	Cisplatin	RPS6KA4	3|4|7	14	4.67	**0.99**	0.99	**46.67**	0
UFSP2	Cisplatin	NME1	5|3|4	12	4	**0.99**	0.99	**40**	0
UFSP2	Cisplatin	EVC2	3|4|5	12	4	**0.99**	0.99	**40**	0
UFSP2	Cisplatin	DHCR24	3|4|3	10	3.33	**0.97**	0.97	**33.33**	0.01
UFSP2	Cisplatin	BAP1	4|2|4	10	3.33	**0.93**	0.93	**33.33**	0.01
UFSP2	Cisplatin	PURB	3|3|2	8	2.67	**0.91**	0.91	**26.67**	0.01
UFSP2	Cisplatin	OXA1L	4|2|2	8	2.67	**0.87**	0.87	**26.67**	0.02
UFSP2	Cisplatin	EPS15	2|2|2	6	2	**0.81**	0.81	**20**	0.02
UFSP2	Cisplatin	RAB5B	12|0|13	25	8.33	**0.67**	0.67	**83.33**	0.03
UFSP2	Cisplatin	U2AF1	12|0|10	22	7.33	**0.67**	0.67	**73.33**	0.05
UFSP2	Cisplatin	PRKACB	12|0|8	20	6.67	**0.67**	0.67	**66.67**	0.09
UFSP2	Cisplatin	AHCYL1	9|11|0	20	6.67	**0.67**	0.67	**66.67**	0.06
UFSP2	Cisplatin	AP3B2	9|0|9	18	6	**0.67**	0.67	**60**	0.08
UFSP2	Cisplatin	CTNNB1	5|8|0	13	4.33	**0.67**	0.67	**43.33**	0.11
UFSP2	Cisplatin	YTHDF3	0|6|6	12	4	**0.67**	0.67	**40**	0.1
UFSP2	Cisplatin	ACTN2	0|7|4	11	3.67	**0.66**	0.66	**36.67**	0.12
UFSP2	Cisplatin	KIF13B	0|6|4	10	3.33	**0.66**	0.66	**33.33**	0.13
UFSP2	Cisplatin	PSMD10	4|5|0	9	3	**0.66**	0.66	**30**	0.14
UFSP2	Cisplatin	ERGIC1	0|4|5	9	3	**0.66**	0.66	**30**	0.14

UFSP2	Cisplatin	SEC61A2	4|4|0	8	2.67	**0.66**	0.66	**26.67**	0.15
UFSP2	Cisplatin	GOLGA4	4|0|4	8	2.67	**0.66**	0.66	**26.67**	0.15
UFSP2	Cisplatin	CBX8	0|17|16	33	11	**0.66**	0.66	**3**	0.13
UFSP2	Cisplatin	GLRX3	0|3|6	9	3	**0.65**	0.65	**30**	0.16
UFSP2	Cisplatin	ARFGEF2	5|0|3	8	2.67	**0.65**	0.65	**26.67**	0.17
UFSP2	Cisplatin	SPCS2	4|3|0	7	2.33	**0.65**	0.65	**23.33**	0.18
UFSP2	Cisplatin	ARHGEF40	3|4|0	7	2.33	**0.65**	0.65	**23.33**	0.18
UFSP2	Cisplatin	TMEM263	0|3|4	7	2.33	**0.65**	0.65	**23.33**	0.18
UFSP2	Cisplatin	MB21D2	3|0|3	6	2	**0.64**	0.64	**20**	0.19
UFSP2	Cisplatin	SNX3	3|0|3	6	2	**0.64**	0.64	**20**	0.19
UFSP2	Cisplatin	PDLIM1	3|0|3	6	2	**0.64**	0.64	**20**	0.19
UFSP2	Cisplatin	WDR81	3|0|3	6	2	**0.64**	0.64	**20**	0.19
UFSP2	Cisplatin	RAP1A	18|25|20	63	21	**0.61**	0.61	**5.25**	0.21
UFSP2	Cisplatin	MUC16	2|0|9	11	3.67	**0.6**	0.6	**36.67**	0.21
UFSP2	Cisplatin	TKT	4|0|2	6	2	**0.6**	0.6	**20**	0.21
UFSP2	Cisplatin	MORC3	2|4|0	6	2	**0.6**	0.6	**20**	0.21
UFSP2	Cisplatin	SPTB	0|2|4	6	2	**0.6**	0.6	**20**	0.21
UFSP2	Cisplatin	UBE2S	6|2|7	15	5	**0.59**	0.59	**7.5**	0.26
UFSP2	Cisplatin	KIAA1671	3|0|2	5	1.67	**0.59**	0.59	**16.67**	0.23
UFSP2	Cisplatin	PANK4	3|0|2	5	1.67	**0.59**	0.59	**16.67**	0.23
UFSP2	Cisplatin	POGLUT2	3|0|2	5	1.67	**0.59**	0.59	**16.67**	0.23
UFSP2	Cisplatin	PM20D2	3|0|2	5	1.67	**0.59**	0.59	**16.67**	0.23
UFSP2	Cisplatin	COQ8B	2|3|0	5	1.67	**0.59**	0.59	**16.67**	0.23
UFSP2	Cisplatin	CRYBG3	3|0|2	5	1.67	**0.59**	0.59	**16.67**	0.23
UFSP2	Cisplatin	SPOUT1	0|2|3	5	1.67	**0.59**	0.59	**16.67**	0.23
UFSP2	Cisplatin	ITPR2	0|3|2	5	1.67	**0.59**	0.59	**16.67**	0.23
UFSP2	Cisplatin	SPAG5	0|2|3	5	1.67	**0.59**	0.59	**16.67**	0.23
UFSP2	Cisplatin	CAVIN1	0|3|2	5	1.67	**0.59**	0.59	**16.67**	0.23

UFSP2	Cisplatin	EIF5	2|2|0	4	1.33	**0.54**	0.54	**13.33**	0.26
UFSP2	Cisplatin	KIAA0355	2|0|2	4	1.33	**0.54**	0.54	**13.33**	0.26
UFSP2	Cisplatin	OSBP	2|2|0	4	1.33	**0.54**	0.54	**13.33**	0.26
UFSP2	Cisplatin	SLC39A7	2|2|0	4	1.33	**0.54**	0.54	**13.33**	0.26
UFSP2	Cisplatin	ARHGAP1	2|2|0	4	1.33	**0.54**	0.54	**13.33**	0.26
UFSP2	Cisplatin	ZNF148	2|2|0	4	1.33	**0.54**	0.54	**13.33**	0.26
UFSP2	Cisplatin	RYR1	2|2|0	4	1.33	**0.54**	0.54	**13.33**	0.26
UFSP2	Cisplatin	LPP	0|2|2	4	1.33	**0.54**	0.54	**13.33**	0.26
UFSP2	Cisplatin	LMF2	0|2|2	4	1.33	**0.54**	0.54	**13.33**	0.26
UFSP2	Cisplatin	FHL3	0|2|2	4	1.33	**0.54**	0.54	**13.33**	0.26
UFSP2	Cisplatin	PPP6R3	7|4|8	19	6.33	**0.53**	0.53	**6.33**	0.29

Table 3.S9. High confidence hits obtained in UFL1-miniturboID proteomics.

Bait	Condition	Prey	Spec	SpecSum	AvgSpec	AvgP	SaintScore	FoldChange	BFDR
UFL1	NT	CDK5RAP3	94|91|89	274	91.33	**1**	1	**913.33**	0
UFL1	NT	DDRGK1	82|84|81	247	82.33	**1**	1	**823.33**	0
UFL1	NT	MTDH	88|81|73	242	80.67	**1**	1	**806.67**	0
UFL1	NT	STIM1	86|78|82	246	82	**1**	1	**10.25**	0
UFL1	NT	SRPRA	101|98|92	291	97	**1**	1	**4.93**	0
UFL1	NT	EMD	52|52|50	154	51.33	**1**	1	**7.33**	0
UFL1	NT	BCAP31	31|29|32	92	30.67	**1**	1	**18.4**	0
UFL1	NT	KTN1	21|21|15	57	19	**1**	1	**190**	0
UFL1	NT	PTBP3	16|16|14	46	15.33	**1**	1	**153.33**	0
UFL1	NT	SRP54	41|37|35	113	37.67	**1**	1	**6.28**	0
UFL1	NT	GNB2	16|12|10	38	12.67	**1**	1	**126.67**	0
UFL1	NT	ANKLE2	8|9|8	25	8.33	**1**	1	**83.33**	0
UFL1	NT	LEMD3	10|7|8	25	8.33	**1**	1	**83.33**	0
UFL1	NT	LRRC59	9|7|8	24	8	**1**	1	**80**	0
UFL1	NT	GNA13	6|5|5	16	5.33	**1**	1	**53.33**	0
UFL1	NT	APBB1	4|7|5	16	5.33	**1**	1	**53.33**	0
UFL1	NT	ACTN3	4|5|6	15	5	**1**	1	**50**	0
UFL1	NT	HERC2	15|20|20	55	18.33	**0.99**	0.99	**7.86**	0
UFL1	NT	VEZT	6|6|3	15	5	**0.99**	0.99	**50**	0
UFL1	NT	MRPL16	3|6|4	13	4.33	**0.99**	0.99	**43.33**	0
UFL1	NT	ZNF292	5|3|5	13	4.33	**0.99**	0.99	**43.33**	0
UFL1	NT	CLN3	4|4|3	11	3.67	**0.99**	0.99	**36.67**	0
UFL1	NT	PSMA4	3|3|6	12	4	**0.98**	0.98	**40**	0
UFL1	NT	USP16	3|3|5	11	3.67	**0.98**	0.98	**36.67**	0
UFL1	NT	FNDC3A	5|3|3	11	3.67	**0.98**	0.98	**36.67**	0

UFL1	NT	SNAP47	3|5|3	11	3.67	**0.98**	0.98	**36.67**	0
UFL1	NT	MOSPD2	3|3|3	9	3	**0.97**	0.97	**30**	0.01
UFL1	NT	RNF121	3|3|3	9	3	**0.97**	0.97	**30**	0.01
UFL1	NT	TACC1	2|5|4	11	3.67	**0.94**	0.94	**36.67**	0.01
UFL1	NT	FAR1	4|2|3	9	3	**0.93**	0.93	**30**	0.01
UFL1	NT	SMPD4	4|2|3	9	3	**0.93**	0.93	**30**	0.01
UFL1	NT	RANBP1	2|3|3	8	2.67	**0.93**	0.93	**26.67**	0.01
UFL1	NT	POLR2H	2|3|3	8	2.67	**0.93**	0.93	**26.67**	0.01
UFL1	NT	TMED5	2|3|3	8	2.67	**0.93**	0.93	**26.67**	0.01
UFL1	NT	RPAP3	13|20|14	47	15.67	**0.92**	0.92	**11.75**	0.02
UFL1	NT	ALG6	4|2|2	8	2.67	**0.89**	0.89	**26.67**	0.02
UFL1	NT	TEX264	3|2|2	7	2.33	**0.88**	0.88	**23.33**	0.02
UFL1	NT	CDKAL1	2|2|2	6	2	**0.84**	0.84	**20**	0.02
UFL1	NT	GREB1L	2|2|2	6	2	**0.84**	0.84	**20**	0.02
UFL1	NT	CAMLG	13|16|13	42	14	**0.82**	0.82	**8.4**	0.03
UFL1	NT	RTN4	10|7|4	21	7	**0.79**	0.79	**10.5**	0.04
UFL1	NT	SRPRB	24|28|33	85	28.33	**0.75**	0.75	**3.15**	0.04
UFL1	NT	SOAT1	4|6|6	16	5.33	**0.7**	0.7	**8**	0.04
UFL1	NT	CSNK2A3	16|0|17	33	11	**0.67**	0.67	**110**	0.05
UFL1	NT	RAB12	10|0|13	23	7.67	**0.67**	0.67	**76.67**	0.06
UFL1	NT	LYN	8|7|0	15	5	**0.67**	0.67	**50**	0.06
UFL1	NT	NEB	0|6|6	12	4	**0.67**	0.67	**40**	0.07
UFL1	NT	MUC16	5|5|0	10	3.33	**0.67**	0.67	**33.33**	0.07
UFL1	NT	DTNB	6|4|0	10	3.33	**0.66**	0.66	**33.33**	0.08
UFL1	NT	PRKCA	0|4|5	9	3	**0.66**	0.66	**30**	0.09
UFL1	NT	PSIP1	4|4|0	8	2.67	**0.66**	0.66	**26.67**	0.09
UFL1	NT	PRIM2	0|3|5	8	2.67	**0.66**	0.66	**26.67**	0.1
UFL1	NT	DOCK4	0|5|3	8	2.67	**0.66**	0.66	**26.67**	0.1

UFL1	NT	COL6A1	0|4|4	8	2.67	**0.66**	0.66	**26.67**	0.09
UFL1	NT	EXOC1	3|4|0	7	2.33	**0.65**	0.65	**23.33**	0.11
UFL1	NT	DHX36	3|4|0	7	2.33	**0.65**	0.65	**23.33**	0.11
UFL1	NT	GOLPH3	0|4|3	7	2.33	**0.65**	0.65	**23.33**	0.11
UFL1	NT	EIF5	3|0|3	6	2	**0.65**	0.65	**20**	0.12
UFL1	NT	C1orf27	3|3|0	6	2	**0.65**	0.65	**20**	0.12
UFL1	NT	VAPB	3|0|3	6	2	**0.65**	0.65	**20**	0.12
UFL1	NT	UQCR10	3|0|3	6	2	**0.65**	0.65	**20**	0.12
UFL1	NT	NEURL4	0|3|3	6	2	**0.65**	0.65	**20**	0.12
UFL1	NT	STK11IP	0|3|3	6	2	**0.65**	0.65	**20**	0.12
UFL1	NT	IFI16	0|3|3	6	2	**0.65**	0.65	**20**	0.12
UFL1	NT	RPS6KA4	2|5|0	7	2.33	**0.61**	0.61	**23.33**	0.15
UFL1	NT	CCNB1	4|2|0	6	2	**0.61**	0.61	**20**	0.15
UFL1	NT	DAP3	2|0|3	5	1.67	**0.6**	0.6	**16.67**	0.15
UFL1	NT	POLDIP2	3|2|0	5	1.67	**0.6**	0.6	**16.67**	0.15
UFL1	NT	URB2	3|0|2	5	1.67	**0.6**	0.6	**16.67**	0.15
UFL1	NT	SCD	3|2|0	5	1.67	**0.6**	0.6	**16.67**	0.15
UFL1	NT	lacZ	2|0|3	5	1.67	**0.6**	0.6	**16.67**	0.15
UFL1	NT	INTS2	2|0|3	5	1.67	**0.6**	0.6	**16.67**	0.15
UFL1	NT	COX3	2|0|3	5	1.67	**0.6**	0.6	**16.67**	0.15
UFL1	NT	LSG1	2|3|0	5	1.67	**0.6**	0.6	**16.67**	0.15
UFL1	NT	RPAP1	2|0|3	5	1.67	**0.6**	0.6	**16.67**	0.15
UFL1	NT	NR2F2	0|2|3	5	1.67	**0.6**	0.6	**16.67**	0.15
UFL1	NT	JAGN1	0|2|3	5	1.67	**0.6**	0.6	**16.67**	0.15
UFL1	NT	NME1	0|2|3	5	1.67	**0.6**	0.6	**16.67**	0.15
UFL1	NT	TTF2	0|3|2	5	1.67	**0.6**	0.6	**16.67**	0.15
UFL1	NT	SNX3	0|2|3	5	1.67	**0.6**	0.6	**16.67**	0.15
UFL1	NT	RTN3	2|0|2	4	1.33	**0.56**	0.56	**13.33**	0.2

UFL1	NT	ELMOD2	2|2|0	4	1.33	**0.56**	0.56	**13.33**	0.2
UFL1	NT	SLC30A7	2|2|0	4	1.33	**0.56**	0.56	**13.33**	0.2
UFL1	NT	UQCC1	2|0|2	4	1.33	**0.56**	0.56	**13.33**	0.2
UFL1	NT	DUS3L	2|0|2	4	1.33	**0.56**	0.56	**13.33**	0.2
UFL1	NT	TM9SF4	2|2|0	4	1.33	**0.56**	0.56	**13.33**	0.2
UFL1	NT	SPTLC1	2|0|2	4	1.33	**0.56**	0.56	**13.33**	0.2
UFL1	NT	PIK3C3	2|0|2	4	1.33	**0.56**	0.56	**13.33**	0.2
UFL1	NT	PZP	2|2|0	4	1.33	**0.56**	0.56	**13.33**	0.2
UFL1	NT	TMEM263	0|2|2	4	1.33	**0.56**	0.56	**13.33**	0.2
UFL1	NT	TOR1AIP2	0|2|2	4	1.33	**0.56**	0.56	**13.33**	0.2
UFL1	NT	NMD3	0|2|2	4	1.33	**0.56**	0.56	**13.33**	0.2
UFL1	NT	DOCK11	0|2|2	4	1.33	**0.56**	0.56	**13.33**	0.2
UFL1	NT	STAU2	5|6|7	18	6	**0.54**	0.54	**6**	0.23
UFL1	NT	GRAMD1A	8|6|8	22	7.33	**0.54**	0.54	**5.5**	0.23
UFL1	NT	TARS2	3|6|4	13	4.33	**0.53**	0.53	**6.5**	0.24
UFL1	NT	SYAP1	13|14|12	39	13	**0.52**	0.52	**3**	0.24
Bait	**Condition**	**Prey**	**Spec**	**SpecSum**	**AvgSpec**	**AvgP**	**SaintScore**	**FoldChange**	**BFDR**
UFL1	Cisplatin	CDK5RAP3	76|86|76	238	79.33	**1**	1	**793.33**	0
UFL1	Cisplatin	DDRGK1	81|75|82	238	79.33	**1**	1	**793.33**	0
UFL1	Cisplatin	MTDH	65|64|72	201	67	**1**	1	**670**	0
UFL1	Cisplatin	STIM1	73|69|72	214	71.33	**1**	1	**9.73**	0
UFL1	Cisplatin	SRPRA	84|95|86	265	88.33	**1**	1	**4.42**	0
UFL1	Cisplatin	EMD	49|53|50	152	50.67	**1**	1	**6.33**	0
UFL1	Cisplatin	PTBP3	15|19|17	51	17	**1**	1	**170**	0
UFL1	Cisplatin	BCAP31	30|29|33	92	30.67	**1**	1	**15.33**	0
UFL1	Cisplatin	SRP54	31|36|29	96	32	**1**	1	**6.4**	0
UFL1	Cisplatin	KTN1	13|9|15	37	12.33	**1**	1	**123.33**	0

UFL1	Cisplatin	CCDC88C	10|9|13	32	10.67	**1**	1	**106.67**	0
UFL1	Cisplatin	HERC2	23|27|22	72	24	**1**	1	**6**	0
UFL1	Cisplatin	LRRC59	9|6|6	21	7	**1**	1	**70**	0
UFL1	Cisplatin	ANKLE2	6|7|6	19	6.33	**1**	1	**63.33**	0
UFL1	Cisplatin	TMED5	4|4|4	12	4	**0.98**	0.98	**12**	0
UFL1	Cisplatin	NAV2	4|3|10	17	5.67	**0.98**	0.98	**56.67**	0
UFL1	Cisplatin	RTN4	6|4|3	13	4.33	**0.98**	0.98	**43.33**	0
UFL1	Cisplatin	ITPR2	5|3|4	12	4	**0.92**	0.92	**12**	0
UFL1	Cisplatin	RPS6KA4	3|6|2	11	3.67	**0.91**	0.91	**36.67**	0.01
UFL1	Cisplatin	VAPB	2|3|6	11	3.67	**0.91**	0.91	**36.67**	0.01
UFL1	Cisplatin	CAMLG	11|13|11	35	11.67	**0.9**	0.9	**11.67**	0.02
UFL1	Cisplatin	MOSPD2	3|2|3	8	2.67	**0.9**	0.9	**26.67**	0.02
UFL1	Cisplatin	SNAP47	2|5|2	9	3	**0.85**	0.85	**30**	0.02
UFL1	Cisplatin	FNDC3A	2|2|5	9	3	**0.85**	0.85	**30**	0.02
UFL1	Cisplatin	NEURL4	3|2|2	7	2.33	**0.84**	0.84	**23.33**	0.03
UFL1	Cisplatin	CDKAL1	2|3|2	7	2.33	**0.84**	0.84	**23.33**	0.03
UFL1	Cisplatin	DNAJA2	2|2|3	7	2.33	**0.84**	0.84	**23.33**	0.03
UFL1	Cisplatin	ZMYM4	2|2|3	7	2.33	**0.84**	0.84	**23.33**	0.03
UFL1	Cisplatin	GNB2	15|0|14	29	9.67	**0.67**	0.67	**96.67**	0.05
UFL1	Cisplatin	PRKACB	0|10|12	22	7.33	**0.67**	0.67	**73.33**	0.06
UFL1	Cisplatin	AHCYL1	0|7|9	16	5.33	**0.67**	0.67	**53.33**	0.07
UFL1	Cisplatin	ATP5MF-PTCD1	6|0|9	15	5	**0.67**	0.67	**50**	0.08
UFL1	Cisplatin	TMEM165	6|9|0	15	5	**0.67**	0.67	**50**	0.08
UFL1	Cisplatin	SYNE1	0|6|7	13	4.33	**0.67**	0.67	**43.33**	0.09
UFL1	Cisplatin	RAB2B	4|0|5	9	3	**0.66**	0.66	**30**	0.1
UFL1	Cisplatin	ATP6	4|4|0	8	2.67	**0.66**	0.66	**26.67**	0.11
UFL1	Cisplatin	IFI16	4|3|1	8	2.67	**0.65**	0.65	**26.67**	0.11

UFL1	Cisplatin	USH2A	0|3|4	7	2.33	**0.65**	0.65	**23.33**	0.11
UFL1	Cisplatin	ARFGEF2	0|3|4	7	2.33	**0.65**	0.65	**23.33**	0.11
UFL1	Cisplatin	TMEM263	3|3|1	7	2.33	**0.64**	0.64	**23.33**	0.13
UFL1	Cisplatin	GGCX	3|3|1	7	2.33	**0.64**	0.64	**23.33**	0.13
UFL1	Cisplatin	RNF121	3|3|0	6	2	**0.64**	0.64	**20**	0.13
UFL1	Cisplatin	SIKE1	3|0|3	6	2	**0.64**	0.64	**20**	0.13
UFL1	Cisplatin	HCAR1	3|0|3	6	2	**0.64**	0.64	**20**	0.13
UFL1	Cisplatin	DCAF13	2|5|1	8	2.67	**0.59**	0.59	**26.67**	0.16
UFL1	Cisplatin	POGLUT2	2|4|1	7	2.33	**0.59**	0.59	**23.33**	0.16
UFL1	Cisplatin	UTP6	3|4|1	8	2.67	**0.59**	0.59	**8**	0.18
UFL1	Cisplatin	POTEA	0|2|4	6	2	**0.59**	0.59	**20**	0.16
UFL1	Cisplatin	PHEX	0|2|4	6	2	**0.59**	0.59	**20**	0.16
UFL1	Cisplatin	ERGIC3	3|1|2	6	2	**0.58**	0.58	**20**	0.18
UFL1	Cisplatin	ORMDL1	3|0|2	5	1.67	**0.58**	0.58	**16.67**	0.18
UFL1	Cisplatin	PDAP1	2|0|3	5	1.67	**0.58**	0.58	**16.67**	0.18
UFL1	Cisplatin	SPATA2	0|3|2	5	1.67	**0.58**	0.58	**16.67**	0.18
UFL1	Cisplatin	PM20D2	0|3|2	5	1.67	**0.58**	0.58	**16.67**	0.18
UFL1	Cisplatin	GRAMD1A	5|7|3	15	5	**0.55**	0.55	**7.5**	0.21
UFL1	Cisplatin	NMD3	2|0|2	4	1.33	**0.52**	0.52	**13.33**	0.21
UFL1	Cisplatin	SNAP29	2|2|0	4	1.33	**0.52**	0.52	**13.33**	0.21
UFL1	Cisplatin	SLC25A22	2|0|2	4	1.33	**0.52**	0.52	**13.33**	0.21
UFL1	Cisplatin	PSMD10	2|0|2	4	1.33	**0.52**	0.52	**13.33**	0.21
UFL1	Cisplatin	POR	2|0|2	4	1.33	**0.52**	0.52	**13.33**	0.21
UFL1	Cisplatin	SAMM50	0|2|2	4	1.33	**0.52**	0.52	**13.33**	0.21
UFL1	Cisplatin	BAIAP2L1	0|2|2	4	1.33	**0.52**	0.52	**13.33**	0.21
UFL1	Cisplatin	PPP1R15B	0|2|2	4	1.33	**0.52**	0.52	**13.33**	0.21

Table 3.S10. Gene ontology analysis of C1orf27-miniturboID dataset related to figure 3.4 D

GO-BP C1orf27-miniturboID			
Term	**P-value**	**Adj.P-value**	**Comb.Score**
endoplasmic reticulum organization (GO:0007029)	1.24E-07	5.15E-05	831.224524
protein localization to endoplasmic reticulum (GO:0070972)	2.26E-06	4.71E-04	1995.531785
protein insertion into ER membrane (GO:0045048)	3.06E-05	0.004254024	609.3848607
membrane organization (GO:0061024)	4.48E-05	0.00466874	148.8618672
protein localization to organelle (GO:0033365)	8.49E-05	0.007082775	185.7789586
endoplasmic reticulum membrane organization (GO:0090158)	1.72E-04	0.011985332	1115.711982
reticulophagy (GO:0061709)	2.04E-04	0.012128466	994.8008726
positive regulation of intracellular signal transduction (GO:1902533)	2.38E-04	0.012410292	66.69835802
nuclear membrane organization (GO:0071763)	4.44E-04	0.020552969	584.5396586
nuclear envelope organization (GO:0006998)	5.44E-04	0.02266962	509.1807072
negative regulation of proteasomal ubiquitin-dependent protein catabolic process	0.001191416	0.042681373	298.6314482
regulation of intracellular estrogen receptor signaling pathway (GO:0033146)	0.001269534	0.042681373	285.9396773
organelle disassembly (GO:1903008)	0.001432948	0.042681373	263.1750199
protein insertion into membrane (GO:0051205)	0.001432948	0.042681373	263.1750199
regulation of intracellular steroid hormone receptor signaling pathway	0.001695896	0.04386518	234.3909225
negative regulation of proteasomal protein catabolic process (GO:1901799)	0.001788269	0.04386518	225.9742243
negative regulation of ubiquitin-dependent protein catabolic process (GO:2000059)	0.001788269	0.04386518	225.9742243
positive regulation of ATPase activity (GO:0032781)	0.002181178	0.05053063	196.9523632
positive regulation of nucleocytoplasmic transport (GO:0046824)	0.002611196	0.057308887	173.7550503
positive regulation of I-kappaB kinase/NF-kappaB signaling (GO:0043123)	0.002775146	0.057428268	69.37960931
mitotic nuclear membrane organization (GO:0101024)	0.003200178	0.057428268	150.6516411
mitotic nuclear membrane reassembly (GO:0007084)	0.003200178	0.057428268	150.6516411
IRE1-mediated unfolded protein response (GO:0036498)	0.003451592	0.057428268	142.8237897
endoplasmic reticulum to Golgi vesicle-mediated transport (GO:0006888)	0.003464139	0.057428268	61.5866945
nuclear membrane reassembly (GO:0031468)	0.003580659	0.057428268	139.1630624

unsaturated fatty acid metabolic process (GO:0033559)	0.003580659	0.057428268	139.1630624
membrane lipid biosynthetic process (GO:0046467)	0.004119166	0.061246021	125.9830572
endomembrane system organization (GO:0010256)	0.004249558	0.061246021	55.08584333
selective autophagy (GO:0061912)	0.004259316	0.061246021	123.0126287
regulation of viral genome replication (GO:0045069)	0.005458923	0.07587903	102.9274896
regulation of I-kappaB kinase/NF-kappaB signaling (GO:0043122)	0.005903914	0.076204878	45.85485599
COPII-coated vesicle budding (GO:0090114)	0.005944245	0.076204878	96.76373505
positive regulation of cellular protein localization (GO:1903829)	0.006110262	0.076204878	94.84407585
sphingolipid biosynthetic process (GO:0030148)	0.006620943	0.076204878	89.44759003
positive regulation of proteasomal ubiquitin-dependent protein catabolic process	0.007513763	0.076204878	81.51015037
positive regulation of DNA-binding transcription factor activity (GO:0051091)	0.007639513	0.076204878	39.56505714
protein polyufmylation (GO:1990564)	0.008223548	0.076204878	748.7300223
negative regulation of IRE1-mediated unfolded protein response (GO:1903895)	0.008223548	0.076204878	748.7300223
positive regulation of metallopeptidase activity (GO:1905050)	0.008223548	0.076204878	748.7300223
positive regulation of store-operated calcium channel activity (GO:1901341)	0.008223548	0.076204878	748.7300223
positive regulation of toll-like receptor 9 signaling pathway (GO:0034165)	0.008223548	0.076204878	748.7300223
regulation of morphogenesis of a branching structure (GO:0060688)	0.008223548	0.076204878	748.7300223
enamel mineralization (GO:0070166)	0.008223548	0.076204878	748.7300223
protein K69-linked ufmylation (GO:1990592)	0.008223548	0.076204878	748.7300223
positive regulation by host of viral genome replication (GO:0044829)	0.008223548	0.076204878	748.7300223
positive regulation of cell migration (GO:0030335)	0.009746298	0.077310379	34.2980174
protein ufmylation (GO:0071569)	0.009860378	0.077310379	576.3067827
protein-DNA covalent cross-linking repair (GO:0106300)	0.009860378	0.077310379	576.3067827
negative regulation of endoplasmic reticulum calcium ion concentration	0.009860378	0.077310379	576.3067827
positive regulation of I-kappaB phosphorylation (GO:1903721)	0.009860378	0.077310379	576.3067827
TORC2 signaling (GO:0038203)	0.009860378	0.077310379	576.3067827
endoplasmic reticulum localization (GO:0051643)	0.009860378	0.077310379	576.3067827
protein localization to nuclear envelope (GO:0090435)	0.009860378	0.077310379	576.3067827
calcium ion homeostasis (GO:0055074)	0.01114709	0.077310379	60.6831739

positive regulation of adenylate cyclase activity (GO:0045762)	0.011494589	0.077310379	464.2885874
positive regulation of ER-associated ubiquitin-dependent protein catabolic process	0.011494589	0.077310379	464.2885874
cellular response to platelet-derived growth factor stimulus (GO:0036120)	0.011494589	0.077310379	464.2885874
regulation of I-kappaB phosphorylation (GO:1903719)	0.011494589	0.077310379	464.2885874
regulation of metallopeptidase activity (GO:1905048)	0.011494589	0.077310379	464.2885874
positive regulation of type I interferon-mediated signaling pathway (GO:0060340)	0.011494589	0.077310379	464.2885874
negative regulation by host of viral genome replication (GO:0044828)	0.011494589	0.077310379	464.2885874
protein localization to endoplasmic reticulum exit site (GO:0070973)	0.011494589	0.077310379	464.2885874
positive regulation of vasculature development (GO:1904018)	0.01226918	0.079780587	56.40516715
regulation of proteasomal ubiquitin-dependent protein catabolic process	0.01226918	0.079780587	56.40516715
cellular metal ion homeostasis (GO:0006875)	0.012731366	0.079780587	54.82898989
positive regulation of dendritic cell cytokine production (GO:0002732)	0.013126185	0.079780587	386.1142785
regulation of chemokine (C-C motif) ligand 5 production (GO:0071649)	0.013126185	0.079780587	386.1142785
store-operated calcium entry (GO:0002115)	0.013126185	0.079780587	386.1142785
protein localization to nucleus (GO:0034504)	0.013201104	0.079780587	53.32272621
response to endoplasmic reticulum stress (GO:0034976)	0.014163027	0.080959286	50.50307943
cellular divalent inorganic cation homeostasis (GO:0072503)	0.014408147	0.080959286	49.83554622
regulation of RNA polymerase II regulatory region sequence-specific DNA binding	0.01475517	0.080959286	328.7123935
positive regulation of mitochondrial calcium ion concentration (GO:0051561)	0.01475517	0.080959286	328.7123935
regulation of ER-associated ubiquitin-dependent protein catabolic process	0.01475517	0.080959286	328.7123935
regulation of mammary gland epithelial cell proliferation (GO:0033599)	0.01475517	0.080959286	328.7123935
unsaturated fatty acid biosynthetic process (GO:0006636)	0.01475517	0.080959286	328.7123935
positive regulation of angiogenesis (GO:0045766)	0.015661261	0.082302475	46.70078463
sphingolipid metabolic process (GO:0006665)	0.015661261	0.082302475	46.70078463
regulation of store-operated calcium entry (GO:2001256)	0.016381548	0.082302475	284.9281499
B cell homeostasis (GO:0001782)	0.016381548	0.082302475	284.9281499
cellular response to leucine starvation (GO:1990253)	0.016381548	0.082302475	284.9281499
neuron projection fasciculation (GO:0106030)	0.016381548	0.082302475	284.9281499
nuclear pore complex assembly (GO:0051292)	0.016381548	0.082302475	284.9281499

regulation of toll-like receptor 9 signaling pathway (GO:0034163)	0.018005323	0.085439735	250.5281954
nucleus localization (GO:0051647)	0.018005323	0.085439735	250.5281954
positive regulation of viral release from host cell (GO:1902188)	0.018005323	0.085439735	250.5281954
positive regulation by host of viral process (GO:0044794)	0.018005323	0.085439735	250.5281954
protein targeting (GO:0006605)	0.018030448	0.085439735	41.79775506
regulation of primary metabolic process (GO:0080090)	0.019408383	0.088106493	39.41851503
axonal fasciculation (GO:0007413)	0.019626498	0.088106493	222.8537921
positive regulation of myeloid leukocyte mediated immunity (GO:0002888)	0.019626498	0.088106493	222.8537921
negative regulation by host of viral process (GO:0044793)	0.019626498	0.088106493	222.8537921
defense response to virus (GO:0051607)	0.020255887	0.088106493	38.09244477
cellular calcium ion homeostasis (GO:0006874)	0.021118749	0.088106493	36.83565875
regulation of retrograde protein transport, ER to cytosol (GO:1904152)	0.021245079	0.088106493	200.1543653
alpha-linolenic acid metabolic process (GO:0036109)	0.021245079	0.088106493	200.1543653
negative regulation of endoplasmic reticulum unfolded protein response	0.021245079	0.088106493	200.1543653
positive regulation of ERAD pathway (GO:1904294)	0.021245079	0.088106493	200.1543653
positive regulation of protein exit from endoplasmic reticulum (GO:0070863)	0.021245079	0.088106493	200.1543653
detection of calcium ion (GO:0005513)	0.021245079	0.088106493	200.1543653
positive regulation of cellular catabolic process (GO:0031331)	0.022590536	0.088106493	34.88167364
protein localization to vacuole (GO:0072665)	0.022861069	0.088106493	181.2321988
antiviral innate immune response (GO:0140374)	0.022861069	0.088106493	181.2321988
positive regulation of cyclase activity (GO:0031281)	0.022861069	0.088106493	181.2321988
regulation of IRE1-mediated unfolded protein response (GO:1903894)	0.022861069	0.088106493	181.2321988
nuclear migration (GO:0007097)	0.022861069	0.088106493	181.2321988
nuclear pore organization (GO:0006999)	0.022861069	0.088106493	181.2321988
positive regulation of cytosolic calcium ion concentration (GO:0007204)	0.024411344	0.088106493	32.74450943
positive regulation of lyase activity (GO:0051349)	0.024474471	0.088106493	165.2413349
positive regulation of membrane protein ectodomain proteolysis (GO:0051044)	0.024474471	0.088106493	165.2413349
cellular response to exogenous dsRNA (GO:0071360)	0.024474471	0.088106493	165.2413349
positive regulation of protein export from nucleus (GO:0046827)	0.024474471	0.088106493	165.2413349

positive regulation of response to cytokine stimulus (GO:0060760)	0.024474471	0.088106493	165.2413349
modulation by host of viral genome replication (GO:0044827)	0.024474471	0.088106493	165.2413349
endoplasmic reticulum tubular network organization (GO:0071786)	0.024474471	0.088106493	165.2413349
negative regulation of programmed cell death (GO:0043069)	0.024532314	0.088106493	19.21465358
positive regulation of intracellular protein transport (GO:0090316)	0.024720527	0.088106493	32.40835398
positive regulation of myeloid leukocyte cytokine production involved in immune	0.026085291	0.091408119	151.5680159
positive regulation of TORC1 signaling (GO:1904263)	0.026085291	0.091408119	151.5680159
positive regulation of NF-kappaB transcription factor activity (GO:0051092)	0.026929763	0.091609792	30.19952015
acyl-CoA biosynthetic process (GO:0071616)	0.027693531	0.091609792	139.7566163
establishment of protein localization to endoplasmic reticulum (GO:0072599)	0.027693531	0.091609792	139.7566163
tail-anchored membrane protein insertion into ER membrane (GO:0071816)	0.027693531	0.091609792	139.7566163
regulation of metal ion transport (GO:0010959)	0.027693531	0.091609792	139.7566163
negative regulation of amyloid-beta formation (GO:1902430)	0.027693531	0.091609792	139.7566163
cellular response to growth factor stimulus (GO:0071363)	0.027900344	0.091609792	29.32418193
organonitrogen compound biosynthetic process (GO:1901566)	0.027900344	0.091609792	29.32418193
positive regulation of protein kinase B signaling (GO:0051897)	0.028884962	0.093265379	28.48778746
positive regulation of cell cycle phase transition (GO:1901989)	0.029299196	0.093265379	129.4621222
negative regulation of fibroblast proliferation (GO:0048147)	0.029299196	0.093265379	129.4621222
cellular response to dsRNA (GO:0071359)	0.029299196	0.093265379	129.4621222
negative regulation of canonical Wnt signaling pathway (GO:0090090)	0.030219353	0.094060254	27.42909046
response to fatty acid (GO:0070542)	0.03090229	0.094060254	120.4187098
positive regulation of monocyte chemotaxis (GO:0090026)	0.03090229	0.094060254	120.4187098
positive regulation of neutrophil chemotaxis (GO:0090023)	0.03090229	0.094060254	120.4187098
pore complex assembly (GO:0046931)	0.03090229	0.094060254	120.4187098
negative regulation of amyloid precursor protein catabolic process (GO:1902992)	0.03090229	0.094060254	120.4187098
organelle organization (GO:0006996)	0.031497479	0.094210814	16.21125276
positive regulation of interferon-alpha production (GO:0032727)	0.032502816	0.094210814	112.4184153
lipopolysaccharide-mediated signaling pathway (GO:0031663)	0.032502816	0.094210814	112.4184153
endoplasmic reticulum calcium ion homeostasis (GO:0032469)	0.032502816	0.094210814	112.4184153

regulation of apoptotic process (GO:0042981)	0.032776926	0.094210814	12.28395633
actin filament-based transport (GO:0099515)	0.03410078	0.094210814	105.2963181
calcium ion transport into cytosol (GO:0060402)	0.03410078	0.094210814	105.2963181
calcium-mediated signaling using intracellular calcium source (GO:0035584)	0.03410078	0.094210814	105.2963181
linoleic acid metabolic process (GO:0043651)	0.03410078	0.094210814	105.2963181
positive regulation of transcription regulatory region DNA binding (GO:2000679)	0.03410078	0.094210814	105.2963181
protein stabilization (GO:0050821)	0.035078907	0.094210814	24.16605534
regulation of response to cytokine stimulus (GO:0060759)	0.035696184	0.094210814	98.92003497
fatty-acyl-CoA metabolic process (GO:0035337)	0.035696184	0.094210814	98.92003497
regulation of adenylate cyclase activity (GO:0045761)	0.035696184	0.094210814	98.92003497
positive regulation of granulocyte chemotaxis (GO:0071624)	0.035696184	0.094210814	98.92003497
negative regulation of phosphate metabolic process (GO:0045936)	0.035696184	0.094210814	98.92003497
positive regulation of neutrophil migration (GO:1902624)	0.035696184	0.094210814	98.92003497
positive regulation of peptidase activity (GO:0010952)	0.035696184	0.094210814	98.92003497
regulation of membrane protein ectodomain proteolysis (GO:0051043)	0.035696184	0.094210814	98.92003497
mitochondrial calcium ion homeostasis (GO:0051560)	0.035696184	0.094210814	98.92003497
proteasomal ubiquitin-independent protein catabolic process (GO:0010499)	0.035696184	0.094210814	98.92003497
regulation of peptidase activity (GO:0052547)	0.037289032	0.097184541	93.18213432
regulation of protein export from nucleus (GO:0046825)	0.037289032	0.097184541	93.18213432
negative regulation of Wnt signaling pathway (GO:0030178)	0.039469907	0.102229511	21.82173843
regulation of ryanodine-sensitive calcium-release channel activity (GO:0060314)	0.04046708	0.102271347	83.28452527
positive regulation of ERBB signaling pathway (GO:1901186)	0.04046708	0.102271347	83.28452527
regulation of interferon-alpha production (GO:0032647)	0.04046708	0.102271347	83.28452527
regulation of neutrophil chemotaxis (GO:0090022)	0.04046708	0.102271347	83.28452527
TOR signaling (GO:0031929)	0.042052286	0.105004811	78.99129706
regulation of monocyte chemotaxis (GO:0090025)	0.042052286	0.105004811	78.99129706
positive regulation of toll-like receptor signaling pathway (GO:0034123)	0.043634953	0.106523674	75.06388638
regulation of angiogenesis (GO:0045765)	0.044059459	0.106523674	19.80860412
negative regulation of apoptotic process (GO:0043066)	0.045184913	0.106523674	12.51968666

negative regulation of axonogenesis (GO:0050771)	0.045215085	0.106523674	71.45915608
positive regulation of defense response to virus by host (GO:0002230)	0.045215085	0.106523674	71.45915608
cellular response to acid chemical (GO:0071229)	0.045215085	0.106523674	71.45915608
cellular response to epidermal growth factor stimulus (GO:0071364)	0.045215085	0.106523674	71.45915608
positive regulation of protein import into nucleus (GO:0042307)	0.045215085	0.106523674	71.45915608
cytosolic calcium ion transport (GO:0060401)	0.045215085	0.106523674	71.45915608
protein localization to lysosome (GO:0061462)	0.045215085	0.106523674	71.45915608
regulation of protein kinase B signaling (GO:0051896)	0.045631874	0.106901637	19.20007395
positive regulation of dephosphorylation (GO:0035306)	0.046792684	0.10780414	68.14038433
regulation of calcium ion transmembrane transporter activity (GO:1901019)	0.046792684	0.10780414	68.14038433
positive regulation of viral genome replication (GO:0045070)	0.046792684	0.10780414	68.14038433
fatty-acyl-CoA biosynthetic process (GO:0046949)	0.048367756	0.109171284	65.07612542
regulation of type I interferon-mediated signaling pathway (GO:0060338)	0.048367756	0.109171284	65.07612542
positive regulation of protein import (GO:1904591)	0.048367756	0.109171284	65.07612542
positive regulation of protein modification process (GO:0031401)	0.048433304	0.109171284	18.20133844
negative regulation of axon extension (GO:0030517)	0.049940305	0.110771846	62.23930367
positive regulation of mononuclear cell migration (GO:0071677)	0.049940305	0.110771846	62.23930367
positive regulation of proteolysis involved in cellular protein catabolic process	0.049940305	0.110771846	62.23930367
positive regulation of cell motility (GO:2000147)	0.051296518	0.112459732	17.27917947
negative regulation of developmental growth (GO:0048640)	0.051510333	0.112459732	59.60648671
response to amino acid (GO:0043200)	0.051510333	0.112459732	59.60648671
antigen processing and presentation of peptide antigen via MHC class I	0.053077845	0.115278445	57.15729847
regulation of amyloid-beta formation (GO:1902003)	0.054642845	0.115808368	54.87394129
cellular response to amino acid stimulus (GO:0071230)	0.054642845	0.115808368	54.87394129
positive regulation of protein dephosphorylation (GO:0035307)	0.054642845	0.115808368	54.87394129
apoptotic process (GO:0006915)	0.055490649	0.115808368	16.0792313
regulation of autophagy (GO:0010506)	0.055490649	0.115808368	16.0792313
positive regulation of cell cycle G1/S phase transition (GO:1902808)	0.056205337	0.115808368	52.74080454
regulation of TORC1 signaling (GO:1903432)	0.056205337	0.115808368	52.74080454

response to exogenous dsRNA (GO:0043330)	0.056205337	0.115808368	52.74080454
negative regulation of neurogenesis (GO:0050768)	0.056205337	0.115808368	52.74080454
positive regulation of cytokine-mediated signaling pathway (GO:0001961)	0.057765325	0.115808368	50.744142
regulation of cell cycle G1/S phase transition (GO:1902806)	0.057765325	0.115808368	50.744142
positive regulation of innate immune response (GO:0045089)	0.057765325	0.115808368	50.744142
positive regulation of interferon-beta production (GO:0032728)	0.057765325	0.115808368	50.744142
regulation of defense response to virus by host (GO:0050691)	0.057765325	0.115808368	50.744142
membrane fusion (GO:0061025)	0.057765325	0.115808368	50.744142
regulation of protein import into nucleus (GO:0042306)	0.057765325	0.115808368	50.744142
regulation of axon extension (GO:0030516)	0.060877803	0.120885923	47.11301609
connective tissue development (GO:0061448)	0.060877803	0.120885923	47.11301609
fatty acid derivative biosynthetic process (GO:1901570)	0.06398031	0.125848063	43.89876361
positive regulation of intrinsic apoptotic signaling pathway (GO:2001244)	0.06398031	0.125848063	43.89876361
regulation of canonical Wnt signaling pathway (GO:0060828)	0.065125758	0.126505125	13.84217331
response to growth factor (GO:0070848)	0.065527834	0.126505125	42.42707813
positive regulation of TOR signaling (GO:0032008)	0.065527834	0.126505125	42.42707813
regulation of protein dephosphorylation (GO:0035304)	0.065527834	0.126505125	42.42707813
negative regulation of type I interferon production (GO:0032480)	0.068615444	0.131855484	39.72009676
regulation of fibroblast proliferation (GO:0048145)	0.073228317	0.13943474	36.16635857
positive regulation of response to stimulus (GO:0048584)	0.073228317	0.13943474	36.16635857
negative regulation of cold-induced thermogenesis (GO:0120163)	0.074761012	0.1417061	35.09802438
establishment of protein localization to mitochondrion (GO:0072655)	0.07629125	0.143952268	34.08117343
regulation of interferon-beta production (GO:0032648)	0.077819033	0.146173589	33.11234497
regulation of axonogenesis (GO:0050770)	0.080867252	0.148553498	31.30636634
positive regulation of fat cell differentiation (GO:0045600)	0.080867252	0.148553498	31.30636634
regulation of cellular amine metabolic process (GO:0033238)	0.080867252	0.148553498	31.30636634
regulation of epithelial cell migration (GO:0010632)	0.080867252	0.148553498	31.30636634
negative regulation of protein ubiquitination (GO:0031397)	0.080867252	0.148553498	31.30636634
regulation of release of sequestered calcium ion into cytosol (GO:0051279)	0.082387695	0.149372474	30.46365983

cartilage development (GO:0051216)	0.082387695	0.149372474	30.46365983
regulation of intrinsic apoptotic signaling pathway (GO:2001242)	0.082387695	0.149372474	30.46365983
positive regulation of chemokine production (GO:0032722)	0.0839057	0.151466133	29.65781217
regulation of cellular amino acid metabolic process (GO:0006521)	0.085421269	0.151577315	28.88657397
positive regulation of leukocyte chemotaxis (GO:0002690)	0.085421269	0.151577315	28.88657397
negative regulation of viral genome replication (GO:0045071)	0.085421269	0.151577315	28.88657397
regulation of proteasomal protein catabolic process (GO:0061136)	0.085421269	0.151577315	28.88657397
protein targeting to mitochondrion (GO:0006626)	0.086934406	0.152317846	28.14787128
regulation of cardiac conduction (GO:1903779)	0.086934406	0.152317846	28.14787128
negative regulation of protein modification by small protein conjugation or removal	0.086934406	0.152317846	28.14787128
innate immune response (GO:0045087)	0.088388751	0.153035741	10.26072039
negative regulation of metabolic process (GO:0009892)	0.088445116	0.153035741	27.439789
mitochondrial transport (GO:0006839)	0.088445116	0.153035741	27.439789
negative regulation of cell cycle G2/M phase transition (GO:1902750)	0.089953402	0.154364481	26.76055615
positive regulation of proteolysis (GO:0045862)	0.089953402	0.154364481	26.76055615
regulation of calcium ion transport (GO:0051924)	0.091459268	0.154406943	26.10853271
negative regulation of neuron projection development (GO:0010977)	0.091459268	0.154406943	26.10853271
RNA modification (GO:0009451)	0.091459268	0.154406943	26.10853271
muscle organ development (GO:0007517)	0.091459268	0.154406943	26.10853271
positive regulation of apoptotic signaling pathway (GO:2001235)	0.092962718	0.156312312	25.4821979
positive regulation of interleukin-8 production (GO:0032757)	0.095962383	0.160708087	24.30104522
positive regulation of cysteine-type endopeptidase activity (GO:2001056)	0.097458606	0.162560955	23.74369267
positive regulation of viral process (GO:0048524)	0.098952428	0.164395069	23.20694325
regulation of cellular ketone metabolic process (GO:0010565)	0.100443852	0.164901914	22.68973459
tRNA processing (GO:0008033)	0.100443852	0.164901914	22.68973459
pre-replicative complex assembly (GO:0036388)	0.100443852	0.164901914	22.68973459
regulation of cellular catabolic process (GO:0031329)	0.101932882	0.166039108	22.19107438
tRNA modification (GO:0006400)	0.101932882	0.166039108	22.19107438
negative regulation of G2/M transition of mitotic cell cycle (GO:0010972)	0.103419522	0.167154808	21.71003486

cellular response to nutrient levels (GO:0031669)	0.103419522	0.167154808	21.71003486
positive regulation of protein localization to nucleus (GO:1900182)	0.106385646	0.171284997	20.79739923
negative regulation of viral process (GO:0048525)	0.109342253	0.173724391	19.94551348
positive regulation of multicellular organismal process (GO:0051240)	0.110537129	0.173724391	8.129403237
post-translational protein modification (GO:0043687)	0.110537129	0.173724391	8.129403237
fatty acid biosynthetic process (GO:0006633)	0.110816998	0.173724391	19.54058705
regulation of TOR signaling (GO:0032006)	0.110816998	0.173724391	19.54058705
regulation of endopeptidase activity (GO:0052548)	0.110816998	0.173724391	19.54058705
regulation of hematopoietic stem cell differentiation (GO:1902036)	0.110816998	0.173724391	19.54058705
antigen processing and presentation of exogenous peptide antigen via MHC class I,	0.113759387	0.177669154	18.76960016
cellular response to amino acid starvation (GO:0034198)	0.115227038	0.178623327	18.40238306
NIK/NF-kappaB signaling (GO:0038061)	0.115227038	0.178623327	18.40238306
regulation of transcription from RNA polymerase II promoter in response to	0.116692333	0.178899643	18.04663424
response to amino acid starvation (GO:1990928)	0.116692333	0.178899643	18.04663424
regulation of hematopoietic progenitor cell differentiation (GO:1901532)	0.116692333	0.178899643	18.04663424
positive regulation of interleukin-6 production (GO:0032755)	0.118155274	0.180478935	17.70185463
positive regulation of tumor necrosis factor production (GO:0032760)	0.119615866	0.18138115	17.367573
positive regulation of type I interferon production (GO:0032481)	0.119615866	0.18138115	17.367573
antigen processing and presentation of exogenous peptide antigen via MHC class I	0.121074112	0.182927191	17.04334406
axon development (GO:0061564)	0.122530015	0.183795023	16.72874671
positive regulation of ubiquitin-dependent protein catabolic process (GO:2000060)	0.122530015	0.183795023	16.72874671
regulation of fat cell differentiation (GO:0045598)	0.12398358	0.183989868	16.42338248
lipid biosynthetic process (GO:0008610)	0.12398358	0.183989868	16.42338248
regulation of organelle organization (GO:0033043)	0.12398358	0.183989868	16.42338248
positive regulation of protein phosphorylation (GO:0001934)	0.124579583	0.184177168	7.136798867
regulation of interleukin-8 production (GO:0032677)	0.12543481	0.184177168	16.12687401
positive regulation of tumor necrosis factor superfamily cytokine production	0.12543481	0.184177168	16.12687401
long-chain fatty acid metabolic process (GO:0001676)	0.128330279	0.187767461	15.55901245
anaphase-promoting complex-dependent catabolic process (GO:0031145)	0.129774525	0.188557411	15.28699853

response to insulin (GO:0032868)	0.129774525	0.188557411	15.28699853
positive regulation of protein catabolic process (GO:0045732)	0.131216451	0.18933308	15.02251647
Wnt signaling pathway, planar cell polarity pathway (GO:0060071)	0.131216451	0.18933308	15.02251647
negative regulation of cellular amide metabolic process (GO:0034249)	0.13265606	0.189443757	14.76527602
negative regulation of phosphorylation (GO:0042326)	0.13265606	0.189443757	14.76527602
positive regulation of proteasomal protein catabolic process (GO:1901800)	0.13265606	0.189443757	14.76527602
protein targeting to membrane (GO:0006612)	0.134093356	0.190193638	14.51500132
regulation of transcription from RNA polymerase II promoter in response to stress	0.134093356	0.190193638	14.51500132
regulation of establishment of planar polarity (GO:0090175)	0.135528342	0.191012529	14.27142994
regulation of type I interferon production (GO:0032479)	0.136961022	0.191012529	14.03431214
regulation of cation channel activity (GO:2001257)	0.136961022	0.191012529	14.03431214
regulation of cysteine-type endopeptidase activity involved in apoptotic process	0.136961022	0.191012529	14.03431214
SCF-dependent proteasomal ubiquitin-dependent protein catabolic process	0.136961022	0.191012529	14.03431214
positive regulation of autophagy (GO:0010508)	0.138391399	0.192364045	13.8034101
regulation of stem cell differentiation (GO:2000736)	0.139819478	0.193703396	13.57849725
negative regulation of mitotic cell cycle phase transition (GO:1901991)	0.141245261	0.194387042	13.35935759
regulation of lipid metabolic process (GO:0019216)	0.141245261	0.194387042	13.35935759
regulation of heart contraction (GO:0008016)	0.142668752	0.195700229	13.14578512
positive regulation of epithelial cell migration (GO:0010634)	0.144089955	0.195718278	12.93758324
interleukin-1-mediated signaling pathway (GO:0070498)	0.144089955	0.195718278	12.93758324
cotranslational protein targeting to membrane (GO:0006613)	0.144089955	0.195718278	12.93758324
regulation of cell migration (GO:0030334)	0.145264639	0.196366344	5.996669967
regulation of cell cycle phase transition (GO:1901987)	0.145508873	0.196366344	12.73456428
positive regulation of cold-induced thermogenesis (GO:0120162)	0.148339871	0.199541052	12.34336594
calcium-mediated signaling (GO:0019722)	0.15537763	0.208335922	11.44444364
protein targeting to ER (GO:0045047)	0.156778399	0.208870902	11.27705098
cellular response to organonitrogen compound (GO:0071417)	0.156778399	0.208870902	11.27705098
cellular response to peptide hormone stimulus (GO:0071375)	0.160967202	0.213089916	10.79732988
positive regulation of protein serine/threonine kinase activity (GO:0071902)	0.160967202	0.213089916	10.79732988

response to calcium ion (GO:0051592)	0.162358981	0.2142522	10.64452089
regulation of protein ubiquitination (GO:0031396)	0.165135825	0.217229145	10.34890048
regulation of interleukin-6 production (GO:0032675)	0.166520898	0.218117945	10.20588739
Fc-epsilon receptor signaling pathway (GO:0038095)	0.167903742	0.218117945	10.06594445
regulation of Wnt signaling pathway (GO:0030111)	0.167903742	0.218117945	10.06594445
regulation of protein serine/threonine kinase activity (GO:0071900)	0.167903742	0.218117945	10.06594445
Fc receptor signaling pathway (GO:0038093)	0.169284361	0.218549779	9.928980323
regulation of macroautophagy (GO:0016241)	0.169284361	0.218549779	9.928980323
positive regulation of metabolic process (GO:0009893)	0.170662759	0.219649292	9.794907156
response to lipid (GO:0033993)	0.172038939	0.220467015	9.663640419
calcium ion transport (GO:0006816)	0.173412904	0.220467015	9.53509875
cellular response to lectin (GO:1990858)	0.173412904	0.220467015	9.53509875
stimulatory C-type lectin receptor signaling pathway (GO:0002223)	0.173412904	0.220467015	9.53509875
tumor necrosis factor-mediated signaling pathway (GO:0033209)	0.174784659	0.22153557	9.409203809
positive regulation of cysteine-type endopeptidase activity involved in apoptotic	0.17888669	0.225364802	9.046658483
innate immune response activating cell surface receptor signaling pathway	0.17888669	0.225364802	9.046658483
cellular response to lipopolysaccharide (GO:0071222)	0.180249634	0.226397884	8.930622881
regulation of mRNA catabolic process (GO:0061013)	0.182968945	0.228357625	8.705376343
positive regulation of cell population proliferation (GO:0008284)	0.183753062	0.228357625	4.514447446
positive regulation of epithelial cell proliferation (GO:0050679)	0.184325318	0.228357625	8.596041941
cellular response to organic substance (GO:0071310)	0.184325318	0.228357625	8.596041941
regulation of tumor necrosis factor production (GO:0032680)	0.185679508	0.228357625	8.488821384
non-canonical Wnt signaling pathway (GO:0035567)	0.185679508	0.228357625	8.488821384
defense response to symbiont (GO:0140546)	0.185679508	0.228357625	8.488821384
regulation of phosphorylation (GO:0042325)	0.187031517	0.228357625	8.383658172
platelet degranulation (GO:0002576)	0.187031517	0.228357625	8.383658172
neutrophil degranulation (GO:0043312)	0.187928109	0.228357625	4.387905926
negative regulation of cell growth (GO:0030308)	0.18838135	0.228357625	8.280497738
negative regulation of growth (GO:0045926)	0.18838135	0.228357625	8.280497738

neutrophil activation involved in immune response (GO:0002283)	0.190320369	0.229252089	4.317753496
plasma membrane bounded cell projection organization (GO:0120036)	0.191074498	0.229252089	8.079976131
neutrophil mediated immunity (GO:0002446)	0.192117553	0.229252089	4.266134286
cellular response to insulin stimulus (GO:0032869)	0.19241782	0.229252089	7.982514794
DNA-dependent DNA replication (GO:0006261)	0.19241782	0.229252089	7.982514794
muscle contraction (GO:0006936)	0.19241782	0.229252089	7.982514794
positive regulation of canonical Wnt signaling pathway (GO:0090263)	0.19375898	0.230192292	7.886855761
cellular response to hypoxia (GO:0071456)	0.195097979	0.231124594	7.792953007
protein-DNA complex assembly (GO:0065004)	0.21099872	0.24854934	6.788244088
neuron development (GO:0048666)	0.21099872	0.24854934	6.788244088
regulation of mRNA stability (GO:0043488)	0.214926061	0.252462443	6.568007796
regulation of cytosolic calcium ion concentration (GO:0051480)	0.217533749	0.254807791	6.427179677
regulation of G2/M transition of mitotic cell cycle (GO:0010389)	0.218834442	0.25561334	6.358483438
positive regulation of Wnt signaling pathway (GO:0030177)	0.224016278	0.260935161	6.094565063
positive regulation of protein kinase activity (GO:0045860)	0.225306519	0.261707015	6.031183686
cellular response to interleukin-1 (GO:0071347)	0.226594681	0.262472172	5.968796537
skeletal system development (GO:0001501)	0.230446714	0.264728044	5.787389048
cellular response to starvation (GO:0009267)	0.230446714	0.264728044	5.787389048
T cell receptor signaling pathway (GO:0050852)	0.230446714	0.264728044	5.787389048
cellular protein-containing complex assembly (GO:0034622)	0.243152932	0.278557068	5.239236664
neuron projection development (GO:0031175)	0.246924963	0.282103313	5.089978954
mitochondrion organization (GO:0007005)	0.25192599	0.287030431	4.900686817
defense response to bacterium (GO:0042742)	0.253171206	0.287663196	4.855010529
positive regulation of developmental process (GO:0051094)	0.254414412	0.288290244	4.809967812
regulation of mitotic cell cycle (GO:0007346)	0.255655611	0.288911625	4.765546642
regulated exocytosis (GO:0045055)	0.258132001	0.290921741	4.678522285
negative regulation of cytokine production (GO:0001818)	0.260600401	0.292912041	4.593846925
antigen receptor-mediated signaling pathway (GO:0050851)	0.264288074	0.296258406	4.47105067
regulation of mitotic cell cycle phase transition (GO:1901990)	0.26795791	0.299566886	4.353072137

negative regulation of macromolecule metabolic process (GO:0010605)	0.275244405	0.305160682	4.130562657
cellular response to tumor necrosis factor (GO:0071356)	0.275244405	0.305160682	4.130562657
regulation of programmed cell death (GO:0043067)	0.275244405	0.305160682	4.130562657
positive regulation of cellular process (GO:0048522)	0.275888674	0.305160682	2.579649754
proteasomal protein catabolic process (GO:0010498)	0.288420737	0.318178432	3.764097593
negative regulation of multicellular organismal process (GO:0051241)	0.299028317	0.329010048	3.498733081
regulation of cell growth (GO:0001558)	0.302529981	0.331986847	3.41634835
positive regulation of phosphorylation (GO:0042327)	0.343249197	0.375682192	2.61423876
positive regulation of cell differentiation (GO:0045597)	0.348719042	0.38066974	2.52483738
cellular component assembly (GO:0022607)	0.351979717	0.383225959	2.473279961
regulation of protein phosphorylation (GO:0001932)	0.357379029	0.38809129	2.390629421
protein deubiquitination (GO:0016579)	0.358453644	0.388247194	2.374572111
central nervous system development (GO:0007417)	0.359526517	0.388400408	2.358667682
regulation of cell population proliferation (GO:0042127)	0.361016131	0.389001877	1.656648955
protein modification by small protein removal (GO:0070646)	0.36804709	0.395555764	2.236707737
proteolysis (GO:0006508)	0.379583609	0.406905822	2.08310739
DNA repair (GO:0006281)	0.390915793	0.417979194	1.943950474
MAPK cascade (GO:0000165)	0.396000188	0.422332681	1.884984249
protein polyubiquitination (GO:0000209)	0.407041404	0.433000677	1.763758849
proteasome-mediated ubiquitin-dependent protein catabolic process (GO:0043161)	0.413965458	0.439094999	1.69219907
negative regulation of gene expression (GO:0010629)	0.414948186	0.439094999	1.682306601
cellular response to oxygen-containing compound (GO:1901701)	0.415929316	0.439094999	1.672494056
cellular protein localization (GO:0034613)	0.421782676	0.444149939	1.615249902
positive regulation of cytokine production (GO:0001819)	0.427579136	0.448997644	1.560676354
intracellular protein transport (GO:0006886)	0.428539718	0.448997644	1.551828754
ubiquitin-dependent protein catabolic process (GO:0006511)	0.445565268	0.464505252	1.403699001
positive regulation of transcription by RNA polymerase II (GO:0045944)	0.445568587	0.464505252	1.097271974
negative regulation of cell population proliferation (GO:0008285)	0.468398112	0.487087314	1.228258604
positive regulation of macromolecule metabolic process (GO:0010604)	0.472853974	0.490497779	1.196785434

protein modification by small protein conjugation (GO:0032446)	0.49459556	0.51177754	1.054674282
cellular protein metabolic process (GO:0044267)	0.501367346	0.517500454	1.01399696
cellular protein modification process (GO:0006464)	0.509869517	0.524976762	0.804760611
regulation of intracellular signal transduction (GO:1902531)	0.517914145	0.531946301	0.921039228
nervous system development (GO:0007399)	0.525986618	0.538910122	0.878772594
positive regulation of gene expression (GO:0010628)	0.553220995	0.565424399	0.749458663
protein ubiquitination (GO:0016567)	0.584608204	0.596043083	0.622451264
positive regulation of transcription, DNA-templated (GO:0045893)	0.589087585	0.599145178	0.54307083
negative regulation of cellular process (GO:0048523)	0.612537838	0.621479996	0.525983672
cytokine-mediated signaling pathway (GO:0019221)	0.647159577	0.655013455	0.424349115
negative regulation of transcription by RNA polymerase II (GO:0000122)	0.683136363	0.689752696	0.336217798
regulation of transcription by RNA polymerase II (GO:0006357)	0.721088272	0.72631355	0.26367301
negative regulation of transcription, DNA-templated (GO:0045892)	0.798868423	0.802718391	0.140942207
regulation of gene expression (GO:0010468)	0.839854911	0.841873793	0.0955654
regulation of transcription, DNA-templated (GO:0006355)	0.980366739	0.980366739	0.004896362

Table 3.S11 Gene ontology analysis related to figure 3.5 D and E

GO-BP UFSP2-miniturboID			
Term	**P-value**	**Adj. P-value**	**Comb. Score**
positive regulation of histone phosphorylation (GO:0033129)	4.94E-06	0.001127072	12207.70394
regulation of histone phosphorylation (GO:0033127)	1.48E-05	0.001688375	5554.533472
positive regulation of proteolysis involved in cellular protein catabolic process	1.52E-04	0.009829697	1210.174959
positive regulation of histone modification (GO:0031058)	1.72E-04	0.009829697	1115.711982
regulation of proteasomal protein catabolic process (GO:0061136)	4.64E-04	0.02116405	588.5229122
regulation of translational initiation (GO:0006446)	7.35E-04	0.026597117	435.5732891
negative regulation of gene expression (GO:0010629)	8.17E-04	0.026597117	146.1381612
positive regulation of proteasomal protein catabolic process (GO:1901800)	0.001172876	0.031157031	319.8049846
positive regulation of protein phosphorylation (GO:0001934)	0.001229883	0.031157031	119.0855167
protein polyufmylation (GO:1990564)	0.002996653	0.034143123	2638.914119
late endosome to Golgi transport (GO:0034499)	0.002996653	0.034143123	2638.914119
negative regulation of IRE1-mediated unfolded protein response (GO:1903895)	0.002996653	0.034143123	2638.914119
regulation of mRNA binding (GO:1902415)	0.002996653	0.034143123	2638.914119
DNA replication, synthesis of RNA primer (GO:0006269)	0.002996653	0.034143123	2638.914119
positive regulation of metallopeptidase activity (GO:1905050)	0.002996653	0.034143123	2638.914119
protein K69-linked ufmylation (GO:1990592)	0.002996653	0.034143123	2638.914119
protein ufmylation (GO:0071569)	0.003594998	0.034143123	2044.882815
positive regulation of RNA binding (GO:1905216)	0.003594998	0.034143123	2044.882815
regulation of transmission of nerve impulse (GO:0051969)	0.003594998	0.034143123	2044.882815
positive regulation of I-kappaB phosphorylation (GO:1903721)	0.003594998	0.034143123	2044.882815
histone-serine phosphorylation (GO:0035404)	0.003594998	0.034143123	2044.882815
positive regulation of NF-kappaB transcription factor activity (GO:0051092)	0.003742864	0.034143123	144.8837669
regulation of I-kappaB phosphorylation (GO:1903719)	0.004193015	0.034143123	1657.396457
negative regulation of cytoplasmic translation (GO:2000766)	0.004193015	0.034143123	1657.396457
membrane invagination (GO:0010324)	0.004193015	0.034143123	1657.396457

regulation of metallopeptidase activity (GO:1905048)	0.004193015	0.034143123	1657.396457
negative regulation of neurotransmitter secretion (GO:0046929)	0.004193015	0.034143123	1657.396457
positive regulation of mRNA binding (GO:1902416)	0.004193015	0.034143123	1657.396457
negative regulation of cAMP-dependent protein kinase activity (GO:2000480)	0.004790703	0.034989777	1385.975083
negative regulation of regulated secretory pathway (GO:1903306)	0.004790703	0.034989777	1385.975083
regulation of translation (GO:0006417)	0.0049025	0.034989777	119.727745
negative regulation of RNA catabolic process (GO:1902369)	0.005388063	0.034989777	1185.987693
regulation of RNA polymerase II regulatory region sequence-specific DNA	0.005388063	0.034989777	1185.987693
histone phosphorylation (GO:0016572)	0.005388063	0.034989777	1185.987693
cellular response to hydroxyurea (GO:0072711)	0.005985094	0.034989777	1032.951295
negative regulation of voltage-gated calcium channel activity (GO:1901386)	0.005985094	0.034989777	1032.951295
formation of translation preinitiation complex (GO:0001731)	0.005985094	0.034989777	1032.951295
negative regulation of establishment of protein localization (GO:1904950)	0.005985094	0.034989777	1032.951295
regulation of long-term synaptic depression (GO:1900452)	0.005985094	0.034989777	1032.951295
positive regulation of posttranscriptional gene silencing (GO:0060148)	0.006581796	0.035729751	912.3494182
response to hydroxyurea (GO:0072710)	0.006581796	0.035729751	912.3494182
negative regulation of activated T cell proliferation (GO:0046007)	0.006581796	0.035729751	912.3494182
negative regulation of endoplasmic reticulum unfolded protein response	0.007774217	0.039757195	735.0172993
reticulophagy (GO:0061709)	0.007774217	0.039757195	735.0172993
negative regulation of translational initiation (GO:0045947)	0.008369936	0.039757195	668.1300945
regulation of IRE1-mediated unfolded protein response (GO:1903894)	0.008369936	0.039757195	668.1300945
regulation of cAMP-dependent protein kinase activity (GO:2000479)	0.008369936	0.039757195	668.1300945
dicarboxylic acid catabolic process (GO:0043649)	0.008369936	0.039757195	668.1300945
modulation by host of viral genome replication (GO:0044827)	0.008965327	0.040239747	611.4626003
regulation of cytoplasmic translation (GO:2000765)	0.008965327	0.040239747	611.4626003
positive regulation of DNA-binding transcription factor activity (GO:0051091)	0.009168332	0.040239747	75.93348028
regulation of neurotransmitter transport (GO:0051588)	0.00956039	0.040239747	562.8907982
protein localization to endoplasmic reticulum (GO:0070972)	0.00956039	0.040239747	562.8907982
activation of protein kinase A activity (GO:0034199)	0.010155126	0.040239747	520.8353408

negative regulation of viral entry into host cell (GO:0046597)	0.010155126	0.040239747	520.8353408
negative regulation of phagocytosis (GO:0050765)	0.010155126	0.040239747	520.8353408
positive regulation of cell cycle phase transition (GO:1901989)	0.010749535	0.040239747	484.0984099
positive regulation of CREB transcription factor activity (GO:0032793)	0.010749535	0.040239747	484.0984099
regulation of early endosome to late endosome transport (GO:2000641)	0.010749535	0.040239747	484.0984099
cellular response to glucagon stimulus (GO:0071377)	0.011343616	0.040239747	451.7557081
regulation of synaptic vesicle exocytosis (GO:2000300)	0.011343616	0.040239747	451.7557081
folic acid metabolic process (GO:0046655)	0.011343616	0.040239747	451.7557081
cytoplasmic translational initiation (GO:0002183)	0.011343616	0.040239747	451.7557081
cellular response to nitrogen compound (GO:1901699)	0.011937371	0.040239747	423.0830518
positive regulation of peptidyl-lysine acetylation (GO:2000758)	0.011937371	0.040239747	423.0830518
negative regulation of viral life cycle (GO:1903901)	0.011937371	0.040239747	423.0830518
regulation of protein kinase A signaling (GO:0010738)	0.011937371	0.040239747	423.0830518
cellular response to inorganic substance (GO:0071241)	0.012530798	0.040239747	397.505318
positive regulation of transcription regulatory region DNA binding	0.012530798	0.040239747	397.505318
response to glucagon (GO:0033762)	0.012530798	0.040239747	397.505318
regulation of dendritic spine development (GO:0060998)	0.012530798	0.040239747	397.505318
positive regulation of peptidase activity (GO:0010952)	0.013123899	0.040435798	374.5602037
positive regulation of dendritic spine development (GO:0060999)	0.013123899	0.040435798	374.5602037
regulation of voltage-gated calcium channel activity (GO:1901385)	0.013123899	0.040435798	374.5602037
positive regulation of receptor internalization (GO:0002092)	0.013716674	0.041150022	353.8720301
positive regulation of histone acetylation (GO:0035066)	0.013716674	0.041150022	353.8720301
positive regulation of viral life cycle (GO:1903902)	0.014309122	0.042369869	335.132492
regulation of cAMP-mediated signaling (GO:0043949)	0.014901244	0.043557484	318.0863027
positive regulation of filopodium assembly (GO:0051491)	0.01549304	0.044155165	302.5203443
negative regulation of protein transport (GO:0051224)	0.01549304	0.044155165	302.5203443
negative regulation of cation channel activity (GO:2001258)	0.016084511	0.044183957	288.2553657
nucleobase-containing small molecule interconversion (GO:0015949)	0.016084511	0.044183957	288.2553657
positive regulation of gene silencing by miRNA (GO:2000637)	0.016084511	0.044183957	288.2553657

regulation of protein transport (GO:0051223)	0.016675655	0.044729993	275.1395602
negative regulation of calcium ion transmembrane transporter activity	0.016675655	0.044729993	275.1395602
negative regulation of mRNA catabolic process (GO:1902373)	0.017266474	0.045776234	263.0435442
renal water homeostasis (GO:0003091)	0.018447136	0.047794854	241.4824938
negative regulation of proteasomal ubiquitin-dependent protein catabolic	0.018447136	0.047794854	241.4824938
regulation of intracellular estrogen receptor signaling pathway (GO:0033146)	0.01903698	0.048091429	231.8389989
RNA biosynthetic process (GO:0032774)	0.01903698	0.048091429	231.8389989
regulation of histone acetylation (GO:0035065)	0.019626498	0.048091429	222.8537921
regulation of neurotransmitter secretion (GO:0046928)	0.019626498	0.048091429	222.8537921
regulation of activated T cell proliferation (GO:0046006)	0.020215692	0.048091429	214.4638136
positive regulation of DNA binding (GO:0043388)	0.020215692	0.048091429	214.4638136
organelle disassembly (GO:1903008)	0.020215692	0.048091429	214.4638136
negative regulation of T cell proliferation (GO:0042130)	0.020804561	0.048091429	206.6136938
positive regulation of cell cycle G1/S phase transition (GO:1902808)	0.020804561	0.048091429	206.6136938
cellular response to virus (GO:0098586)	0.020804561	0.048091429	206.6136938
positive regulation of macromolecule metabolic process (GO:0010604)	0.021368359	0.048091429	39.47728665
regulation of receptor internalization (GO:0002090)	0.021393106	0.048091429	199.254625
regulation of cell cycle G1/S phase transition (GO:1902806)	0.021393106	0.048091429	199.254625
regulation of intracellular steroid hormone receptor signaling pathway	0.021981327	0.048091429	192.343425
glutamate receptor signaling pathway (GO:0007215)	0.021981327	0.048091429	192.343425
negative regulation of ubiquitin-dependent protein catabolic process	0.022569223	0.048091429	185.8417561
connective tissue development (GO:0061448)	0.022569223	0.048091429	185.8417561
DNA replication initiation (GO:0006270)	0.022569223	0.048091429	185.8417561
negative regulation of proteasomal protein catabolic process (GO:1901799)	0.022569223	0.048091429	185.8417561
regulation of viral entry into host cell (GO:0046596)	0.023156796	0.048886569	179.7154695
regulation of filopodium assembly (GO:0051489)	0.02433097	0.049977128	168.4701655
regulation of response to DNA damage stimulus (GO:2001020)	0.02433097	0.049977128	168.4701655
endosome organization (GO:0007032)	0.02433097	0.049977128	168.4701655
negative regulation of protein catabolic process (GO:0042177)	0.024917572	0.050725057	163.2992349

positive regulation of receptor-mediated endocytosis (GO:0048260)	0.026089806	0.052641378	153.7498329
positive regulation of response to stimulus (GO:0048584)	0.027260748	0.054521496	145.1329635
regulation of cellular metabolic process (GO:0031323)	0.027845735	0.054731272	141.1340062
regulation of DNA binding (GO:0051101)	0.027845735	0.054731272	141.1340062
regulation of protein metabolic process (GO:0051246)	0.028430399	0.055402829	137.3227634
negative regulation of catabolic process (GO:0009895)	0.029014742	0.055591269	133.6867953
regulation of cellular protein metabolic process (GO:0032268)	0.029014742	0.055591269	133.6867953
negative regulation of transport (GO:0051051)	0.03018246	0.057029354	126.8961017
cartilage development (GO:0051216)	0.030765836	0.057029354	123.721361
endocytic recycling (GO:0032456)	0.030765836	0.057029354	123.721361
negative regulation of protein metabolic process (GO:0051248)	0.030765836	0.057029354	123.721361
positive regulation of cell population proliferation (GO:0008284)	0.031614116	0.057626696	28.56407685
regulation of alternative mRNA splicing, via spliceosome (GO:0000381)	0.031931624	0.057626696	117.7689507
regulation of gene silencing by RNA (GO:0060966)	0.032514035	0.057626696	114.9756685
positive regulation of response to DNA damage stimulus (GO:2001022)	0.032514035	0.057626696	114.9756685
regulation of posttranscriptional gene silencing (GO:0060147)	0.032514035	0.057626696	114.9756685
positive regulation of gene expression (GO:0010628)	0.032604578	0.057626696	27.82574446
regulation of phagocytosis (GO:0050764)	0.034259344	0.060085618	107.2458163
regulation of secretion by cell (GO:1903530)	0.034840472	0.060178997	104.8660242
selective autophagy (GO:0061912)	0.034840472	0.060178997	104.8660242
regulation of gene silencing by miRNA (GO:0060964)	0.039477969	0.067676518	88.68891636
cellular response to light stimulus (GO:0071482)	0.041211758	0.06960208	83.69212377
regulation of plasma membrane bounded cell projection assembly	0.041211758	0.06960208	83.69212377
positive regulation of cellular protein localization (GO:1903829)	0.04178905	0.070058113	82.13254395
positive regulation of synaptic transmission (GO:0050806)	0.042942678	0.071466647	79.15828252
negative regulation of cellular process (GO:0048523)	0.043734808	0.072257509	21.55658276
RNA transport (GO:0050658)	0.044670733	0.073272857	75.02824312
cellular response to UV (GO:0034644)	0.045246116	0.073686531	73.73247947
negative regulation of protein serine/threonine kinase activity (GO:0071901)	0.045821181	0.073973927	72.47436707

positive regulation of proteasomal ubiquitin-dependent protein catabolic process	0.046395928	0.073973927	71.25235747
positive regulation of ubiquitin-dependent protein catabolic process	0.046395928	0.073973927	71.25235747
positive regulation of cellular amide metabolic process (GO:0034250)	0.047544471	0.075278746	68.91085828
positive regulation of plasma membrane bounded cell projection assembly	0.048691746	0.076563572	66.69714422
negative regulation of cellular amide metabolic process (GO:0034249)	0.050410283	0.078722907	63.5950896
positive regulation of neuron projection development (GO:0010976)	0.051554392	0.079045858	61.66019918
retrograde transport, endosome to Golgi (GO:0042147)	0.051554392	0.079045858	61.66019918
positive regulation of cellular process (GO:0048522)	0.052301761	0.079045858	18.34375422
positive regulation of binding (GO:0051099)	0.052697239	0.079045858	59.82286213
negative regulation of translation (GO:0017148)	0.052697239	0.079045858	59.82286213
regulation of mRNA splicing, via spliceosome (GO:0048024)	0.052697239	0.079045858	59.82286213
positive regulation of transport (GO:0051050)	0.053268188	0.079380045	58.93859893
Wnt signaling pathway (GO:0016055)	0.053838822	0.079709425	58.07619178
regulation of epithelial cell proliferation (GO:0050678)	0.054409141	0.079842325	57.23487629
negative regulation of cellular protein metabolic process (GO:0032269)	0.054979145	0.079842325	56.41392257
interleukin-1-mediated signaling pathway (GO:0070498)	0.054979145	0.079842325	56.41392257
response to UV (GO:0009411)	0.057824442	0.083442866	52.59122124
positive regulation of translation (GO:0045727)	0.058392559	0.083732726	51.8788186
positive regulation of cellular protein metabolic process (GO:0032270)	0.059527849	0.083779936	50.50172124
regulation of proteasomal ubiquitin-dependent protein catabolic process	0.059527849	0.083779936	50.50172124
regulation of protein catabolic process (GO:0042176)	0.059527849	0.083779936	50.50172124
mRNA transport (GO:0051028)	0.060661885	0.084852207	49.18491924
positive regulation of cellular metabolic process (GO:0031325)	0.061228433	0.085122455	48.54796116
cellular response to peptide hormone stimulus (GO:0071375)	0.061794667	0.085388995	47.92471293
modulation of chemical synaptic transmission (GO:0050804)	0.063491493	0.087205183	46.13313567
response to endoplasmic reticulum stress (GO:0034976)	0.064056476	0.08745435	45.56071409
regulation of Wnt signaling pathway (GO:0030111)	0.064621146	0.087700127	45.00007231
activation of protein kinase activity (GO:0032147)	0.066313285	0.088937818	43.38546243
histone modification (GO:0016570)	0.066313285	0.088937818	43.38546243

positive regulation of cell projection organization (GO:0031346)	0.068002618	0.090670157	41.86527496
regulation of mRNA catabolic process (GO:0061013)	0.070811946	0.093475768	39.52096422
regulation of apoptotic process (GO:0042981)	0.070926789	0.093475768	13.76547809
positive regulation of epithelial cell proliferation (GO:0050679)	0.07137288	0.093523084	39.07824746
regulation of cell population proliferation (GO:0042127)	0.074651287	0.096264907	13.09450825
DNA-dependent DNA replication (GO:0006261)	0.074731967	0.096264907	36.58651144
positive regulation of macromolecule biosynthetic process (GO:0010557)	0.074731967	0.096264907	36.58651144
negative regulation of inflammatory response to antigenic stimulus	0.078636823	0.100163105	33.99629322
ribonucleoprotein complex assembly (GO:0022618)	0.078636823	0.100163105	33.99629322
regulation of inflammatory response to antigenic stimulus (GO:0002861)	0.079193425	0.100311672	33.65102434
protein localization to organelle (GO:0033365)	0.081971814	0.103257312	32.00830783
regulation of mRNA stability (GO:0043488)	0.084188989	0.105467525	30.78701959
regulation of cytokine production (GO:0001817)	0.086401255	0.107647465	29.64052002
cellular response to interleukin-1 (GO:0071347)	0.089159698	0.110480496	28.30297928
peptidyl-serine phosphorylation (GO:0018105)	0.08971047	0.110562093	28.04732599
skeletal system development (GO:0001501)	0.090811098	0.11131683	27.54722002
regulation of neuron projection development (GO:0010975)	0.094653695	0.115406645	25.90669724
peptidyl-serine modification (GO:0018209)	0.096842776	0.117447622	25.03955069
positive regulation of transcription by RNA polymerase II (GO:0045944)	0.100551705	0.12130047	9.676146067
positive regulation of developmental process (GO:0051094)	0.101206388	0.121447665	23.44072134
negative regulation of immune response (GO:0050777)	0.101750478	0.121461304	23.25255588
positive regulation of cellular biosynthetic process (GO:0031328)	0.102837754	0.122119832	22.88349705
negative regulation of cytokine production (GO:0001818)	0.103923822	0.122770111	22.52384318
negative regulation of macromolecule metabolic process (GO:0010605)	0.110414966	0.129100576	20.54567702
regulation of programmed cell death (GO:0043067)	0.110414966	0.129100576	20.54567702
regulation of signal transduction (GO:0009966)	0.112569084	0.13094771	19.94797785
negative regulation of inflammatory response (GO:0050728)	0.120070897	0.138791077	18.0615127
positive regulation of protein modification process (GO:0031401)	0.121137826	0.138791077	17.81544622
negative regulation of multicellular organismal process (GO:0051241)	0.121137826	0.138791077	17.81544622

positive regulation of cell motility (GO:2000147)	0.124862747	0.142343532	16.9950901
regulation of gene expression (GO:0010468)	0.134206086	0.152233769	7.0530083
membrane organization (GO:0061024)	0.135950852	0.153449477	14.86397018
anterograde trans-synaptic signaling (GO:0098916)	0.137000117	0.153872053	14.68334745
regulation of transcription by RNA polymerase II (GO:0006357)	0.13845422	0.154742952	5.320741187
positive regulation of phosphorylation (GO:0042327)	0.141707371	0.157606247	13.91196561
regulation of protein phosphorylation (GO:0001932)	0.148465195	0.16409722	12.90557234
protein deubiquitination (GO:0016579)	0.148983002	0.16409722	12.83293594
positive regulation of cell migration (GO:0030335)	0.15001775	0.164442534	12.68957688
protein modification by small protein removal (GO:0070646)	0.153630294	0.167357668	12.20711236
DNA metabolic process (GO:0006259)	0.154145221	0.167357668	12.14054113
positive regulation of transcription, DNA-templated (GO:0045893)	0.155890837	0.168450762	5.919504944
proteolysis (GO:0006508)	0.15927872	0.171299756	11.50493877
chemical synaptic transmission (GO:0007268)	0.16895377	0.180851923	10.43187356
cellular response to DNA damage stimulus (GO:0006974)	0.190968571	0.203461842	8.469716046
negative regulation of cell population proliferation (GO:0008285)	0.205184654	0.217591168	7.469744956
negative regulation of programmed cell death (GO:0043069)	0.206156582	0.217609725	7.407505043
phosphorylation (GO:0016310)	0.21533571	0.226251345	6.853503441
regulation of cell migration (GO:0030334)	0.219171416	0.228676368	6.638825567
protein modification by small protein conjugation (GO:0032446)	0.219649669	0.228676368	6.61270617
regulation of nucleic acid-templated transcription (GO:1903506)	0.22963116	0.237981384	6.098068095
regulation of intracellular signal transduction (GO:1902531)	0.232932226	0.240310169	5.93982807
regulation of cellular macromolecule biosynthetic process (GO:2000112)	0.24739595	0.254082327	5.30781648
negative regulation of apoptotic process (GO:0043066)	0.25522111	0.260943556	5.002845648
protein phosphorylation (GO:0006468)	0.260244631	0.264891857	4.81913214
negative regulation of cellular macromolecule biosynthetic process	0.283132201	0.286907297	4.084701888
cytokine-mediated signaling pathway (GO:0019221)	0.315188911	0.317978193	3.278880579
regulation of transcription, DNA-templated (GO:0006355)	0.396648839	0.398396191	1.463853332
cellular protein modification process (GO:0006464)	0.468204656	0.468204656	1.277594747

GO-BP UFL1-miniturboID			
Term	**P-value**	**Adj. P-value**	**Comb. Score**
protein ufmylation (GO:0071569)	3.03405E-05	0.011923807	3846.615893
endoplasmic reticulum membrane organization (GO:0090158)	0.000132781	0.015643732	1319.911549
positive regulation of cellular protein localization (GO:1903829)	0.000146604	0.015643732	298.1322004
endoplasmic reticulum organization (GO:0007029)	0.000159224	0.015643732	286.8762013
protein localization to endoplasmic reticulum (GO:0070972)	0.000240554	0.017841063	879.8573816
establishment of protein localization to endoplasmic reticulum (GO:0072599)	0.000272383	0.017841063	808.9130319
response to endoplasmic reticulum stress (GO:0034976)	0.000532967	0.029922263	161.447879
protein targeting (GO:0006605)	0.000773319	0.036142945	134.5029957
negative regulation of proteasomal ubiquitin-dependent protein catabolic	0.000919668	0.036142945	356.1288723
positive regulation of proteolysis involved in cellular protein catabolic process	0.000919668	0.036142945	356.1288723
protein insertion into ER membrane (GO:0045048)	0.001310124	0.040389352	280.0589703
negative regulation of proteasomal protein catabolic process (GO:1901799)	0.001381668	0.040389352	270.0849651
negative regulation of ubiquitin-dependent protein catabolic process	0.001381668	0.040389352	270.0849651
positive regulation of NF-kappaB transcription factor activity (GO:0051092)	0.001438806	0.040389352	98.45220704
endoplasmic reticulum to Golgi vesicle-mediated transport (GO:0006888)	0.002383672	0.057257935	75.76585354
mitotic nuclear membrane organization (GO:0101024)	0.002476806	0.057257935	180.7220635
mitotic nuclear membrane reassembly (GO:0007084)	0.002476806	0.057257935	180.7220635
IRE1-mediated unfolded protein response (GO:0036498)	0.002672096	0.057344522	171.4217151
nuclear membrane reassembly (GO:0031468)	0.002772381	0.057344522	167.0712817
positive regulation of cysteine-type endopeptidase activity (GO:2001056)	0.003637392	0.068486078	138.0616047
regulation of viral genome replication (GO:0045069)	0.004233909	0.068486078	123.9645789
positive regulation of protein localization to nucleus (GO:1900182)	0.004358303	0.068486078	121.4332914
gland development (GO:0048732)	0.004741579	0.068486078	114.3352279
myeloid leukocyte differentiation (GO:0002573)	0.004741579	0.068486078	114.3352279
positive regulation of DNA-binding transcription factor activity (GO:0051091)	0.005304009	0.068486078	49.07918337

positive regulation of proteasomal ubiquitin-dependent protein catabolic process	0.005836836	0.068486078	98.43781771
positive regulation of ubiquitin-dependent protein catabolic process	0.005836836	0.068486078	98.43781771
negative regulation of phosphorylation (GO:0042326)	0.006881018	0.068486078	87.31670862
protein polyufmylation (GO:1990564)	0.007229642	0.068486078	878.8271482
negative regulation of IRE1-mediated unfolded protein response (GO:1903895)	0.007229642	0.068486078	878.8271482
positive regulation of metallopeptidase activity (GO:1905050)	0.007229642	0.068486078	878.8271482
SRP-dependent cotranslational protein targeting to membrane, translocation	0.007229642	0.068486078	878.8271482
positive regulation of store-operated calcium channel activity (GO:1901341)	0.007229642	0.068486078	878.8271482
positive regulation of toll-like receptor 9 signaling pathway (GO:0034165)	0.007229642	0.068486078	878.8271482
regulation of morphogenesis of a branching structure (GO:0060688)	0.007229642	0.068486078	878.8271482
enamel mineralization (GO:0070166)	0.007229642	0.068486078	878.8271482
protein K69-linked ufmylation (GO:1990592)	0.007229642	0.068486078	878.8271482
positive regulation of intracellular signal transduction (GO:1902533)	0.007590989	0.068486078	27.99378117
cotranslational protein targeting to membrane (GO:0006613)	0.008170316	0.068486078	76.94305785
negative regulation of endoplasmic reticulum calcium ion concentration	0.008669509	0.068486078	677.1245224
positive regulation of histone phosphorylation (GO:0033129)	0.008669509	0.068486078	677.1245224
positive regulation of I-kappaB phosphorylation (GO:1903721)	0.008669509	0.068486078	677.1245224
histone-serine phosphorylation (GO:0035404)	0.008669509	0.068486078	677.1245224
endoplasmic reticulum localization (GO:0051643)	0.008669509	0.068486078	677.1245224
calcium ion homeostasis (GO:0055074)	0.008679731	0.068486078	73.56467544
positive regulation of vasculature development (GO:1904018)	0.009559699	0.068486078	68.44748539
regulation of proteasomal ubiquitin-dependent protein catabolic process	0.009559699	0.068486078	68.44748539
protein targeting to ER (GO:0045047)	0.009740293	0.068486078	67.4936474
cellular metal ion homeostasis (GO:0006875)	0.009922411	0.068486078	66.56128539
positive regulation of adenylate cyclase activity (GO:0045762)	0.01010736	0.068486078	546.0060757
exocrine system development (GO:0035272)	0.01010736	0.068486078	546.0060757
positive regulation of ER-associated ubiquitin-dependent protein catabolic	0.01010736	0.068486078	546.0060757
ribosomal large subunit export from nucleus (GO:0000055)	0.01010736	0.068486078	546.0060757
negative regulation of protein kinase activity by regulation of protein	0.01010736	0.068486078	546.0060757

regulation of I-kappaB phosphorylation (GO:1903719)	0.01010736	0.068486078	546.0060757
regulation of metallopeptidase activity (GO:1905048)	0.01010736	0.068486078	546.0060757
definitive hemopoiesis (GO:0060216)	0.01010736	0.068486078	546.0060757
protein localization to endoplasmic reticulum exit site (GO:0070973)	0.01010736	0.068486078	546.0060757
regulation of protein ubiquitination (GO:0031396)	0.010855687	0.070882454	62.19881367
negative regulation of gene expression (GO:0010629)	0.011083616	0.070882454	32.00347843
cellular divalent inorganic cation homeostasis (GO:0072503)	0.011239503	0.070882454	60.58241533
regulation of RNA biosynthetic process (GO:2001141)	0.011543199	0.070882454	454.4518266
store-operated calcium entry (GO:0002115)	0.011543199	0.070882454	454.4518266
regulation of protein localization to nucleolus (GO:1904749)	0.011543199	0.070882454	454.4518266
positive regulation of angiogenesis (GO:0045766)	0.012224998	0.071830583	56.82627504
intracellular protein transport (GO:0006886)	0.012428696	0.071830583	29.85675004
regulation of RNA polymerase II regulatory region sequence-specific DNA	0.012977027	0.071830583	387.1908225
histone phosphorylation (GO:0016572)	0.012977027	0.071830583	387.1908225
positive regulation of mitochondrial calcium ion concentration (GO:0051561)	0.012977027	0.071830583	387.1908225
regulation of ER-associated ubiquitin-dependent protein catabolic process	0.012977027	0.071830583	387.1908225
regulation of mammary gland epithelial cell proliferation (GO:0033599)	0.012977027	0.071830583	387.1908225
negative regulation of cellular protein catabolic process (GO:1903363)	0.014408847	0.073541257	335.8616723
regulation of store-operated calcium entry (GO:2001256)	0.014408847	0.073541257	335.8616723
B cell homeostasis (GO:0001782)	0.014408847	0.073541257	335.8616723
regulation of histone phosphorylation (GO:0033127)	0.014408847	0.073541257	335.8616723
neuron projection fasciculation (GO:0106030)	0.014408847	0.073541257	335.8616723
nuclear pore complex assembly (GO:0051292)	0.014408847	0.073541257	335.8616723
regulation of toll-like receptor 9 signaling pathway (GO:0034163)	0.015838662	0.077807426	295.5155745
cellular response to cholesterol (GO:0071397)	0.015838662	0.077807426	295.5155745
monocyte differentiation (GO:0030224)	0.015838662	0.077807426	295.5155745
cellular calcium ion homeostasis (GO:0006874)	0.016527964	0.078149668	44.98910449
axonal fasciculation (GO:0007413)	0.017266474	0.078149668	263.0435442
synaptic vesicle fusion to presynaptic active zone membrane (GO:0031629)	0.017266474	0.078149668	263.0435442

digestive system development (GO:0055123)	0.017266474	0.078149668	263.0435442
negative regulation of programmed cell death (GO:0043069)	0.017369044	0.078149668	24.24045084
protein localization to organelle (GO:0033365)	0.017928035	0.078149668	42.19480275
regulation of retrograde protein transport, ER to cytosol (GO:1904152)	0.018692287	0.078149668	236.3979777
negative regulation of endoplasmic reticulum unfolded protein response	0.018692287	0.078149668	236.3979777
positive regulation of ERAD pathway (GO:1904294)	0.018692287	0.078149668	236.3979777
Golgi ribbon formation (GO:0090161)	0.018692287	0.078149668	236.3979777
reticulophagy (GO:0061709)	0.018692287	0.078149668	236.3979777
ribosomal subunit export from nucleus (GO:0000054)	0.018692287	0.078149668	236.3979777
positive regulation of protein exit from endoplasmic reticulum (GO:0070863)	0.018692287	0.078149668	236.3979777
detection of calcium ion (GO:0005513)	0.018692287	0.078149668	236.3979777
regulation of cytokine production (GO:0001817)	0.019870519	0.078273548	38.87726923
protein localization to vacuole (GO:0072665)	0.020116103	0.078273548	214.1775585
activation of cysteine-type endopeptidase activity (GO:0097202)	0.020116103	0.078273548	214.1775585
positive regulation of cyclase activity (GO:0031281)	0.020116103	0.078273548	214.1775585
regulation of IRE1-mediated unfolded protein response (GO:1903894)	0.020116103	0.078273548	214.1775585
nuclear pore organization (GO:0006999)	0.020116103	0.078273548	214.1775585
pancreas development (GO:0031016)	0.020116103	0.078273548	214.1775585
protein modification by small protein conjugation (GO:0032446)	0.02092577	0.07910658	21.50059598
regulation of apoptotic process (GO:0042981)	0.02135532	0.07910658	16.0387767
positive regulation of lyase activity (GO:0051349)	0.021537924	0.07910658	195.3922669
regulation of dephosphorylation (GO:0035303)	0.021537924	0.07910658	195.3922669
positive regulation of protein export from nucleus (GO:0046827)	0.021537924	0.07910658	195.3922669
endoplasmic reticulum tubular network organization (GO:0071786)	0.021537924	0.07910658	195.3922669
positive regulation of protein kinase B signaling (GO:0051897)	0.022679173	0.082526991	34.94728124
cellular response to sterol (GO:0036315)	0.022957753	0.082774284	179.3236456
synaptic vesicle membrane organization (GO:0048499)	0.024375593	0.084560615	165.438216
tail-anchored membrane protein insertion into ER membrane (GO:0071816)	0.024375593	0.084560615	165.438216
regulation of metal ion transport (GO:0010959)	0.024375593	0.084560615	165.438216

negative regulation of amyloid-beta formation (GO:1902430)	0.024375593	0.084560615	165.438216
cellular protein-containing complex assembly (GO:0034622)	0.024547334	0.084560615	32.76222468
positive regulation of cell cycle phase transition (GO:1901989)	0.025791447	0.084560615	153.3319168
positive regulation of CREB transcription factor activity (GO:0032793)	0.025791447	0.084560615	153.3319168
negative regulation of fibroblast proliferation (GO:0048147)	0.025791447	0.084560615	153.3319168
regulation of cellular protein catabolic process (GO:1903362)	0.025791447	0.084560615	153.3319168
response to cholesterol (GO:0070723)	0.027205317	0.084560615	142.6933592
positive regulation of monocyte chemotaxis (GO:0090026)	0.027205317	0.084560615	142.6933592
negative regulation of RNA metabolic process (GO:0051253)	0.027205317	0.084560615	142.6933592
negative regulation of RNA splicing (GO:0033119)	0.027205317	0.084560615	142.6933592
positive regulation of neutrophil chemotaxis (GO:0090023)	0.027205317	0.084560615	142.6933592
nuclear membrane organization (GO:0071763)	0.027205317	0.084560615	142.6933592
pore complex assembly (GO:0046931)	0.027205317	0.084560615	142.6933592
negative regulation of amyloid precursor protein catabolic process	0.027205317	0.084560615	142.6933592
protein stabilization (GO:0050821)	0.027606258	0.084560615	29.73625233
granulocyte differentiation (GO:0030851)	0.028617205	0.084560615	133.2788782
hepaticobiliary system development (GO:0061008)	0.028617205	0.084560615	133.2788782
cellular response to interferon-beta (GO:0035458)	0.028617205	0.084560615	133.2788782
positive regulation of peptidyl-lysine acetylation (GO:2000758)	0.028617205	0.084560615	133.2788782
lipopolysaccharide-mediated signaling pathway (GO:0031663)	0.028617205	0.084560615	133.2788782
endoplasmic reticulum calcium ion homeostasis (GO:0032469)	0.028617205	0.084560615	133.2788782
calcium-mediated signaling using intracellular calcium source (GO:0035584)	0.030027116	0.085791491	124.8951999
intrinsic apoptotic signaling pathway in response to DNA damage by p53 class	0.030027116	0.085791491	124.8951999
nuclear envelope organization (GO:0006998)	0.030027116	0.085791491	124.8951999
positive regulation of transcription regulatory region DNA binding	0.030027116	0.085791491	124.8951999
regulation of adenylate cyclase activity (GO:0045761)	0.03143505	0.085791491	117.3871491
positive regulation of granulocyte chemotaxis (GO:0071624)	0.03143505	0.085791491	117.3871491
negative regulation of phosphate metabolic process (GO:0045936)	0.03143505	0.085791491	117.3871491
positive regulation of neutrophil migration (GO:1902624)	0.03143505	0.085791491	117.3871491

positive regulation of peptidase activity (GO:0010952)	0.03143505	0.085791491	117.3871491
positive regulation of signal transduction by p53 class mediator (GO:1901798)	0.03143505	0.085791491	117.3871491
mitochondrial calcium ion homeostasis (GO:0051560)	0.03143505	0.085791491	117.3871491
negative regulation of apoptotic process (GO:0043066)	0.032469354	0.086620923	15.99052201
positive regulation of histone acetylation (GO:0035066)	0.032841011	0.086620923	110.6287727
regulation of cysteine-type endopeptidase activity (GO:2000116)	0.032841011	0.086620923	110.6287727
mitotic cell cycle checkpoint signaling (GO:0007093)	0.032841011	0.086620923	110.6287727
regulation of protein export from nucleus (GO:0046825)	0.032841011	0.086620923	110.6287727
endomembrane system organization (GO:0010256)	0.033538695	0.087871382	25.24302534
apoptotic nuclear changes (GO:0030262)	0.034245002	0.089127721	104.5168226
regulation of angiogenesis (GO:0045765)	0.034780476	0.089925836	24.4707871
positive regulation of ERBB signaling pathway (GO:1901186)	0.035647025	0.090969356	98.96590014
regulation of neutrophil chemotaxis (GO:0090022)	0.035647025	0.090969356	98.96590014
regulation of protein kinase B signaling (GO:0051896)	0.036040136	0.091379182	23.73435633
regulation of monocyte chemotaxis (GO:0090025)	0.037047083	0.092735692	93.90478963
mononuclear cell differentiation (GO:1903131)	0.037047083	0.092735692	93.90478963
positive regulation of toll-like receptor signaling pathway (GO:0034123)	0.038445178	0.095626298	89.27365553
negative regulation of axonogenesis (GO:0050771)	0.039841313	0.096652075	85.02187553
response to interferon-beta (GO:0035456)	0.039841313	0.096652075	85.02187553
regulation of phosphatase activity (GO:0010921)	0.039841313	0.096652075	85.02187553
protein localization to lysosome (GO:0061462)	0.039841313	0.096652075	85.02187553
positive regulation of dephosphorylation (GO:0035306)	0.041235492	0.098814318	81.10634814
positive regulation of viral genome replication (GO:0045070)	0.041235492	0.098814318	81.10634814
positive regulation of small GTPase mediated signal transduction (GO:0051057)	0.042627715	0.101531467	77.49015815
regulation of autophagy (GO:0010506)	0.043960635	0.101759228	19.95248369
negative regulation of axon extension (GO:0030517)	0.044017987	0.101759228	74.14151495
negative regulation of DNA binding (GO:0043392)	0.044017987	0.101759228	74.14151495
positive regulation of mononuclear cell migration (GO:0071677)	0.044017987	0.101759228	74.14151495
negative regulation of response to biotic stimulus (GO:0002832)	0.044017987	0.101759228	74.14151495

negative regulation of developmental growth (GO:0048640)	0.045406309	0.103148436	71.03290112
liver development (GO:0001889)	0.045406309	0.103148436	71.03290112
regulation of intracellular estrogen receptor signaling pathway (GO:0033146)	0.045406309	0.103148436	71.03290112
antigen processing and presentation of peptide antigen via MHC class I	0.046792684	0.103311938	68.14038433
positive regulation of histone modification (GO:0031058)	0.046792684	0.103311938	68.14038433
signal transduction by p53 class mediator (GO:0072331)	0.046792684	0.103311938	68.14038433
regulation of histone acetylation (GO:0035065)	0.046792684	0.103311938	68.14038433
mitotic G2 DNA damage checkpoint signaling (GO:0007095)	0.046792684	0.103311938	68.14038433
membrane organization (GO:0061024)	0.047789758	0.103462331	18.51878538
regulation of amyloid-beta formation (GO:1902003)	0.048177116	0.103462331	65.44305725
positive regulation of protein dephosphorylation (GO:0035307)	0.048177116	0.103462331	65.44305725
organelle disassembly (GO:1903008)	0.048177116	0.103462331	65.44305725
protein insertion into membrane (GO:0051205)	0.048177116	0.103462331	65.44305725
positive regulation of cell cycle G1/S phase transition (GO:1902808)	0.049559606	0.105280676	62.92257879
negative regulation of neurogenesis (GO:0050768)	0.049559606	0.105280676	62.92257879
regulation of cell cycle G1/S phase transition (GO:1902806)	0.050940157	0.107056052	60.5627958
intrinsic apoptotic signaling pathway by p53 class mediator (GO:0072332)	0.050940157	0.107056052	60.5627958
regulation of intracellular steroid hormone receptor signaling pathway	0.052318772	0.109368497	58.34942939
regulation of axon extension (GO:0030516)	0.053695453	0.110483315	56.26981346
negative regulation of innate immune response (GO:0045824)	0.053695453	0.110483315	56.26981346
connective tissue development (GO:0061448)	0.053695453	0.110483315	56.26981346
positive regulation of intrinsic apoptotic signaling pathway (GO:2001244)	0.056443026	0.114933208	52.46795162
synaptic vesicle exocytosis (GO:0016079)	0.056443026	0.114933208	52.46795162
central nervous system development (GO:0007417)	0.057304102	0.115334373	15.69037684
positive regulation of cell migration (GO:0030335)	0.05768249	0.115334373	15.59484067
response to growth factor (GO:0070848)	0.057813922	0.115334373	50.72663121
regulation of protein dephosphorylation (GO:0035304)	0.057813922	0.115334373	50.72663121
regulation of ubiquitin-dependent protein catabolic process (GO:2000058)	0.059182896	0.116878784	49.08062328
negative regulation of protein catabolic process (GO:0042177)	0.059182896	0.116878784	49.08062328

cellular response to glucose starvation (GO:0042149)	0.060549948	0.118980648	47.52264366
intracellular protein transmembrane transport (GO:0065002)	0.061915083	0.121057849	46.04611786
cellular response to radiation (GO:0071478)	0.063278302	0.121309135	44.64509756
positive regulation of RNA metabolic process (GO:0051254)	0.063278302	0.121309135	44.64509756
mitotic G2/M transition checkpoint (GO:0044818)	0.063278302	0.121309135	44.64509756
zymogen activation (GO:0031638)	0.063278302	0.121309135	44.64509756
erythrocyte differentiation (GO:0030218)	0.064639609	0.122131568	43.31418865
regulation of fibroblast proliferation (GO:0048145)	0.064639609	0.122131568	43.31418865
positive regulation of nucleocytoplasmic transport (GO:0046824)	0.064639609	0.122131568	43.31418865
regulation of DNA binding (GO:0051101)	0.065999005	0.123512424	42.0484888
regulation of protein localization to nucleus (GO:1900180)	0.065999005	0.123512424	42.0484888
establishment of protein localization to mitochondrion (GO:0072655)	0.067356494	0.123696739	40.84353327
negative regulation of MAP kinase activity (GO:0043407)	0.067356494	0.123696739	40.84353327
cellular response to alcohol (GO:0097306)	0.067356494	0.123696739	40.84353327
cellular response to ionizing radiation (GO:0071479)	0.067356494	0.123696739	40.84353327
regulation of gene expression (GO:0010468)	0.068487139	0.12518812	7.540426606
regulation of axonogenesis (GO:0050770)	0.07141754	0.128160243	37.55409845
regulation of epithelial cell migration (GO:0010632)	0.07141754	0.128160243	37.55409845
negative regulation of protein ubiquitination (GO:0031397)	0.07141754	0.128160243	37.55409845
intrinsic apoptotic signaling pathway in response to DNA damage	0.07141754	0.128160243	37.55409845
cartilage development (GO:0051216)	0.072767424	0.128818008	36.55469109
regulation of intrinsic apoptotic signaling pathway (GO:2001242)	0.072767424	0.128818008	36.55469109
myeloid cell differentiation (GO:0030099)	0.072767424	0.128818008	36.55469109
negative regulation of cysteine-type endopeptidase activity (GO:2000117)	0.074115414	0.130615953	35.59880662
regulation of cyclin-dependent protein kinase activity (GO:1904029)	0.075461511	0.130644819	34.68379512
positive regulation of leukocyte chemotaxis (GO:0002690)	0.075461511	0.130644819	34.68379512
negative regulation of viral genome replication (GO:0045071)	0.075461511	0.130644819	34.68379512
regulation of proteasomal protein catabolic process (GO:0061136)	0.075461511	0.130644819	34.68379512
protein targeting to mitochondrion (GO:0006626)	0.076805719	0.131237597	33.80721303

regulation of cardiac conduction (GO:1903779)	0.076805719	0.131237597	33.80721303
negative regulation of protein modification by small protein conjugation or	0.076805719	0.131237597	33.80721303
positive regulation of interleukin-1 beta production (GO:0032731)	0.078148039	0.132380083	32.96680367
mitochondrial transport (GO:0006839)	0.078148039	0.132380083	32.96680367
regulation of calcium ion transport (GO:0051924)	0.080827029	0.133431139	31.38630877
negative regulation of neuron projection development (GO:0010977)	0.080827029	0.133431139	31.38630877
RNA modification (GO:0009451)	0.080827029	0.133431139	31.38630877
positive regulation of protein binding (GO:0032092)	0.080827029	0.133431139	31.38630877
membrane lipid biosynthetic process (GO:0046467)	0.080827029	0.133431139	31.38630877
muscle organ development (GO:0007517)	0.080827029	0.133431139	31.38630877
cellular protein localization (GO:0034613)	0.08190754	0.133431139	11.13433323
positive regulation of apoptotic signaling pathway (GO:2001235)	0.082163704	0.133431139	30.64249755
selective autophagy (GO:0061912)	0.082163704	0.133431139	30.64249755
mitotic DNA damage checkpoint signaling (GO:0044773)	0.082163704	0.133431139	30.64249755
positive regulation of interleukin-1 production (GO:0032732)	0.086162477	0.138778088	28.57715052
double-strand break repair via nonhomologous end joining (GO:0006303)	0.086162477	0.138778088	28.57715052
negative regulation of endopeptidase activity (GO:0010951)	0.08749166	0.139207377	27.93925167
positive regulation of Ras protein signal transduction (GO:0046579)	0.08749166	0.139207377	27.93925167
positive regulation of viral process (GO:0048524)	0.08749166	0.139207377	27.93925167
regulation of innate immune response (GO:0045088)	0.088818975	0.139636014	27.32446318
tRNA processing (GO:0008033)	0.088818975	0.139636014	27.32446318
positive regulation of multicellular organismal process (GO:0051240)	0.088826981	0.139636014	10.26253333
regulation of RNA metabolic process (GO:0051252)	0.090144427	0.140026719	26.7316145
regulation of cellular catabolic process (GO:0031329)	0.090144427	0.140026719	26.7316145
tRNA modification (GO:0006400)	0.090144427	0.140026719	26.7316145
negative regulation of G2/M transition of mitotic cell cycle (GO:0010972)	0.091468017	0.141523349	26.1596111
negative regulation of cellular catabolic process (GO:0031330)	0.095427642	0.147070836	24.55874441
negative regulation of viral process (GO:0048525)	0.09674381	0.147365572	24.0604974
neutrophil chemotaxis (GO:0030593)	0.09674381	0.147365572	24.0604974

COPII-coated vesicle budding (GO:0090114)	0.09674381	0.147365572	24.0604974
response to ionizing radiation (GO:0010212)	0.099370603	0.149877742	23.11221794
protein transport (GO:0015031)	0.099524019	0.149877742	9.129763299
positive regulation of protein phosphorylation (GO:0001934)	0.100431693	0.149877742	9.043628353
granulocyte chemotaxis (GO:0071621)	0.100681231	0.149877742	22.66073522
regulation of hydrolase activity (GO:0051336)	0.100681231	0.149877742	22.66073522
ubiquitin-dependent ERAD pathway (GO:0030433)	0.100681231	0.149877742	22.66073522
sphingolipid biosynthetic process (GO:0030148)	0.101990018	0.151253122	22.22346028
regulation of RNA splicing (GO:0043484)	0.104602078	0.154543671	21.38907034
positive regulation of protein modification by small protein conjugation or	0.105905355	0.154724181	20.99080931
neutrophil migration (GO:1990266)	0.105905355	0.154724181	20.99080931
positive regulation of type I interferon production (GO:0032481)	0.105905355	0.154724181	20.99080931
negative regulation of protein serine/threonine kinase activity (GO:0071901)	0.107206801	0.156045454	20.60445933
axon development (GO:0061564)	0.108506417	0.156201546	20.2295229
negative regulation of NF-kappaB transcription factor activity (GO:0032088)	0.108506417	0.156201546	20.2295229
regulation of neuron differentiation (GO:0045664)	0.108506417	0.156201546	20.2295229
negative regulation of protein modification process (GO:0031400)	0.111100173	0.159351708	19.51203228
regulation of cyclin-dependent protein serine/threonine kinase activity	0.112394317	0.159461973	19.16860956
regulation of gene expression, epigenetic (GO:0040029)	0.112394317	0.159461973	19.16860956
positive regulation of protein ubiquitination (GO:0031398)	0.112394317	0.159461973	19.16860956
regulation of interleukin-1 beta production (GO:0032651)	0.113686642	0.160715288	18.83486025
negative regulation of defense response (GO:0031348)	0.116265843	0.163772317	18.19487976
regulation of Ras protein signal transduction (GO:0046578)	0.117552725	0.163823478	17.88794432
negative regulation of cellular amide metabolic process (GO:0034249)	0.117552725	0.163823478	17.88794432
positive regulation of proteasomal protein catabolic process (GO:1901800)	0.117552725	0.163823478	17.88794432
ERAD pathway (GO:0036503)	0.118837797	0.164448079	17.5892715
protein targeting to membrane (GO:0006612)	0.118837797	0.164448079	17.5892715
negative regulation of binding (GO:0051100)	0.120121063	0.165640623	17.29855098
regulation of type I interferon production (GO:0032479)	0.121402524	0.165684184	17.01548741

regulation of cysteine-type endopeptidase activity involved in apoptotic process	0.121402524	0.165684184	17.01548741
positive regulation of autophagy (GO:0010508)	0.122682182	0.165684184	16.7397995
positive regulation of binding (GO:0051099)	0.122682182	0.165684184	16.7397995
negative regulation of protein kinase activity (GO:0006469)	0.122682182	0.165684184	16.7397995
SRP-dependent cotranslational protein targeting to membrane (GO:0006614)	0.122682182	0.165684184	16.7397995
organelle organization (GO:0006996)	0.123372177	0.166045429	7.250686448
regulation of heart contraction (GO:0008016)	0.126510371	0.168518988	15.95437137
negative regulation of cellular protein metabolic process (GO:0032269)	0.127782846	0.168518988	15.70562743
positive regulation of epithelial cell migration (GO:0010634)	0.127782846	0.168518988	15.70562743
hemopoiesis (GO:0030097)	0.127782846	0.168518988	15.70562743
negative regulation of MAPK cascade (GO:0043409)	0.127782846	0.168518988	15.70562743
interleukin-1-mediated signaling pathway (GO:0070498)	0.127782846	0.168518988	15.70562743
regulation of MAP kinase activity (GO:0043405)	0.131589542	0.172958829	14.9954785
calcium-mediated signaling (GO:0019722)	0.137898415	0.180046767	13.9205088
intrinsic apoptotic signaling pathway (GO:0097193)	0.137898415	0.180046767	13.9205088
positive regulation of transcription by RNA polymerase II (GO:0045944)	0.14281611	0.185850104	4.730922225
response to calcium ion (GO:0051592)	0.144163024	0.186983724	12.96318759
regulation of Wnt signaling pathway (GO:0030111)	0.149143043	0.192174478	12.27028968
regulation of protein serine/threonine kinase activity (GO:0071900)	0.149143043	0.192174478	12.27028968
histone modification (GO:0016570)	0.152859684	0.19631979	11.78823899
positive regulation of gene expression (GO:0010628)	0.154030948	0.196621316	5.626527528
calcium ion transport (GO:0006816)	0.154095078	0.196621316	11.63417077
sphingolipid metabolic process (GO:0006665)	0.155328731	0.197554018	11.4832524
negative regulation of response to external stimulus (GO:0032102)	0.15779083	0.199394843	11.19051065
regulation of protein binding (GO:0043393)	0.15779083	0.199394843	11.19051065
positive regulation of cysteine-type endopeptidase activity involved in apoptotic	0.159019279	0.200303131	11.04851796
cellular response to lipopolysaccharide (GO:0071222)	0.160245999	0.201203442	10.90933625
positive regulation of epithelial cell proliferation (GO:0050679)	0.163915799	0.204504473	10.50789792
cellular response to organic substance (GO:0071310)	0.163915799	0.204504473	10.50789792

defense response to symbiont (GO:0140546)	0.165135621	0.205374365	10.3792142
regulation of phosphorylation (GO:0042325)	0.166353725	0.206236637	10.25298125
negative regulation of cell growth (GO:0030308)	0.167570113	0.206442177	10.12913434
negative regulation of growth (GO:0045926)	0.167570113	0.206442177	10.12913434
positive regulation of macromolecule biosynthetic process (GO:0010557)	0.171209003	0.209611023	9.771294622
muscle contraction (GO:0006936)	0.171209003	0.209611023	9.771294622
Golgi organization (GO:0007030)	0.17241855	0.210436305	9.656386866
defense response to virus (GO:0051607)	0.176036973	0.214187401	9.32401455
positive regulation of cellular catabolic process (GO:0031331)	0.18561158	0.225139972	8.519736899
negative regulation of DNA-binding transcription factor activity (GO:0043433)	0.187988394	0.227321351	8.335436586
positive regulation of cytosolic calcium ion concentration (GO:0007204)	0.192721947	0.232326702	7.98483309
positive regulation of intracellular protein transport (GO:0090316)	0.193901166	0.232326702	7.900734333
regulation of cytosolic calcium ion concentration (GO:0051480)	0.193901166	0.232326702	7.900734333
brain development (GO:0007420)	0.196254616	0.234431806	7.736577923
negative regulation of protein phosphorylation (GO:0001933)	0.198601431	0.23651625	7.577612216
cellular response to interleukin-1 (GO:0071347)	0.202109254	0.239058236	7.348406791
regulation of signal transduction by p53 class mediator (GO:1901796)	0.20327523	0.239058236	7.274364134
regulation of cell differentiation (GO:0045595)	0.20327523	0.239058236	7.274364134
peptidyl-serine phosphorylation (GO:0018105)	0.20327523	0.239058236	7.274364134
cellular response to growth factor stimulus (GO:0071363)	0.205602249	0.239058236	7.129667682
skeletal system development (GO:0001501)	0.205602249	0.239058236	7.129667682
cellular response to starvation (GO:0009267)	0.205602249	0.239058236	7.129667682
organonitrogen compound biosynthetic process (GO:1901566)	0.205602249	0.239058236	7.129667682
double-strand break repair (GO:0006302)	0.212544001	0.246400567	6.721032562
negative regulation of canonical Wnt signaling pathway (GO:0090090)	0.21369525	0.247006569	6.656412982
peptidyl-serine modification (GO:0018209)	0.21828402	0.251570733	6.407172324
positive regulation of I-kappaB kinase/NF-kappaB signaling (GO:0043123)	0.220568698	0.253460522	6.287841142
mitochondrion organization (GO:0007005)	0.225118729	0.25793487	6.059082054
positive regulation of developmental process (GO:0051094)	0.227384117	0.259555386	5.949403908

negative regulation of immune response (GO:0050777)	0.228514411	0.259555386	5.895688436
regulation of mitotic cell cycle (GO:0007346)	0.228514411	0.259555386	5.895688436
positive regulation of cellular biosynthetic process (GO:0031328)	0.230770213	0.261362229	5.790434766
negative regulation of cytokine production (GO:0001818)	0.233019645	0.263151496	5.687994768
negative regulation of Wnt signaling pathway (GO:0030178)	0.243063737	0.273707875	5.259186292
positive regulation of transcription, DNA-templated (GO:0045893)	0.24433741	0.274356006	2.589345621
negative regulation of macromolecule metabolic process (GO:0010605)	0.246383456	0.275081529	5.127004365
regulation of programmed cell death (GO:0043067)	0.246383456	0.275081529	5.127004365
negative regulation of transcription by RNA polymerase II (GO:0000122)	0.261121936	0.290710824	2.813147386
negative regulation of multicellular organismal process (GO:0051241)	0.268158377	0.296862654	4.360334561
positive regulation of protein modification process (GO:0031401)	0.268158377	0.296862654	4.360334561
regulation of cell growth (GO:0001558)	0.271371763	0.299576132	4.260212714
positive regulation of cell motility (GO:2000147)	0.275635094	0.303430229	4.131926555
regulation of I-kappaB kinase/NF-kappaB signaling (GO:0043122)	0.278816775	0.306075398	4.039422511
apoptotic process (GO:0006915)	0.286188312	0.313292497	3.835103847
regulation of canonical Wnt signaling pathway (GO:0060828)	0.308885431	0.337199929	3.283104072
cellular component assembly (GO:0022607)	0.316964873	0.345061482	3.110884031
regulation of protein phosphorylation (GO:0001932)	0.321968132	0.349539989	3.009819831
regulation of cell cycle (GO:0051726)	0.351252803	0.38028196	2.492251438
DNA repair (GO:0006281)	0.353161072	0.381297531	2.462398955
proteasome-mediated ubiquitin-dependent protein catabolic process	0.37472031	0.403465977	2.152783217
positive regulation of cytokine production (GO:0001819)	0.387501854	0.416088056	1.990649739
post-translational protein modification (GO:0043687)	0.39647669	0.424564956	1.885141623
regulation of transcription by RNA polymerase II (GO:0006357)	0.399627643	0.42677626	1.184241144
cellular response to DNA damage stimulus (GO:0006974)	0.40091636	0.426992221	1.835300462
negative regulation of transcription, DNA-templated (GO:0045892)	0.402595147	0.427621331	1.355367489
negative regulation of cell population proliferation (GO:0008285)	0.426051232	0.451315725	1.579427713
positive regulation of macromolecule metabolic process (GO:0010604)	0.430280639	0.454570675	1.540367943
cellular protein modification process (GO:0006464)	0.44196096	0.465658599	1.120283917

phosphorylation (GO:0016310)	0.443613491	0.466150005	1.423930643
regulation of cell migration (GO:0030334)	0.450166437	0.471774426	1.370197434
cellular protein metabolic process (GO:0044267)	0.457449435	0.478131989	1.312993555
regulation of nucleic acid-templated transcription (GO:1903506)	0.467805109	0.487658907	1.235941215
nervous system development (GO:0007399)	0.481059522	0.500149186	1.14411414
negative regulation of nucleic acid-templated transcription (GO:1903507)	0.493994939	0.512242773	1.061217755
regulation of cellular macromolecule biosynthetic process (GO:2000112)	0.496993013	0.513995406	1.04288722
positive regulation of cell population proliferation (GO:0008284)	0.501457989	0.517251941	1.016174171
neutrophil degranulation (GO:0043312)	0.506618769	0.520598583	0.986146699
cellular response to cytokine stimulus (GO:0071345)	0.5073518	0.520598583	0.981953652
neutrophil activation involved in immune response (GO:0002283)	0.509544588	0.521487039	0.969515518
neutrophil mediated immunity (GO:0002446)	0.51172795	0.522361258	0.957285302
protein phosphorylation (GO:0006468)	0.51750447	0.526889266	0.925653975
protein ubiquitination (GO:0016567)	0.537896317	0.546235795	0.821897469
negative regulation of cellular macromolecule biosynthetic process	0.552808325	0.559932143	0.753143065
negative regulation of cellular process (GO:0048523)	0.565312041	0.571125019	0.699667769
cytokine-mediated signaling pathway (GO:0019221)	0.599633526	0.604246091	0.570092723
positive regulation of cellular process (GO:0048522)	0.602024867	0.605104278	0.561914002
regulation of transcription, DNA-templated (GO:0006355)	0.646670363	0.648320032	0.397942373
regulation of cell population proliferation (GO:0042127)	0.677069479	0.677069479	0.350625464

Table 3.S12 Triple intersection of proteomics dataset related to figure 3.S5 B

C1orf27	**UFSP2**	**UFL1**	**C1orf27 & UFL1**	**UFSP2 & UFL1**	**C1orf27 & UFSP2 & UFL1**
UFSP2	**C1orf27**	**CDK5RAP3**	MTDH	RPS6KA4	**DDRGK1**
VEZT	PRKAR1A	PTBP3	CAMLG		**TMEM263**
MAVS	MB21D2	SRP54	KTN1		
TACC1	**NME1**	GNB2	ANKLE2		
PSMA4	FMR1	LRRC59	VAPB		
SYAP1	PM20D2	**HERC2**	BCAP31		
AKAP1	PRIM2	FNDC3A	STIM1		
VAPA	SNX3	SNAP47	EMD		
TOR1AIP1	EIF5	RNF121	SRPRA		
SYNE2		TMED5	CDKAL1		
TEX264		NEURL4	RTN4		
TMEM214		IFI16	MOSPD2		
NRDC		NMD3			
FADS2		GRAMD1A			
TOR1AIP2					
SCD					
JPH1					
RRAGB					
DNAJA2					

Table 3.S13 Primers and sgRNAs sequences used in this study.

Oligos used in NGS library preparation-nested PCR										
Outer-PCR										
outer_TKO_v1-F	AGGGCCTATTTCCCATGATTCCTT									
outer_TKO_v1-R	TCAAAAAAGCACCGACTCGG									
Inner-PCR										
Forward-i5										
Truseq_**i5_1**	AATGATACGGCGACCACCGAGATCTACACTATAGCCTACACTCTTTCCCTACACGACGCTCTTCCGATCTTGTGGAAAGGACGAGGTACCG									
Truseq_**i5_2**	AATGATACGGCGACCACCGAGATCTACACATAGAGGCACACTCTTTCCCTACACGACGCTCTTCCGATCTTGTGGAAAGGACGAGGTACCG									
Truseq_**i5_3**	AATGATACGGCGACCACCGAGATCTACACCCTATCCTACACTCTTTCCCTACACGACGCTCTTCCGATCTTGTGGAAAGGACGAGGTACCG									
Truseq_**i5_4**	AATGATACGGCGACCACCGAGATCTACACGGCTCTGAACACTCTTTCCCTACACGACGCTCTTCCGATCTTGTGGAAAGGACGAGGTACCG									
Reverse-i7										
Truseq_**i7_1**	CAAGCAGAAGACGGCATACGAGATCGAGTAATGTGACTGGAGTTCAGACGTGTGCTCTTCCGATCTATTTTAACTTGCTATTTCTAGCTCTAAAAC									
Truseq_**i7_2**	CAAGCAGAAGACGGCATACGAGATTCTCCGGAGTGACTGGAGTTCAGACGTGTGCTCTTCCGATCTATTTTAACTTGCTATTTCTAGCTCTAAAAC									
Truseq_**i7_3**	CAAGCAGAAGACGGCATACGAGATAATGAGCGGTGACTGGAGTTCAGACGTGTGCTCTTCCGATCTATTTTAACTTGCTATTTCTAGCTCTAAAAC									
Truseq_**i7_4**	CAAGCAGAAGACGGCATACGAGATGGAATCTCGTGACTGGAGTTCAGACGTGTGCTCTTCCGATCTATTTTAACTTGCTATTTCTAGCTCTAAAAC									
Truseq_**i7_5**	CAAGCAGAAGACGGCATACGAGATTTCTGAATGTGACTGGAGTTCAGACGTGTGCTCTTCCGATCTATTTTAACTTGCTATTTCTAGCTCTAAAAC									
Truseq_**i7_6**	CAAGCAGAAGACGGCATACGAGATACGAATTCGTGACTGGAGTTCAGACGTGTGCTCTTCCGATCTATTTTAACTTGCTATTTCTAGCTCTAAAAC									

Table 3.S14 Software and packages used in this study.

Software-Package	Source	Reference
MAGecK 0.5.9.5	https://sourceforge.net/p/mageck/wiki/Home/	(Li et al, 2014)
DrugZ	https://github.com/hart-lab/drugz	(Colic et al, 2019)
R-Studio 22.07.1	https://www.r-project.org/	R software
GSEA 4.3.0	https://www.gsea-msigdb.org/gsea/index.jsp	(Subramanian et al, 2005; Mootha et al, 2003)
Graphpad-Prism 9.3.1	https://www.graphpad.com/scientific-software/prism/	GraphPad
Snapgene 6.0.6	https://www.snapgene.com	Dotmatics
Adobe Photoshop 22.1.0	https://www.adobe.com/products/illustrator.html	Adobe
Adobe Illustrator 25.0.1	https://www.adobe.com/products/photoshop.html	Adobe
ProHits	https://prohits.ircm.qc.ca/Prohits/	(Liu et al, 2017)
SAINTexpress v3.6.1	https://prohits.ircm.qc.ca/Prohits/	(Choi et al, 2011)
ProHits-viz	https://prohits-viz.org/	(Knight et al, 2017)